Pseudopeptidic Macrocyclic Systems with Preorganized Cavities

Ferran Esteve Franch

Directors:

Prof. Santiago V. Luis Lafuente

Dra. Belén Altava Benito

Tutor:

Prof. Eduardo García-Verdugo Cepeda

Castelló de la Plana, July 2022

UNIVERSITAT JAUME·I

Programa de Doctorado en Química Sostenible

Escuela de Doctorado de la Universitat Jaume I

Pseudopeptidic Macrocyclic Systems with Preorganized Cavities

Memoria presentada por Ferran Esteve Franch para optar al grado de doctor por la Universitat Jaume I

Ferran Esteve Franch	Santiago V. Luis Lafuente	Belén Altava Benito

Castelló de la Plana, Abril de 2022.

Financiación

Licencias

Agradecimientos

Me gustaría agradecer a todas las personas que han aparecido en mi vida durante esta etapa de formación, así como a las que ya estaban presentes desde antes de empezarla. Esta tesis, al igual que yo, tiene un poco de cada uno de vosotros.

En primer lugar, quiero mostrar mi enorme gratitud a los profesores del grupo de Química Sostenible y Supramolecular de la Universitat Jaume I. Gracias Maribel, por estar siempre pendiente, por enseñarme lo que es la resiliencia, y por tener las palabras correctas en cada momento en que las he necesitado. Gracias Santiago, por contagiarme de tu pasión por la química, por ayudarme a levantarme en las situaciones de frustración tan presentes durante el doctorado y por ser un ejemplo a seguir como persona y como profesional. Gracias Belén, por estar siempre presente en el día a día, por ayudarme con todas las dudas que me han surgido y por demostrarme que con constancia todo es más fácil de conseguir. Gracias Eduardo, por los millones de ideas, por todas las conversaciones que me han hecho crecer tanto como químico como persona, y por hacerme notar la confianza que siempre has tenido en mí.

Quería agradecer también a todos los miembros del grupo con los que he coincidido. Mi primera mentora en el laboratorio, Adriana, que empezó siendo compañera y ha terminado siendo amiga. Gracias por hacer tan fácil el compartir esta etapa contigo. A Iván, gracias por los momentos compartidos tanto en el laboratorio como en los congresos, cenas, comidas, pádel, etc. Muchas gracias Edgar, por tantas risas juntos, por compartir tu sentido del humor conmigo, y por las clases gratuitas de elegancia en el tenis y fútbol sala. No me puedo olvidar de don David, gracias por tu sabiduría y por tu tranquilidad, has sido la dosis de calma necesaria durante esta etapa de formación. Gracias por aguantar mis ataques sonámbulos que ahora nos traen tantos buenos momentos, eres el compañero de habitación más "tuanis" que se puede pedir. Gracias Dani, por tantas carcajadas en el laboratorio y por siempre tener una visión más cercana a la vida "fuera" de la universidad, tus consejos siempre se agradecen. Gracias a Raúl y Maria por estar siempre dispuestos a ayudar tanto en el laboratorio

como fuera de él, sois dos ejemplos de humildad y trabajo. En cuanto a los miembros actuales del grupo, Samira, Nyhad, Jose Juan, Armando, Sergio, Marc, Julián, os agradezco la compañía diaria y toda la ayuda que me habéis prestado y os deseo mucha suerte en vuestras etapas. También me gustaría resaltar el papel de los alumnos de TFG y TFM que me han ayudado durante estos años, Adrian, Alex, Irene, Juan, Miguel, Iván, Andrea y David, sin vosotros este trabajo no hubiera sido posible.

A los miembros del departamento de Química Inorgánica y Orgánica y de Química Física y Analítica, por ser un ejemplo de cooperación. A los miembros de los grupos de investigación vecinos, por todos los momentos compartidos en las cenas y comidas de becarios. A Eva, por compartir conmigo cada comida durante estos últimos 5 años, gracias por escuchar y por todos tus consejos, y por siempre preocuparte por nosotros. A mis antiguos compañeros de la carrera y del máster, por estar presentes en estas dos etapas que me han llevado a estar dónde me encuentro actualmente, sin vosotros el camino hubiera sido más complicado.

A todos los técnicos de los servicios centrales de la Universitat Jaume I, por estar siempre disponibles para realizar todos los análisis necesarios. En especial, me gustaría agradecer el trato recibido por parte de Cristian, Gabriel, Ricard, José Miguel y Cristina, gracias por la cercanía mostrada, por tener paciencia y por ayudarme siempre en todo lo posible.

También quiero mostrar mi especial gratitud al prof. Jean-Marie Lehn, por darme la oportunidad de unirme a su querido grupo durante la estancia internacional. Aunque sólo hayan sido 3 meses, el poder compartir tiempo a su lado ha sido realmente enriquecedor. Como ya te he comentado muchas veces, mi enorme gratitud para Annia, por hacer realidad esta estancia y por toda la ayuda incondicional prestada. Gracias a todos los miembros de Labo Lehn, por hacerme sentir uno más desde el momento que llegué. Especialmente, a Tanguy, Maria Jesús, Artem, Paulo, Meixia, Bogdan, Chengyi, Cyril y Jean-Louis, por compartir tantos momentos juntos.

A mis amigos del alboroto, por siempre hablar tan poco de estos temas, gracias por ser la evasión necesaria. Aunque la filtración de la piña colada cada vez sea más

evidente, las amistades del filtrado cada vez són más puras y cristalinas. Gracias en especial a Xavi, Sergio, David, Ángel, Mauro, Adrián, Guillem, Rafa, Josevi i Juan, por estar siempre. Andrés, te quedas fuera de esa lista porque, de forma muy afortunada, podrías estar en cualquier párrafo de estos agradecimientos. Gracias por ser amigo, vecino, compañero, confidente y familia desde siempre.

A mi pareja, Maria. Siempre he sido mucho de charrar, pero contigo he aprendido a hablar. Eres como una fase estacionaria universal, da igual lo complicada que sea la mezcla inicial de problemas, siempre consigues separarlos de forma sensata y cambiar mi percepción, haciendo que cada fracción pase de problema a solución con tus consejos. Gracias por apostar por mí, por tu confianza, por tu ayuda, por tu amor. Gracias por aparecer y quedarte, por quemar etapas a mi lado y por ayudarme a crecer. Eres la mejor persona que conozco, y por eso doy gracias a la química por juntar nuestros caminos. Gracias también a Ana, Ricardo, José Luis e Isabel por hacerme sentir uno más de la familia.

Finalmente, quiero agradecer todo el apoyo que mi familia me ha brindado. Vuestra confianza en mí me empuja a esforzarme cada día un poco más. Por muy lejos que estemos, cada uno de vosotros sois ganadores en vuestras pequeñas batallas, y de vosotros he aprendido que siempre hay que luchar por lo que se desea. En especial, gracias a mis iaios, Vicente y Julieta. Iaio, seguramente ya hayas leído está tesis por internet mucho antes de que yo la haya escrito, eres un ejemplo de superación y de constancia. Iaia, siempre presente, siempre al tanto, siempre escuchando, la persona con el corazón más puro que se pueda tener. A mi hermano Borja, por soportarme, quererme y aceptarme desde que era pequeño. Gracias por tu paciencia, por acompañarme en todo momento, y por tu bondad. Gracias también a Miriam, por cuidarlo y hacerle feliz. Finalmente, a mis padres Ximo y Amparo, gran parte de lo que soy es el resultado de todos vuestros esfuerzos. Sois el claro ejemplo de que la responsabilidad y el cachondeo pueden ir juntos de la mano, gracias por vuestro apoyo cuando lo he necesitado y cuando no, por defenderme, y por hacerme sentir querido.

Abbreviations

3D – Three-dimensional

ACS – American chemical society

Asp – Aspartic acid

ATR – Attenuated total reflection

CA – Carbonic anhydrase

CC – Cyclic carbonates

CCDC - Cambridge crystallographic data centre

CD – Circular dichroism

CGC – Critical gelation concentration

CGT – Critical gelation temperature

COSY – Correlation spectroscopy

CPME – Cyclopentyl methyl ether

DCC – Dynamic combinatorial chemistry

DCvC - Dynamic covalent chemistry

DCLs – Dynamic combinatorial libraries

DFT – Density functional theory

DNA - Deoxyribonucleic acid

DOSY – Diffusion-ordered spectroscopy

EA – Elemental analysis

e.e. – Enantiomeric excess

FT – Fourier transform

GC – Gas chromatography

h – Hours

H-bonding – Hydrogen bonding

HBA – Hydrogen bond acceptor

HBD – Hydrogen bond donor

His – Histidine

HMBC - Heteronuclear multiple bond correlation

HPLC – High performance liquid chromatography

HRMS – High resolution mass spectrometry

HSQC - Heteronuclear single quantum coherence

IR – Infrared spectroscopy

LHSV - Liquid hourly space velocity

LMWG – Low molecular weight gelators

LVER – Linear viscoelastic region

MEI – Macrocyclization Environmental Impact

min – Minutes

MMFF - Merck molecular force field

nm - Nanometres

NMR – Nuclear magnetic resonance

NOESY - Nuclear overhauser effect spectroscopy

NPs – Nanoparticles

ORD – Optical rotatory dispersion

PDB – Protein data bank

Phe/F – Phenylalanine

PS-DVB - Polystyrene-divinylbenzene

RIC- Reactants interaction complex

RNA - Ribonucleic acid

rpm – Revolutions per minute

r.t. – Room temperature

SDG – Sustainable development goals

Ser – Serine

SO – Styrene oxide

SC – Styrene carbonate

SPMs – Shape persistent macrocycles

TGA – Thermogravimetric analysis

TOF – Turn over frequency

TON – Turn over number

TOS – Time on stream

Trp – Tryptophane

TS – Transition state

UN – United Nations

UV – Ultraviolet

Val/V – Valine

Vis – Visible

Resumen de la Tesis

La presente tesis doctoral se engloba dentro del área de la Química Supramolecular y más concretamente en el campo de la Química Bioinspirada. El principal objetivo es el diseño y desarrollo de nuevos sistemas seudopeptídicos macrocíclicos, con cavidades en su estructura, ya que estos compuestos cíclicos son muy interesantes por sus propiedades químicas. Conjuntamente, siempre se intenta interrelacionar la Química Supramolecular y la Química Sostenible, o bien buscando metodologías sintéticas más respetuosas para el medio ambiente, o bien utilizando los compuestos diseñados para aplicaciones sostenibles, como puede ser la conversión de CO_2. La memoria de la tesis se ha estructurado en 10 capítulos dónde los resultados y su discusión se han redactado siguiendo el formato de artículos científicos a partir del trabajo de investigación desarrollado. Los resultados obtenidos han permitido la publicación de dos artículos en la revista *Journal of Organic Chemistry,* de la editorial ACS, así como un artículo en la revista *Green Chemistry*, de la editorial Royal Society of Chemistry, otro en la revista *Advanced Sustainable Systems*, de la editorial Wiley, y, por último, un artículo en la revista *Chem* de la editorial Cell-press. Asimismo, el trabajo desarrollado ha permitido la elaboración de una patente española. El manuscrito en el que se describen de forma más detallada los resultados incluidos en la patente ha sido enviado a la revista *Angewandte Chemie International Edition,* perteneciente a la editorial Wiley. Del mismo modo, los resultados obtenidos en el diseño de nuevas especies seudopeptídicas capaces de formar hidrogeles supramoleculares se han enviado a la revista *Materials Chemistry Frontiers* de la editorial Royal Society of Chemistry. En la sección previa al resumen de la tesis se pueden encontrar las abreviaciones y símbolos empleados recurrentemente a lo largo de este trabajo, ordenados alfabéticamente.

El primer capítulo contiene una introducción sobre los temas más relevantes que se tratan en esta tesis, con la finalidad de contextualizar al lector y mostrarle los antecedentes para que pueda comprender la importancia de los resultados obtenidos. A continuación, en el capítulo segundo, se exponen y detallan los objetivos generales de la tesis, de forma que el lector pueda visualizar la evolución del proyecto partiendo

de las metas fijadas al inicio de esta etapa. A partir de esa sección, se detalla la discusión de los resultados obtenidos en las diferentes etapas del proyecto, durante los 7 capítulos sucesivos.

En el capítulo 3 se describe la síntesis de macrociclos seudopeptídicos de diferente tamaño que contienen en su estructura un grupo hexahidropirrolo[3,4-*f*]isoindólico. La longitud de la cadena hidrocarbonada del espaciador alifático demostró ser determinante para la selectividad de la reacción. Tal y como se demostró mediante las diferentes técnicas espectroscópicas y modelización molecular, cuanto mayor era la distancia entre los grupos amida del seudopéptido de cadena abierta, menos favorecida se encontraba la conformación en forma de U y, por tanto, menor era el rendimiento del macrociclo [1+1] deseado. Por otro lado, el anión bromuro que actuaba como grupo saliente en cada una de las cuatro reacciones S_N2 favorecía claramente la macrociclación al inducir una disposición espacial óptima para el intermedio de reacción. Sin embargo, cuando se utilizaba cloruro como grupo saliente se obtuvieron productos de naturaleza polimérica, indicando que la presencia de este anión más básico conllevaba una pérdida de preorganización para la ciclación. Este trabajo permitió la publicación de un artículo en la revista *Journal of Organic Chemistry*.

En busca de mejorar la sostenibilidad de este método sintético, y tomando ventaja del efecto catalítico promovido por los aniones bromuro, se diseñó un protocolo sintético en flujo continuo para los macrociclos descritos en el capitulo 3. Con este objetivo en mente, se funcionalizó una resina Merrifield comercial con una amina secundaria para obtener un soporte polimérico de naturaleza básica. Esta resina se utilizó para producir el macrociclo en flujo continuo, obteniendo productividades casi 20 veces más elevadas que las alcanzables por la síntesis tradicional. Además, se diseñó un sistema en flujo que combinaba la síntesis con el aislamiento del producto, recuperando el 85% del disolvente utilizado en la reacción. De este modo, el impacto medioambiental de la macrociclación se redujo drásticamente. Ambas mejoras quedan reflejadas en el capítulo 4. Esta investigación se pudo publicar en la revista especializada *Journal of Organic Chemistry*.

En el capítulo 5 se utilizaron los macrociclos que contienen el grupo hexahidropirrolo[3,4-*f*]isoindólico como catalizadores para la síntesis de carbonatos cíclicos empleando epóxidos y dióxido de carbono como reactivos. El sistema multicomponente organocatalítico era el resultado de combinar los seudopéptidos cíclicos con una sal orgánica que actuaba como fuente de especies nucleofílicas. Los resultados catalíticos demostraban una tendencia inesperada, ya que la actividad era mayor en presencia de los aniones menos nucleófilos. Gracias a los diferentes estudios supramoleculares se pudo elucidar la naturaleza de este comportamiento catalítico, observándose que en presencia del anión cloruro (especie menos nucleófila pero más básica) los seudopéptidos macrociclos de cadena corta eran capaces de preorganizar los diferentes componentes de reacción en una disposición espacial óptima para su transformación, imitando el *modus operandi* de las enzimas. En este capítulo también se estudió el efecto de la cavidad en la estructura seudopeptídica, así como el tamaño de la misma, y la basicidad de los grupos amino presentes en los organocatalizadores. Este estudio se publicó en la revista *Green Chemistry*.

De nuevo, con el objetivo principal de mejorar la sostenibilidad del proceso catalítico de conversión de CO_2, se diseñó una nueva generación de macrociclos seudopeptídicos (capítulo 6). Estos nuevos compuestos contenían en su estructura, además de una cavidad con elevada densidad funcional, un brazo adicional que permitía su inmovilización covalente en un soporte polimérico. Con esta aproximación también se consiguió soportar la fuente de aniones nucleofílicos en la misma matriz, de forma que se reducían los residuos en comparación con el sistema descrito en el capítulo 5. El diseño del sistema permitió elegir una matriz hidrofóbica que favoreciera las interacciones supramoleculares entre los componentes catalíticos, obteniendo valores de TON y TOF elevados incluso a presiones de dióxido de carbono bajas. Este modelo sinzimático heterogéneo se pudo reciclar durante 5 ciclos catalíticos sin pérdida aparente de actividad, ya que las interacciones no-covalentes son reversibles y el sistema no sufría de desactivación durante el proceso. Este trabajo se publicó en la revista *Advanced Sustainable Systems*.

Estos resultados catalíticos, aunque prometedores, seguían teniendo la principal limitación de la necesidad de temperaturas de aproximadamente 100 °C para funcionar. En el capítulo 7 se describen unos complejos bimetálicos seudopeptídicos capaces de llevar a cabo la reacción incluso a temperatura ambiente, sin necesitar además ningún co-catalizador. Los compuestos homobimetálicos quirales demostraron ser eficientes en la resolución cinética de epóxidos, obteniendo carbonatos cíclicos con buena enantioselectividad. En este proyecto se estudiaron también las fuerzas no-covalentes que permitían alcanzar actividades catalíticas tan elevadas. También se evaluó el efecto de los sustituyentes del aminoácido utilizado, obteniéndose los mejores resultados para los seudopéptidos derivados de la fenilalanina. Tal y como se esperaba, variando la quiralidad de los centros estereogénicos de los complejos seudopeptídicos se consiguió modular la enantiopreferencia de la reacción de cicloadición de CO_2 a los epóxidos. Esta investigación permitió la redacción de un manuscrito listo para ser enviado a la revista *Angew. Chem. Int. Ed.,* y también la publicación de una patente española.

En el capítulo 8 se describe el trabajo realizado durante el periodo de estancia investigadora internacional en el *Institut de Science et d'Ingénierie Supramoléculaires* (Strasbourg, Francia), bajo la supervisión del prof. Jean-Marie Lehn. El proyecto se basaba en sintetizar criptandos seudopeptídicos dinámicos mediante la reacción de formación de iminas. Los resultados obtenidos demostraron que en presencia de disolventes apolares se favorecía la encapsulación de dos moléculas de agua en el interior de la cavidad, llevando a resultados casi cuantitativos para las cajas moleculares [3+2] deseadas. Por el contrario, la utilización de disolventes polares llevaba al sistema a la formación de productos poliméricos que actuaban como trampa cinética del sistema dinámico. Los seudopéptidos bicíclicos obtenidos demostraban sufrir una fuerte inducción de quiralidad helicoidal, ya que solo un tipo de enantiómero rotacional se podía observar para cada criptando homoléptico en cuanto a la quiralidad del carbono α. La naturaleza reversible de este tipo de enlaces admitía procesos de reordenamiento entre criptandos de diferente quiralidad, obteniendo las cajas moleculares seudopeptídicas homoquirales como productos

termodinámicamente favorecidos. Estos resultados permitieron la redacción de un manuscrito que ha sido aceptado en la revista *Chem*.

El capítulo 9 describe los avances tecnológicos alcanzados en el diseño de nuevos materiales biocompatibles basados en compuestos seudopeptídicos de cadena abierta. Los tetra-seudopéptidos homolépticos derivados de L-Phe eran capaces de formar una red tridimensional en disoluciones acuosas, incluso utilizando concentraciones de hidrogelante bajas. Estos superhidrogelantes, además, podían experimentar transiciones gel-sol dependiendo del pH de la disolución acuosa, siendo clasificados como materiales inteligentes. Este tipo de variación estructural también se promovía al absorber CO_2, ya que las especies carbamato formadas al reaccionar con los grupos amino terminales limitaban el ensamblaje correcto de los seudopéptidos.

Finalmente, en el capítulo 10 y último, se exponen las conclusiones más relevantes derivadas del trabajo descrito en cada uno de los capítulos que conforman esta tesis.

Summary of the Thesis

The present Doctoral Thesis is included within the area of Supramolecular Chemistry and, more specifically, in the field of Bioinspired Chemistry. The main objective is the design and development of new pseudopeptidic systems bearing cavities in their structure, since these cyclic compounds are extremely interesting due to their physicochemical properties. Besides, there is always a clear correlation between Supramolecular Chemistry and Sustainable Chemistry during this project, either looking for more environmentally friendly synthetic methodologies, or using the compounds designed for sustainable applications, such as CO_2 conversion. The thesis is structured in 10 chapters where the results and discussions are presented following the scientific articles format. The results obtained allowed for the publication of two articles in the "Journal of Organic Chemistry", from the ACS publisher, as well as an article in the "Green Chemistry" journal, from the Royal Society of Chemistry publisher. Another manuscript was published in the "Advanced Sustainable Systems" journal, from the Wiley publishing house, and, finally, an additional article has been recently accepted in "Chem" from the Cell-press publishing house. Likewise, the work carried out has allowed for the elaboration of a Spanish patent. The manuscript in which the results embodied in the patent are described in higher detail has been submitted to the journal "Angewandte Chemie International Edition", belonging to the Wiley publishing house. In a similar manner, the results obtained in the design of new pseudopeptide species capable of forming supramolecular hydrogels have been submitted to the journal "Materials Chemistry Frontiers" of the Royal Society of Chemistry publisher. In the section prior to the abstract of the thesis you can find the abbreviations and symbols used recurrently throughout this work, alphabetically arranged.

The first chapter contains an introduction describing the most relevant topics discussed in this thesis, with the aim of contextualizing the reader and highlighting the relevance of the results obtained. Next, in the second chapter, the general objectives of the thesis are exposed, so that the reader can visualize the evolution of the research based on the goals set at the beginning of this project. From this section

on, the discussion of the results obtained in the different research works of the project is detailed over 7 consecutive chapters.

Chapter 3 discusses the syntheses of pseudopeptidic macrocycles of different sizes that contain an hexahydropyrrolo[3,4-*f*]isoindolic group within their structure. The length of the hydrocarbon chain of the aliphatic spacer was crucial for reaching high yields in the macrocyclization reaction. As demonstrated through different spectroscopic techniques and molecular modelling, the greater the distance between the amide groups of the open-chain pseudopeptide, the less favoured the U-turn preorganization and, therefore, the lower the yield of the desired [1+1] macrocycle. On the other hand, the bromide anion that acted as leaving group in each of the four S_N2 reactions was clearly encouraging macrocyclization, as it induced an optimal spatial conformation for the reaction intermediate. However, when chloride was used as the leaving group, products of polymeric nature were obtained, indicating that the presence of this more basic anion entailed a loss of preorganization for cyclization. This work allowed for the publication of a research article in the "Journal of Organic Chemistry".

Seeking to improve the sustainability of these macrocyclizations, and bearing in mind the catalytic effect promoted by bromide anion, a continuous-flow synthetic protocol was designed for the macrocycles presented in chapter 3. The first objective was to develop a basic polymeric support by functionalizing a commercially available Merrifield resin with a secondary amine. This polymer was used to produce the macrocycle under continuous-flow conditions, obtaining productivities almost 20 times higher than those attainable by traditional batch synthesis. In addition, a promising flow system was designed that combined the synthesis of the macrocycle with its isolation, recovering 85% of the solvent used in the reaction. In this way, the environmental impact of the macrocyclization was remarkably reduced, as evidenced by a new environmental metric proposed (MEI score). All these interesting results are explained in higher detail in chapter 4. This research was published in the specialized journal "Journal of Organic Chemistry".

In Chapter 5, macrocycles containing the hexahydropyrrolo[3,4-*f*]isoindolic group were used as catalysts for the synthesis of cyclic carbonates using epoxides and carbon dioxide as reagents. The multicomponent organocatalytic system was relied on the combination of the cyclic pseudopeptides with an organic salt that acted as a nucleophilic source. The catalytic results revealed an unexpected trend, as the activity was higher in the presence of the less nucleophilic anions. Thanks to the different supramolecular studies, it was possible to elucidate the nature of this catalytic behaviour. In the presence of the chloride anion (the least nucleophilic but most basic species), macrocyclic pseudopeptides were capable of preorganizing the different reaction components in an optimal spatial arrangement for their transformation, imitating the *modus operandi* of enzymes. In this chapter we also studied the effect of the cavity of the pseudopeptidic structure, as well as its size, and the basicity of the amino groups present in the peptidomimetic compounds. This study was published in the journal "Green Chemistry".

Again, with the main objective of improving the sustainability of the catalytic CO_2 conversion, a new generation of pseudopeptidic macrocycles was designed (Chapter 6). These new compounds contained in their structure, together with the cavity with high functional density, an additional pendant arm that allowed their covalent immobilization on polymeric supports. With this approach, it was also possible to also immobilize the source of nucleophilic anions in the same matrix, reducing the waste generated compared to the system described in chapter 5. The design of the system was based on an hydrophobic matrix that favoured supramolecular interactions between catalytic components, obtaining high TON and TOF values even at low carbon dioxide pressures. This heterogeneous synzymatic model could be recycled for 5 catalytic cycles without apparent loss of activity, since the non-covalent interactions are reversible. This work was published in the journal "Advanced Sustainable Systems".

These catalytic results, although promising, still required temperatures of ca. 100 °C to promote high CO_2 conversions. Chapter 7 describes pseudopeptidic bimetallic complexes capable of carrying out the reaction even at room temperature, without

the need of any co-catalyst. These chiral homobimetallic compounds proved to be also efficient in the kinetic resolution of epoxides, obtaining cyclic carbonates with good enantioselectivity. In this project, the non-covalent forces that allowed for reaching such remarkable catalytic activities were also studied. The effect of the amino acid sidechains used was also evaluated, obtaining the best results for pseudopeptides derived from phenylalanine. As expected, varying the chirality of the stereogenic centres of the pseudopeptidic complexes modulated the enantiopreference obtained in the cycloaddition of CO_2 to epoxides. This research has been submitted to "Angewandte Chemie International Edition", and it also permitted the publication of a Spanish patent.

Chapter 8 summarizes the work carried out during the period of international research stay at the *Institut de Science et d'Ingénierie Supramoléculaires* (Strasbourg, France), under the supervision of prof. Jean-Marie Lehn. The project was consisted of synthesizing dynamic pseudopeptidic cryptands through reversible reactions of imine formation. The results obtained showed that the presence of apolar solvents favoured the encapsulation of two water molecules inside the cavity, leading to almost quantitative yields for the desired [3+2] molecular cages. On the contrary, the use of polar solvents led to the formation of polymeric products that acted as a kinetic trap for the dynamic system. The bicyclic pseudopeptides undergone a strong helical chirality induction, since only one type of rotational enantiomer was observed for each homoleptic cryptand, as ruled by the α-carbon chirality. The reversible nature of this type of bonds allowed for rearrangement processes between cryptands of different chirality, obtaining homochiral pseudopeptidic macrobicycles as thermodynamically favoured products. These results are described in manuscript that has been accepted in the journal "Chem".

Chapter 9 illustrates the technological advances achieved in the design of new biocompatible materials based on open-chain pseudopeptidic compounds. Homoleptic tetra-pseudopeptides derived from L-Phe permitted the formation of a three-dimensional network in aqueous solutions, even at low gelator concentrations. These superhydrogels also endured gel-sol transitions depending on the pH of the

aqueous solution, being classified as intelligent materials. This type of structural variation was also promoted by CO_2 absorption, as the carbamate derivatives formed upon its reaction with the terminal amino groups of the pseudopeptide hampered the correct self-assembly.

Finally, in chapter 10, the most relevant conclusions derived from the work described in each of the chapters that are encompassed in this thesis are presented.

Scientific Divulgation

The results obtained throughout the development of the current PhD Thesis have led to five publications in high impact scientific journals and the publication of a Spanish patent:

➢ **Authors**: Ferran Esteve, Belén Altava, Michael Bolte, M. Isabel Burguete, Eduardo García-Verdugo, Santiago V. Luis
   Title: Highly selective anion template effect in the synthesis of constrained pseudopeptidic macrocyclic cyclophanes
   Reference: *J. Org. Chem.*, **2020**, 85, 1138-1145. doi: 10.1021/acs.joc.9b03048

➢ **Authors**: Ferran Esteve, Belén Altava, M. Isabel Burguete, Michael Bolte, Eduardo García-Verdugo, Santiago V. Luis
   Title: Pseudopeptidic Macrocycles as Cooperative Minimalistic Synzyme Systems for the Remarkable Activation and Conversion of CO_2 in the Presence of Chloride Anion
   Reference: *Green Chem.* **2020**, 22, 4697-4705. doi: 10.1039/D0GC01449D

➢ **Authors**: Ferran Esteve, Adrian Escrig, Raul Porcar, Santiago V. Luis, Belén Altava, Eduardo García-Verdugo
   Title: Immobilized Supramolecular Systems as Efficient Synzymes for CO_2 Activation and Conversion
   Reference: *Adv. Sustain. Syst.* **2022**, 2100408. doi: 10.1002/adsu.202100408

➢ **Authors**: Ferran Esteve, Raul Porcar, Santiago V. Luis, Belén Altava, Eduardo García-Verdugo
   Title: Continuous flow processes as an enabling tool for the synthesis of constrained pseudopeptidic macrocycles
   Reference: *J. Org. Chem.*, **2022**, *87*, 3519-3528. doi: 10.1021/acs.joc.1c03081

➢ **Authors**: Ferran Esteve, Santiago V. Luis, Belén Altava, Eduardo García-Verdugo
   Title: One-component bimetallic pseudopeptidic complexes for CO_2 conversion
   Reference: *P202230050.*

➢ **Authors**: Ferran Esteve, Belén Altava, Eduardo García-Verdugo, Santiago V. Luis, Jean-Marie Lehn
   Title: Doubly Chiral Pseudopeptidic Macrobicyclic Molecular cages: Water-assisted Dynamic Covalent Self-Assembly and Chiral Self-sorting
   Reference: *Chem*, **2022**, Accepted. doi: 10.1016/j.chempr.2022.04.007

Additional research articles are being prepared to be published in relevant scientific journals:

- ➤ **Authors**: Ferran Esteve, Raul Porcar, Michael Bolte, Belén Altava, Eduardo García-Verdugo, Santiago V. Luis
  Title: Highly Active and Enantioselective Multifunctional One-Component Supramolecular Catalysts for the Cycloaddition of CO_2 to Epoxides
  Reference: *Angew. Chem. Int. Ed.*, **2022**, Submitted.

- ➤ **Authors**: Ferran Esteve, Alexis Villanueva-Antolí, Belén Altava, Eduardo García-Verdugo, Santiago V. Luis
  Title: Unravelling the supramolecular driving forces in the formation of CO_2-responsive pseudopeptidic low molecular weight hydrogelators
  Reference: *Mater. Chem. Front.,* **2022**, Submitted.

- ➤ **Authors**: Ferran Esteve, Belén Altava, Santiago V. Luis, Eduardo García-Verdugo
  Title: Are macrocyclizations sustainable? A novel metric and synthetic approaches towards green processes.
  Reference: *Green Chem.*, **2022**, Submitted.

- ➤ **Authors**: Ferran Esteve, Belén Altava, Santiago V. Luis, Eduardo García-Verdugo
  Title: Basically, nucleophilicity matters little: unravelling the supramolecular driving forces in enzyme-like CO_2 conversion
  Reference: *Appl. Energy*, **2022**, Manuscript under preparation.

Some of the results have also been presented in numerous scientific congresses and conferences, from both national and international relevance:

- ➢ **Authors**: F. Esteve, R. Porcar, A. Escrig, B. Altava, E. García-Verdugo, S. V. Luis
  Title: Preorganized pseudopeptidic systems for CO_2 activation and conversion
  Participation: oral presentation
  Congress: XXVII Seminario Internacional en Ciencias Naturales para el Desarrollo
  City: Costa Rica   **Year**: 2022

- ➢ **Authors**: F. Esteve, R. Porcar, B. Altava, E. García-Verdugo, S. V. Luis
  Title: Flow Chemistry as Enabling Tool for more Productive and Environmentally Friendly Macrocyclizations
  Participation: poster
  Congress: 5th EuCheMS Conference on Green and Sustainable Chemistry
  City: Thessaloniki, Greece   **Year**: 2021

- ➢ **Authors**: F. Esteve, R. Porcar, B. Altava, E. García-Verdugo, S. V. Luis
  Title: Greener macrocyclizations: highly productive flow synthesis of cyclic pseudopeptides
  Participation: oral presentation
  Congress: 25th Annual Green Chemistry & Engineering Conference
  City: United States of America   **Year**: 2021

- ➢ **Authors**: F. Esteve, R. Porcar, B. Altava, M. I. Burguete, E. García-Verdugo, S. V. Luis
  Title: Pseudopeptidic Macrocycles as Effective Cooperative Synzymatic Ssystems for Conversion of CO_2
  Participation: poster
  Congress: 1st SupraMat Network Conference
  City: Tarragona, Spain   **Year**: 2021

- ➢ **Authors**: F. Esteve, R. Porcar, B. Altava, M. I. Burguete, E. García-Verdugo, S. V. Luis
  Title: Macrocyclic Pseudopeptides as Cooperative Synzimatic Systems for Efficient Conversion of CO_2
  Participation: oral presentation
  Congress: 23 Conferencia de Química
  City: Santiago de Cuba, Cuba   **Year**: 2020

➢ **Authors**: F. Esteve, R. Porcar, B. Altava, M. I. Burguete, E. García-Verdugo, S. V. Luis
Title: Pseudopeptidic Macrocyclic Compounds as Active Organocatalysts for CO2 conversion
Participation: poster
Congress: 4th EuCheMS Conference on Green and Sustainable Chemistry
City: Tarragona, Spain   **Year**: 2019

➢ **Authors**: F. Esteve, B. Altava, M. I. Burguete, S. V. Luis
Title: Supramolecularly Assisted Synthesis of Pseudopeptidic Macrocyclic Compounds: The Influence of Halide Anions
Participation: poster
Congress: XIII International Workshop on sensors and molecular recognition
**City**: Valencia, Spain   **Year**: 2019

➢ **Authors:** A. Valls, B. Altava, F. Esteve, M. I. Burguete, S. V. Luis
Title: Supramolecularly Assisted Synthesis of Pseudopeptidic Receptors
Participation: poster
Congress: XXXVII Reunión Bienal de la RSEQ
City: San Sebastian, Spain   **Year:** 2019

➢ **Authors**: F. Esteve, B. Altava, M. I. Burguete, S. V. Luis
Title: Supramolecularly Assisted Synthesis of Pseudopeptidic Macrocyclic Compounds
Participation: poster
Congress: International Symposium on Macrocyclic and Supramolecular Chemistry
City: Lecce, Italy   **Year**: 2019

➢ **Authors**: B. Altava, M. I. Burguete, F. Esteve, S. V. Luis
Title: Supramolecularly Assisted Synthesis of Pseudopeptidic Macrocyclic Compounds
Participation: poster
Congress: International Simposium on Setting their Table: Women and the Periodic Table of Elements
City: Murcia, Spain   **Year**: 2019

> **Authors**: F. Esteve, B. Altava, M. I. Burguete, S. V. Luis
> **Title:** Modulated Synthesis of Chiral Macrocyclic Compounds Derived from Pseudopeptides
> **Participation**: poster
> **Congress:** XV Simposio Jóvenes Investigadores Químicos, RSEQ-Sigma Aldrich (Merck)
> **City**: Toledo, Spain   **Year**: 2018

> **Authors**: F. Esteve, A. Valls, B. Altava, M. I Burguete, L. González, S. V. Luis, I. Peña
> **Title:** Studies in Aqueous Media of Self-assembled Bis-imidazolium Salts Based on Pseudopeptidic Compounds
> **Participation**: poster
> **Congress:** XII International Workshop on sensors and molecular recognition
> **City**: Valencia, Spain   **Year**: 2018

> **Authors:** F. Esteve, A. Valls, B. Altava, M. I Burguete, S. V. Luis
> **Title:** Reception of Biological Anions through Tripodal Ionic Liquids Derived from Natural Amino Acids
> **Participation:** poster
> **Congress:** XIV Simposio de Investigadores Jóvenes Químicos, RSEQ-Sigma Aldrich (Merck)
> **City:** Badajoz, Spain   **Year:** 2017
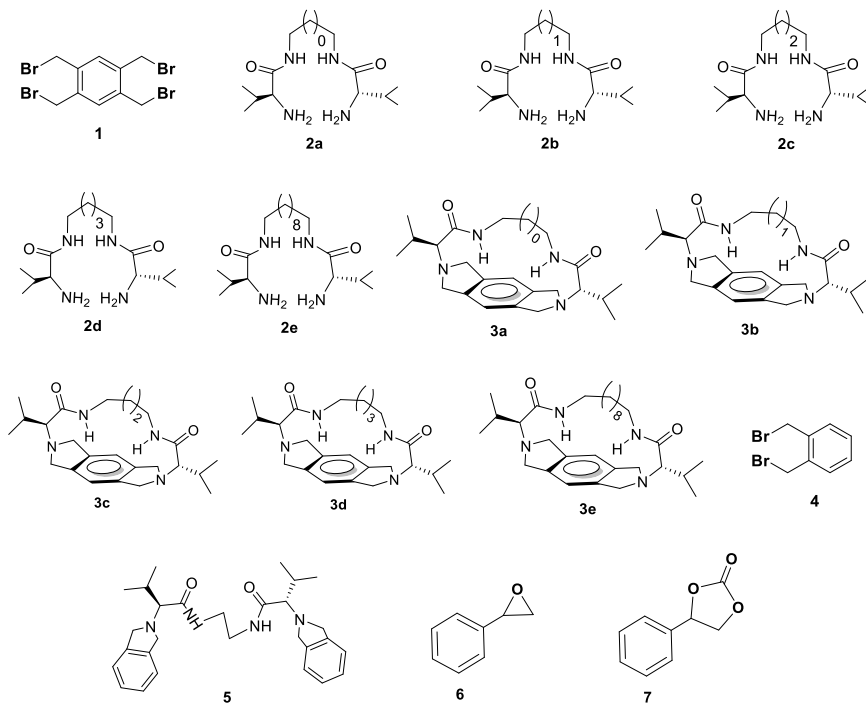
Structure of the Compounds Considered in this Work

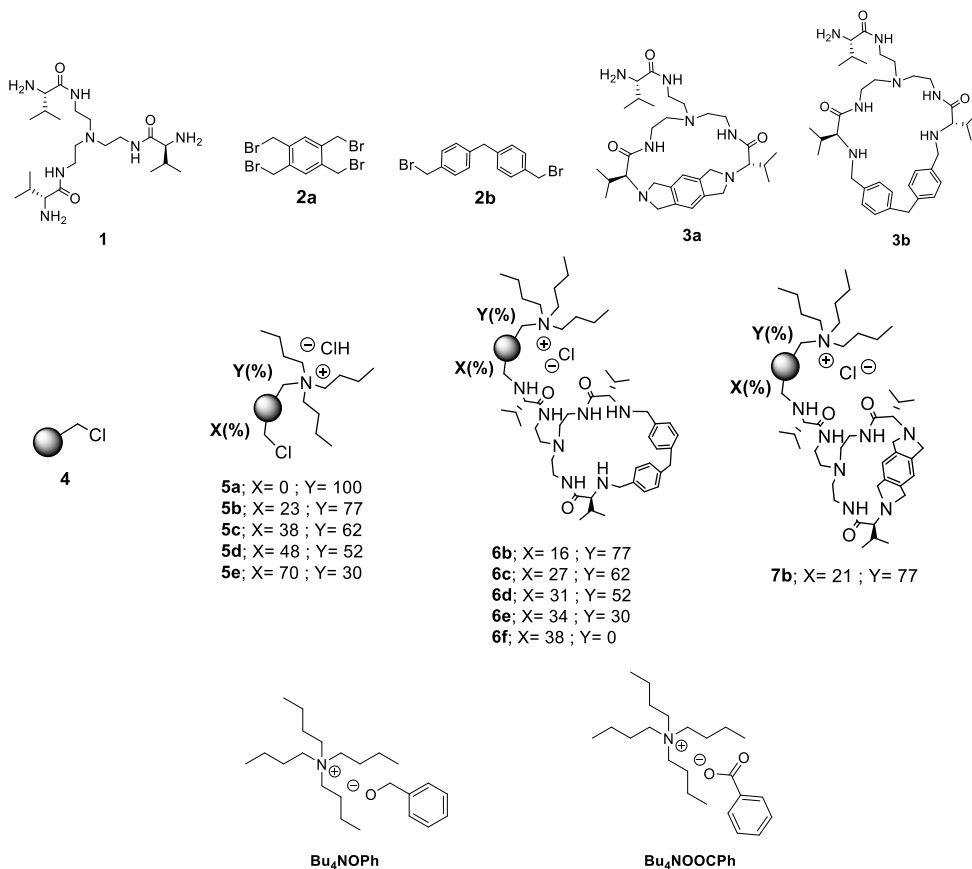**Chapter 3:** Highly Selective Anion Template Effect in the Synthesis of Constrained Pseudopeptidic Macrocyclic Cyclophanes.

1a   1b   1c

1d   1e   2

3a   3b   3c

3d   3e   5a
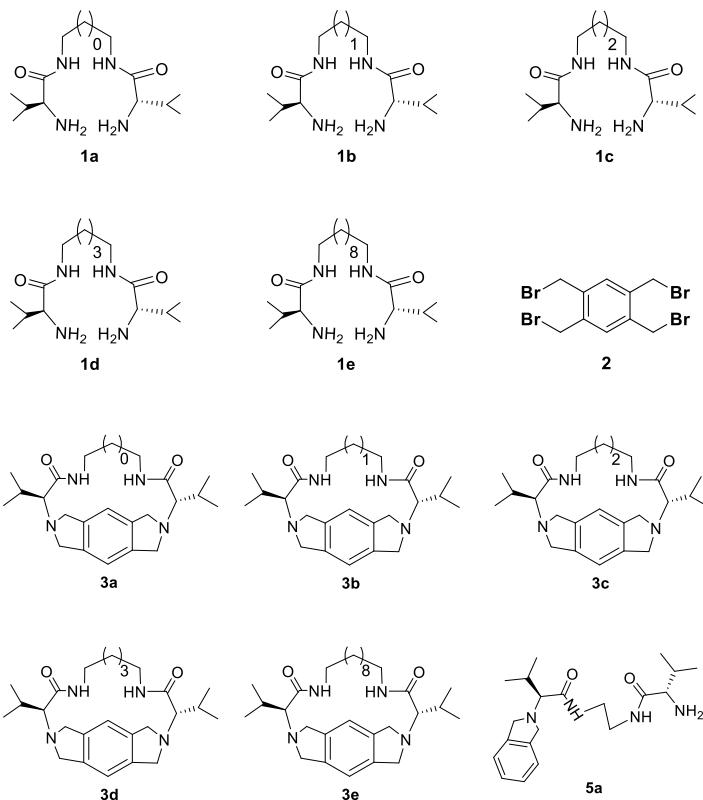
Chapter 4: Continuous Flow Processes as an Enabling Tool for the Synthesis of Constrained Pseudopeptidic Macrocycles.
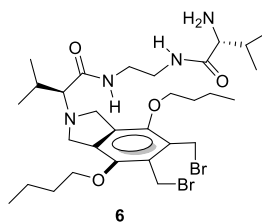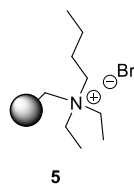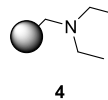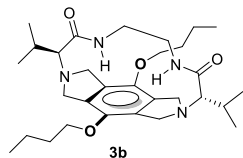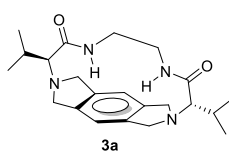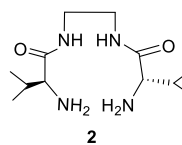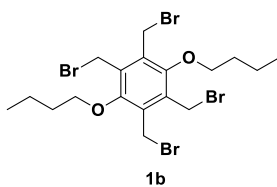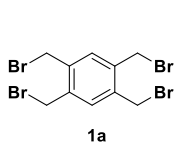
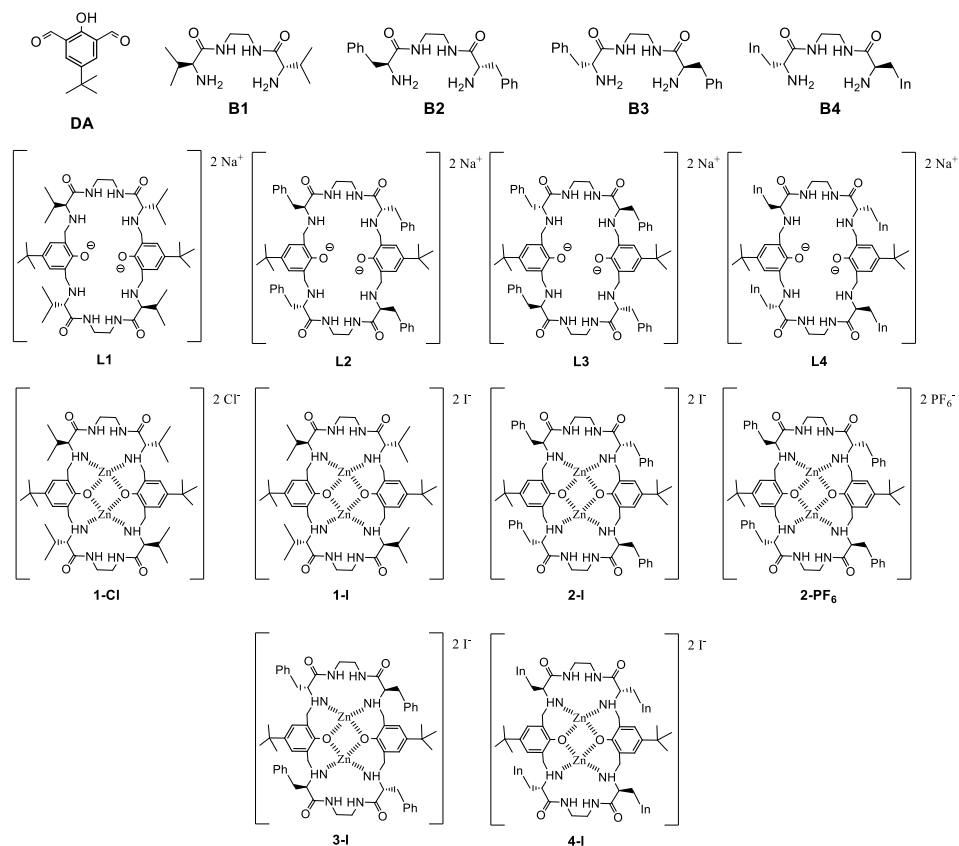**Chapter 5:** Pseudopeptidic Macrocycles as Cooperative Minimalistic Synzyme Systems for the Remarkable Activation and Conversion of CO_2 in the Presence of Chloride Anion.
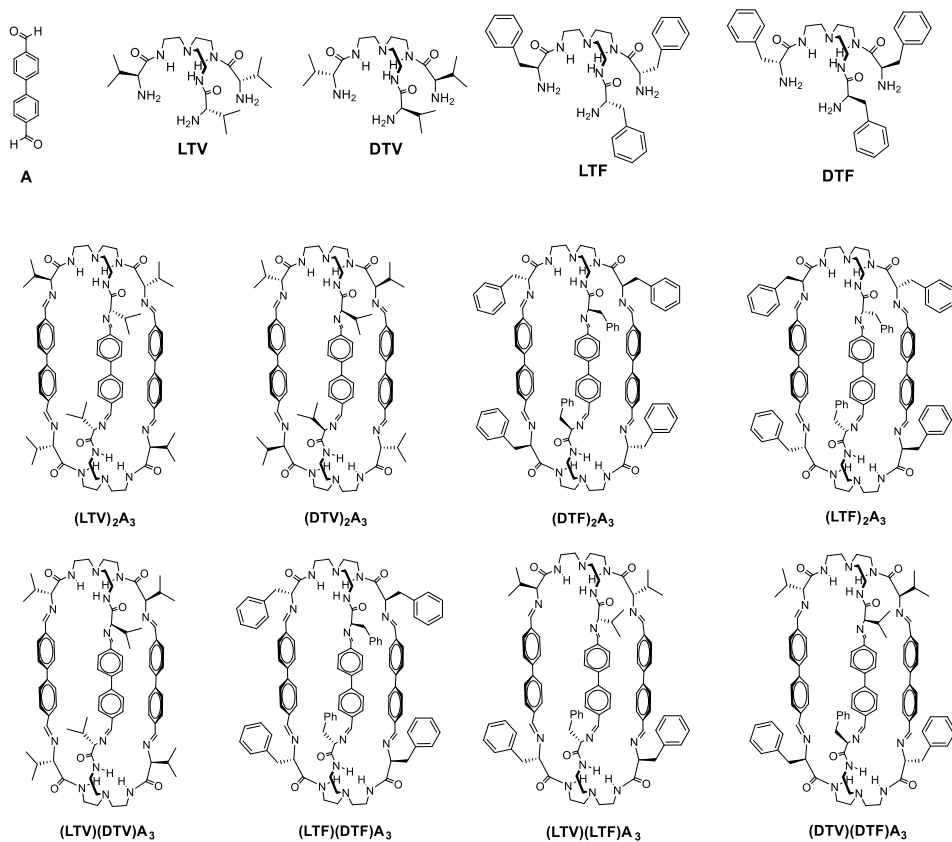
Chapter 6: Immobilized Supramolecular Systems as Efficient Synzymes for CO_2 activation and Conversion.

1

2a

2b

3a

3b

4

5a; X= 0 ; Y= 100
5b; X= 23 ; Y= 77
5c; X= 38 ; Y= 62
5d; X= 48 ; Y= 52
5e; X= 70 ; Y= 30

6b; X= 16 ; Y= 77
6c; X= 27 ; Y= 62
6d; X= 31 ; Y= 52
6e; X= 34 ; Y= 30
6f; X= 38 ; Y= 0

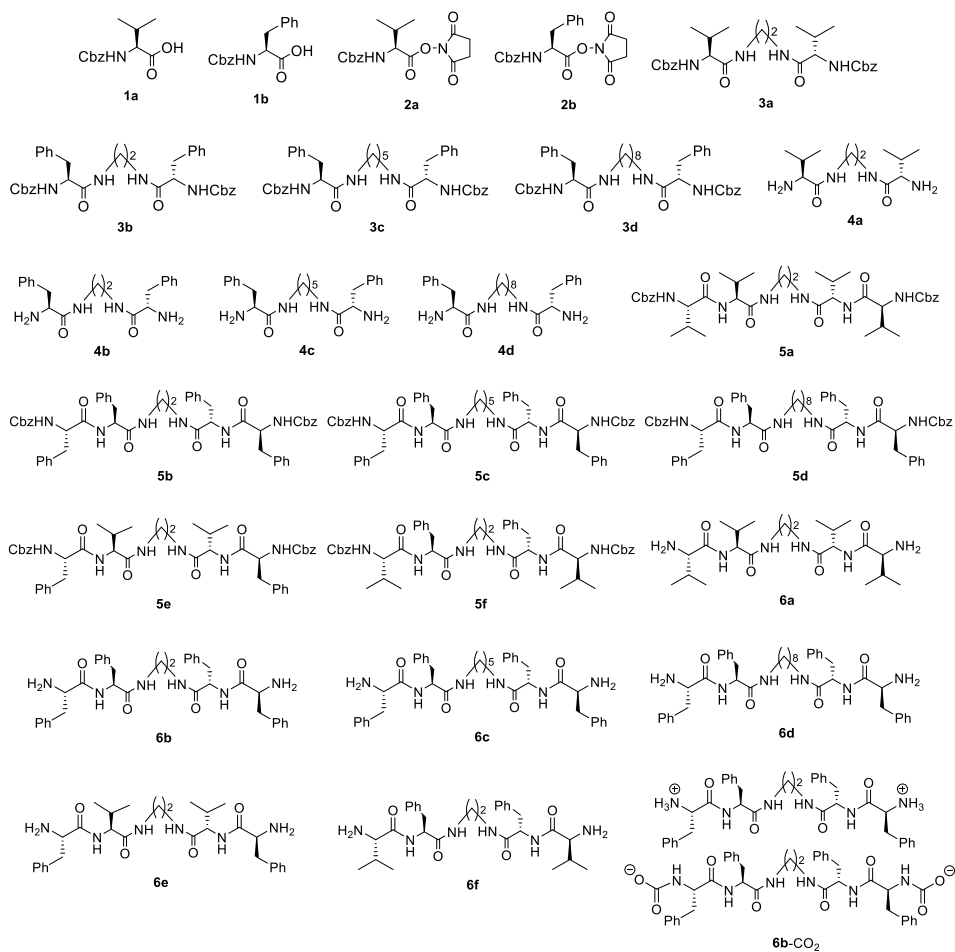**7b**; X= 21 ; Y= 77

Bu₄NOPh

Bu₄NOOCPh

Chapter 7: Highly Active and Enantioselective Multifunctional One-Component Supramolecular Catalysts for the Cycloaddition of CO_2 to Epoxides.

DA
B1
B2
B3
B4

L1
L2
L3
L4

1-Cl
1-I
2-I
2-PF₆

3-I
4-I

Chapter 8: Doubly Chiral Pseudopeptidic Macrobicyclic Molecular cages: Water-assisted Dynamic Covalent Self-Assembly and Chiral Self-sorting.

A   **LTV**   **DTV**   **LTF**   **DTF**

$(LTV)_2A_3$ $(DTV)_2A_3$ $(DTF)_2A_3$ $(LTF)_2A_3$

$(LTV)(DTV)A_3$ $(LTF)(DTF)A_3$ $(LTV)(LTF)A_3$ $(DTV)(DTF)A_3$

Chapter 9: Unravelling the Supramolecular Driving Forces in the Formation of CO_2-Responsive Pseudopeptidic Low Molecular Weight Hydrogelators.

INDEX

Chapter 1

General Introduction

1.1. Supramolecular chemistry

Supramolecular chemistry is a relatively recent domain of chemistry, frequently defined as the "non-covalent chemistry" or the "chemistry beyond molecules".[1] These non-covalent interactions are comparatively weaker than covalent bonds, although they have been proved to be essential in a wide range of fundamental biological functions.[2] Supramolecular interactions include, among others, electrostatic interactions, hydrogen bonding, van der Waals forces, π-interactions, hydrophobic interactions or halogen bonding.[3]

However, before delving further into this topic, it is important to set the discovery of these interactions in their historical background. At the end of the nineteenth century, the forces between molecules were being studied by authors such as J. D. van der Waals (Nobel Prize in Physics in 1910) and H. E. Fischer (Nobel Prize in Chemistry in 1902). In 1894, Fischer postulated the fundamental roots of supramolecular chemistry when he suggested that substrate-enzyme interactions could be defined in terms of the "lock and key" principle, paving the way for understanding host-guest chemistry and molecular recognition (Figure 1.1).
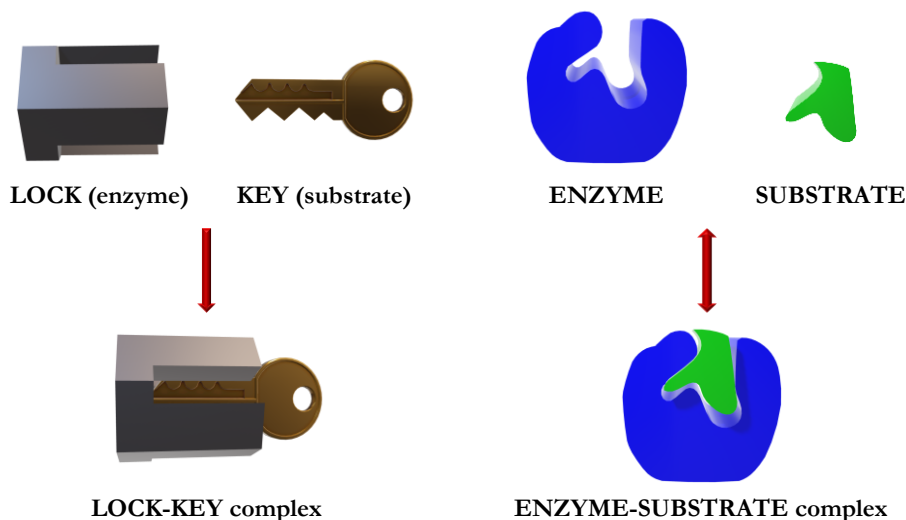
Figure 1.1. Visual representation of the "Lock and key" concept introduced by H. E. Fischer in 1894.

After some years of experimentation, chemists began to better comprehend these kinds of interactions beyond specific individual molecules. In the first decades of the twentieth century, concepts such as hydrogen bonding were demonstrated,[4] and after the discovery of crown ethers by C. J. Pedersen,[5] there was an increase of the interest towards understanding weak forces and their chemical nature, properties, and potential applications. These oxygenated compounds were outstanding because, within their two-dimensional arrangement, an electron rich cavity was formed. Hence, they were able to locate cationic guests, in particular alkaline cations, in the interior of their pocket, an achievement that had not been obtained before. Furthermore, depending on the specific structure of the ethers they could reach selectivity for the recognition of specific ions with different sizes (Figure 1.2).
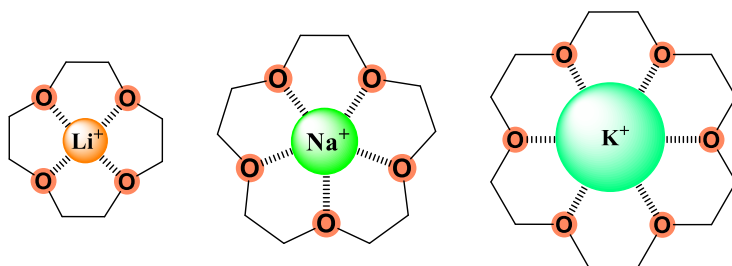
Figure 1.2. Cationic guests in the crown ethers cavities (hosts), the different sizes of the intramolecular cavities provide selectivity to cations with different ionic radii.

The term "supramolecular chemistry" was first introduced by J. M. Lehn. His studies in this area led him to win the Nobel Prize in Chemistry in 1987 together with D. J. Cram and C. J. Pedersen, for their work in the design of molecules with structure-specific interactions. The three of them also advanced in the knowledge of the differences and interrelations between molecular and supramolecular chemistry (Figure 1.3).[6] Whereas molecular chemistry precisely designs synthetic protocols to obtain complex molecules by means of creating or breaking covalent bonds, supramolecular chemistry permits the synthesis of even more complex "supermolecules", relying on non-covalent interactions between the components.[7]
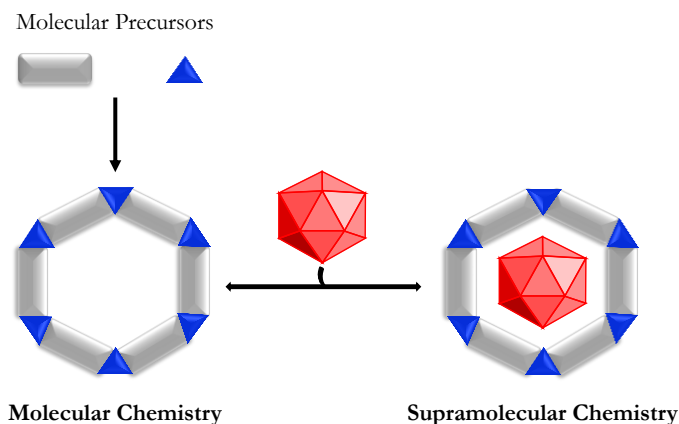
Figure 1.3. Comparison between the scope of molecular and supramolecular chemistry.

Since then, three main themes have driven the development of supramolecular chemistry.[1a] At first, the main objective was to merely synthesize molecular receptors for selective molecular recognition, relying on design and preorganization.[8] Those supramolecular procedures were used for implementing information storage and processing. Subsequently, on the grounds of experience gained in non-covalent interactions, self-assembly processes were used for programming systems. Self-organization is based on the spontaneous but controlled assembly of complex supramolecular architectures.[9] The third theme was established in the dynamic character of supramolecular chemistry, as a result of the reversibility of the non-covalent interactions which build up the supramolecular complexes. This approach led to chemical diversity and evolution, obtaining a wide range of substances from relatively small libraries of components by exchanging, incorporating or extruding components, and thus these findings gave place to the so-called *Dynamic Combinatorial Chemistry* (DCC).[10]

This field has recently received an upsurge of interest as the correct use of chemical knowledge has resulted in the design of sophisticated systems to be used for different applications such as molecular recognition,[11] developing chemical sensors,[12] and the synthesis of self-assembled gels and materials.[13] Together with the development of a huge number of theoretical concepts, a revolution has also occurred in characterisation techniques,[14] that allow researchers to follow the

processes involved and to study, for example, the conformations adopted and the nature of the intermolecular forces. Supramolecular chemists must know concepts not only from inorganic and organic chemistry to synthesize the molecular precursors, but also from physical chemistry and computational modelling to understand the properties and behaviours of the supramolecular complexes.[15] Consequently, this field has a noticeable interdisciplinary character, impinging on a broad range of other areas such as pharmacology, physics, biology, material science and energy storage (Figure 1.4).
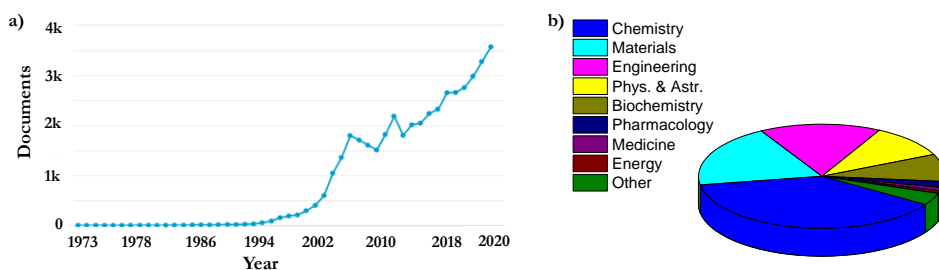
Figure 1.4. a) Number of publications (1k = 1000) discussing supramolecular processes over the last 50 years (Search "Supramolecular" as a keyword in Scopus database). b) Supramolecular publications classified by area (Adapted from the search "Supramolecular" as a keyword in Scopus database).

Nowadays, it is feasible to synthesize molecules with well-designed binding sites, achieving a superior level of refinement and control. In less than 40 years, this chemistry discipline has evolved from designing simple cation receptors to complex molecular machines.[16] In fact, such influence had the development of the aforementioned molecular motors that The Royal Swedish Academy of Sciences decided to award the Nobel Prize in Chemistry 2016 to J. P. Sauvage, J. F. Stoddart and B. L. Feringa for "*the design and synthesis of molecular machines*".[17]

1.1.1.   Non-covalent interactions

The main difference between a non-covalent and a covalent bond is that the former does not involve sharing electrons. Therefore, non-covalent interactions tend

to be weaker than the covalent ones, although this type of bonds play a crucial role in Nature.[18] For instance, achieving the optimal spatial disposition for proteins[19] and for DNA[20] is only possible by means of non-covalent interactions. Very often, strong binding can be achieved through the involvement of multiple non-covalent bonds. Besides, it is important to bear in mind that the environment -particularly the solvent- is a key factor influencing supramolecular forces, as depending on the nature of the surrounding media the strength of interaction can drastically change. [21]

Non-covalent bonds range from strong coordinative bonds with energies up to hundreds of kJ/mol to weak van der Waals forces of only a few kJ/mol. The strongest interactions (100-350 kJ/mol) correspond to ion-ion forces, which are fundamentally affected by the charges, extent of delocalization, and distances between the components. Therefore, although no directionality is present in this type of electrostatic interaction, the geometric factor is essential when successfully assembling two oppositely charged ions. Another type of supramolecular interaction is named as ion-dipole, in which a polar molecule interacts with an ionic compound. A similar scenario is found in the dipole-dipole pair, albeit in this case two polar molecules interact through their dipoles. Ion-dipole and dipole-dipole interactions are partially directional and weaker than ion-ion forces, with respective energies of 50-200 and 5-50 kJ/mol.[22]

On the other hand, there are some supramolecular forces which much depend on the orientation of the components, such as hydrogen and halogen bonding, with energies of 4-120 and 200 kJ/mol, respectively. This directionality is the fundamental tool that allows chemists to precisely design complementary hosts for a specific guest. As abovementioned, hydrogen bonding is crucial in most biological functions, and thus it has been commonly named as "*the key interaction in supramolecular chemistry*".[23] A clear parallelism can be observed between hydrogen and halogen bonds as, in both cases, an electron rich centre (hydrogen/halogen bond acceptor) must be spatially close to a hydrogen attached to an electronegative atom or to a halogen (hydrogen/halogen bond donor).[24] Interestingly, it must be noted that the strength

of these interactions can be extremely decreased by incorporating a competitive effector.

Within the directional supramolecular forces, one may also include the interactions involving π-systems, which can non-covalently bind cations, anions, and other π-moieties. The cation-π interaction is based on the attraction between an electron poor cation and the π-cloud located above and below an aromatic ring,[25] amounting an energy of ca. 5-80 kJ/mol. Anion-π[26] and π-π interactions are weaker (2-40 and 2-50 kJ/mol, respectively) as they rely on the polarizability of the electron cloud of a π-system to create a positive dipolar moment that further interacts with an electron rich anion/aromatic scaffold.[27] The weakest noncovalent interactions are those of van de Waals type, with energies lower than 5 kJ/mol. These forces arise from the interaction of an electron cloud polarized by adjacent nuclei, so they quickly vanish with longer distances between interacting molecules.

Table 1.1. Summary of the types and properties of the main supramolecular forces.[22]

Interaction	Directionality	Bond energy (kJ/mol)
Ion - Ion	Non-directional	100 - 350
Ion - Dipole	Partially directional	50 - 200
Dipole - Dipole	Partially directional	5 - 50
Hydrogen Bonding	Directional	4 - 120
Cation - π	Directional	5 - 80
Anion - π	Directional	2 - 40
π - π	Directional	2 - 50
Metal Coordination	Directional	100 - 300
Van der Waals	Non-directional	≤ 5
Halogen bonding	Directional	≈ 200

Finally, although the line between supramolecular and molecular chemistry is blurry in this case, metal coordination can be also classified as a noncovalent interaction. In fact, these types of metallic complexes present bond energies similar to the ion-dipole systems, even higher in some cases (ca. 100-300 kJ/mol). The high

energy related to these interactions is the consequence of dative bonds between the ligands and the metal ion, presenting a great covalent contribution. Therefore, metal coordination could be described as a subtype of ion-dipole force but with higher covalent character. The bond energies for each non-covalent interaction are detailed in Table 1.1.

1.1.2. Pseudopeptides and supramolecular chemistry

One of the main building blocks used by Nature to create complex systems are amino acids, as they present large functional densities and an intrinsic variability provided by the sidechains. Although a limited number of amino acids exist in Nature, their combination in long peptidic chains allow for the formation of an infinite number of structures. These large molecules with multiple properties and roles are the result of millions of years of natural evolution, through which the only arrangements that have persisted are the ones providing an essential function.[28]

Not surprisingly, the functionality of proteins and enzymes does not only rely on the composition of the peptidic chain, but also in the spatial distribution of the components. In fact, the vast majority of amino acids are involved in the correct preorganization of the macromolecule, whereas only a few units form the active pocket.[29] These astonishing systems are the result of specific non-covalent interactions, selective recognition, and self-assembly of the different components. The protein folding hypothesis was first introduced by K. A. Dill and it assumed that the native state of a protein corresponds to a single well-defined tertiary structure, which is the minimum energy state.[30] Therefore, many non-native states corresponding to partially/incorrectly folded proteins would be trapped in different local minima, obtaining the so-called folding funnel (Figure 1.5). Several research lines have focused on the prediction of these folding profiles, with the aid of computational methods.[31]
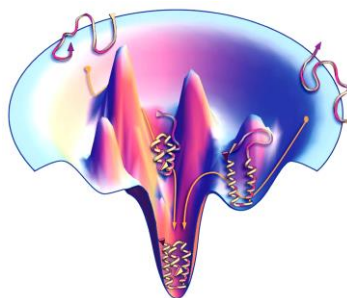
Figure 1.5. Example of a funnel-shaped energy landscape with many high-energy unfolded structures.[32]

Considering that artificially designing those macromolecules would be time demanding and expensive, the development of small molecular models has allowed to shed light on the properties of proteins determined by structural parameters and factors.[33] Although different types of peptidomimetics can be found in the literature,[34] the ideal scenario would be to use the knowledge gathered from natural sources to combine biotic and abiotic moieties in low molecular weight compounds to achieve the desired function.[28,35]

Metal-containing biomolecules are extremely important and frequent in Nature. For instance, iron complexes are used in the transport of oxygen (haemoglobin), magnesium complexes are crucial in the photosynthesis (chlorophyll), and cobalt complexes (vitamin B_{12}) are necessary for the synthesis of red blood cells.[36] Systematic studies were carried out in order to elucidate the nature of the metal complexation by proteins and peptides. The experiments were initiated by the observation of several metal ions being able to induce deprotonation and metal ion coordination of the peptidic amide groups, resulting in high stability metal complexes.[37] Besides, the oxygen atoms of the amide groups were also found to be exceptional binding sites for metal ions in neutral ligands.[38]

Therefore, metal coordination chemistry was one of the first areas in which peptidomimetics offered remarkable advances. At the end of the 20th Century, C. J. Burrows,[39] J. D. Kilburn,[40] and W. C. Still developed metal complexes of novel pseudopeptidic systems with C_2 symmetry that revealed the potential of these

supermolecules as biomimetic metalloenzymes.[41] Some years later, R. Polt and co-workers designed bis(iminoamide) complexes active in the diethylzinc addition to benzaldehyde.[42] In this regard, our group has developed promising C_2 symmetric bis(aminoamide) ligands derived from both natural and non-natural amino acids, with the general structure illustrated in Chart 1.1.[43]
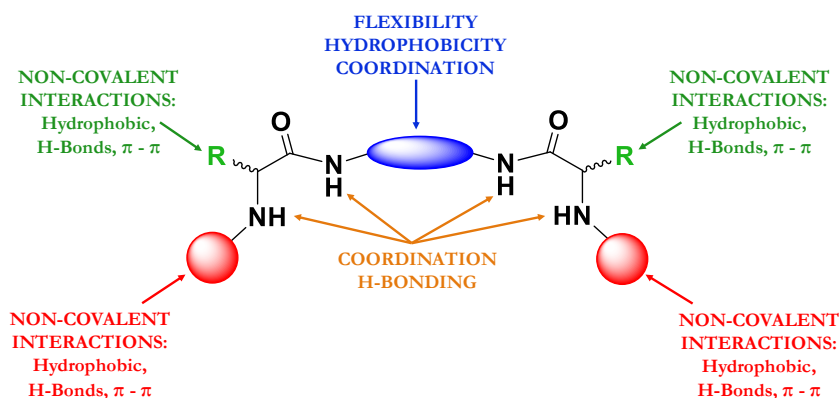
Chart 1.1. General structure of symmetric C_2 bis(aminoamide) ligands.

In these structures, amino and amide group functionalities can participate in metal complexation with different coordination capabilities,[28] in a similar manner to the tetradentate ligands commonly found in coenzymes and catalytic models.[44] Moreover, the different binding sites are connected through a chiral backbone, which can be easily tuned by changing the amino acid sidechain or the spacer (section highlighted in blue, Chart 1.1), providing a high structural and conformational flexibility.[45] Apart from being active in several enantioselective catalytic reactions,[46] some metal complexes have been also proved as chemical sensors.[47]

In conjunction with the development of metallic peptidomimetics, supramolecular catalysis has also been attained through well-designed metal-free pseudopeptides. Although a reduced number of pseudopeptidic organocatalysts can be found in literature, some results are quite remarkable.[48] Asymmetric aldol reactions catalysed by L-proline derived pseudopeptides have gained interest over the past two decades.[49] In this regard, J. Mlynarski research group designed highly selective C_2-symmetric pseudopeptides active in aldolic reactions in the presence of

an excess of water.[50] Rather extraordinary were also the results obtained by A. J. Pearson and co-workers, whose pseudopeptidic bifunctional organocatalyst containing both L-proline and acidic sites within its structure (see Chart 1.2) afforded high yields and excellent enantioselectivities of the desired products after 5 days of reaction. [51]
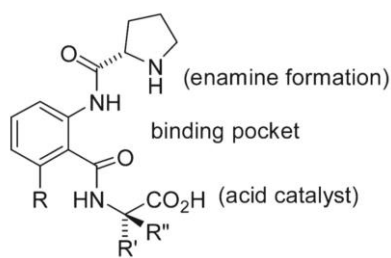
Chart 1.2. Bifunctional organocatalyst for the aldol reaction developed by A. J. Pearson.[51]

However, while designing novel catalysts is one of the major challenges as a consequence of their industrial impact,[52] the study of self-organized complex structures is fundamental to better understand biological behaviours.[53] In fact, self-assembly processes exist widely in Nature, that uses them to generate functional systems such as the DNA double helix[54] or the folding of linear peptides to form well-defined nanostructures.[55] Therefore, studying the self-assembling processes undergone by pseudopeptides could serve not only as a proof of concept for mimicking Nature, but also as a sustainable manner to obtain added-value materials. The main characteristic of these materials is their reversibility, as they are built up of non-covalent interactions that can be ceased with external stimuli.[56]

In this regard, the proper design of low molecular weight peptides and pseudopeptides has allowed their self-assembly under physiological conditions to form hydrogels with important applications in tissue engineering[57] and L-lysine based amphiphilic organogelators.[28,58] Taking into account the presence of many functional groups and the design flexibility of the ligands developed in our group (Chart 1.1), potential self-assembly applications of these bis(aminoamides) have also been studied. For example, S. Verma and co-workers predicted the formation of fibres by means of π-π interactions between phenylalanine (Phe) aromatic sidechains of C_2 and

C_3 pseudopeptides.[59] Similar structures have been studied by C. Tomasini and her group, providing relevant advances in the design of biocompatible hydrogels and self-healing materials using bolamphiphilic pseudopeptides.[60]

The Sustainable and Supramolecular Chemistry group at the Universitat Jaume I has also reported interesting self-assembly results regarding linear pseudopeptides, leading to promising biocompatible organogels and/or hydrogels.[61] In addition, the effect of the pH in the self-organization of gemini amphiphilic pseudopeptides,[62] as well as their interaction with macromolecules of biological relevance (lipidic membranes) was explored.[63] In a similar manner, the impact of the amino acid sidechain in the self-assembly patterns of C_2-symmetric pseudopeptides was also studied. Combining solid state and solution studies it was possible to elucidate the nature of the different patterns obtained, both for Val and Phe derivatives.[64] On this behalf, a new family of tetra-pseudopeptides has been developed in Chapter 9. These compounds presented remarkable hydrogelation properties even at low concentrations. In addition, the materials presented a sol-gel transition depending on the pH of the medium, making them the ideal candidates for CO_2-responsive gels.

It must also be noted that some of the abovementioned open-chain pseudopeptides have been proved to be useful as chemical sensors for target molecules of different nature. For example, a detailed study of anion recognition and transport by C_2 and C_3 symmetric pseudopeptides was reported in 2015 (Figure 1.6).[65] In this study, the capability of different urea and thiourea derivatives to interact and transport anions was assayed and compared with the results obtained for the analogous bis(aminoamides).
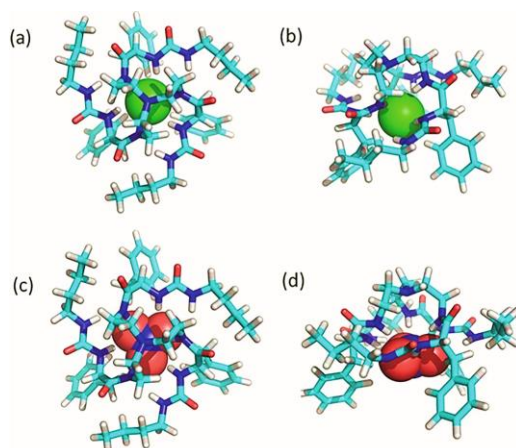
Figure 1.6. Top and side views of the optimized structures of the supramolecular complexes of C_3-symmetric pseudopeptides with chloride (a, b) and nitrate (c, d).[65]

Another important example was the research reported in 2016, in which a fluorescent *on-off* pH sensor was meticulously designed. A pyrene-based pseudopeptide helped for intracellular pH sensing with the aid of a confocal fluorescent microscope as, upon protonation, a folded conformation was adopted resulting in an intense excimer emission centred at 490 nm (345 nm excitation wavelength).[66]

1.2.   Macrocyclic compounds

Macrocycles are generally defined as molecules containing a cyclic framework of at least twelve atoms. While some natural existing macrocycles can present cavities consisting of more than 50 atoms, the most common natural ring sizes comprise 14-, 16- and 18-membered cyclic frameworks.[67] These cyclic molecular entities display a combination of molecular recognition and complexation properties with vital implications in Nature and for host-guest/supramolecular chemistry.[68] The main driving force for the tight binding with the substrate is the decrease in the degrees of conformational freedom, providing the macrocycle with a higher preorganization and functional density than the open-chain analogues.[69]

Since the accidental discovery of the crown ethers by C. J. Pedersen more than half a century ago,[5] the chemistry of synthetic macrocycles designed for specific and highly selective host-guest complexation has experienced a rapid development. The essential breakthrough provided by crown ethers in the 1960s led to other scientists developing novel synthetic receptors containing at least one cavity within their structure. For example, the research pioneered by D. J. Cram on macrocyclic cyclophanes, spherands, and carcerands that were able to interact not only with alkali and alkaline earth metal cations, but also with small organic molecules.[70] Roughly contemporarily, E. H. Simmons and C. H. Park designed macrobicyclic molecular cages containing tertiary amino groups, which upon protonation could locate halide anions within their cavities (Figure 1.8b).[71]

Figure 1.8. Examples of macrocyclic hosts for metal ions. a) C. J. Pedersen's crown ethers, b) E. H. Simmon's and C. H. Park's macrobicyclic diamines, and c) J. M. Lehn's 3D-cryptands.

Later on, J. M. Lehn demonstrated that complete encapsulation of metal cations could be achieved by novel three-dimensional (3D) receptors he called cryptands,[72] inspired by both C. J. Pedersen's crown ethers and E. H. Simmons' and C. H. Park's macrobicyclic diamines (Figure 1.8c).

Following this work, other researchers, as for instance F. Vögtle, became active in synthesizing shape- and size ion-selective receptors, and throughout the 1980s research in the area gathered a rapid pace with concepts such as mechanically interlocked molecular architectures emerging.[73]

However, more than half a century before those investigations, the three native states (α, β and γ) of natural occurring cyclodextrins had already been characterised by F. Schardinger in 1904.[74] Cyclic dextrins were found to be the result of starch degradation. This crystalline fermented product presented astonishing properties such as water and acid resistance.[75] After a period of doubt and many years of exploration, cyclodextrins are nowadays one of the better understood macrocycles in host-guest systems (Figure 1.9) and have found many applications in molecular encapsulation of substrates of different nature.[76]
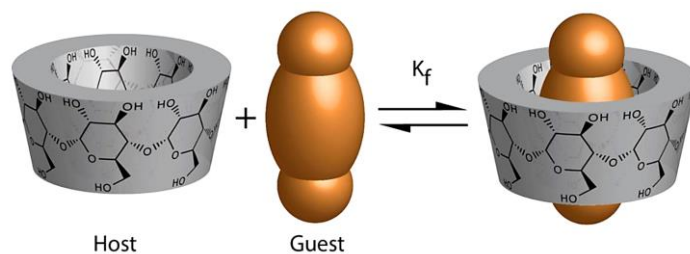
Figure 1.9. Schematic illustration of the association of free cyclodextrin ("host") and substrate ("guest") to form the substrate-cyclodextrin complex.[75]

During the subsequent decades, an enormous number of synthetic macrocyclic compounds have been described. Among others, special attention should be paid to torands, calixerenes, cucurbiturils, pillararenes, and new cyclophanes. The synthesis of such complex systems has given rise to a considerable increase in the research activity regarding macrocyclic chemistry, especially in relation to molecular recognition and self-assembling processes. Nowadays, a wide range of macrocycles

can be found in literature, ranging from two-dimensional to 3D, from flexible to rigid structures, from inert to stimuli-responsive systems, and from monofunctional to multifunctional scaffolds.[68]

The development of precise stimuli-responsive macrocyclic compounds has served as a powerful tool to mimic Nature. It is well known that life is intimately connected with motion at all length scales - from the taxis of a bacterium to the regular oscillation of a beating heart, all the way to the mechanics of the human body. This is the result of molecules consuming fuel and channelling the energy into certain modes of molecular movement. Therefore, the proper design of macrocycles has offered a more realistic insight into the dynamics of different biological processes, nearly reaching the sophistication and versatility allowed by Nature's rules of molecular motion.[77] Although the motion of covalently bonded molecular systems has been greatly studied by researchers such as R. T. Kelly and B. E. Dial, the field in which macrocycles have provided significant advances is in controlling motion in supramolecular systems. Nonetheless, the control of such non-covalent assemblies is demanding, as the stability of the desired assembly must be maintained by restriction of bulk exchange.[78]

A nice example of controlled molecular motion was published in 2010 by B. L. Feringa and D.-H. Qu.[79] In their work, they developed a self-complexing pseudorotaxane that imitated the rotary motor system of ATPases. The rotary motion was based on light-driven conformational changes, and the lockable property was achieved by acid-base equilibrium that controlled the highly selective intramolecular self-complexation (Figure 1.10).
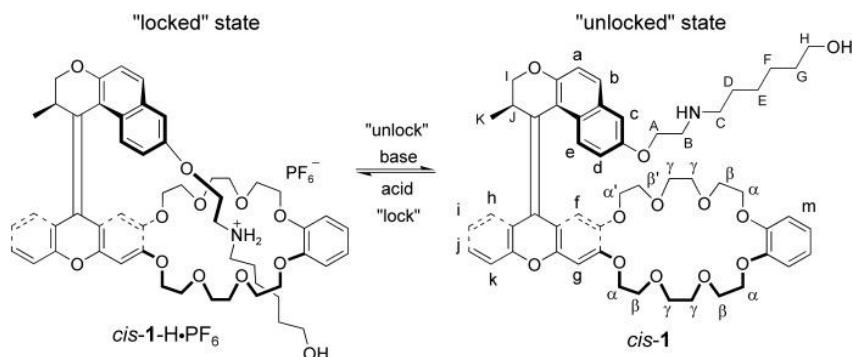
Figure 1.10. Chemical structure of the lockable light-driven molecular motor and the acid-base-controlled locking-unlocking movements.[79]

Considering the elegant conformational changes and the complex chemical structures of the macrocyclic compounds, as important as a precise design is the correct characterisation of the different states adopted. X-ray crystallography can provide a detailed picture of static conformation in the solid phase; however, crystal packing can significantly affect conformation, and caution is required when attempting to rationalize a conformation adopted in solution using crystallographic data. Nuclear Magnetic Resonance (NMR) spectroscopy has been routinely used for conformational analysis of macrocycles in solution, in conjunction with other spectroscopic techniques such as infrared (IR), circular dichroism (CD) or ultraviolet (UV). Moreover, researchers tend to support their experimental data with computational modelling and calculations, as it facilitates the vision of the conformations adopted.[69a]

1.2.1. Macrocyclization synthetic approaches

Despite macrocyclic compounds have been found to be useful in a wide range of applications, one of the main bottlenecks for their use is their often-tedious synthetic and purification protocols.[80] As a matter of fact, affording high yields for the desired cyclic structures is not always trivial, as the intramolecular cyclization steps must compete with intermolecular dimerization / oligomerization processes.[81] Notwithstanding, macrocyclic structures of different sizes can be found in Nature,

demonstrating that their synthesis is favourable under certain conditions. For example, the antibiotics vancomycin,[82] tyrocidine A,[83] and cyclosporine A,[84] as well as the oxytocin hormone and its related neuropeptide vasopressin,[85] contain macrocyclic scaffolds within their structure.

In 1953, P. J. Flory detected ring formation in some polymerization reactions, although the cyclic products were solely obtained when the ring contained six or more atoms and under diluted conditions.[86] This observation was in good agreement with the preceding work of P. Ruggly and K. Ziegler, which revealed that high-dilution techniques favoured the formation of cycles in the cyclization reaction of small organic molecules.[87] Considering the two general ring-closure scenarios, high dilution techniques shall improve the efficiency of the macrocyclization step in both unimolecular (Figure 1.11a) and bimolecular synthetic approaches (Figure 1.11b). As a matter of fact, high-dilution techniques shall lead to higher macrocyclization efficiencies for the unimolecular approach because of the increased effective concentration. It should be mentioned that the monomeric ring formation is unimolecular in the reactant, whereas the formation of higher condensates and chain polymers proceeds bimolecularly.[88]
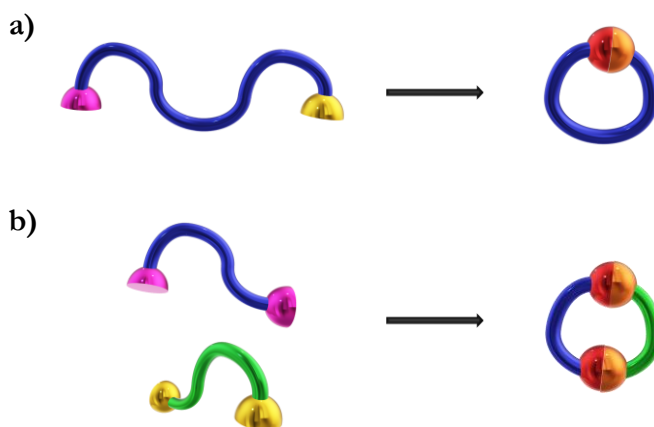

Figure 1.11. Schematic representation of the most common ring closure techniques for the preparation of macrocycles: a) unimolecular approach, and b) bimolecular approach.[88]

On the other hand, more sophisticated methodologies are needed to afford high yields of the desired macrocycles in bimolecular approaches. In those cases, using

exact stoichiometric quantities of reagents is crucial, so the formation of the macrocyclic species is not precluded. Moreover, in line with the unimolecular approach, a decrease in the reaction concentration favours the bimolecular reaction over the competing multimolecular dimerization/oligomerization.

1.2.1.1. *Preorganization*

Generally, competing oligomerization processes are favoured by entropic factors, as many different conformations allow for oligomerization while only a few ones favour macrocyclization. Macrocyclizations could be achieved, with moderate yields, combining high-dilution techniques with stepwise protection/deprotection protocols.[89] However, these concepts are against the sustainability principles introduced by P. T. Anastas and J. C. Warner.[90] Therefore, the development of more elegant and greener methodologies has received much attention in macrocyclic chemistry. In point of fact, macrocyclization reactions were found to be much more efficient if the reagents involved in the cyclization step presented complementary conformations. In this regard, the concept of preorganized conformations was first introduced by D. J. Cram, who postulated the principle of preorganization and defined it as follows: "*the more highly hosts and guests are organized for binding and low solvation prior to their complexation, the more stable will be their complexes*".[91] Although this methodology was firstly applied in molecular recognition and host-guest chemistry,[92] it has also provided remarkable improvements in macrocyclization reactions, as the correct design of the reagents can lead to higher cyclization efficiencies. Hence, a general approach towards successful macrocyclizations is to use open-chain precursors preorganized in a folded conformation that allows the two reacting sites of the open chain precursor to be spatially close.[93] This arrangement, with the appropriate orientation, provides an unambiguous trajectory of attack, making the cyclization a faster process compared with the intermolecular process.[94] Taking the example illustrated in Figure 1.11, a correct design of the reagents could improve the preorganization of the reacting groups, favouring the cyclic products (Figure 1.12).

Figure 1.12. Schematic representation of the preorganized reagents for: a) unimolecular macrocyclization, and b) bimolecular cyclization.

Several preorganization strategies rely on designing rigidized reagents, in which an optimal "locked" conformation is achieved. This methodology often results in shape persistent macrocycles (SPMs). In the case of bimolecular macrocycliations, after the first intermolecular reaction takes place (when discussing bimolecular macrocyclizations), the subsequent intramolecular cyclization step can be triggered by the intrinsic rigid conformation of the open-chain intermediate.[95] In order to achieve such rigidized structures, many examples involve rigidized aromatic moieties, acetylenic units, and allenic subunits.[96]

On the other hand, some examples can be found in which the optimal conformations are attained by means of supramolecular interactions. H-bonding has been widely used as a driving force for intramolecular folding, affording well-established conformations.[96,97] For instance, K. Hiratani and co-workers prepared a new family of macrocycles through the amidation of di(acid chloride) derivatives with different diamino compounds, highlighting the crucial role of intramolecular hydrogen bonds in preorganizing the reaction intermediate.[98] Other intramolecular interactions such as π-π or metal coordination also rendered adequate folding of the open-chain precursors.[99, 100]

S. V. Luis group has designed, for the last 20 years, several preorganized bis(aminoamides) displaying appropriate arrangements for macrocyclization. In 2003, they reported the synthesis of [1+1] pseudopeptidic macrocycles driven by

both intramolecular hydrogen bonding and solvophobic effects in the key reaction intermediate. Quite interestingly, the expected cyclic products were obtained in moderate-good yields after thorough purification, but the reactions were carried out at relatively high concentrations (8.2 mM).[43] Later on, the synthesis of larger [2+2] macrocycles was studied by reacting different bis(aminoamides) with terephthaldehyde. Although complex mixtures were obtained when using achiral aliphatic spacers for the pseudopeptidic open-chain precursor, the pseudopeptides containing chiral cyclohexane-1,2-amine as spacer led to good yields in the macrocyclization. Conformational studies of the predicted intermediate demonstrated the proximity of the reactive groups involved in the intramolecular cyclization, as a result of H-bonding and imine conjugation. Besides, using the pseudopeptidic diastereomer resulted in a drastic decrease in the efficiency of the macrocyclization, indicating a clear match/mismatch outcome.[101] The last example was published in 2014, in which a detailed study of the effect of the amino acid sidechain in the macrocyclization reaction was performed. The nature of the chiral groups of the amino acids was proved to be of paramount importance in the preorganization of the reagents and the cyclization intermediates. Indeed, an increase in the number of substituents on the α carbon atom (quaternary amino acids) significantly decreased the macrocyclization reaction rate.[102]

1.2.1.2. *Template effect*

An interesting alternative for the cases in which the precursors are not precisely preorganized is the use of templating elements that promote a favourable conformation. In this regard, the most frequent mechanism for templated-macrocyclizations is the precursor(s) wrapping around the templating agent, approaching the two final reactive ends leading to the macrocycle. Hence, the introduction of the template helps to change the unfavoured disposition and to induce an appropriate conformation for the macrocyclization step (Figure 1.13).
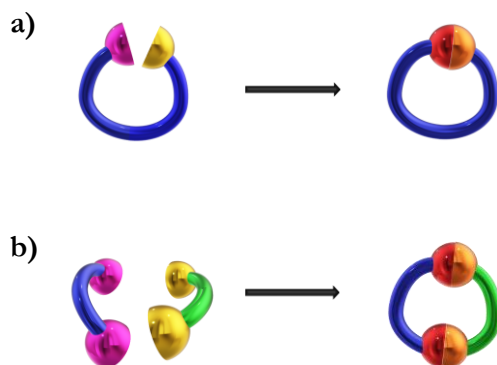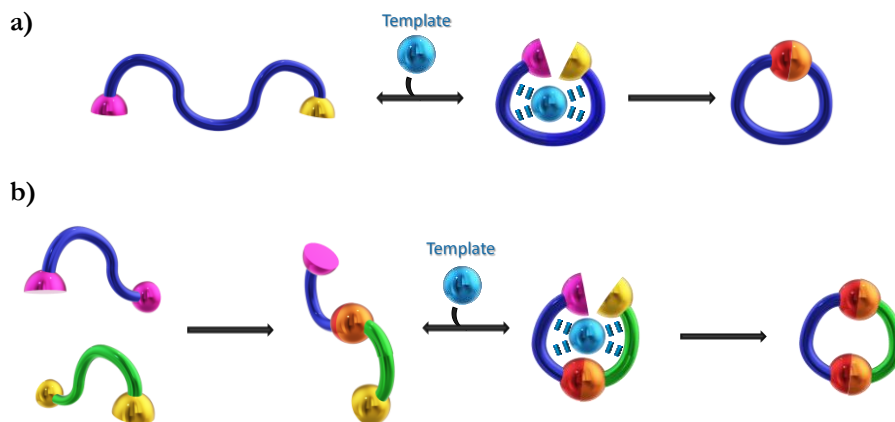
Figure 1.13. Schematic representation of the template effect in: a) unimolecular macrocyclization, and b) bimolecular cyclization.

The template effect can be classified into two well-defined types, namely kinetic and thermodynamic templates, depending on the reversibility of the macrocyclization reaction.[96,103]

> ➢ Kinetic templates: Operate on irreversible reactions by stabilizing the main transition states / intermediates leading to the desired product.
> ➢ Thermodynamic or equilibrium templates: Operate on reversible conditions. Templates preferentially shift the equilibrium distribution towards the formation of the desired product.

The employment of template processes has been of great significance since the mid-1960s. They have allowed the synthesis of compounds that are difficult or even impossible to obtain from their components by traditional methods.[104] Numerous examples of template-driven macrocyclizations can be found in literature, ranging from metallic to anionic based templates.[105]

Metal templated macrocyclization arose at the end of the 20th Century, when the need of synthesizing different crown ethers with high purity and yields was extremely on demand.[106] Still, several recent studies highlight the crucial role of different alkaline and alkaline earth metals in the highly efficient syntheses of novel crown ethers derivatives.[107] In conjunction with the development of crown ethers,

researchers such as D. H. Busch and E. K. Barefield designed nickel-based templated syntheses of tetraaza-cyclic compounds.[108] Those preliminary studies have been deeply understood and expanded to the metal templated synthesis of macrocycles based on transition metal as, for instance, zinc, cobalt, copper or cadmium.[109]

The use of anions as templates for macrocyclizations is also a subject of interest as they have been proved as highly efficient in these processes.[96] Not surprisingly, taking account of the excellent affinities achieved by macrocyclic hosts towards certain anions, exploiting the potential template effects of such anions has also received much attention. P. D. Beer and co-workers developed sophisticated anion templated syntheses of interpenetrated and interlocked structures, claiming the fundamental role of the open-chain intermediate affinity towards the desired anion and the nature of the anion itself.[110] In 2017, the synthesis of chiral C_2-symmetric macrocyclic ureas was afforded in excellent yields as a result of the favourable conformation adopted upon anion recognition by the urea and amino groups of the reaction intermediate.[111] In addition, the synthesis of a thermodynamically unfavoured inverted-hemicucurbituril has also been recently reported by R. Aav's group. In this study, the selectivity of the reaction is clearly affected by the formation of two different diastereomeric intermediates, with different affinities towards chloride anion. Therefore, by incrementing the amount of halide anion introduced, the product distribution could be modified, indicating an effective anionic templation.[112]

In this regard, our research group has developed several anionic templates of both thermodynamic and kinetic nature. The syntheses of [2+2] pseudopeptidic macrocycles by reductive amination of rigid aromatic dialdehydes with C_2-symmetric bis(aminoamides) was favoured when using an anionic dicarboxylate template.[113] As a matter of fact, thermodynamically unfavoured macrocycles could be synthesized using the correct dicarboxylate species, counterbalancing the "mismatch" effect of the configurations of the stereogenic centres at the spacer and at the amino acid derived fragments.[114] More sophisticated [3+2] molecular cages could be efficiently

obtained using tricarboxylate anionic compounds as the template (Figure 1.14). The formation of [3+2] macrobicyclic compounds through imine condensation is usually challenging, as larger oligomers, interlocked structures or dynamic mixtures can be obtained. However, the addition of benzene-1,3,5-tricarboxylate as its tetrabutylammonium salt led to a faster reaction, achieving yields higher than 80% of the desired cage in 3 hours of reaction.[115]
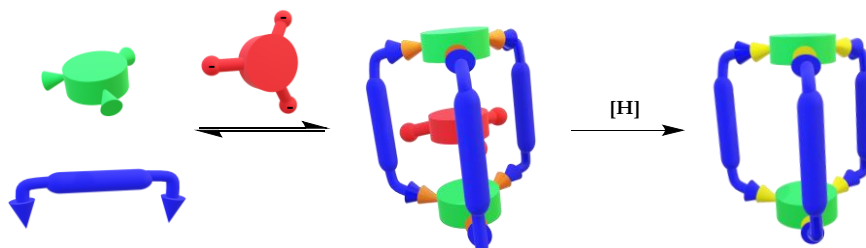
Figure 1.14. Schematic representation of the template-assisted synthesis of [3+2] pseudopeptidic molecular cages. Blue: bis(aminoamides), green: trialdehyde, red: tricarboxylate template, orange and yellow: imino and amino groups formed, respectively.[115]

Similar dynamic pseudopeptidic cages have been synthesized *via* imine condensation between tripodal open-chain pseudopeptides and dialdehyde species. The autocatalytic thermodynamic template-effect of the water generated has been precisely studied, obtaining the best yields in hydrophobic solvents. This water encapsulation was also responsible for the high fidelity chiral self-sorting experienced by the macrobicycles (see Chapter 8).[116]

Considering that some macrocyclization reactions involve S_N2 irreversible conditions, the use of kinetic anionic templates has also been investigated by S. V. Luis' group. In 2012, pyridine-containing pseudopeptidic macrocycles were efficiently synthesized, observing a remarkable synergetic effect between the preorganization of the open-chain pyridinic precursor and anionic templation. Depending on the size of the final macrocycle, either bromide or chloride anions were found to selectively provide the fastest reaction profiles, whereas other anions such as fluoride or acetate were less active as templating species.[117] Later on, the effects of different aliphatic spacers as well as the change of the amino acid sidechains

were studied, taking account of the template effects involving the bromide anions present in the reaction as side-products of the nucleophilic substitutions.[102]

The performance of anionic kinetic templates was also assayed in amide bond formation reactions. Macrocyclic isophthalamide-containing pseudopeptidic compounds were obtained through cyclization processes involving two consecutive amide bond formation reactions. This design provided the macrocycles with four potentially convergent amide groups that could favour the interaction with anions under neutral conditions. The poor yields of the desired macrocycles obtained in the absence of templates were significantly increased upon addition of one equivalent of different halide anions, with the templating effect following the order Cl⁻ > Br⁻ > I⁻. The noteworthy effect of chloride compared with bromide and iodide anions was the result of a stronger coordination of chloride due to its smaller radius and the greater Coulomb attraction.[118] The efficiency of the chloride anion as a kinetic template in peptidic amide formation reactions was also demonstrated by G. Speranza's group some years later.[119]

Recently, the highly selective anion-templated syntheses of constrained macrocyclic pseudopeptides have been accomplished through four consecutive S_N2 reactions. In contrast to the previous reported template-mediated macrocyclizations, the introduction of chloride anion led to the formation of products of oligomeric nature, because of the drastic conformational change in the reaction intermediate provided by this halide anion (see Chapter 3).[120]

1.2.1.3. *Flow chemistry as an enabling tool*

Inspired by the many advantages that flow chemistry has offered to chemical syntheses,[121] some research groups have assayed macrocyclization reactions in small-scale flow reactors (Figure 1.15).[122] This synthetic approach appears currently as a necessity, as the environmental impact of every chemical transformation should be considered and approaches for their decrease should be developed. In this regard, flow chemistry meets many of the green chemistry principles, as it generally reduces energy requirements, the amount of chemical waste generated, and the exposure to

hazardous chemicals or intermediates.[123] In addition, continuous processes permit better control of mass-transfer, temperature, and stoichiometry. This latter aspect is of paramount importance when discussing bi- or multi-molecular macrocyclizations, as the reagent stoichiometries can modify the selectivity outcome.[124]
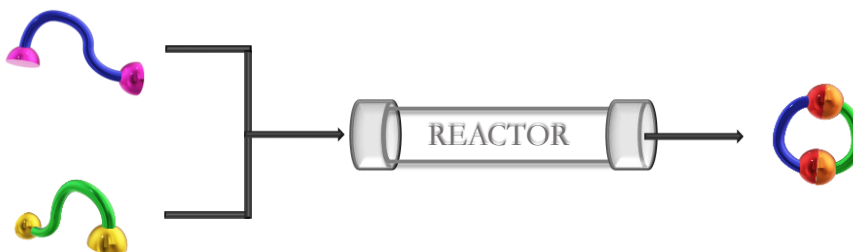
Figure 1.15. Schematic representation of a continuous-flow bimolecular macrocyclization.

In spite of these benefits, flow macrocyclization is still a seldom exploited field, as this type of reactions present some additional chemical requirements.[125] For instance, if oligomers are formed during the reaction, they can precipitate inside the flow reactor. The precipitate would block the system, hampering the attainment of high productivities. Therefore, flow macrocyclization procedures are mainly suitable for reactions in which the selectivity towards the desired macrocycle is high. The most daunting challenge is, however, the low productivities attainable under high-dilution conditions. Some research groups have devoted many efforts to perform high- concentration macrocyclizations under batch conditions, obtaining promising results in this regard.[126] S. K. Collins and co-workers described in 2016 a Glaser-Hay flow macrocyclization for the production of an Ivorenolide A precursor. The cyclization step was performed at relatively high concentrations (24 mM), and the yield of the product was ca. 2 times higher when using continuous flow conditions than for the batch protocol.[127]

One of the most important aspects for flow systems is the design of the experimental set-up.[128] A rich engineering background is important to optimally organize the components of the system, to select appropriate materials for each piece, and to decide which auxiliary equipment is needed for the reaction. For example, one may wonder if the reaction needs different temperatures in some sections of the set-

up, which would be the most appropriate mixer, whether the isolation step can be coupled to the reactor, etc. In terms of the reactor design, different approaches can be found in literature (Figure 1.16).
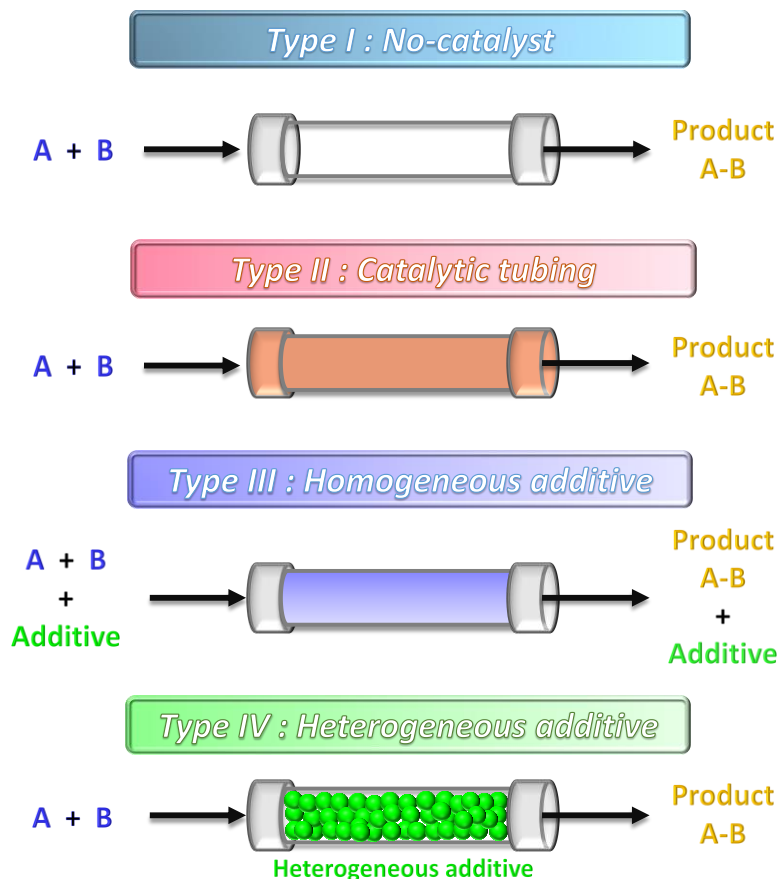
Figure 1.16. Description of the most common reactor designs for flow macrocyclizations. The additive encompasses catalytic, basic, acid, and other auxiliar species.

Some flow macrocyclizations have been performed with remarkable productivities using type I reactors for the continuous production of macrocycles. This simplistic approach has been generally employed in photoinduced macrocyclizations. Limited light penetration is always problematic when performing photochemical reactions under batch conditions, and this problem can be even significantly worse for macrocyclizations because of the low concentrations. Therefore, the high surface-to-volume ratio and homogeneous irradiation could

enhance the efficiency in continuous-flow macrocyclizations.[122] K. Zhang *et al.* reported in 2016 a highly productive and effortless scalable flow process for the production of cyclic polymers. The scale of the reaction was ca. 250 times greater under flow conditions than for the batch methodology, while the residence time was reduced 15 times without modifying the yield attained (90%). Thus, the flow macrocyclization promoted superior productivities even at larger scales.

Type II and type III reactors have been widely applied to alkyne-azide cycloaddition macrocyclizations. S. K. Collins and co-workers described in 2015 a continuous process for the synthesis of macrocyclic triazoles based on click-chemistry. In the project, the authors used CuI as homogeneous catalyst, in the presence of different ligands such as triethylamine or ethylenediamine. The macrocyclization step was performed at relatively high concentrations (30 mM), obtaining a 4-fold increase in productivity compared to the batch processes.[129] Not many years before the latter project, a different scenario was proposed by A. R. Bogdan and K. James. These authors were able to synthesize macrocyclic triazoles with the aid of copper tubing, that acted as the catalyst for the alkyne-azide cycloaddition. By using this novel copper-surface design, the productivity of the reaction augmented from 3.9 to 18.3 g_{prod}/L·h, under the continuous-flow process.[130] Lastly, I. R. Baxendale *et al.* reported in 2020 a packed column reactor containing K_2CO_3 that allowed for scaling-up the synthesis of cyclic substituted 2-oxazolines. This sort of design can be classified as type IV reactors, as the inorganic base smoothly permitted the intramolecular cyclization with yields > 70% even at gram scale. Thereby, the authors were able to produce 5 g of cyclic species in approximately 8 hours.[131]

Having a closer look to the herein described flow macrocyclization examples, it can be noted that most of the reported methodologies were employed for unimolecular macrocyclizations. Nevertheless, some inspiring works can also be found targeting multimolecular flow macrocyclizations. As an example, C. J. Doonan and co-workers synthesized in 2015 a carbon-based molecular cage *via* three-fold homocoupling macrocyclization. The reaction can be classified as a type III flow

macrocyclization, as the catalytic species were pumped through the reactor in the same phase as the reagents. With the continuous-flow approach the authors demonstrated that the amount of copper species could be significantly reduced, thus decreasing the chemical waste generated in the process. Moreover, the authors envisaged that the amount of auxiliary substances could be further reduced to sub-stoichiometric quantities when using immobilized copper species.[132] T. Fodi and co-workers described also in 2016 an efficient flow macrocyclization for obtaining pyridino-18-crown-6-ethers. The alkylation embodied a KOH packed-bed reactor (type IV reactor), which represented a much safer methodology than the ones previously described employing NaH as the base. The higher productivities obtained, as compared to the batch syntheses, were assigned to the lower residence times required to render the crown ethers with the desired yield.[133]

Chapter 4 of the present thesis shows our efforts to develop efficient flow-macrocyclizations for the production of constrained pseudopeptidic macrocycles. The flow protocol prompted a 17-fold increase in productivity when compared to the analogous batch system. In addition, the environmental impact was reduced more than 2 orders of magnitude by *in-situ* combining the flow-synthesis with macrocycle isolation.

1.2.2. Pseudopeptidic macrocycles

Protein-protein interactions (PPIs) execute many fundamental cellular functions and have served as prime drug targets over the last two decades.[134] Yet, the growing appreciation of complex PPIs, which are not easily addressed using small molecules, demands the development of inhibitors that are more sophisticated than traditional small molecules. Consequently, one of the main fields of application of peptidomimetic macrocycles is the design of active therapeutic agents.[135] This is the result of several unique features of the peptide-based cyclic compounds, as are, for example, their large polar surface areas that facilitate cellular permeability and bioavailability.[67] Moreover, another pharmacological advantage relies on the higher

level of preorganization of bioactive conformations compared with open-chain compounds, thereby avoiding entropic losses upon binding that would decrease affinity.[69a] In this regard, the work carried out by researchers such as L. Gentilucci and C. Palomo must be pinpointed.[136]

Pseudopeptidic macrocycles have also opened a new window of opportunities in building up dynamic combinatorial libraries (DCLs). In fact, DCLs have served as simplified minimalistic models of complex evolutionary biological processes, proposing the generation of dynamic mixtures of components that can rapidly exchange and interconvert. DCLs can thus be adaptive and able to express changes in the whole system as a response to different external stimuli, as, for instance, a change in the conditions or the addition of chemical effectors.[137] Therefore, the best adapted member of the library amplifies at the expense of the other congeners. One of the main requisites for rapid interconversions is the presence of reversible bonds within the structure of the components, and principally imino (C=N) and disulphide (S-S) bonds have been studied. The availability of natural amino acids containing in their sidechains such groups (i. e. cysteine) has rendered pseudopeptidic compounds with promising properties in this field.[138]

Another area in which cyclic peptidomimetics have contributed with remarkable improvements is in the design of molecular hosts. During the first decade of this century, different peptide-based macrocycles proved to be active in the molecular recognition of different substrates as nitromethane,[139] carboxylic acids,[140] quinuclidines,[141] or even water molecules.[142] Recognition of phosphate and sulphate are two crucial cases to study for understanding how nature designs proteins to bind these anions selectively. An example is the naturally occurring Phosphate Binding Protein of 34 kD a single tight phosphate-binding site is present, in which the phosphate ion is held tightly by means of hydrogen bonding and electrostatic interactions.[143] Trying to mimic this astonishing natural process, G. Haberhauer and co-workers developed in 2009 different azole-containing cyclic peptides tremendously useful in binding dihydrogen phosphate anions in a 1:1 stoichiometry.[144] In a similar manner, S. Kubik and co-workers designed in 2010 a

pseudopeptidic molecular container for the highly selective recognition of sulphate anions, even in competitive environments. The triply linked bis-cyclopeptide was able to locate anions within its cavity by means of hydrogen bonding with the amide groups.[145] Even more elegant anion recognition examples have been accomplished in the last ten years, as is, for instance, pyrophosphate recognition by unguisin A.[146]

On this subject, S. V. Luis' group has devoted significant research efforts to design macrocyclic pseudopeptidic receptors for various anions. In 2012, with the collaboration of R. Vilar's group, a fluorescent acridine-based macrocyclic receptor was carefully designed in order to provide high selectivity towards dihydrogen phosphate. The high preorganization of the macrocyclic compounds rendered tighter associations with the guests, as compared with analogous open-chain pseudopeptides. Moreover, the anion complexation could be straightforwardly assayed by fluorescent studies, as intense fluorescence emissions could be observed upon conversion of the acridine moiety of the receptor into the strongly emitting acridinium fluorophore.[147] Similar acridine-based macrocycles were posteriorly found to selectively bind tryptophan in very acidic aqueous media. Interestingly, the supramolecular complex was formed despite the two components were positively charged, indicating the crucial role of solvent molecules and counterions involved in the supramolecular interactions.[148] Also in 2012, a new family of C_3-symmetric pseudopeptidic cages were able not only to interact with chloride anion, but also to transport it throughout lipidic membranes. In this project, the affinity towards the halide anion could be tuned by modifying the structural components of the molecular cage, as is, for instance, the sidechain of the amino acid scaffold or the substitution in the aromatic lid of the cage (Figure 1.17).[149] The recognition of more sophisticated substrates as N-protected dipeptides,[150] natural amino acids[151] or other amino acid derived compounds[152] have likewise been accomplished with different C_2 and C_3-symmetric cyclic peptidomimetics.
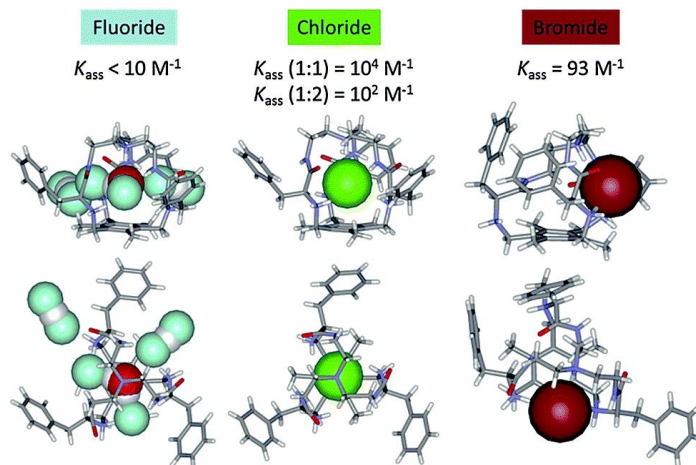
Figure 1.17. Small C_3-symmetric tripodal cages as receptors of halide anions. Solution binding constants and upper and side views of the corresponding pseudopeptidic cage complexes for fluoride (light blue), chloride (green) and bromide (dark red) as observed in solid state.[138c]

Additionally, interesting results have also been reported in the study of self-assembly processes of several macrocyclic pseudopeptides. Small [1+1] peptidomimetic cyclophanes showed to be strong organogelators for esters and aromatic solvents such as benzene, toluene, styrene, and anisole.[153] Quite surprisingly, the intrinsic molecular chirality of the cycles was often transferred to the assembled fibres, as each enantiomer of the macrocyclic pseudopeptides provided fibres with opposite helicity.[154] Regarding bigger [2+2] macrocyclic pseudopeptides, the exact combination of the spacer and the sidechain of the amino acid was demonstrated as essential. For example, some valine cyclic derivatives tend to form fibrillar materials when they contained short aliphatic spacers and a *meta*-substituted aromatic subunit, in contrast with the phenylalanine derivatives that rather self-assembled in vesicles. These macrocycles resulted in amorphous materials when the pH of the medium reached acidic conditions. In contrast, when *para*-substituted aromatic scaffolds were present, the opposite tendency was observed. Neutral conditions led to the formation of amorphous solids, whereas upon acidification of the medium, crystalline and fibrillar structures were obtained for Val and Phe derivatives, respectively. [28,155]

1.3. Supramolecular catalysis

A catalyst is, by concept, a compound that accelerates the rate of a certain reaction, without being consumed. This is the result of the alternative energetic pathway provided by the catalytic species, which involve lower activation energies than the non-catalysed mechanism.[156] Although the concept of "catalyst" was introduced by J. J. Berzelius in 1835, catalytic processes date back to the dawn of civilization, when the production of alcohol by fermentation arose.[157] After two centuries of evolution, unimaginable levels of sophistication have been accomplished in catalysis. The many advantages that catalysis has provided to industrial processes are guided by both higher efficiencies and the noteworthy environmental benefits. In fact, the major cause of industrial waste, particularly in fine chemicals and pharmaceuticals manufacture, was the use of stoichiometric non-reusable reagents in organic synthesis. Catalytic processes have clearly replaced those archaic stoichiometric methodologies, as a result of the lower energy-consumption requirements and the higher selectivities achieved. Therefore, the implementation of catalysis has enormously contributed to the decrease of the industrial waste streams.[158]

Taking into account the many catalytic examples reported up to date, it is intuitive to set a parallelism between catalysis and supramolecular chemistry. As a matter of fact, catalysts bring together the various substrates (recognition + preorganization) by means of non-covalent interactions.[159] Even though the definition of supramolecular catalysis is not trivial, this field has become a recognized subdiscipline nestling between catalysis and supramolecular chemistry. The activity of supramolecular catalysts shall be characterised by their capability to accelerate the reaction through reversible interactions such as hydrogen and halogen bonding, van de Waals forces and π-π interactions. Additionally, as aforementioned (Section 1.1.1), coordination complexes can also be considered as supramolecular catalysts as the reactions are activated by Lewis acid-base pairs between the substrates, ligands, and the metallic core.[160]

The supramolecular catalytic activity often relies on non-easily predictable weak interactions (cation-π, CH-π, NH-π) and steric repulsions that play a crucial role in the catalytic cycle, often precluding the precise design of the catalytic species. Moreover, considering the many species and potential interactions of the so-called "catalytic pool" (ligands, substrates, solvent molecules, metals, and counterions), determining the catalytic mechanistic pathway can be extremely challenging. Hence, unambiguous control experiments and suitable analytical techniques are essential to accurately elucidate the nature of the non-covalent interactions.[161]

Supramolecular catalysts have demonstrated capability to accelerate reaction rates based on different principles. For example, the concept of preorganization can be critical in this regard, as if the host molecule is able to optimally organize the components of the reaction in a well-defined position, no major conformational changes are required for the reaction to occur.[162] In other cases, the enhancement of the reaction rate is the result of stabilization of the transition state by the supramolecular catalyst.[163] One of the main drawbacks of this approach, however, is that generally the rigid catalytic cavities hamper the conformational adjustment for perfect transition state stabilization.[160] Ultimately, the rate of reaction can be extremely augmented as a result of the increase in the effective local concentration. This is in fact a predominant factor in bimolecular reactions, as if the catalyst is able to encapsulate the reagents in a small pocket, the probability of the reaction to occur is tremendously increased.[164]

This section has been divided into three main topics: organometallic, organocatalytic, and synzymatic supramolecular catalysts. Nevertheless, it goes without saying that the distinction between the three subgroups is far from trivial, as some systems could be classified into more than one specific group.

1.3.1. Metalloorganic supramolecular catalysts

In metal catalysis, the whole catalytic pool (the ligand, the counterion, and the metal units) can be involved in the mechanism at a given stage. Thus, non-covalent interactions such as hydrogen bonding, Lewis acid-Lewis base, electrostatic, and hydrophobic forces might be adjusted to properly tune the final catalytic properties of the system.[161] An inspiring example showing modulable catalytic performance was reported by J. N. H. Reek and co-workers in 2001. This work demonstrated that changing the self-sorting properties in a Lewis acid-Lewis base system drastically affected to the catalytic performance in the asymmetric hydroformylation of unfunctionalized internal alkenes.[165] At this point, it is important to distinguish between the different coordination spheres found in metallic complexes. The first coordination sphere consists of the solvent molecules and the coordinating groups of the ligands that are directly connected to the metal. The counterions and the remote portion of the ligand backbone, together with other molecules that interact with the ligands by means of non-covalent interactions, form the second coordination sphere. The control of the process in terms of reactivity and selectivity depends on the mutual interactions between all the components at both coordination spheres.[166]

Self-assembly processes can be used very efficiently to produce in a simple way catalytic organometallic systems, some of them of high complexity, containing constrained spaces very well-suited for efficient catalytic transformations.[167] One of the leading experts in this field is M. Fujita, whose group has designed several complicated organometallic cages by self-organization of the initial pieces.[168] The properties of the cages can be easily tuned by changing the ligands and the coordination modes in the micro-environment of the metal. For instance, chirality could be easily added to the molecular cages,[169] and the cavity volume could be straightforwardly modified by adjusting the N-Pd-N bite angles.[170] Unsurprisingly, some of these molecular cages presented catalytic activity for a wide range of reactions. Diels-Alder reactions were attained within the cavity of the cyclic assembly.

The cage could successfully encapsulate the reactants through non-covalent interactions in less than 5 minutes and, upon increasing the temperature to 80 °C, the Diels-Alder product formation was completed after 5 hours of reaction. The stereoselectivity towards the *syn*-conformation of the adduct was assigned to the presence of π-π interactions, that stabilized both the transition state and the final product (Figure 1.18b).[171]
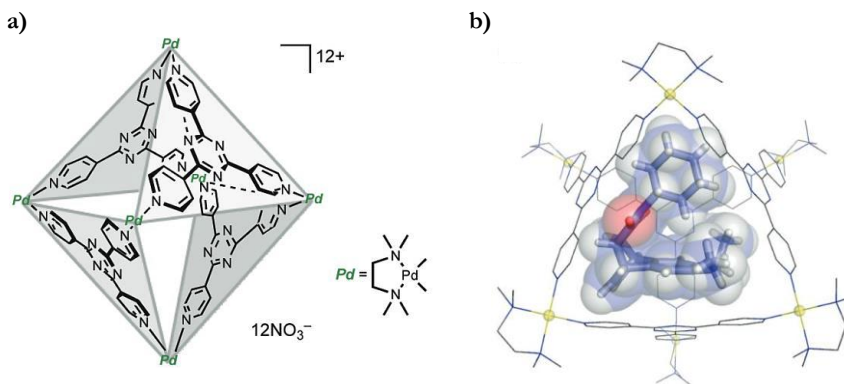

Figure 1.18. a) General structure of the Pd-cage reported by Fujita's group. b) Crystal structure of the Diels-Alder product within the cavity of the self-assembled coordination complex.[171]

In addition, other chemical transformations have been achieved in the cavities of self-assembled molecular cages. Ranging from Knoevenagel to hydrolysis reactions, many examples can be found in literature in which the acceleration of the reaction rate is the result of, among other features, proper preorganization, stabilization of the intermediates, and increased effective concentration.[167a] These substrate-ligand interactions leading to encapsulated reagents have been further exploited, allowing for the design of molecular complexes with recognition sites for specific substrates. In 2006, R. H. Crabtree *et. al.* reported a selective C-H oxidation of ibuprofen in which a target functional group of the substrate was used to interact with the catalyst scaffold. The authors meticulously designed a catalyst scaffold derived from Kemp's triacid combined with a terpyridine ligand site for manganese. Upon formation of the catalyst-substrate adduct through dual hydrogen bonds, one

particular benzylic position of ibuprofen was placed over the Mn centre and thus, the selectivity for oxidation of that specific position was higher than 98% (Figure 1.19).[172]
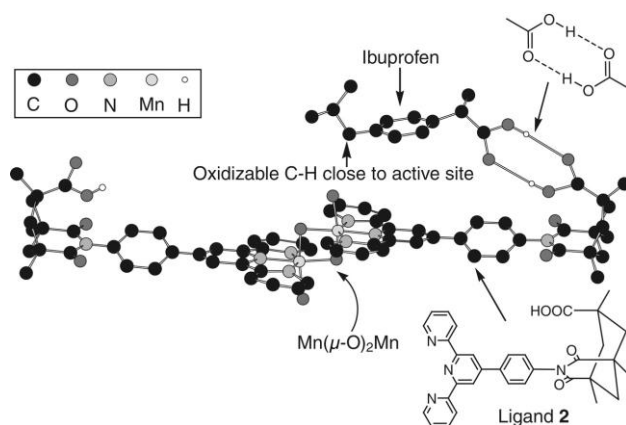

Figure 1.19. Molecular modelling of dimanganese catalyst docked with H-bonded ibuprofen (substrate).[172c]

Later on, in a similar manner, hydrogen bonded assisted site-selective epoxidation of 3-vinylquinolones was accomplished with high enantioselectivities using a Ru(II)-porphyrin as catalyst.[173] P. R. Schreiner and co-workers designed in 2019 a rhodium bimetallic catalyst which was active in site-selective nitrenoid insertions, as a result of remote hydrogen bonding between a post-functionalized urea-based ligand and the substrate of reaction.[174] Interestingly enough, regioselective reactions have also been obtained through the use of non-covalent interactions different from hydrogen bonding. For instance, a fascinating example was published in which electrostatic interactions defined the site-selectivity cross-coupling at remote positions. The presence of a sulfonylated phosphine ligand in a palladium complex allowed the differentiation between initially equivalent chlorides of different dichloroarenes. This was the result of attractive electrostatic interactions between the sulfonate group and the cation associated with the deprotonated substrate, guiding the Pd-catalysed cross-coupling reaction to the halide in *meta-* position of the arene.[175]

Supramolecular interactions between ligands can also play an essential role in the catalytic properties of the complexes. Back in 1980s, C. F. Roobeek and P. W. N. M. van Leeuwen introduced the concept of ligand-ligand non-covalent interactions

when studying secondary phosphine oxides. Upon coordination to a soft transition-metal, *cis*-coordinated phosphine ligands can interact by means of hydrogen bonding between the O-H (hydrogen bond donor site) of a neutral ligand and the oxygen atom of the neighbouring secondary phosphine oxide in its anionic configuration (hydrogen bond acceptor site). Thus, the initially monodentate phosphine ligands were found to be acting as quasi-chelates in the complexes, which provided catalytic activity in the hydroformylation of alkenes and the hydrogenation of alkenes and aldehydes.[176] Other quasi-chelate examples relied on the well-established tautomer system 2-pyridone/2-hydroxypyridine.[177] Hydrogen bonding between ligands has also been recently elucidated in [Cp*Ru] complexes, proven as crucial in controlling the regioselectivity in hydrometallation reactions of unsymmetrical alkynes. The [Ru-Cl] unit of the catalyst served as a hydrogen bond acceptor, leading to a highly favourable organization of the catalyst with bound propargylic alkyne through an interligand hydrogen bond. This precise arrangement resulted in a highly preorganized complex that enhanced both regioselectivity and reaction rates.[172a,178]

1.3.2. Supramolecular organocatalysts

Organocatalytic protocols arose at the end of the 20th Century and have gained lots of adherents since then.[179] In fact, the Royal Swedish Academy of Sciences decided to award the Nobel Prize in Chemistry 2021 to B. List and D. W. C. MacMillan for "*the development of asymmetric organocatalysis*".[180] From a sustainable point of view, the use of purely organic compounds as catalysts aims to decrease the depletion of scarcely abundant transition and noble metals. Nonetheless, replacing metal-based catalysts is not an easy task, as achieving the activities and selectivities accomplished in the presence of metallic scaffolds is quite challenging for compounds of merely organic nature.

Traditional organocatalysis is not considered as a supramolecular discipline because the interactions in the catalytic systems usually involve creating and breaking reversible covalent bonds.[161] This is the case of the well-established chemistry of

reaction activation using secondary amine containing organocatalysts. For instance, L-proline and several derivatives have provided remarkable advances in asymmetric catalysis.[181] However, as the rate acceleration relies on the formation of covalent enamine or iminium species, substoichiometric catalytic loadings (10-20 mol%) are required to obtain great results. Although the synthesis of added-value enantiopure compounds can be attained, the high loadings needed cannot compete with the infinitely minor catalytic loadings (<0.5 mol%) used in organometallic catalysis.

Therefore, the design of organocatalytic compounds able to accelerate reactions by means of supramolecular interactions is of paramount importance. Pioneer work in this field was carried out by R. Breslow and co-workers, who studied the catalytic effect of cyclodextrins in Diels-Alder reactions. They observed that the addition of nitrosobenzene with 1,3-cyclohexadiene, and that of methylvinylketone with 1,3-cyclopentadiene, were much faster in water than in other organic solvents such as formamide or ethylene glycol. This observation was the result of solvophobic binding of the reactants in the presence of polar solvents. Thus, the potential organocatalytic performance of cyclodextrins was assayed, considering their hydrophobic inner cavity as a possible active site. Not surprisingly, the reaction rate was tremendously enhanced in the presence of β-cyclodextrin, whereas when α-cyclodextrin was used instead, it rather acted as an inhibitor. Molecular modelling studies revealed that the hydrophobic pocket of β-cyclodextrin was big enough to stabilize the transition state, but the highly energetic intermediate could not be properly located in the smaller cavity of the α-architecture.[182] On this subject, K. B. Sharpless and co-workers demonstrated that reactions that took more than 24 hours in organic solvents could be completed within minutes in the presence of water. The organic compounds involved were insoluble in water, so the reaction rate enhancement relied on both hydrophobic effects and increased effective concentration of the reactants.[183] From that very moment, a new field of research arose in which reactions were carried out "on water". Such reactions are predominantly ruled by the hydrophobic character of the reagents, that tends to accelerate the reaction rates in the presence of water.[184]

Considering the huge impact that C. J. Pedersen's crown ethers had in supramolecular chemistry, it is not surprising that one of the first organocatalytic supramolecular systems comprised those oxygenated cyclic compounds. In D. J. Sam and H. E. Simmon's preliminary studies, some crown ethers were catalytically active in potassium permanganate-mediated oxidations by acting as phase transfer reagents.[185] Several examples can be found in which complexation of the cation by the crown ethers leads to more nucleophilic/basic "naked" anions, accelerating S_N2 and E2 reactions.[186] Although this methodology has been widely applied over the years, the work published in 2021 by G.-W. Kim and co-workers will be further discussed.[187] In their research, the authors explored the organocatalytic properties of crown ethers in S_N2 fluorinations. The complexation of an alkali metal, namely Cs^+, by the macrocycle rendered an activated fluoride anion. The study revealed high efficiency for both intermolecular and intramolecular activation, relying on the crown ether units acting as Lewis base promoters.

H. Jing *et. al.* designed in 2018 appropriate-size crown ethers for the complexation of the cationic counterions of N-heterocycle anions. Thus, the enhanced nucleophilic character of the anion allowed capturing CO_2 to form a carbamate intermediate, which further reacted with cyclic epoxides to form valuable organic carbonates without the need of any co-catalysts.[188] This experiment demonstrates the high level of sophistication recently reached in crown ether organocatalysis, developing novel supramolecular catalysts for important and diverse reactions such as nitrite anion reduction via electron transfer, regioselective functionalization of unactivated C-H bonds, or Diels-Alder additions.[189]

The last part of this section is committed to the study of hydrogen bonded assisted organocatalysis. This branch of supramolecular organocatalysis dates back to 1998, with the first example published by E. N. Jacobsen and M. S. Sigman. In their work, they proved the organocatalytic activity of chiral Schiff-bases in enantioselective Strecker reactions, both in solution and on solid phase. Quite interestingly, the catalytic activity merely relied on the hydrogen bonding donor properties of the thiourea group present in the structure of the ligand, as was

posteriorly demonstrated.[190] At the same time, E. J. Corey and M. J. Grogan reported a chiral C_2-symmetric guanidine bifunctional catalyst also active in Strecker reactions. In this case, one of the NH groups of the guanidine moiety was intermolecularly hydrogen bonded to the nitrogen atom of the initial imine, enhancing the electrophilic character of the carbon, and thus accelerating the reaction rate.[191]

During the first quarter of the 21st century, several fascinating hydrogen bond donor (HBD) catalysts have been synthesized. The thiourea derived organocatalysts introduced by E. N. Jacobsen were found active in other asymmetric reactions such as Baylis-Hillman,[192] or Mannich reactions.[193] Subsequent investigations have focused on the design of appropriately preorganized HBD sites within different structures, in order to create organocatalytic nanoreactors.[194] H.-Y. Chen's group described the syntheses of two *endo*-functionalized organic cages exhibiting good size selectivity and catalytic activity for Friedel-Crafts reactions.
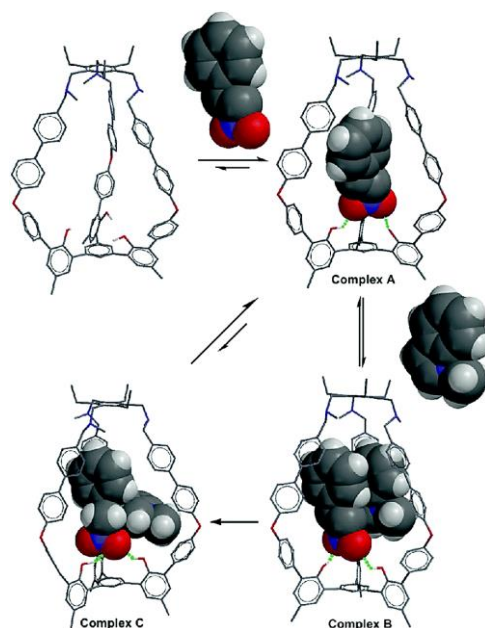

Figure 1.20. Optimized structures of the Friedel-Craft reaction pathway in the cage.[195]

The cavity could accommodate the different species without product inhibition, as the increase in the steric hindrance lowered the binding affinity of the product, compared with the reagent, regenerating the cage. In the catalytic mechanism, the

three endohedral phenol groups acted as active HBD sites to accelerate the reaction rate (Figure 1.20).[195]

Heterogenous HBD catalysts have also been obtained, as for instance the Zn-based MOF described in 2019 by S. K. Mandal and D. Markad. The catalytic activity of the porous material purely relied on hydrogen bonding between the primary amide groups and the nitro group of the reagent, activating the substrate for Friedel-Crafts alkylation. Additionally, the catalyst could be recovered without losing its activity up to 4 times, surpassing most of the previously reported results regarding heterogenous organocatalytic Friedel-Crafts reactions.[196] Taking into account the fundamental correspondences between hydrogen and halogen bonding, some contributions have been made in the last 5 years concerning halogen bond donor catalysis.[197]

On the other hand, scarce examples can be found in literature regarding hydrogen bond acceptor (HBA) organocatalysts. This is quite surprising considering that, in addition to the hydrogen donor, an acceptor with a lone electron pair is the essential partner in hydrogen bonding. Ma's group reported the very first example of HBA assisted organocatalysis, consisting of a C_2-symmetric chiral bisoxazoline. Biologically active agents could be catalytically synthesized through enantioselective aldol reactions in the presence of the chiral bisoxazoline.[198]

Having described the most relevant approaches in this area, it must be mentioned that supramolecular organocatalysis often involves multifunctionality, combining within the structure of the catalyst several active sites for non-covalent interactions.[161] Although supramolecular forces are relatively weak, appropriate design of catalytic species can provide synergic effects to enhance the reaction rate.[199] As an example, Z. Li *et. al.* studied in 2018 the catalytic performance of a cavitand in the ring-opening cyclization of epoxy alcohols. Comparing the activity of the cavitand with an open-chain analogue, the more rigid compound promoted higher rates and regioselectivities because of the proper preorganization of the groups. Thorough DFT calculations proved that the catalytic activity depended on the

combination of HBD and HBA sites, together with CH-π interactions that stabilized the TS of the desired product.[200]

1.3.3. Synzymatic supramolecular catalysts

As Nature has served as a dominant source of inspiration in the area of supramolecular chemistry, it is not surprising that enzymes have served as natural prototypes for the design of supramolecular catalysts.[201] Consequently, much effort has been invested in creating systems that can mimic enzymatic catalysis, the so-called synzymes (synthetic enzymes).[202] These artificial catalysts must present the correct preorganization to locate the reagents with optimal arrangements, as well as a high desolvation power to enhance the stabilization of the transition state within the active pocket. However, the unrivalled ability of enzymes to accelerate the rates of chemical reactions by staggering amounts (up to 10^{20} times the rate of the uncatalyzed reaction), is still a distant scenario for the synthetic systems. Nonetheless, the design of synzymatic systems has not only served as a proof of concept for the way enzymes work, but it has also provided advantages regarding some vulnerabilities of the biological analogues.[203] Enzymes frequently present low thermal stability, low tolerance to experimental conditions, poor substrate versatility and diversity, poor adaptability to abiotic reactions, and high cost of preparation and purification.[204]

Two different approaches can be followed for developing synzymes. The first strategy is based on designing a molecular system that is made up of similar components to the ones found in the active pocket of the natural enzyme. In this way, if the structure of the designed molecule resembles the micro-environment found in the enzyme, the catalyst should imitate the catalytic performance of the enzyme (Figure 1.21).[205]
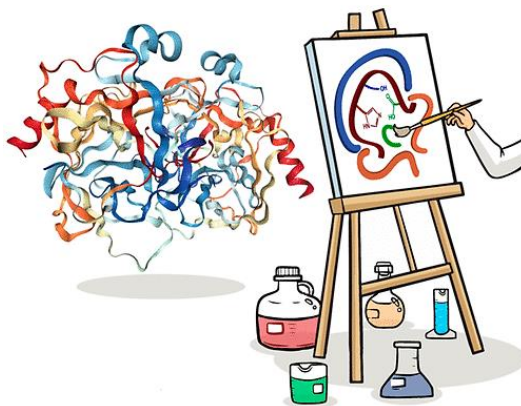
Figure 1.21. Artistic representation of enzyme mimicking by carefully designing the active pocket.[206]

This methodology has proven challenging, as mimicking a whole catalytic cavity can be exceedingly complicated for some enzymatic systems.[207] Interestingly enough, however, the mechanistic pathways of enzymes such as chymotrypsin hydrolases or the enzyme family of cytochrome P-450, have been deeply understood.[208] The remarkable catalytic activity of chymotrypsin-like enzymes relies on three main factors: the active site consisting of a catalytic triad (Ser-His-Asp), stabilization of the transition state through hydrogen bonding of the amide and amino functionalities of the peptidic backbone, and the hydrophobic environment.[206] D. J. Cram and his team developed a wonderful example of a synthetic serine protease mimic, containing a precisely aligned catalytic triad as well as a suitable binding pocket.[209] However, as aforementioned, preparing this system required more than 30 synthetic steps, limiting the relevance of this approach.

A different scenario is found when synthetic compounds are able to simulate enzymatic behaviours without having structural semblance to the natural catalyst. For example, hydrolase activities have been attained with transition metal-based synzymes. D. N. Reinhoudt and co-workers developed in 2005 novel triazamacrocyclic ligands that were attached to different calix[4]arene based platforms. Effects such as the flexibility of the whole system as well as the position of the metal complexes were investigated in order to shed light on the mechanism in some hydrolytic processes.[210] In more recent studies, the hydrolase activity of

mononuclear iron complexes,[211] and dinuclear nickel complexes,[212] have been demonstrated.

In 2004, J. Rebek and A. Gissot reported a monofunctionalized cavitand able to catalyse the aminolysis of a choline derivative. A pyridone scaffold was added to the bowl-shaped structure, as it is a well-known bifunctional catalyst for the breakdown of tetrahedral intermediates. Additionally, the cavity provided the shape and the non-covalent interactions to stabilize the transition state, creating a unique environment with high substrate specificity.[213]

One of the main fields of application of synzymatic systems is in CO_2 conversion. It is well known that the continuous emission of carbon dioxide into the atmosphere is causing global warming, which is a major issue nowadays. Consequently, the concept of anthropogenic CO_2 capture, activation and conversion, in combination with other simple molecules, into added-value chemical products that can compensate for the energetic and economic costs of its capture is currently receiving increasing attention. In fact, carbon dioxide is an abundant, naturally occurring, non-toxic, low-cost and renewable carbon source which can be used as C_1 building block. [214] Considering the sluggish reactivity of CO_2 and its high stability, the design of efficient catalysts is of general interest.[215]

In Nature, the hydrolysis of carbon dioxide into bicarbonate and protons is one of the fastest enzymatic reactions, accurately carried out by carbonic anhydrase. The active pocket of the enzyme consists of a Zn(II) metallic core coordinated to three imidazolium residues (His-triad) of the macromolecule, with a water molecule or hydroxide anion (depending on the pH) completing the distorted tetrahedral arrangement of the complex (Figure 1.22).[216] This enzyme catalyses other processes involving hydration of aldehydes, pyruvate and alkyl pyruvates as well as the hydrolysis of carboxylic, sulfonic, carbonic and phosphoric esters.[217]
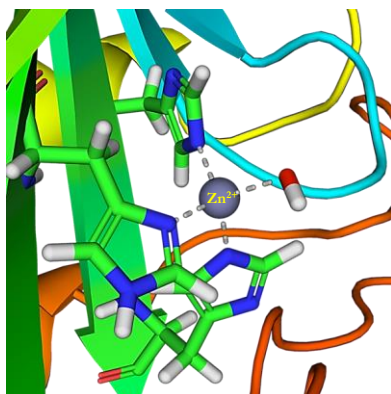
Figure 1.22. Carbonic anhydrase active site at basic pH, observing a hydroxide anion (PDB:1CA2).

Notably, carbonic anhydrase mimics have been proposed as potential catalysts for carbon capture and sequestration from the environment.[218] Most commonly, these synzymes contain Zn(II) metalorganic complexes, though a few examples with other abundant and inexpensive metals have also been reported. Early examples were based on metallic complexes of cyclodextrins derivatives, as cyclic dextrins were one of the most we---studied supramolecular systems. For instance, I. Tabushi and Y. Kuroda reported in 1984 a bis(histamino)-π-cyclodextrin-Zn^{2+}-imidazole complex as a moderately active carbonic anhydrase mimic. An insight in the mechanistic pathway demonstrated a critical reduction in the catalytic activity as a result of the fast carbamation of the free imidazolium groups, together with a pH drop and bicarbonate inhibition.[219] Since then, several biomimetic complexes have been developed to reproduce the specific $[Zn(His)_3(OH_2)]^{2+}$ coordination core, although dicationic zinc aqua model complexes have proven extremely difficult to stabilize. Most classical models only succeeded in stabilizing Zn-hydroxo species because of the high Lewis-acidity of the Zn(II) centre bound to only four neutral ligands. In strong contrast, a very stable dicationic zinc-aqua complex was obtained using the calix[6]tris(imidazole) ligand in 2001. Despite the complex did not render hydrolytic activity, it served to study the binding properties of such constrained metallic centres.[208b,220]

More sophisticated studies have been attained in the recent years.[221] MOFs and Zn-clusters have proved to efficiently reproduce some carbonic anhydrase catalytic processes.[218,222] The emergence of stimuli-responsive molecular machines has allowed to better control the catalytic activity of synzymatic systems. For instance, S. Bandyopadhyay and M. Saha built a photoresponsible carbonic anhydrase mimic. Using light as stimulus is convenient as it offers excellent spatio-temporal control and it can operate without any physical contact. This elegantly designed photoswitchable catalyst consisted of a bisimidazole-azobenzene scaffold which, upon irradiation, shifted the conformation from *cis-* to *trans-*. The *cis*-isomer performed tremendously greater catalytic activities than the *trans*-isomer, as a result of a bidentate coordination of the imidazole groups to the Zn(II) metallic core. In contrast, the *trans*-configuration led to the formation of polymeric complexes, which were found less active in the ester hydrolysis. Additionally, the catalytic activity was much enhanced by the introduction of an ionic polymeric co-catalyst that helped in the stabilization of the oxyanion transition state.[223]

Nowadays, carbonic anhydrase mimics are used not only for conversion of CO_2 into bicarbonate but also for the formation of added-value chemicals. For instance, the catalytic conversion of carbon dioxide into cyclic carbonates has been extensively studied, as the products find many utilities such as raw materials for green polymers, electrolytes in lithium-ion batteries and as benign solvents.[224] The most established mechanism for the reaction encompasses an oxirane (**R** in Figure 1.23) ring-opening step by a nucleophilic species (**Nu** in Figure 1.23), leading to the phenolate intermediate (**I1** in Figure 1.23). The phenolate thus attacks to the carbon dioxide molecule, obtaining a carboxylate intermediate (**I2** in Figure 1.24). Finally, the oxygen atom of the carboxylate intermediate attacks to the vicinal electrophilic carbon (substituted with the leaving group, CH_2-Nu) producing the desired cyclic carbonate (**P** in Figure 1.23).[225] The regioselectivity of the ring-opening step, namely α- or β-attack, much depends on the nature of both the epoxide and the catalyst introduced.[226]
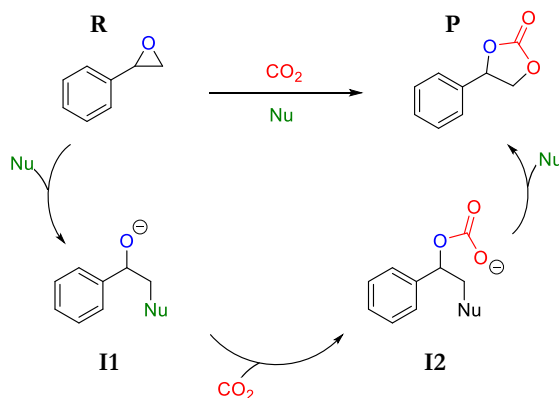
Figure 1.23. Most established mechanism for the cycloaddition of CO_2 to styrene oxide in the presence of a nucleophile. The β-attack mechanism has been displayed in this case.

This reaction has been successfully achieved in the presence of Lewis acids, Lewis bases, nucleophiles, and more sophisticated multifunctional/multicomponent catalysts.[227] Considering the many interacting sites of enzymes, some bioinspired enzyme mimics have provided remarkable advantages on this behalf. For instance, in 2019, Liu *et. al.* designed amide-functionalized heterometallic helicate cages that were able to efficiently convert CO_2 into the desired cyclic carbonate. The robust synzyme could be easily recycled for up to 5 runs, and its high catalytic activity was based on the well-oriented multiple Lewis-basic and Lewis-acid active sites of the cage.[228]

In this regard, an organocatalytic synzymatic system has been recently reported by our research group. The efficiency of the cycloaddition of CO_2 to epoxides was significantly improved by the presence of highly constrained pseudopeptidic macrocycles, which could be recycled for up to 3 times. The activity relied on synergetic effects involving an optimal preorganization of the whole catalytic pool and the Lewis-basic sites present in the macrocyclic structures, which captured carbon dioxide (see Chapter 5). This system was further developed, envisaging that the use of a hydrophobic solid-solvent could promote stronger non-covalent interactions between the active-sites and the substrates.[229] With this objective in mind, we decided to design macrocyclic pseudopeptides bearing a pendant arm

within their structure, so they could be easily immobilized onto polymeric supports.[230] As expected, these heterogeneous organocatalysts were active in the cycloaddition of CO_2 to terminal epoxides, promoting high TON and TOF values even at moderate reaction conditions (see Chapter 6).

Combining the many advantages provided by the pseudopeptidic functional groups with the well-known catalytic benefits of metallic centres, we also designed a series of macrocyclic organometallic catalysts with a high level of preorganization. These Zn(II)-derived compounds were found active in the cycloaddition of carbon dioxide to epoxides, even at room temperature, in the absence of auxiliary co-catalysts (Chapter 7). Interestingly, the catalysts promoted good enantioselectivities for the desired cyclic carbonates through kinetic resolution of oxiranes.

1.4. References

1- (a) Lehn, J. M. Toward Self-Organization and Complex Matter. *Science* **2002**, *295*, 2400-2403. (b) Lehn, J. M. Perspectives in supramolecular chemistry - From molecular recognition towards molecular information processing and self-organization. *Angew. Chem. Int. Ed.* **1990**, *29*, 1304-1319. (c) Lehn, J. M. Supramolecular Chemistry - Scope and Perspectives Molecules, Supermolecules, and Molecular Devices (Nobel Lecture). *Angew. Chem. Int. Ed.* **1988**, *27*, 89-112.

2- Klug, A. From Macromolecules to Biological Assemblies (Nobel Lecture). *Angew. Chem. Int. Ed.* **1983**, *22*, 565-582.

3- Nguyen, S. T.; Gin, D. L.; Hupp, J. T.; Zhang, X. Supramolecular chemistry: Functional structures on the mesoscale. *Proc. Natl. Acad. Sci.* **2001**, *98*, 11849-11850.

4- (a) Stahl, N.; Jencks, W. P. Hydrogen bonding between solutes in aqueous solution. *J. Am. Chem. Soc.* **1986**, *108*, 4196-4205. (b) Latimer, W. M.; Rodebush, W. H. Polarity and ionization from the standpoint of the Lewis theory of valence. *J. Am. Chem. Soc.* **1920**, *7*, 1419-1433. (c) Moore, T. S.; Winmill, T. F. The state of amines in aqueous solution. *J. Chem. Soc., Trans.* **1912**, *101*, 1635-1676.

5- Pedersen, C. J. Cyclic Polyethers and Their Complexes with Metal Salts. *J. Am. Chem. Soc.* **1967**, *89*, 7017-7036.

6- Steed, J. W.; Atwood, J. L. *Supramolecular Chemistry*. Wiley: 2013.

7- Lehn, J. M., Supramolecular Chemistry. *Science* **1993**, *260*, 1762-1763.

8- (a) Gohlke, H.; Klebe, G. Approaches to the Description and Prediction of the Binding Affinity of Small-Molecule Ligands to Macromolecular Receptors. *Angew. Chem. Int. Ed.* **2002**, *41*, 2644-2676. (b) Gellman, S. H. Introduction: Molecular Recognition. *Chem. Rev.* **1997**, *97*, 1231-1232.

9- (a) Zhao, X.; Zhang, S. Molecular designer self-assembling peptides. *Chem. Soc. Rev.* **2006**, *35*, 1105-1110. (b) Pochan, D.; Scherman, O. Introduction: Molecular Self-Assembly. *Chem. Rev.* **2021**, *121*, 13699-13700.

10- (a) Frei, P.; Hevey, R.; Ernst, B. Dynamic Combinatorial Chemistry: A New Methodology Comes of Age. *Chem. Eur. J.* **2019**, *25*, 60-73. (b) Barboiu, M.; Aastrup, T. *Constitutional Dynamic Chemistry*. Springer: 2012. (c) Lehn, J. M. From supramolecular chemistry towards constitutional dynamic chemistry and adaptive chemistry. *Chem. Soc. Rev.* **2007**, *36*, 151-160. (d) Lehn, J. M.; Eliseev, A. V. Dynamic Combinatorial Chemistry. *Science* **2001**, *291*, 2331-2332.

11- (a) Ariga, K.; Ito, H.; Hill, J. P.; Tsukube, H. Molecular recognition: from solution science to nano/materials technology. *Chem. Soc. Rev.* **2012**, *41*, 5800-5835. (b) Beer, P. D.; Gale, P. A. Anion Recognition and Sensing: The State of the Art and Future Perspectives. *Angew. Chem. Int. Ed.* **2001**, *40*, 486-516.

12- (a) Anichini, C.; Czepa, W.; Pakulski, D.; Aliprandi, A.; Ciesielski, A.; Samori, P. Chemical sensing with 2D materials. *Chem. Soc. Rev.* **2018**, *47*, 4860-4908. (b) Persch, E.; Dumele, O.; Diederich, F. Molecular Recognition in Chemical and Biological Systems. *Angew. Chem. Int. Ed.* **2015**, 54, 2-40.

13- (a) Chen, H.; Stoddart, J. F. From molecular to supramolecular electronics. *Nat. Rev. Mater.* **2021**, *6*, 804-828. (b) Amabilino, D. B.; Smith, D. K.; Steed, J. W. Supramolecular materials. *Chem. Soc. Rev.* **2017**, *46*, 2404-2420.

14- (a) Kaufmann, E. N. Characterisation of Materials. Wiley: 2012. (b) Silva, M. V. Historical Development of NMR and LC-NMR. Wiley: 2011.

15- Beer, P. D.; Gale, P. A.; Smith, D. K. *Supramolecular Chemistry*. Oxford University Press: 1999.

16- (a) Erbas-Cakmak, S.; Leigh, D. A.; McTernan, C. T.; Nussbaumer, A. L. Artificial Molecular Machines. *Chem. Rev.* **2015**, *115*, 10081-10206. (b) Diederich, F. 40 Years of Supramolecular Chemistry. *Angew. Chem. Int. Ed.* **2007**, *46*, 68-69.

17- https://www.nobelprize.org/prizes/chemistry/2016/press-release/

18- Uhlenheuer, D. A.; Petkau, K.; Brunsveld, L. Combining supramolecular chemistry with biology. *Chem. Soc. Rev.* **2010**, *39*, 2817-2826.

19- (a) Kobko, N.; Dannenberg, J. J. Cooperativity in Amide Hydrogen Bonding Chains. Relation between Energy, Position, and H-Bond Chain Length in Peptide and Protein Folding Models. *J. Phys. Chem. A* **2003**, *107*, 10389-10395. (b) Rose, G. D. Hydrogen Bonding, Hydrophobicity, Packing and Protein Folding. *Annu. Rev. Biophys. Biomol. Struct.* **1993,** *22*, 381-415.

20- (a) Feng, B.; Sosa, R. P.; Martensson, A. K. F.; Jiang, K.; Tong, A.; Dorfman, K. D.; Takahasi, M.; Lincoln, P.; Bustamante, C. J.; Westerlund, F.; Nordén, B. Hydrophobic catalysis and a potential biological role of DNA unstacking induced by environment effects. Proc. Natl. Acad. Sci. U S A. **2019**, *116*, 17169-17174. (b) Cleaves, H. J. *Watson–Crick Pairing*. Springer: 2011.

21- (a) Würthner, F. Solvent Effects in Supramolecular Chemistry: Linear Free Energy Relationships for Common Intermolecular Interactions. *J. Org. Chem.* **2022**, *87*, 1602–1615**.** (b) Schneider, H. J. Binding Mechanisms in Supramolecular Complexes. *Angew. Chem. Int. Ed.* **2009**, *48*, 3924-3977.

22- Schalley, C. A. *Analytical Methods in Supramolecular Chemistry*. Wiley: 2007.

23- Jeffrey, G. A. *An Introduction to Hydrogen Bonding*. Oxford University Press: 1997.

24- Cavallo, G.; Metrangolo, P.; Milani, R.; Pilati, T.; Priimagi, A.; Resnati, G.; Terraneo, G. The Halogen Bond. *Chem. Rev.* **2016**, *116*, 2478-2601.

25- Dougherty, D. A. The Cation-π Interaction. *Acc Chem Res.* **2013**, *46*, 885-893.

26- Schottel, B. L.; Chifotides, H. T.; Dunbar, K. R. Anion-π interactions. *Chem. Soc. Rev.* **2008**, *37*, 68-83.

27- Hunter, C. A.; Sanders, J. K. M. The nature of π-π interactions. *J. Am. Chem. Soc.* **1990**, *112*, 5525-5534.

28- (a) Sheehan, F.; Sementa, D.; Jain, A.; Kumar, M.; Tayarani-Najjaran, M.; Kroiss, D.; Ulijn, V. Peptide-Based Supramolecular Systems Chemistry, *Chem. Rev.* **2021**, *121*, 13869-13914. (b) Luis, S. V.; Alfonso, I. Bioinspired Chemistry Based on Minimalistic Pseudopeptides. *Acc. Chem. Res.* **2014**, *47*, 112-124.

29- Lapidoth, G.; Khersonsky, O.; Lipsh, R.; Dym, O.; Albeck, S.; Rogotner, S.; Fleishman, S. J. Highly active enzymes by automated combinatorial backbone assembly and sequence design. *Nat. Commun.* **2018**, article number: 2780.

30- Dill, K. A. Theory for the folding and stability of globular proteins. *Biochemistry* **1985**, *24*, 1501-1509.

31- (a) Shi, G.; Wüst, T.; Landau, D. P. Elucidating thermal behavior, native contacts, and folding funnels of simple lattice proteins using replica exchange Wang-Landau sampling. *J. Chem. Phys.* **2018**, *149*, 164913-164921. (b) Istrail, S.; Schwartz, R.; King, J. Lattice Simulations of Aggregation Funnels for Protein Folding. *J. Comput. Biol.* **1999,** *6*, 143-162.

32- Dill, K. A.; MacCallum, J. L. The Protein-Folding Problem, 50 Years On. *Science* **2012**, *338*, 1042-1046.

33- Wu, Y. D.; Gellman, S., Peptidomimetics. *Acc. Chem. Res.* **2008**, *41*, 1231-1232.

34- (a) Pelay-Gimeno, M.; Glas, A.; Koch, O.; Grossmann, T. N. Structure-Based Design of Inhibitors of Protein-Protein Interactions: Mimicking Peptide Binding Epitopes. *Angew. Chem. Int. Ed.* **2015**, *54*, 8896-8927. (b) Azzarito, V.; Long, K.; Murphy, N. S.; Wilson, A. J. Inhibition of α-helix-mediated protein-protein interactions using designed molecules. *Nat. Chem.* **2013**, *5*, 161-173. (c) Ripka, A. S.; Rich, D. H. Peptidomimetic design. *Curr. Opin. Chem. Biol.* **1998***, 2,* 441-452.

35- Alfonso, I. From simplicity to complex systems with bioinspired pseudopeptides. *Chem. Commun.* **2016**, *52*, 239-250.

36- Lawrance, G. A., Introduction to Coordination Chemistry. Wiley: 2013.

37- (a) Sóvágó, I.; Kállay, C.; Várnagy, K. Peptides as complexing agents: Factors influencing the structure and thermodynamic stability of peptide complexes. *Coord. Chem. Rev.* **2012**, *256*, 2225-2233. (b) Burger, K. *Biocoordination Chemistry*. Ellis Horwood: 1990.

38- Sigel, H.; Martin, R. B. Coordinating properties of the amide bond. Stability and structure of metal ion complexes of peptides and related ligands. *Chem. Rev.* **1982**, *82*, 385-426.

39- Wagler, T. R.; Fang, Y.; Burrows, C. J. Optically active difunctionalized dioxocyclam macrocycles: ligands for nickel-catalyzed oxidation of alkenes. *J. Org. Chem.* **1989**, *54*, 1584-1589.

40- Fessmann, T.; Kilburn, J. D. Identification of Sequence-Selective Receptors for Peptides with a Carboxylic Acid Terminus. *Angew. Chem. Int. Ed.* **1999**, *38*, 1993-1996.

41- Still, W. C. Discovery of Sequence-Selective Peptide Binding by Synthetic Receptors Using Encoded Combinatorial Libraries. *Acc. Chem. Res.* **1996**, *29*, 155-163.

42- (a) Polt, R.; Kelly, B. D.; Dangel, B. D.; Tadikonda, U. B.; Ross, R. E.; Raitsimring, A. M.; Astashkin, A. V. Optically Active 4- and 5-Coordinate Transition Metal Complexes of Bifurcated Dipeptide Schiff Bases. *Inorg. Chem.* **2003**, *42*, 566-574. (b) Dangel, B. D.; Polt, R. Catalysis by Amino Acid-Derived Tetra coordinate Complexes: Enantioselective Addition of Dialkylzincs to Aliphatic and Aromatic Aldehydes. *Org. Lett.* **2000**, *2*, 3003-3006.

43- Becerril, J.; Bolte, M.; Burguete, M. I.; Galindo, F.; García-España, E.; Luis, S. V.; Miravet, J. F. Efficient Macrocyclization of U-Turn Preorganized Peptidomimetics: The Role of Intramolecular H-Bond and Solvophobic Effects. *J. Am. Chem. Soc.* **2003**, *125*, 6677-6686.

44- Meyer, F; Kozlowski, H. *Comprehensive Coordination Chemistry II: From Biology to Nanotechnology.* Elsevier: 2004.

45- (a) Gorla, L.; Martí-Centelles, V.; Altava, B.; Burguete, M. I.; Luis, S. V. Cu2+recognition by N,N'-benzylatedbis(amino amides). *Dalton Trans.* **2017**, *46*, 2660-2669. (b) Gorla, L.; Martí-Centelles, V.; Freimuth, L.; Altava, B.; Burguete, M. I.; Luis, S. V. Cu2+, Zn2+, and Ni2+ Complexes of C2-Symmetric Pseudopeptides with an Aromatic Central Spacer. *Inorg. Chem.* **2016**, *55*, 7617-7629. (c) Marti, I.; Ferrer, A.; Escorihuela, J.; Burguete, M. I.; Luis, S. V. Copper(II) complexes of bis(amino amide) ligands: effect of changes in the amino acid residue. *Dalton Trans.* **2012**, *41*, 6764-6776.

46- (a) Escorihuela, J.; Burguete, M. I.; Luis, S. V. Enantioselective nickel-catalyzed conjugate addition of dialkylzinc to chalcones using chiral α-amino amides. *Tetrahedron Lett.* **2008**, *49*, 6885-6888. (b) Burguete, M. I.; Collado, M.; Escorihuela, J.; Galindo, F.; García-Verdugo, E.; Luis, S. V.; Vicent, M. a. J. Nickel complexes from α-amino amides as efficient catalysts for the enantioselective Et2Zn addition to benzaldehyde. *Tetrahedron Lett.* **2003**, *44*, 6891-6894.

47- Burguete, M. I.; Galindo, F.; Luis, S. V.; Vigara, L. A turn-on fluorescent indicator for citrate with micromolar sensitivity. *Dalton Trans.* **2007**, *36*, 4027-4033.

48- (a) Weseliński, Ł.; Słyk, E.; Jurczak, J. The highly enantioselective 1,3-dipolar cycloaddition of alkyl glyoxylate-derived nitrones to E-crotonaldehyde catalyzed by hybrid diamines. *Tetrahedron Lett.* **2011**, *52*, 381-384. (b) Postnikova, B. J.; Anslyn, E. V. Asymmetric enolate alkylation via templation with chiral synthetic receptors. *Tetrahedron Lett.* **2004**, *45*, 501-504.

49- Trost, B. M.; Brindle, C. S. The direct catalytic asymmetric aldol reaction. *Chem. Soc. Rev.* **2010**, *39*, 1600-1632.

50- Paradowska, J.; Pasternak, M.; Gut, B.; Gryzło, B.; Mlynarski, J. Direct Asymmetric Aldol Reactions Inspired by Two Types of Natural Aldolases: Water-Compatible Organocatalysts and Zn(II) Complexes. *J. Org. Chem.* **2011**, *77*, 173-187.

51- Pearson, A. J.; Panda, S. N-Prolinylanthranilamide Pseudopeptides as Bifunctional Organocatalysts for Asymmetric Aldol Reactions. *Org. Lett.* **2011**, *13*, 5548-5551.

52- Joshi, S.; Ranade, V. *Industrial Catalytic Processes for Fine and Specialty Chemicals.* Elsevier: 2016.

53- Kushner, D. J. Self-assembly of biological structures. *Bacteriol Rev.* **1969**; *33*, 302-345.

54- Watson, J. D.; Crick, F. H. C. Molecular structure of nucleic acids: a structure for deoxyribose nucleic acid. *Am. J. Psychiatry* **2003**, *160*, 623-624.

55- Voet, D.; Voet, J. G. *Biochemistry;* 2nd Ed. John Wiley & Sons, Inc.: 1994.

56- (a) Kumar, M.; Ing, N. L.; Narang, V.; Wijerathne, N. K.; Hochbaum, A. I.; Ulijn, R. V. Amino-acid-encoded biocatalytic self-assembly enables the formation of transient conducting nanostructures. *Nat. Chem.* **2018**, *10*, 696-703. (b) Sevim, S.; Sorrenti, A.; Franco, C.; Furukawa, S.; Pané, S.; DeMello, A. J.; Puigmartí-Luis, J. Self-assembled materials and supramolecular chemistry within microfluidic environments: from common thermodynamic states to non-equilibrium structures. *Chem. Soc. Rev.* **2018**, *47*, 3788-3803.

57- Silva, G. A.; Czeisler, C.; Niece, K. L.; Beniash, E.; Harrington, D. A.; Kessler, J. A.; Stupp, S. I. Selective Differentiation of Neural Progenitor Cells by High-Epitope Density Nanofibers. *Science* **2004**, *303*, 1352-1355.

58- Suzuki, M.; Hanabusa, K. L-lysine-based low-molecular-weight gelators. *Chem. Soc. Rev.* **2009**, 38, 967-975.

59- Ghosh, S.; Adler-Abramovich, L.; Gazit, E.; Verma, S. Spacer driven morphological twist in Phe-Phe dipeptide conjugates. *Tetrahedron* **2013**, *69*, 2004-2009.

60- (a) Giuri, D.; Barbalinardo, M.; Zanna, N.; Paci, P.; Montalti, M.; Cavallini, M.; Valle, F.; Calvaresi, M.; Tomasini, C. Tuning Mechanical Properties of Pseudopeptide Supramolecular Hydrogels by Graphene Doping. *Molecules* **2019**, *24*, 4345-4356. (b) Zanna, N.; Merlettini, A.; Tomasini, C. Self-healing hydrogels triggered by amino acids. *Org. Chem. Front.* **2016**, *3*, 1699-1704. (c) Angelici, G.; Falini, G.; Hofmann, H.-J.; Huster, D.; Monari, M.; Tomasini, C. A Fiberlike Peptide Material Stabilized by Single Intermolecular Hydrogen Bonds. *Angew. Chem. Int. Ed.* **2008**, *47*, 8075-8078.

61- (a) Valls, A.; Altava, B.; Aseyev, V.; García-Verdugo, E.; Luis, S. V. Imidazolium based gemini amphiphiles derived from L-valine. Structural elements and surfactant properties. *J. Mol. Liq.* **2021**, *341*, article number: 117434. (b) Valls, A.; Castillo, A.; Porcar, R.; Hietala, S.; Altava, B.; García-Verdugo, E.; Luis, S. V. Urea-Based Low-Molecular-Weight Pseudopeptidic Organogelators for the Encapsulation and Slow Release of (R)-Limonene. *J. Agric. Food Chem.* **2020**, *68*, 7051-7061.

62- Korchowiec, B.; Gorczyca, M.; Korchowiec, J.; Rubio-Magnieto, J.; Lotfallah, A. H.; Luis, S. V.; Rogalska, E. A The effect of protonation in a family of peptide based gemini amphiphiles on the interaction in Langmuir films. *J. Mol. Liq.* **2019**, *284*, 357-365.

63- Gorczyca, M.; Korchowiec, B.; Korchowiec, J.; Trojan, S.; Rubio-Magnieto, J.; Luis, S. V.; Rogalska, E. A Study of the Interaction between a Family of Gemini Amphiphilic Pseudopeptides and Model Monomolecular Film Membranes Formed with a Cardiolipin. *J. Phys. Chem. B* **2015**, *119*, 6668-6679.

64- Gorla, L.; Martí-Centelles, V.; Altava, B.; Burguete, M. I.; Luis, S. V. The role of the side chain in the conformational and self-assembly patterns of C2-symmetric Val and Phe pseudopeptidic derivatives. *CrystEngComm* **2019**, *21*, 2398-2408.

65- Martí, I.; Burguete, M. I.; Gale, P. A.; Luis, S. V. Acyclic Pseudopeptidic Hosts as Molecular Receptors and Transporters for Anions. *Eur. J. Org. Chem.* **2015**, *23*, 5150-5158.

66- Faggi, E.; Serra-Vinardell, J.; Pandey, M. D.; Casas, J.; Fabriàs, G.; Luis, S. V.; Alfonso, I. Pseudopeptidic fluorescent on-off pH sensor based on pyrene excimer emission: Imaging of acidic cellular organelles. *Sens. Actuators B Chem.* **2016**, *234*, 633-640.

67- Yudin, A. K. Macrocycles: lessons from the distant past, recent developments, and future directions. *Chem Sci.* **2015**, 6, 30-49.

68- Liu, Z.; Nalluri, S. K. M.; Stoddart, J. F. Surveying macrocyclic chemistry: from flexible crown ethers to rigid cyclophanes. *Chem. Soc. Rev.* **2017**, *46*, 2459-2478.

69- (a) Appavoo, S. D.; Huh, S.; Diaz, D. B.; Yudin, A. K. Conformational Control of Macrocycles by Remote Structural Modification. *Chem. Rev.* **2019**, *119*, 9724-9752. (b) Bogdan, A. R.; Jerome, S. V.; Houk, K. N.; James, K. Strained Cyclophane Macrocycles: Impact of Progressive Ring Size Reduction on Synthesis and Structure. *J. Am. Chem. Soc.* **2012**, *134*, 2127-2138.

70- Cram, D. J. The design of molecular hosts, guests, and their complexes. *Science* **1988**, *240*, 760-767.

71- (a) Simmons, H. E.; Park, C. H. Macrobicyclic amines. I. Out-in isomerism of 1,(k+2)-diazabicyclo[k.l.m]alkanes. *J. Am. Chem. Soc.* **1968**, *90*, 2428-2429. (b) Simmons, H. E.; Park, C. H. Macrobicyclic amines. II. out-out in-in Prototropy in 1, (k + 2)-diazabicyclo [k.l.m] alkaneammonium ions. *J. Am. Chem. Soc.* **1968**, *90*, 2429-2431. (c) Simmons, H. E.; Park, C. H. Macrobicyclic amines. III. Encapsulation of halide ions by in,in-1,(k + 2)-diazabicyclo[k.l.m.]alkane ammonium ions. . *J. Am. Chem. Soc.* **1968**, *90*, 2431-2432.

72- (a) Lehn, J. M. Supramolecular Chemistry: Receptors, Catalysts, and Carriers. *Science* **1985**, *227*, 849-856. (b) Lehn, J. M. Cryptates: the chemistry of macropolycyclic inclusion complexes. *Acc. Chem. Res.* **1978**, *11*, 49-57.

73- (a) Vögtle, F.; Alfter, F. *Supramolecular chemistry: an introduction.* Wiley: 1991. (b) Vögtle, F.; Weber, E. *Host Guest Complex Chemistry: Macrocycles.* Springer: 1985.

74- Schardinger, F. Azetongärung. *Wien. Klin. Wochenschr.,* **1904**, *17*, 207-209.

75- Crini, G. Review: A History of Cyclodextrins. *Chem. Rev.* **2014**, *114*, 10940-10975.

76- Hui, B. Y.; Zain, N. N. M.; Mohamad, S.; Prabu, S.; Osman, H.; Raoov, M. A comprehensive molecular insight into host-guest interaction of Phenanthrene with native and ionic liquid modified beta-cyclodextrins: Preparation and characterisation in aqueous medium and solid state. *J. Mol. Struct.* **2020**, *1206*, 127675-127685. (b) Morin-Crini, N.; Crini, G. Environmental applications of water insoluble betacyclodextrinepichlorohydrin polymers. *Prog. Polym. Sci.* **2013**, *38*, 344-368. (c) Szejtli, J. Introduction and General Overview of Cyclodextrin Chemistry. *Chem. Rev.* **1998**, *98*, 1743-1754. (d) Szejtli, J. Utilization of Cyclodextrins in Industrial Products and Processes. *J. Mater. Chem.* **1997**, *7*, 575-587.

77- Lancia, F.; Ryabchun, A.; Katsonis, A. Life- like motion driven by artificial molecular machines. *Nat. Rev. Chem.* **2019**, *3*, 536-551.

78- Erbas-Cakmak, S.; Leigh, D. A.; McTernan, C. T.; Nussbaumer, A. L. Artificial Molecular Machines. *Chem. Rev.* **2015**, *115*, 10081-10206.

79- Qu, D.-H.; Feringa, B. L. Controlling Molecular Rotary Motion with a Self-Complexing Lock. *Angew. Chem. Int. Ed.* **2010**, *49*, 1107-1110.

80- Li, F.; Gan, Q.; Xue, L.; Wang, Z. M.; Jiang, H. H-bonding directed one-step synthesis of novel macrocyclic peptides from ε-aminoquinolinecarboxylic acid. *Tetrahedron Lett.* **2009**, *50*, 2367-2369.

81- Bastings, M.; de Greef, T.; van Dongen, J.; Merkx, M.; Meijer, E. Macrocyclization of enzyme-based supramolecular polymers. *Chem. Sci.* **2010**, *1*, 79-88.

82- Levine, D. Vancomycin: A history. *Clin. Infect. Dis.* **2006**, *42*, S5-S12.

83- Kohli, R.; Walsh, C.; Burkart, M. Biomimetic synthesis and optimization of cyclic peptide antibiotics. *Nature* **2002**, *418*, 658-661.

84- Schreiber, S.; Crabtree, G. The mechanism of action of cyclosporin A and FK506. *Immunol. Today* **1992**, *13*, 136-142.

85- Poulain, D.; Oliet, S.; Theodosis, D. *Vasopressin And Oxytocin: From Genes To Clinical Applications.* Elsevier: 2002.

86- Flory, P. J. *Principles of Polymer Chemistry.* Ithaca: 1953.

87- (a) Ziegler, K.; Eberle, H.; Ohlinger, H. Über vielgliedrige Ringsysteme. I. Die präparativ ergiebige Synthese der Polymethylenketone mit mehr als 6 Ringgliedern. *Justus Liebigs Ann. Chem.* **1933**, *504*, 94-130. (b) Ruggli, P. Über einen Ring mit dreifacher Bindung. *Justus Liebigs Ann. Chem.* **1912**, *392*, 92-100.

88- Laurent, B.; Grayson, S. Synthetic approaches for the preparation of cyclic polymers. *Chem. Soc. Rev.* **2009**, *38*, 2202-2213.

89- Mortensen, K. T.; Osberger, T. J.; King, A.; Sore, H. F.; Spring, D. R. Strategies for the Diversity-Oriented Synthesis of Macrocycles. *Chem. Rev.* **2019**, *119*, 10288-10317.

90- Anastas, P. T.; Warner, J. C. *Green Chemistry: Theory and Practice*. Oxford University Press: 1998.

91- Cram, D. J.; Cram, J. M. *Container Molecules and their Guests*. The Royal Society of Chemistry: 1994

92- (a) McGrath, J. M.; Pluth, M. D. Understanding the Effects of Preorganization, Rigidity, and Steric Interactions in Synthetic Barbiturate Receptors. *J. Org. Chem.* **2014**, *79*, 711-71. (b) Lehn, J. M. Toward complex matter: Supramolecular chemistry and self-organization. *Proc. Natl. Acad. Sci. U. S. A.* **2002**, *99*, 4763-4768.

93- (a) Tiwari, V. K.; Kumar, A.; Schmidt, R. R. Disaccharide-Containing Macrocycles by Click Chemistry and Intramolecular Glycosylation. *Eur. J. Org. Chem.* **2012,** *15*, 2945-2956. (b) Gening, M.; Titov, D.; Grachev, A.; Gerbst, A.; Yudina, O.; Shashkov, A.; Chizhov, A.; Tsvetkov, Y.; Nifantiev, N. Synthesis, NMR, and conformational studies of cyclic oligo-(1→6)-β-D-Glucosamines. *Eur. J. Org. Chem.* **2010**, 2465-2475. (c) Velasco-Torrijos, T.; Murphy, P. Metathesis of structurally preorganized bivalent carbohydrates. Synthesis of macrocyclic and oligomeric scaffolds. *Org. Lett.* **2004**, *6*, 3961-3964.

94- (a) Hill, R.; Rai, V.; Yudin, A. Macrocyclization of linear peptides enabled by amphoteric molecules. *J. Am. Chem. Soc.* **2010***, 132*, 2889-2891. (b) Colombo, S.; Coluccini, C.; Caricato, M.; Gargiulli, C.; Gattuso, G.; Pasini, D. Shape selectivity in the synthesis of chiral macrocyclic amides. *Tetrahedron* **2010**, *66*, 4206-4211.

95- (a) Hayase, N.; Nogami, J.; Shibata, Y.; Tanaka, K. Synthesis of a Strained Spherical Carbon Nanocage by Regioselective Alkyne Cyclotrimerization. *Angew. Chem.* **2019**, *131*, 9539-9542. (b) Kim, S.; Castillo, H. D.; Lee, M.; Mortensen, R. D.; Tait, S. L.; Lee, D. From Foldable Open Chains to Shape-Persistent Macrocycles: Synthesis, Impact on 2D Ordering, and Stimulated Self-Assembly. *J. Am. Chem. Soc.* **2018**, *14*, 4726-4735. (c) Zhang, L.; Hughes, D. L.; Cammidge, A. N. Discotic Triphenylene Twins Linked through Thiophene Bridges: Controlling Nematic Behavior in an Intriguing Class of Functional Organic Materials. *J. Org. Chem*. **2012**, *77*, 4288-4297.

96- Martí-Centelles, V.; Pandey, M. D.; Burguete, M. I.; Luis, S. V. Macrocyclization Reactions: The Importance of Conformational, Configurational, and Template-Induced Preorganization. *Chem. Rev.* **2015**, *115*, 8736-8834.

97- (a) Meshcheryakov, D.; Arnaud-Neu, F.; Bohmer, V.; Bolte, M.; Cavaleri, J.; Hubscher-Bruder, V.; Thondorf, I.; Werner, S. Cyclic Tetraureas With Variable Flexibility-Synthesis, Crystal Structures and Properties. *Org. Biomol. Chem.* **2008**, *6*, 3244-3255. (b) Blankenstein, J.; Zhu, J. Conformation-Directed Macrocyclization Reactions. *Eur. J. Org. Chem.* **2005**, *10*, 1949-1964. (c) Carver, F. J.; Hunter, C. A.; Shannon, R. J. Directed Macrocyclisation Reactions. *J. Chem. Soc., Chem. Commun.* **1994**, *10*, 1277-1280.

98- Gong, W.-T.; Hiratani, K.; Oba, T.; Ito, S. A Convenient And Efficient Route for the Synthesis of Amidecrownophanes Via 1:1 Macrocyclization of Di(Acid Chloride) With Diamine Derivatives. *Tetrahedron Lett.* **2007**, *48*, 3073-3076.

99- Katagiri, K.; Tohaya, T.; Masu, H.; Tominaga, M.; Azumaya, I. Effect of Aromatic-Aromatic Interactions on the Conformational Stabilities of Macrocycle and Preorganized Structure during Macro-cyclization. *J. Org. Chem.* **2009**, *74*, 2804-2810.

100- (a) Evans, N. H.; Serpell, C. J.; Christensen, K. E.; Beer, P. D. Amide and Urea Ferrocene-Containing Macrocycles Capable of the Electro-chemical Sensing of Anions. *Eur. J. Inorg. Chem.* **2012**, *6*, 939-944. (b) Fujita, M.; Tominaga, M.; Hori, A.; Therrien, B. Coordination Assemblies from a Pd(II)-Cornered Square Complex. *Acc. Chem. Res.* **2005**, *38*, 369-378. (c) Chowdhury, S.; Schatte, G.; Kraatz, H.-B. Synthesis, Structure And Electrochemistry of Ferrocene−Peptide Macrocycles. *Dalton Trans.* **2004**, 11, 1726-1730.

101- Bru, M.; Alfonso, I.; Burguete, M. I.; Luis, S. V. Efficient syntheses of new chiral peptidomimetic macrocycles through a configurationally driven preorganization. *Tetrahedron Lett.* **2005**, *46*, 7781-7785.

102- Martí-Centelles, V.; Burguete, M. I.; Cativiela, C.; Luis, S. V. The Role of the Amino Acid-Derived Side Chain in the Preorganization of C2-Symmetric Pseudopeptides: Effect on S_N2 Macrocyclization Reactions. *J. Org. Chem.* **2014**, *79*, 559-570.

103- Thompson, M. C.; Busch, D. H. Reactions of Coordinated Ligands. IX. Utilization of the Template Hypothesis to Synthesize Macrocyclic Ligands in Situ. *J. Am. Chem. Soc.* **1964**, *86*, 3651-3656.

104- Gerbeleu, N. V.; Arion, V. B.; Burgess, J. *Template Synthesis of Macrocyclic Compounds.* Wiley: 1999.
105- (a) Yang, S.; Miyachi, A.; Matsuno, T.; Muto, H.; Sasakawa, H.; Ikemoto, K.; Isobe, H. Metal-Templated Oligomeric Macrocyclization via Coupling for Metal-Doped π-Systems. *J. Am. Chem. Soc.* **2021**, *143*, 15017-15021. (b) Diederich, F.; Stang, P. J. *Templated organic synthesis.* Wiley: 2000.

106- Pedersen, C. J. Macrocyclic Polyethers: Dibenzo-18-Crown-6 Polyether and Dicyclohexyl-18-Crown-6 Polyether. *Org. Synth.* **1972**, *52*, 66-74.

107- (a) Dankert, F.; Donsbach, C.; Rienmüller, J.; Richter, R. M.; von Hänisch, C. Alkaline Earth Metal Template (Cross-)Coupling Reactions with Hybrid Disila-Crown Ether Analogues. *Chem. Eur. J.* **2019**, *25*, 15934-15943. (b) Dankert, F.; Donsbach, C.; Mais, C.-N.; Reuter, K.; von Hänisch, C. Alkali and Alkaline Earth Metal Derivatives of Disila-Bridged Podands: Coordination Chemistry and Structural Diversity. *Inorg. Chem.* **2018**, *57*, 351-359.

108- (a) Barefield, E. K. New Synthesis of 1,4,8,11-Tetraazacyclote-tradecane (Cyclam) Via the Nickel(II) Complex. *Inorg. Chem.* **1972**, *11*, 2273-2274. (b) Karn, J. L.; Busch, D. H. Nickel (II) Complexes of the Tetradentate Macrocycle 2,12-Dimethyl-3,7,11,17-Tetraazabicyclo(11.3.1) Heptadeca-1 (17),2,11,13,15-Pentaene. *Nature* **1966**, *211*, 160-162.

109- (a) Rivera, D. G.; Ojeda-Carralero, G. M.; Reguera, L.; van der Eycken, E. Peptide macrocyclization by transition metal catalysis, *Chem. Soc. Rev.* **2020**, *49*, 2039-2059. (b) Mikhailov, O. V. Molecular structures of M(II) chelates with compartmental (N,N)-, (N,O)- And (N,S)-donor ligands and articulated metal chelate cycles. *Rev. Inorg. Chem.* **2018**, *38*, 163-191. (c) Fabbrizzi, L.; Licchelli, M.; Mosca, L.; Poggi, A. Template Synthesis of Azacyclam Metal Complexes Using Primary Amides as Locking Fragments. *Coord. Chem. Rev.* **2010**, *254*, 1628-1636.

110- (a) Bunchuay, T.; Docker, A.; Martinez-Martinez, A. I.; Beer, P. D. A Potent Halogen-Bonding Donor Motif for Anion Recognition and Anion Template Mechanical Bond Synthesis. *Angew. Chem. Int. Ed.* **2019**, *39*, 13823-13827. (b) Evans, N. H.; Beer, P. D. Advances in Anion Supramolecular Chemistry: From Recognition to Chemical Applications. *Angew. Chem. Int. Ed.* **2014**, *53*, 11716-11754. (c) Beer, P. D.; Sambrook, M. R.; Curiel, D. Anion-templated assembly of interpenetrated and interlocked structures. *Chem. Commun.* **2006**, 20, 2105-2117.

111- Leczycka-Wilk, K.; Dabrowa, K.; Cmoch, P.; Jarosz, S. Chloride-Templated Macrocyclization and Anion-Binding Properties of C2-Symmetric Macrocyclic Ureas from Sucrose. *Org. Lett.* **2017**, *19*, 4596-4599.

112- Prigorchenko, E.; Kaabel, S.; Narva, T.; Baskir, A.; Fomitsenko, M.; Adamson, J.; Järving, I.; Rissanen, K.; Tamm, T.; Aav, R. Formation and trapping of the thermodynamically unfavoured inverted-hemicucurbit[6]uril. *Chem. Commun.* **2019**, *55*, 9307-9310.

113- (a) Alfonso, I.; Bolte, M.; Bru, M.; Burguete, M. I.; Luis, S. V.; Rubio, J. Supramolecular Control for the Modular Synthesis of Pseudopeptidic Macrocycles through an Anion-Templated Reaction. *J. Am. Chem. Soc.* **2008**, *130*, 6137-6144. (b) Bru, M.; Alfonso, I.; Burguete, M. I.; Luis, S. V. Anion-Templated Syntheses of Pseudopeptidic Macrocycles. *Angew. Chem. Int. Ed.* **2006**, *45*, 6155-6159.

114- Bru, M.; Alfonso, I.; Bolte, M.; Burguete, M. I.; Luis, S. V. Structurally Disfavoured Pseudopeptidic Macrocycles Through Anion Templation. *Chem. Commun.* **2011**, *47*, 283-285.

115- Moure, A.; Luis, S. V.; Alfonso, I. Efficient Synthesis of Pseudopeptidic Molecular Cages. *Chem. Eur. J.* **2012**, *18*, 5496-5500.

116- (a) Jedrzejewska, H.; Szumna, A. Making a Right or Left Choice: Chiral Self-Sorting as a Tool for the Formation of Discrete Complex Structures. *Chem. Rev.* **2017**, *117*, 4863-4899. (b) Liu, M.; Zhang, L.; Wang, T. Supramolecular Chirality in Self-Assembled Systems. *Chem. Rev.* **2015**, *115*, 7304-7397.

117- Martí-Centelles, V.; Burguete, M. I.; Luis, S. V. Template Effects in SN2 Displacements for the Preparation of Pseudopeptidic Macrocycles. *Chem. Eur. J.* **2012**, *18*, 2409-2422.

118- Martí-Centelles, V.; Burguete, M. I.; Luis, S. V. Macrocycle Synthesis by Chloride-Templated Amide Bond Formation. *J. Org. Chem.* **2016**, *81*, 2143-2147.

119- Vidovic, N.; Horvat, G.; Riva, D.; Rinkovec, T.; Cindro, N.; Tomisic, V.; Speranza, G. Chloride-Assisted Peptide Macrocyclization. *Org. Lett.* **2020**, *22*, 2129-2134.

120- Esteve, F.; Altava, B.; Bolte, M.; Burguete, M. I.; García-Verdugo, E.; Luis, S. V. Highly Selective Anion Template Effect in the Synthesis of Constrained Pseudopeptidic Macrocyclic Cyclophanes, *J. Org. Chem.* **2020**, *85*, 1138-1145.

121- (a) Guidi, M.; Seeberger, P. H.; Gilmore, K. How to approach flow chemistry. *Chem. Soc. Rev.* **2020**, *49*, 8910-8932. (b) Luis, S. V.; Garcia-Verdugo, E. *Flow Chemistry: Integrated Approaches for Practical Applications Ed.* RSC: 2019.

122- (a) Jones, C. D.; Kershaw Cook, L. J.; Marquez-Gamez, D.; Luzyanin, K. V.; Steed, J. W.; Slater, A. G. High-Yielding Flow Synthesis of a Macrocyclic Molecular Hinge. *J. Am. Chem. Soc.* **2021**, *143*, 7553-7565. (b) Godin, E.; Morin, E.; Collins, S. K. Continuous flow macrocyclization. *Aldrichimica Acta* **2018**, *51*, 35-46.

123- Vaccaro, L. *Sustainable Flow Chemistry: Methods and Applications.* Wiley: 2017.

124- Diac, A.; Matache, M.; Grosu, I.; Hadade, N. D. Naphthalenediimide - A Unique Motif in Macrocyclic and Interlocked Supramolecular Structures. *Adv. Synth. Catal.* **2018**, *360*, 817-845.

125- Bédard, A.-C.; Régnier, S.; Collins, S. K. Continuous flow macrocyclization at high concentrations: synthesis of macrocyclic lipids. *Green Chem.* **2013**, *15*, 1962-1966.

126- (a) Sytniczuk, A.; Dabrowski, M.; Banach, L.; Urban, M.; Czarnocka-Sniadala, S.; Milewski, M.; Kajetanowicz, A.; Grela, K. At Long Last: Olefin Metathesis Macrocyclization at High Concentration. *J. Am. Chem. Soc.* **2018**, *140*, 28, 8895-8901. (b) Collins, J. C.; Farley, K. A.; Limberakis, C.; Liras, S.; Price, D.; James, K. Macrocyclizations for Medicinal Chemistry: Synthesis of Druglike Macrocycles by High-Concentration Ullmann Coupling. *J. Org. Chem.* **2012**, *77*, 11079-11090. (c) Bédard, A.-C.; Collins, S. K. Microwave accelerated Glaser-Hay macrocyclizations at high concentrations. *Chem. Commun.* **2012**, *48*, 6420-6422.

127- de Leseleuc, M.; Godin, E.; Parisien-Collete, S.; Lévesque, A.; Collins, S. K. Catalytic Macrocyclization Strategies Using Continuous Flow: Formal Total Synthesis of Ivorenolide A. *J. Org. Chem.* **2016**, *81*, 6750-6756.

128- Taylor, C. J.; Baker, A.; Chapman, M. R.; Reynolds, W. R.; Jolley, K. E.; Clemens, G.; Smith, G. E.; Blacker, A. J.; Chamberlain, T. W.; Christie, S. D. R.; Tylor, B. A.; Bourne, R. A. Flow chemistry for process optimisation using design of experiments. *J. Flow. Chem.* **2021**, *11*, 75-86.

129- Bédard, A.-C.; Santandrea, J.; Collins, S. K. Efficient Continuous-Flow Synthesis of Macrocyclic Triazoles. *J. Flow Chem.* **2015**, *5*, 142-144.

130- Bogdan, A. R.; James, K. Efficient Access to New Chemical Space Through Flow-Construction of Druglike Macrocycles Through Copper-Surface-Catalyzed Azide-Alkyne Cycloaddition Reactions. *Chem. Eur. J.* **2010**, *16*, 14506-14512.

131- Ruggeri, M.; Dombrowski, A. W.; Djuric, S. W.; Baxendale, I. R. Rearrangement of 3 Hydroxyazetidines into 2 Oxazolines. *J. Org. Chem.* **2020**, *85*, 7276-7286.

132- Kitchin, M.; Konstas, K..; Sumby, C. J.; Czyz, M. L.; Valente, P.; Hill, M. R.; Polyzos, A.; Doonan, C. J. Continuous flow synthesis of a carbon-based molecular cage macrocycle via a three-fold homocoupling reaction. *Chem. Commun.* **2015**, *51*, 14231-14234.

133- Fodi, T.; Kupai, J.; Túrós, G.; Németh, T.; Rojik, E.; Riethmüller, E.; Balogh, G. T.; Huszthy, P. Application of flow chemistry to macrocyclization of crown ethers. *J. Flow Chem.* **2016**, *6*, 297-301.

134- Lee, A. C.-L.; Harris, J. L.; Khanna, K. K.; Hong, J.-H. A Comprehensive Review on Current Advances in Peptide Drug Development and Design. *Int. J. Mol. Sci.* **2019**, *20*, 2383-2403.

135- Mabonga, L.; Kappo, A. P. Peptidomimetics: A Synthetic Tool for Inhibiting Protein-Protein Interactions in Cancer. *Int. J. Pept. Res. Ther.* **2020**, *26*, 225-241.

136- (a) Zabala-Uncilla, N.; Miranda, J. I.; Laso, A.; Fernandez, X.; Ganboa, J. I.; Palomo, C. Linear and Cyclic Depsipeptidomimetics with β-Lactam Cores: A Class of New αvβ3 Integrin Receptor Inhibitors. *ChemBioChem* **2017**, *18*, 654-665. (b) De Marco, R.; Tolomelli, A.; Juaristi, E.; Gentilucci, L. Integrin Ligands with α/β-Hybrid Peptide Structure: Design, Bioactivity, and Conformational Aspects. *Med. Res. Rev.* **2016**, *36*, 389-424.

137- Holub, J.; Vantomme, G.; Lehn, J.-M. Training a Constitutional Dynamic Network for Effector Recognition: Storage, Recall, and Erasing of Information. *J. Am. Chem. Soc.* **2016**, *138*,11783-11791.

138- (a) Lafuente, M.; Alfonso, I.; Solà, J. Structurally Selective Assembly of a Specific Macrobicycle from a Dynamic Library of Pseudopeptidic Disulfides. *ChemSystemsChem* **2019**, *1*, 25-31. (b) Atcher, J.; Solà, J.; Alfonso, I. Pseudopeptidic compounds for the generation of dynamic combinatorial libraries of chemically diverse macrocycles in aqueous media. *Org. Biomol. Chem.* **2017**, *15*, 213-219. (c) Alfonso, I. From simplicity to complex systems with bioinspired pseudopeptides. *Chem. Commun.* **2016**, *52*, 239-250.

139- Kuberski, B.; Szumna, A. A self-assembled chiral capsule with polar interior. *Chem. Commun.* **2009**, 1959-1961.

140- Szumna, A. Chiral Encapsulation by Directional Interactions. *Chem. Eur. J.* **2009**, *15*, 12381-12388.

141- Butterfield, S. M.; Rebek, J. A Synthetic Mimic of Protein Inner Space: Buried Polar Interactions in a Deep Water-Soluble Host. J. Am. Chem. Soc. **2006**, *128*, 15366-15367.

142- Szumna, A. Water co-encapsulation in an inverted molecular capsule. *Chem. Commun.* **2009**, *28,* 4191-4193.

143- Borges, A.; Gillespie, D.; Nag, A. Biological applications of amide and amino acid containing synthetic macrocycles. *Supramol. Chem.* **2019**, *31*, 575-596.

144- Schnopp, M.; Ernst, S.; Haberhauer, G. Anion Recognition by Neutral Macrocyclic Azole Amides. *Eur. J. Org. Chem.* **2009**, *2*, 213-222.

145- Fiehn, T.; Goddard, R.; Seidel, R. W.; Kubik, S. A Cyclopeptide-Derived Molecular Cage for Sulfate Ions That Closes with a Click. *Chem. Eur. J.* **2010**, *16*, 7241-7255.

146- Ariawan, A. D.; Webb, J. E. A.; Howe, E. N. W.; Gale, P. A.; Thordarson, P.; Hunter, L. Cyclic peptide unguisin A is an anion receptor with high affinity for phosphate and pyrophosphate. *Org. Biomol. Chem.* **2017**, *15*, 2962-2967.

147- Martí-Centelles, V.; Burguete, M. I.; Galindo, F.; Izquierdo, M. A.; Kumar, D. K.; White, A. J. P.; Luis, S. V.; Vilar, R. Fluorescent Acridine-Based Receptors for H_2PO_4-. *J. Org. Chem.* **2012**, *77*, 490-500.

148- Martí-Centelles, V.; Izquierdo, M. A.; Burguete, M. I.; Galindo, F.; Luis, S. V. Recognition of Free Tryptophan in Water by Synthetic Pseudopeptides: Fluorescence and Thermodynamic Studies. *Chem. Eur. J.* **2014**, *20*, 7465-7478.

149- Martí, I.; Rubio, J.; Bolte, M.; Burguete, M. I.; Vicent, C.; Quesada, R.; Alfonso, I.; Luis, S. V. Tuning Chloride Binding, Encapsulation, and Transport by Peripheral Substitution of Pseudopeptidic Tripodal Small Cages. *Chem. Eur. J.* **2012**, *18*, 16728-16741.

150- (a) Faggi, E.; Moure, A.; Bolte, M.; Vicent, C.; Luis, S. V.; Alfonso, I. Pseudopeptidic Cages as Receptors for N-Protected Dipeptides. *J. Org. Chem.* **2014**, *79*, 4590-4601. (b) Alfonso, I.; Bolte, M.; Bru, M.; Burguete, M. I.; Luis, S. V.; Vicent, C. Molecular recognition of N-protected dipeptides by pseudopeptidic macrocycles: a comparative study of the supramolecular complexes by ESI-MS and NMR. *Org. Biomol. Chem.* **2010**, *8*, 1329-1339.

151- Izquierdo, M. A.; Wadhavane, P. D.; Vigara, L.; Burguete, M. I.; Galindo, F.; Luis, S. V. The interaction of amino acids with macrocyclic pH probes of pseudopeptidic nature. *Photochem. Photobiol. Sci.* **2017**, *16*, 1320-1326.

152- (a) Faggi, E.; Vicent, C.; Luis, S. V.; Alfonso, I. Stereoselective recognition of the Ac-Glu-Tyr-OH dipeptide by pseudopeptidic cages. *Org. Biomol. Chem.* **2015**, *13*, 11721-11731. (b) Alfonso, I.; Burguete, M. I.; Galindo, F.; Luis, S. V.; Vigara, L. Unraveling the Molecular Recognition of Amino Acid Derivatives by a Pseudopeptidic Macrocycle: ESI-MS, NMR, Fluorescence, and Modeling Studies. *J. Org. Chem.* **2009**, *74*, 6130-6142.

153- (a) Becerril, J.; Burguete, M. I.; Escuder, B.; Galindo, F.; Gavara, R.; Luis, S. V.; Miravet, J. F.; Peris, G. Self-Assembly of Small Peptidomimetic Cyclophanes. *Chem. Eur. J.* **2004**, *10*, 3879-3890. (b) Becerril, J.; Burguete, M. I.; Escuder, B.; Luis, S. V.; Miravet, J. F.; Querol, M. Minimalist Peptidomimetic Cyclophanes as Strong Organogelators. *Chem. Commun.* **2002**, *7*, 738-739.

154- Becerril, J.; Escuder, B.; Gavara, R.; Luis, S. V.; Miravet, J. F. Understanding the Expression of Molecular Chirality in the Self-Assembly of a Peptidomimetic Organogelator. *Eur. J. Org. Chem.* **2005**, *3*, 481-485.

155- Alfonso, I.; Bru, M.; Burguete, M. I.; García-Verdugo, E.; Luis, S. V. Structural Diversity in the Self-Assembly of Pseudopeptidic Macrocycles. *Chem. Eur. J.* **2010**, *16*, 1246-1255.

156- Laidler, K. J.; Meiser, J. H. *Physical chemistry.* Benjamin/Cummings: 1982.

157- Lindström, B.; Pettersson, L. J. A Brief History of Catalysis. *CATTECH* **2003**, *7*, 130-138.

158- Arthur, R.; Arends, I.; Hanelfeld, U. *Green Chemistry and Catalysis.* Wiley-VCH: 2007.

159- Olivo, G.; Capocasa, G.; Del Giudice, D.; Lanzalunga, O.; Di Stefano, S. New horizons for catalysis disclosed by supramolecular chemistry. *Chem. Soc. Rev.* **2021**, 50, 7681-7724.

160- Van Leeuwen, P. W. N. M. *Supramolecular Catalysis.* Wiley-VCH: 2008.

161- Raynal, M.; Ballester, P.; Vidal-Ferran, A.; van Leeuwen, P. W. N. M. Supramolecular catalysis. Part 1: non-covalent interactions as a tool for building and modifying homogeneous catalysts. *Chem. Soc. Rev.* **2014**, *43*, 1660-1733.

162- Lehn, J. M.; Sirlin, C. Molecular Catalysis: Enhanced Rates of Thiolysis with High Structural and Chiral Recognition in Complexes of a Reactive Macrocyclic Receptor Molecule. *J. C. S. Chem. Comm.* **1978**, *21*, 949-951.

163- Yoshizawa, M.; Tamura, M.; Fujita, M. Diels-Alder in Aqueous Molecular Hosts: Unusual Regioselectivity and Efficient Catalysis. *Science* **2006**, *312*, 251-254.

164- (a) Xu, J.; Zhang, Y.; Zhang, J.; Li, Y.; Li, B.; Qiu, H.; Zhang, P.; Yin, S. Constructing a triangular metallacycle with salen–Al and its application to a catalytic cyanosilylation reaction. *Chem. Commun.* **2021**, *57*, 10399-10402. (b) Kang, J.; Rebek, J. Acceleration of a Diels-Alder Reaction by a Self-Assembled Molecular Capsule. *Nature* **1997**, *385*, 50-52.

165- Slagt, V. F.; Reek, J. N. H.; Kamer, P. C. J.; van Leeuwen, P. W. N. M. Assembly of Encapsulated Transition Metal Catalyst. *Angew. Chem. Int. Ed.* **2001**, *40*, 4271-4274.

166- Dudev, T.; Dudev, M.; Lim, C. First-Second Shell Interactions in Metal Binding Sites in Proteins: A PDB Survey and DFT/CDM Calculations. *J. Am. Chem. Soc.* **2003**, *125*, 3168-3180.

167- (a) Fang, Y.; Powell, J. A.; Li, E.; Wang, Q.; Perry, Z.; Kirchon, A.; Yang, X.; Xiao, Z.; Zhu, C.; Zhang, L.; Huang, F.; Zhou, H.-C. Catalytic reactions within the cavity of coordination cages. *Chem. Soc. Rev.* **2019**, *48*, 4707-4730. (b) Brown, C. J.; Toste, F. D.; Bergman, R. G.; Raymond, K. N. Supramolecular Catalysis in Metal–Ligand Cluster Hosts. *Chem. Rev.* **2015**, *115*, 3012-3035.

168- (a) Fujita, D.; Suzuki, R.; Fujii, Y.; Yamada, M.; Nakama, T.; Matsugami, A.; Hayashi, F.; Weng, J.-K.; Yagi-Utsumi, M.; Fujita, M. Protein stabilization and refolding in a gigantic self-assembled cage. *Chem* **2021**, *7*, 2672-2683. (b) Domoto, Y.; Abe, M.; Fujita, M. A Highly Entangled (M3L2)8 Truncated Cube from the Anion-Controlled Oligomerization of a π-Coordinated M3L2 Subunit. *J. Am. Chem. Soc.* **2021**, *143*, 8578-8582.

169- Nishioka, Y.; Yamaguchi, T.; Kawano, M.; Fujita, M. Asymmetric [2 + 2] Olefin Cross Photoaddition in a Self-Assembled Host with Remote Chiral Auxiliaries. *J. Am. Chem. Soc.* **2008**, *130*, 8160-8161.

170- Fang, Y.; Murase, T.; Sato, S.; Fujita, M. Noncovalent Tailoring of the Binding Pocket of Self-AssembledCages by Remote Bulky Ancillary Groups. *J. Am. Chem. Soc.* **2013**, *135*, 613-615.

171- Murase, T.; Horiuchi, S.; Fujita, M. Naphthalene Diels-Alder in a Self-Assembled Molecular Flask. *J. Am. Chem. Soc.* **2010**, *132¸* 2866-2867.

172- (a) Davis, H. J.; Phipps, R. J. Harnessing non-covalent interactions to exert control over regioselectivity and site-selectivity in catalytic reactions. *Chem. Sci.* **2017**, *8*, 864-877. (b) Balcells, D.; Moles, P.; Blakemore, J. D.; Raynaud, C.; Brudvig, G. W.; Crabtree, R. H.; Eisenstein, O. Molecular recognition in Mn-catalyzed C-H oxidation. Reaction mechanism and origin of selectivity from a DFT perspective. *Dalton Trans.* **2009**, *30*, 5989-6000. (c) Das, S.; Incarvito, C. D.; Crabtree, R. H.; Brudvig, G. W. Molecular Recognition in the Selective Oxygenation of Saturated C-H Bonds by a Dimanganese Catalyst. *Science* **2006**, *312*, 1941-1943.

173- (a) Fackler, P.; Huber, S. M.; Bach, T. Enantio- and Regioselective Epoxidation of Olefinic Double Bonds in Quinolones, Pyridones, and Amides Catalyzed by a Ruthenium Porphyrin Catalyst with a Hydrogen Bonding Site. *J. Am. Chem. Soc.* **2012**, *134*, 12869-12878. (b) Fackler, P.; Berthold, C.; Voss, F.; Bach, T. Hydrogen-Bond-Mediated Enantio- and Regioselectivity in a Ru-Catalyzed Epoxidation Reaction. *J. Am. Chem. Soc.* **2010**, *132*, 15911-15913.

174- Berndt, J.-P.; Radchenko, Y.; Becker, J.; Logemann, C.; Bhandari, D. R.; Hrdina, R.; Schreiner, P. R. Site-selective nitrenoid insertions utilizing postfunctionalized bifunctional rhodium(II) catalysts. *Chem. Sci.* **2019**, *10*, 3324-3329.

175- (a) Golding, W. A.; Phipps, R. J. Electrostatically-directed Pd-catalysis in combination with C-H activation: site-selective coupling of remote chlorides with fluoroarenes and fluoroheteroarenes. *Chem. Sci.* **2020**, *11*, 3022-3027. (b) Golding, W. A.; Pearce-Higgins, R.; Phipps, R. J. Site-Selective Cross-Coupling of Remote Chlorides Enabled by Electrostatically Directed Palladium Catalysis. *J. Am. Chem. Soc.* **2018**, *140*, 13570-13574.

176- (a) Dubrovina, N. V.; Börner, A. Enantioselective catalysis with chiral phosphine oxide preligands. *Angew. Chem. Int. Ed.* **2004**, *43*, 5883-5886. (b) Van Leeuwen, P. W. N. M.; Roobeek, C. F.; Wife, R. L.; Frijns, J. H. G. Platinum hydroformylation catalysts containing diphenylphosphine oxide ligands. *J. Chem. Soc. Chem. Commun.* **1986**, *1*, 31-33.

177- Carboni, S.; Gennari, C.; Pignataro, L.; Piarulli, U. Supramolecular ligand–ligand and ligand–substrate interactions for highly selective transition metal catalysis. *Dalton trans.* **2011**, *40*, 4355-4373.

178- Rummelt, S. M.; Radkowski, K.; Rosca, D.-A.; Fürstner, A. Interligand Interactions Dictate the Regioselectivity of trans-Hydrometalations and Related Reactions Catalyzed by [Cp*RuCl]. Hydrogen Bonding to a Chloride Ligand as a Steering Principle in Catalysis. *J. Am. Chem. Soc.* **2015**, *137*, 5506-5519.

179- (a) List, B. Introduction: Organocatalysis. *Chem. Rev.* **2007**, *107*, 5413-5415. (b) Gaunt, M. J.; Johansson, C. C. C.; McNally, A.; Vo, N. T. Enantioselective organocatalysis. *Drug Discov. Today* **2007**, *12*, 8-27.

180- https://www.nobelprize.org/prizes/chemistry/2021/press-release/

181- (a) North, M. *Sustainable Catalysis: Without Metals or Other Endangered Elements, Part 1*. Royal Society of chemistry: 2015. (b) Kumar, P.; Jha, V.; Gonnade, R. Proline-Catalyzed Asymmetric Synthesis of *syn-* and *anti-*1,3-Diamines. *J. Org. Chem.* **2013**, *78*, 11756-11764. (c) Córdova, A.; Notz, W.; Barbas, C. F. Proline-Catalyzed One-Step Asymmetric Synthesis of 5-Hydroxy-(2E)-hexenal from Acetaldehyde. *J. Org. Chem.* **2002**, *67*, 301-303.

182- Breslow, R.; Guo, T. Diels-Alder Reactions in Nonaqueous Polar Solvents. Kinetic Effects of Chaotropic and Antichaotropic Agents and of β-Cyclodextrin. *J. Am. Chem. Soc.* **1988**, *110*, 5613-5617. (b) Rideout, D. C.; Breslow, R. Hydrophobic acceleration of Diels-Alder reactions. *J. Am. Chem. Soc.* **1980**, *102*, 7816-7817.

183- Narayan, S.; Muldoon, J.; Finn, M: G.; Fokin, V. V.; Kolb, H. C.; Sharpless, K. B. "On Water": Unique Reactivity of Organic Compounds in Aqueous Suspension. *Angew. Chem. Int. Ed.* **2005**, *44*, 3275-3279.

184- (a) Song, C. E.; Park, S. J.; Hwang, I.-S.; Jung, M. J.; Shim, S. Y.; Bae, H. Y.; Jung, J. Y. Hydrophobic chirality amplification in confined water cages. *Nat. Commun.* **2019**, *851*, article number: 851. (b) Organic synthesis reactions on-water at the organic-liquid water interface. *Biomol. Chem.* **2016**, *14*, 9945-9960. (c) Chanda, A.; Fokin, V. V. Organic Synthesis "On Water". *Chem. Rev.* **2009**, *109*, 725-748.

185- Sam, D. J.; Simmons, H. E. Crown polyether chemistry. Potassium permanganate oxidations in benzene. *J. Am. Chem. Soc.* **1972**, *94*, 4024-4025.

186- Gokel, G. W.; Durst, H. D. Principles and Synthetic Applications in Crown Ether Chemistry. *Synthesis* **1976**, *3*, 168-184.

187- Oh, Y.-H.; Yun, W.; Kim, C.-H.; Jang, S.-W.; Lee, S.-S.; Lee, S.; Kim, D.-W. Inter- and Intra-Molecular Organocatalysis of SN2 Fluorination by Crown Ether: Kinetics and Quantum Chemical Analysis. *Molecules* **2021**, *26*, article number: 2947.

188- Wang, J.; Liang, Y.; Zhou, D.; Ma, J.; Jing, H. New crown ether complex cation ionic liquids with N-heterocycle anions: preparation and application in CO2 fixation. *Org. Chem. Front.* **2018**, *5*, 741-748.

189- Di Stefano, S.; Capocasa, G.; Mandolini, L. Supramolecular Catalysts Featuring Crown Ethers as Recognition Units. *Eur. J. Org. Chem.* **2020**, *23*, 3340-3350.

190- (a) Vachal, P.; Jacobsen, E. N. Structure-Based Analysis and Optimization of a Highly Enantioselective Catalyst for the Strecker Reaction. *J. Am. Chem. Soc.* **2002**, *124,* 10012-10014. (b) Sigman, M. S.; Jacobsen, E. N. Schiff Base Catalysts for the Asymmetric Strecker Reaction Identified and Optimized from Parallel Synthetic Libraries. *J. Am. Chem. Soc.* **1998**, *120*, 4901-4902.

191- Corey, E. J.; Grogan, M. J. Enantioselective Synthesis of α-Amino Nitriles from N-Benzhydryl Imines and HCN with a Chiral Bicyclic Guanidine as Catalyst. *Org. Lett.* **1999**, *1*, 157-160.

192- Sohtome, Y.; Tanatani, A.; Hashimoto, Y.; Nagasawa, K. Development of bis-thiourea-type organocatalyst for asymmetric Baylis–Hillman reaction. *Tetrahedron Lett.* **2004**, *45*, 5589-5592.

193- Wenzel, A. G.; Jacobsen, E. N. Asymmetric Catalytic Mannich Reactions Catalyzed by Urea Derivatives: Enantioselective Synthesis of β-Aryl-β-Amino Acids. *J. Am. Chem. Soc.* **2002**, *124*, 12964-12965.

194- (a) Mayfield, A. B.; Metternich, J. B.; Trotta, A. H.; Jacobsen, E. N. Stereospecific Furanosylations Catalyzed by Bis-thiourea Hydrogen-Bond Donors. *J. Am. Chem. Soc.* **2020**, *142*, 4061-4069. (b) Fastnacht, K. V.; Spink, S. S.; Dharmaratne, N. U.; Pothupitiya, J. U.; Datta, P. P.; Kiesewetter, E. T.; Kiesewetter, M. K. Bis- and Tris-Urea H-Bond Donors for Ring-Opening Polymerization: Unprecedented Activity and Control from an Organocatalyst. *ACS Macro Letters* **2016,** *5*, 982-986.

195- Chen, H.-Y.; Gou, M.; Wang, J.-B. De novo *endo*-functionalized organic cages as cooperative multi-hydrogen-bond-donating catalysts. *Chem. Commun.* **2017**, *53*, 3524-3526.

196- Markad, D.; Mandal, S. K. Design of a Primary-Amide-Functionalized Highly Efficient and Recyclable Hydrogen-Bond-Donating Heterogeneous Catalyst for the Friedel-Crafts Alkylation of Indoles with β-Nitrostyrenes. *ACS Catal.* **2019**, *9*, 3165-3173.

197- (a) Xu, C.; Rao, V. U. B.; Weigen, J.; Loh, C. C. J. A robust and tunable halogen bond organocatalyzed 2-deoxyglycosylation involving quantum tunnelling. *Nat. Commun.* **2020**, *11*, article number: 4911. (b) Perera, M. D.; Aakeröy, C. B. Organocatalysis by a multidentate halogen-bond donor: an alternative to hydrogen-bond based catalysis. *New J. Chem.* **2019**, *43*, 8311-8314. (c) Szell, P. M. J.; Zablotny, S.; Bryce, D. L. Halogen bonding as a supramolecular dynamics catalyst. *Nat. Commun.* **2019**, *10*, article number: 916. (d) Bergamaschi, G.; Lascialfari, L.; Pizzi, A.; Martinez-Espinoza, M. I.; Demitri, N.; Milani, A.; Gori, A.; Metrangolo, P. A halogen bond-donor amino acid for organocatalysis in water. *Chem. Commun.* **2018**, *54*, 10718-10721.

198- Yang, Z.-Y.; Zeng, J.-L.; Ren, N.; Meng, W.; Nie, J.; Ma, J.-A. C2-Symmetric Chiral Bisoxazolines as Hydrogen-Bond-Acceptor Catalysts in Enantioselective Aldol Reaction of β-Carbonyl Acids with Trifluoroacetaldehyde Hemiacetals. *Org. Lett.* **2016**, *18*, 6364-6367

199- Okino, T.; Hoashi, Y.; Takemoto, Y. Enantioselective Michael Reaction of Malonates to Nitroolefins Catalyzed by Bifunctional Organocatalysts. *J. Am. Chem. Soc.* **2003**, *125*, 12672-12673.

200- Xu, L.; Fang, G.; Tao, J.; Ye, Z.; Xu, S.; Li, Z. Molecular Mechanism and Solvation Effect of Supramolecular Catalysis in a Synthetic Cavitand Receptor with an Inwardly Directed Carboxylic Acid for Ring-Opening Cyclization of Epoxy Alcohols. *ACS Catal.* **2018**, *8,* 11910-11925.

201- Meeuwissen, J.; Reek, J. N. H. Supramolecular catalysis beyond enzyme mimics. *Nat. Chem.* **2010**, *2*, 615-621.

202- Oliveira, G. H. C.; Ramos, L. M.; de Paiva, R. K. C.; Passos, S. T. A.; Simoes, M. M.; Machado, F.; Correa, J. R.; Neto, B. A. D. Synthetic enzyme-catalyzed multicomponent reaction for Isoxazol-5(4H)-one Syntheses, their properties and biological application; why should one study mechanisms?. *Org. Biomol. Chem.* **2021**, *19*, 1514-1531.

203- Kuah, E.; Toh, S.; Yee, J.; Ma, Q.; Gao, Z. Enzyme Mimics: Advances and Applications. *Chem. Eur. J.* **2016**, *22*, 8404-8430.

204- Yin, Y.; Dong, Z.; Luo, Q.; Liu, J. Biomimetic catalysts designed on macromolecular scaffolds. *Prog. Polym. Sci.* **2012***, 37,* 1476-1509.

205- (a) Yang, J.; Gabriele, B.; Belvedere, S.; Huang, Y.; Breslow, R. Catalytic Oxidations of Steroid Substrates by Artificial Cytochrome P-450 Enzymes. *J. Org. Chem.* **2002**, *67*, 5057-5067. (b) Wolfe, J.; Nemeth, D.; Costero, A.; Rebek, J. Convergent Functional Groups: Catalysis of Hemiacetal Cleavage in a Synthetic Molecular Cleft. *J. Am. Chem. Soc.* **1988**, *110*, 983-984.

206- Nothling, M. D.; Xiao, Z.; Bhaskaran, A.; Blyth, M. T.; Bennet, C. W.; Coote, M. L.; Connal, L. A. Synthetic Catalysts Inspired by Hydrolytic Enzymes. *ACS Catal.* **2019**, *9*, 168-187.

207- Pluth, M. D.; Bergman, R. G.; Raymond, K. R. Acid Catalysis in Basic Solution: A Supramolecular Host Promotes Orthoformate Hydrolysis. *Science* **2007**, *316*, 85-88.

208- (a) Pereira, M. M.; Dias, L. D.; Calvete, M. J. F. Metalloporphyrins: Bioinspired Oxidation Catalysts. *ACS Catal.* **2018**, *8*, 10784-10808. (b) Rebilly, J.-N.; Colasson, B.; Bistri, O.; Over, D.; Reinaud, O. Biomimetic cavity-based metal complexes. *Chem. Soc. Rev.* **2015**, 44, 467-489.

209- Cram, D. J.; Katz, H. E.; Dicker, I. B. Host-Guest Complexation. 31. A Transacylase Partial Mimic. *J. Am. Chem. Soc.* **1984**, *106*, 4987-5000.

210- Cacciapaglia, R.; Casnati, A.; Mandolini, L.; Reinhoudt, D. N.; Salvio, R.; Sartori, A.; Ungaro, R. Catalysis of Diribonucleoside Monophosphate Cleavage by Water Soluble Copper(II) Complexes of Calix[4]arene Based Nitrogen Ligands. *J. Am. Chem. Soc.* **2006**, *128*, 12322-12330. (b) Cacciapaglia, R.; Casnati, A.; Mandolini, L.; Reinhoudt, D. N.; Salvio, R.; Sartori, A.; Ungaro, R. Calix[4]arene-Based Zn2+ Complexes as Shape- and Size-Selective Catalysts of Ester Cleavage. *J. Org. Chem.* **2005**, *70*, 5398-5402.

211- Heying, R. S.; da Silva, M. P.; Wecker, G. S.; Peralta, R. A.; Bortoluzzi, A. J.; Neves, A. Unusual hydrolase-like activity of a mononuclear Fe(III) complex. *Inorg. Chem. Commun.* **2019**, *102*, 245-250.

212- Chaves, C. C. V.; Farias, G.; Formagio, M. D.; Neves, A.; Peralta, R. M.; Mikcha, J. M. G.; de Souza, B.; Peralta, R. A. Three new dinuclear nickel(II) complexes with amine pendant-armed ligands: Characterisation, DFT study, antibacterial and hydrolase-like activity. *Inorg. Chim. Acta* **2020***, 507*, 119559-119572.

213- Gissot, A.; Rebek, J. A Functionalized, Deep Cavitand Catalyzes the Aminolysis of a Choline Derivative. *J. Am. Chem. Soc.* **2004**, *126*, 7424-7425.

214- Suleman, S.; Younus, H. A.; Ahmad, N.; Khattak, Z. A. K.; Ullah, H.; Chaemchuen, S.; Verpoort, F. CO2 insertion into epoxides using cesium salts as catalysts at ambient pressure. *Catal. Sci. Technol.* **2019**, *9*, 3868-3873.

215- Mirabaud, A.; Martinez, A.; François, B.; Dutasta, J.-P.; Dufaud, V. A new heterogeneous host–guest catalytic system as an eco-friendly approach for the synthesis of cyclic carbonates from CO_2 and epoxides. *New J. Chem.* **2018**, *42*, 16863-16874.

216- (a) Kim, C. U.; Song, H.; Avvaru, B. S.; Gruner, S. M.; Park, S.; McKenna, R. Tracking solvent and protein movement during CO2 release in carbonic anhydrase II crystals. *Proc. Natl. Acad. Sci. U. S. A.* **2016**, *113*, 5257-5262. (b)Eriksson, A. E.; Jones, T. A.; Liljas, A. Refined structure of human carbonic anhydrase II at 2.0 Å resolution. *Proteins* **1988**, *4*, 274-282.

217- Aresta, M.; Schloss, J. V. *Enzymatic and Model Carboxylation and Reduction Reactions for Carbon Dioxide Utilization*. Springer: 1990.

218- Wright, A. M.; Wu, Z.; Zhang, G.; Mancuso, J. L.; Comito, R. J.; Day, R. W.; Hendon, C. H.; Miller, J. T.; Dinca, M. A Structural Mimic of Carbonic Anhydrase in a Metal-Organic Framework. *Chem* **2018**, *4*, 2894-2901.

219- Tabushi, I.; Kuroda, Y. Bis(histamino)cyclodextrin-Zn-Imidazole Complex as an Artificial Carbonic Anhydrase. *J. Am. Chem. Soc.* **1984**, *106*, 4580-4584.

220- Sénèque, O.; Rager, M. N.; Giorgi, M.; Reinaud, O. Supramolecular Stabilization of a Tris(imidazolyl) Zn-Aqua Complex Evidenced by X-ray Analysis: A Structural Model for Mono-Zinc Active Sites of Enzymes. *J. Am. Chem. Soc.* **2001**,*123*, 8442-8443.

221- (a) Kumar, R.; Sahoo, S. C.; Nanda, P. K. A *µ4*-Oxo Bridged Tetranuclear Zinc Complex as an Efficient Multitask Catalyst for CO2 Conversion. *Eur. J. Inorg. Chem.* **2021**, *11*, 1057-1064. (b) Liang, S.; Wu, X.-L.; Zong, M.-H.; Lou, W.-Y. Zn-triazole coordination polymers: Bioinspired carbonic anhydrase mimics for hydration and sequestration of CO2. *Chem. Eng. J.* **2020**, *398*, article number: 125530.

222- Huang, Y.; Zhang, S.; Chen, H.; Zhao, L.; Zhang, Z.; Cheng, P.; Chen, Y. A Zinc Coordination Complex Mimicking Carbonic Anhydrase for CO2 Hydrolysis and Sequestration. *Inorg. Chem.* **2019**, *58*, 9916-9921.

223- Saha, M.; Bandyopadhyay, S. Reversible photoresponsive activity of a carbonic anhydrase mimic. *Chem. Commun.* **2019**, *55*, 3294-3297.

224- Maeda, C.; Sasaki, S.; Takaishi, K.; Ema, T. Calix[4]pyrroles as macrocyclic organocatalysts for the synthesis of cyclic carbonates from epoxides and carbon dioxide. *Catal. Sci. Technol.* **2018**, *8*, 4193-4198.

225- (a) Wang, T.-T.; Xie, Y.; Deng, W.-Q. Reaction Mechanism of Epoxide Cycloaddition to CO$_2$ Catalyzed by Salen-M (M = Co, Al, Zn). *J. Phys. Chem. A* **2014**, *118*, 9239-9243. (b) North, M.; Pasquale, R. Mechanism of cyclic carbonate synthesis from epoxides and CO2. *Angew. Chem. Int. Ed.* **2009**, *48*, 2946-2948.

226- Castro-Gómez, F.; Salassa, G.; Kleij, A. W.; Bo, C. A DFT Study on the Mechanism of the Cycloaddition Reaction of CO2 to epoxides Catalyzed by Zn(Salphen) Complexes. *Chem. Eur. J.* **2013**, *19*, 6289-6298.

227- (a) Guo, L.; Lamb, K. J.; North, M. Recent developments in organocatalysed transformations of epoxides and carbon dioxide into cyclic carbonates. *Green Chem.* **2021**, *23*, 77-118. (b) Zhang, F.; Wang, Y.; Zhang, X.; Liu, H.; Han, B. Recent advances in the coupling of CO2 and epoxides into cyclic carbonates under halogen-free condition. *Green Chem. Eng.* **2020**, *2*, 82-93. (c) Shaikh, R. R.; Pornpraprom, S.; D'Elia, V. Catalytic Strategies for the Cycloaddition of Pure, Diluted, and Waste CO2 to Epoxides under Ambient Conditions. *ACS Catal.* **2018**, *8*, 419-450. (d) Lu, X.-B.; Darensbourg, D. J. Cobalt catalysts for the coupling of CO2 and epoxides to provide polycarbonates and cyclic carbonates. *Chem. Soc. Rev.* **2012**, *41*, 1462-1484. (e) Clegg, W.; Harrington, R. W.; North, M.; Pasquale, R. Cyclic Carbonate Synthesis Catalysed by Bimetallic Aluminium–Salen Complexes. *Chem. Eur. J.* **2010**, *16*, 6828-6843.

228- Wang, L.; Zhang, R.; Han, Q.; Xu, C.; Chen, W.; Yang, H.; Gao, G.; Qin, W.; Liu, W. Amide-functionalized heterometallic helicate cages as highly efficient catalysts for CO_2 conversion under mild conditions. *Green Chem.* **2018**, *20*, 5311-5317.

229- (a) Sun, Q.; Wang, S.; Aguila, B.; Meng, X.; Ma, S.; Xiao, F.-S. Creating solvation environments in heterogeneous catalysts for efficient biomass conversion. *Nat. Commun.* **2018**, *9*, article number: 3236. (b) Arca, H. A.; Gomes, G. C. C.; Mota, C. J. A. Solid solvents: activation parameters for the rearrangement of cyclopropylcarbinyl bromide on mordenite zeolite. *New J. Chem.* **2014**, *38*, 2760-2762.

230- Altava, B.; Burguete, M. I.; Frías, J. C.; García-España, E.; Luis, S. V.; Miravet, J. F. Preparation of Polymer-Supported Polyazamacrocycles. The Role of the Polymeric Matrix in the Preparation of Polymer-Supported Polyazamacrocycles, *Ind. Eng. Chem. Res.* **2000**, *39*, 3589-3595.

Chapter 2

Objectives

As has been previously mentioned, this PhD is framed in between the areas of Supramolecular Chemistry and Sustainable Chemistry. The general targets of this thesis have been:

➢ To meticulously design pseudopeptidic systems bearing in their structures preorganized cavities.

➢ To develop greener synthetic protocols for challenging macrocyclizations and macrobicyclizations, based on flow chemistry, the use of templating agents, and the use of preorganized reagents.

➢ To characterize and elucidate the conformational features of the different macrocycles considering their supramolecular properties with the combined use of a wide range of spectroscopic techniques and theoretical calculations.

➢ To study the viability of the different systems to act as enzyme-like catalysts for CO_2 conversion.

➢ To explore the feasibility of the final cyclic products to perform as host molecules for selective molecular recognition of relevant substrates.

Starting from these overall goals of the PhD, the specific objectives that were established for each of the chapters of the present thesis are summarized below.

The specific objectives for Chapter 3 (Highly selective anion template effect in the synthesis of constrained pseudopeptidic macrocyclic cyclophanes), which is framed in the field of template-assisted macrocyclizations, were established as follows:

➢ To synthesize a series of constrained pseudopeptidic macrocycles bearing in their structure the hexahydropyrrolo[3,4-*f*]isoindolocyclophane scaffold.

➢ To characterize the C_2-symmetric cyclic pseudopeptides by means of spectroscopic and solid-state X-ray analyses.

> ➢ To study the kinetic profiles for the macrocyclization reactions, evaluating the role of the aliphatic spacer length and the halide anion introduced in the system.
>
> ➢ To design an open-chain analogue for corroborating the catalytic template-effect of the macrocyclization leaving groups, i.e., bromide anions.

In terms of Chapter 4 (Continuous flow processes as an enabling tool for the synthesis of constrained pseudopeptidic macrocycles), that can be categorized in the field of flow chemistry, the specific goals were:

> ➢ To synthesize an appropriate supported base for performing the macrocyclization reaction using continuous-flow protocols.
>
> ➢ To design a flow set-up for the macrocyclization, taking into account the intrinsic requirements of the reaction.
>
> ➢ To optimize the reaction conditions, flow rate and residence time, for affording the desired yields of the products.
>
> ➢ To design a new flow set-up combining both the synthesis and isolation of the macrocycles.
>
> ➢ To evaluate the advantages promoted by flow chemistry in comparison with the batch macrocyclization, measuring the productivity and E-Factor for both conditions.
>
> ➢ To introduce a simple environmental metric for scrutinization of macrocyclization reactions in terms of their environmental implications.

The main objectives for Chapter 5 (Pseudopeptidic macrocycles as cooperative minimalistic synzyme systems for the remarkable activation and conversion of CO_2 in the presence of chloride anion), that is framed in the field of supramolecular and enzyme-like catalysis, were:

➢ To assay the catalytic activity of the macrocycles described in chapter 3 as organocatalysts in the transformation of epoxides to cyclic carbonates using CO_2.

➢ To study the effect of the aliphatic spacer length in the preorganization of the catalytic active groups and, therefore, in the catalytic efficiency of the bicomponent system.

➢ To elucidate the supramolecular forces governing the catalytic activity of the enzyme-like systems by means of spectroscopic techniques and molecular modelling.

➢ To analyse the applicability of the most active system in the cycloaddition of CO_2 to different epoxides, and to design an appropriate recycling protocol.

In a similar manner, the specific goals for Chapter 6 (Immobilized supramolecular systems as efficient synzymes for CO_2 activation and conversion), which can also be framed in the area of enzyme-like supramolecular catalysis, are described below.

➢ To synthesize a new family of pseudopeptidic macrocycles bearing in their structure a functional pendant arm.

➢ To evaluate the catalytic properties of the macrocycles for the homogeneous cycloaddition of CO_2 to styrene oxide, in the presence of a nucleophile source.

➢ To immobilize the macrocyclic pseudopeptides, together with a nucleophile source, on PS-DVB polymeric resins. Thereafter, to characterize the multicomponent materials obtained.

➢ To study the catalytic properties of these novel materials as heterogenous synzymes for the cycloaddition of CO_2 to epoxides.

➢ To develop a protocol for recycling the materials and to assay the reusing properties for such catalysts.

The main objectives for Chapter 7 (Bioinspired one-component catalysts for the enantioselective cycloaddition of CO_2 to epoxides), which describes the use of bioinspired organometallic catalysts, were identified as follows:

- ➢ To design a series of pseudopeptidic ligands with a cavity that can complex metallic ions.
- ➢ To synthesize and characterize the corresponding bimetallic Zn^{2+} complexes for the different pseudopeptidic macrocycles.
- ➢ To evaluate the efficiency of these novel organometallic compounds as one-component catalysts for the cycloaddition of CO_2 to terminal epoxides.
- ➢ To elucidate the catalytic mechanism.

The main objectives of Chapter 8 (Doubly chiral pseudopeptidic macrobicyclic molecular cages: water-assisted dynamic covalent self-Assembly and chiral self-sorting), that can be framed in the field of dynamic covalent chemistry and template-assisted macrocyclizations, were established as:

- ➢ To synthesize a new family of dynamic pseudopeptidic cryptand-like compounds through imine condensation reactions.
- ➢ To study the selectivity changes promoted by different chemical effectors, as for instance, the solvent used as reaction medium.
- ➢ To evaluate the self-sorting properties for the dynamic library of cryptands.
- ➢ To elucidate the main supramolecular driving forces for the high-fidelity homochiral self-sorting observed.

Finally, the main objectives of Chapter 9 (Unravelling the supramolecular driving forces in the formation of CO2-responsive pseudopeptidic low molecular weight hydrogelators), that is focused on the design of bioinspired responsive materials, were set as follows:

➤ To synthesize a new family of homoleptic and heteroleptic tetra-pseudopeptides.

➤ To study the gelating properties of the pseudopeptidic compounds both in aqueous and organic solvents.

➤ To evaluate the supramolecular sites of the different open-chain pseudopeptides.

➤ To assay the effect on the supramolecular self-assembly of external stimuli like pH and CO_2.

Chapter 3

Highly selective anion template effect in the synthesis of constrained pseudopeptidic macrocyclic cyclophanes
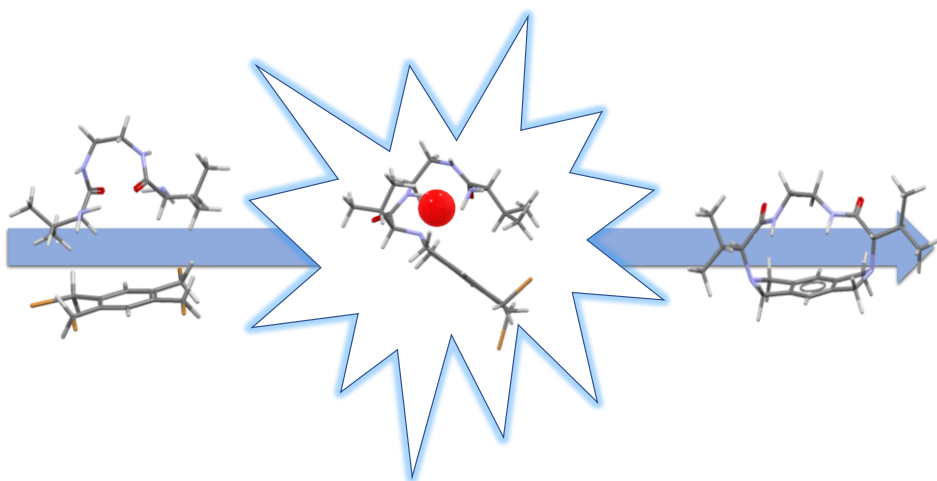
3.1. Main text

3.1.1. Abstract

Herein, we report the synthesis of a novel family of constrained pseudopeptidic macrocyclic compounds containing the hexahydropyrrolo[3,4-*f*]isoindolocyclophane scaffold and involving four coupled substitution reactions in the macrocyclization process. Although the increase in the number of steps involved in the macrocyclization could lead to a larger number of possible side products, the optimization of the methodology and the study of the driving forces have made it possible to obtain the desired macrocycles in excellent yields. A thorough computational study has been carried out to understand the macrocyclization process, and the results obtained nicely agree with experimental data. Moreover, the bromide anion had a clear catalytic template effect in the macrocyclization reaction, and surprisingly, the chloride anion had a negative template effect in opposition to the results obtained for analogous macrocycles. The parameters responsible for the specific kinetic template effect observed have been studied in detail.

3.1.2. Introduction

Macrocyclic compounds play an important role in Nature, having found important applications in host-guest chemistry, catalysis, sensing, and for planning and construction of new materials,[1] and, particularly, cyclopeptides have been shown to take part in important biological functions.[2]

The synthesis of macrocyclic compounds usually requires an important synthetic effort, the macrocyclization step being often yield-limiting.[3] This step needs to efficiently compete with intermolecular dimerization and oligomerization processes and requires an efficient preorganization of the intermediate species.[4] In this regard, it has been described that a U-turn preorganization in pseudopeptides can favour the intramolecular processes over the intermolecular ones, providing simple routes for the preparation of the related macrocyclic structures.[5] As a matter

of fact, the presence of folded conformations has been associated with the outcome of macrocyclization reactions in many peptides and pseudopeptides.[6] Several structural units such as urea, proline residues, rigid aromatic units, and so on have been associated with the formation of α-, β-, γ-, or related U-turns.[7] Such arrangements, with the appropriate orientation, provide an unencumbered trajectory of attack, accelerating the intramolecular macrocyclization process. Polycations, oligoamides, and peptidic structures can develop strong supramolecular interactions with anions,[8] facilitating their appropriate folding and providing access to efficient macrocyclization processes.[9] The selection of a suitable anion can be crucial, as anions can act either as kinetic or as thermodynamic templates, stabilizing the corresponding transition state or final macrocycle through specific supramolecular interactions.[10]

In the framework of previous studies on minimalistic pseudopeptidic compounds,[11,12] the efficient preparation of macrocyclic structures was achieved through the reaction of C_2-symmetric pseudopeptides with bis(halomethyl)arenes. This was based, in some cases, on the proper conformational and configurational preorganization of open-chain precursors,[13] whereas, in other instances, the use of anionic templates allowed high-yielding macrocyclization processes, even for systems for which conformational or configurational factors were unfavorable.[14] The first generations of polyazacyclophanes prepared in this way were highly dynamic, behaving as minimalistic models of molecular rotors,[15] and displayed interesting self-assembly,[16] molecular recognition, and sensing properties.[11,17] In this context, the design and preparation of more rigid related systems is of interest, considering the role of preorganization in supramolecular properties.[18]

Herein, we report the synthesis of a novel family of conformationally constrained pseudopeptidic macrocycles (**3**), for which the macrocyclization requires four consecutive substitution reactions competing with the corresponding intermolecular processes and where the role of the halide anions present is key to achieve excellent results.

3.1.3.   Experimental section

General.

NMR experiments were carried out at 400 or 300 MHz for ^{1}H and 100 or 75 MHz for [13]C. Chemical shifts are reported in ppm from tetramethylsilane using the solvent resonance as the internal standard. Fourier transform infrared (FT-IR) spectra were recorded using an attenuated total reflection (ATR) adapter. High resolution mass spectrometry (HRMS) were recorded with a Q-TOF instrument. Rotatory power was determined with a digital polarimeter (Na: 589 nm). Melting points were measured using a standard apparatus and are uncorrected.

Open-chain pseudopeptidic compounds **1** were prepared following literature procedures.[13]

General Macrocyclization Reaction Conditions.

*Synthesis of **3a**.* Open-chain pseudopeptide **1a** (119 mg, 0.459 mmol) and tetrakis(bromomethyl)-benzene **2** (217 mg, 0.459 mmol) were dissolved in acetonitrile (155 mL), together with 6 equivalents of Cs_2CO_3 (897 mg, 2.754 mmol). The reaction mixture was refluxed on a heating mantle with magnetic stirring for 2.5 h, and then the solvent was evaporated under vacuum. The resulting residue was treated with basic water (pH ≈ 11), centrifuging the final suspension at 3000 rpm for 8 min, and the solid afforded pure **3a**. Yield (150 mg, 85.2%, 0.392 mmol); mp >300 °C; $[\alpha]_D^{25}$ -32.8° (c = 0.5, MeOH); IR (ATR): 3263, 3053, 1623, 1531 cm^{-1}; ^{1}H NMR (400 MHz, CD_3OD): δ 0.78 (d, J = 6.5 Hz, 6H), 1.10 (d, J = 6.6 Hz, 6H), 1.95-2.07 (m, 2H), 2.51 (d, J = 10.3 Hz, 2H), 2.94-3.14 (m, 4H), 3.82-3.93 (m, 4H), 4.24−4.29 (m, 4H), 7.06 (s, 2H); ^{13}C{^{1}H} NMR (100 MHz, CD_3OD): δ 20.1, 20.1, 31.5, 40.9, 55.0, 62.6, 77.3, 117.9, 141.9, 142.8, 175.3; HRMS (ESI/Q-TOF) m/z: [M + H]+ calcd for $C_{22}H_{33}N_4O_2$, 385.2604; found, 385.2598.

*Synthesis of **3b**.* This compound was obtained as described above starting from **1b**. Yield 78.0%; mp >300 °C; $[\alpha]_D^{25}$ -65.2° (c = 0.5, MeOH); IR (ATR) 3337, 3071, 1621, 1541 cm^{-1}; ^{1}H NMR (400 MHz, CD_3OD): δ 0.41 (m, 2H), 0.81 (d, J = 6.5 Hz,

6H), 1.10 (d, J = 6.6 Hz, 6H), 1.96-2.09 (m, 2H), 2.38 (ddd, J = 12.8, 9.8, 7.6 Hz, 2H), 2.52 (d, J = 10.7 Hz, 2H), 2.91 (ddd, J = 12.8, 9.5, 7.4 Hz, 2H), 3.85 (d, J = 14.9 Hz, 2H), 4.14 (d, J = 15.4 Hz, 4H), 4.48 (dd, J = 28.4, 15.2 Hz, 4H), 6.90 (s, 2H); $^{13}C\{^1H\}$ NMR (100 MHz, CD$_3$OD): δ 20.1, 20.1, 28.5, 29.8, 37.9, 53.2, 61.5, 77.0, 116.8, 142.2, 173.5; HRMS (ESI/Q-TOF) m/z: [M + H]$^+$ calcd for C$_{23}$H$_{35}$N$_4$O$_2$, 399.2760; found, 399.2762.

Synthesis of **3c**. This compound was obtained as described above starting from **1c**. Yield 69.0%; mp >300 °C; [α]$_D^{25}$ -63.2° (c = 0.5, MeOH); IR (ATR) 3356, 3070, 1629, 1540 cm^{-1}; ^1H NMR (400 MHz, CD$_3$OD): δ 0.84 (d, J = 6.6 Hz, 6H), 0.88-1.04 (m, 4H), 1.10 (d, J = 6.6 Hz, 6H), 2.03 (dq, J = 10.3, 6.6 Hz, 2H), 2.67 (d, J = 10.4 Hz, 2H), 2.69-2.77 (m, 2H), 3.13 (dt, J = 13.3, 7.4 Hz, 2H), 3.97 (d, J = 14.7 Hz, 2H), 4.12 (d, J = 14.8 Hz, 2H), 4.44 (dd, J = 16.4 Hz, 4H), 6.94 (s, 2H); $^{13}C\{^1H\}$ NMR (100 MHz, CD$_3$OD): δ 20.2, 20.3, 26.9, 30.5, 40.1, 53.6, 61.5, 76.7, 116.9, 141.0, 141.3, 174.1; HRMS (ESI/Q-TOF) m/z: [M + H]$^+$ calcd for C$_{24}$H$_{37}$N$_4$O$_2$, 413.2917; found, 413.2915.

Synthesis of **3d**. This compound was obtained as described above starting from **1d**. Yield after purification by flash chromatography using CH$_2$Cl$_2$:MeOH (95:5) as the eluent mixture 31.7%; mp >300 °C; [α]$_D^{25}$ +20.8° (c = 0.2, MeOH); IR (ATR) 3288, 3075, 1625, 1547 cm^{-1}; ^1H NMR (400 MHz, CD$_3$OD): δ 0.85 (d, J = 6.5 Hz, 6H), 1.05-0.93 (m, 4H), 1.08 (d, J = 6.6 Hz, 6H), 1.13-1.26 (m, 2H), 2.06 (dp, J = 10.7, 6.5 Hz, 2H), 2.60 (dt, J = 13.4, 6.6 Hz, 2H), 2.71 (d, J = 10.7 Hz, 2H), 2.79-2.93 (m, 2H), 3.96 (d, J = 14.0 Hz, 2H), 4.20 (d, J = 13.9 Hz, 2H), 4.24-4.39 (m, 4H), 6.97 (s, 2H); $^{13}C\{^1H\}$ NMR (100 MHz, CD$_3$OD): δ 20.1, 20.2, 26.1, 29.2, 30.4, 40.8, 53.1, 60.5, 75.3, 117.2, 140.6, 140.8, 173.1; HRMS (ESI/Q-TOF) m/z: [M + H]$^+$ calcd for C$_{25}$H$_{39}$N$_4$O$_2$, 427.3073; found, 427.3070.

Synthesis of **3e**. This compound was obtained as described above starting from **1e**. Yield after purification by flash chromatography using CH$_2$Cl$_2$/MeOH (90:10) as the eluent mixture 28.7%; mp >300 °C; [α]$_D^{25}$ -9.9° (c = 0.1, MeOH); IR (ATR) 3290, 3077, 1632, 1546 cm^{-1}; 1H NMR (400 MHz, CD$_3$OD): δ 0.68-0.8 (m, 4H), 0.86-0.96

(m, 8H), 1.00-1.12 (m, 12H), 1.27-1.41 (m, 4H), 1.42-1.53 (m, 2H), 2.08-2.20 (m, 2H), 2.85 (d, J = 10.1 Hz, 2H), 2.89-2.96 (m, 2H), 3.51-3.60 (m, 2H), 4.07-4.20 (m, 8H), 7.01 (s, 2H); ^{13}C{^{1}H} NMR (100 MHz, CD$_3$OD): δ 20.0, 20.1, 28.0, 28.8, 30.9, 31.3, 31.3, 39.3, 55.6, 62.7, 72.8, 117.0, 139.3, 172.1; HRMS (ESI/Q-TOF) m/z: [M + H]$^{+}$ calcd for C$_{30}$H$_{49}$N$_4$O$_2$, 497.3856; found, 497.3863.

Synthesis of **5a**. Compound **1a** (352 mg, 1.363 mmol), α,α'-dibromo-o-xylene **4** (249 mg, 0.908 mmol) were dissolved in acetonitrile (250 mL) in the presence of Cs$_2$CO$_3$ (1775 mg, 5.448 mmol), and the reaction mixture was refluxed on a heating mantle with magnetic stirring for 5 h. The solvent was then evaporated under vacuum and the resulting solid was purified by flash chromatography using CH$_2$Cl$_2$/MeOH (92:8) as the eluent mixture. Yield (99 mg, 30.2%, 0.275 mmol); mp 117-119 °C; [α]$_D^{25}$ -21.6° (c = 0.2, MeOH); IR (ATR): 3291, 3069, 1639, 1539 cm^{-1}; ^{1}H NMR (400 MHz, CD$_3$CN): δ 0.78 (d, J = 6.8 Hz, 3H), 0.91 (d, J = 7.0 Hz, 3H), 0.94 (d, J = 6.7 Hz, 3H), 1.01 (d, J = 6.8 Hz, 3H), 2.00-2.17 (m, 2H), 2.91 (d, J = 6.8 Hz, 1H), 3.13 (d, J = 4.4 Hz, 1H), 3.22-3.34 (m, 4H), 3.88-4.09 (m, 4H), 7.06 (s, 1H), 7.20 (m, 4H), 7.46 (s, 1H); ^{13}C{^{1}H} NMR (100 MHz, CD$_3$OD): δ 17.7, 18.8, 19.4, 20.5, 30.1, 32.3, 39.4, 40.4, 56.7, 60.9, 74.1, 123.2, 127.8, 140.6, 173.9, 174.3; HRMS (ESI/Q-TOF) m/z: [M + H]$^{+}$ calcd for C$_{20}$H$_{33}$N$_4$O$_2$, 361.2604; found, 361.2605.

Crystal Structures.

Single crystals suitable for X-ray crystallography were obtained by slow evaporation of a solution of the macrocyclic compound in methanol. A suitable crystal was selected and mounted on a SuperNova, Dual, Cu at zero, Atlas diffractometer. The structure was solved with the SHELXT 2014/5[26] structure solution program and refined with the SHELXL-2018/3[27] refinement package. Artwork representations were processed using MERCURY[28] software.

3.1.4.   Results and discussion

Open-chain pseudopeptides **1a-e** were prepared starting from the corresponding commercially available protected amino acid as has been previously described.[13]

The macrocyclization between **1a** and tetrakis-(bromomethyl)benzene **2** (Scheme 3.1) was assayed under different conditions (Supporting Information, Table S3.1). Best yields, as determined by ^{1}H NMR, were obtained using Cs_2CO_3 as the base and CH_3CN as the solvent (95% yield after 3 h of reaction at 90 °C, entry 11, Table S3.1). It has to be mentioned that in the absence of Cs_2CO_3 the maximum yield obtained was 50%, suggesting that **1a** acted as the base neutralizing the ammonium salts formed after each N-alkylation, as has been observed before for related macrocyclization processes (entry 7, Table S3.1).[10d]
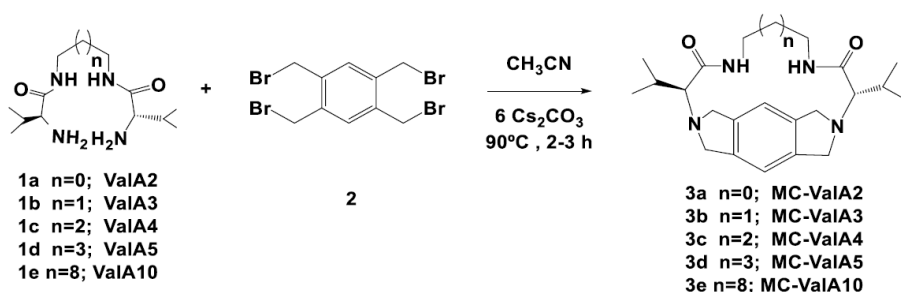
Scheme 3.1. Syntheses of pseudopeptidic macrocycles

The ESI-MS (+) of the crude of the reaction showed an intense peak at m/z 385.2 associated with [**3a** + H]$^+$ and the complete absence of signals corresponding to the open-chain intermediate or the [2 + 2] or other [n + n] macrocycles. The small peak observed at m/z 769.5 was assigned to the [**3a** + **3a** + H]$^+$ cluster, as confirmed by MS/MS experiments (Supporting Information, Figure S3.1).[19] When apolar solvents like 1,2-dimethoxyethane, $CHCl_3$, or toluene were assayed, no reaction could be observed, which can be assigned to the lack of solubility of either the reagents or the base needed. On the other hand, when ethanol or DMF was used, a noteworthy decrease in the efficiency of the macrocyclization was detected, most likely associated

with the interference with the hydrogen bonding patterns that can be essential for a proper preorganization of the intermediates.

Figure 3.1 shows the ^{1}H NMR spectra obtained for the reaction between **1a** and **2** at different reaction times (90 °C, CD$_3$CN).
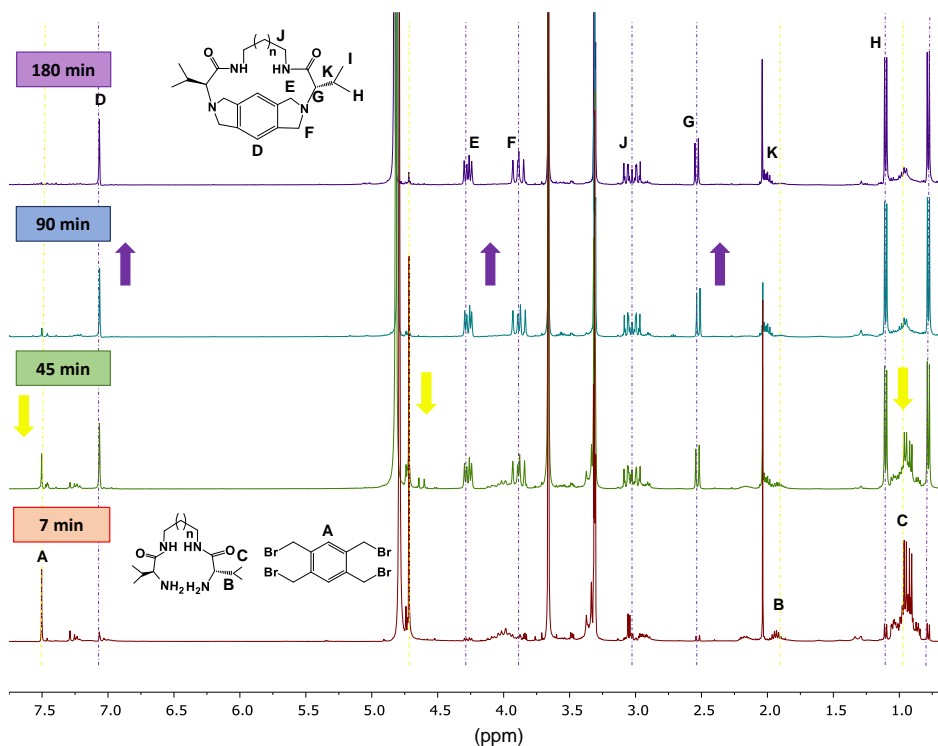
Figure 3.1. ^{1}H NMR spectra for the reaction between **1a** and **2** in CD$_3$CN at 90 °C. Upward arrows indicate macrocycle **3a** formation, and downward arrows indicate disappearance of open-chain precursor **1a** and tetrakis(bromomethyl)benzene **2**.

The disappearance of reagents was followed by monitoring the HA aromatic signal for **2** and the H$_B$ and H$_C$ valine signals for **1a**. The formation of **3a** was followed through the appearance of the signals for the aromatic (H$_D$), benzylic (H$_E$, H$_F$), chiral (H$_G$), and valine (H$_H$ and H$_I$) protons. It must be noted that, upon cyclization, significant upfield shifts were observed for the signals of the methylene groups (H$_J$) of the central spacer, in good agreement with the results observed for other related polyaza[n]cycloalcanes[20] and cyclic pseudopeptides.[13] The large anisotropy observed for the two hydrogen atoms of different methylene groups confirms also a high level

of conformational constraint. It must be noted that no relevant peaks for other species were detected during this transformation, which highlights the remarkable selectivity of this macrocyclization process where once the first N-C bond is formed the intramolecular formation of the other three N-C bonds needs to compete efficiently with related intermolecular reactions, leading to oligomers or polymers.

As could be expected, a significant effect of the nature of the spacer on the macrocyclization yield was observed at 3 mM concentration (Table 3.1). For open-chain pseudopeptides with longer aliphatic spacers (n ≥ 1), the selectivity decreases as the length of the spacer increases, with the formation of poly- or oligomeric side products, as evidenced by ESI-MS and ^1H NMR spectra (Supporting Information, Figures S3.2 and S3.3). Still, although longer aliphatic chains can disfavour the intramolecular hydrogen-bonding that leads to a favourable U-fold preorganization, cyclization yields were also good for precursors **1d-e** (>50% selectivity). The presence of amide functionalities seems to play a key role in such remarkable macrocyclization yields, as confirmed by results obtained using α,ω-diamines instead of diamino-diamides **1**. Thus, for instance, the reaction using 1,8-diaminooctane yielded a highly insoluble oligomeric/polymeric material with the total absence of the macrocyclic product.

Table 3.1. Yield obtained for the macrocyclization reaction between **1a-e** and **2**.[a]

Entry	Macrocycle	Conversion (%)[b]	Selectivity (%)[b]	Isolated yield (%)
1	**3a**	>99	99	85[c]
2	**3b**	>99	90	78[c]
3	**3c**	>99	76	69[c]
4	**3d**	>99	59	32[d]
5	**3e**	>99	51	29[d]

[a] CH_3CN, 3 h of reaction, 90 °C. [b] Determined by ^1H NMR. [c] Isolated yield after treatment with basic water. [d] Isolated yield after chromatographic purification.

Computational studies were also carried out to shed light on these processes. For this purpose, the open-chain intermediates, generated from **1a-e** after the two initial S_N2 reactions had taken place with the formation of the isoindoline structure,

were fully optimized using molecular mechanics at the Merck Molecular Force Field (MMFF) level of theory with the Spartan08 program (Figure 3.2).[21] All intermediates displayed folded conformations driven by intramolecular hydrogen bonds. For compounds with shorter spacers (Figure 3.2a,b), the minimum energy conformers contained intramolecular hydrogen bonds involving the amide NH groups and the primary and ternary amine groups at both ends of the pseudopeptidic chain. This achieved U-turn conformations with the two amide groups in *syn*-disposition.
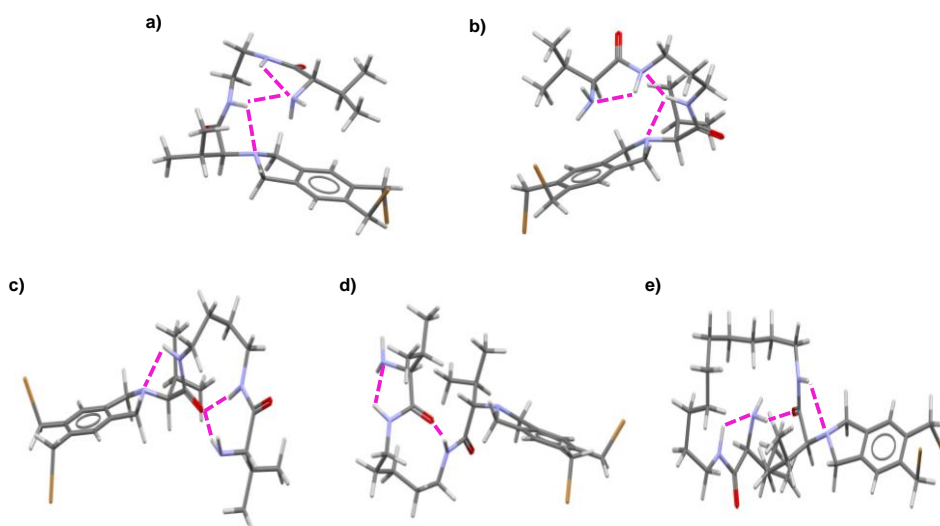
Figure 3.2. Minimum energy conformers calculated for the corresponding intermediates when precursors **1a-e** were used.

On the contrary, for compounds containing larger spacers (4, 5, and 10 methylene units, Figure 3.2c-e), the hydrogen bond between one amide NH and the ternary amine group was preserved, but the hydrogen bonding of the second amide NH involved the participation of one amide CO as the hydrogen bond acceptor, directly or through a $NH\cdots NH_2\cdots OC$ array (Figure 3.2e). This resulted in the two amide groups displaying an anti-disposition. As a result of these conformational preferences, the distance between the nitrogen atom of the primary amino group and the closest carbon atoms of the bromomethyl subunits was significantly shorter for precursors **1a,b** than for **1c-e** (6.37, 4.74, 9.73, 10.96, and 11.61 Å, respectively). These shorter C-N distances for **1a,b** should correlate with an increased probability

for the intramolecular cyclization reaction in good agreement with experimental results. For the non-pseudopeptidic 1,8-diamineoctane, the minimized structure showed an almost extended conformation in agreement with the low probability of the intramolecular cyclization observed experimentally (Supporting Information, Figure S3.4).

On the other hand, the smaller involvement of the nitrogen lone pairs of the primary amino groups in the intermediates displaying longer spacers is in good agreement with the higher reactivity observed for the corresponding pseudopeptides. High-performance liquid chromatography (HPLC) analysis allowed monitoring the conversion of tetrakis(bromomethyl)-benzene (**2**). For precursors **1c**-**e**, the total consumption of **2** was achieved after 2 h of reaction, whereas almost 3 h were needed for **1a,b** (Figure 3.3).
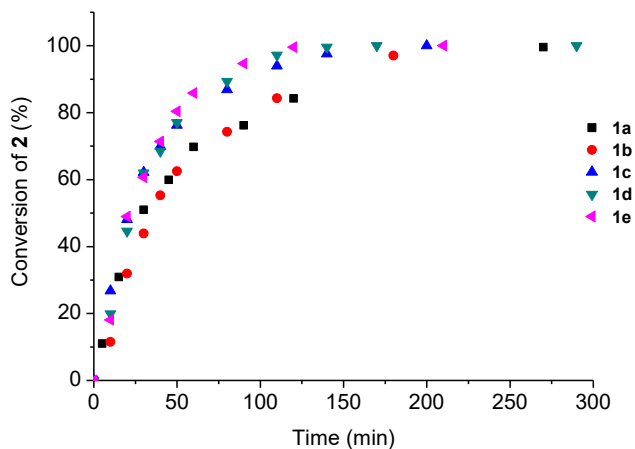
Figure 3.3. Kinetic profiles of the macrocyclization reaction between **1a**-**e** (3 mM) and **2** (3 mM), using acetonitrile as the solvent at 90 °C. The conversion was determined by HPLC.

Furthermore, ESI-MS analysis of the reaction crude obtained in competitive experiments using an equimolecular mixture **1a-e** (1 equiv each) and **2** (1 equiv) (CH$_3$CN, 24 h, Supporting Information, Figure S3.5a) revealed that the preference for the formation of the corresponding [1 + 1] macrocycles followed the order **3a** > **3b** > **3c** > **3d** > **3e** (Supporting Information, Figure S3.5b). This confirmed the strong selectivity toward the macrocyclization process for the open-chain

pseudopeptides with the shorter central aliphatic spacers, despite their slightly lower reactivity.

All the macrocyclic products could be purified to isolate the pure compounds in 29-85% yields and were fully characterised by spectroscopic and ESI-MS techniques. Further confirmation of the expected structures was obtained by X-ray diffraction. Single crystals suitable for this technique were obtained for compounds **3a**, **3b**, and **3e** by slow evaporation of methanol. Only a partial resolution could be achieved for the crystal obtained from **3d**, but the results also confirmed the formation of the macrocyclic structure Figure 3.4 shows the molecular structures for **3a**, **3b**, and **3e** (see also Supporting Information, Figures S3.13–S3.15).
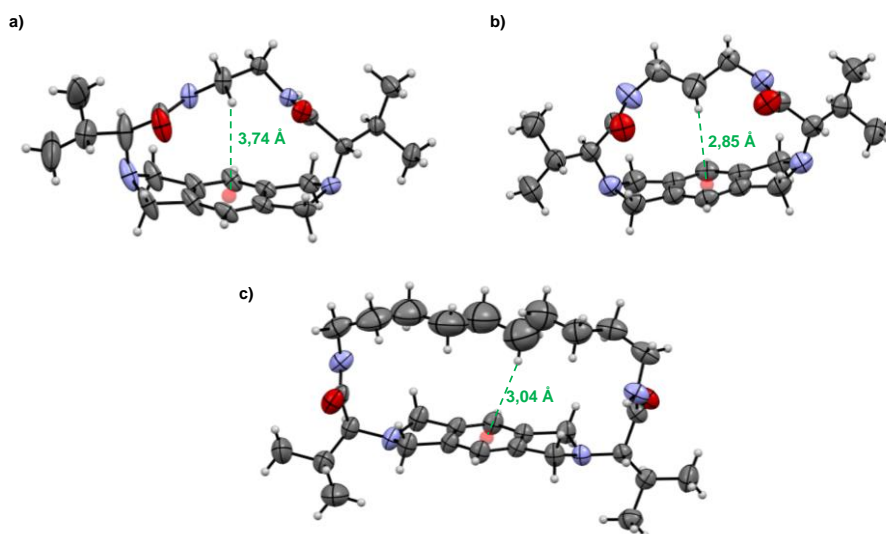
Figure 3.4. Molecular structures of macrocycles a) **3a**, b) **3b**, and c) **3e**. Distances from the centroid of the aromatic moiety to the closest H of the aliphatic spacer have been highlighted in green. Ellipsoids at 50% of probability.

As can be observed in Figure 3.4, the amide groups are essentially coplanar for the largest macrocyclic compound **3e** (amide-amide angle 21°), whereas for **3a** and **3b** the amides lay in almost perpendicular planes (67 and 87°, respectively, Supporting Information, Figure S3.16). Remarkable differences are observed in the structure of the five-membered rings. For **3a** and **3b**, the nitrogen atom is located

above the aromatic ring plane, whereas for **3e** both nitrogen atoms are below this plane. An intermediate situation is present in the partly resolved structure of **3d**, with each nitrogen atom located at a different side of the aromatic plane (Supporting Information, Figure S3.17). The presence of intramolecular aromatic-H contacts is highlighted in Figure 3.4, with centroid-H distances following the order **3b** < **3e** < **3a**.

For macrocycles **3a** and **3b**, the packing is stabilized by strong parallel amide-amide H-bonds in columnar stacks providing well-defined β-sheet-like arrangements. However, for compound **3e**, the amide groups are in an antiparallel disposition with the hydrogen bonding network involving amide-amide H-bonds between one molecule and four adjacent ones (Supporting Information, Figure S3.18). Hydrophobic interactions that are essential for the structural stability of biomolecules in water,[22] in particular for the organization and assembly of peptides and proteins,[23] are also key for the final 3D packing as in other pseudopeptidic systems.[24] Hydrophobic interactions involve preferentially weak isopropyl-isopropyl and isopropyl-aromatic contacts for **3a** and **3b**, whereas **3e** displays aromatic-methylene and isopropyl-methylene contacts involving the long aliphatic spacer (Supporting Information, Figures S3.19−S3.21).

As much as four bromide anions are generated for each macrocycle formed, an anion effect can be expected for this process according to previous results in this field.[9-13] When the macrocyclization using **1a** was carried out in the presence of 10 equiv of NEt₄Br, a clear increase in the reaction rate was observed (100% conversion and 96% yield after 1.5 h against ca. 65% yield in the absence of added salt). A similar kinetic effect was observed for **1d**, whereas for **1e** the effect was very minor (Supporting Information, Figure S3.6). Nevertheless, no significant differences in the final selectivity were detected after adding 10 equiv of NEt₄Br (entries 1, 2, and 3 Table 3.2 vs entries 1, 4, and 5 Table 3.1). This suggests that one main effect of adding an excess of bromide anions can be the increase of the nucleophilic character of the primary amino groups by efficiently competing with them in the hydrogen bonding

to the amide N-H fragments, which agrees well with NMR data (Supporting Information, Figure S3.7).

Table 3.2. Macrocyclization yields obtained in the presence of an excess of anions.[a]

Entry	Macrocycle	X⁻	Conversion (%)	Selectivity (%)[b]
1	**3a**	Br⁻	>99	96
2	**3d**	Br⁻	>99	59
3	**3e**	Br⁻	>99	47
4	**3a**	I⁻	>99	82
5	**3a**	Cl⁻	>99	nd[c]

[a] CH₃CN, 1.5 h of reaction, 90 °C. [b] Determined by ¹H NMR. [c] Not detected.

In spite of the NMR titration data showing that chloride associates more strongly with 1a than bromide (Supporting Information, Figure S3.7), the addition of an excess of chloride anions also increased the rate for the conversion of **2** but, rather surprisingly, produced a remarkable decrease in the efficiency of the macrocyclization for **1a** (Table 3.2, entry 5), leading mainly to the formation of polymeric species as was observed by ¹H NMR (ESI Figure S3.8). Interestingly, this noteworthy negative effect of the chloride anion was also confirmed when the macrocyclization between **1a** and tetrakis(chloromethyl)benzene was studied, as only oligomeric compounds were again obtained. Alternatively, an excess of iodide anions also produced an increase in the rate but led to a slight decrease of the macrocyclization yield (Table 3.2, entry 4). This indicates that the basicity of the anions leading to an increase in the nucleophilicity of the primary groups is not the primary reason responsible of the efficient macrocyclization and that bromide (and to a lower extent iodide) must play a specific role in the preorganization of the intermediate species leading to macrocycle formation.

The role of other anions was also analysed, in particular considering that different anion topologies could lead to different macrocyclization products.[14b] In this regard, carboxylate anions like acetate or terephthalate were studied as potential templates but no significant effect was observed. In both cases, ca. 80% yields of the

[1 + 1] macrocycle were obtained after 3 h, highlighting that the formed bromide anion plays a key role in the process. As an analogue to the open-chain intermediate preceding the macrocyclization, the pseudopeptide **5a** was prepared from **1a** and bis(bromomethyl)benzene (Supporting Information, Scheme S3.1). The ^{1}H NMR titration in CD_3CN of **5a** with Br$^-$, I$^-$, and Cl$^-$, as their NEt_4X salts, led to significant downfield shifts of the signals for the amine NH_2, amide NH, C*H and benzylic protons. As expected, the higher $\Delta\delta$ values were observed for the amide protons, in particular for those closer to the aromatic ring (Supporting Information, Figure S3.9). For this amide signal, the maximum observed downfield shifts after addition of 16 equiv of anion were $\Delta\delta$ (NH) = 1.02 (Cl$^-$), 0.45 (Br$^-$) and 0.10 ppm (I$^-$). All $\Delta\delta$ values followed the order anticipated for the basicity of the corresponding anion, being rather small in the case of iodide. Thus, it was clear that although the reactivity of the amino groups can be related with the basicity of the anions, the selectivity in the macrocyclization is not associated with a stronger interaction with a given anion. Interestingly, in the sample from the titration with Cl$^-$, the ^{1}H NMR spectrum changed dramatically after 1 week, showing a significant broadening and splitting of most signals (Supporting Information, Figure S3.10), suggesting the formation of supramolecular aggregates involving **5a** and the chloride anion. In good agreement with this, DOSY experiments revealed a significantly slower diffusion for the aged sample (Supporting Information, Figure S3.11). CD also provided interesting data. Figure 3.5 shows the CD spectra of **5a** obtained in the absence and presence of 10 equiv of the different anions. The CD spectra of **5a** and **5a** in the presence of chloride were similar, displaying a strong negative CD signal at 223 nm assigned to n-π transitions and a weak negative CD signal at 265 nm attributed to π-π transitions.[25] On the contrary, the CD spectra of **5a** in the presence of bromide and iodide did not present the negative CD signal at 223 nm, but only the weak negative signal associated to the aromatic moiety at 270 nm.
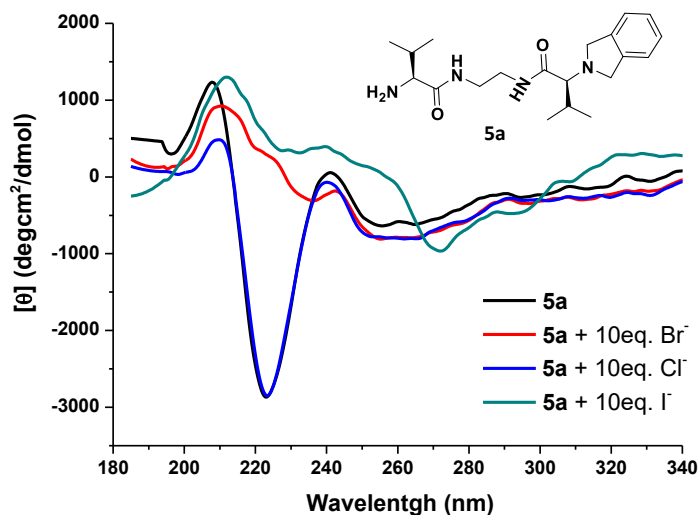
Figure 3.5. Partial CD spectra of **5a** (0.1 mM in CH$_3$CN) in the absence and presence of 10 equiv of different anions.

The results obtained indicate a different preorganization of the intermediate during the macrocyclization process as a function of the interaction with the different anions. According to computational calculations, compound **5a** (Supporting Information, Figure S3.12) presents a minimum energy conformer with the amide groups in antiparallel disposition, facilitating the formation of β-sheet-like aggregates, and justifying the presence of the strong negative CD-band at 223 nm.[25] The addition of the most basic and more strongly interacting chloride anion seems to stabilize this antiparallel disposition of amide groups and the formation of aggregates, presenting some similarities to β-sheets. The use of the less coordinating and larger bromide and iodide anions can provide a fully different arrangement with the two amide fragments coordinated to the anions. The parallel disposition of the dipoles for the two amide fragments could explain the disappearance of the corresponding CD signal. If the same considerations are applied to the intermediates in the intramolecular macrocyclization process (Figure 3.6), it seems clear that the conformation developed through the interaction with bromide (and to a lesser extension iodide) is more appropriately preorganized for the macrocyclization than the one developed in the presence of chloride. Thus, bromide and iodide can act as appropriate

macrocyclization templates, whereas chloride acts as an inhibitor (antitemplate) for the same process.
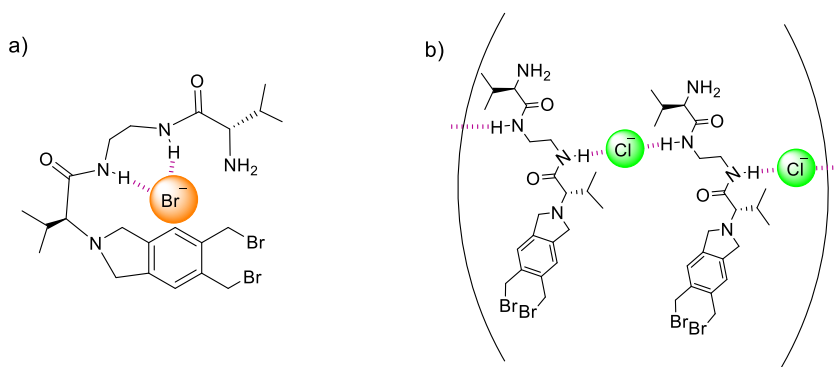
Figure 3.6. Proposed preorganization of the intermediates during the macrocyclization process in the presence of bromide or chloride template anions. R = H, **5a**. R = CH₂Br, macrocyclization intermediate.

3.1.5.   Conclusions

The synthesis of a new family of conformationally constrained pseudopeptidic macrocyclic cyclophanes has been carried out in remarkable good yields in CH_3CN using Cs_2CO_3 as the base. As evidenced from experimental results and computational calculations, the appearance of properly preorganized intermediates is facilitated by intramolecular H-bonding involving amide and amine functionalities, but also by the presence of the bromide anion that is generated in the process. The presence of anions provides a general kinetic effect, increasing the reactivity of the starting bis(aminoamide). However, a remarkable differential effect is observed according to the nature of the anion. Whereas bromide, and to a lower extent iodide, seems to act as an efficient template facilitating the [1 + 1] macrocyclization process, chloride plays an antitemplate role, hampering the corresponding cyclization and favouring oligomerization reactions. Our results indicate that the smaller size of the chloride anion and its higher basicity and coordinating capacity is at the origin of this behaviour. Whereas chloride can favour strong intermolecular associations of the open-chain intermediate through $NH_{amide}\cdots Cl^-\cdots NH_{amide}$ hydrogen bonds, the

larger size of the bromide and iodide anions allows establishing intramolecular $NH_{amide}\cdots X\cdots NH_{amide}$ hydrogen bonds that facilitate an appropriate folding of the intermediate for macrocyclization.

3.1.6. References

1- (a) Gao, W.-X.; Zhang, H.-N.; Jin, G.-X.; Supramolecular catalysis based on discrete heterometallic coordination-driven metallacycles and metallacages. *Coord. Chem. Rev.* **2019**, *386*, 69-84. (b) Ye, Z.; Yang, Z.; Wang, L.; Chen, L.; Cai, Y.; Deng, P.; Feng, W.; Li, X.; Yuan, L. A Dynamic Hydrogen-Bonded Azo-Macrocycle for Precisely Photo-Controlled Molecular Encapsulation and Release. *Angew. Chem., Int. Ed.* **2019**, *58*, 12519-12523. (c) Liu, Z.; Nalluri, S. K. M.; Stoddart, J. F. Surveying macrocyclic chemistry: from flexible crown ethers to rigid cyclophanes. *Chem. Soc. Rev.* **2017**, *46*, 2459-2478. (d) Joshi, T.; Graham, B.; Spiccia, L. Macrocyclic metal complexes for metalloenzyme mimicry and sensor development. *Acc. Chem. Res.* **2015**, *48*, 2366-2379. (e) Rezaeivala, M.; Keypour, H. Schiff base and non-Schiff base macrocyclic ligands and complexes incorporating the pyridine moiety-The first 50 years. *Coord. Chem. Rev.* **2014**, *280*, 203-253. (f) Mewis, R. E.; Archibald, S. J. Biomedical applications of macrocyclic ligand complexes. *Coord. Chem. Rev.* **2010**, *254*, 1686-1712.

2- (a) Leroux, M.; Vorherr, T.; Lewis, I.; Schaefer, M.; Koch, G.; Karaghiosoff, K.; Knochel, P. Late-Stage Functionalization of Peptides and Cyclopeptides Using Organozinc Reagents. *Angew. Chem., Int. Ed.* **2019**, *58*, 8231-8234. (b) Jafara, M. R.; Yu, H.; Wickware, J. M.; Lin, Y.-S.; Derda, R. Light-responsive bicyclic peptides. *Org. Biomol. Chem.* **2018**, *16*, 7588-7594. (c) D'Amato, A.; Volpe, R.; Vaccaro, M. C.; Terracciano, S.; Bruno, I.; Tosolini, M.; Tedesco, C.; Pierri, G.; Tecilla, P.; Costabile, C.; Della Sala, G.; Izzo, I.; De Riccardis, F. Cyclic Peptoids as Mycotoxin Mimics: An Exploration of Their Structural and Biological Properties. *J. Org. Chem.* **2017**, *82*, 8848-8863. (d) Thakkar, A.; Trinh, T. B.; Pei, D. Global Analysis of Peptide Cyclization Efficiency. *ACS Comb. Sci.* **2013**, *15*, 120-129.

3- (a) Jurczak, J.; Sobczuk, A.; Dabrowa, K.; Lindner, M.; Niedbała, P. An Indirect Synthetic Approach toward Conformationally Constrained 20-Membered Unclosed Cryptands via Late-Stage Installation of Intraannular Substituents. *J. Org. Chem.* **2018**, *83*, 13560-13567. (b) Hammershøj, P.; Beldring, K.; Nielsen, A. R.; Fristrup, P.; Clausen, M. H. Observations on the Influence of Precursor Conformations on Macrocyclization Reactions. *Eur. J. Org. Chem.* **2016**, *8*, 1533-1540. (c) Segawa, Y.; Miyamoto, S.; Omachi, H.; Matsuura, S.; Šenel, P.; Sasamori, T.; Tokitoh, N.; Itami, K. Concise synthesis and crystal structure of [12]cycloparaphenylene. *Angew. Chem., Int. Ed.* **2011**, *50*, 3244-3248. (d) Reyes, S.; Pattarawarapan, M.; Roy, S.; Burgess, K. Preferred Secondary Structures as a Possible Driving Force for Macrocyclization.

Tetrahedron **2000**, *56*, 9809-9818. (e) Miller, S. J.; Blackwell, H. E.; Grubbs, R. H. Application of Ring-Closing Metathesis to the Synthesis of Rigidified Amino Acids and Peptides. *J. Am. Chem. Soc.* **1996**, *118*, 9606-9614. (f) Still, W. C.; Galynker, I. Stereospecific synthesis of the C30-C43 segment of palytoxin by macrocyclically controlled remote asymmetric induction. *J. Am. Chem. Soc.* **1982**, *104*, 1774−1776.

4- Martí-Centelles, V.; Luis, S. V.; Burguete, M. I.; Pandey, M. Macrocyclization Reactions: The Importance of Conformational, Configurational and Template-Induced Preorganization. *Chem. Rev.* **2015**, *115*, 8736-8834.

5- (a) Yuan, L.; Zeng, H.; Yamato, K.; Sanford, A. R.; Feng, W.; Atreya, H. S.; Sukumaran, D. K.; Szyperski, T.; Gong, B. Helical Aromatic Oligoamides: Reliable, Readily Predictable Folding from the Combination of Rigidified Structural Motifs. *J. Am. Chem. Soc.* **2004**, *126*, 16528-16537. (b) Cavelier-Frontin, F.; Pepe, G.; Verducci, J.; Siri, D.; Jacquier, R. Prediction of the best linear precursor in the synthesis of cyclotetrapeptides by molecular mechanic calculations. *J. Am. Chem. Soc.* **1992**, *114*, 8885-8890.

6- (a) Horne, W. S.; Gellman, S. H. Foldamers with Heterogeneous Backbones. *Acc. Chem. Res.* **2008**, *41*, 1399-1408. (b) Hecht, S.; Huc, I. Foldamers: Structure, Properties, and Applications; Wiley-VCH: Weinheim, 2007. (c) Nakanishi, H.; Kahn, M. in *Bioorganic Chemistry: Peptides and Proteines*; Hecht, S. M. Ed.; Oxford University Press: New York, 1998, Chapter 12. (d) Liu, Z.-P.; Rizo, J.; Gierasch, L. M. Protein folding. In *Bioorganic Chemistry: Peptides and Proteines*; S. M. Hecht, Ed.; Oxford University Press: New York, 1998, Chapter 6. (e) Gellman, S. H. Foldamers: A Manifesto. *Acc. Chem. Res.* **1998**, *31*, 173-180.

7- (a) Wellhöfer, I.; Frydenvang, K.; Kotesova, S.; Christiansen, A. M.; Laursen, J. S.; Olsen, C. A. Functionalized Helical β-Peptoids. *J. Org. Chem.* **2019**, *84*, 3762-3779. (b) Hjelmgaard, T.; Dissing, M. M.; Andersen, J.-M.; Frydenvang, K.; Nielsen, J. Advances towards Aromatic Oligoamide Foldamers: Synthesis and X-ray Structures of Dimeric Arylopeptoids with Conformation-Directing Side Chains Hjelmgaard. *Eur. J. Org. Chem.* **2014**, 3971-3975. (c) Martinek, T. A.; Fülöp, F. Peptidic Foldamers: Ramping Up Diversity. *Chem. Soc. Rev.* **2012**, *41*, 687-702. (d) Horne, W. S. Peptide and peptoid foldamers in medicinal chemistry. *Drug Discovery* **2011**, *6*, 1247-1262. (e) Nowick, J. S.; Insaf, S. The Propensies of Amino Acids to Form Parallel β-Sheets. *J. Am. Chem. Soc.* **1997**, *119*, 10903-10908.

8- (a) Tyszka, A.; Pikus, G.; Dąbrowa, K.; Jurczak, J. Late-Stage Functionalization of (R)-BINOL-Based Diazacoronands and Their Chiral Recognition of α-Phenylethylamine Hydrochlorides. *J. Org. Chem.* **2019**, *84*, 6502-6507. (b) Eytel, L. M.; Fargher, H. A.; Haley, M. M.; Johnson, D. W. The road to aryl CH-anion binding was paved with good intentions: fundamental studies, host design, and historical perspectives in CH hydrogen bonding. *Chem. Commun.* **2019**, *55*, 5195-5206. (c) Mungalpara, D.; Stegmüller, S.; Kubik, S. A neutral halogen bonding macrocyclic

anion receptor based on a pseudocyclopeptide with three 5-iodo-1,2,3-triazole subunits. *Chem. Commun.* **2017**, *53*, 5095-5098. (d) Dabrowa, K.; Ulatowski, F.; Lichosyt, D.; Jurczak, J. Catching the chloride: searching for non-Hofmeister selectivity behavior in systematically varied polyamide macrocyclic receptors. *Org. Biomol. Chem.* **2017**, *15*, 5927-5943. (e) Tamaki, K.; Ishigami, A.; Tanaka, Y.; Yamanaka, M.; Kobayashi, K. Self-Assembled Boronic Ester Cavitand Capsules with Various Bis(catechol) Linkers: Cavity-Expanded and Chiral Capsules. *Chem. Eur. J.* **2015**, *21*, 13714-13722.

9- (a) Łęczycka-Wilk, K.; Dąbrowa, K.; Cmoch, P.; Jarosz, S. Chloride-Templated Macrocyclization and Anion-Binding Properties of C-2-Symmetric Macrocyclic Ureas from Sucrose. *Org. Lett.* **2017**, *19*, 4596-4599. (b) Martí-Centelles, V.; Burguete, M. I.; Luis, S. V. Macrocycle Synthesis by Chloride-Templated Amide Bond Formation. *J. Org. Chem.* **2016**, *81*, 2143-2147. (c) Katayev, E. A.; Kolesnikov, G. V.; Arnold, R.; Lavrov, H. V.; Khrustalev, V. N. Templating Irreversible Covalent Macrocyclization by Using Anions. *Chem. Eur. J.* **2013**, *19*, 3710-3714. (d) Katayev, E. A.; Pantos, G. D.; Reshetova, M. D.; Khrustalev, V. N.; Lynch, V. M.; Ustynyuk, Y. A.; Sessler, J. L. Anion-Induced Synthesis and Combinatorial Selection of Polypyrrolic Macrocycles. *Angew. Chem., Int. Ed.* **2005**, *44*, 7386-7390. (e) Garbleu, N. V.; Arion, V. B.; Burgess, J. Template Synthesis of Macrocyclic Compounds; Wiley: Weinheim, 1999.

10- (a) Kaabel, S.; Stein, R. S.; Järving, I.; Friščić, T.; Aav, R. Size-Control by Anion Templating in Mechanochemical Synthesis of Hemicucurbiturils in the Solid State. *Angew. Chem. Int. Ed.* **2019**, *58*, 6230-6234. (b) Batiste, S. M.; Johnston, J. N. Evidence for Ion-Templation During Macrocyclooligomerization of Depsipeptides. *J. Am. Chem. Soc.* **2018**, *140*, 4560-4568. (c) Satake, A.; Ishizawa, Y.; Katagiri, H.; Kondo, S. Chloride Selective Macrocyclic Bisurea Derivatives with 2,2'-Binaphthalene Moieties as Spacers. *J. Org. Chem.* **2016**, *81*, 9848-9857. (d) Martí-Centelles, V.; Burguete, M. I.; Luis, S. V. Template Effects in S_N2 Displacements for the Preparation of Pseudopeptidic Macrocycles. *Chem. Eur. J.* **2012**, *18*, 2409-2422. (e) Lankshear, M. D.; Beer, P. D. Strategic Anion Templation. *Coord. Chem. Rev.* **2006**, *250*, 3142-3160. (f) Gimeno, N.; Vilar, R. Anions as templates in coordination and supramolecular chemistry. *Coord. Chem. Rev.* **2006**, *250*, 3161-3189. (g) Vilar, R. Anion-Templated Synthesis. *Angew. Chem., Int. Ed.* **2003**, *42*, 1460-1477.

11- Luis, S. V.; Alfonso, I. Bioinspired Chemistry Based on Minimalistic Pseudopeptides. *Acc. Chem. Res.* **2014**, *47*, 112-124.

12- Valls, A.; Altava, B.; Burguete, M. I.; Escorihuela, J.; Martí-Centelles, V.; Luis, S. V. Supramolecularly assisted synthesis of chiral tripodal imidazolium compounds. *Org. Chem. Front.* **2019**, *6*, 1214-1225.

13- Bru, M.; Alfonso, I.; Burguete, M. I.; Luis, S. V. Efficient syntheses of new chiral peptidomimetic macrocycles through a configurationally driven preorganization. *Tetrahedron Lett.* **2005**, *46*, 7781-7785.

14- (a) Moure, A.; Luis, S. V.; Alfonso, I. Efficient synthesis of pseudopeptidic molecular cages. *Chem. Eur. J.* **2012**, *18*, 5496-5500. (b) Alfonso, I.; Bolte, M.; Bru, M.; Burguete, M. I.; Luis, S. V.; Rubio, J. Supramolecular Control for the Modular Synthesis of Pseudopeptidic Macrocycles through an Anion Templated Reaction. *J. Am. Chem. Soc.* **2008**, *130*, 6137-6144.

15- Alfonso, I.; Burguete, M. I.; Galindo, F.; Luis, S. V.; Vigara, L. Molecular Rotors as Simple Models to Study Amide NH-Aromatic Interactions and Their Role in the Folding of Peptide-like Structures. *J. Org. Chem.* **2007**, *72*, 7947-7956.

16- Wadhavane, P. D.; Galian, R. E.; Izquierdo, M. A.; Aguilera-Sigalat, J.; Galindo, F.; Schmidt, L.; Burguete, M. I.; Pérez-Prieto, J.; Luis, S. V. Photoluminescence enhancement of CdSe quantum dots: A case of organogel-nanoparticle symbiosis. *J. Am. Chem. Soc.* **2012**, *134*, 20554-20563.

17- Martí-Centelles, V.; Burguete, M. I.; Galindo, F.; Izquierdo, M. A.; Kumar, D. K.; White, A. J. P.; Luis, S. V.; Vilar, R. Fluorescent acridine-based receptors for $H_2PO_4^-$. *J. Org. Chem.* **2012**, *77*, 490-500.

18- (a) Gaeta, M.; Raciti, D.; Randazzo, R.; Gangemi, C. M. A.; Raudino, A.; D'Urso, A.; Fragalà, M. E.; Purrello, R. Chirality Enhancement of Porphyrin Supramolecular Assemnbly Driven by a Template Preorganization Effect. *Angew. Chem., Int. Ed.* **2018**, *57*, 10656-10660. (b) Wang, Z.; Liang, C.; Shang, Y.; He, S.; Wang, L.; Yang, Z. Narrowing the diversification of supramolecular assemblies by preorganization. *Chem. Commun.* **2018**, *54*, 2751-2754. (c) Cram, D. J. Preorganization-From Solvents to Spherands. *Angew. Chem., Int. Ed.* **1986**, *25*, 1039-1057.

19- (a) Pan, H. A non-covalent dimer formed in electrospray ionisation mass spectrometry behaving as a precursor for fragmentations. *Rapid Commun. Mass Spectrom.* **2008**, *22*, 3555-3560. (b) König, S.; Fales, H. M. Formation and Decomposition of Water Clusters as Observed in a Triple Quadrupole Mass Spectrometer. *J. Am. Soc. Mass Spectrom.* **1998**, *9*, 814-822.

20- Andrés, A.; Burguete, M. I.; García-España, E.; Luis, S. V.; Miravet, J. F.; Soriano, C. Polyazacyclophanes. 2,6,9,13-Tetraaza[14]paracyclophane as a cationic and anionic receptor. *J. Chem. Soc., Perkin Trans.* **1993**, *2*, 749-755.

21- Deppmeier, B. J.; Driessen, A. J.; Hehre, T. S.; Hehre, W. J.; Johnson, J. A.; Klunzinger, P. E.; Leonard, J. M.; Pham, I. N.; Pietro, W. J.; Jianguo, Y. Spartan08, build 132 (Mar 27 2009), Wavefunction Inc.: Irvine CA, 2009.

22- (a) Jiang, L.; Cao, S.; Cheung, P. P.-H.; Zheng, X.; Leung, C. W. T.; Peng, Q.; Shuai, Z.; Tang, B. Z.; Yao, S.; Huang, X. Real-time monitoring of hydrophobic aggregation reveals a critical role of cooperativity in hydrophobic effect. *Nat. Commun.* **2017**, *8*, 15639-15647. (b) Kinoshita, M.; Hayashi, T. Unified elucidation of the entropy-driven and -opposed hydrophobic effects. *Phys. Chem. Chem. Phys.* **2017**, *19*, 25891-25904. (c) Ball, P. Water is an active matrix of life for cell and molecular biology. *Proc. Natl. Acad. Sci. U.S.A.* **2017**, *114*, 13327-13335. (d) Pratt, L. R.; Pohorille, A. Hydrophobic Effects and Modeling of Biophysical Aqueous Solution Interfaces. *Chem. Rev.* **2002**, *102*, 2671-2692.

23- (a) Hirota, S.; Lin, Y. -W. Design of artificial metalloproteins/ metalloenzymes by tuning noncovalent interactions. *J. Biol. Inorg Chem.* **2018**, *23*, 7-25. (b) Tomasini, C.; Zanna, N. Oxazolidinonecontaining pseudopeptides: Supramolecular materials, fibers, crystals, and gels. *J. Pept. Sci.* **2017**, *108*, No. e22898. (c) Macedi, E.; Meli, A.; De Riccardis, F.; Rossi, P.; Smith, V. J.; Barbour, L. J.; Izzo, I.; Tedesco, C. Molecular recognition and solvatomorphism of a cyclicpeptoid: formation of a stable 1D porous framework. *CrystEngComm* **2017**, *19*, 4704-4708. (d) Jang, Y.; Champion, J. A. Self-Assembled Materials Made from Functional Recombinant Proteins. *Acc. Chem. Res.* **2016**, *49*, 2188-2198. (e) Levy, Y.; Onuchic, J. N. Mechanisms of Protein Assembly: Lessons from Minimalist Models. *Acc. Chem. Res.* **2006**, *39*, 135-142.

24- Gorla, L.; Martí-Centelles, V.; Altava, B.; Burguete, M. I.; Luis, S. V. The role of the side chain in the conformational and selfassembly patterns of C_2-symmetric Val and Phe pseudopeptidic derivatives. *CrystEngComm* **2019**, *21*, 2398-2408.

25- (a) Ranjbar, B.; Gill, P. Circular Dichroism Techniques: Biomolecular and Nanostructural Analyses- A Review. *Chem. Biol. Drug Des.* **2009**, *74*, 101-120. (b) Bulheller, B. M.; Miles, A. J.; Wallace, B. A.; Hirst, J. D. Charge-transfer transitions in the vacuumultraviolet of protein circular dichroism spectra. *J. Phys. Chem. B* **2008**, *112*, 1866-1874. (c) Kelly, S. M.; Jess, T. J.; Price, N. C. How to study proteins by circular dichroism. *Biochim. Biophys. Acta* **2005**, *1751*, 119-139. (d) Lowe, S. L.; Pandey, R. R.; Czlapinski, J.; Kie-Adams, G.; Hoffmann, M. R.; Thomasson, K. A.; Pierce, K. S. Dipole interaction model predicted pi-pi* circular dichroism of cyclo(LPro)$_3$ using structures created by semi-empirical, ab initio, and molecular mechanics methods. *J. Pept. Res.* **2003**, *61*, 189-201.

26- Sheldrick, G. M.; A short history of SHELX. *Acta Crystallogr., Sect. A: Found. Crystallogr.* **2008**, *64*, 112-122.

27- Sheldrick, G. M. Crystal structure refinement withSHELXL. *Acta Crystallogr., Sect. C: Struct. Chem.* **2015**, *71*, 3-8.

28- Macrae, C. F.; Bruno, I. J.; Chisholm, J. A.; Edgington, P. R.; McCabe, P.; Pidcock, E.; Rodriguez-Monge, L.; Taylor, R.; van de Streek, J.; Wood, P. A. Mercury

CSD 2.0- new features for the visualization and investigation of crystal structures. *J. Appl. Crystallogr.* **2008**, *41*, 466-470.

3.2. Supporting information

Table S3.1. Macrocyclization yields obtained for the reaction between **1a** (3 mM) and **2** (3 mM).

Entry	Solvent	Base[a]	Temp. (ºC)	Time (min)	Yield (%)[b]
1	EtOH	KOH	88	420	<25
2	DMF	KOH	160	60	<45
3	CH_3CN	-	88	120	ca. 50
4	CH_3CN	Et_3N	93	60	-
5	CH_3CN	Na_2CO_3	88	200	60
6	CH_3CN	$(NH_4)_2CO_3$	88	420	ca. 50
7	CH_3CN	Cs_2CO_3	88	180	95

[a] 6 equiv. [b] Determined by ^{1}H NMR
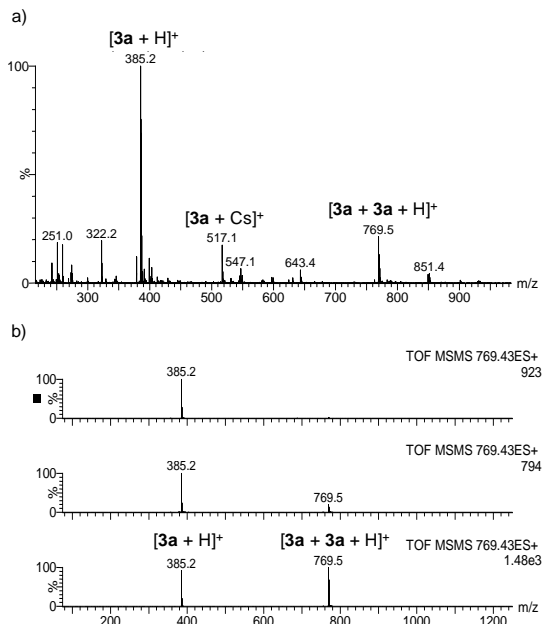
Figure S3.1. a) ESI-MS (+) of the crude of the reaction between **1a** (3 mM) and **2** (3 mM) after 3 h. b) ESI MS/MS (+) of the peak at m/z 769.5 corresponding to [**3a** + **3a** + H]$^+$.
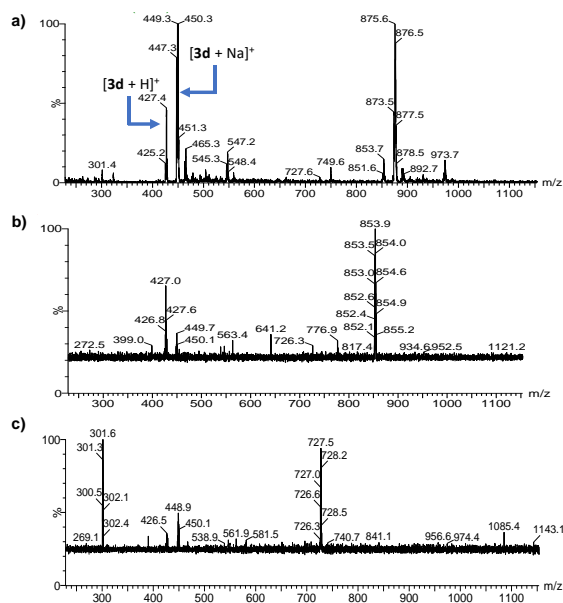
Figure S3.2. a) ESI-MS (+) of the crude of the reaction between **1d** (3 mM) and **2** (3 mM) after 3 h. b) ESI MS/MS (+) of the peak at 853.9 m/z corresponding to a side-product of the reaction. c) ESI MS/MS (+) of the peak at 727.5 m/z corresponding to a second side-product of the reaction.
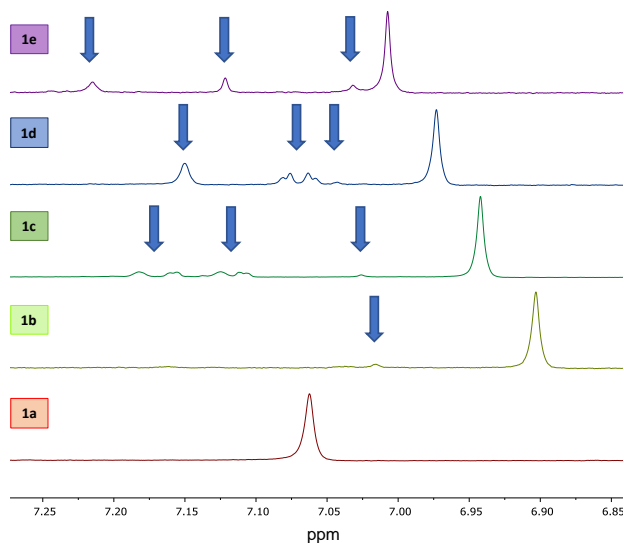
Figure S3.3. Partial ^{1}H NMR (400 MHz) spectra of the crude after 3h of macrocyclization reactions at 90 °C in acetonitrile from precursors **1a-e** (3 mM) and **2** (3 mM). Arrows indicate the proton signals associated to the formation of side products. Deuterated solvent: CD$_3$OD.
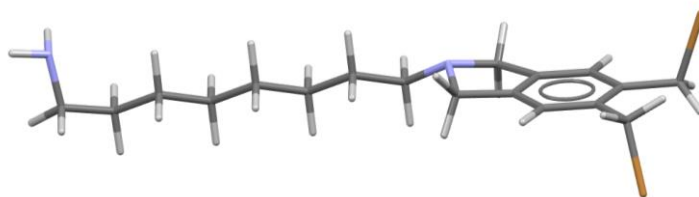
Figure S3.4. Minimum energy conformer calculated (MMFF level of theory using Spartan08) for the hypothetic intermediate of the reaction between **2** and 1,8-diaminooctane.
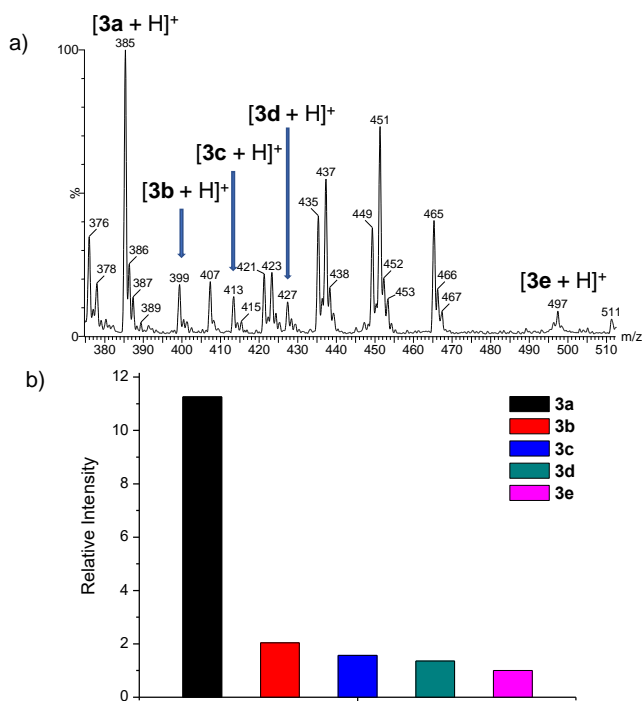
Figure S3.5. a) ESI-MS (+) competitive studies involving the reaction of **1a-e** (3 mM each) and tetrakisbromomethylbenzene **2** (3 mM) in acetonitrile at 90 °C. b) Relative intensity of the peaks corresponding to the desired [1+1] macrocycles **3a-e.**
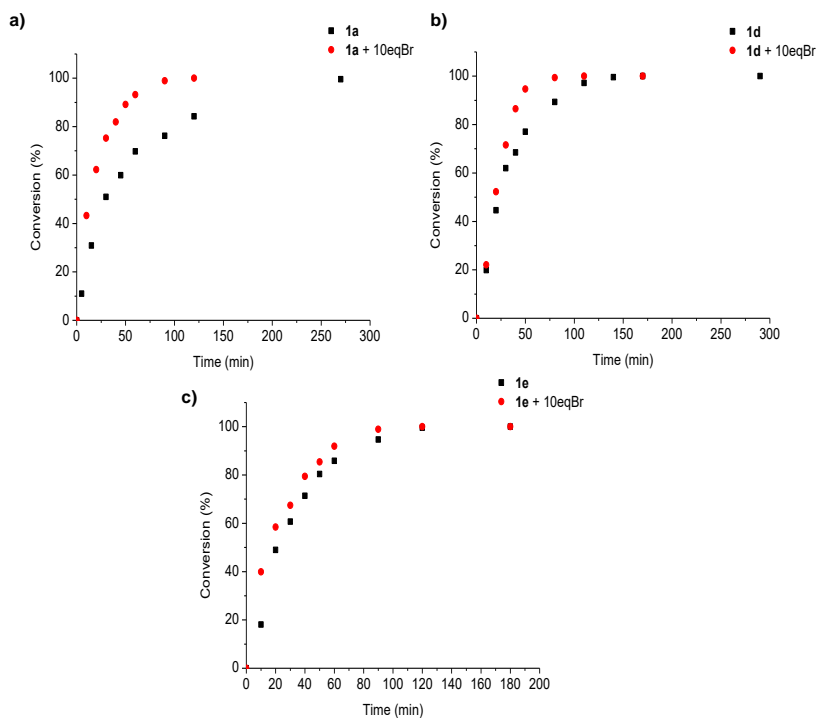
Figure S3.6. Kinetic profiles for the conversion of tetrakisbromomethylbenzene **2** (as followed by HPLC) in the absence (black) and presence (red) of added bromide (10 equiv. as its tetraethylammonium salt) in the reaction with **1a** a), **1d** b) and **1e** c). Conditions: Acetonitrile, 90 ºC, 3mM concentration.
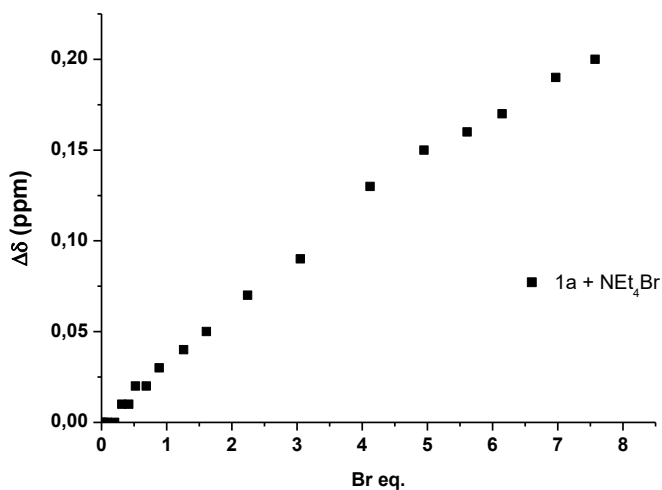
Figure S3.7. ^{1}H NMR titration (NH$_{amide}$ signal) of **1a** (7mM) with tetrabutylammonium bromide in CD$_3$CN.
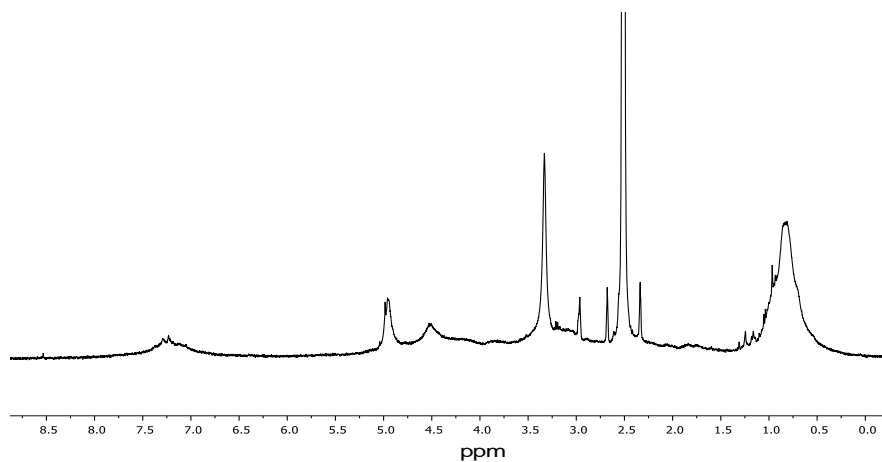
Figure S3.8. Partial ^{1}H NMR spectrum (DMSO-d_6) of the crude of the reaction in acetonitrile (90 °C) between **1a** (3 mM) and **2** (3 mM) in the presence of 10 equiv. of Cl$^-$.
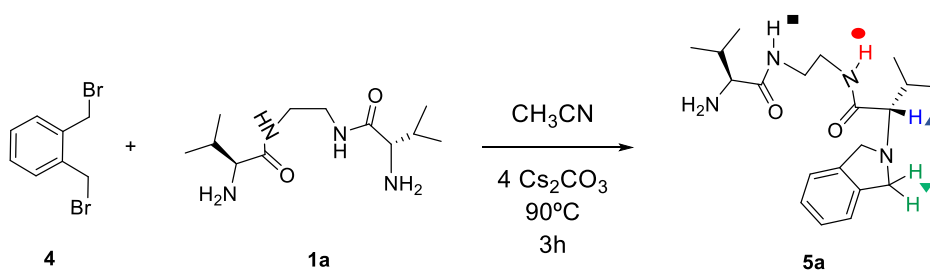
Scheme S3.1. Synthesis of **5a** as a model for the open chain intermediates in the macrocyclization reactions.
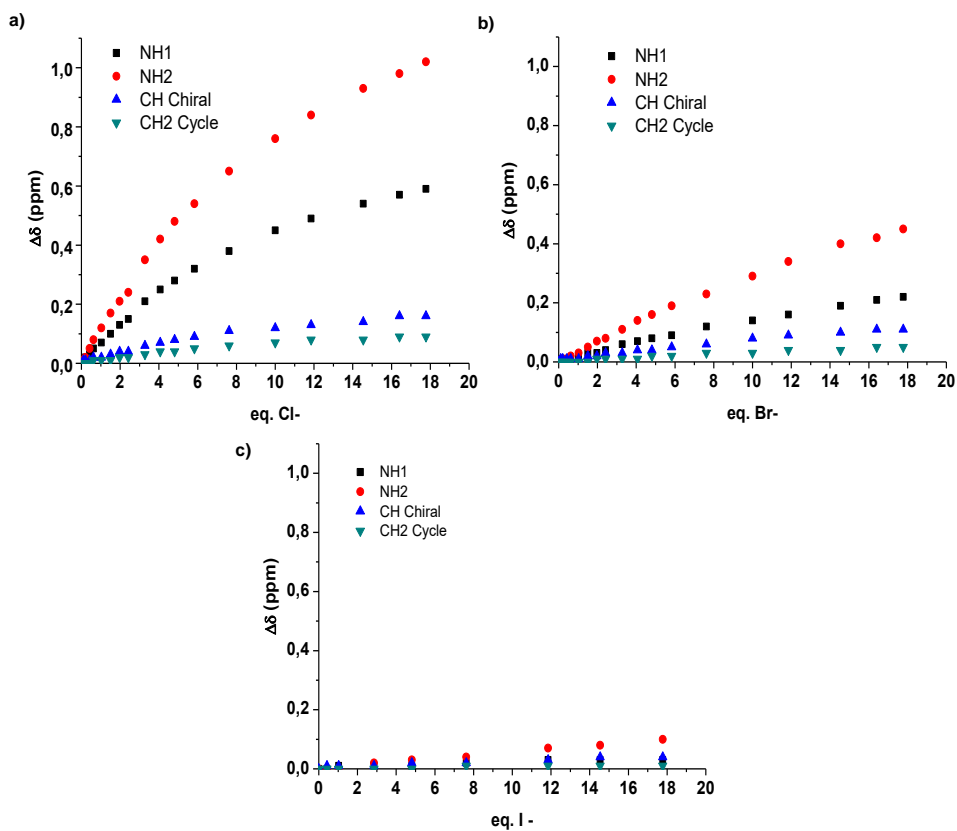
Figure S3.9. Plots of Δδ against concentration for the titration of **5a** (7 mM) with different anions in CD$_3$CN. a) NEt$_4$Cl, b) NEt$_4$Br and c) NEt$_4$I.
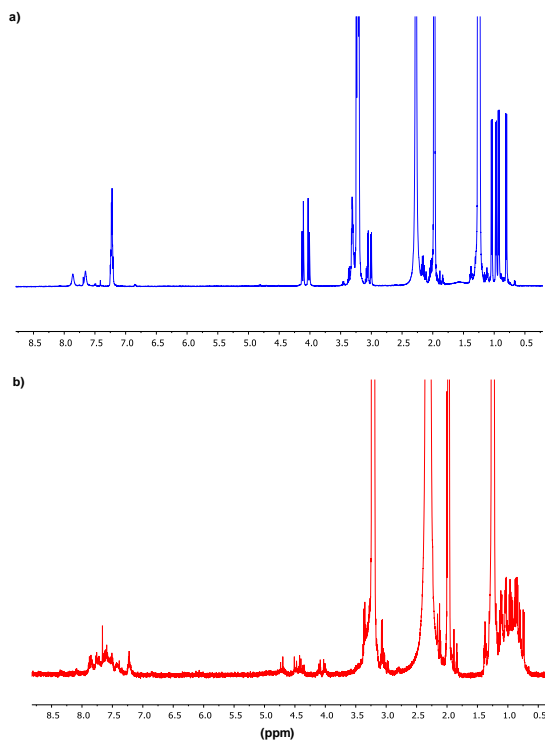
Figure S3.10. a) ^{1}H NMR (500 MHz) spectrum of the initial mixture of **5a** (7 mM in CD$_3$CN) with 10 equiv. of NEt$_4$Cl. b) ^{1}H NMR (500 MHz) spectrum of the same sample after one weak.
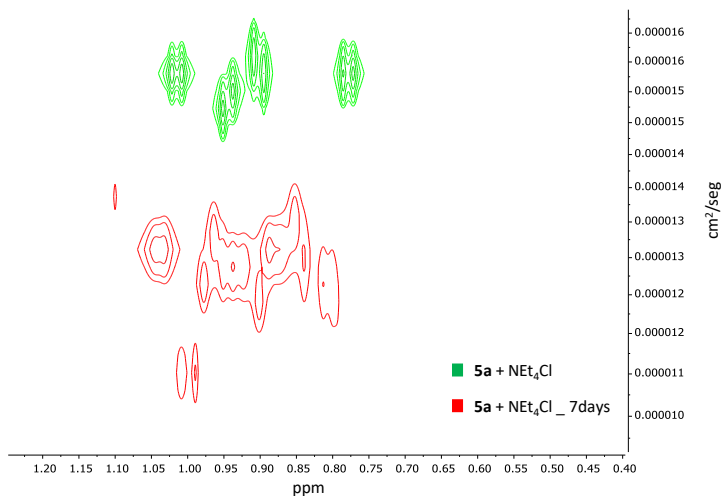
Figure S3.11. Partial DOSY spectrum (0.4 – 1.2 ppm range) of **5a** + Cl$^-$ after initial mixing (green) and after 7 days (red).
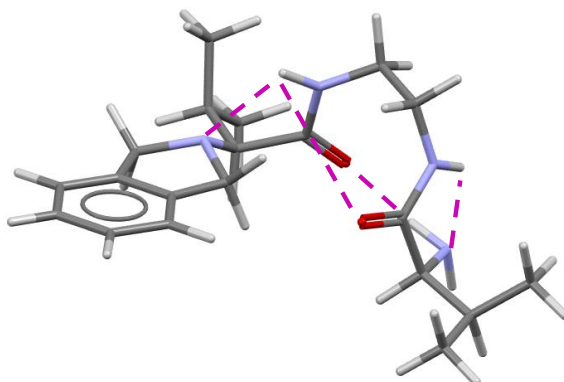
Figure S3.12. Minimum energy conformer (MMFF, Spartan08) for **5a** highlighting the detected hydrogen bonds.
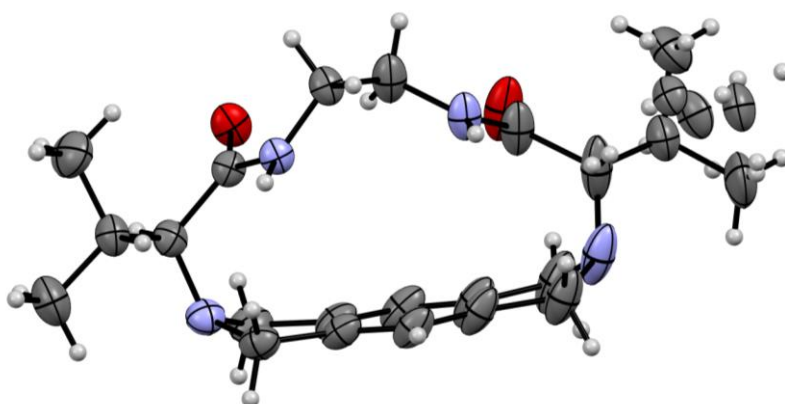
Figure S3.13. Thermal ellipsoid plot for the crystal structure of **3a**. Ellipsoids at 50% of probability.
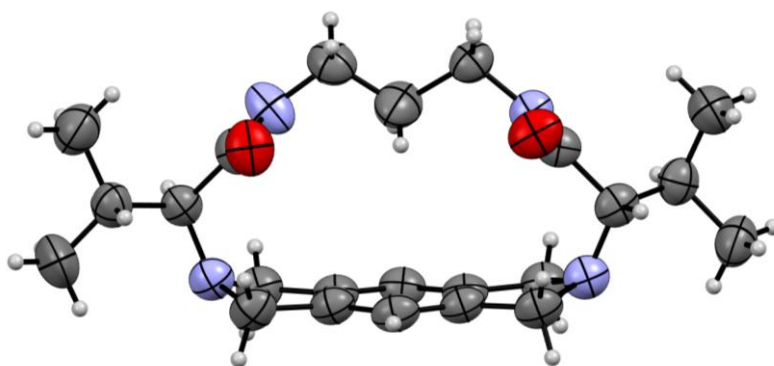
Figure S3.14. Thermal ellipsoid plot for the crystal structure of **3b**. Ellipsoids at 50% of probability.
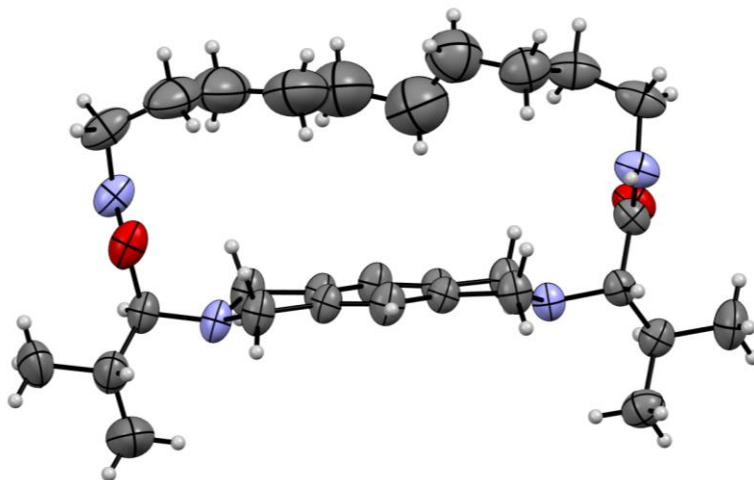
Figure S3.15. Thermal ellipsoid plot for the crystal structure of **3e**. Ellipsoids at 50% of probability.
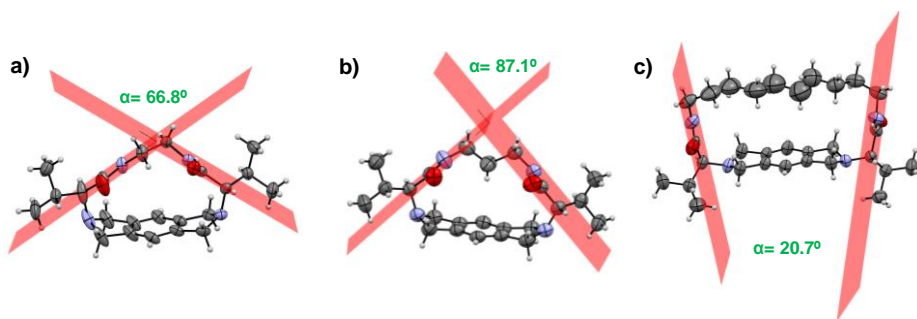
Figure S3.16. Amide bond planes found in the crystal structures of a) **3a**, b) **3b** and c) **3e**.
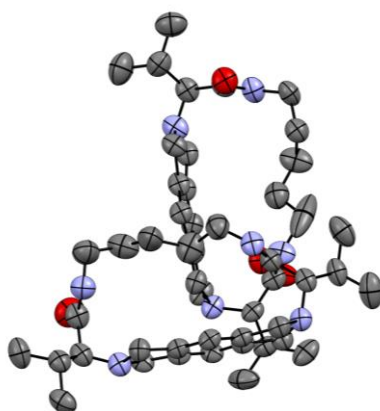
Figure S3.17. Partially resolved molecular structure of the macrocycle **3d**. Hydrogens and solvent molecules have been removed for clarity. Ellipsoids at 50% of probability.
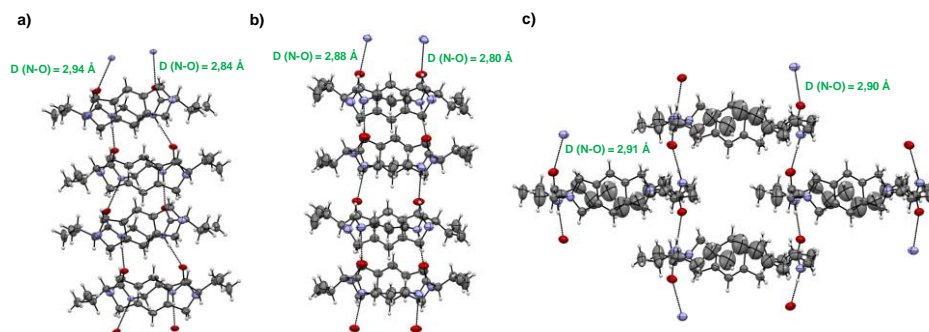
Figure S3.18. Hydrogen bonding networks in the formation of columnar stacks for a) **3a**, b) **3b** and c) **3e**.
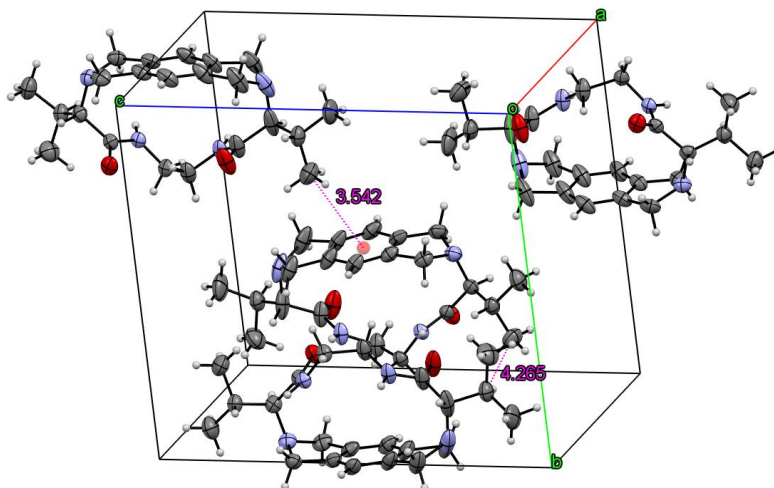
3a

Figure S3.19. Packing observed in the crystal structures of **3a** highlighting the observed hydrophobic intermolecular interactions.
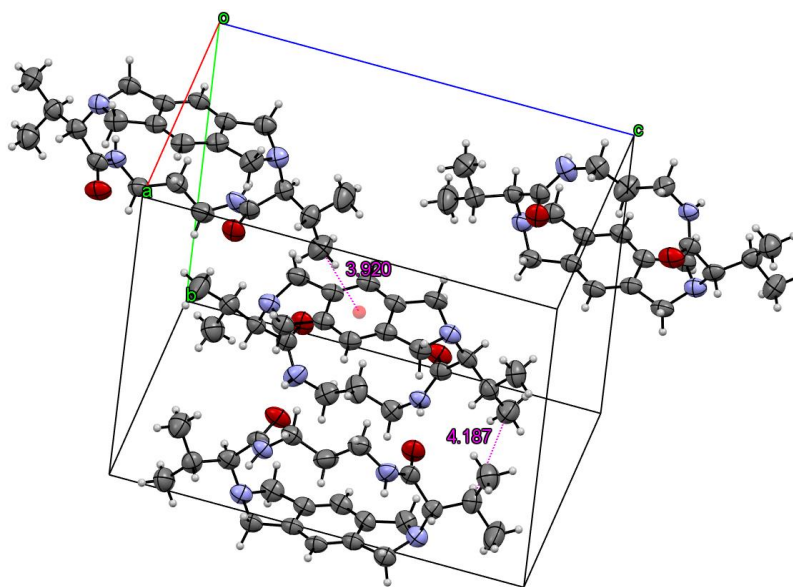
3b

Figure S3.20. Packing observed in the crystal structures of **3b** highlighting the observed hydrophobic intermolecular interactions.

3e
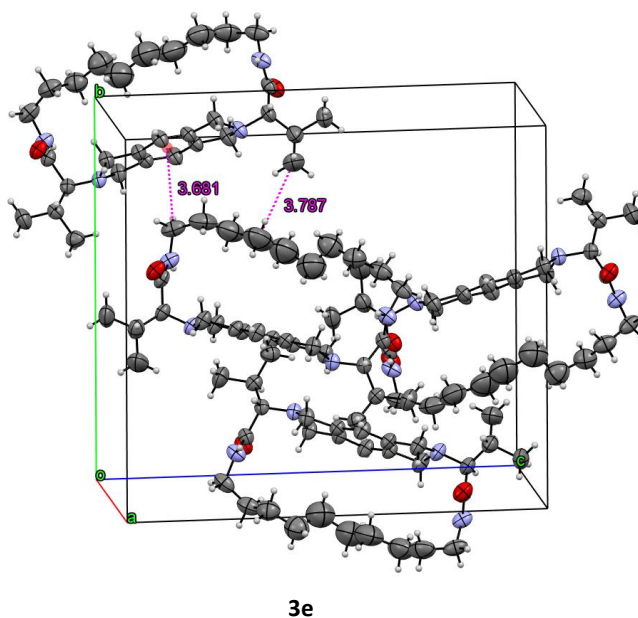
Figure S3.21. Packing observed in the crystal structures of **3e** highlighting the observed hydrophobic intermolecular interactions.
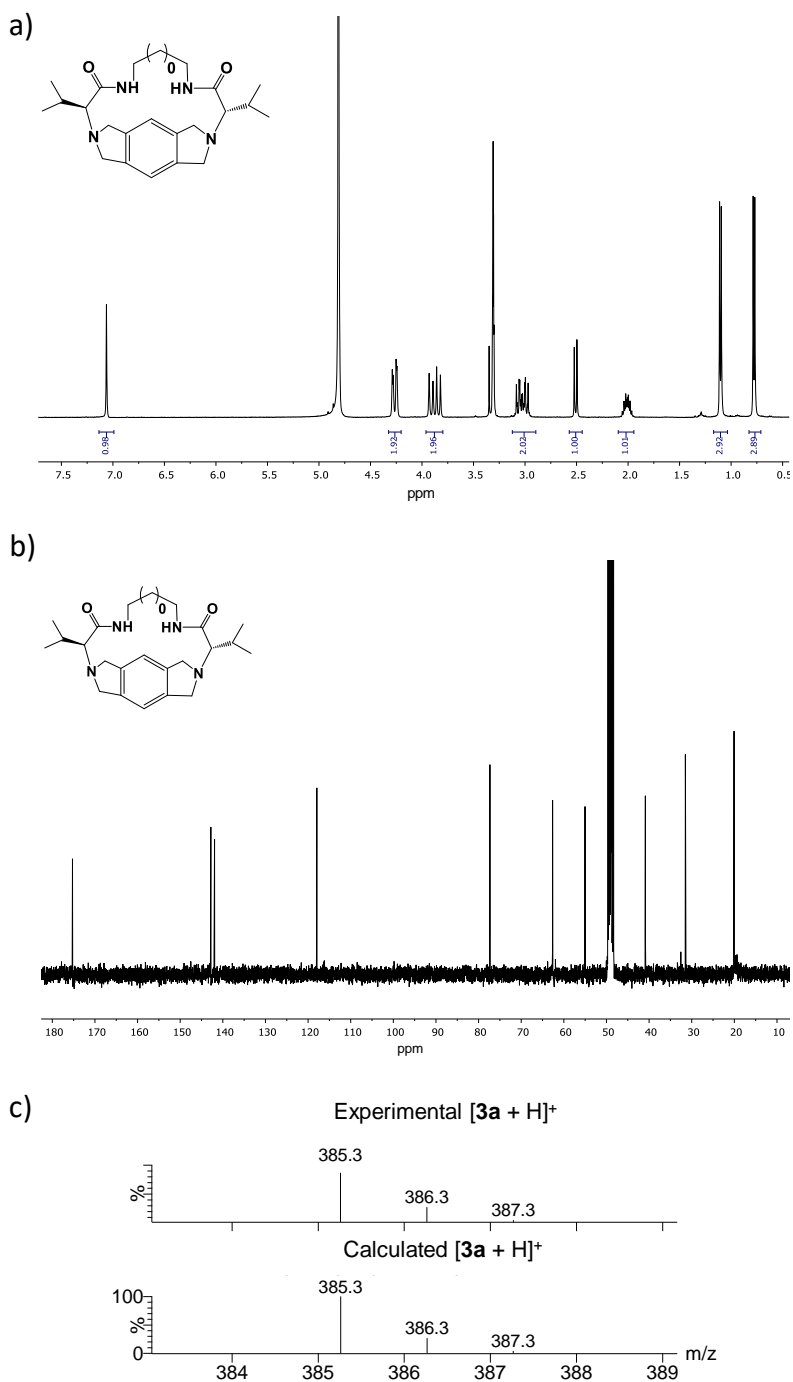
Figure S3.22. a) ^{1}H NMR (400 MHz, CD$_3$OD); b) ^{13}C{^{1}H} NMR (100 MHz, CD$_3$OD) and c) HRMS (ESI/Q-TOF, CH$_3$OH) of **3a**.
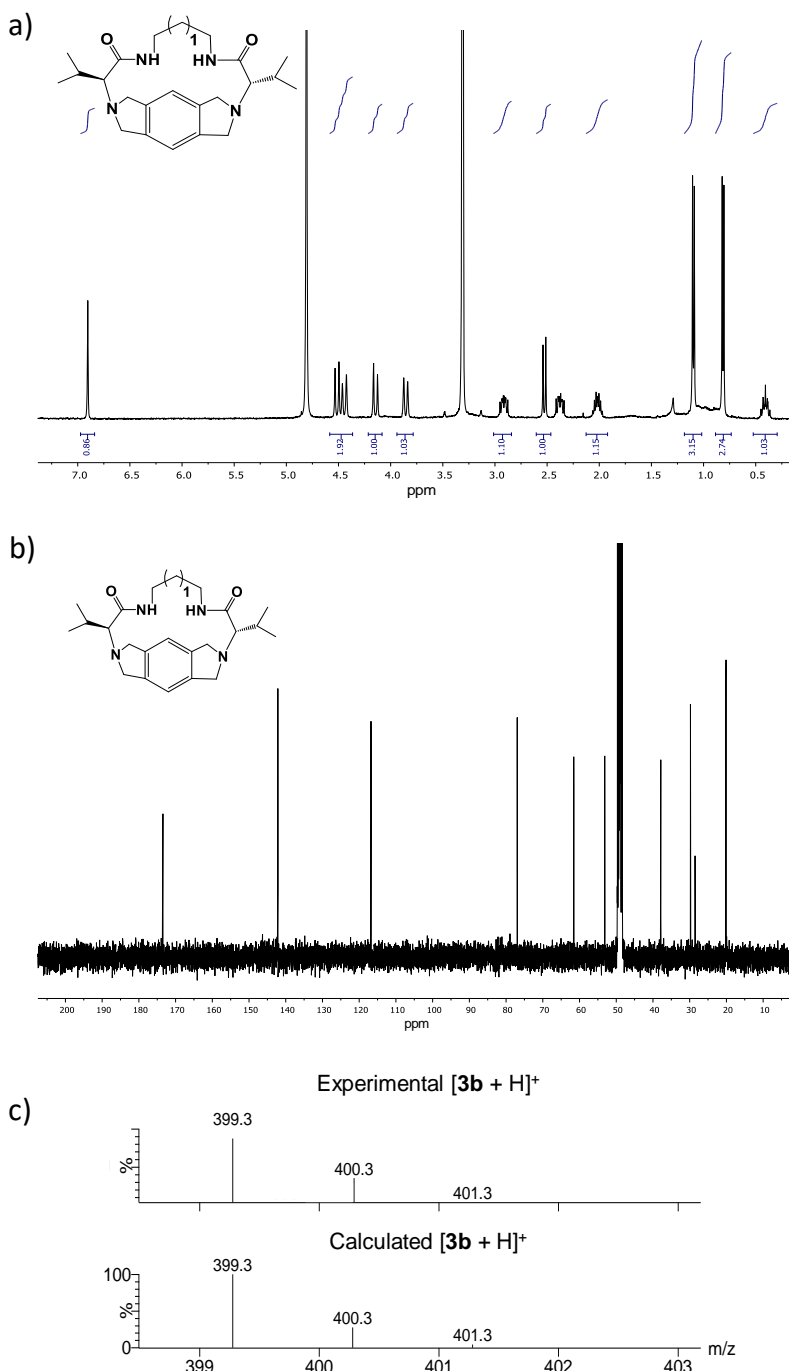
Figure S3.23. a) ¹H NMR (400 MHz, CD₃OD); b) ¹³C{¹H} NMR (100 MHz, CD₃OD) and c) HRMS (ESI/Q-TOF, CH₃OH) of **3b**.
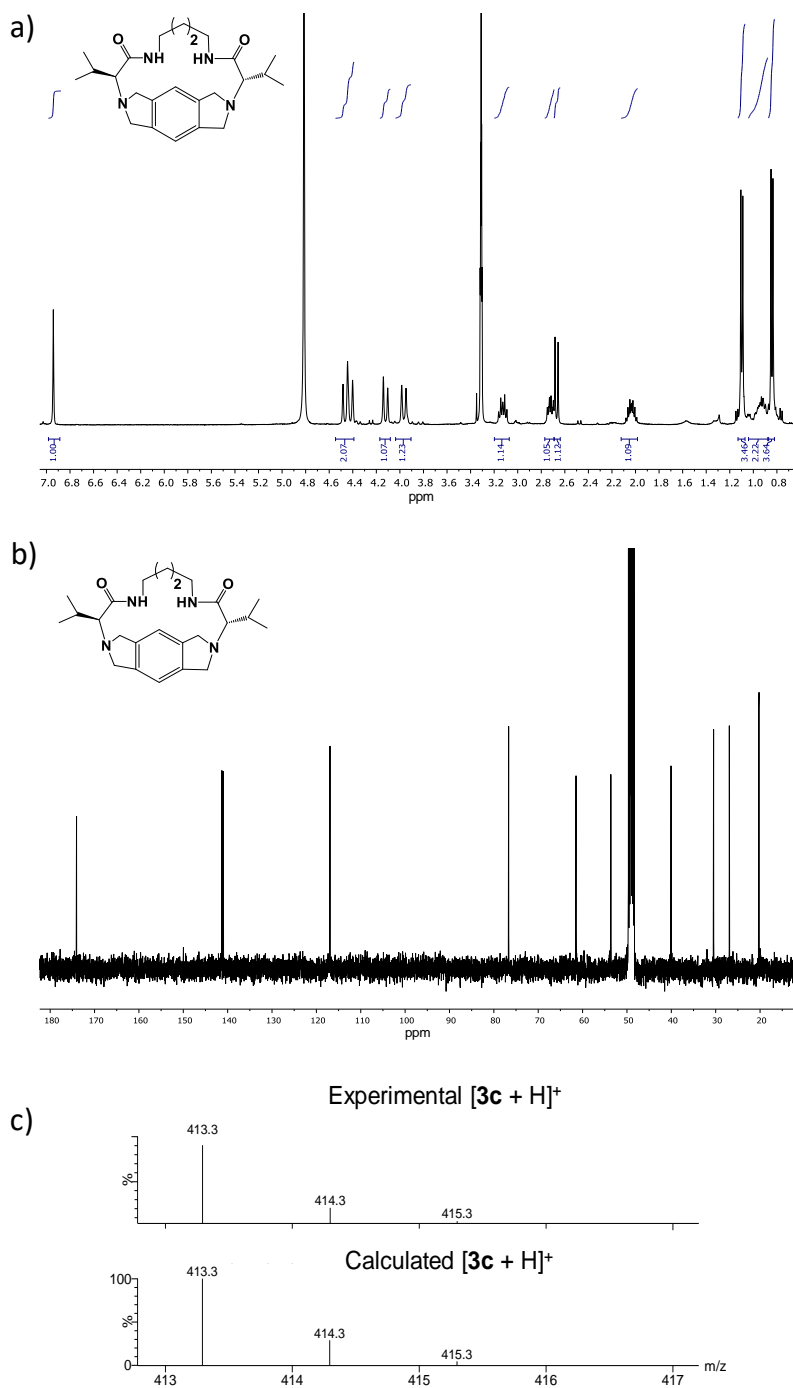
Figure S3.24. a) ¹H NMR (400 MHz, CD₃OD); b) ¹³C{¹H} NMR (100 MHz, CD₃OD) and c) HRMS (ESI/Q-TOF, CH₃OH) of **3c**.

a)

b)

c)

Experimental [**3d** + H]⁺

Calculated [**3d** + H]⁺
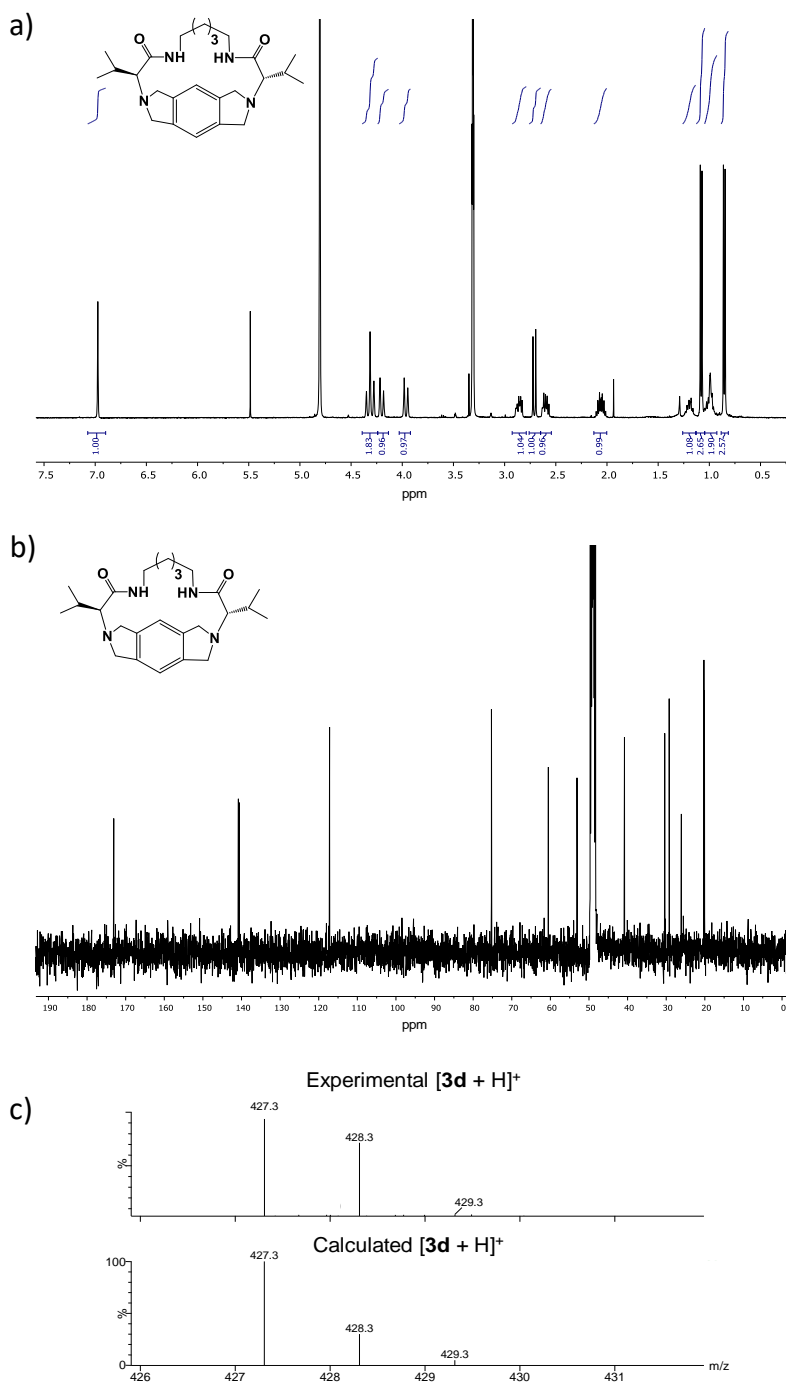
Figure S3.25. a) ¹H NMR (400 MHz, CD₃OD); b) ¹³C{¹H} NMR (100 MHz, CD₃OD) and c) HRMS (ESI/Q-TOF, CH₃OH) of **3d**.
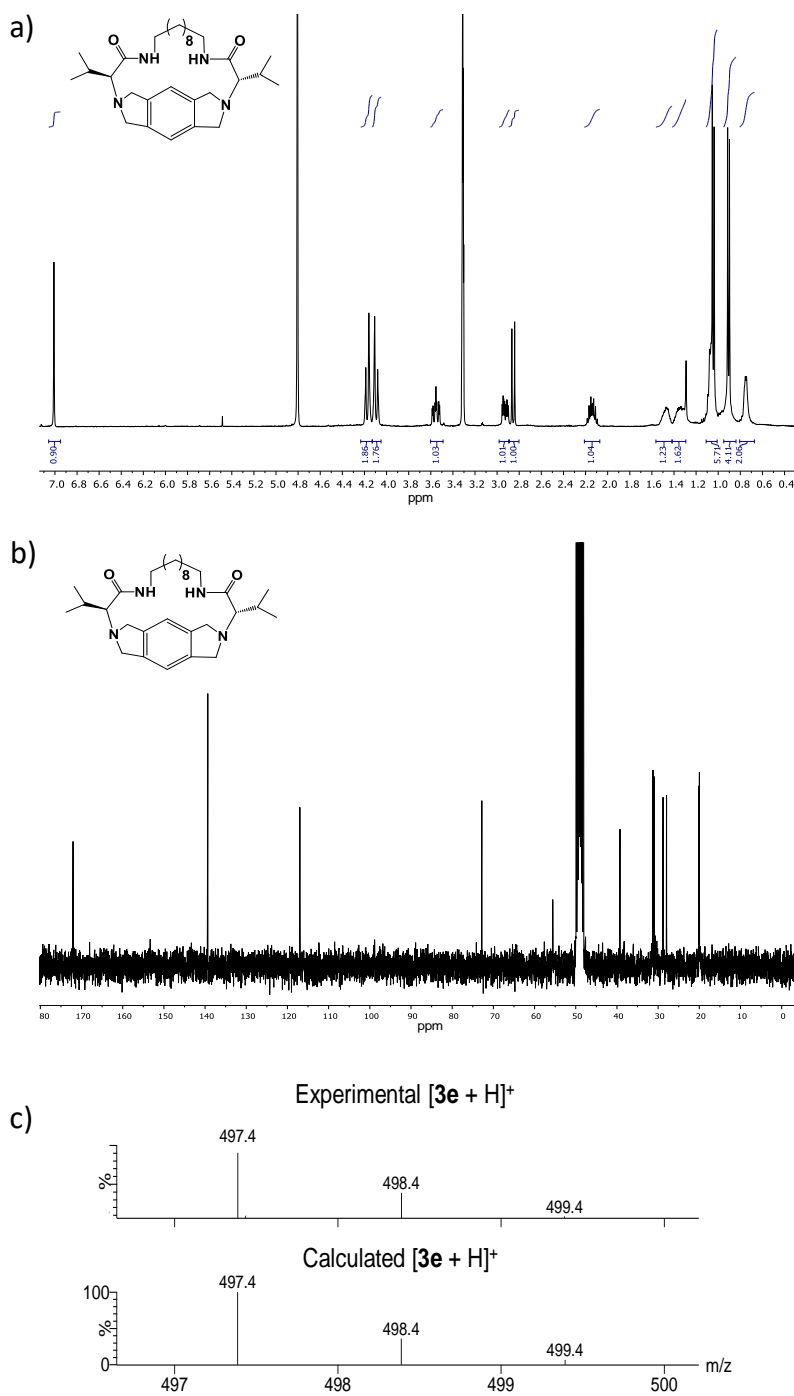
Figure S3.26. a) ^{1}H NMR (400 MHz, CD$_3$OD); b) ^{13}C{^{1}H} NMR (100 MHz, CD$_3$OD) and c) HRMS (ESI/Q-TOF, CH$_3$OH) of **3e**.

a)

b)

c)
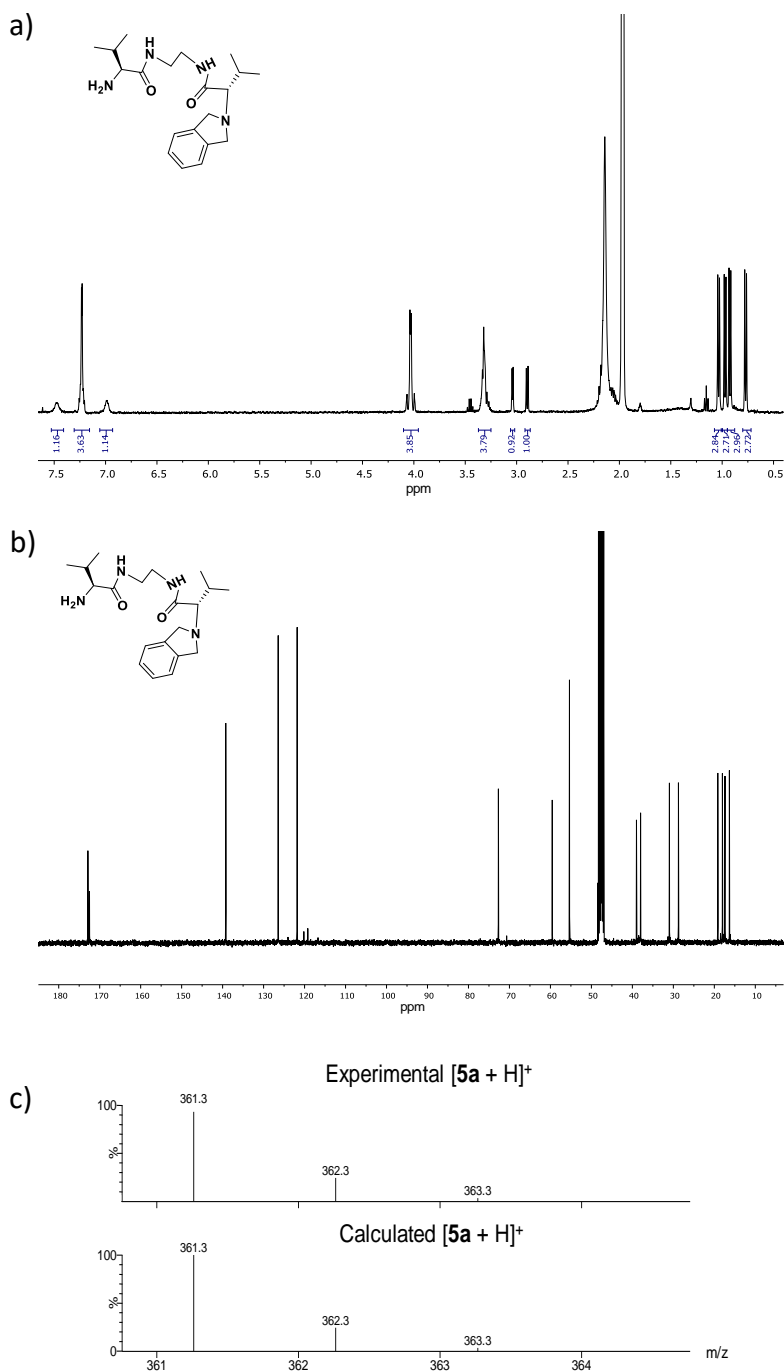
Figure S3.27. a) ^{1}H NMR (400 MHz, CD$_3$CN); b) ^{13}C{^{1}H} NMR (100 MHz, CD$_3$CN) and c) HRMS (ESI/Q-TOF, CH$_3$OH) of **5a**.

Chapter 4

Continuous Flow Processes as an Enabling Tool for the Synthesis of Constrained Pseudopeptidic Macrocycles
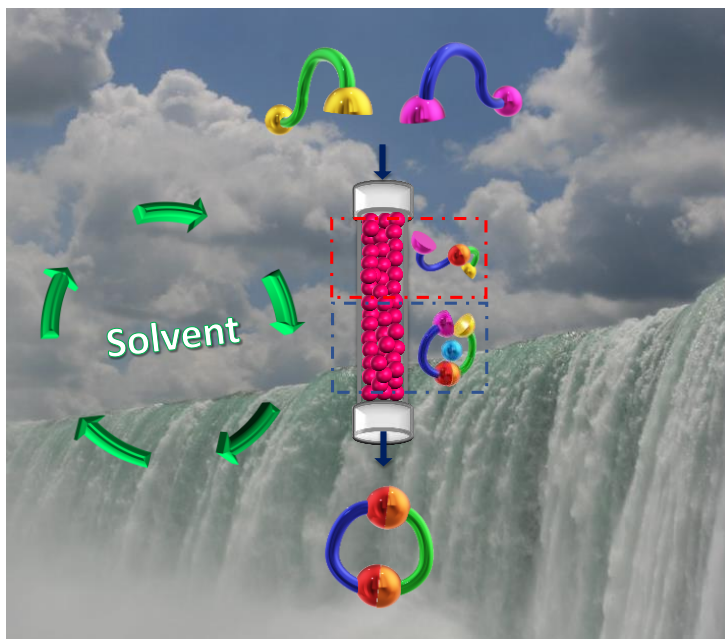
4.1.   Main text

4.1.1.   Abstract

Herein we report our efforts to develop a continuous flow methodology for the efficient preparation of pseudopeptidic macrocyclic compounds containing the hexahydropyrrolo-[3,4-*f*]-isoindolocyclophane scaffold and involving four coupled substitution reactions in the macrocyclization process. Appropriate design of a supported base permitted the continuous production of the macrocycles even at large scales, taking advantage of the positive template effect promoted by the bromide anions. In addition, the use of flow protocols allowed a ca. 20-fold increase in productivity as well as reducing the environmental impact almost 2 orders of magnitude, in comparison with the related batch macrocyclization process.

4.1.2.   Introduction

Success in the synthesis of macrocyclic structures with good yields involves a delicate balance of kinetic and thermodynamic factors.[1] The most usual approach to the preparation of macrocyclic structures is based on kinetically favouring intramolecular versus intermolecular reactions. According to their different kinetic laws, this can be achieved by modifying the relative concentrations of the active species. Thus, the use of high-dilution conditions is often required to favour the macrocyclization process.[2] In some cases, the prevalence of an appropriate conformation of the immediate precursor, providing a favourable preorganization for the macrocyclization step, can be an essential factor for the process to be high yielding.[3] Alternatively, the proper conformation can be induced by the presence of a second species (template).[4] A supramolecular preorganization event, as induced by a template, incorporates molecular information from the guest to the formed supramolecular species. But even in systems and approaches where the structural or induced conformations of the open-chain precursors favour the macrocyclization reaction, the effect of reaction conditions are still critical for success. The well-documented application of small-scale flow reactors has often proved to offer

considerable advantages over batch reactor designs in synthetic processes.[5] Continuous flow reactions permit very efficient heat transfer and, therefore, good control of the reaction temperature, avoiding the problems associated with highly exothermic reactions. Mass transfer is also enhanced due to the lower reaction volume and increased contact area, and the use of dangerous or air- and moisture-sensitive compounds can be facilitated by the sealed reactors.[6] Optimization of reaction conditions is eased by an appropriate control of the residence time, and the scale-up can be achieved by simply pumping, mixing, and quenching the reagents continuously through the reactor for longer periods of time.[7] Thus, this approach allows a shortening of the time from research to development and production.[8] Macrocyclization processes under continuous flow conditions is a seldom explored field of research. There are, however, a few precedents in the literature highlighting the opportunities provided by continuous flow processes for the synthesis of macrocycles.[9] In general, the macrocyclizations considered took place through either intermolecular or intramolecular bond formation enabled by transition metal catalysts. Hence, carbon−carbon bond forming macrocyclizations have been achieved by a Glaser−Hay coupling,[10] or by an azide−acetylene cycloaddition reaction at high temperature, which did not proceed under batch conditions.[11] In the case of intermolecular macrocyclizations, different chiral and achiral pyridino-18-crown-6 ethers were synthesized by alkylation of various alcohols in the presence of pyridine diiodides in a continuous-flow Williamson type synthesis using KOH as the base in a packed bed reactor. This provided a cheaper and less dangerous method with higher yields and in shorter times than the ones reported using NaH as a base in batch conditions.[12]

In a similar manner, the use of a K_2CO_3 packed bed reactor enabled the preparation in high yields and high purities of C_2-symmetric chiral PyBox. The macrocyclization reaction relied on amide formation of chlorinated chelidamic acids in the presence of different amino alcohols, and the results obtained by flow processes were not attainable under batch conditions.[13] Continuous flow methodologies have also been applied for the preparation of cage molecules via a 3-

fold homocoupling macrocyclization reaction or by dynamic covalent imine forming reactions.[14,15] These reduced number of precedents suggest that continuous flow methodologies pave the way to develop more efficient macrocyclization reactions. The success of this underexploited approach is based on the precise control of reagent concentration via static mixers, the use of supported reagents and catalysts, and the superior heat and mass transfer only achievable under flow conditions. As such our efforts have been devoted to developing a continuous flow methodology for the preparation of constrained macrocyclic pseudopeptides.

4.1.3. Experimental section

General.

NMR experiments were carried out at 400 or 300 MHz for ^{1}H and 100 or 75 MHz for [13]C. Chemical shifts are reported in ppm from tetramethylsilane using the solvent resonance as the internal standard. FT-IR spectra were recorded using an ATR adapter. HRMS were recorded with a Q-TOF instrument. Optical rotation was determined with a digital polarimeter (Na: 589 nm). Melting points were measured using a standard apparatus and are uncorrected. Unless otherwise stated, all reagents were commercially available and not purified before use. The pseudopeptidic reagent **2** was prepared following literature procedures.[23]

*General procedure for synthesis of compound **1b**.*

The aromatic reagent **1b** was obtained according to literature procedures (Scheme S2).[21] The overall yield for the reaction was 22% (3.765 g). Characterisation: IR (ATR) 2960, 1434, 1274, 1020, 632 cm^{-1}; ^{1}H NMR (400 MHz, CDCl$_3$) δ 4.76 (s, 8H), 4.16 (t, J = 6.6 Hz, 4H), 1.89−1.94 (m, 4H), 1.58−1.62 (m, 4H), 1.05 (t, J = 7.4 Hz, 6H); ^{13}C{^{1}H} NMR (100 MHz, CDCl$_3$) δ 153.8, 133.4, 75.1, 32.5, 23.4, 19.3, 14.1. The structure of the compound was confirmed by single crystal X-ray diffraction (Figure S4.10: see also Table S4.1 in Supplemental CD). CCDC number: 2084454.

*General procedure for synthesis of compound **4**.*

The macroporous Merrifield resin (5.00 g, 5.5 mmol Cl/g, 27.5 mmol of Cl) was introduced in a round-bottom flask (50 mL). DMF (10 mL) and diethylamine (17.1 mL, 165 mmol) were then added, and the mixture was heated at 80 °C on a heating mantle with gentle stirring overnight. The reaction crude was filtered off under a vacuum and the resin was washed with DMF (3×), MeOH (3×), and CH_2Cl_2 (3×). After vacuum drying at 50 °C for 5 h, 5.71 g of resin were obtained (95%, 26.1 mmol of amine). Characterisation: absence of C−Cl band (1264 cm^{-1}) in the FT-IR spectrum (Figure S4.11); the full absence of C−Cl bonds was also confirmed by a negative NBP test (Figure S4.12);[24] Calcd %N for full conversion 6.4%; Exp. 6.6%. TGA decomposition temperature >350 °C.

*General procedure for synthesis of compound **5**.*

Resin **4** (1.5 g, 6.9 mmol) was introduced in a round-bottom flask (25 mL). DMF (4 mL) and n-bromobutane (3.0 mL, 27.6 mmol) were added and the mixture was heated at 80 °C on a heating mantle with gentle stirring overnight. The reaction crude was filtered off under a vacuum and the resin was washed with DMF (3×), MeOH (3×), and CH_2Cl_2 (3×). After vacuum drying at 50 °C for 12 h, 2.74 g of resin were obtained (97%, 26.1 mmol of ammonium salt). Characterisation: appearance of a broad band at 2800−2200 cm^{-1}, representative of ammonium salts (Figure S4.13); negative NBP test (Figure S4.14);[24] Calcd %N for full conversion 4.1%, Exp. 4.4%. TGA decomposition temperature >200 °C.

Batch syntheses.

*Synthesis of **3a** using Cs_2CO_3 as the base.* Pseudopeptide **2** (132 mg, 0.512 mmol) and **1a** (242 mg, 0.512 mmol) were dissolved in acetonitrile (255 mL), and Cs_2CO_3 (1000 mg, 3.069 mmol, 6 equiv) was added. The reaction mixture was refluxed on a heating mantle with magnetic stirring for 3 h, and then the solvent was evaporated under a vacuum. The resulting residue was treated with distilled water, centrifuging

the final suspension at 3000 rpm for 8 min to afford pure **3a** as a solid. Yield: 167 mg (0.434 mmol, 85%). For complete characterisation see ref 16.

*Synthesis of **3a** using **4** as the base.* Pseudopeptide **2** (197 mg, 0.765 mmol) and **1a** (362 mg, 0.765 mmol) were dissolved in acetonitrile (383 mL), and the supported base **4** (1000 mg, 4.588 mmol, 6 equiv) was added. The reaction mixture was refluxed on a heating mantle with gentle magnetic stirring for 2.5 h, and then the basic resin was filtered off. The resulting residue was evaporated under a vacuum to yield pure **3a** as a yellowish solid. Yield: 241 mg (0.627 mmol, 82%).

*Synthesis of **3b** using Cs_2CO_3 as the base.* Pseudopeptide **2** (132 mg, 0.512 mmol) and **1b** (304 mg, 0.512 mmol) were dissolved in acetonitrile (255 mL), and Cs_2CO_3 (1000 mg, 3.069 mmol, 6 equiv) was added. The reaction mixture was refluxed on a heating mantle with magnetic stirring for 6 h, and then the solvent was evaporated under a vacuum. The resulting residue was treated with distilled water, centrifuging the final suspension at 3000 rpm for 8 min, and the resultant solid was purified by flash chromatography using $MeOH:CH_2Cl_2$ as the eluent. Yield: 8 mg (0.015 mmol, 3%). Characterisation: $[\alpha]_D^{25}$ +9.6° (c = 0.1, MeOH); IR (ATR) 3310, 1645, 1523, 1290, 1239 cm^{-1}; ^1H NMR (400 MHz, CDCl$_3$) δ 5.71 (s, 1H), 4.34 (d, J = 15.1 Hz, 1H), 4.21 (d, J = 14.5 Hz, 1H), 3.95 (d, J = 15.3 Hz, 1H), 3.81−3.91 (m, 3H), 3.24−3.21 (m, 1H) 3.13−3.10 (m, 1H), 2.36 (d, J = 10.0 Hz, 1H), 2.06−2.11 (m, 1H), 1.61−1.65 (m, 2H), 1.43−1.45 (m, 2H), 1.09 (d, J = 6.7 Hz, 3H), 0.95 (t, J = 7.3 Hz, 3H), 0.79 (d, J = 6.5 Hz, 3H); $^{13}C\{^1H\}$ NMR (100 MHz, CDCl$_3$) δ 173.2, 145.9, 134.2, 133.4, 72.6, 59.7, 52.9, 41.1, 32.3, 30.6, 20.0, 19.7, 19.3, 14.0; HRMS (ESI/Q-TOF) m/z [M + H]$^+$ calcd for $C_{30}H_{48}N_4O_4$, 529.3754, found 529.3752.

*Synthesis of **3b** using **4** as the base.* Pseudopeptide **2** (197 mg, 0.765 mmol) and **1b** (454 mg, 0.765 mmol) were dissolved in acetonitrile (383 mL), and the supported base **4** (1000 mg, 4.588 mmol, 6 equiv) was added. The reaction mixture was refluxed on a heating mantle with gentle magnetic stirring for 6 h, and then the basic resin was filtered off. The resulting residue was evaporated under a vacuum, and the resulting

solid was purified by flash chromatography using MeOH:CH₂Cl₂ as the eluent (Tables S4.2 and S4.3 in Supplemental CD). Yield: 12 mg (0.023 mmol, 3%).

*Synthesis of **6** using **4** as the base.* Pseudopeptidic intermediate **6** could be isolated and fully characterised from the chromatographic protocol of the reaction between **2** and **1b**. Characterisation: $[\alpha]_D^{25}$ −6.8° (c = 0.1, MeOH); IR (ATR) 3298, 1636, 1542, 1262, 653 cm⁻¹; ¹H NMR (400 MHz, CDCl₃) δ 7.18 (s, 1H), 4.74−4.83 (m, 2H), 4.15−4.17 (m, 1H), 3.84−3.86 (m, 1H), 3.66−3.72 (m, 2H), 3.35−3.37 (m, 1H), 3.00 (d, J = 4.7 Hz, 1H), 1.82−1.84 (m, 2H), 1.53−1.59 (m, 2H), 1.04 (d+t, J = 6.6, 5.7 Hz, 6H), 0.93 (d, J = 6.8 Hz, 3H); ¹³C{¹H} NMR (100 MHz, CDCl₃) δ 173.6, 154.0, 134.5, 132.0, 75.5, 71.8, 46.1, 32.7, 31.7, 23.9, 19.9, 19.4, 18.6, 14.1; HRMS (ESI/Q-TOF) m/z [M + H]⁺ calcd for $C_{30}H_{50}Br_2N_4O_4$, 689.2277, found 689.2286.

Kinetic profiles.

Each reaction was performed in a twin-neck round-bottom flask on a heating mantle. Different aliquots were withdrawn from the flask at the desired times and injected in a HPLC instrument in order to determine the conversion of the aromatic reagent **1a** or **1b**, with the appropriate calibrates

Flow equipment.

Syringe pumps from kdScientific and Hamilton 25 mL syringes were used. Glass Omnifit columns with variable length and an internal diameter of 0.7854 cm were used as the reactor. For the scale-up experiment, an ISMATEC-REGLO Digital peristaltic pump was used to pump the reagents with a total flow of 1160 μL/min. The reactor could be kept at 80 °C by recirculating water with a Julabo F-83 instrument.

Flow optimization.

Stock solutions (4 mM) of the different reagents were accurately prepared in 500 mL volumetric flasks. These solutions were separately introduced in the system with two syringe pumps and were mixed before the reactor with a T-shaped piece.

The resultant 2 mM reaction mixture was run through an Omnifit (006RG-10-10) column packed with 1000 mg of **4**, resulting in a 2.16 mL basic reactor. This column was immersed in a 500 mL beaker and thermostatted with water at 80 °C (Figure S4.15). Adjusting the flows provided by the syringe pumps, the effect of the residence time could be elucidated. All the residence times were determined with the breakthrough of compounds. The final solutions were injected in the HPLC instrument to determine the effectiveness of the reaction.

Flow-distillation methodology.

A distillation setup was easily connected to the flow system described in the "Flow optimization" section. The tubing at the exit of the reactor was introduced into a 100 mL twin-neck round-bottom flask through one of the necks of the flask. A distillation setup was mounted in the other neck of the flask, allowing the solvent to be recovered in a separate flask, and reused for the preparation of new stock solutions (Figure S4.16). The temperature of the distillation flask on a heating mantle was set at 95 °C, so the distillation temperature was stabilized at 81 °C to yield pure acetonitrile in almost a stationary regime. For **1a**, at the end of the process, crystals of pure **3a** were recovered from the distillation flask. In the case of **1b**, the resultant brownish solid residue of the distillation was purified by flash chromatography to afford pure **3b**.

Flow syntheses.

*Flow Synthesis of **3a**.* The solutions of **1a** and **2** in acetonitrile (4 mM) were pumped through an Omnifit (006RG-10- 10) column packed with 1000 mg of **4** for 10 h. This column was immersed in a 500 mL beaker with water at 80 °C. The residence time was set to 10.7 min by adjusting the total flow to 200 μL/min. While the solvent outcoming from the reactor was being distilled, the formation of crystals could be observed at the bottom of the distillation flask. After recovering and drying off the crystals, pure **3a** was obtained (63 mg, 69% yield, 0.165 mmol). With this system, 85% of the acetonitrile pumped through the system was recovered.

Flow Synthesis of **3b**. The solutions of **1b** and **2** in acetonitrile (4 mM) were pumped through an Omnifit (006RG-10-10) column packed with 1000 mg of **4** for 10 h. This column was immersed in a 500 mL beaker with water at 80 °C. The residence time was set to 10.7 min, by adjusting the total flow to 200 µL/min. After 10 h, the resultant brownish solid was purified by flash chromatography, using MeOH:CH$_2$Cl$_2$ as eluent to yield **3b** as a white solid (Tables S4.4 and S4.5 in Supplemental CD). Yield: 24 mg (0.045 mmol, 19%).

Scaled-up Flow Synthesis of **3a**. The solutions of **1a** and **2** in acetonitrile (4 mM) were pumped through an Omnifit (006EZ-10-33- AF) column packed with 6000 mg of **4** for 17 h. The reactor was kept at 80 °C by recirculation of water around the reactor (Figure S4.17). The residence time was set to 10.7 min, by adjusting the total flow to 1160 µL/min. The resulting residue was evaporated under a vacuum to yield pure **3a** as a yellowish solid (891 mg, 2.319 mmol, 98% yield).

Crystal structures.

Single crystals suitable for X-ray crystallography were obtained by slow evaporation of an acetonitrile solution of **1b**. A suitable crystal was selected and mounted on a SuperNova, Dual, Cu at zero, Atlas diffractometer. The structure was solved with the SHELXT 2014/5[25] structure solution program and refined with the SHELXL-2018/3[26] refinement package. Artwork representations were processed using MERCURY[27] software.

4.1.4.   Results and discussion

We have recently reported a highly selective anion-templated synthesis of a conformationally constrained pseudopeptidic macrocyclic cyclophane (**3a**).[16] The optimal preorganization of the reagents and the intermediate, together with the positive template effect of the bromide anion, provided an efficient macrocyclization reaction with excellent yield and selectivity (higher than 95%) in CH$_3$CN using Cs$_2$CO$_3$ as the base. This macrocyclic system can act as an efficient organocatalyst

for the conversion of CO_2 under relatively mild conditions.[17] In an attempt to develop new structures of this family, the synthesis of **3b** was attempted under batch conditions, although unsuccessfully. Most likely, the lower macrocyclization efficiency attained when using **1b** is the result of the steric hindrance provided by the additional groups on the aromatic scaffold. In the search of alternative approaches and to provide an easier scale-up for the synthesis of these pseudopeptidic macrocyclic cyclophanes (**3**), the use of flow chemistry was considered.

Although the use of packed bed reactors using inorganic bases has been formerly reported,[12,13] the partial solubility of Cs_2CO_3 in CH_3CN hampered this approximation, as some leaching could not be avoided. Thus, to develop this macrocyclization under continuous-flow, the design of an appropriate immobilized base to substitute the Cs_2CO_3 was envisaged. Among the different solid supported bases,[18] the polymer immobilized tertiary amine **4** was selected as it was easily obtained by modification of a Merrifield resin (chloromethyl polystyrene-divinylbenzene macroporous resin, 5.5 mmol Cl/g nominal loading) with diethylamine (see Scheme S4.1 and Figures S4.11 and S4.12 for the synthesis and characterisation of **4**). The efficiency of this supported base was initially evaluated in the macrocyclization reaction between **2** and **1a** under batch conditions (Scheme 4.1) in the presence of **4** instead of Cs_2CO_3 (6 equiv in both cases).

1a: R = -H
1b: R = -O-$(CH_2)_3$-CH_3

2

4

3a: R = -H
3b: R = -O-$(CH_2)_3$-CH_3
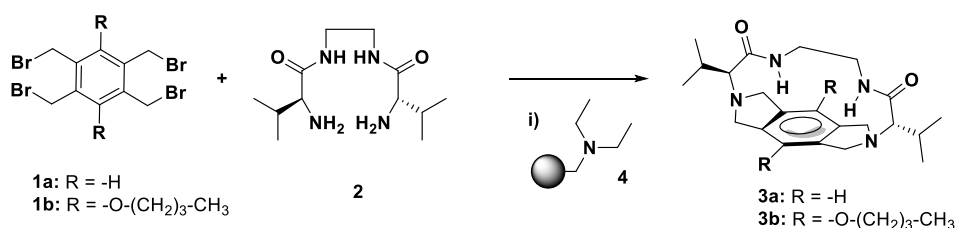
Scheme 4.1. Macrocyclization reaction between **1a-b** and **2**. i) 3 h, 80 ºC, 6 equivalents of base in CH_3CN, 2 mM.

After 3 h of reaction, the crude was filtered off and the solvent was removed under a vacuum, affording pure **3a** in 82% isolated yield. The supported base was straightforwardly recovered from the reaction crude and analysed by IR

spectroscopy. The FT-IR-ATR spectrum of the used base showed the appearance of a broad band at $2800-2400$ cm^{-1} corresponding to the formation of ammonium salts (Figure S4.1).[19] The reactivation of the protonated resin could be attained by simply washing the resin with a 0.5 M KOH methanolic solution, observing the disappearance of the ammonium broad bands in the IR spectrum (Figure S4.1). The base could be used again in the macrocyclization reaction for 15 runs without any decrease in the efficiency. These initial results support the use of **4** as suitable replacement of Cs$_2$CO$_3$. Indeed, when the kinetic profiles of the reaction in the presence of **4** or Cs$_2$CO$_3$ were compared, a slightly faster profile was obtained using **4** instead of Cs$_2$CO$_3$, reaching NMR yields higher than 90% in 2 h (Figure S4.2).

Once the efficiency of **4** as a supported base was proved for the macrocyclization under batch conditions, its behaviour under continuous-flow conditions was evaluated. The experimental setup is shown in Figure 4.1 (see also Figure S4.15).
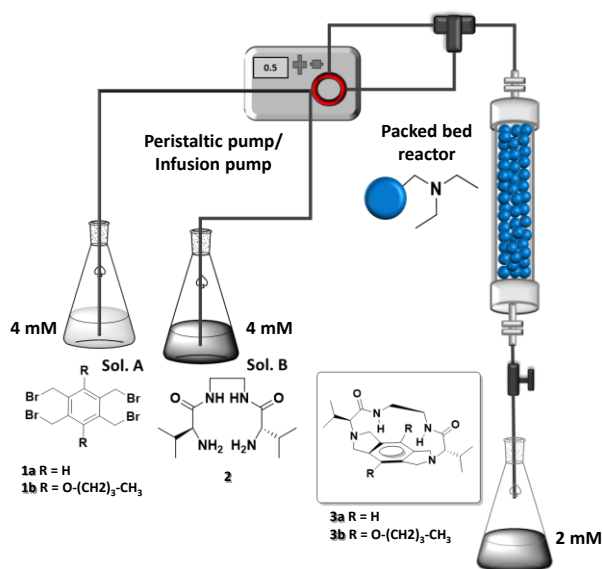
Figure 4.1. Schematic representation of the flow set-up for the continuous flow macrocyclization. Solution A: **1**, 4 mM in CH$_3$CN. Solution B: **2**, 4 mM in CH$_3$CN. Infusion pumps were generally used for the experiments. Peristaltic pumps were used for scale-up experiments.

The two reagents (4 mM solutions in CH_3CN) were pumped separately (solutions A and B) and mixed before entering the packed bed reactor. Noteworthy, if both reagents were mixed before pumping, part of the initial bis(aminoamide) **2** acted as the base. This led to the formation of the desired macrocycle but also to the precipitation of corresponding dishydrobromide salt of **2** with the blockage of the flow reactor. It should also be pointed out that a higher concentration of the reagents reduced the efficacy of the macrocyclization and led to precipitation of the final macrocycle. Thus, the final concentration at the mixing point was fixed to 2 mM in CH_3CN.

The reaction mixture was pumped through a packed bed reactor loaded with the supported base **4** (4.7 mmol amine/g) at different flow rates while heated at 80 °C. Table 4.1 illustrates the results obtained. The use of a 1000 µL/min flow rate (entry 1, Table 4.1) led to promising NMR yields of 69% with only 2.1 min of residence time, demonstrating the suitability of the reaction setup to convert the reagents into the desired macrocycle. The increase in residence time from 2.1 to 10.7 min by reducing the total flow rate from 1000 to 400 µL/min (entries 1 to 3, Table 4.1) resulted in progressive increments of the NMR yields of the desired [1 + 1] cyclic pseudopeptide **3a**.

Table 4.1. Optimization for the Macrocyclization between **1a** and **2** under flow conditions.[a]

Entry	Total flow (µl/min)[b]	Residence time (min)	Yield (%)[c]
1	1000	2.1	69
2	700	3.1	79
3	400	5.4	91
4	200	10.7	99

[a] All the experiments were carried out for 1 gram of basic resin **4**. Column volume: 2.16 mL.
[b] Total flow rate corresponds to equal flow rates of each reagent to maintain a ratio of 1:1. [c] ¹H NMR yields. Yields calculated for aliquots taken after pumping a volume of reagents equal to at least three times the packed void volume of the reactor.

To our delight, a 99% NMR yield was attained for a total flow of 200 µL/min using a reactor of only 2.16 mL (entry 4 in Table 4.1). This result is outstanding as

under batch conditions, reaction times of ca. 2 h are required to achieve a similar yield.

To assess the macrocyclization efficiency under batch and flow conditions, the volumetric productivity per gram of base for both systems was calculated considering the yields of the isolated product (see Experimental Section for details). Remarkably, comparing the productivity of the flow-based process (4.303 g_{3a}/g_{base}·L·h) with the ones obtained in batch conditions using either Cs_2CO_3 (0.216 g_{3a}/g_{base}·L·h) or the supported base **4** (0.252 g_{3a}/g_{base}·L·h) indicated an almost 20- time increase on productivity in favour of the flow process (Figure 4.2).
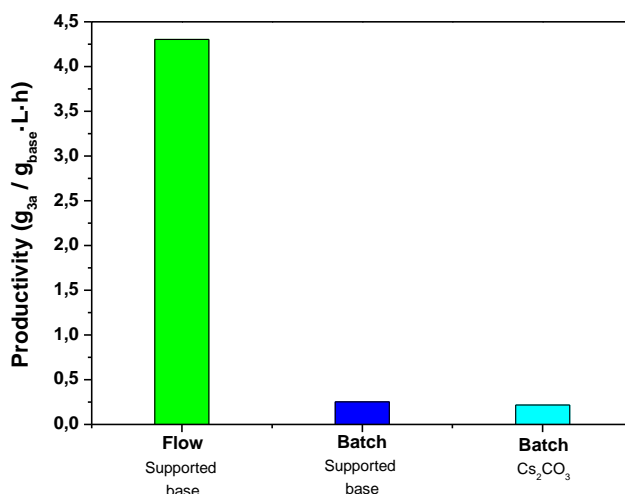
Figure 4.2. Productivities obtained using acetonitrile as solvent (2 mM final concentrations of **1a** and **2**) at 80 °C. Batch conditions: caesium carbonate (light blue), **4** (blue); flow conditions with **4** (green). Reaction times: 10.7 min for flow conditions, 2.5 h for batch conditions using **4**, and 3 h for batch conditions using Cs_2CO_3.

This enhancement on the reaction productivity is likely to be related with the higher local concentration of the base in the flow setup. For instance, in the reactor of 2.16 mL, at a flow rate of 200 µL/min, an instant ratio of 1300 mol of base/mol of **2** can be achieved, while in the batch process the ratio was fixed to 6 mol of base/mol of **2**. A second possible effect can be attributed to the formation of the corresponding supported salt bromide (R₃NHBr) during the process. This salt can play a double role, as previously demonstrated for this macrocyclization.[16] The

bromide anion acts as an efficient template facilitating the [1 + 1] macrocyclization process. The strong intramolecular associations of the open-chain intermediate through $NH_{amide} \cdots Br^- \cdots NH_{amide}$ hydrogen bonds provide its appropriate folding favouring macrocyclization and thus hampering oligomerization reactions. Additionally, the bromide salt can enhance the kinetics of the macrocyclization by increasing the nucleophilic character of the terminal amino groups of **2**.

To analyse the effects of the supported base and its conjugated acid formed during the reaction, the macrocyclization process was studied at moderate yields of **3a**. Figure 4.3 shows the evolution of reaction profile in terms of yield of **3a** *vs* the time on stream (TOS) obtained by pumping the reagents (total flow = 400 µL/min) through a packed bed reactor of 0.87 mL (packed void volume; residence time = 2.2 min). The results showed that at early times on stream the reaction achieves an NMR yield of ca. 70%. The high excess of the base in comparison with the pseudopeptide **2** is likely to contribute to this good yield in a short contact time (2.2 min). As the time on stream increases, the basic supported reagent is consumed and transformed into its corresponding conjugated acid. Thus, a steady decrease in activity after a certain time on stream should be expected. However, a significant increase on the NMR yield was observed during the first 7 h of continuous production of macrocycle **3a**, rendering a maximum value of 81% after 450 min on the stream. This initial steady enhancement of the NMR yield with time can be attributed to the generation of the ammonium bromide salts, triggering the template-assisted macrocyclization.[16] It must be noted that this maximum represents the optimal ratio between the amount of base needed for the process to occur efficiently and the amount of bromide template favoring the macrocyclization. After this point, the amount of ammonium bromide continues increasing with the concomitant decrease in the amount of available base. This leads to a decrease in NMR yield. Such a decrease is initially slow, between 450 and 725 min, showing a slope similar but with opposite sign to the one observed from 0 to 450 min. Overall, during this first stage (0−725 min, orange in Figure 4.3) the system is quite efficient as the concentration of both participant

species, the base and the bromide salt, are kept sufficiently high as compared to that of the reagents pumped.
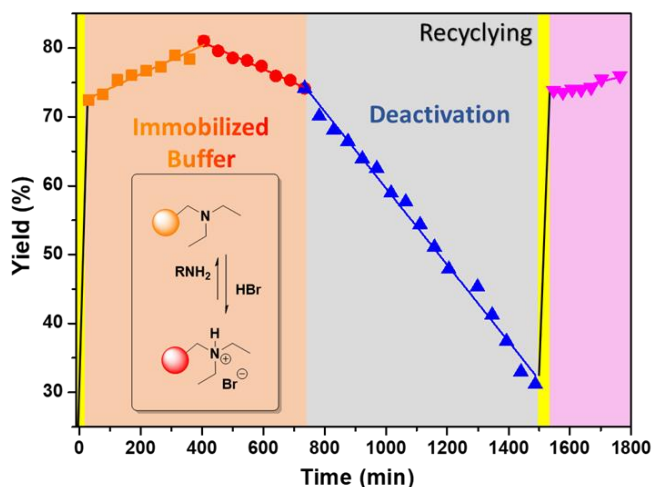
Figure 4.3. Macrocyclization yield of **3a** *vs* TOS. The ranges marked in yellow correspond to the loading of the reagents in the reactor and the reactivation process. The area highlighted in orange is assigned to the regime in which concentration of the NR_3 / R_3NHBr supported species are high enough. Time ranges in grey correspond to the deactivation of the supported base. The time range marked in pink corresponds to the macrocyclization after the reactivation of the basic resin, being comparable to the situation in the first (orange) stage Conditions: 400 μL/min (2 mM) for 2.2 minutes. Yields for **3a** were determined by ^{1}H NMR.

After 750 min on stream, the concentration of the basic sites onto the support becomes too small, and the NMR yields suffer a more drastic decrease with time until reaching a value of only ca. 35% after 1500 min. At this point, the amount of reagents fed to the reactor corresponded to the theoretical value of base loaded. At this time, the flow of the reagents was stopped and 30 mL of a 0.5 M solution of KOH in methanol was pumped through the reactor at 1000 μL/min, allowing to fully recover the supported base (as previously corroborated in Figure S4.1). When the pumping of the reagents was restarted, similar yields to those initially observed were obtained (pink region in Figure 4.3).

In the view of these results, and to prove the positive effect produced by the in-situ generation of the bromide ammonium salt, a packed bed reactor was loaded with a polymer cocktail,[20] containing an equimolar mixture of supported amine (**4**) and an

analogous supported bromide salt (**5**, Scheme S4.1). The macrocyclization was carried out under the same conditions reported above. The efficiency of the system, in terms of productivity, for the initial 150 min was constant and as high as the best obtained for the initial setup using only the supported base **4**. After a certain period, the productivity of the system decayed in a similar way to that previously observed for the supported base **4** (Figure S4.3). These results confirmed that the presence of the supported bromide enhanced the efficiency of the macrocyclization reaction.

Encouraged by these improvements, the continuous flow synthesis of an analogous pseudopeptidic macrocycle **3b** was also evaluated. The macrocyclization reaction between **2** and **1b** was more challenging due to the electronic and steric factors introduced by the presence of the butoxy groups. Compound **1b** was obtained as reported in the literature with a 22% yield (Scheme S4.2).[21] Indeed, under batch conditions, even when the macrocycle **3b** could be isolated and fully characterised by spectroscopic techniques, only a poor isolated yield (3% of **3b**) was obtained. The lower macrocyclic efficiency can be attributed to the poorer preorganization of the reaction intermediate **6** in which only one of the terminal amino groups of **2** had reacted with two adjacent bromomethyl groups of 1b (Scheme 4.2). This favours the intermolecular reactions instead of the intramolecular process, resulting in a wide range of oligomeric/ polymeric side products detected by MS, NMR, and flash chromatography (Figure 4.4 and Figure S4.4) with a poor selectivity toward the desired macrocycle (Table 4.2).
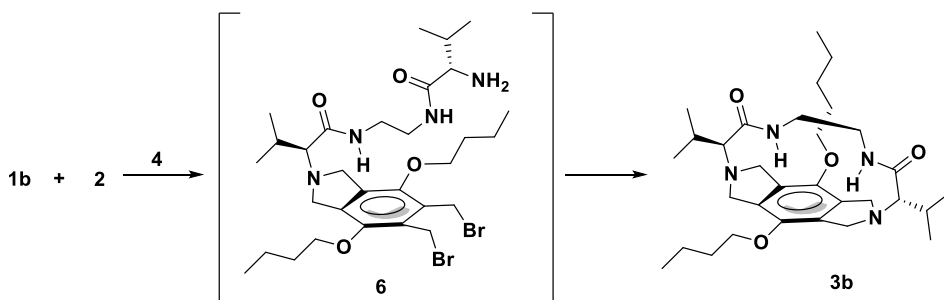
Scheme 4.2. Macrocyclization reaction between **1b** and **2**. Reaction conditions: 3 h, 80 °C, 6 equiv of **4** in CH$_3$CN, 2 mM in **1b** and **2**.
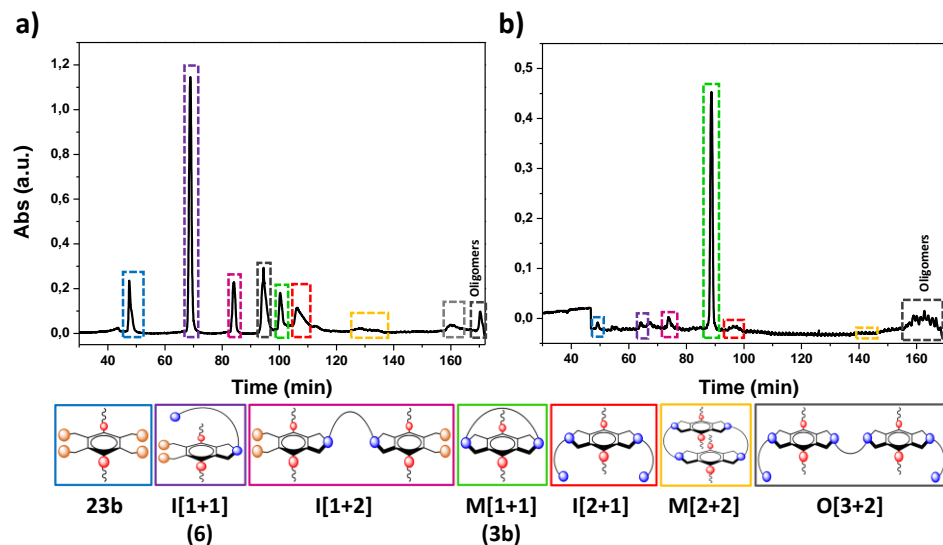
Figure 4.4. Flash chromatograms (UV-wavelength: 220 nm) obtained for the purification of the crude of the macrocyclization reaction between **2** and **1b**, using CH_2Cl_2 and MeOH as the eluents. The predominant component of each fraction has been highlighted. Peaks in green correspond to the desired [1 + 1] macrocycle **3b**. a) Batch conditions. b) Continuous flow system.

Clear evidence of the reduced macrocyclization efficiency for **3b** was the detection and isolation in a ca. 5% yield of the open-chain [1 + 1] intermediate **6** (Table 4.2 and Scheme 4.2). In the case of the cyclization between **1a** and **2**, the analogous intermediate could not be detected nor isolated, as the preorganization of the reagents and the template and catalytic effect of the bromide permitted the four substitution reactions to take place almost simultaneously.[16]

When the reaction was performed following the same optimization protocol described for the synthesis of **3a** under flow conditions, using **4** as supported base, a significant increase in the conversion of **1b** was observed, as compared with the one attained under batch conditions (Figure S4.5). In fact, conversions above 95% were obtained using a flow rate of 200 µL/min, corresponding with a residence time of 10.7 min, while the conversion under batch conditions was only 70% after 1 h. This remarkable acceleration of the reaction led to a reduced number of side products (Figure 4.4 and Table 4.2). Again, the higher actual concentration of base and the

presence of the bromide anions must contribute to this improved performance. The 19% isolated yield obtained for **3b**, under flow conditions, represents a ca. 6-time improvement in comparison with the yield obtained under batch conditions (3%).

Table 4.2. Comparison of the product distribution obtained under batch and flow conditions for the reaction between **1b** and **2**.[a]

Entry	Product	Product distribution (%)	
		Batch	*Flow*
1	I [1+1] (**6**)	5	1
2	I [1+2]	4	2
3	M [1+1] (**3b**)	5	20
4	I [2+1]	19	3
5	M [2+2]	7	2
6	O [3+2]	8	2
7	Oligomers/Polymers	42	60
8	Others	10	10

[a] I = intermediate, M = macrocycle, O = oligomer. Numbers in brackets [n+m] correspond to the stoichiometric factor for **2** (n) and **1b** (m); See Figure 4.4 for the identification of the different species. [b] Product distribution calculated after separation and purification by flash chromatogram using CH_2Cl_2 and MeOH as the eluents. Product distribution for the impure fractions has been calculated as their most abundant component identified by ESI-MS(+) and/or ^{1}H NMR. Batch conditions: 3 h, 80 °C, 6 equivalents of **4** in CH_3CN, 2 mM in **1b** and **2**. Flow conditions: total flow 200 μL/min, 80 °C, CH_3CN (2 mM final concentration), residence time: 10.7 min.

This led to remarkable higher productivities. Whereas the productivity under batch conditions for the synthesis of **3b** using **4** as supported base was 0.014 $g_{3b}/g_{base}·L·h$, it could be increased up to 1.126 $g_{3b}/g_{base}·L·h$ with the continuous flow methodology, corresponding to a ca. 80-time increase. These results highlight how the continuous flow processes can be exploited for enhancing the yield, selectivity, and productivity of the macrocyclization reactions in comparison with the reaction under batch conditions.

The continuous flow process also provided significant advantages for the simple production of the macrocycle at the gram scale. When a 3-time scale-up of the macrocyclization under batch conditions was assayed, a reduction of the isolated yield

of **3a** from 85% to 43% was observed. However, under flow conditions, using a reactor of 12.4 mL loaded with 6 g of the supported base **4** and a total flow (provided by a peristaltic pump) of 1160 µL/min for 17 h, it was possible to synthesize up to 0.891 g of **3a**, corresponding with a 98% isolated yield (see Experimental Section for additional details).

The continuous flow macrocyclization process enabled by the supported base opens the possibility to integrate, in a single process, the synthesis of the macrocycle, its purification, and the separation and reuse of the solvent used in excess. This integration may contribute to increase the sustainability of the process even when high-dilution conditions are used. With this idea in mind, the continuous flow system was coupled with a distillation setup (Figure 4.5).
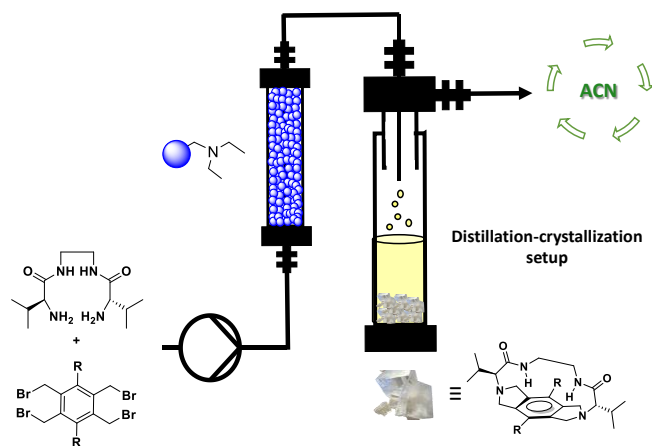
Figure 4.5. Integration into the flow process of a distillation-crystallization set-up for the synthesis of constrained pseudopeptidic macrocycles. The amount of acetonitrile recovered (up to 85%) was used to form the subsequent reagent solutions.

This simple setup allowed to obtain a stationary stream of high purity recovered solvent (Figure S4.6). The average distillation flow of the distillation stream was of 198 µL/min, in good agreement with the macrocyclization flow input (200 µL/min). The total recovery over the time on stream reached up to 85% as some solvent remained on the distillation device. Additionally, the continuous distillation of the solvent afforded a continuous increase in the concentration of the macrocycle in the final solution. This resulted in the formation of crystals in the distillation flask

(Figures S4.7 and S4.8). The chemical composition of the crystals was determined by NMR and IR analyses, indicating that the only product formed was **3a** with a 69% isolated yield (Figure S4.9).

Inspired by former environmental metrics,[22,28] a simple and new metric that simultaneously accounts for the macrocyclization efficiency in terms of productivity and waste generated during the synthesis and isolation of the macrocycles can be defined. The Macrocyclization Environmental Impact (MEI) can be calculated by Equation 4.1, with the higher the value obtained, the higher the environmental impact of the process.

$$\text{MEI} = \text{E-Factor} / \text{Productivity} \quad (g_{waste} \times L \times h / g_{macrocycle}^2) \quad \text{(Eq. 4.1)}$$

In this equation the amount of waste should include the residues generated in both the synthesis and the isolation of the macrocycle. The productivity will be the grams of products obtained divided by the reactor volume (L) and time (h). As evidenced by the equation, the ideal scenario would be to have a macrocyclization with low E-Factor and high productivity, yielding modest MEI values.

In general, the higher is the amount of waste generated per gram of macrocycle the higher the MEI value would be, emphasizing the need to decrease the waste produced. This is of major importance in macrocyclizations, where large amounts of solvent waste are generated due to the low concentrations required and to the tedious purification protocols generally involved. Hence, the cost and CO_2 footprint associated with purchasing, evaporating, and disposing such additional volume of solvent is indirectly considered, as well as the larger equipment and safety issues related with its handling. Another drawback of employing high-dilution conditions is the prolonged reaction times often needed for attaining high macrocyclization yields, significantly reducing the productivity for the whole process. In the light of these considerations, the MEI score must take into account the dilution and time

requirements to achieve the optimised yield, with the higher these parameters are, the lower the macrocyclization efficiency, and, therefore, the higher the score of the MEI.

In order to validate the applicability of the proposed metric, we evaluated the environmental implications for the different approaches discussed in this chapter (Table 4.3). For instance, a remarkable decrease of 1 order of magnitude for the E-Factor was observed when comparing the batch and flow syntheses of **3a** (see entries 1−3 in Table 4.3), illustrating the advantages of flow-integrated synthesis and isolation. In a similar trend, the coupled flow synthesis-isolation for **3b** resulted in a much lower environmental impact for the macrocyclization (entries 5 and 6, Table 4.3).

Table 4.3. Summary of the macrocyclization efficiencies in terms of productivity and E-Factor obtained for macrocycles **3a** and **3b**.[a]

Entry	Comp.	Meth.	Yield (%)	Productivity $(g_P/L \cdot h)$	E-Factor	MEI $(g_w \cdot L \cdot h/g_P)$
1		Batch	82	0.252	1033	4099
2	**3a**	Flow	98	4.303	1030	239
3		Flow[a]	69	2.977	155	52
4		Batch	3	0.014	371209	26514929
5	**3b**	Batch	3	0.014	1033[b]	73786
6		Flow[a]	19	1.126	155[b]	138

[a] Including reaction, purification or crystallisation, and solvent recovery. [b] The waste generated during the chromatographic purification has not been considered in the waste calculation. Reaction conditions: 80 °C, 6 equivalents of **4** in CH_3CN, 2 mM in **1b** and **2**.

One may realize that E-Factor values did not allow for distinction between the results in entries 1, 2, and 5. In such cases, the MEI scores fostered valuable information. The much lower MEI values obtained in the flow synthesis of **3a** compared with the values for the batch syntheses of **3a** and **3b** permits easy classification of the most damaging macrocyclization. These MEI scores (entry 5 > entry 1 > entry 2) are in good accordance with the productivity trend, with a difference of more than 2 orders of magnitude between the extreme scenarios. In

addition, results presented in entries 1, 4, and 5 (Table 4.3) reveal the drastic environmental implications related with chromatographic protocols. These preliminary results highlight the paramount role of designing novel techniques for increasing the macrocyclization efficiency and selectivity.

4.1.5.   Conclusions

The present results highlight that conducting macrocyclizations in continuous flow can offer several important advantages. This has been illustrated for the flow syntheses of constrained pseudopeptidic macrocycles. The higher productivity and lower environmental impact obtained under flow conditions can be correlated with the more efficient template effect within the packed bed reactor, and with the integration of the isolation and solvent reuse in a simple setup. To the best of our knowledge, this is the first system reported up to date integrating macrocyclization, crystallization with high quality crystals, and solvent recovery under flow conditions. These continuous-flow macrocyclizations can be easily scaled-up by simply pumping the reaction mixture continuously through the reactor for a given period of time. Besides, we have postulated a simple metric for quantification of the macrocyclization environmental impact. The MEI scores seemed to be useful even in the cases where well-established environmental metrics did not allow for scrutinization.

4.1.6.   References

1- Martí-Centelles, V.; Pandey, M. D.; Burguete, M. I.; Luis, S. V. Macrocyclization Reactions: The Importance of Conformational, Configurational, and Template-Induced Preorganization. *Chem. Rev.* **2015**, *16*, 8736-8834.

2- (a) Ziegler, K.; Eberle, H.; Ohlinger, H. Über vielgliedrige Ringsysteme. I. Die präparativ ergiebige Synthese der Polymethylenketone mit mehr als 6 Ringgliedern. *Justus Liebigs Ann. Chem.* **1933**, *504*, 94-130. (b) Ruggli, P. Über einen Ring mit dreifacher Bindung. *Justus Liebigs Ann. Chem.* **1912**, *392*, 92-100.

3- (a) Yang, Y.; Ying, H.; Li, Z.; Wang, J.; Chen, Y.; Luo, B.; Gray, D. L.; Ferguson, A.; Chen, Q.; Z, Y.; Cheng, J. Near quantitative synthesis of urea macrocycles enabled by bulky N-substituent. *Nat. Commun.* **2021**, *12*, article number: 1572. (b) Wu, Z. H.; Hu, T.; He, L.; Gong, B. One-pot formation of aromatic tetraurea macrocycles. *Org. Lett.* **2012**, *14*, 2504-250. (c) Bru, M.; Alfonso, I.; Burguete, M. I.; Luis, S. V. Efficient syntheses of new chiral peptidomimetic macrocycles through a configurationally driven preorganization. *Tetrahedron Lett.* **2005**, *46*, 7781-7785.

4- (a) Bols, P. S.; Anderson, H. L. Template-Directed Synthesis of Molecular Nanorings and Cages. *Acc. Chem. Res.* **2018**, *51*, 2083-2092. (b) Rotger, M. C.; Piña, M. N.; Frontera, A.; Martorell, G.; Ballester, P.; Deyà, P. M.; Costa, A. Conformational Preferences and Self-Template Macrocyclization of Squaramide-Based Foldable Modules. *J. Org. Chem.* **2004**, *69*, 2302-2308.

5- (a) Plutschack, M. B.; Pieber, B.; Gilmore, K.; Seeberger, P. H. The Hitchhiker's Guide to Flow Chemistry. *Chem. Rev.* **2017**, *117*, 11796-11893. (b) Baxendale, I. R.; Ley, S. V.; Smith, C. D.; Tranmer, G. K. A flow reactor process for the synthesis of peptides utilizing immobilized reagents, scavengers and catch and release protocols. *Chem. Commun.* **2006**, *46,* 4835-4837.

6- Luis, S. V.; Garcia-Verdugo, E., Eds.; *Flow Chemistry: Integrated Approaches for Practical Applications*, 1st Ed., RSC publishing: London, 2019.

7- Akwi, F. M.; Watts, P. Continuous flow chemistry: where are we now? Recent applications, challenges and limitations. *Chem. Commun.* **2018**, *54*, 13894-13928

8- Gutmann, B.; Cantillo, D.; Kappe, C. O. Continuous-Flow Technology-A Tool for the Safe Manufacturing of Active Pharmaceutical Ingredients. *Angew. Chem. Int. Ed.* **2015**, *54*, 6688-6729.

9- (a) Ruggeri, M.; Dombrowski, A. W.; Djuric, S. W.; Baxendale, I. R. Rearrangement of 3-Hydroxyazetidines into 2-Oxazolines. *J. Org. Chem.* **2020**, *85*, 7276−7286. (b) Godin, E.; Morin, E.; Collins, S. K. Continuous flow macrocyclization. *Aldrichimica Acta* **2018**, *51*, 35-46. (c) Mifune, Y.; Nakamura, H.; Fuse, S. A rapid and clean synthetic approach to cyclic peptides via micro-flow peptide chain elongation and photochemical cyclization: synthesis of a cyclic RGD peptide. *Org. Biomol. Chem.* **2016**, *14*, 11244-11249.

10- Bédard, A. C.; Régnier, S.; Collins, S. K. Continuous flow macrocyclization at high concentrations: synthesis of macrocyclic lipids, *Green Chem*. **2013**, *15*, 1962-1966.

11- Bogdan, A. R.; James, K. Efficient Access to New Chemical Space Through Flow-Construction of Druglike Macrocycles Through Copper-Surface-Catalyzed Azide-Alkyne Cycloaddition Reactions. *Chem. Eur. J.* **2010**, *16*, 14506-14512.

12- Fodi, T.; Kupai, J.; Túrós, G.; Németh, T.; Rojik, E.; Riethmüller, E.; Balogh, G. T.; Huszthy, P. Application of flow chemistry to macrocyclization of crown ethers. *J. Flow Chem.* **2016**, *6*, 297-301.

13- Battilocchio, C.; Baumann, M.; Baxendale, I. R.; Biava, M.; Kitching, M. O.; Ley, S. V.; Martin, R. E.; Ohnmacht, S. A.; Tappin, N. D. C. Scale-Up of Flow-Assisted Synthesis of C$_2$-Symmetric Chiral PyBox Ligands. *Synthesis* **2012**, *4*, 635-647.

14- Kitchin, M.; Konstas, K..; Sumby, C. J.; Czyz, M. L.; Valente, P.; Hill, M. R.; Polyzos, A.; Doonan, C. J. Continuous flow synthesis of a carbon-based molecular cage macrocycle via a three-fold homocoupling reaction. *Chem. Commun.* **2015**, *51*, 14231-14234.

15- Briggs, M. E.; Slater, A. G.; Lunt, N.; Jiang, S.; Little, M. A.; Greenaway, R. L; Hasell, T.; Battilocchio, C.; Ley, S. V.; Cooper, A. I. Dynamic flow synthesis of porous organic cages. *Chem. Commun.* **2015**, *51*, 17390-17393.

16- Esteve, F.; Altava, B.; Bolte, M.; Burguete, M. I.; García-Verdugo, E.; Luis, S. V. Highly Selective Anion Template Effect in the Synthesis of Constrained Pseudopeptidic Macrocyclic Cyclophanes. *J. Org. Chem.* **2020**, *85*, 1138-1145.

17- Esteve, F.; Altava, B.; Bolte, M.; Burguete, M. I.; García-Verdugo, E.; Luis, S. V. Pseudopeptidic macrocycles as cooperative minimalistic synzyme systems for the remarkable activation and conversion of CO$_2$ in the presence of the chloride anion. *Green Chem.* **2020**, *22*, 4697-4705.

18- Bing, W.; We, M. Recent advances for solid basic catalysts: Structure design and catalytic performance. *J. Sol. State Chem.* **2019**, *269*, 184-194.

19- (a) Socrates, G. *Infrared Characteristic Group Frequencies*. New York, *Wiley*, 1994. (b) Oxton, I. A.; Knop, O. Infrared Spectra of the Ammonium Ion in Crystals. I. Ammonium Hexachloroplatinate(IV) and Hexachlorotellurate(IV). *Can. J. Chem.* **1975**, *53*, 2675-2682.

20- Sans, V.; Gelat, F.; Karbass, N.; Burguete, M. I.; García-Verdugo, E.; Luis, S. V. Polymer Cocktail: A Multitask Supported Ionic Liquid-Like Species to Facilitate Multiple and Consecutive C-C Coupling Reactions. *Adv. Synth. Catal.* **2010**, *352*, 3012-3021.

21- Kawai, H.; Utamura, T.; Motoi, E.; Takahasi, T.; Sugino, H.; Tamura, M.; Ohkita, M.; Fujiwara, K.; Saito, T.; Tsuji, T.; Suzuki, T. Hydrindacene-Based Acetylenic

Macrocycles with Horizontally and Vertically Ordered Functionality Arrays. *Chem. Eur. J.* **2013**, *19*, 4513-4524.

22- Sheldon, R. A. The E factor 25 years on: the rise of green chemistry and sustainability. *Green Chem.* **2017**, *19*, 18-43.

23- Becerril, J.; Bolte, M.; Burguete, M. I.; Galindo, F.; Garcia-España, E.; Luis, S. V.; Miravet, J. F. Efficient Macrocyclization of U-Turn Preorganized Peptidomimetics: The Role of Intramolecular H-Bond and Solvophobic Effects. *J. Am. Chem. Soc.* **2003**, *125*, 6677-6686.

24- Altava, B.; Burguete, M. I.; Galindo, F.; Gavara, R.; Luis, S. V. A Sensitive Colorimetric Method for the Study of Polystyrene Merrifield Resins and Chloromethylated Macroporous Monolithic Polymers. *J. Comb. Chem.* **2004**, *6*, 859-861.

25- Sheldrick, G. M. A short history of SHELX. *Acta Crystallogr. A* **2008**, *64*, 112-122.

26- Sheldrick, G. M. Crystal structure refinement with SHELXL. *Acta Crystallogr. C* **2015**, *71*, 3-8.

27- Macrae, C. F.; Bruno, I. J.; Chisholm, J. A.; Edgington, P. R.; McCabe, P.; Pidcock, E.; Rodriguez Monge, L.; Taylor, R.; van de Streek, J.; Wood, P. A. New Features for the Visualization and Investigation of Crystal Structures. *J. Appl. Crystallogr.* **2008**, *41*, 466-470.

28- Collins, J. C.; James, K. Emac – a comparative index for the assessment of macrocyclization efficiency. *Med. Chem. Commun.* **2012**, *3*, 1489-1495.

4.2. Supporting information
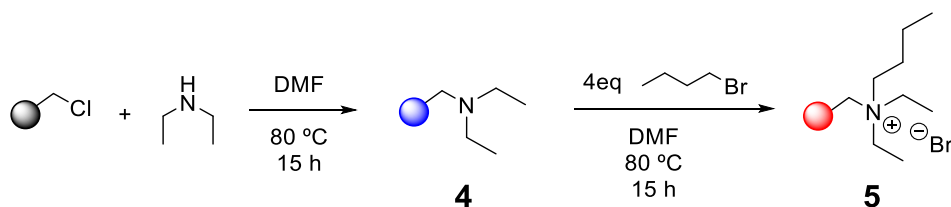
Scheme S4.1. Synthesis of the polymeric supported base (**4**) and template (**5**). The reactions were performed in an orbital stirrer.
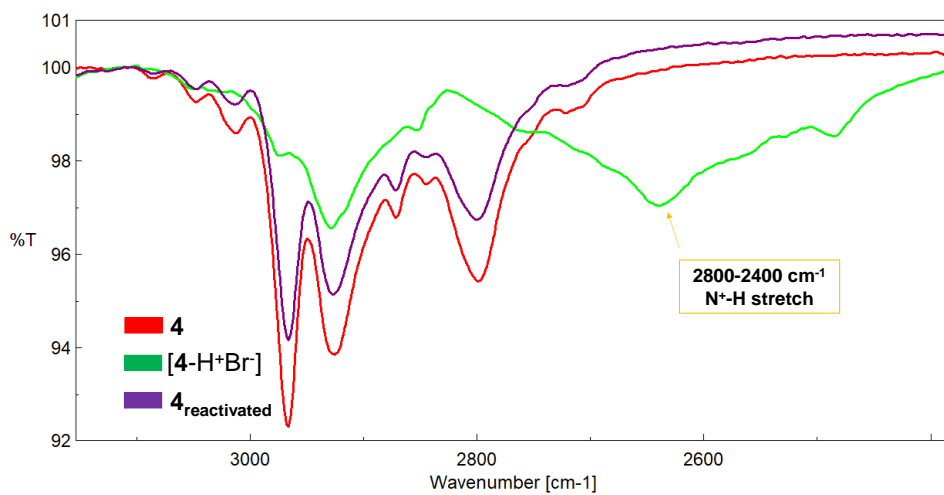
Figure S4.1. Partial IR spectra of **4** (red), the resin after being filtered-off [4-H⁺Br⁻] (green), and the resin after basic treatment **4**reactivated (purple).
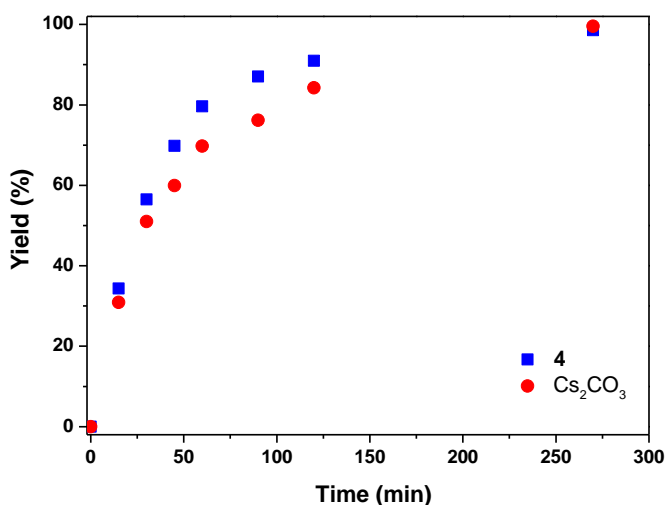
Figure S4.2. Kinetic profiles when using 6 equivalents of **4** (blue) or caesium carbonate (red) under batch conditions, with a selectivity >99% towards **3a**. Reaction conditions: 80 ºC, 2 mM for **1a** and **2** in CH_3CN. Yields for **3a** were calculated by ^1H NMR spectroscopy.
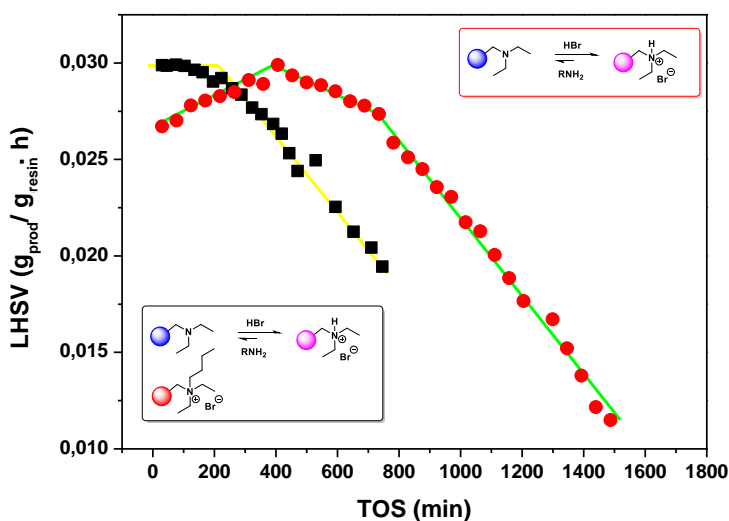
Figure S4.3. Productivity profiles vs time on stream (TOS). a) Red dots: Supported base **4** (1 g). b) black squares: cocktail mixture of **4** and **5** in a 1:1 molar ratio (1g in total). Conditions: 400 mL/min (2 mM in **1a** and **2**) for 2.2 minutes. LHSV calculated using the yields determined by HPLC, the weight of the polymeric resin and the residence time.
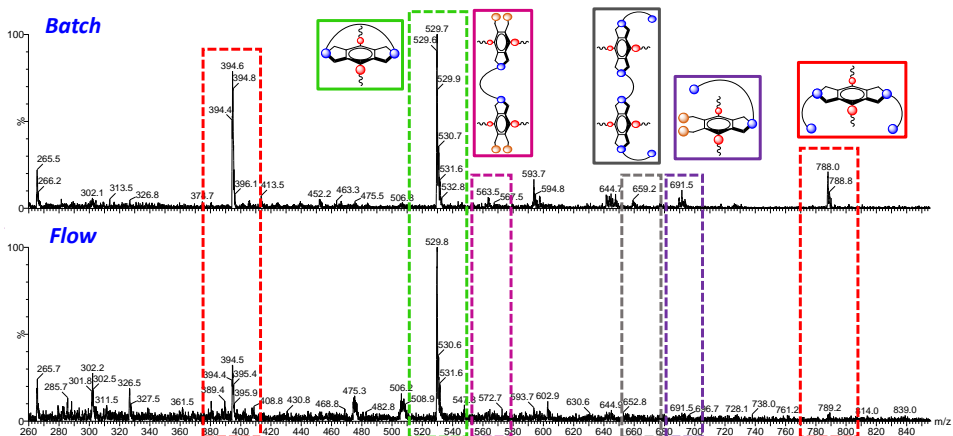
Figure S4.4. MS-ESI(+) comparison between the reaction crudes obtained under batch conditions (above) and flow conditions (below) using **4** as base.
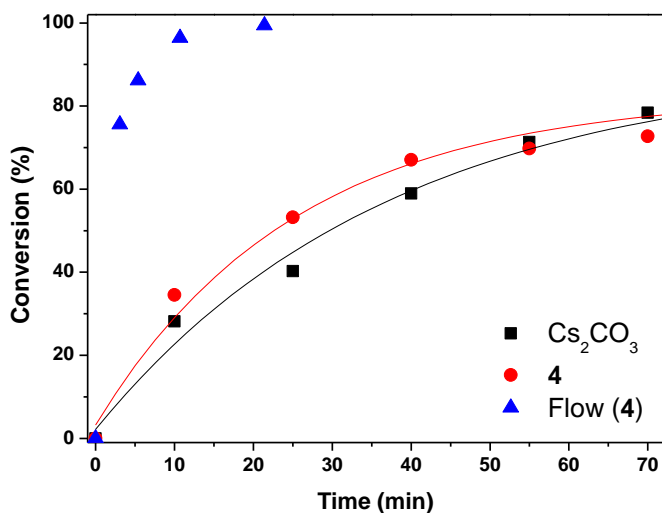
Figure S4.5. Conversion profiles for **1b** obtained with the different conditions assayed for the synthesis of **3b**. Black: Inorganic base under batch conditions; Red: Basic resin **4** under batch conditions; Blue: Basic resin **4** under flow conditions. All the experiments were carried out with 6 equivalents of the respective base. The blue points correspond to the conversions achieved for the different residence times obtained adjusting the flow. Conversions determined by HPLC. Reaction conditions: 80 °C, 2 mM in acetonitrile for **1b** and **2**.
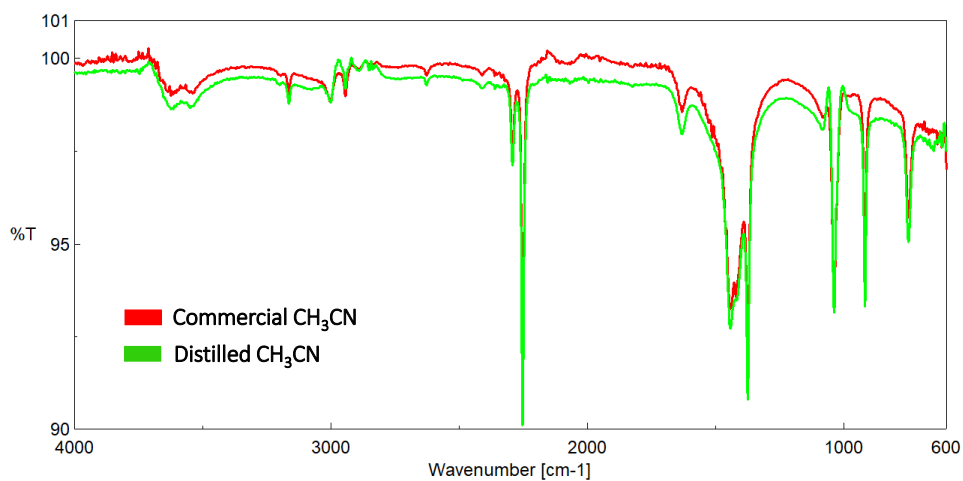
Figure S4.6. IR spectra comparison between commercial acetonitrile (red spectrum) and the distilled fraction of the flow macrocyclization (green spectrum).
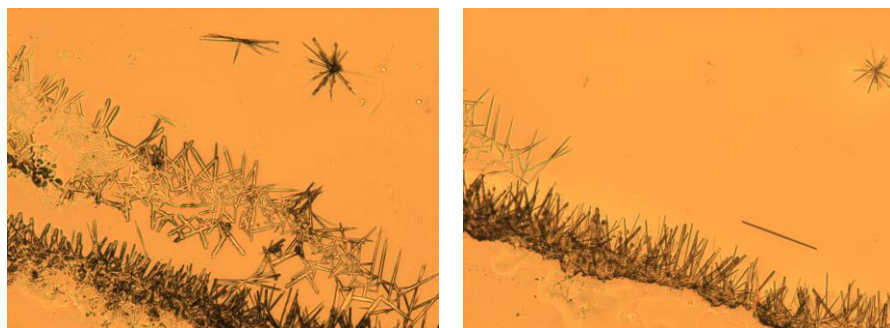
Figure S4.7. Optical microscopy pictures (40x1) of the **3a** crystals obtained in the reaction crudes after slow evaporation of acetonitrile.
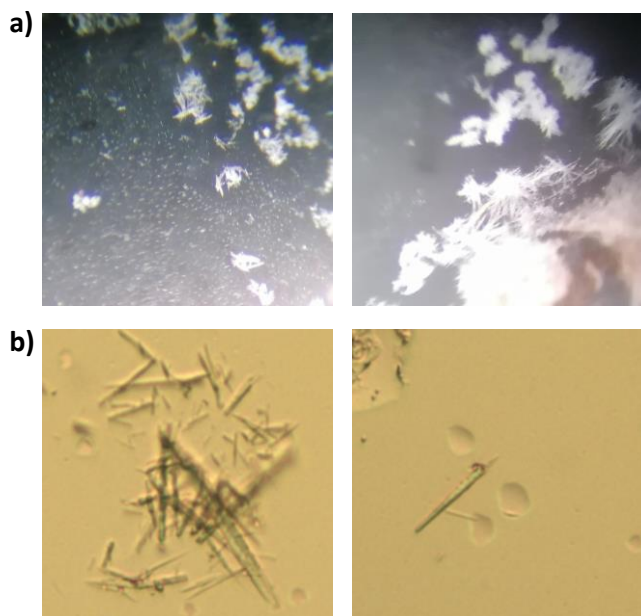
Figure S4.8. a) Optical microscopy (10x2) pictures of the flow distillation flask walls. b) Optical microscopy pictures (40x2) of the **3a** crystals obtained, extracted from the distillation flask with immersion oil.
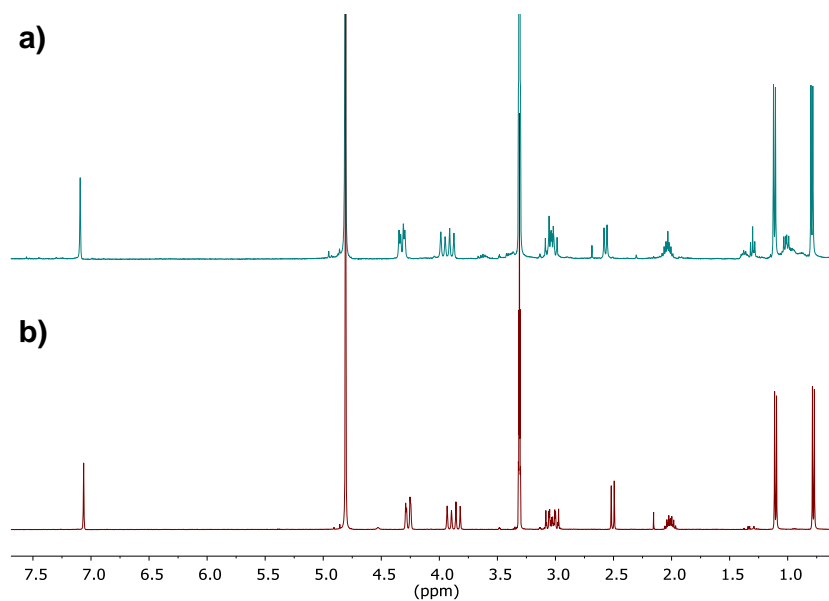
Figure S4.9. ^{1}H NMR (400 MHz, 7 mM in CD$_3$OD) of the reaction crude for a) scaled-up macrocyclization reaction between **1a** and **2**. b) flow-distillation set-up leading to high quality crystals of **3a**.
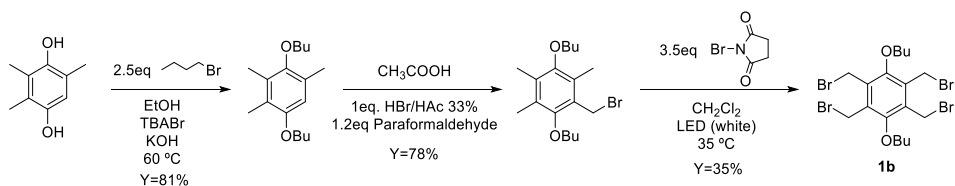
Scheme S4.2. Synthetic route for **1b**. See reference 21 for more details.
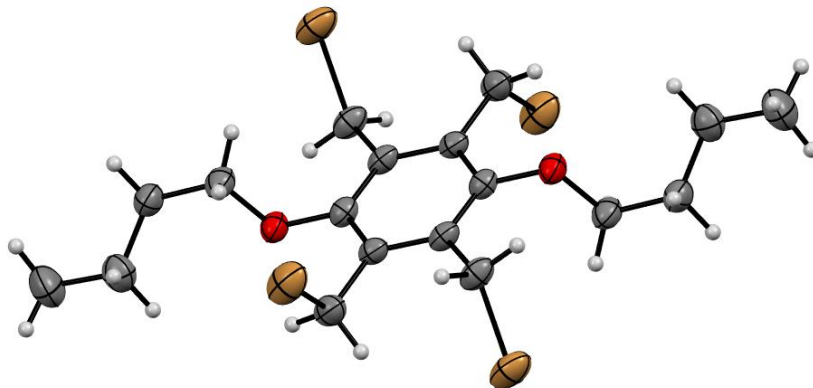
Figure S4.10. Thermal ellipsoid plot of **1b**. Ellipsoids at 50% of probability.
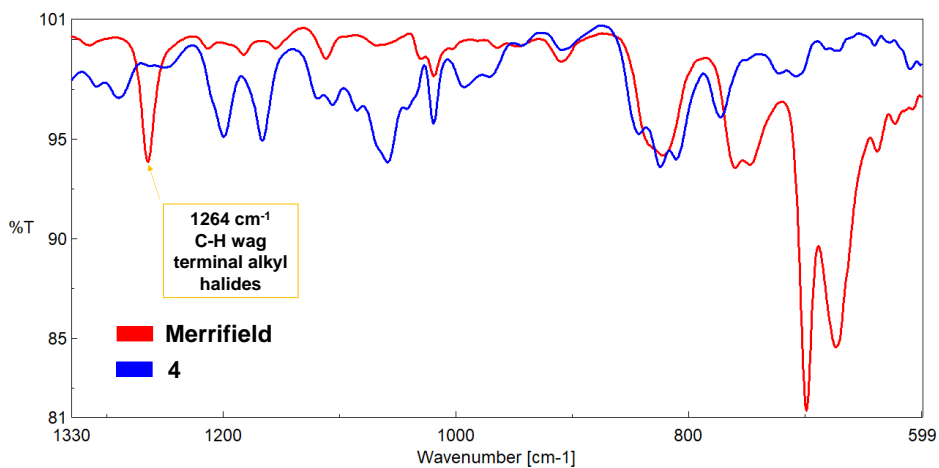
Figure S4.11. Partial IR spectra for the starting Merrifield resin (5.5 mmol of Cl/g nominal loading) and **4** (blue spectrum). Disappearance of the C-Cl characteristic band has been highlighted in orange.
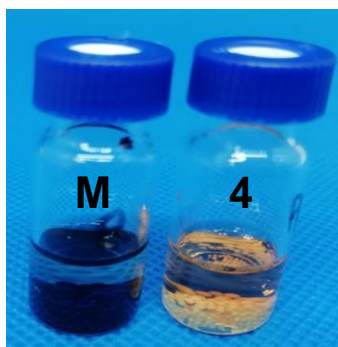
Figure S4.12. Picture of the NBP test carried out for the supported base **4** (right vial)). The control NBP test for the initial Merrifield (M) resin has also been included (left vial) showing the development of colour associated to the presence of C-Cl groups.
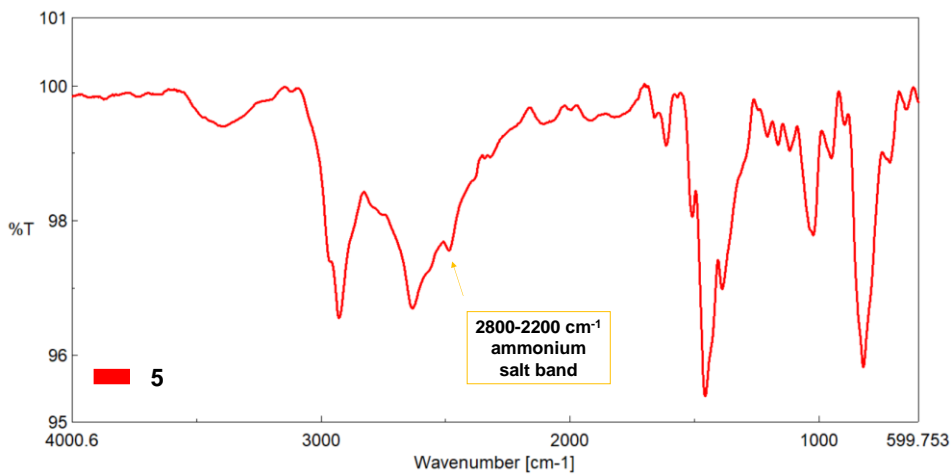
Figure S4.13. Partial IR spectra for **5**. The presence of a broad band at 2800-2200 cm^{-1} characteristic of ammonium salts has been highlighted in orange.
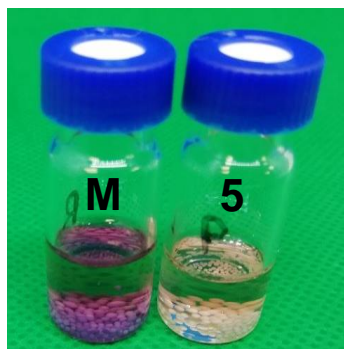
Figure S4.14. Picture of the NBP test carried out for the supported base **5** (right vial). The control NBP test for the initial Merrifield (M) resin has also been included (left vial) showing the development of colour associated to the presence of C-Cl groups.
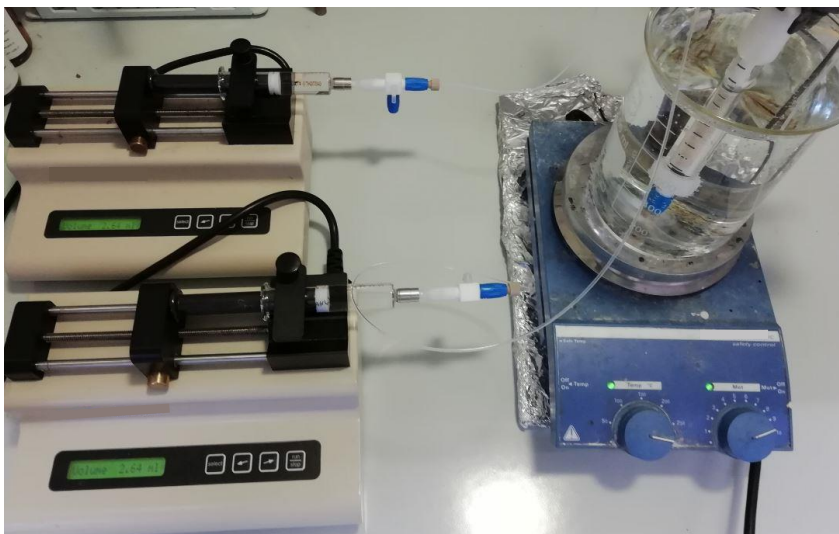
Figure S4.15. Flow system used for the macrocyclization reaction in CH$_3$CN, in a water bath at 80 °C.
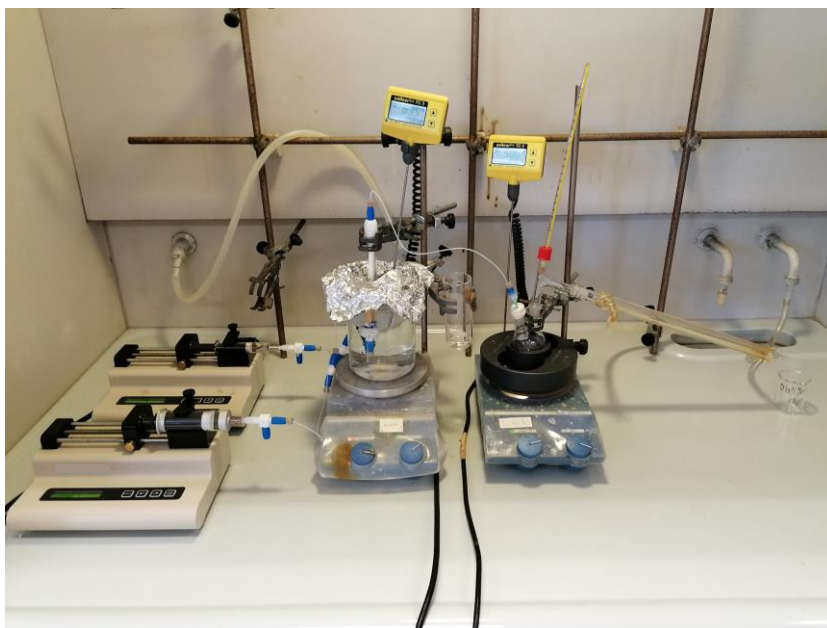
Figure S4.16. Flow system containing a distillation setup. The recovered acetonitrile was reused to obtain the solutions of the reagents.
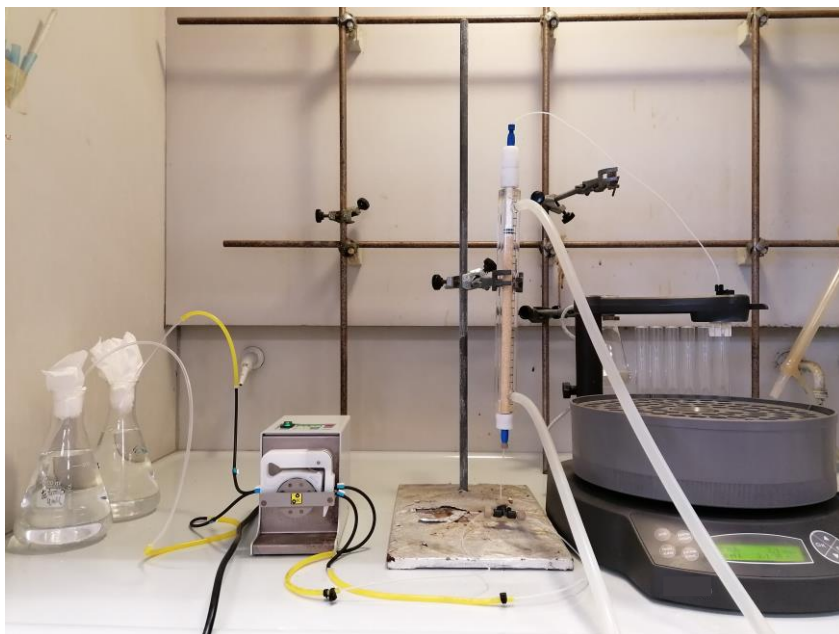
Figure S4.17. Scaled-up flow setup for the synthesis of **3a** in gram scale.

a)

3b R = O-(CH$_2$)$_3$-CH$_3$

b)

3b R = O-(CH$_2$)$_3$-CH$_3$

c)

Calculated [**3b** + H]$^+$

529.4
530.4
531.4

Experimental [**3b** + H]$^+$

529.4
530.4
531.4

m/z
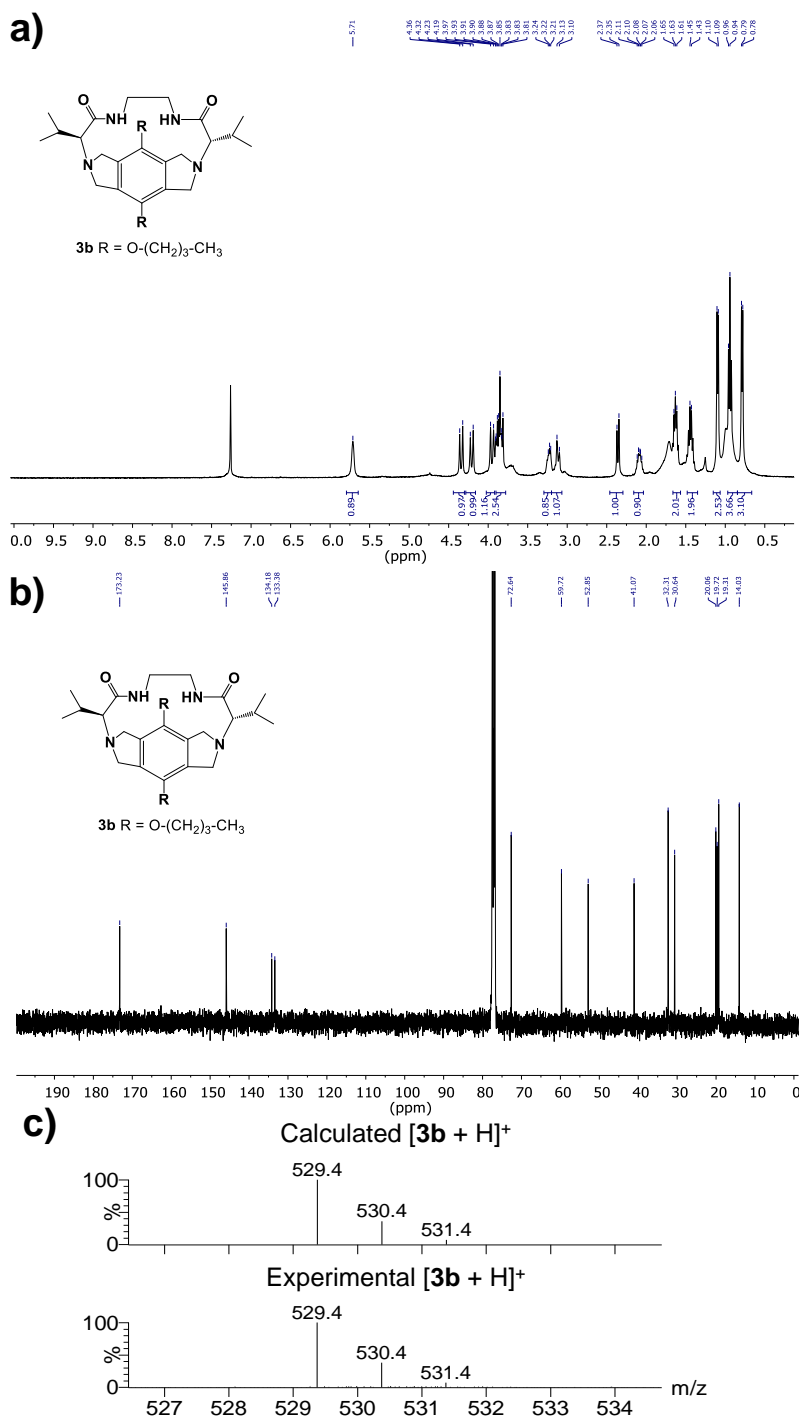
Figure S4.18. a) ^{1}H NMR (CDCl$_3$, 400 MHz), b) ^{13}C{^{1}H} NMR (CDCl$_3$, 100 MHz) and c) HRMS data for **3b**.
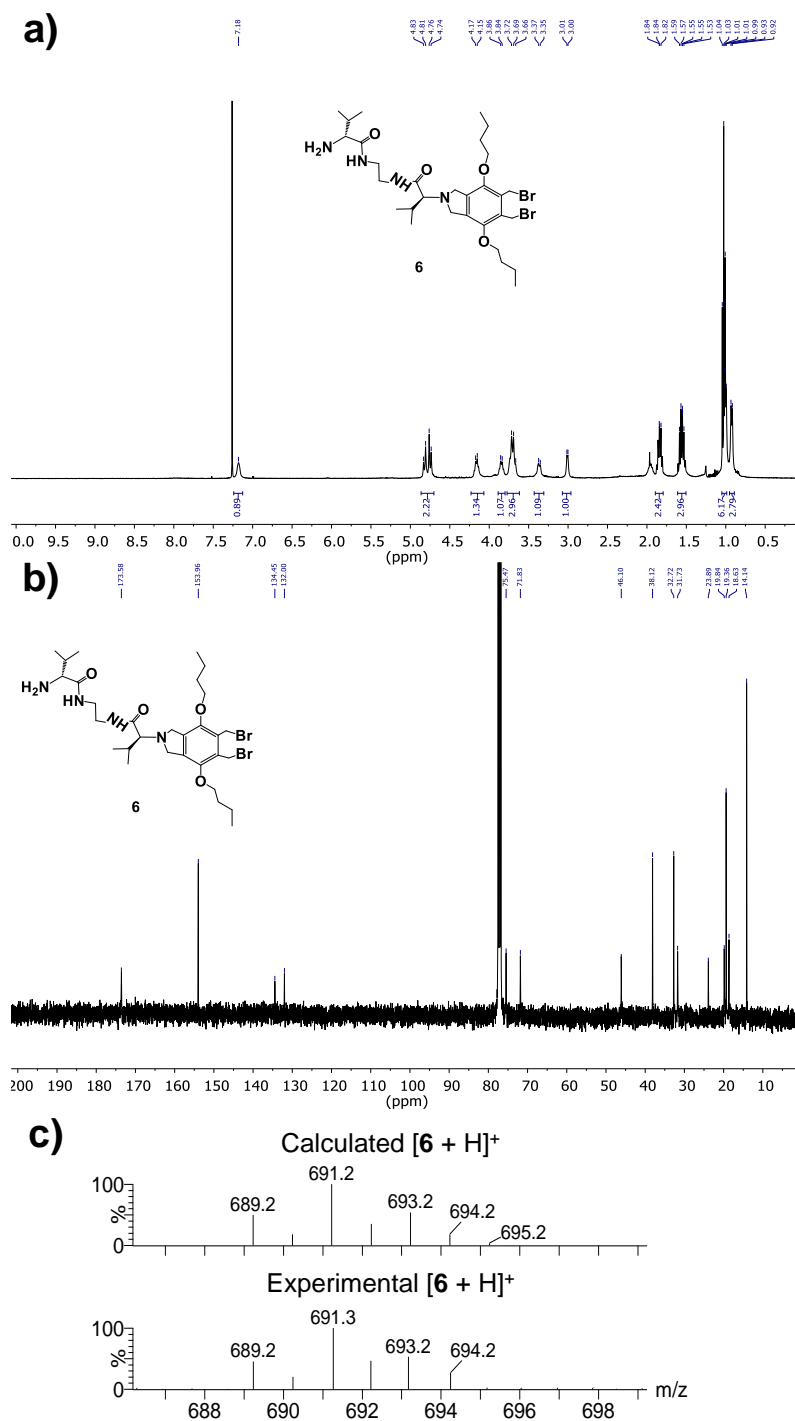
Figure S4.19. a) ^{1}H NMR (CDCl$_3$, 400 MHz), b) ^{13}C{^{1}H} NMR (CDCl$_3$, 100 MHz) and c) HRMS data for **6**.

a)

1b R = O-(CH$_2$)$_3$-CH$_3$

b)

1b R = O-(CH$_2$)$_3$-CH$_3$
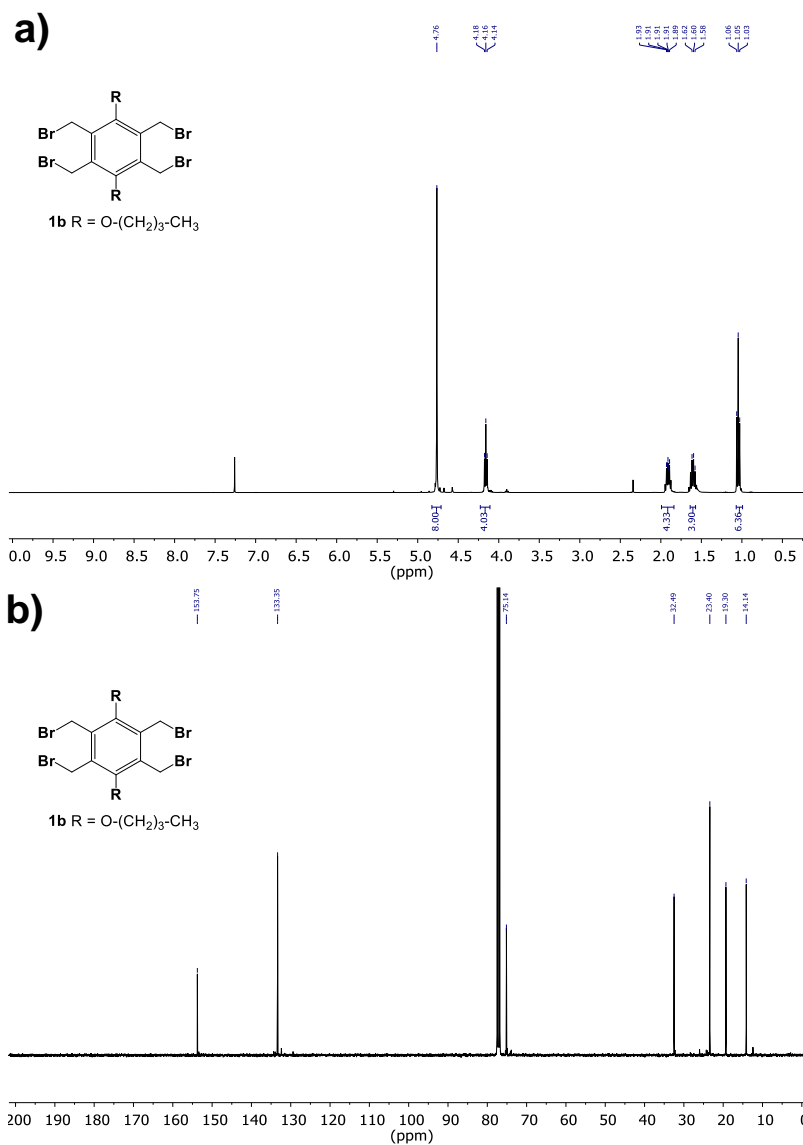
Figure S4.20. a) ^{1}H NMR (CDCl$_3$, 400 MHz) and b) ^{13}C{^{1}H} NMR (CDCl$_3$, 400 MHz) data for **1b**.
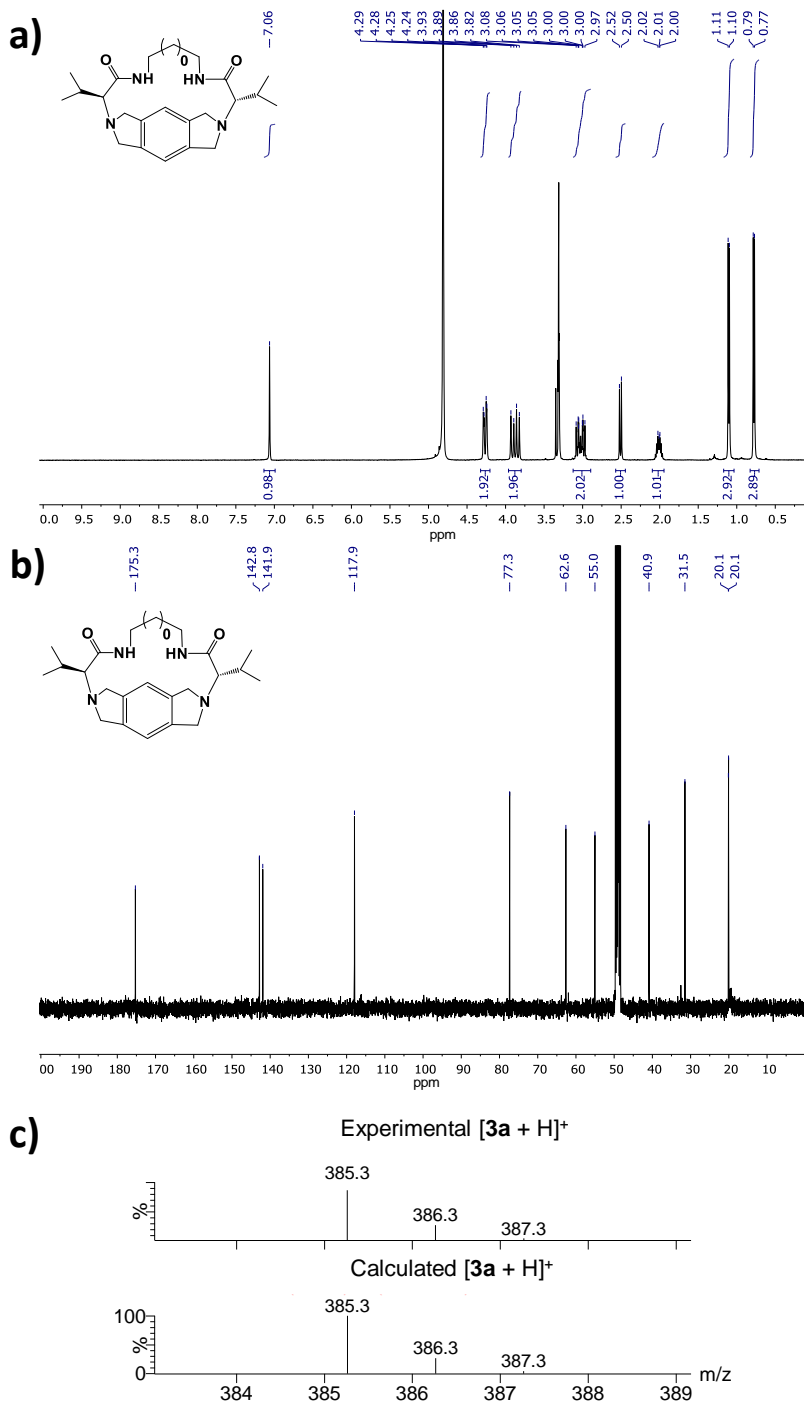
Figure S4.21. a) ¹H NMR (CD₃OD, 400 MHz), b) ¹³C{¹H} NMR (CD₃OD, 100 MHz) and c) HRMS data for **3a**.

Chapter 5

Pseudopeptidic Macrocycles as Cooperative Minimalistic Synzyme Systems for the Remarkable Activation and Conversion of CO$_2$ in the Presence of Chloride Anion
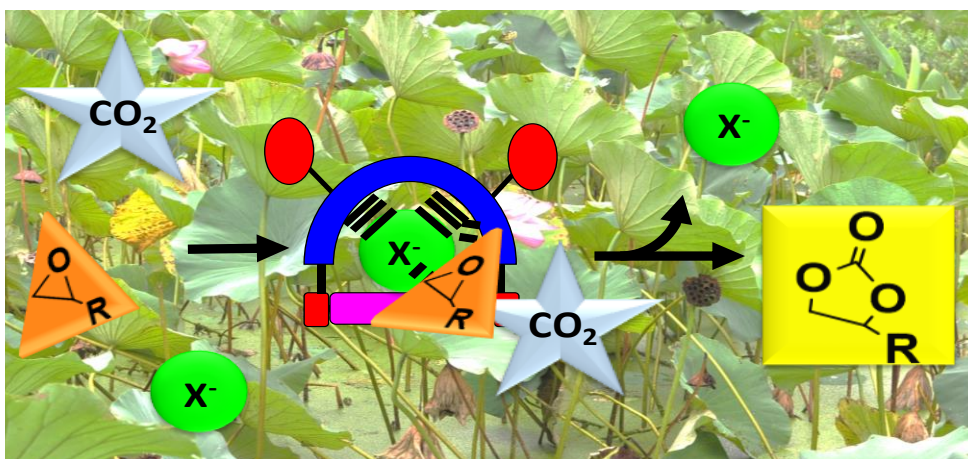
5.1. Main text

5.1.1. Abstract

A series of pseudopeptidic compounds have been assayed as organocatalyts for the conversion of CO_2 into organic carbonates through a cooperative multifunctional mechanism. Conformationally constrained pseudopeptidic macrocycles **3a** and **3b** have been revealed to be excellent synzymes for this purpose, being able to provide a suitable preorganization of the different functional elements and reaction components to activate the CO_2 molecule and stabilize the different anionic intermediates involved, through a series of cooperative supramolecular interactions. As a result, remarkable catalytic efficiencies are found at low CO_2 pressures and moderate temperatures, with TON and TOF values surpassing those reported for other organocatalytic supramolecular systems under similar conditions. The process works well for monosubstituted epoxides. The involvement of the different structural elements has been analysed in detail and preliminary studies show the potential for recovery and reuse of these catalytic systems.

5.1.2. Introduction

Nature has developed smart and complex systems working under elaborate self-regulation protocols and mild conditions and producing reduced waste. Many of them are based on the self-organization and self-assembly of a few simple building blocks.[1] Clear examples are provided by enzymes, which are highly sophisticated catalysts that Nature has optimized over billions of years. Their unique self-organization affords specific 3D-arrangements of individual functional groups allowing the required supramolecular and cooperative interplay of the various active-site functionalities within the enzyme. This often enables a precise location of the reacting substrates/reagents within the 3D-environment of the active site of the enzyme leading to highly efficient transformations in terms of both activity and selectivity.[2]

Developing abiotic systems able to mimic the efficiency of these natural structures is an important goal in Green Chemistry,[3] and a broad range of synthetic supramolecular systems displaying enzymatic activity, often referred to as synzymes, has been reported.[4] As in natural enzymes, the catalytic activity of these systems can provide selective substrate recognition and is dominated by supramolecular interactions.[5] In this field, macrocyclic cavities have been often exploited as minimalistic enzymatic mimics, taking advantage of the higher degree of preorganization of the functionalities present, which represents a key element of the active sites of enzymes.[6]

Achieving such a preorganization is not always easy and macrocyclizations often represent a synthetic challenge.[7] However, efficient macrocyclization strategies based on conformational, configurational or template-induced self-organization have been developed for the preparation of minimalistic macrocyclic pseudopeptides.[8,9] Despite their simplicity, as well as the high molecular diversity attainable and the presence of a high level of well-defined functionality,[10] these macrocycles have not been yet exploited as supramolecular organocatalytic systems. On the other hand, the conversion of CO_2 into valuable chemicals represents a challenge of great current interest in Green Chemistry, from different perspectives.[11] A variety of catalytic approaches have been reported for the reaction between CO_2 and epoxides to form cyclic carbonates,[12-15] a family of compounds of interest for a variety of different applications. [16] Here we report the initial results for the evaluation of some macrocyclic pseudopeptidic systems (**3**, Scheme 5.1), in the presence of tetra-alkyl-ammonium chlorides, as supramolecular synzymes for the activation and conversion of CO_2 into carbonates in the presence of epoxides. When appropriately adjusted, the different structural elements of these minimalistic pseudopeptides like the nature of the central spacers, the amino acid sidechains, and the groups attached to the amino functions, can facilitate a precise and well-defined self-assembly of the halide, the epoxide and CO_2 in a minimalistic cooperative supramolecular interplay with the macrocyclic host, providing a highly efficient catalytic transformation of CO_2 into the corresponding cyclic carbonates.
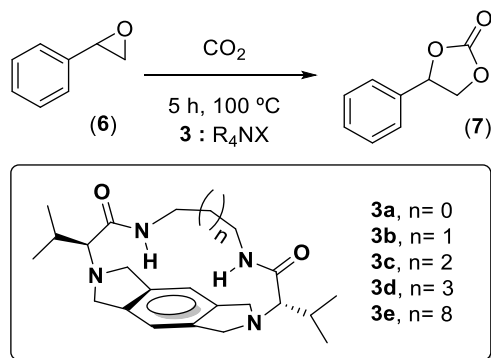
Scheme 5.1. Cycloaddition of carbon dioxide to styrene oxide catalysed by the supramolecular systems **3** : R₄NX.

5.1.3. Experimental section

General.

NMR experiments were carried out at 500, 400 or 300 MHz for ^{1}H and 125, 100 or 75 MHz for ^{13}C. Chemical shifts are reported in ppm from tetramethylsilane using the solvent resonance as the internal standard. Fourier transform infrared spectra (FT-IR) were recorded using an attenuated total reflection (ATR) adapter. High resolution mass spectrometry (HRMS) was recorded with a Q-TOF instrument. Rotatory power was determined with a digital polarimeter (Na: 589 nm). Melting points were measured using a standard apparatus and are uncorrected.

Open-chain pseudopeptidic compounds **2** were prepared following literature procedures,[8c] as well as the macrocyclic structures **3**.[17]

Two different set-ups were used for the cycloaddition reaction with CO_2. The first one, employed for the reaction at atmospheric pressure, used a standard round bottom flask with a CO_2 balloon (100% CO_2) as gas supply. The second one, for the reactions under pressure, used a Berghof R-300 high pressure reactor connected to a pressurized CO_2 source and a back-pressure regulator from Jasco (see Figure S5.11)

Synthesis of (2S,2'S)-N,N'-(ethane-1,2-diyl)bis(2-(isoindolin-2-yl)-3-methylbutanamide.

*Synthesis of **5**.* Compound **2a** (101 mg, 0.391 mmol) and α,α'-dibromo-o-xylene (**4**) (215 mg, 0.782 mmol) were dissolved in acetonitrile (65 mL) in the presence of Cs_2CO_3 (764 mg, 2.346 mmol), and the reaction mixture was refluxed on a heating mantle with magnetic stirring for 5 hours. The solvent was then evaporated under vacuum and the resulting residue was treated with basic water (pH ≈ 11), to afford pure **5** as a solid after centrifugation of the resulting suspension at 3000 rpm for 8 min. Yield (140 mg, 77.3%, 0.302 mmol); m.p. = 168-169 °C; $[\alpha]_D^{25}$ = -41.7° (c = 0.4, CH_3CN); IR (ATR): 3297, 2959, 1641, 1544 cm^{-1}; ^1H NMR (400 MHz, CD_3CN) δ = 0.91 (d, J = 6.7 Hz, 6H), 0.98 (d, J = 6.8 Hz, 6H), 2.86 (d, J = 6.7 Hz, 2H), 3.29-3.33 (m, 4H), 3.95-4.03 (m, 8H), 7.00 (s, 2H), 7.15-7.22 (m, 8H), $^{13}C\{^1H\}$ NMR (100 MHz, CD_3CN) δ = 18.4, 20.4, 29.8, 39.9, 56.5, 74.1, 123.1, 127.5, 140.8, 172.4; HRMS (ESI/Q-TOF) m/z: $[M+H]^+$ calcd for $C_{28}H_{38}N_4O_2$ 463.3703; found 463.3706.

*General procedure for the reaction of **6** with CO_2 in the presence of pseudopeptides and Bu_4NCl.*

8.7 mmol of styrene oxide, 0.087 mmol of Bu_4NCl and 0.0087 mmol of the corresponding pseudopeptide were added to a 25 mL twin-necked round bottom flask. The system was purged with dry N_2 and CO_2, leaving two CO_2 balloons (100% CO_2) as gas supply. The mixture was refluxed on a heating mantle with magnetic stirring for 5 hours at 100 °C. Finally, a sample of the crude was collected and analyzed by NMR. The conversion of **6** into **7** could be calculated, considering the integration of the signal at 3.88 ppm for the disappearance of **6** and the one for the signal at 5.67 ppm for the formation of **7**.

IR kinetic experiments.

The same procedure above was carried out but using just one CO_2 balloon (100% CO_2) and closing the second neck with a septum. Samples at defined times were directly collected through the septum with a syringe and directly analysed by FT-IR. The conversion of **6** into **7** could be calculated, using the area of the bands at

1440-1510 cm^{-1} (νC-C stretching, aromatic ring) as the reference and the area of the band at 1020–1100 cm^{-1} (νC-O asymmetric vibration) for the formation of **7**.

Crystal structures.

Single crystals suitable for X-ray crystallography were obtained by slow evaporation of a methanol solution of [**3a**·2HCl]. A crystal was selected and mounted on a SuperNova, Dual, Cu at zero, Atlas diffractometer. The structure was solved with the SHELXT 2014/5[18] structure solution program and refined with the SHELXL-2018/3[19] refinement package. Artwork representations were processed using MERCURY[20] software. The refined structure of [**3a**·2HCl] has been registered in CCDC with the deposition number 1995455.

Molecular modelling.

Lowest energy conformations for the different species considered were calculated at the MMFF level of theory using Spartan08.[21] Stationary points were confirmed by subsequent frequency calculation. All vibrational frequencies were positive.

5.1.4.   Results and discussion

In previous supramolecular catalytic systems evaluated for this process, a common strategy has been the use of supramolecular hosts able to strongly bind cations, affording in this way activated anions (e.g. "naked" X$^-$),[22-24] In the present case, however, the design elements for the organocatalytic pseudopeptides considered took into account their multifunctional and highly preorganized character and their capacity to develop cooperative supramolecular interactions with the three species involved in the process: the nucleophilic species (halide anions), the epoxide and the CO_2 molecules. Such interactions could include NH$_{amide}$···X···HN$_{amide}$, O$_{epoxide}$···HN$_{amide}$ and N$_{amine}$···CO_2 and cooperate to locate the three components in close proximity (A1, Figure 5.1), within a supramolecular complex, and with an

appropriate orientation as to facilitate low energy pathways for the desired reaction, fully mimicking the behaviour of many enzymatic sites.

A common mechanism reported for the activation of CO_2 has been its interaction with a Lewis base, in particular tertiary amines.[25,26] Thus, the $N_{amine}\cdots CO_2$ interaction can also contribute to this activation (A2, Figure 5.1). Besides, Brønsted or Lewis acid sites have been used to activate the epoxide,[27] sometimes involving bifunctional or multifunctional systems,[15b,28,29] and accordingly the $O_{epoxide}\cdots HN_{amide}$ can contribute to activate the epoxide. The selected synzymatic structure **3** has a high modularity (size of the macrocyclic cavity, conformational preferences, polarity, etc.) as to enable a fast optimization of the catalytic efficiency.
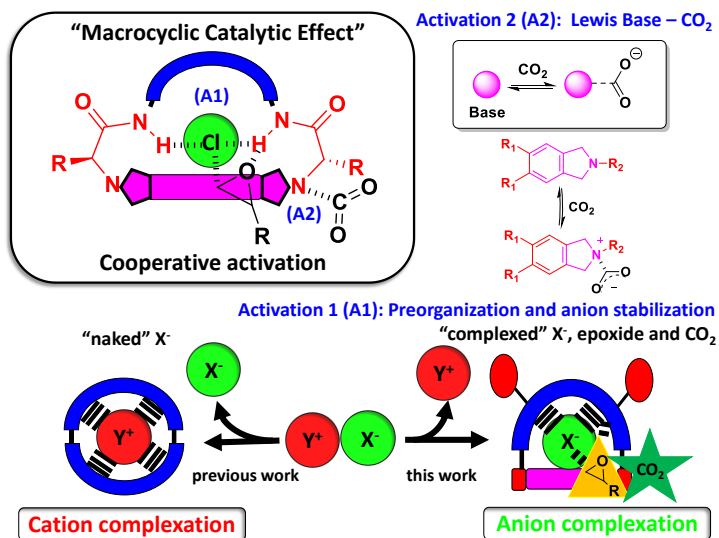
Figure 5.1. Pseudopeptidic macrocycles as minimalistic synzymes for the conversion of CO_2 through a cooperative multifunctional activation mechanism. A1: preorganization of the reactive components (amide and amine sites). A2: activation of the inert CO_2 species by a Lewis base (amine sites).

Constrained macrocycles **3**, prepared as previously reported from open chain C_2-symmetric pseudopeptides **2** and *tetrakis*(-bromomethyl)arenes **1** (Scheme S5.1), have two amide groups appropriately located as to cooperatively interact with anions and potentially with the oxygen atom of epoxides, and in close proximity of

conformationally restricted amino groups that could participate in the activation of CO_2 molecules.[17]

Following this design, the pseudopeptidic macrocycle **3a** was initially tested in combination with Bu$_4$NX salts for the synthesis of the organic carbonate **7** (Scheme 5.1). The selection of the L-valine derivative was based in the excellent results observed in the synthesis of **3a** from **2a** and in the suitability of its solubility properties, as most of these pseudopeptidic compounds have a rather limited solubility in styrene oxide (SO). The results obtained from the initial screening at 100 °C and ambient pressure (CO_2 balloon) using **3a** and SO as an epoxide of moderate-low reactivity,[13a] are summarized in Table 5.1. After 5 h and in the absence of the macrocycle, conversions into carbonate were 49% for Bu$_4$NI, 59% for Bu$_4$NBr and 65% for Bu$_4$NCl (entries 1-3, Table 5.1). It must be noted that in the absence of the tetrabutylammonium salt no reaction took place when **3a** was added (entry 4, Table 5.1). The use, under the same conditions, of an equimolecular mixture of both **3a** and Bu$_4$NX (1 mol% each relative to **6**) led to a significant increase in the activity in the case of Bu$_4$NCl, reaching a 93% conversion (entry 7, Table 5.1) while the observed improvements where minor for Bu$_4$NBr and Bu$_4$NBr (entries 5 and 6, Table 5.1). A complete selectivity towards the formation of **7** was observed and the formation of other species was not detected by ^{1}H NMR. The decomposition of tetraalkylammonium salts has been reported in some catalytic processes involving the same reaction, but the formation of tributyl amine was not detected up to the detection limit of the techniques used.[30] It should be also noted that the crude of reactions with conversion close or lower than 50% were also analysed by chiral HPLC. In all the cases, neither the epoxide nor the carbonate showed any enantioselectivity excluding the enantiopreference of the macrocycle for a given enantiomeric epoxide, which seems reasonable considering the temperatures used.

The same high conversion was maintained when the amount of macrocycle was reduced from 1 to 0.1 mol%, while keeping a 1 mol% loading of Bu$_4$NCl (entry 8, Table 5.1). However, in this case, the TON with respect to the **3a** was significantly higher, reaching a value of 930. Reducing also the loading of Bu$_4$NCl to 0.1 mol%,

keeping a 1 : 1 **3a** : Bu$_4$NCl molar ratio, led to an important reduction in conversion (22%, entry 9, Table 5.1). When the same experiment was performed at 10 bar of CO$_2$, a 73% conversion was observed. This result highlighted again the synergic effects between Bu$_4$NCl and the macrocycle **3a**, as in the absence of the macrocycle only a 45% conversion was observed (entries 11 and 12, Table 5.1).

Table 5.1. Screening of **3a**/Bu$_4$NX mixtures for the reaction between styrene oxide (**6**) and CO$_2$ to afford **7**.[a]

Entry	Bu$_4$NX (mol%)	3a (mol%)	Conversion (%)[b]	TON (Bu$_4$NX)	TON (3a)
1	X=I, (1)	-	49	49	-
2	X=Br, (1)	-	59	59	-
3	X=Cl, (1)	-	65	65	-
4	-	1	4	-	4
5	X=I, (1)	1	53	53	53
6	X=Br, (1)	1	67	67	67
7	X=Cl, (1)	1	93	93	93
8	X=Cl, (1)	0.1	93	93	930
9	X=Cl, (0.1)	0.1	22	220	220
10	X=Cl, (0.1)	-	16	160	-
11	X=Cl, (0.1)[c]	-	45	450	-
12	X=Cl, (0.1)[c]	0.1	73	730	730
13	X=Cl, (0.1)[c]	0.01	76	760	7600

[a] 1 mL epoxide **6** (8.7 mmol), p(CO$_2$)= CO$_2$ balloon, 100 °C, 5 h. [b] Conversions determined by ^{1}H RMN, selectivity for **7** >99.9 % in all cases. [c] p(CO$_2$)= 10 bar.

A ca. 1.5 times increase in conversion was always observed, for all the conditions assayed, when 1 equivalent of **3a** was added to Bu$_4$NCl. At 10 bar of CO$_2$ the amount of macrocycle could be further reduced to 0.01 mol%, while keeping a 1 : 10 **3a** : Bu$_4$NCl molar ratio, with the conversion to carbonate being 76% after 5 h. This represents achieving excellent TON and TOF values of 7600 and 1520 h^{-1}. Although some comparable or higher TON and TOF values have been described for transition metal-based catalysts (Table S5.2), often at higher pressures and temperatures,[14,31] the results presented here significantly surpass those found for organocatalytic and

supramolecular catalytic systems, in particular when epoxides of moderate-low reactivity like SO are involved (for a detailed comparison see Table S5.1).[22,23,27-29] Some remarkable examples of organocatalytic systems being able to achieve high conversions/yields of cyclic carbonates (>90%) at ambient pressure and temperature have been reported. It must be noted, however, that most often they involve the use of more reactive epoxides like glycidyl or propylene oxides and, besides, commonly use 2-10% catalyst loadings and extended reaction times (20-24 h) which leads to significantly reduced TON and TOF values.[25,27-29]

The catalytic performance of several tetraalkylammonium chlorides (R_4NCl) in the presence or absence of **3a** was also assayed (Table S5.3). For both Bu_4NCl and Et_4NCl the presence of the macrocycle **3a** (0.1 mol%) led again to an increase in conversion of ca. 1.5 times and to good TON values of 930 and 800, respectively (entries 4 and 5, Table S5.3). However, no reaction was observed for Me_4NCl, most likely for the lack of solubility of this salt in the reaction medium (entry 6, Table S5.3).

Although the initial solvent free conditions should be preferred according to the principles of green chemistry, the reaction was also studied in 2-MeTHF and acetonitrile (Table S5.4). Both are non protic polar solvents in which nucleophiles can be relatively "free" making them more reactive. The lack of an adequate solubility of the ammonium salt and the macrocycle precluded an efficient reaction in 2-MeTHF. Results improved, however, in acetonitrile. At 1 bar of CO_2 and 80 °C, with a 2.4 M concentration of epoxide, the conversion was 18% after 3 h in the presence of 1 mol% of Bu_4NCl and was increased more than three times when 0.1 mol% of **3a** was added (60% conversion, entries 5 and 6, Table S5.4). When using only 0.01 mol% of macrocycle **3a**, the conversion after 3 h reached 39%, which again corresponds with excellent TON and TOF values of 3900 and 1300 h^{-1}, respectively (entry 7, Table S5.4).

As mentioned above, entries 1-3 in Table 5.1 reveal that for the **3a** : Bu_4NX system the reactivity order was $Cl^- > Br^- \gg I^-$. This follows the basicity order and not the nucleophilicity order as found for other supramolecular receptors.[23c] Being the

more basic anion, chloride is expected to interact stronger with receptors **3** through hydrogen bonding to the amide NH fragments, as shown in related pseudopeptides,[8,32] and this should make chloride less available to react. Thus, the mechanism involved cannot rely on the activation of the nucleophile, but on the capacity of **3a** to correctly preorganize all the reacting species at short distances and with the correct orientation as to significantly enhance the reaction rate. The stronger binding of Cl⁻ (in comparison with Br⁻ and I⁻) can favour the adoption of the required conformation in the macrocyclic pseudopeptide not achievable with the other two anions.

Thus, ^{1}H NMR titrations in benzene-d_6 (ESI, Figure S5.1) showed that upon addition of Bu$_4$NCl, the NH amide proton signal underwent a large downfield shift ($\Delta\delta$ = 2.74 ppm). This variation is consistent with the development of strong NH$_{amide}$···Cl···HN$_{amide}$ H-bonding interactions (log β = 3.15 ± 0.01). The interaction of **3a** with other halide anions was much smaller. After addition of 10 equivalents of Bu$_4$NX the observed downfield shifts for the amide protons ($\Delta\delta_{(NH)}$) were 1.43 and 0.19 ppm for Br⁻ and I⁻, respectively (Table S5.5). The corresponding binding constants were too low to be accurately determined. Significant changes were also observed for the signals corresponding to the methine of the stereogenic carbon ($\Delta\delta$ = 0.87 ppm), to the aromatic protons ($\Delta\delta$ = 0.39 ppm) and to one of the isoindolinic protons -appearing as two AB systems in the 3.3 – 4.6 ppm region- that shifted downfield from 3.42 ppm to 4.32 ppm, strongly reducing the anisochrony of the AB system (Figure S5.1 and S5.2). Overall, this suggests important conformational changes upon complexation with Cl⁻.

In the same way, the strong negative signal at 285 nm observed in the CD of **3a** in benzene (0.5 mM) essentially disappeared after addition of 10 equivalents of Bu$_4$NCl (Figure 5.2) while the effect was less intense in the presence of Bu$_4$NBr and minor for Bu$_4$NI (Figure S5.3). This CD signal is assignable to π-π* transitions of the aromatic group located in a chiral environment and, as well known from studies related to proteins and other biomolecules, is very sensible to changes in the

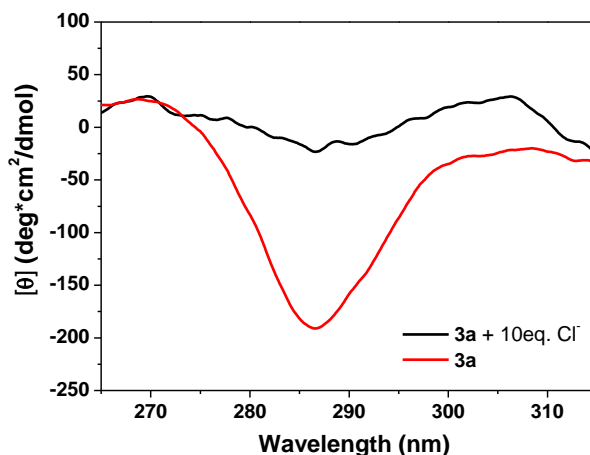environment and mobility and to the presence of additional groups at short distances.[33]

Figure 5.2. CD spectra in benzene (0.5 mM) for **3a** (red) and **3a** + 10 equivalents of Bu$_4$NCl (black).

Molecular modelling of the [**3a** + Cl$^-$] complex shows that in the most stable conformation both amide groups of the macrocycle adopt a *syn*-disposition and strongly interact with the halide anion (Figure 5.3).[21] The conformation observed in the macrocycle is similar to the one found in its X-Ray structure,[17] although the two carbonyl groups display longer distances to the corresponding methylene groups of the isoindolinic rings, in particular in one of the cases (Figure S5.4) which agrees well with the changes observed in ^{1}H NMR.
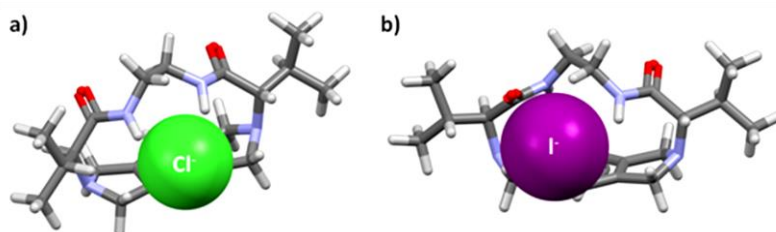
Figure 5.3. Lowest energy conformers calculated for a) [**3a** + Cl$^-$] complex highlighting the amide groups are in *syn*-disposition. b) [**3a** + I$^-$] complex highlighting the amide groups in *anti*-disposition.

In contrast, for the most stable conformation calculated for the [**3a** + I$^-$] complex, the amide groups adopt an *anti*-disposition, where only one amide group is

interacting with the iodide anion (Figure 5.3). It must be noted that only in the *syn*-disposition of the amide groups it is possible to facilitate the location of the epoxide on the same side of the halide and close to the activated CO_2 as envisaged in the catalyst design.

The level of structural preorganization of **3a**, being a conformationally constrained macrocycle can be relevant for the results obtained. To evaluate a possible "macrocyclic effect",[34] the open chain pseudopeptidic compound **5**, displaying the same functional groups and the same connectivity than **3a**, but lacking the constraints associated to the macrocyclic structure, was synthetized (Scheme S5.1) and tested.

The course of the model reaction catalysed by Bu_4NCl or by this salt in the presence of **3a** or **5** (0.1 equivalents relative to Bu_4NCl) was monitored by FT-ATR-IR spectroscopy (Figure S5.5). The conversion *vs.* time profiles confirmed the importance of the macrocyclic structure, showing that the higher conversion obtained after 5 h for the supramolecular system **3a** : Bu_4NCl (65% for Bu_4NCl alone, 73% in the presence of **5** and 93% in the presence of **3a**) was associated to a faster reaction rate (Figure 5.4). Thus, for instance, after one hour of reaction TOF values reached 380 h^{-1} for Bu_4NCl, 480 h^{-1} for **5** : Bu_4NCl and 630 h^{-1} for **3a** : Bu_4NCl.
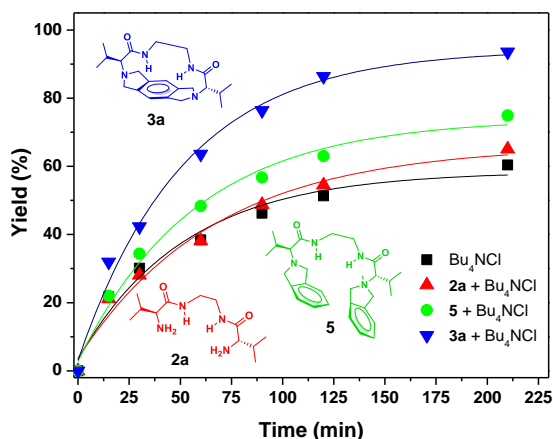
Figure 5.4. Conversion vs time profiles obtained for the reaction between **6** and CO_2 as monitored by FT-ATR-IR. Catalysts: 1 mol% Bu_4NCl and 0.1 mol% of **2a**, **3a** or **5**. Reaction conditions: solventless, 100 °C, 5 h, CO_2 balloon.

The results shown in Figure 5.4 also confirmed the importance of the tertiary amine groups in the activation of CO_2 molecules.[25,26] When the related pseudopeptide **2a** presenting primary amino groups was assayed, an irrelevant catalytic effect was observed (red points, Figure 5.4). Furthermore, the double salt [**3a**·2HCl], was obtained by treatment of **3a** with the stoichiometric amount of HCl in methanol (Scheme S5.1). This salt could maintain the main structural features of [**3a** + Cl⁻] but lacking the activating role of the tertiary amines. The ¹H NMR spectrum of this salt in DMSO-d_6 (Figure S5.6) showed the appearance of a new signal for the ammonium proton (R_3N^+H) at 10.45 ppm. Additionally, the amide signal was shifted downfield ($\Delta\delta_{NH} = 1.3$ ppm), indicating the presence of NH_{amide}···Cl⁻ interactions. The X-Ray crystal structure of [**3a**·2HCl] contained two molecules in the asymmetric unit, with *syn-* and *anti-*arrangements of the amide groups (Figure S5.7, see also Figure S5.12). Both structures exhibit Cl⁻···HN_{amide} hydrogen bonds, particularly the one with the *syn-* amide groups that seems to display an appropriate preorganization of the cavity. However, no formation of the carbonate **7** was obtained when **6** was heated in the presence of 1 mol% of salt [**3a**·2HCl], highlighting the importance of these tertiary amino groups.

The length of the central aliphatic spacer linking the two amino acid fragments is another structural element defining the conformational flexibility of compounds **3** and, accordingly, their level of preorganization. Hence, important differences were found as a function of the length of the spacer in macrocycles **3a-e** demonstrating that a reduction in the preorganization of the macrocyclic cavity is critical, leading to less active systems. Compounds with shorter spacers (n = 0 or 1, **3a** and **3b**) afforded efficient catalytic systems (conversion > 90%, entries 1 and 2, Table 5.2), while for spacers of intermediate length (n = 2 or 3, **3c** and **3d**) some decrease in conversion was observed (ca. 80% conversion, entries 3 and 4, Table 5.2). Finally, the macrocycle with the largest spacer (n = 8) afforded a strong decay in activity (52% conversion, entry 5, Table 5.2).

Table 5.2. Screening of macrocyclic catalysts mixtures for the reaction between styrene oxide (**6**) and CO_2 to afford **7**.[a]

Entry	Macrocycle[b]	Spacer -$(CH_2)_{n+2}$-	3 : Bu₄NCl molar ratio	Conversion (%)[c]
1	3a	0	1 : 10	93
2	3b	1	1 : 10	96
3	3c	2	1 : 10	83
4	3d	3	1 : 10	79
5	3e	8	1 : 10	52

[a] 1 mL epoxide 6 (8.7 mmol), 1 mol% of Bu₄NCl, 1 : 10 macrocycle : Bu₄NCl molar ratio, CO_2 balloon, 100 °C, 5 h. Conversion achieved for BuN₄Cl alone 65%. [b] Obtained as previously reported in ref. 17. [c] Conversions determined by ^1H NMR, selectivity for 7 >99.9 % in all the cases.

The increase in mobility associated to the length of the spacer in compounds 3 was highlighted by the changes observed for the signals from the four protons of the isoindolinic rings in ^1H NMR spectra. As mentioned, they are observed in all solvents as two well-differentiated AB systems, the signals for the protons directed towards the macrocyclic cavity, and accordingly affected by the shielding cone of the $C=O_{amide}$ fragments, appearing at higher field. In CD₃OD (Figure S5.2), the larger anisochrony was observed for compounds with the shorter spacers (3b, $\Delta\delta$ = 0.59 and 0.37) and decreased significantly for the macrocycles with the larger spacers (3d and 3e). For 3e the spectrum changes to an apparent AB single system, suggesting a high degree of conformational flexibility allowing the rotation of the aromatic unit, accompanied by the inversion at the nitrogen atoms, with respect to the macrocyclic main plane.[35]

Besides, the CD spectrum for the less active macrocycle 3e (larger spacer) was like that of 3a but, in this case, the effect of the addition of Bu₄NCl was minor. For the intermediate macrocycle 3d the CD signal was essentially absent, which can be associated to the coexistence of several conformations as suggested by X-Ray data and molecular modelling studies,[17] and no significant changes were observed in the presence of chloride anion (Figure S5.3). Thus, the formation of a strong [3a + Cl⁻] complex displaying a highly restricted conformational mobility and an appropriate preorganization seems to be a requisite for the higher activity of 3a in this catalytic process, despite the reduced reactivity of the anion in such a complex. The larger spacers would allow, for instance, and *anti*-disposition of the amide groups and the

location of chloride and epoxide coordinated on opposite sides of the macrocyclic cavity, precluding a direct interaction of these two components of the reaction.

According to literature data, hydrogen bonding between the oxygen atom of SO and the amide hydrogens can activate the epoxide.[15,28,29] ^{1}H NMR titrations of **3a** with **6** in C_6D_6 did not show significant changes that could be attributed to the formation of the corresponding complex. However, ^{1}H NMR spectra obtained for the [3a + Cl^{-} + **6**] system in benzene-d_6 in ratios similar to those in the catalytic experiments (2 mM of **3a**, 20 mM of Bu$_4$NCl and 240 mM of **6**) suggested the formation of a ternary complex (Figure S5.8). Thus, the complex signal for the methylene protons closer to the ammonium (R-CH$_2$-N[+]R$_3$) experienced an upfield shift ($\Delta\delta = 0.05$ ppm), associated to the weakening of the ion pair, that is appreciably larger than the one observed in the absence of **6**. Despite the large excess of **6** present, a minor downfield shift was also observed for the protons of the epoxide ring suggesting the presence of a weak interaction Cl^{-}···HCHOR$_{epoxide}$.

In agreement with this, molecular modelling for [**3a** + Cl^{-} + **6**] showed that in the lowest energy species the rigidly preorganized cavity of **3a** facilitates a cooperative but asymmetric H-bonding of both *syn*-amide groups with the chloride anion, while **6** is located displaying short NH$_{amide}$···O distances, adopting a suitable conformation for the nucleophilic attack on the less hindered carbon atom and contributing to the shielding of the anion from its interaction with Bu$_4$N[+] (Figure 5.5a).

In contrast, in the lowest energy species for [**3e** + Cl^{-} + **6**] only one of the two *anti*-amides interacts with the chloride anion, while the epoxide is located closer to the macrocycle but adopting an orientation much less favourable for the reaction to occur, as the CO_2 molecule that could be interacting with one of the amino groups should not be appropriately located (Figure 5.5b).
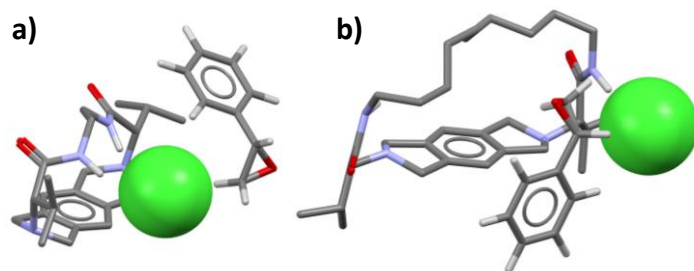
Figure 5.5. Lowest energy conformers calculated (MMFF level of theory) for the supramolecular species a) [**3a** + Cl⁻ + **6**] and b) [**3e** + Cl⁻ + **6**]. Non-essential hydrogen atoms are omitted for clarity.

In the light of the former results, the observed catalytic activity seems to rely on a cooperative multifunctional mechanism based on an efficient preorganization of the different components and participating groups: amide, tertiary amine, anion, epoxide and CO_2 (Figure S5.9). According to the general mechanism established for the synthesis of cyclic carbonates from epoxides and carbon dioxide, the mechanism depicted in Figure 5.6 can be considered.[30] After formation of the [**3a** + Cl⁻] complex (**A**), interaction with the epoxide can lead to the formation of the [**3a** + Cl⁻ + **6**] supramolecular species (**B**), while CO_2 can be activated by tertiary amino groups in close proximity leading to the intermediate **C**. The attack of the chloride to the less hindered carbon atom of the epoxide produces the requisite intermediate **D**, which subjected to the insertion of CO_2 generates the intermediate **E**. Both, the alkoxide and the alkylcarbonate anions, in intermediates **D** and **E**, can be stabilised by interaction with the amide groups, reducing the energy required for the ring-opening of the epoxide, which is considered the rate determining step. Finally, the corresponding cyclic carbonate is obtained through an intramolecular cyclization step to give the [**3a** + Cl⁻ + **7**] species (**F**), from which the catalytic [**3a** + Cl⁻] complex (**A**) is regenerated. Nevertheless, more detailed studies, including in depth kinetic analyses and high-level computational studies, are needed to fully analyse these mechanistic details, although this is out of the scope of this initial work.

Figure 5.6. Proposed mechanism for the cycloaddition of styrene oxide and CO_2 catalysed by the supramolecular system **3a** : R_4NX.

The coupling reactions of CO_2 with several epoxides (Fig. 5.7) were also investigated under the optimized conditions. In general, excellent conversions (>90%) were found for reactive and moderately reactive monosubstituted epoxides (entries 1-4, Table 5.3). Only for cyclohexene oxide a lower conversion was observed (18%), as a result of its lower reactivity associated to the steric hindrance present (entry 5, Table 5.3).[36] In this case, 15 hours were required for a complete conversion of the epoxide in the desired carbonate.

Figure 5.7. Structures of the epoxides assayed.

Table 5.3. Cycloaddition of CO_2 to different epoxides catalysed by **3a** : BuN_4Cl.[a]

Entry	Epoxide	Conversion (%)[b]	TON (3a)	TON (Bu₄NCl)
1	6	93	930	93
2	8	94	940	94
3	9	99	990	99
4	10	98	980	98
5	11	18 (99)[c]	180 (990)[c]	18 (99)[c]

[a] Reaction conditions: solventless, 100 °C, 5 h, CO_2 balloon; 1 mol% of BuN_4Cl, 0.1 mol% of **3a**. [b] Conversions determined by ^1H NMR. [c] Conversions determined by ^1H NMR after 15 h of reaction without solvent, 100 °C using a CO_2 balloon.

Finally, the reusability of the catalyst was also assayed using styrene oxide as the substrate at the optimized reaction conditions (Figure S5.10). The pseudopeptidic macrocycle **3a** could be recovered almost quantitatively by precipitation with cyclopentyl methyl ether (CPME) and could be used after centrifugation and decantation of the solution with only a minor decrease in the conversion of **6** into **7** being observed after three reuses. After the recycling protocol, the integrity of the organocatalyst was corroborated by NMR and MS analyses, with no significant changes observed as compared to the spectra of freshly prepared **3a**. Considering the small scale of the experiments, these results support the feasibility of this methodology to isolate and reuse the catalytic system.

5.1.5. Conclusions

Overall, the present results show that pseudopeptidic macrocycles represent a remarkable and unique scaffold for the development of a synzymatic approach allowing the efficient conversion of CO_2 into organic carbonates achieving high TON and TOF values surpassing the best values reported for supramolecular systems under related conditions. Despite the reduced reactivity that could be associated to the interaction of the chloride anion with the amide NH fragments, the conformational restrictions defined by the macrocyclic structure, along with the very high functional density, facilitate an appropriate supramolecular preorganization,

with suitable distances and orientations, of the three components involved: the nucleophilic anion, the epoxide and one molecule of CO_2. Simultaneously, the tertiary amino groups can activate the CO_2 molecules, while the amide functionalities could activate the epoxide and stabilize the different anionic intermediates formed, leading to the cooperative involvement of the different structural elements, fully mimicking the behaviour found in enzymatic sites. Similar catalytic activities are observed for monosubstituted epoxides, while the activity decreases with cyclohexene oxide. A preliminary approach has been developed allowing the recovery and reuse of the catalytic system. Additional work is needed to fully disclose the mechanistic aspects of the process involved, but the present results provide a new promising entry to the development of efficient metal-free processes for the conversion of CO_2 into cyclic carbonates from epoxides.

5.1.6. References

1- (a) Huang, Z.; Kang, S. K.; Banno, M.; Yamaguchi, T.; Lee, D.; Seok, C.; Yashima, E.; Lee, M. Pulsating Tubules from Noncovalent Macrocycles. *Science* **2012**, *337*, 1521-1526. (b) Schaller, V.; Bausch, A. R. A fresh twist for self-assembly. *Nature* **2012**, *481*, 268-269. (c) Smith, K. H.; Tejeda-Montes, E.; Poch, M.; Mata, A. Integrating top-down and self-assembly in the fabrication of peptide and protein-based biomedical materials. *Chem. Soc. Rev.* **2011**, *40*, 4563-4577. (d) Moore, J. S.; Kraft, M. L. Synchronized Self-Assembly. *Science* **2008**, *320*, 620-621; (e) Segalman, R. A. Directing Self-Assembly Toward Perfection. *Science* **2008**, *321*, 919-920.

2- Fersht, A. *Structure and Mechanism in Protein Science: A Guide to Enzyme Catalysis and Protein Folding; Freeman*, W. H.; New York, 1999.

3- (a) Wang, L.; Zhang, R.; Han, Q.; Xu, C.; Chen, W.; Yang, H.; Gao, G.; Qin, W.; Liu, W. Amide-functionalized heterometallic helicate cages as highly efficient catalysts for CO_2 conversion under mild conditions. *Green Chem.* **2018**, *20*, 5311-5317. (b) Cao, X.; Teong, S. P.; Wu, D.; Yi, G.; Su, H.; Zhang, Y. An enzyme mimic ammonium polymer as a single catalyst for glucose dehydration to 5-hydroxymethylfurfural. *Green Chem.* **2015**, *17*, 2348-2352. (c) Rothenberg, G.; Clark, J. H. On oxyhalogenation, acids, and non-mimics of bromoperoxidase enzymes. *Green Chem.* **2000**, *2*, 248–251.

4- (a) Kuah, E.; Toh, S.; Yee, J.; Ma, Q.; Gao, Z. Enzyme Mimics: Advances and Applications. *Chem. Eur. J.* **2016**, *22*, 8404-8430. (b) Dong, Z.; Luo, Q.; Liu, J.

Artificial enzymes based on supramolecular scaffolds. *Chem. Soc. Rev.* **2012**, *41*, 7890-7908. (c) Wiester, M. J.; Ulmann, P. A.; Mirkin, C. A. Enzyme mimics based upon supramolecular coordination chemistry. *Angew. Chem. Int. Ed.* **2011**, *50*, 114-137.

5- (a) Zhu, Y.; Rebek, J.; Yu, Y. Cyclizations catalyzed inside a hexameric resorcinarene capsule. *Chem. Commun.* **2019**, *55*, 3573-3577. (b) Wu, N. W.; Petsalakis, I. D.; Theodorakopoulos, G.; Yu, Y.; Rebek, J. Cavitands as Containers for α,ω-Dienes and Chaperones for Olefin Metathesis. *Angew. Chem. Int. Ed.* **2018**, *57*, 15091-15095. (c) Wu, N. W.; Rebek, J. Cavitands as Chaperones for Monofunctional and Ring-Forming Reactions in Water. *J. Am. Chem. Soc.* **2016**, *138*, 7512-7515.

6- (a) Nath, B. D.; Takaishi, K.; Ema, T. Macrocyclic multinuclear metal complexes acting as catalysts for organic synthesis. *Catal. Sci. Technol.* **2020**, *10*, 12-34. (b) Raynal, M.; Ballester, P.; Vidal-Ferran, A.; van Leeuwen, P. W. N. M. Supramolecular catalysis. Part 2: artificial enzyme mimics. *Chem. Soc. Rev.* **2014**, *43*, 1734-1787.

7- Martí-Centelles, V.; Pandey, M. D.; Burguete, M. I.; Luis, S. V. Macrocyclization Reactions: The Importance of Conformational, Configurational, and Template-Induced Preorganization. *Chem. Rev.* **2015**, *115*, 8736-8834.

8- (a) Marti-Centelles, V.; Burguete, M. I.; Luis, S. V. Macrocycle Synthesis by Chloride-Templated Amide Bond Formation. *J. Org. Chem.* **2016**, *81,* 2143-2147. (b) Marti-Centelles, V.; Burguete, M. I.; Luis, S. V. Template Effects in S_N2 Displacements for the Preparation of Pseudopeptidic Macrocycles. *Chem. Eur. J.* **2012**, *18,* 2409-2422. (c) Becerril, J.; Bolte, M.; Burguete, M. I.; Galindo, F.; Garcia-España, E.; Luis, S. V.; Miravet, J. F. Efficient Macrocyclization of U-Turn Preorganized Peptidomimetics: The Role of Intramolecular H-Bond and Solvophobic Effects. *J. Am. Chem. Soc.* **2003**, *125*, 6677-6686.

9- (a) Bru, M.; Alfonso, I.; Bolte, M.; Burguete, M. I.; Luis, S. V. Structurally disfavoured pseudopeptidic macrocycles through anion templation. *Chem. Commun.* **2011**, *47*, 283-285. (b) Alfonso, I.; Bolte, M.; Bru, M.; Burguete, M. I.; Luis, S. V.; Rubio, J. Supramolecular Control for the Modular Synthesis of Pseudopeptidic Macrocycles through an Anion-Templated Reaction. *J. Am. Chem. Soc.* **2008**, *130*, 6137-6144.

10- Luis, S. V.; Alfonso, I. Bioinspired Chemistry Based on Minimalistic Pseudopeptides. *Acc. Chem. Res.* **2014**, *47*, 112-124.

11- (a) Delafontaine, L.; Asset, T.; Atanassov, P. Metal-Nitrogen-Carbon Electrocatalysts for CO_2 Reduction towards Syngas Generation. *ChemSusChem* **2020**, *13*, 1688-1698. (b) Ronda-Lioret, M.; Rothenberg, G.; Shiju, N. R. A Critical Look at Direct Catalytic Hydrogenation of Carbon Dioxide to Olefins. *ChemSusChem* **2019**, *12*, 3896-3914. (c) Tomkins, P.; Mueller, T. E. Evaluating the carbon inventory, carbon fluxes and carbon cycles for a long-term sustainable world. *Green Chem.* **2019**,

21, 3994-4013. (d) Chen, Y.; Mu, T. Conversion of CO_2 to value-added products mediated by ionic liquids. *Green Chem.* **2019**, *21*, 2544-2574. (e) Leclaire J.; Heldebrant, D. J. A call to (green) arms: a rallying cry for green chemistry and engineering for CO_2 capture, utilisation and storage. *Green Chem.* **2018**, *20*, 5058-5081. (f) Song, Q.-W.; Zhou, Z.-H.; He, L.-N. Efficient, selective and sustainable catalysis of carbon dioxide *Green Chem.* **2017**, *19*, 3707-3728. (g) Fiorani, G.; Guo, W.; Kleij, A. W. Sustainable conversion of carbon dioxide: the advent of organocatalysis. *Green Chem.* **2015**, *17*, 1375-1389.

12- (a) Shaikh, R. R.; Pornpraprom, S.; D'Elia, V. Catalytic Strategies for the Cycloaddition of Pure, Diluted, and Waste CO_2 to Epoxides under Ambient Conditions. *ACS Catal.* **2018**, *8*, 419-450. (b) Alves, M.; Grignard, B.; Mereau, R.; Jerome, C.; Tassaing, T.; Detrembleur, C. Organocatalyzed coupling of carbon dioxide with epoxides for the synthesis of cyclic carbonates: catalyst design and mechanistic studies. *Cat. Sci Tech.* **2017**, 7, 2651-2684. (c) Buttner, H.; Longwitz, L.; Steinbauer, J.; Wulf, C.; Werner, T. Recent Developments in the Synthesis of Cyclic Carbonates from Epoxides and CO_2. *Top. Curr. Chem.* **2017**, *375*, Article Number: 50.

13- (a) Subramanian, S.; Oppenheim, J.; Kim, D.; Nguyen, T. S.; Silo, W. M. H.; Kim, B.; Goddard III, W. A.; Yavuz, C. T. Catalytic Non-redox Carbon Dioxide Fixation in Cyclic Carbonates *Chem*, **2019**, *5*, 3232-3242. (b) Xie, Y.; Zhang, Z.; Jiang, T.; He, J.; Han, B.; Wu, T.; Ding, K. CO_2 cycloaddition reactions catalyzed by an ionic liquid grafted onto a highly cross-linked polymer matrix. *Angew. Chem. Int. Ed.* **2007**, *46*, 7255-7258.

14- (a) Takaishi, K.; Nath, B. D.; Yamada, Y.; Kosugi H.; Ema, T. Unexpected Macrocyclic Multinuclear Zinc and Nickel Complexes that Function as Multitasking Catalysts for CO_2 Fixations. *Angew. Chem. Int. Ed.* **2019**, *58*, 9984-9988. (b) Castro-Osma, J. A.; Lamb, K. J.; North, M. Cr(salophen) Complex Catalyzed Cyclic Carbonate Synthesis at Ambient Temperature And Pressure. *ACS Catal.* **2016**, *6*, 5012-5025. (c) Maeda, C.; Taniguchi, T.; Ogawa, K.; Ema, T. Bifunctional Catalysts Based on *m*-Phenylene-Bridged Porphyrin Dimer and Trimer Platforms: Synthesis of Cyclic Carbonates from Carbon Dioxide and Epoxides. *Angew. Chem. Int. Ed.* **2015**, *54*, 134-138. (d) Dharman, M. M.; Yu, J.-I.; Ahn, J.-Y.; Park, D.-W. Selective production of cyclic carbonate over polycarbonate using a double metal cyanide-quaternary ammonium salt catalyst system. *Green Chem.* **2009**, *11,* 1754-1757.

15- (a) Zhou, H.; Zhang, H.; Mu, S.; Zhang, W.-Z.; Ren, W.-M.; Lu, X.-B. Highly regio- and stereoselective synthesis of cyclic carbonates from biomass-derived polyols via organocatalytic cascade reaction. *Green Chem.* **2019**, *21*, 6335-6341. (b) Li, Y.-D.; Cui, D.-X.; Zhu, J.-C.; Huang, P.; Tian, Z.; Jia, Y.-Y.; Wang, P.-A. Bifunctional phase-transfer catalysts for fixation of CO_2 with epoxides under ambient pressure. *Green Chem.* **2019**, *21*, 5231-5237.

16- (a) Kamphuis, A. J.; Picchioni, F.; Pescarmona, P. P. CO_2-fixation into cyclic and polymeric carbonates: principles and applications. *Green Chem.* **2019**, *21*, 406-448. (b) Liu, X.; de Vries, J. G.; Werner, T. Transfer hydrogenation of cyclic carbonates and polycarbonate to methanol and diols by iron pincer catalysts. *Green Chem.* **2019**, *21*, 5248-5255. (c) Yadav, N.; Seidi, F.; Crespy, D.; D'Elia V. Polymers Based on Cyclic Carbonates as Trait d'Union Between Polymer Chemistry and Sustainable CO_2 Utilization. *ChemSusChem,* **2019**, *12*, 724-754. (d) Ding, Y.; Tian, J.; Chen, W.; Guan, Y.; Xu, H.; Li, X.; Wu, H.; Wu, P. One-pot synthesized core/shell structured zeolite@copper catalysts for selective hydrogenation of ethylene carbonate to methanol and ethylene glycol. *Green Chem.* **2019**, *21*, 5414-5426.

17- Esteve, F.; Altava, B.; Bolte, M.; Burguete, M. I.; García-Verdugo E.; Luis, S. V. Highly Selective Anion Template Effect in the Synthesis of Constrained Pseudopeptidic Macrocyclic Cyclophanes. *J. Org. Chem.* **2020**, *85*, 1138-1145.

18- Sheldrick, G. M. A short history of SHELX. *Acta Crystallogr. A,* **2008**, *64*, 112-122.

19- Sheldrick, G. M. Crystal structure refinement with SHELXL. *Acta Crystallogr. C,* **2015**, *71*, 3-8.

20- Macrae, C. F.; Bruno, I. J.; Chisholm, J. A.; Edgington, P. R.; McCabe, P.; Pidcock, E.; Rodriguez Monge, L.; Taylor, R.; van de Streek, J.; Wood, P. A. New Features for the Visualization and Investigation of Crystal Structures. *J. Appl. Crystallogr.* **2008**, *41*, 466-470.

21- (a) Calculated using Spartan08 software at the MMFF level of theory. Deppmeier, B. J.; Driessen, A. J.; Hehre, T. S.; Hehre, W. J.; Johnson, J. A.; Klunzinger, P. E.; Leonard, J. M.; Pham, I. N.; Pietro W. J.; Jianguo, Y. Spartan '08, build 132 (Mar 27 2009), Wavefunction Inc.: Irvine CA, 2009. (b) Halgren, T. A. Merck molecular force field. I. Basis, form, scope, parameterization, and performance of MMFF94. *J. Comp. Chem.,* **1996**, *17*, 490-519.

22- (a) Mirabaud, A.; Martinez, A.; Bayard, F.; Dutasta, J.-P.; Dufaud, V. A new heterogeneous host-guest catalytic system as an eco-friendly approach for the synthesis of cyclic carbonates from CO_2 and epoxides. *New J. Chem.* **2018**, *42*, 16863-16874. (b) Wang, J.; Liang, Y.; Zhou, D.; Ma, J.; Jing, H. New crown ether complex cation ionic liquids with N-heterocycle anions: preparation and application in CO_2 fixation. *Org. Chem. Front.* **2018**, *5*, 741-748. (c) Mirabaud, A.; Mulatier, J.-C.; Martinez, A.; Dutasta, J.-P.; Dufaud, V. Merging host-guest chemistry and organocatalysis for the chemical valorization of CO_2., *Cat. Today* **2017**, *281*, 387-391. (d) Mirabaud, A.;

Mulatier, J.-C.; Martinez, A.; Dutasta, J. P.; Dufaud, V. Investigating Host–Guest Complexes in the Catalytic Synthesis of Cyclic Carbonates from Styrene Oxide and CO_2. *ACS Catal.* **2015**, *5*, 6748-6752.

23- (a) Maeda, C.; Sasaki, S.; Takaishia, K.; Ema, T. Calix[4]pyrroles as macrocyclic organocatalysts for the synthesis of cyclic carbonates from epoxides and carbon dioxide. *Catal. Sci. Technol.* **2018**, *8*, 4193-4198. (b) Martínez-Rodríguez, L.; Garmilla, J. O.; Kleij, A. W. Cavitand-Based Polyphenols as Highly Reactive Organocatalysts for the Coupling of Carbon Dioxide and Oxiranes. *ChemSusChem* **2016**, *9*, 749-755. (c) Shi, J.; Song, J.; Ma, J.; Zhang, Z.; Fan, H.; Han, B. Effective synthesis of cyclic carbonates from CO2 and epoxides catalyzed by KI/cucurbit[6]uril, *Pure Appl. Chem.* **2013**, *85*, 1633-1641. (d) Song, J.; Zhang, Z.; Han, B.; Hu, S.; Li, W.; Xie, Y. Synthesis of cyclic carbonates from epoxides and CO_2 catalyzed by potassium halide in the presence of β-cyclodextrin. *Green Chem.* **2008**, *10*, 1337-1341.

24- Desens, W.; Kohrt, C.; Frank, M.; Werner, T. Highly Efficient Polymer-Supported Catalytic System for the Valorization of Carbon Dioxide. *ChemSusChem* **2015**, *8*, 3815-3822.

25- Wang, L.; Zhang, G.; Kodama, K.; Hirose, T. An efficient metal- and solvent-free organocatalytic system for chemical fixation of CO_2 into cyclic carbonates under mild conditions. *Green Chem.* **2016**, *18*, 1229-1233.

26- (a) Chen, C.; Zhang, J.; Li, G.; Shen, P.; Jin, H.; Zhang, N. Two coordination polymers constructed from a multidentate carboxylic acid ligand with a tertiary amine serve as acid–base catalysts for the synthesis of chloropropene carbonate from CO_2 under atmospheric pressure. *Dalton Trans.* **2014**, *43*, 13965-13971. (b) Yang, Z. Z.; He, L. N.; Zhao, Y. N.; Li, B.; Yu, B. CO_2 capture and activation by superbase/polyethylene glycol and its subsequent conversion *Energy Environ. Sci.* **2011**, *4*, 3971-3975. (c) Meredith, J. C.; Johnston, K. P.; Seminario, J. M.; Kazarian, S. G.; Eckert, C. A. Quantitative Equilibrium Constants between CO_2 and Lewis Bases from FTIR Spectroscopy. *J. Phys. Chem.* **1996**, *100*, 10837-10848.

27- (a) Andrea, K. A.; Kerton, F. M. Triarylborane-Catalyzed Formation of Cyclic Organic Carbonates and Polycarbonates. *ACS Catal.* **2019**, *9*, 1799-1809. (b) Yingcharoen, P.; Kongtes, C.; Arayachukiat, S.; Suvarnapunya, K.; Vummaleti, S. V. C.; Wannakao, S.; Cavallo, L.; Poater, A.; D' Elia, V. Assessing the pKa-Dependent Activity of Hydroxyl Hydrogen Bond Donors in the Organocatalyzed Cycloaddition of Carbon Dioxide to Epoxides: Experimental and Theoretical Study. *Adv. Synth. Catal.* **2019**, *361*, 366-373. (c) Sodpiban, O.; Del Gobbo, S.; Barman, S.; Aomchad, V.; Kidkhunthod, P.; Ould-Chikh, S.; Poater, A.; D'Elia, V.; Basset, J.-M. Synthesis of well-defined yttrium-based Lewis acids by capturing a reaction intermediate and

catalytic application for cycloaddition of CO_2 to epoxides under atmospheric pressure. *Catal. Sci. Technol.* **2019**, *9*, 6152-6165. (d) Takaishi, K.; Okuyama, T.; Kadosaki, S.; Uchiyama, M.; Ema, T. Hemisquaramide Tweezers as Organocatalysts: Synthesis of Cyclic Carbonates from Epoxides and CO_2. *Org. Lett.* **2019**, *21*, 1397-1401. (e) Wu, X.; Chen, C.; Guo, Z.; North, M.; Whitwood, A. C. Metal- and Halide-Free Catalyst for the Synthesis of Cyclic Carbonates from Epoxides and Carbon Dioxide. *ACS Catal.* **2019**, *9*, 1895-1906. (f) Arayachukiat, S.; Kongtes, C.; Barthel, A.; Vummaleti, S. V. C.; Poater, A.; Wannakao, S.; Cavallo, L.; D'Elia, V. Ascorbic Acid as a Bifunctional Hydrogen Bond Donor for the Synthesis of Cyclic Carbonates from CO_2 under Ambient Conditions. *ACS Sustainable Chem. Eng.* **2017**, *5*, 6392-6397.

28- Liu, S.; Suematsu, N.; Maruoka, K.; Shirakawa, S. Design of bifunctional quaternary phosphonium salt catalysts for CO_2 fixation reaction with epoxides under mild conditions. *Green Chem.* **2016**, *18*, 4611-4615.

29- Liu, N.; Xie, Y.-F.; Wang, C.; Li, S.-J.; Wei, D.; Li, M.; Dai, B. Cooperative Multifunctional Organocatalysts for Ambient Conversion of Carbon Dioxide into Cyclic Carbonates. *ACS Catal.* **2018**, *8*, 9945-9957.

30- (a) Clegg, W.; Harrington, R. W.; North, M.; Pasquale, R. Cyclic Carbonate Synthesis Catalysed by Bimetallic Aluminium-Salen Complexes. *Chem. Eur. J.* **2010**, *16*, 6828-6843. (b) North, M.; Pasquale, R. Mechanism of Cyclic Carbonate Synthesis from Epoxides and CO_2. *Angew. Chem. Int. Ed.* **2009**, *48*, 2946-2948.

31- (a) Wang, L.; Xu, C.; Han, Q.; Tang, X.; Zhou, P.; Zhang, R.; Gao, G.; Xu, B.; Qin, W.; Liu, W. Ambient chemical fixation of CO_2 using a highly efficient heterometallic helicate catalyst system. *Chem. Commun.* **2018**, *54*, 2212-2215. (b) Whiteoak, C. J.; Kielland, N.; Laserna, V.; Escudero-Adán, E. C.; Martin, E.; Kleij, A. W. A Powerful Aluminum Catalyst for the Synthesis of Highly Functional Organic Carbonates. *J. Am. Chem. Soc.* **2013**, *135*, 1228-1231.

32- (a) Martí, I.; Bolte, M.; Burguete, M. I.; Vicent, C.; Alfonso, I.; Luis, S. V. Tight and Selective Caging of Chloride Ions by a Pseudopeptidic Host. *Chem. Eur. J.* **2014**, *20*, 7458-7464. (b) Martí, I.; Rubio, J.; Bolte, M.; Burguete, M. I.; Vicent, C.; Quesada, R.; Alfonso, I.; Luis, S. V. Tuning Chloride Binding, Encapsulation, and Transport by Peripheral Substitution of Pseudopeptidic Tripodal Small Cages. *Chem. Eur. J.* **2012**, *18*, 16728-16741.

33- (a) Pescitelli, G.; Di Bari, L.; Berova, N. Conformational aspects in the studies of organic compounds by electronic circular dichroism. *Chem. Soc. Rev.* **2011**, *40*, 4603-4625. (b) Ranjbar, B.; Gill, P. Circular Dichroism Techniques: Biomolecular and Nanostructural Analyses- A Review. *Chem. Biol. Drug Des.* **2009**, *74*, 101-120. (c)

Bulheller, B. M.; Rodger, A.; Hirst, J. D. Circular and linear dichroism of proteins. *Phys. Chem. Chem. Phys.* **2007**, *9*, 2020-2035. (d) Kelly, S. M.; Jess, T. J.; Price, N. C. How to study proteins by circular dichroism. *Biochim. Biophys. Acta* **2005**, *1751*, 119-139. (e) Kelly, S. M.; Price, N. C. The Use of Circular Dichroism in the Investigation of Protein Structure and Function. *Curr. Prot. Pept. Sci.* **2000**, 1, 349-384.

34- (a) Guo, H.; Zhang, L.-W.; Zhou, H.; Meng, W.; Ao, Y.-F.; Wang, D.-X.; Wang, Q.-Q. Substrate-Induced Dimerization Assembly of Chiral Macrocycle Catalysts toward Cooperative Asymmetric Catalysis. *Angew. Chem. Int. Ed.* **2020**, *59*, 2623-2627. (b) Evans, N. H.; Beer, P. D. Advances in Anion Supramolecular Chemistry: From Recognition to Chemical Applications. *Angew. Chem. Int. Ed.* **2014**, *53*, 11716-11754. (c) Cabbiness, D. K.; Margerum, D. W. Macrocyclic effect on the stability of copper(II) tetramine complexes. *J. Am. Chem. Soc.* **1969**, *91*, 6540-6541.

35- Alfonso, I.; Burguete, M. I.; Galindo, F.; Luis, S. V.; Vigara, L. Molecular Rotors as Simple Models to Study Amide NH-Aromatic Interactions and Their Role in the Folding of Peptide-like Structures. *J. Org. Chem.* **2007**, *72*, 7947-7956.

36- Tappe, N. A.; Reich, R. M.; D'Elia, V.; Kühn, F. E. Current advances in the catalytic conversion of carbon dioxide by molecular catalysts: an update. *Dalton Trans.* **2018**, *47*, 13281-13313.

5.2. Supporting information
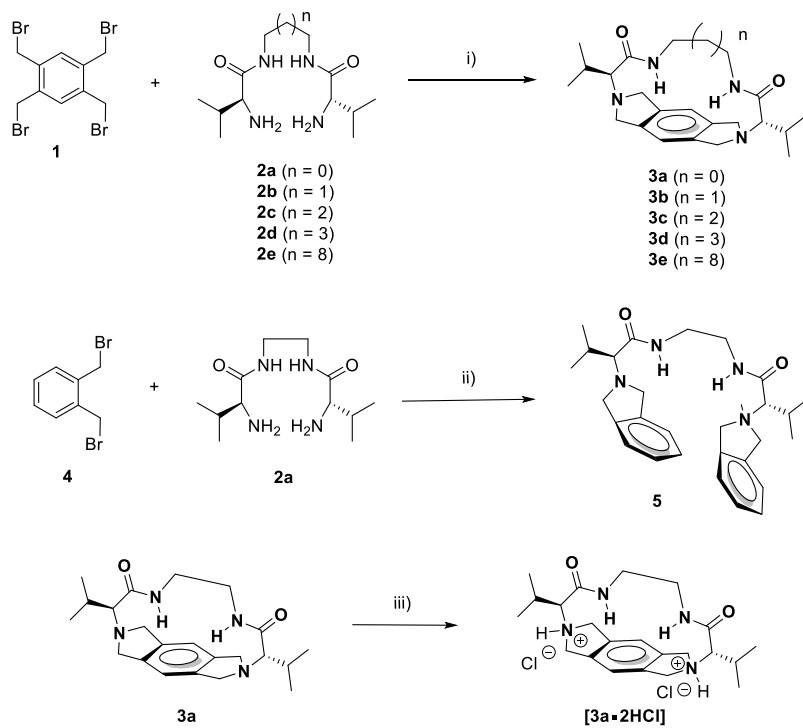
Scheme S5.1. Synthesis of macrocyclic systems and related analogues. i) CH$_3$CN, 2-3 h, 90 °C. ii) CH$_3$CN, 5 h, 90 °C. iii) CH$_3$OH, 1 h, 25 °C.

Table S5.1. Comparation of the results in this work with some selected organocatalytic/supramolecular examples for the reaction between styrene oxide (**6**) and CO$_2$ to afford **7**.
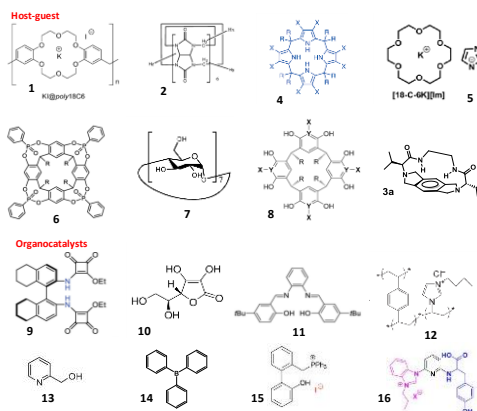
Entry	Ref.	Catalyst	T (°C)	P (bar)	% cat	Time (h)	Conv. (%)	TON	TOF
1	1	Polycrown ether 18C6 (**1**) - KI	100	10	2	3	89	44.5	14.8
2	2	curcurbit[6]uril (**2**) - KI	120	40	1.5 KI 0.1 g CB[6]	5	95	63.3	12.7
3	3	calix[4]pyrrole (R= CH3- X= H) (**4**) - Bu$_4$NI	100	17	1	15	98	98	6.5
4	4	IL+crown ether [18-C-6-K][Im] (**5**)	100	10	1	6	93	93.5	15.6
5	5	Tetraphosphonate Cavitand (R = C3H7) (**6**) - Bu$_4$NCl	100	1	1 (**6**) - 1 co-cat	24	85	85	3.5
		Tetraphosphonate Cavitand (R = C3H7) (**6**) - Me$_4$NCl					25	25	1
		Tetraphosphonate Cavitand (R = C3H7) (**6**) - Me$_4$NBr					58	58	2.4
		Tetraphosphonate Cavitand (R = C3H7) (**6**) - Me$_4$NI					92	92	3.8
6	6	β-CD (**7**) - KI	120	60	2.5 KI	12	94	37.6	3.1
7	7	Cavitand-Based Polyphenols (**8**) - Bu$_4$NI	50	10	1.5 (**8**) - 5 Bu$_4$NI (MEK)	18	93	62	3.4
		1,2-Epoxyhexane instead of **6** (solventless)	80	10	0.01 (**8**) - 1.6 Bu$_4$NI	18	74	7400	411
8	This work	Macrocycle **3a**- Bu$_4$NCl	100	10	0.01 of **3a** - 0.1 Cl	5	76	7600	1525
			80	1	0.01 of **3a** - 1 Cl (ACN)	3	39	3900	1300
9	8	Hemisquaramide (**9**) - Bu$_4$NI	30	1	2 (**9**) - 5 Bu$_4$NI	24	92	18.4	0.8
10	9	Ascorbic acid (**10**) - Bu$_4$NI	60	1	2 (**10**) - 4 Bu$_4$NI	23	96	48	2.1
11	10	Salophens (**11**)	120	10	10	24	100	10	0.4
					5 (2-MeTHF)	24	90	18	0.8
12	11	PILs (**12**)	110	60	0.526	7	79	150	21.5
13	12	2-Pyridinemethanol (**13**)	25	1	8 (**13**) + 8 Bu$_4$NI	18	91	11.4	0.6
14	13	Triarylboranes (**14**) Propylene oxide instead of **6**	100	1	0.025 (**14**) + 0.1 PPNCl	24	31	1240	52
		Glycidyl chloride instead of **6**	100	20	0.025 (**14**) + 0.1 PPNCl	3	76	3040	1013
15	14	Phosphonium salts (**15**)	60	1	1	24	92	92	3.8
16	15	Organic pincers (**16**)	25	1	4	24	62	15.5	0.65

References

1: T. Werner and coworkers, *ChemSusChem*, 2015, **8**, 3815-3822; **2:** B. Han and coworkers, *Pure Appl. Chem.*, 2013, **85**, 1633-1641; **3:** T. Ema and coworkers, *Cat. Sci. Technol.*, 2018, **8**, 4193-4198; **4:** H. Jing and coworkers, *Org. Chem Front.*, 2018, **5**, 741-748; **5:** J.-P. Dutasta, V. Dufaud and coworkers, *ACS Catal.*, 2015, **5**, 11, 6748-6752; **6:** B. Han and coworkers, *Green Chem.*, 2008, **10**, 1337–1341; **7:** A. W. Kleij and coworkers, *ChemSusChem*, 2016, **9**, 749-755; **8:** T. Ema and coworkers, *Org. Lett.,* 2019, **21**, 1397-1401; **9:** V. D'Elia and coworkers, *ACS Sustainable Chem. Eng.*, 2017, **5**, 6392-6397; **10:** M. North and coworkers, *ACS Catal.*, 2019, **9**, 1895-1906; **11:** B. Han and coworkers, *Angew. Chem. Int. Ed.*, 2007, **46**, 7255-7258; **12:** T. Hirose and coworkers, *Green Chem.*, 2016, **18**, 1229-1233; **13:** F. M. Kerton and coworkers, *ACS Catal.*, 2019, **9**, 1799-1809; **14:** S. Shirakawa and coworkers, *Green Chem.*, 2016, **18**, 4611-4615; **15:** N. Liu and coworkers, *ACS Catal.,* 2018, **8**, 9945-9957.

Table S5.2. Selected metal-based catalytic systems for the reaction between styrene oxide (**6**) and CO_2 to afford **7**.
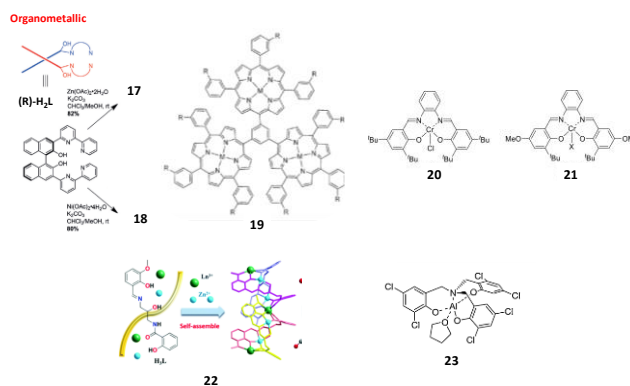
Entry	Ref.	Catalyst	T (ºC)	P (bar)	% cat	Time (h)	Conv. (%)	TON	TOF
1	16	Multinuclear complexes **17** (Zn) **18** (Ni)	120 120	150 150	0.1 0.1	24 24	70 97	700 970	29 40
2	17	Trimer Porphyrin Platforms (**19**) (Zn, R = O(CH₂)₆NBu₃Br)	120	250	0.002	9	96	48000	5333
3	18	Cr(salophen) **20** - Bu₄NBr	25		2.5 (**16**) - 5 Bu₄NBr	6	65	25.8	4.3
		21 (X = Br) - Bu₄NBr			2.5 (**17**) - 5 Bu₄NBr	6	71	28.2	4.7
4	19	Zn₃[Co(CN)₆]₂ - Bu₄NCl	100	3.4	0.1 (Zn) - 1 Bu₄NCl	6	43	430	71.7
5	20	heterometallic helicate complex (**22**) - Bu₄NBr	120	10	0.025 (**18**) – 0.75 Bu₄NBr	1	96	3840	3840
					0.0025 (**18**) – 0.5 Bu₄NBr	1	67	26800	26800
6	21	Al-complex (**23**) – Bu₄NI (4-Fluorostyrene oxide)	70	10	0.05 (**19**) - 0.25 Bu₄NI	18	93	1860	103
		1,2-epoxyhexane instead of **6**			0.0005 (**19**) - 0.5 Bu₄NI	2	24	48000	24000
					0.0005 (**19**) - 0.5 Bu₄NI	18	56	112000	6222

References

16: T. Ema and coworkers, *Angew. Chem. Int. Ed.*, 2019, **58**, 9984-9988; **17:** T. Ema and coworkers, *Angew. Chem. Int. Ed.*, 2015, **54**, 134-138; **18:** M. North and coworkers, *ACS Catal.*, 2016, **6**, 5012-5025; **19:** D.-W. Park and coworkers, *Green Chem.*, 2009, **11**, 1754-1757; **20:** W. Liu and coworkers, *Chem. Commun.*, 2018, **54**, 2212-2215; **21:** A. W. Kleij and coworkers, *J. Am. Chem. Soc.*, 2013, **135**, 1228-1231.

Table S5.3. Effect of the nature of the alkyl group in the **3a** : R$_4$NCl catalytic system for the reaction between styrene oxide (**6**) and CO$_2$ to afford **7**.[a]

Entry	R$_4$NCl (mol%)	3a (mol%)	Conversion[b] (%)	TON (3a)
1	X = Bu, (1)	-	65	-
2	X = Et, (1)	-	54	-
3	X = Me, (1)	-	0	-
4	X = Bu, (1)	0.1	93	930
5	X = Et, (1)	0.1	80	800

[a] Reaction conditions: 1 mL epoxide **6** (8.7 mmol), p(CO$_2$)=1 bar (CO$_2$ balloon), 5 h, 100 °C.
[b] Conversions determined by ^{1}H NMR, selectivity for **7** was >99.9 %.

Table S5.4. Effect of the solvent for the reaction between styrene oxide (**6**) and CO$_2$ to afford **7**.[a]

Entry	Bu$_4$NCl (mol%)	3a (mol%)	Solvent	Time (h)	Conversion[b] (%)	TON (Bu$_4$NCl)	TON (3a)
1	1	-	MeTHF	1	3	3	-
2	1	0.1	MeTHF	1	3	3	30
3	1	-	ACN	1	9	9	-
4	1	0.1	ACN	1	25	25	250
5	1	-	ACN	3	18	18	-
6	1	0.1	ACN	3	59	59	590
7	1	0.01	ACN	3	39	39	3900

[a] Reaction conditions: 80 °C, 2.4 M of **6** in the solvent, p(CO$_2$)=1 bar. [b] Conversions determined by ^{1}H NMR, selectivity for **7** was >99.9 %.
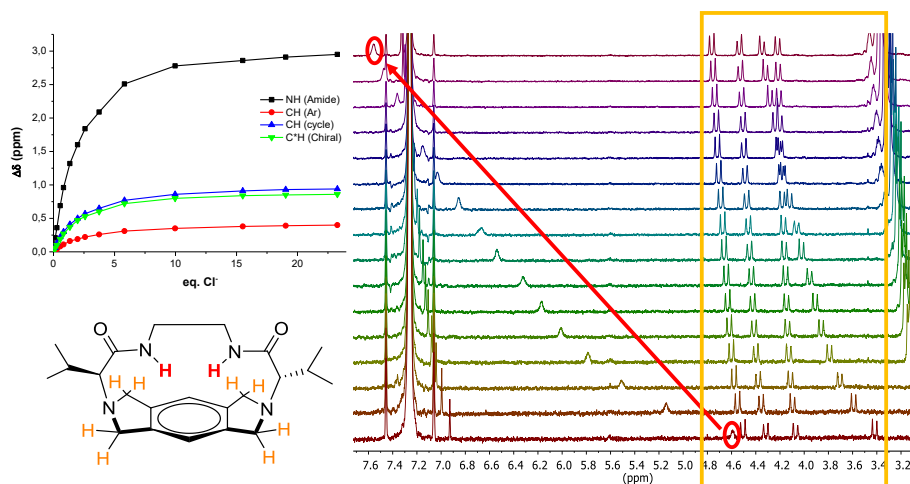
Figure S5.1. Partial ¹H NMR spectra for the titration of **3a** with Bu₄NCl. The downfield shift highlighted in red corresponds to the NH$_{amide}$ signal. Solvent: benzene-d_6 (0.5 mM).
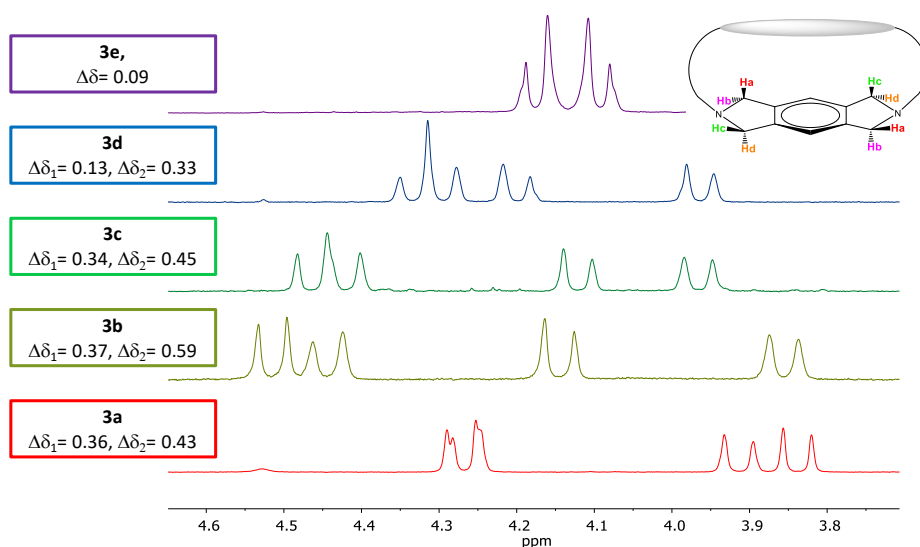
Figure S5.2. Partial ¹H NMR (400 MHz) spectra (signals for the isoindolinic protons) of the macrocyclic pseudopeptides **3a-e**, 6 mM in CD₃OD. $\Delta\delta_1$ and $\Delta\delta_2$ correspond to the difference in chemical shifts between Ha and Hb and/or Hc and Hd.
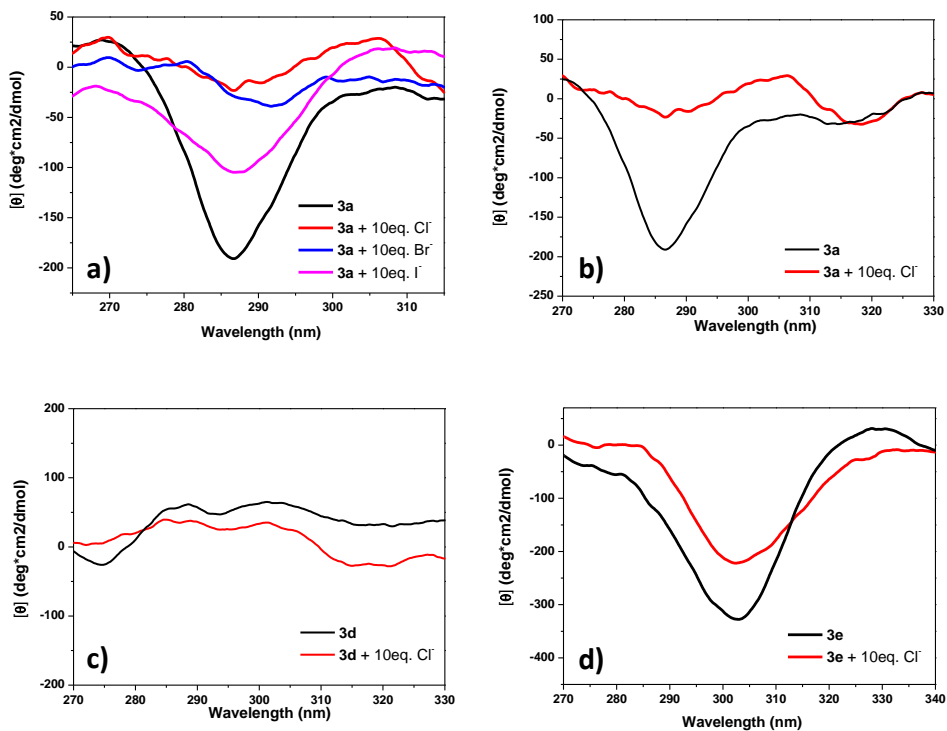
Figure S5.3. a) CD spectra of **3a** in the presence of 10 eq. of Bu$_4$NX; b)-d) CD spectra of **3a**, **3d** and **3e** in the absence and presence of 10 eq. of chloride anion.
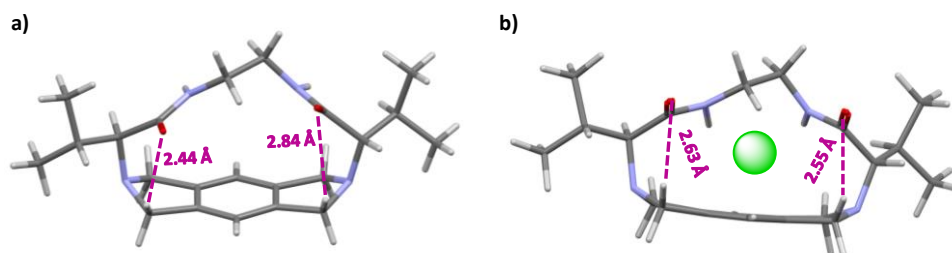
Figure S5.4. a) Structure of **3a** found in the crystal structure (*syn*-disposition of the amide groups). b) Lowest energy conformation for [**3a** + Cl⁻] calculated using Spartan08 at the MMFF (Merck Molecular Force Field) level of theory. The lines display the distances between each C=O group and the closest hydrogen atom of the isoindolinic ring.

Table S5.5. Shifts observed for the NH_{amide} signals in the presence of 10 equivalent of Bu_4NX.[a]

Entry	Bu₄NX: 3a	Cl	Br	I
1	$\Delta\delta$(NH) ppm	2.74	1.43	0.19

[a] Solvent: benzene-d_6 (0.5mM).
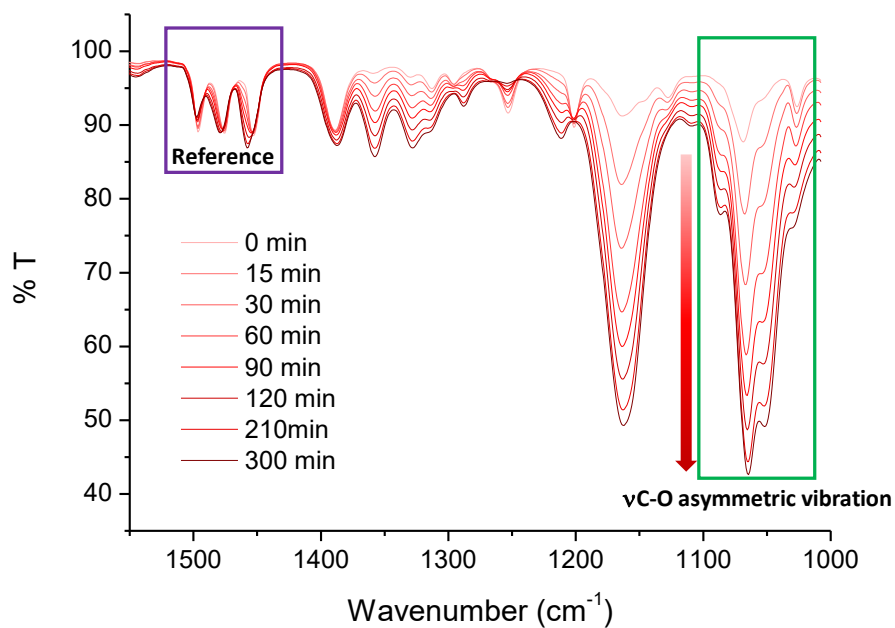
Figure S5.5. Partial FT-ATR-IR spectra used to obtain the kinetic profiles for the reaction between styrene oxide (**6**) and CO_2 to afford **7**. Reaction conditions: solventless, 100 °C, 5 h, CO_2 balloon.
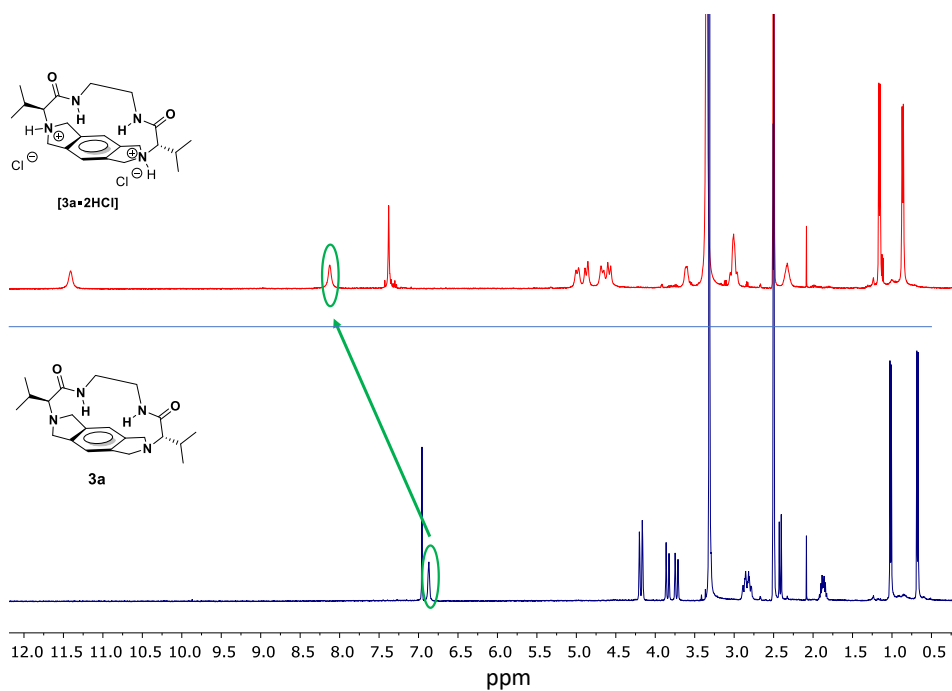
Figure S5.6. ^{1}H NMR (400 MHz, 30 °C) spectra of **3a** and **[3a·2HCl]** using DMSO-d$_6$ as the solvent (9 mM). The downfield shift observed for the NH$_{amide}$ has been highlighted in green.
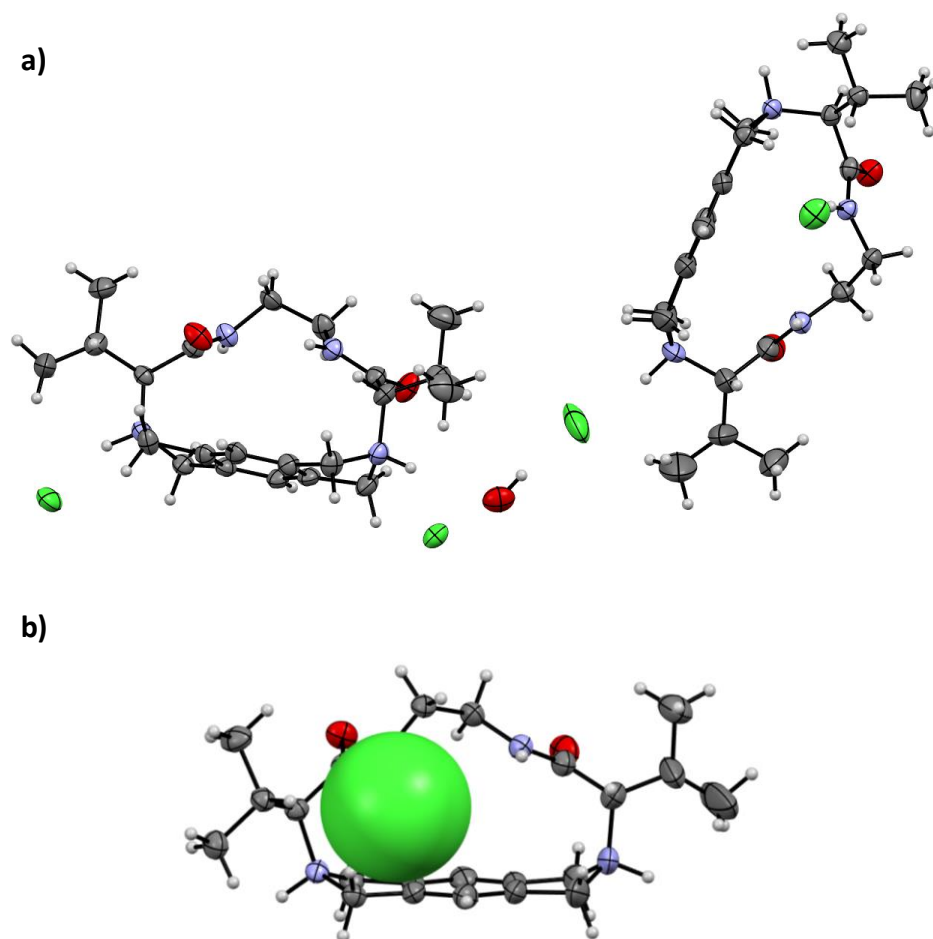
Figure S5.7. a) Unit cell for the crystal structure of the [**3a·2HCl**] salts displaying the two conformations present (*syn-* and *anti*-disposition of the amide groups). Ellipsoids at 50% of probability. Chloride anions are highlighted in green. One of the chloride anions can adopt two slightly different positions; only one is shown for clarity. b) Representation of the structure for the conformer with the *syn*-disposition of the amide groups highlighting the position of the chloride anion (CPK representation) interacting with the amide groups. The second chloride anion has been deleted for clarity.
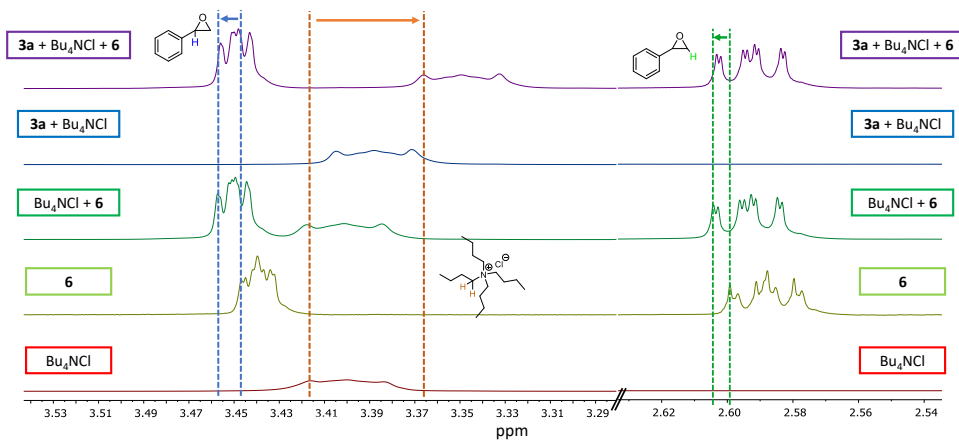
Figure S5.8. Partial ^1H NMR (500 MHz) spectra for Bu4NCl, **6** and the mixtures [Bu4NCl + **6**], [**3a** + Bu4NCl] and [**3a** + Bu4NCl + **6**] in C_6D_6. [**6**] = 240 mM; [Bu4NCl] = 20 mM; [**3a**] = 2 mM (samples in 1mL of C_6D_6).
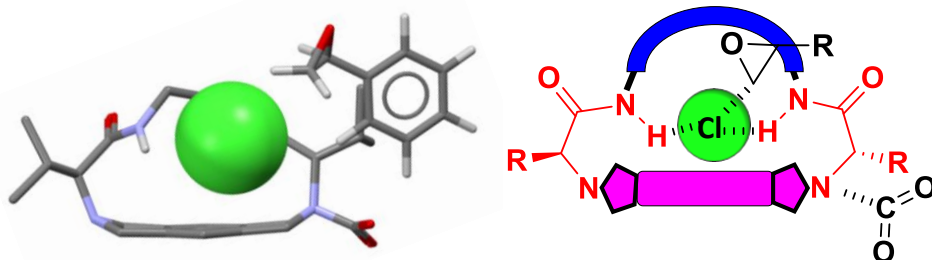
Figure S5.9. Lowest energy conformer calculated for the [**3a** + Cl- + **6**] species in the presence of CO_2 activated by the tertiary amino group. MMFF level of theory. Non-essential hydrogen atoms are omitted for clarity.
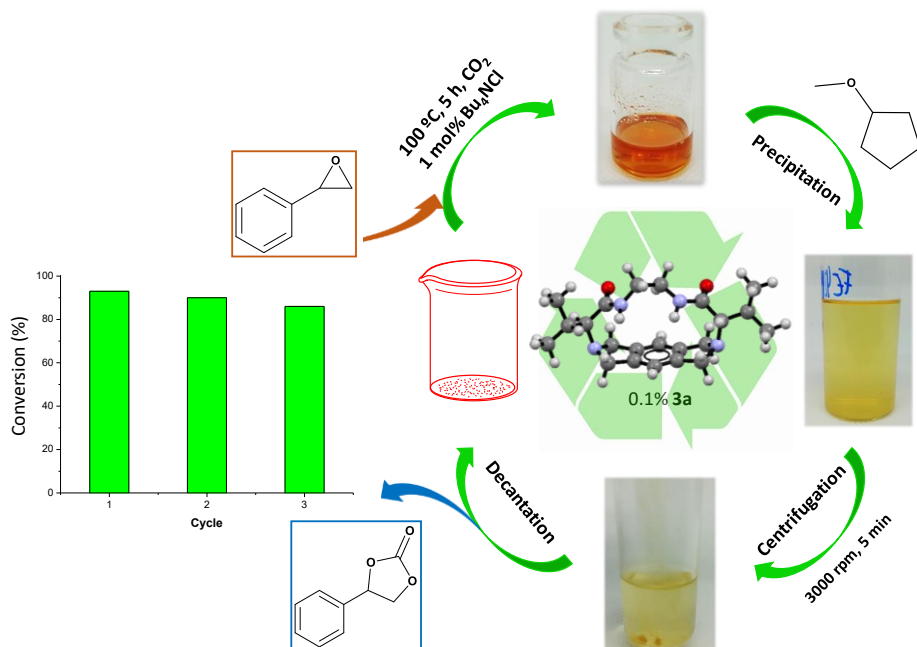
Figure S5.10. Schematic representation of the protocol for catalyst **3a** recycling.
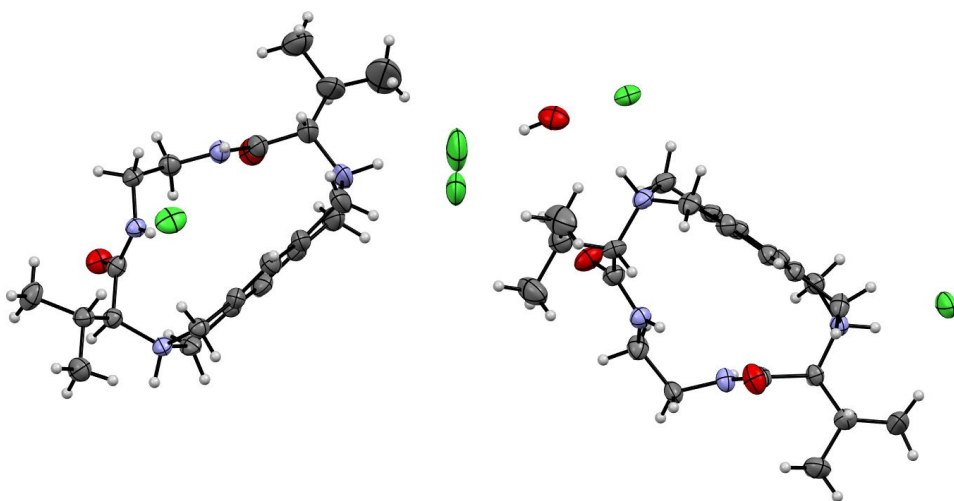
Figure S5.11. Thermal ellipsoid plot for the crystal structure of [**3a·2HCl**]. Ellipsoids at 50% of probability.
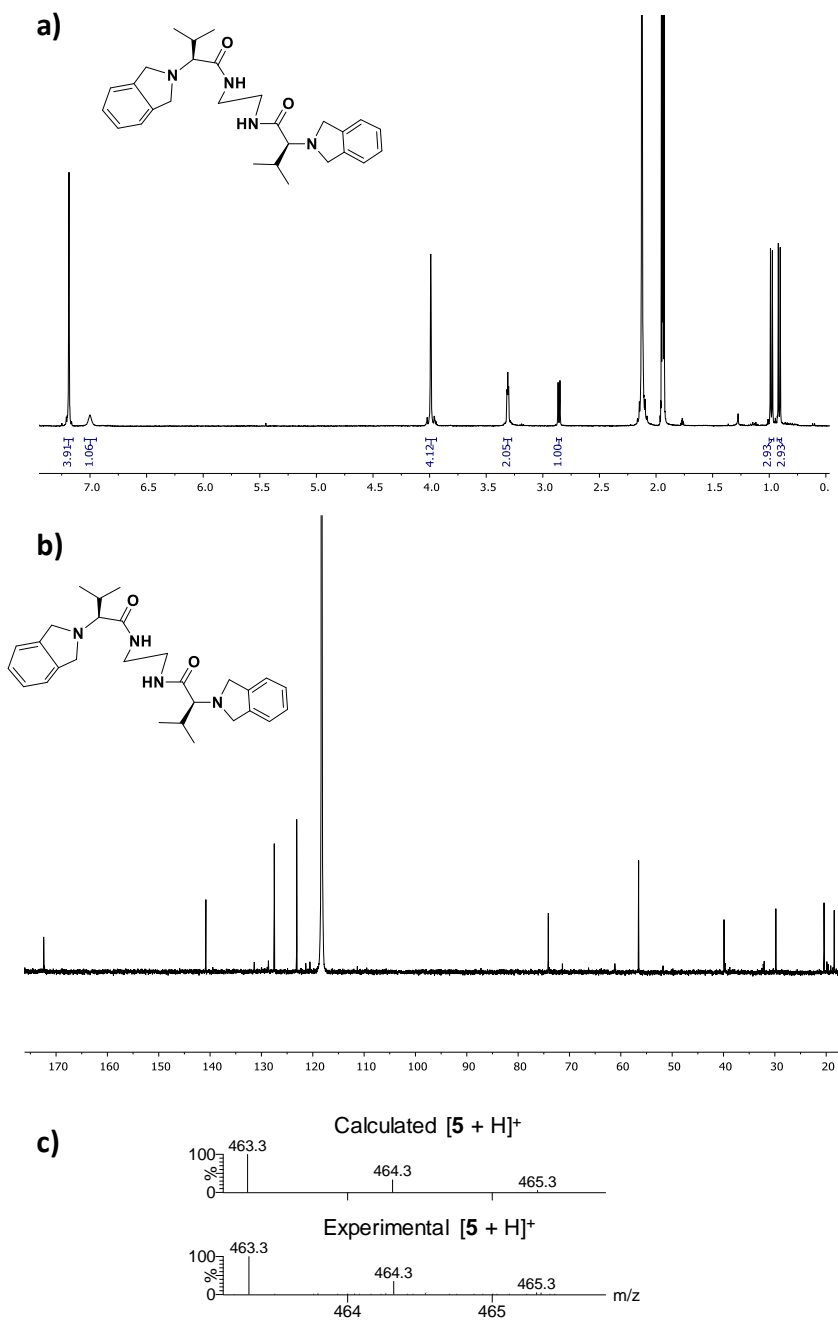
Figure S5.12. a) ^{1}H NMR (400 MHz, CD$_3$CN); b) ^{13}C{^{1}H} NMR (100 MHz, CD$_3$CN) and c) HRMS (ESI/Q-TOF, CH$_3$OH) for pseudopeptide **5**.

Chapter 6

Immobilized Supramolecular Systems as Efficient Synzymes for CO_2 activation and Conversion

HYDROPHOBIC SOLID-SOLVENT

ACTIVE POCKET
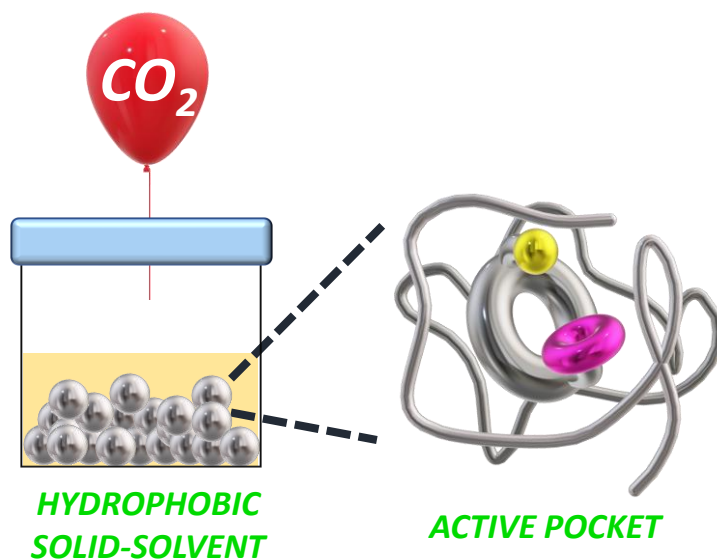
6.1. Main text

6.1.1. Abstract

Supramolecular catalysis can provide distinct advantages for the catalytic conversion of CO_2 into carbonates by cycloaddition to epoxides. For example, the absence of metals in the catalytic site, and the easy design for optimization. The incorporation of multiple functionalities in pseudopeptidic macrocycles with a pendant arm allows catalytic systems to be obtained where halide anions (nucleophilic activating agents for epoxides), hydrogen bond acceptor sites (activating agents for epoxides and stabilizing sites for anionic intermediates), and amine groups (Lewis basic sites for activating CO_2) are in proximity. This allows a high activity in the cycloaddition of CO_2 to styrene oxide under mild conditions (turnover number (TON) = 900, CO_2 balloon, 100 °C, 5 h). The primary amino groups in the arm facilitate the immobilization of these macrocyclic structures in cross-linked polymeric matrices containing ammonium halide fragments. Such multifunctional insoluble polymers afford excellent catalytic results with high TON and turnover frequency values and remarkable productivities (>10 $g_{prod}/g_{resin}\cdot$h). This activity is maintained for a variety of epoxides and is retained after several catalytic runs. Their performance is significantly higher than those reported for most heterogenous supramolecular catalytic systems for CO_2 transformation into carbonates.

6.1.2. Introduction

Enzymes can induce remarkable reactivity in catalytic transformations, while maintaining high selectivity, based on the presence of a well-defined network of reversible noncovalent forces.[1] Indeed, enzymes are a major inspiration for supramolecular chemistry. Therefore, it is not surprising that enzymes have served as prototypes for the meticulous design of supramolecular catalysts.[2] In recent years, many efforts have been devoted to developing abiotic systems able to mimic such catalytic proficiencies by means of host-guest supramolecular interactions.[3] However,

finding highly active supramolecular catalytic systems is not a trivial task. In enzymes, their tertiary structure defines a shielded catalytic pocket, allowing strong noncovalent forces even in highly competitive environments (i.e., water).[4] On the contrary, for an abiotic supramolecular catalytic system, the host-guest interactions (i.e., hydrogen bonding, halogen bonding, π-π-stacking, dipolar aggregation, and solvophobic forces) that define the supramolecular microenvironment facilitating an active and selective transformation are usually very sensitive to the nature of the solvents.[5] Thus, it is important that solvent effects are taken into account when designing new supramolecular catalytic systems. Very often, the behaviour of such systems is enhanced using non-competitive organic solvents, which can be highly toxic and/or display high boiling points (toluene, dimethyl sulfoxide, etc.), and under relatively dilute conditions, leading to an increased usage of solvents. This results in both waste generation and an increased energy demand for the separation steps, often overpassing the one involved in the targeted chemical transformation. A promising solution to overcome these issues is the use of solid solvents. These systems are organic/inorganic materials that provide a solvent-like solid medium, onto which host molecules can be grafted in a controlled manner defining, at the molecular scale, the microenvironment required to favour the host–guest supramolecular interactions. Although some bioinspired solid solvents have shown promising results on this behalf, this is still a seldom explored field.[6]

The growing emissions of carbon dioxide to the atmosphere have triggered the blossoming of technologies for its capture, activation, and conversion into added value chemicals.[7,8] Nevertheless, the high kinetic and thermal stability of CO_2 appears as a major challenge.[9] Hence, the development of new catalysts for CO_2 transformation, able to work at mild process conditions with good performance, and being also reusable and easily separable, is of high industrial interest.[10,11] Among the different added-value products that have been obtained using carbon dioxide,[12-14] cyclic carbonates (CC) are one of the most popular.[15] Several metal-based systems have been reported as highly active in the catalytic conversion of CO_2 to CC, under mild conditions.[16-20] Organocatalytic processes can be considered as greener catalytic

approaches, as they avoid issues related to metal contamination, and, in the last decade, a variety of metal-free systems have been designed as sustainable alternatives for catalysed CC formation.[21] Immobilization of catalytic species on solid matrices has become, likewise, a common method to decrease the environmental impact, facilitating the recovery and reuse of the catalysts.[22-24] Currently, however, the reported heterogenous catalysts require harsh reaction conditions, which highlights the need of further developments in this field to achieve practical applications.[25,26] In this context, examples of supramolecular catalytic systems evaluated for this process are seldom.[27-29] Most of them rely on a host able to strongly bind cations, affording activated anions (i.e., "naked" X^-) that increase, in this way, their nucleophilicity in the initial epoxide ring-opening step.[30-32] Even more scarce is the use of immobilized supramolecular systems for the cycloaddition of CO_2 to epoxides.[33-35]

Herein, we report a new supramolecular (metal-free) system presenting high activity in the cycloaddition of carbon dioxide to epoxides under mild conditions, in the absence of additional solvents/cocatalysts. The immobilization of a pseudopeptidic macrocyclic host and halide nucleophiles in a polymeric matrix provided a suitable microenvironment and afforded excellent catalytic systems with improved practical application. The experimental results revealed that the polystyrene matrix enhanced the supramolecular interactions between the active catalytic pockets and the substrates. Mechanistic insights were studied by spectroscopic techniques, demonstrating the paramount role of the noncovalent interactions in the activity of the macrocyclic organocatalysts. Besides, the material could be easily recovered and applied to a wide range of epoxides with well-differentiated chemical properties. This greener approach addresses the UN's Sustainable Development Goals (SDGs) 9, 11, and 13 encompassing waste reduction and conversion of environmentally hazardous species.

6.1.3. Experimental section

General.

NMR experiments were carried out at 400 or 300 MHz for ^{1}H and 125, 100, or 75 MHz for [13]C. Chemical shifts were reported in ppm from tetramethylsilane using the solvent resonance as the internal standard. FTIR were recorded using a JASCO instrument with an ATR adapter. RAMAN analyses were performed using a Witec instrument. HRMS was recorded with a Q-TOF instrument. Optical rotation was determined with a digital polarimeter (Na: 589 nm). Melting points were measured using a standard apparatus and were uncorrected. Open-chain pseudopeptidic compounds **2** were prepared following literature procedures,[8c] as well as the macrocyclic structures **3**.[17]

General Procedure for the Synthesis of Macrocyclic Pseudopeptides.

*Synthesis of **3a**:* Open-chain pseudopeptidic compound **1** was prepared following literature procedures.[48] Compound **1** (0.263 g, 0.594 mmol) and caesium carbonate (1.161 g, 3.564 mmol) were placed in a 250 mL twin-necked round bottom flask under an inert atmosphere, using dry acetonitrile (198 mL) as solvent. Then, the bromomethyl aromatic reagent **2a** (0.281 g, 0.594 mmol) was dissolved in dry CH_3CN (15 mL) and added dropwise. The reaction mixture was refluxed for 3 h. The resultant suspension was filtered, and the solution was dried under reduced pressure. The white solid obtained was purified by flash chromatography (CH_2Cl_2/MeOH as the eluent) affording pure **3a**. Yield: 16% (0.054 g, 0.095 mmol). Characterisation: white solid, mp = 183 °C; $[\alpha]_D^{20}$ = −24.9 (c = 0.1, CH_3OH); ^{1}H NMR (400 MHz, CD_3OD, δ): 6.94 (s, 2H), 4.34 (dd, J = 19.2, 14.5 Hz, 4H), 4.19 (d, J = 14.1 Hz, 2H), 3.97 (d, J = 13.8 Hz, 2H), 3.75 (d, J = 6.1 Hz, 1H), 3.24–3.12 (m, 3H), 2.74–2.64 (m, 5H), 2.22–2.12 (m, 3H), 2.06 (dt, J = 10.7, 6.6 Hz, 2H), 1.85–1.73 (m, 2H), 1.09 (d, J = 6.6 Hz, 6H), 1.04 (dd, J = 17.0, 6.9 Hz, 6H), 0.85 (d, J = 6.5 Hz, 6H); ^{13}C NMR (75 MHz, CD_3OD, δ): δ = 171.8, 171.6, 139.7, 139.1, 116.3, 73.7, 59.3, 59.1, 54.2, 51.5, 37.0, 35.0, 31.3, 28.0, 18.9, 18.7, 18.2, 16.5; ATR-FTIR:

3325, 3040, 2980, 1632, 1525, 1450 cm^{-1}; HRMS (ESI) m/z: [**3a** + H]$^+$ calcd for C$_{31}$H$_{52}$N$_7$O$_3$, 570.4126; found, 570.4128.

Synthesis of ***3b***: Prepared following the procedure described above. Yield: 34% (0.099 g, 0.156 mmol). Characterisation: white solid, mp = 156 °C; [α]$_D^{20}$ = −15.6 (c = 0.1, CH$_3$OH); ^{1}H NMR (400 MHz, CD$_3$OD, δ): 7.25 (d, 2H, J = 8.0 Hz), 7.08 (d, 2H, J = 8.0 Hz), 4.00 (d, J = 13.7 Hz, 1H), 3.92 (s, 1H), 3.55 (d, J = 13.7 Hz, 1H), 3.25–3.16 (m, 2H), 3.06–2.95 (m, 1H), 2.89 (t, J = 7.0 Hz, 1H), 2.85 (d, J = 5.0 Hz, 1H), 2.54 (q, J = 6.6 Hz, 1H), 2.44 (t, J = 6.9 Hz, 2H), 2.07–1.92 (m, 2H), 0.99 (d, J = 6.9 Hz, 3H), 0.98–0.93 (m, 3H), 0.92 (d, J = 6.7 Hz, 3H); ^{13}C NMR (75 MHz, CD$_3$OD, δ): δ = 176.7, 176.4, 141.6, 138.8, 129.9, 68.9, 61.7, 58.3, 54.6, 53.4, 38.0, 38.1, 33.3, 32.9, 25.2, 19.8, 18.5, 17.8; ATR-FTIR: 3310, 3075, 2955, 1643, 1511, 1464 cm^{-1}; HRMS (ESI) m/z: [**3b** + H]$^+$ calcd for C$_{36}$H$_{57}$N$_7$O$_3$, 636.4601; found, 636.4605.

General Procedure for the Immobilization of Tributylamine.

Resin **5**: Merrifield resin **4** (microporous, 1% DVB cross-linking, 3.9 mmol g^{-1} Cl loading) (0.600 g, 2.340 mmol) was introduced in a 12 mL vial. The polymer was swelled with DMF (3 mL), and tributylamine (0.867 g, 4.680 mmol) was added to the resultant suspension. The vial was introduced in an orbital agitator and heated to 60 °C with a constant agitation of 150 rpm. After 12 h of reaction, the functionalized resin was filtered and washed with DMF, MeOH, and CH$_2$Cl$_2$. The final material was dried overnight under reduced pressure at 50 °C. Yield: 92%. The degree of functionalization (DF) was determined by RAMAN, FTIR, and EA. The presence or absence of chloromethyl groups was also evaluated by the NBP test. TGA analyses revealed the thermal stability of the materials. See the Supporting Information for detailed characterisation.

*General Procedure for the Immobilization of **3**.*

*Synthesis of **6f**.* Resin **4** (0.090 g, 0.351 mmol) was introduced in a 12 mL vial. The polymer was swelled with DMF (2 mL), and DIPEA (0.045 g, 0.351 mmol) was added to this suspension. Compound **3b** (0.223 g, 0.351 mmol) was separately dissolved in DMF (1 mL) and then added to the vial containing the polymer. The vial was introduced in an orbital agitator and heated to 80 °C with a constant agitation of 150 rpm. After 18 h of reaction, the resin was filtered and washed with DMF, MeOH, and CH_2Cl_2. The final material was dried overnight under reduced pressure at 50 °C. Yield: 95%. The DF was determined by RAMAN, FTIR, and EA. The presence or absence of chloromethyl groups was evaluated by the NBP test. TGA analyses revealed the thermal stability of the materials. See the Supporting Information for detailed characterisation of the resins.

Characterisation of the resins.

*Resin **5a**.* This material was synthesized following the experimental procedure described in the main manuscript. IR: absence of band at 1264 cm^{-1}. RAMAN: absence of band at 1268 cm^{-1}. Negative NBP Test. Decomposition temperature: 180 °C (TGA). Elemental analysis theoretical %N = 3.2, experimental = 3.3. IR bands: 3024, 2953, 1480, 1376, 863. Raman bands: 3063, 2923, 1610, 1193, 1005.

*Resin **5b**.* This material was synthesized following the experimental procedure described in the main manuscript. IR: presence of band at 1264 cm^{-1}. RAMAN: presence of band at 1268 cm^{-1}. Positive NBP Test. Decomposition temperature: 181 °C (TGA). Elemental analysis theoretical %N = 2.9, experimental = 2.5. IR bands: 3024, 2953, 1480, 1376, 1264, 863. Raman bands: 3063, 2923, 1610, 1268, 1193, 1005.

*Resin **5c**.* This material was synthesized following the experimental procedure described in the main manuscript. IR: presence of band at 1264 cm^{-1}. RAMAN: presence of band at 1268 cm^{-1}. Positive NBP Test. Decomposition temperature: 182

°C (TGA). Elemental analysis theoretical %N = 2.5, experimental = 2.0. IR bands: 3024, 2953, 1480, 1376, 1264, 863. Raman bands: 3063, 2923, 1610, 1268, 1193, 1005.

Resin **5d**. This material was synthesized following the experimental procedure described in the main manuscript. IR: presence of band at 1264 cm^{-1}. RAMAN: presence of band at 1268 cm^{-1}. Positive NBP Test. Decomposition temperature: 215 °C (TGA). Elemental analysis theoretical %N = 2.0, experimental = 1.7. IR bands: 3024, 2953, 1480, 1376, 1264, 863. Raman bands: 3063, 2923, 1610, 1268, 1193, 1005.

Resin **5e**. This material was synthesized following the experimental procedure described in the main manuscript. IR: presence of band at 1264 cm^{-1}. RAMAN: presence of band at 1268 cm^{-1}. Positive NBP Test. Decomposition temperature: 227 °C (TGA). Elemental analysis theoretical %N = 1.3, experimental = 0.9. IR bands: 3024, 2953, 1480, 1376, 1264, 863. Raman bands: 3063, 2923, 1610, 1268, 1193, 1005.

Resin **6b**. This material was synthesized following the experimental procedure described in the main manuscript. IR: absence of band at 1264 cm^{-1}. RAMAN: absence of band at 1268 cm^{-1}. Negative NBP Test. Decomposition temperature: 183 °C (TGA). Elemental analysis theoretical %N = 4.6, experimental = 3.4. IR bands: 3024, 2953, 1664, 1480, 1376, 854. Raman bands: 3063, 2923, 1610, 1193, 1005.

Resin **6c**. This material was synthesized following the experimental procedure described in the main manuscript. IR: absence of band at 1264 cm^{-1}. RAMAN: absence of band at 1268 cm^{-1}. Negative NBP Test. Decomposition temperature: 186 °C (TGA). Elemental analysis theoretical %N = 6.9, experimental = 4.9. IR bands: 3024, 2953, 1664, 1480, 1376, 854. Raman bands: 3063, 2923, 1610, 1193, 1005.

Resin **6d**. This material was synthesized following the experimental procedure described in the main manuscript. IR: absence of band at 1264 cm^{-1}. RAMAN: absence of band at 1268 cm^{-1}. Negative NBP Test. Decomposition temperature: 235

°C (TGA). Elemental analysis theoretical %N = 8.6, experimental = 5.5. IR bands: 3024, 2953, 1664, 1480, 1376, 854. Raman bands: 3063, 2923, 1610, 1193, 1005.

*Resin **6e**.* This material was synthesized following the experimental procedure described in the main manuscript. IR: absence of band at 1264 cm^{-1}. RAMAN: absence of band at 1268 cm^{-1}. Negative NBP Test. Decomposition temperature: 273 °C (TGA). Elemental analysis theoretical %N = 9.9, experimental = 4.8. IR bands: 3024, 2953, 1664, 1480, 1376, 854. Raman bands: 3063, 2923, 1610, 1193, 1005.

*Resin **6f**.* This material was synthesized following the experimental procedure described in the main manuscript. IR: absence of band at 1264 cm^{-1}. RAMAN: absence of band at 1268 cm^{-1}. Negative NBP Test. Decomposition temperature: 430 °C (TGA). Elemental analysis theoretical %N = 11.4, experimental = 4.3. IR bands: 3024, 1660, 1443, 810. Raman bands: 3063, 2923, 1610, 1193, 1005.

*Resin **7b**.* This material was synthesized following the experimental procedure described in the main manuscript. IR: absence of band at 1264 cm^{-1}. RAMAN: absence of band at 1268 cm^{-1}. Negative NBP Test. Decomposition temperature: 188 °C (TGA). Elemental analysis theoretical %N = 4.3, experimental = 3.9. IR bands: 3024, 2953, 1670, 1460, 1376, 857. Raman bands: 3063, 2923, 1610, 1193, 1005.

General Procedures for CO_2 Fixation with Epoxides.

The desired resins (≈0.5 mol% for the loading of chloride anion) and the epoxides were added into a twin-necked round bottom flask at room temperature. Then, the system was purged with three CO_2 balloons. Fresh CO_2 was charged in the reactor with two additional balloons and the flask was placed into an oil bath at 100 °C. After the reaction was completed and cooled at room temperature, the excess CO_2 was vented. The crude product was separated through filtration. The conversion of epoxides to cyclic carbonates was obtained by ^{1}H NMR (Bruker 400 MHz), and the selectivity for cyclic carbonates was always >99.9%.

Recycling Study.

After the reaction, the catalyst was recovered by filtration, washed with ethanol, and dried overnight under reduced pressure. Afterward, the resin was used for the next run without further treatment. The same study was performed for five runs.

Molecular Modeling.

Lowest energy conformations for the different species considered were calculated at the MMFF level of theory using Spartan08.[58,59] The stationary points were confirmed by subsequent frequency calculation. All vibrational frequencies were positive. See the Supporting Information for detailed computational data.

6.1.4. Results and discussion

6.1.4.1. Synthesis of the Pseudopeptidic Macrocycles

We have recently reported organocatalytic synzymatic systems based on pseudopeptidic macrocycles bearing in their structure hydrogen bond donor (HBD) and Lewis-basic groups.[36] This bioinspired approach was highly active in the cycloaddition of CO_2 to epoxides, as the pseudopeptides were able to optimally pre-organize the reaction components in a confined space, favouring their reaction. Nonetheless, large amounts of co-catalysts acting as nucleophilic source are generally needed for such supramolecular systems, resulting in separation hurdles and increased waste.[37] Thus, we envisaged that modifying the structure of the pseudopeptidic macrocycles by adding a pendant arm could enable their immobilization on a solid resin jointly with a nucleophilic source, reducing such limitations and providing the added advantages associated with immobilized catalysts.

The syntheses of the macrocycles were carried out (Scheme 6.1) by reacting the pseudopeptidic tripodal reagent **1** with aromatic species bearing bromomethyl groups, namely, 1,2,4,5-(tetrakisbromomethyl)benzene (**2a**) or bis(4-

(bromomethyl)phenyl)methane (**2b**). These macrocyclization reactions were a major challenge, as the intramolecular macrocycle formation competes with other intermolecular reactions.[38] The use of high-dilution techniques,[39] although reducing this problem, only allowed the isolation of the desired [1+1] macrocycles with 16% and 34% yield, for **3a** and **3b**, respectively.
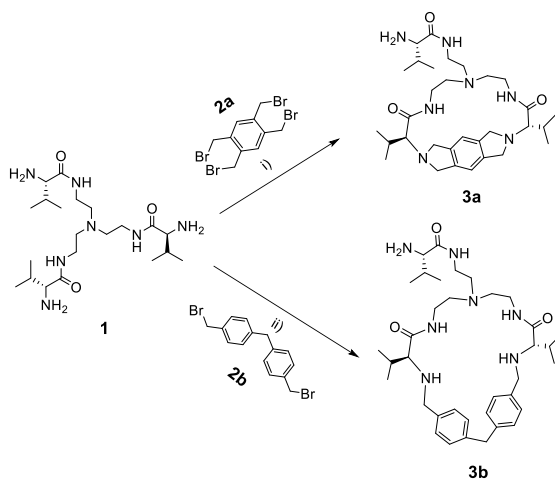
Scheme 6.1. Macrocyclization reaction between **1** and the two aromatic compounds. Reaction conditions (i) 3 mM for **1**, 3 mM for **2a**, and 18 mM of Cs_2CO_3 in CH_3CN at 82 °C (reflux) for 3 h. (ii) 3 mM for **1**, 3 mM for **2b**, and 18 mM of Cs_2CO_3 in CH_3CN at 82 °C (reflux) for 3 h.

Inspired by previous works on templated macrocyclizations,[40,41,42] we decided to investigate if the addition of anionic species to the reaction medium could result in any improvement in the yields. Thus, when **1** (3 mM in CH_3CN) was reacted with **2b** (3 mM in CH_3CN) in the presence of 10 equivalents of Bu_4NBr (30 mM in CH_3CN), a final yield of 48% was attained. Evaluating the kinetic profile of the untemplated and templated reactions, faster conversions for **2b** were obtained in the presence of the 10 equivalents of the bromide salt (Figure S6.1). The kinetic enhancement can be explained by the enhanced nucleophilicity of the terminal amino groups when the anion is hydrogen bonded to the N-H amide fragments in substitution of the amino groups. On the other hand, this interaction of the amide groups with the anion favours the appropriate folding of the open-chain intermediate, approaching the two reactive ends in a template effect.[43] However, in

the case of **2a**, no improvement was attained. The molecular models of the open-chain reaction intermediates for both macrocyclizations suggested important differences regarding the template effect of the bromide anion (Figure S6.2). The bromide anion triggered a positive effect, in the case of **3b**, reducing the distance between the reactive groups (see ESI Figure S6.2c vs. S6.2d), whereas for **3a** the $H_2N\cdots CH_2Br$ distance was larger in the presence of the bromide than in its absence (Figure S6.2a and S6.2b).

6.1.4.2. Evaluation of the Macrocyclic Systems as Catalysts under Homogenous Conditions

The obtained pseudopeptidic macrocycles were assayed as catalysts in the cycloaddition of CO_2 to styrene oxide. Different tetrabutylammonium salts were selected as the nucleophile source, with all reactions being carried out under solventless conditions. Table 6.1 shows the results obtained for the different systems studied. Moderate yields were obtained when the reaction was performed in the presence of 1 mol% of Bu_4NCl or Bu_4NI (Entries 1 and 2, Table 6.1). Adding 0.1 mol% of **3a** or **3b** to 1 mol% of Bu_4NCl resulted in a 1.7- and 1.8-fold increase in yields, respectively (Entries 1, 3 and 4, Table 6.1).

Table 6.1. Screening of $3/Bu_4NX$ mixtures for the reaction between styrene oxide and CO_2 to afford styrene carbonate.[a]

Entry	Bu_4NX (mol%)	Macrocycle (mol%)	Yield (%)[b]	TON (Bu_4NX)	TON (3)
1	X = Cl, (1)	-	65	65	-
2	X = I, (1)	-	49	49	-
3	X = Cl, (1)	**3a** (0.1)	81	81	810
4	X = Cl, (1)	**3b** (0.1)	90	90	900
5	X = I, (1)	**3a** (0.1)	52	52	520
6	X = I, (1)	**3b** (0.1)	56	56	560
7	X = Cl, (0.1)	-	16	160	-
8	X = Cl, (0.1)	**3b** (0.1)	36	360	360

[a] 500 µL styrene epoxide (4.35 mmol), $p(CO_2)$= CO_2 balloon, 100 ºC, 5 h. [b] Yields determined by ^1H NMR, selectivity for styrene carbonate was >99.9 % in all cases.

These results corresponded to turnover number (TON) values higher than 800 in the presence of the macrocycles. On the other hand, no significant improvement was observed when mixing the pseudopeptidic macrocycles with the iodide salt (see Entries 2, 5, and 6 in Table 6.1). This poor catalytic activity in the presence of iodide anion was assigned to its lower basicity, preventing the formation of hydrogen bonds with the pseudopeptides.[36] The most active catalytic system (Bu_4NCl + **3b**), promoted a ≈2.3-fold increase in yields at lower catalytic loadings, although the yields for the desired organic carbonates were low for the reaction times studied (Entries 7 and 8 in Table 6.1). Slightly higher TON values were reported for macrocycles related to **3a** but lacking the pendant arm.[36] However, it must be noted that catalytic activity was sensitive to the macrocycle size, with best results obtained for the smallest cavities (TON = 930 for the macrocycle having three methylene groups in the spacer linking the two amino acid moieties). The introduction of the pendant arm requires the use of a larger diethylene amino spacer, comparable in length with the macrocycle containing five methylene groups in the spacer. In this specific case, the obtained TON value was 790, confirming a slightly improved catalytic behaviour for **3a** (TON = 810).

As the epoxide can also interact with HBD sites, the presence in the macrocycles of basic amino groups can play a key role in the catalytic cycle. Lewis bases are well known as CO_2 fixation species, activating the carbon dioxide molecule by formation of the corresponding carbamate.[44,45] Therefore, macrocycles **3** could act as efficient synzymatic systems in a similar way to the one previously described for related pseudopeptidic systems, contributing to organize in close proximity and with an appropriate orientation of the different substrates and catalytic elements.[36] Figure 6.1 depicts a plausible mechanism for the cycloaddition of CO_2 to styrene oxide in the presence of **3b**.[46] The first step should be the formation of the active supramolecular host–guest adduct between the halide anion and the macrocycle (**A**). In the presence of an excess of styrene epoxide, a new supramolecular adduct can be formed through the interaction of the lone pairs of the oxygen with one of the HBD fragments (**B**). This facilitates ring opening at the epoxide through the attack of the chloride anion.

The alkoxylate intermediate formed can be stabilized by hydrogen bonding to the amide groups (**C**). The amine fragments in the structure (one primary, two secondary, and one tertiary) can fix the CO_2 near the formed alkoxylate (species **D**). The attack of the nucleophilic oxygen atom of the alkoxylate to the activated carbon dioxide molecule would form a carboxylate intermediate, which again should be stabilized by the HBD groups (**E**). Finally, this carboxylate intermediate undergoes a ring-closure reaction, releasing chloride as the leaving group, and affording the supramolecular complex of the carbonate (**F**) that finally liberates styrene carbonate with the recovering of the initial complex **A**.
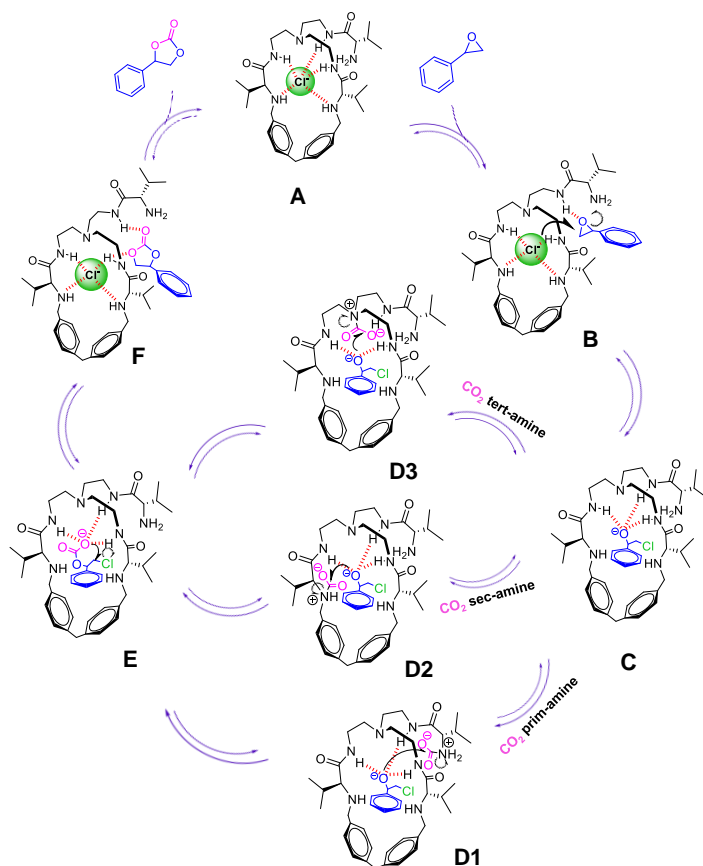
Figure 6.1. Postulated mechanism for the cycloaddition of CO_2 to styrene oxide in the presence of **3b** and chloride anion. The carbon dioxide molecule has been highlighted in pink. The macrocyclic structure is drawn in black, whereas the molecular structures of styrene oxide, styrene carbonate, and their relative intermediates have been marked in blue.

The potential supramolecular interactions in this system were studied in more detail for **3b**, the macrocycle displaying the higher catalytic activity.^{1}H NMR titration experiments with Bu$_4$NCl, using benzene-d$_6$ as solvent,[47] revealed an association constant of 218 ± 1 m^{-1}, suggesting a tight host-guest interaction between the basic chloride anion and the pseudopeptidic structure. The signals of the acidic amide protons of the macrocycle shifted ≈0.6 ppm downfield indicating a strong hydrogen bonding (Figure S6.3a, Supporting Information).[48] A noteworthy downfield shift was also experienced by the aromatic and benzylic protons as well as by the protons of the stereogenic carbon atoms (Figure S6.3b, Supporting Information), suggesting that the chloride anion was located within the cavity. Thus, the resulting supramolecular system contains an efficient nucleophile and HBD groups that could also contribute to stabilize the anionic reaction intermediates formed after the ring-opening step.[46] To explore this issue, alkoxylate and carboxylate species, structurally connected to the expected intermediates were prepared as their tetrabutylammonium salts (Scheme S6.1, Supporting Information).[49]
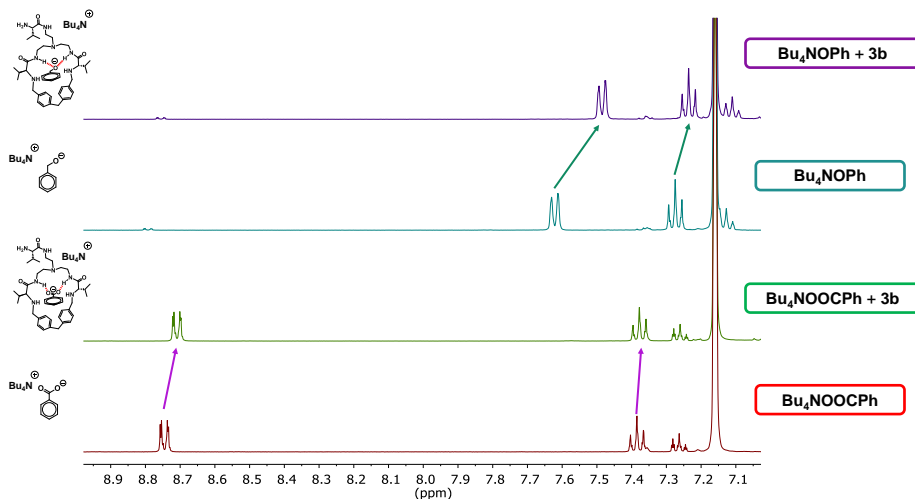
Figure 6.2. Partial ^{1}H NMR spectra for **Bu$_4$NOOCPh** and **Bu$_4$NOPh** in the absence (red and light blue spectra, respectively) and presence (green and purple spectra, respectively) of **3b**. All experiments were carried out in a 400 MHz instrument, using C$_6$D$_6$ as the solvent. Concentrations: 10 mM for the tetrabutylammonium salts and 1 mM for **3b**. Relevant shifts have been marked with arrows.

The ^{1}H NMR spectra obtained in C_6D_6 for mixtures containing a 10:1 ratio of the corresponding tetrabutylammonium salt and **3b** are presented in Figure 6.2. The signal for the protons in *ortho* position to the anionic group experienced the biggest shift in the presence of the host. The upfield shift was more significant in the alkoxylate than for the carboxylate ($\Delta\delta = -0.14$ vs -0.05 ppm), following the basicity trend. Some differences were also noted for the signals of macrocycle **3b** (Figure S6.4, Supporting Information), though the shifts were less pronounced. Besides, the host-guest [**3b**-**Bu₄NOOCPh**] complex was stable enough as to be characterised by high-resolution mass spectrometry (HRMS) (ESI⁻), showing a peak at 756.4823 m/z with an excellent correlation with the isotopic pattern predicted for the host-guest adduct $C_{43}H_{62}N_7O_5^-$ (Figure S6.5, Supporting Information). These data confirm the potential of **3b** to form supramolecular complexes with the different anionic species of the catalytic cycle.

6.1.4.3.   Immobilization of the Macrocycles on Hydrophobic Supports

The structure of macrocycles **3** contains primary amine groups (also secondary amine groups in **3b**), which allowed their immobilization onto polystyrene-divinylbenzene (PS-DVB) gel type Merrifield resins through substitution reactions using the -CH₂-Cl as the grafting linker. The insoluble PS-DVB backbone facilitates that, upon immobilization, the catalytic system could be easily separated from the reaction products and reused in consecutive catalytic cycles. Furthermore, these Merrifield resins have been proved to allow the development of multifunctional heterogenous systems.[50] Such multifunctional materials can display the two components needed for the catalytic system, namely, the macrocycle and the nucleophilic source (i.e., the chloride salt). Finally, the PS-DVB matrix provides the confinement of the catalytic system in a hydrophobic microenvironment. Thus, the solid matrix can mimic the effect of a hydrophobic solvent like toluene, favouring the corresponding supramolecular host-guest interactions between the immobilized macrocycle and anionic species.[6]

The synthetic protocol was based on a two-step immobilization (Scheme 6.2).[50] First, a controlled amount of tributylamine was allowed to react with the chloromethyl groups of the support to form the corresponding ammonium salt. The resulting chloride counterions could serve as active nucleophiles for the catalysis. To optimize the loading and ratio of the two functional sites, polymer **4** (3.9 mmol Cl g^{-1} of resin) was reacted with 1, 0.9, 0.7, 0.5, and 0.3 equivalents of tributylamine, obtaining ammonium-derived resins **5a**, **5b**, **5c**, **5d**, and **5e**. Elemental analyses showed a good correlation between the experimental and the theoretical nitrogen content obtained for this initial step (Table S6.1, Supporting Information).
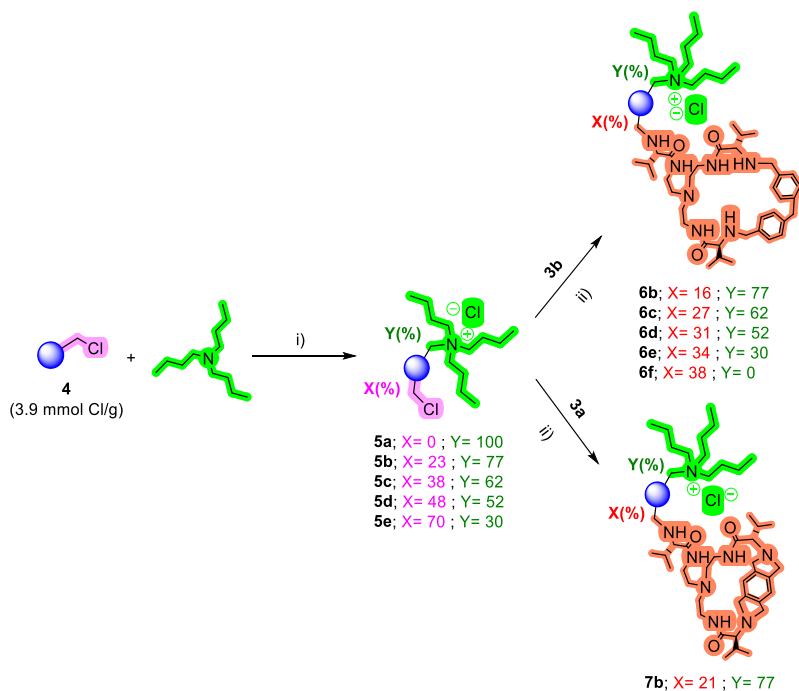
Scheme 6.2. Synthesis of the bifunctional polymeric materials. i) Reaction conditions: DMF, 60 °C, 150 rpm, 12 h. ii) Reaction conditions: DMF, 1 eq. DIPEA, 80 °C, 150 rpm, 18 h. The first step corresponds to the functionalization of the Merrifield resin (**4**) with increasing amounts of tributylamine. The second step corresponds to the immobilization of the macrocyclic pseudopeptides **3**. X and Y values have been determined by elemental analyses, RAMAN, and FTIR spectroscopy.

The immobilization of the macrocycles was performed in a similar manner, adding the equivalents needed for a complete conversion of the remnant

chloromethyl groups. The reaction course was followed by Fourier transform infrared spectroscopy-attenuated total reflection (FTIR-ATR) and RAMAN spectroscopy,[51] observing the disappearance of the characteristic signals for the chloromethyl groups (Figures S6.6 and S6.7, Supporting Information). The appearance of bands characteristic of the functional groups present in the macrocycles was observed in the FTIR-ATR spectra, as is, for instance, the intense band at 1664 cm^{-1} for the CO-NH amide I absorption band (Figure S6.6, Supporting Information). Colorimetric NBP (4-(para-nitrobenzyl)pyridine) tests were also performed to confirm the absence of chloromethyl groups for all the resins (Figure S6.8, Supporting Information).[52] Experimental macrocycle loadings obtained by elemental analyses were lower than those calculated for quantitative transformations (Table 6.2). This can be related with cross-linking processes happening during the immobilization of multifunctional compounds.[53]

Table 6.2. Loading and swelling studies for the different resins synthesized.

Entry	Resin	Theoretical 3 (%) loading	Experimental 3 (%) loading	Anchoring (%)	Swelling (%)[b,c]
1	**5a**	0	0	100	53
2	**6b**	23	17	73	11
3	**6c**	38	27	70	8
4	**6d**	48	31	65	2
5	**6e**	70	34	48	0
6	**6f**	100	38	38	2
7	**7b**	23	21	91	28

[a] Values have been calculated using the %N values obtained in the elemental analyses of the resins. [b] Swelling measured in styrene oxide, using optical microscopy. [c] Values measured as: [(Size$_{wet}$ − Size$_{dry}$)/Size$_{dry}$ × 100].

In this regard, **3a** and **3b** present several amine groups that could react with the -CH$_2$-Cl fragments in the polymer producing the grating of the macrocycle by multiple sites.[54] In agreement with this, the reaction of **3b** and 1 equivalent of chloromethyl benzene (dimethylformamide (DMF), 18 h, 80 °C) afforded a complex mixture of N-benzylation products, as detected by electrospray ionization mass spectrometry (ESI-MS) and ^{1}H NMR (Figure S6.9, Supporting Information). This

additional cross-linking was confirmed by swelling studies in styrene oxide (Table 6.2) revealing a decrease in swelling with the incorporation of the macrocycle, particularly relevant for higher functionalization degrees (Figure S6.10, Supporting Information). It must be noted that an additional noncovalent cross-linking can be achieved in these multifunctional polymers through supramolecular interactions between the macrocycle and the chloride-supported anion. Interestingly, the cross-linking detected was lower for **3a** than for **3b** (Entries 2 and 7 in Table 6.2), as corresponds to the lower nucleophilicity of the tertiary amino groups in **3a**.

Thermogravimetric analysis (TGA) of the functionalized resins revealed that all the polymers were stable until temperatures > 170 °C. Therefore, the catalytic activity of all these materials could be assayed at 100 °C without any associated degradation/decomposition issue.

6.1.4.4. Heterogenous Catalysis Experiments

To test the efficiency of those immobilized catalysts, the cycloaddition of CO_2 to styrene oxide was performed under identical experimental conditions than those used for the homogenous systems (Table 6.3). As expected, the Merrifield resin **4** was not able to promote the formation of the desired styrene carbonate (Entry 1, Table 6.3). In the same way, resin **6f** containing the supported macrocycle but not chloride, only produced traces of the product (Entry 4, Table 6.3). Entries 2 and 3 in the table show that the supported tetraalkylammonium salt by itself can trigger the process, although with modest yields (<35%). To our delight, the multifunctional material **6b** achieved a 2.2-fold increase in the yield relative to **5a** (Entries 3 and 5, Table 6.3). A progressive increase in yield was observed when raising the loading of supported macrocycle, reaching a 79% yield for resin **6e** (Entries 5-8). Despite the lower yields, the catalytic results for **6b** were remarkable, as the TON values for Cl⁻ and **3b** were 86 and 411, respectively, and the productivity for the process was 4.42 g_{prod}/g_{resin} h.

Table 6.3. Catalytic results for the different macrocycle: tetraalkylammonium supported resins in the cycloaddition of CO_2 to styrene oxide.

Entry	Resin	Cl⁻ (mol%)[b]	3 (mol%)[b]	Yield (%)[c]	TON (Cl⁻)	TON (3)	Productivity ($g_{prod}/g_{resin}\cdot h$)[d]
1	**4**	1	-	0	-	-	0
2	**5a**	1	-	31	31	-	2.03
3	**5a**	0.50	-	17	34	-	2.22
4	**6f**	-	0.19	2	-	4	0.26
5	**6b**	0.43	0.09	37	86	411	4.42
6	**6c**	0.44	0.19	44	100	232	3.86
7	**6d**	0.52	0.31	69	133	223	4.50
8	**6e**	0.50	0.57	79	158	139	3.33
9	**7b**	0.43	0.12	85	198	709	10.16

[a] 500 µL styrene epoxide (4.35 mmol), $p(CO_2)$= CO_2 balloon, 100 ºC, 5 h. [b] Catalytic loading relative to styrene oxide. Unless stated in the table, all experiments were carried out at ≈0.5 mol% chloride anion, readjusting the mass of resin weighted. [c] Yields determined by ¹H NMR, selectivity for styrene carbonate was >99.9 % in all cases. [d] Calculated considering the yield, the mass of resin introduced, and the reaction time.

Resin **7b** derived from **3a** rendered higher yields than resins **6** (Entry 9 vs Entry 5, Table 6.3). In this case, the lower degree of cross-linking can allow for a better diffusion of the reagents and, additionally, the anchored macrocycle displays a higher conformational preorganization. For **7b**, the productivity achieved was as high as 10.16 g_{prod}/g_{resin} h, with TON values of 198 for Cl⁻ and 709 for **3a**. Therefore, the supported organocatalytic system **7b** was very active in this process, overcoming the low reactivity of styrene oxide even under mild conditions (CO_2 balloon and 100 °C). Comparing this system with other supramolecular heterogenous catalysts reported for the cycloaddition of CO_2 to styrene oxide, **7b** promoted higher TON and turnover frequency (TOF) values at lower CO_2 pressures (Table S6.2 and Figure S6.11, Supporting Information).

To probe the importance of the cooperativity of the functional sites confined in the multifunctional resin, a control experiment was carried out using a polymer cocktail,[55] prepared by mixing **5a** and **6f** in a 1:1 molar ratio (Figure 6.3). In this system, the direct interaction between functional groups in two different solid phases

is not possible.[56, 57] Thus, under the same conditions reported in Table 6.3, the yield for the desired carbonate was only 18%, which is comparable to the result obtained for **5a** alone (Entry 3 in Table 6.3). This result confirms the relevance of the heterogenous synzymatic system proposed, allowing a close proximity of the functional groups involved in the catalytic cycle (Figure 6.3).
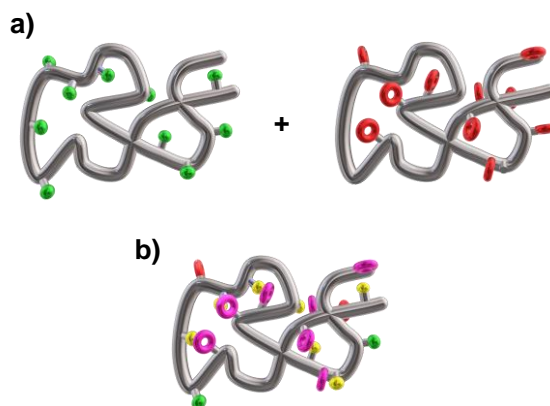
Figure 6.3. Schematic representation of the polymeric chains of the support for a) resins **5a** and **6f** mixed separately in the reactor; b) multifunctional resin containing the supported macrocyclic structure and tetraalkylammonium chloride moieties (**6b–6e** and/or **7b**). Colour code: red circles for macrocycles **3**, green balls for ammonium chloride salt, pink circles and yellow balls represent the activated **3**:Cl⁻ supramolecular complex.

Given the heterogenous nature of these multifunctional supramolecular organocatalysts, a straightforward recovery protocol was designed (Figure 6.4a). After 5 h of reaction, the polymeric beads of **7b** were filtered from the reaction crude and washed with EtOH. After drying the resin for 24 h at 50 °C and reduced pressure, it could be reused in the cycloaddition of CO_2 to styrene oxide without any apparent loss of activity (Figure 6.4b). The integrity of the catalyst was studied using IR spectroscopy, confirming that neither the reagents/products nor the intermediates were adsorbed in the material (Figure S6.12, Supporting Information).
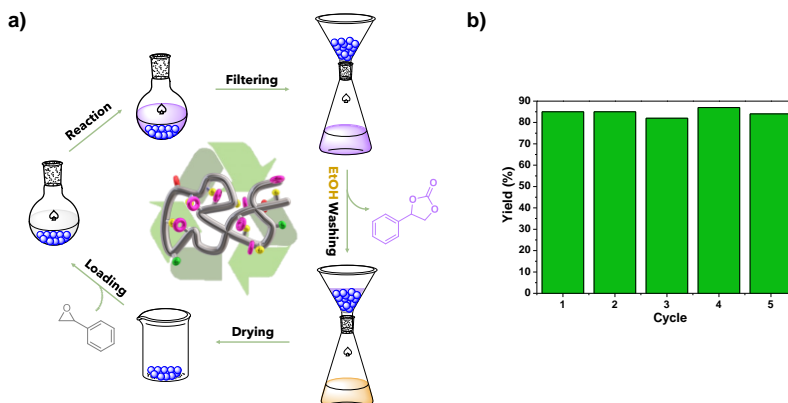
Figure 6.4. a) Recyclability protocol designed for resin **7b**, based on filtering, washing with ethanol, and drying under vacuum. b) NMR yields obtained for the desired styrene carbonate in successive runs. Reaction conditions: 500 μL styrene epoxide (4.35 mmol), 12 mg of resin (0.43 mol% in Cl⁻), p(CO$_2$) = CO$_2$ balloon, 100 °C, 5 h.

To test the general applicability of **7b**, several epoxides were evaluated under the optimized reaction conditions. The substrate scope included internal and terminal epoxides, with well-differentiated reactivity (Figure 6.5). Results confirmed that the immobilized supramolecular system promotes quantitative yields for the most reactive propylene and butylene oxide. Besides, excellent results were also achieved for other terminal epoxides such as glycidol, epichlorohydrin, and phenyl glycidyl ether (TOF values of 166 h^{-1}).
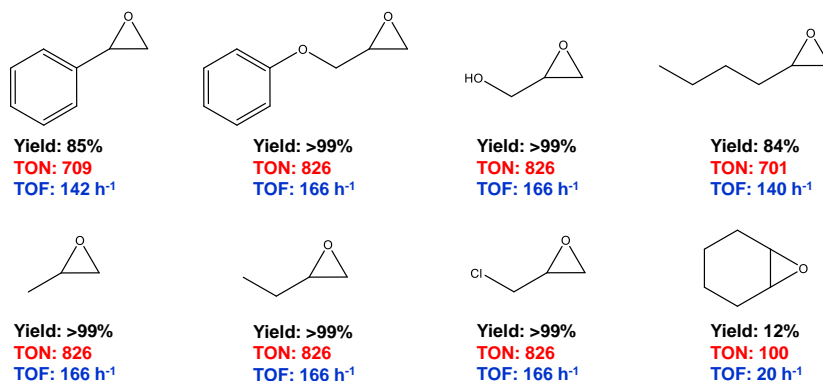
Figure 6.5. Substrate scope in the presence of resin **7b**. Reaction conditions: 500 μL of epoxide, 0.43 mol% in chloride anion for **7b**, p(CO$_2$) = CO$_2$ balloon, 100 °C, 5 h.

The multifunctional heterogenous synzyme was also able to afford high yields for the less reactive 1,2-epoxyhexane (84% in 5 h). When the activity of **7b** was examined for an internal epoxide like cyclohexene oxide, a 12% yield was obtained. This result is in good accordance with the lower reactivity of such internal epoxides.

6.1.5. Conclusions

A series of novel pseudopeptidic macrocycles bearing pendant arms in their structure have been synthesized. These compounds presented a high capacity for supramolecular interactions and interesting catalytic properties in the homogenous cycloaddition of CO_2 to styrene oxide, in the presence of halide anions. The rationale design of the pseudopeptides allowed for their immobilization on hydrophobic supports, along with ammonium chloride fragments, which provided an excellent catalytic performance of the resulting multifunctional systems. Comparing the homogenous results with the heterogenous ones, an opposite trend was observed for compounds **3a** and **3b**. Whereas **3b** was the most active in homogenous phase, **3a** provided better results upon immobilization. This can be associated with the higher cross-linking afforded by the immobilization of **3b**, decreasing the diffusion efficiency of the reagents and products through the polymeric matrix. The most active material **7b** was tested for a wide-range of terminal epoxides, resulting in TOF values higher than 130 h⁻¹ in all cases, despite the low pressures of CO_2 used. Moreover, the catalyst could be recycled and reused without apparent loss of activity, for at least five runs, decreasing the environmental impact of the system.

6.1.6. References

1- Ringe, D.; Petsko, G. A. How enzymes work. *Science* **2009**, *320*, 1428-1429.

2- Meeuwissen, J.; Reek, J. N. H. Supramolecular catalysis beyond enzyme mimics. *Nat. Chem.* **2010**, *2*, 615-621.

3- Raynal, M.; Ballester, P.; Vidal-Ferran, A.; van Leeuwen, P. W. N. M. Supramolecular catalysis. Part 2: artificial enzyme mimics. *Chem. Soc. Rev.* **2014**, *43*, 1734-1787.

4- Dong, J.; Davies, A. P. Molecular Recognition Mediated by Hydrogen Bonding in Aqueous Media. *Angew. Chem. Int. Ed.* **2021**, *60*, 8035-8048.

5- Würthner, F. Solvent Effects in Supramolecular Chemistry: Linear Free Energy Relationships for Common Intermolecular Interactions. *J. Org. Chem.* **2022**, 87, 1602-1615.

6- Sun, Q.; Wang, S.; Aguila, B.; Meng, X.; Ma, S.; Xiao, F.-S. Creating solvation environments in heterogeneous catalysts for efficient biomass conversion. *Nat. Commun.* **2018**, *9*, 3236.

7- Osman, A. I.; Hefny, M.; Abdel Maksoud, M. I. A.; Elgarahy, A. M.; Rooney, D. W. Recent advances in carbon capture storage and utilisation technologies: a review. *Environ. Chem. Lett.* **2021**, *19*, 797-849.

8- Cavalleri, M.; Panza, N.; di Biase, A.; Tseberlidis, G.; Rizzato, S.; Abbiati, G.; Caselli, A. [Zinc(II)(Pyridine-Containing Ligand)] Complexes as Single-Component Efficient Catalyst for Chemical Fixation of CO_2 with Epoxides. *Eur. J. Org. Chem.* **2021**, *19*, 2764-2771.

9- Shi, Y.; Pan, B.-W.; Zhou, Y.; Zhou, J.; Liu, Y.-L.; Zhou, F. Catalytic enantioselective synthesis using carbon dioxide as a C1 synthon. *Org. Biomol. Chem.* **2020**, *18*, 8597-8619.

10- Claver, C.; Yeamin, M. B.; Reguero, M.; Masdeu-Bultó, A. M. Recent advances in the use of catalysts based on natural products for the conversion of CO_2 into cyclic carbonates. *Green Chem.* **2020**, *22*, 7665-7706.

11- Artz, J.; Müller, T. E.; Thenert, K.; Kleinekorte, J.; Meys, R.; Sternberg, A.; Bardow, A.; Leitner, W. Sustainable Conversion of Carbon Dioxide: An Integrated Review of Catalysis and Life Cycle Assessment. *Chem. Rev.* **2018**, *118*, 434–504

12- Lin, S.; Diercks, C. S.; Zhang, Y. B.; Kornienko, N.; Nichols, E. M.; Zhao, Y.; Paris, A. R.; Kim, D.; Yang, P.; Yaghi, O. M.; Chang, C. J. Covalent organic frameworks comprising cobalt porphyrins for catalytic CO_2 reduction in water. *Science*, **2015**, *349*, 1208-1213.

13- Xie, J.-N.; Yu, B.; Guo, C.-X.; He, L.-N. Copper(i)/phosphine-catalyzed tandem carboxylation/annulation of terminal alkynes under ambient pressure of CO_2: one-pot access to 3a-hydroxyisoxazolo[3,2-a]isoindol-8(3aH)-ones. *Green Chem.* **2015**, *17*, 4061-4067.

14- Docherty, S. R.; Copéret, C. Deciphering Metal-Oxide and Metal-Metal Interplay via Surface Organometallic Chemistry: A Case Study with CO_2 Hydrogenation to Methanol. *J. Am. Chem. Soc.* **2021**, *143*, 6767–6780

15- Li, P.; Cao, Z. Catalytic coupling of CO_2 with epoxide by metal macrocycles functionalized with imidazolium bromide: insights into the mechanism and activity regulation from density functional calculations. *Dalton Trans.* **2019**, *48*, 1344-1350.

16- North, M.; Pasquale, R. Mechanism of Cyclic Carbonate Synthesis from Epoxides and CO_2. *Angew. Chem. Int. Ed.* **2009**, *48*, 2946-2948.

17- Whiteoak, C. J.; Kielland, N.; Laserna, V.; Escudero-Adan, E. C.; Martin, E.; Kleij, A. W. A Powerful Aluminum Catalyst for the Synthesis of Highly Functional Organic Carbonates. *J. Am. Chem. Soc.* **2013**, *135*, 1228-1231.

18- Ema, T.; Miyazaki, Y.; Shimonishi, J.; Maeda, C.; Hasegawa, J. Y. Bifunctional Porphyrin Catalysts for the Synthesis of Cyclic Carbonates from Epoxides and CO_2: Structural Optimization and Mechanistic Study. *J. Am. Chem. Soc.* **2014**, *136*, 15270-15279.

19- Liu, J.; Yang, G.; Liu, Y.; Zhang, D.; Hu, X.; Zhang, Z. Efficient conversion of CO_2 into cyclic carbonates at room temperature catalyzed by Al-salen and imidazolium hydrogen carbonate ionic liquids. *Green Chem.* **2020**, *22*, 4509-4515

20- Castro-Osma, J. A.; Lamb, K. J.; North, M. Cr(salophen) Complex Catalyzed Cyclic Carbonate Synthesis at Ambient Temperature And Pressure. *ACS Catal.* **2016**, *6*, 5012-5025.

21- Fiorani, G.; Guo, W.; Kleij, A. W. Sustainable conversion of carbon dioxide: the advent of organocatalysis. *Green Chem.* **2015**, *17*, 1375-1389.

22- Liu, M. S.; Lu, X. Y.; Jiang, Y. C.; Sun, J. M.; Arai, M. Zwitterionic Imidazole-Urea Derivative Framework Bridged Mesoporous Hybrid Silica: A Highly Efficient Heterogeneous Nanocatalyst for Carbon Dioxide Conversion. *ChemCatChem.* **2018**, *10*, 1860-1868.

23- North, M.; Villuendas, P.; Young, C. A Gas-Phase Flow Reactor for Ethylene Carbonate Synthesis from Waste Carbon Dioxide. *Chem. Eur. J.* **2009**, *15*, 11454-11457.

24- Meléndez, J.; North, M.; Villuendas, P.; Young, C. One-component bimetallic aluminium(salen)-based catalysts for cyclic carbonate synthesis and their immobilization. *Dalton Trans.* **2011**, *40*, 3885-3902.

25- Chen, Y.; Xu, P.; Arai, M.; Sun, J. Cycloaddition of Carbon Dioxide to Epoxides for the Synthesis of Cyclic Carbonates with a Mixed Catalyst of Layered Double Hydroxide and Tetrabutylammonium Bromide at Ambient Temperature. *Adv. Synth. Catal.* **2019**, *361*, 335-344.

26- Zhang, J.; Li, X.; Zhu, Z.; Chang, T.; Fu, X.; Hao, Y.; Meng, X.; Panchal, B.; Qin, S. Hydroxylamino-Anchored Poly(Ionic Liquid)s for CO_2 Fixation into Cyclic Carbonates at Mild Conditions. *Adv. Sustainable Syst.* **2021**, *5*, 2000133.

27- Maeda, C.; Sasaki, S.; Takaishi, K.; Ema, T. Calix[4]pyrroles as macrocyclic organocatalysts for the synthesis of cyclic carbonates from epoxides and carbon dioxide. *Catal. Sci. Technol.* **2018**, *8*, 4193-4198.

28- Martínez-Rodríguez, L.; Garmilla, J. O.; Kleij, A. W. Cavitand-Based Polyphenols as Highly Reactive Organocatalysts for the Coupling of Carbon Dioxide and Oxiranes. *ChemSusChem* **2016**, *9*, 749-755.

29- Song, J.; Zhang, Z.; Han, B.; Hu, S.; Li, W.; Xie, Y. Synthesis of cyclic carbonates from epoxides and CO_2 catalyzed by potassium halide in the presence of *β*-cyclodextrin. *Green Chem.* **2008**, *10*, 1337-1341.

30- Wang, J.; Liang, Y.; Zhou, D.; Ma, J.; Jing, H. New crown ether complex cation ionic liquids with N-heterocycle anions: preparation and application in CO_2 fixation. *Org. Chem. Front.* **2018**, *5*, 741-748.

31- Mirabaud, A.; Mulatier, J.-C.; Martinez, A.; Dutasta, J.-P.; Dufaud, V. Merging host-guest chemistry and organocatalysis for the chemical valorization of CO_2. *Catal. Today* **2017**, *281*, 387-391.

32- Mirabaud, A.; Mulatier, J.-C.; Martinez, A.; Dutasta, J.-P.; Dufaud, V. Investigating Host-Guest Complexes in the Catalytic Synthesis of Cyclic Carbonates from Styrene Oxide and CO_2. *ACS Catal.* **2015**, *5*, 6748-6752.

33- Mirabaud, A.; Martinez, A.; Bayard, F.; Dutasta, J.-P.; Dufaud, V. A new heterogeneous host–guest catalytic system as an eco-friendly approach for the synthesis of cyclic carbonates from CO_2 and epoxides. *New J. Chem.* **2018**, *42*, 16863-16874.

34- Dong, T.; Zheng, Y.-J.; Yang, G.-W.; Zhang, Y.-Y.; Li, B.; Wu, G.-P. Crosslinked Resin-Supported Bifunctional Organocatalyst for Conversion of CO_2 into cyclic Carbonates. *ChemSusChem* **2020**, *13*, 4121-4127.

35- Desens, W.; Kohrt, C.; Frank, M.; Werner, T. Highly Efficient Polymer-Supported Catalytic System for the Valorization of Carbon Dioxide. *ChemSusChem* **2015**, *8*, 3815-3822.

36- Esteve, F.; Altava, B.; Burguete, M. I.; Bolte, M.; García-Verdugo, E.; Luís, S. V. Pseudopeptidic macrocycles as cooperative minimalistic synzyme systems for the remarkable activation and conversion of CO_2 in the presence of the chloride anion. *Green Chem.* **2020**, *22*, 4697-4705.

37- Takaishi, K.; Okuyama, T.; Kadosaki, S.; Uchiyama, M.; Ema, T. Hemisquaramide Tweezers as Organocatalysts: Synthesis of Cyclic Carbonates from Epoxides and CO_2. *Org. Lett.* **2019**, *21*, 1397-1401.

38- Martí-Centelles, V.; Pandey, M. D.; Burguete, M. I.; Luis, S. V. Macrocyclization Reactions: The Importance of Conformational, Configurational, and Template-Induced Preorganization. *Chem. Rev.* **2015**, *115*, 8736-8834.

39- Rossa, L.; Vögtle, F. Synthesis of Medio- And Macrocyclic Compounds By High Dilution Principle Techniques, In *Cyclophanes I. Topics in Current Chemistry*, Vol. 113; Springer: 1983.

40- Guillier, K.; Caytan, E.; Dorcet, V.; Mongin, F.; Dumont, E.; Chevallier, F. A Halogen-Bond Donor Catalyst for Templated Macrocyclization. *Angew. Chem. Int. Ed.* **2019**, *58*,14940-14943.

41- Leczycka-Wilk, K.; Dabrowa, K.; Cmoch, P.; Jarosz, S. Chloride-Templated Macrocyclization and Anion-Binding Properties of C_2-Symmetric Macrocyclic Ureas from Sucrose. *Org. Lett.* **2017**, *19*, 4596-4599.

42- Martí-Centelles, V.; Burguete, M. I.; Luis, S. V. Macrocycle Synthesis by Chloride-Templated Amide Bond Formation. *J. Org. Chem.* **2016**, *81*, 2143-2147.

43- Esteve, F.; Altava, B.; Bolte, M.; Burguete, M. I.; García-Verdugo, E.; Luís, S. V. Highly Selective Anion Template Effect in the Synthesis of Constrained Pseudopeptidic Macrocyclic Cyclophanes. *J. Org. Chem.* **2020**, *85*, 1138-1145.

44- Bui, M.; Adjiman, C. S.; Bardow, A.; Anthony, E. J.; Boston, A.; Brown, S.; Fennell, P. S.; Fuss, S.; Galindo, A.; Hackett, L. A.; Hallett, J. P.; Herzog, H. J.; Jackson, G.; Kemper, J.; Krevor, S.; Maitland, G. C.; Matuszewski, M.; Metcalfe, I. S.; Petit, C.; Puxty, G.; Reimer, J.; Reiner, D. M.; Rubin, E. S.; Scott, S. A.; Shah, N.; Smit, B.; Trusler, J. P. M.; Webley, P.; Wilcox, J.; Dowell, N. M. Carbon capture and storage (CCS): the way forward. *Energy Environ. Sci.* **2018**, *11*, 1062-1176.

45- Lashaki, M. J.; Khiavi, S.; Sayari, A. Stability of amine-functionalized CO_2 adsorbents: a multifaceted puzzle. *Chem. Soc. Rev.* **2019**, *48*, 3320-3405.

46- North, M.; Pasquale, R.; Young, C. Synthesis of cyclic carbonates from epoxides and CO_2. *Green Chem.* **2010**, *12*, 1514-1539.

47- Caution: Benzene is a very toxic solvent and must be avoided when possible. In this case, however, titrations in other available deuterated solvents that could provide a similar environment to that of styrene oxide, e.g. toluene-d_8, did not provide enough information.

48- Martí, I.; Bolte, M.; Burguete, M. I.; Vicent, C.; Alfonso, I.; Luis, S. V. Tight and Selective Caging of Chloride Ions by a Pseudopeptidic Host. *Chem. Eur. J.* **2014**, *20*, 7458-7464.

49- Nagae, H.; Aoki, R.; Akutagawa, S.; Kleemann, J.; Tagawa, R.; Schindler, T.; Choi, G.; Spaniol, T. P.; Tsurugi, H.; Okuda, J.; Mashima, K. Lanthanide Complexes Supported by a Trizinc Crown Ether as Catalysts for Alternating Copolymerization of Epoxide and CO_2:Telomerization Controlled by Carboxylate Anions. *Angew. Chem. Int. Ed.* **2018**, *57*, 2492-2496.

50- Sans, V.; Gelat, F.; Burguete, M. I.; García-Verdugo, E.; Luis, S. V. Polymer-supported Pd-NHC complexes: Strategies for the development of multifunctional systems. *Catal. Today* **2012**, *196*, 137-147.

51- Altava, B.; Burguete, M. I.; García-Verdugo, E.; Luis, S. V.; Vicent, M. J. The use of NIR-FT-Raman spectroscopy for the characterisation of polymer-supported reagents and catalysts. *Tetrahedron* **2001**, *57*, 8675-8683.

52- Altava, B.; Burguete, M. I.; Galindo, F.; Gavara, R.; Luis, S. V. A Sensitive Colorimetric Method for the Study of Polystyrene Merrifield Resins and Chloromethylated Macroporous Monolithic Polymers. *J. Comb. Chem.* **2004**, *6*, 859-861.

53- Altava, B.; Burguete, M. I.; Frías, J. C.; García-España, E.; Luis, S. V.; Miravet, J. F. Preparation of Polymer-Supported Polyazamacrocycles. The Role of the Polymeric Matrix in the Preparation of Polymer-Supported Polyazamacrocycles. *Ind. Eng. Chem. Res.* **2000**, *39*, 3589-3595.

54- Adrian, F. M.; Altava, B.; Burguete, M. I.; Luis, S. V.; Salvador. R. V. Synthetic methods for the preparation of polystyrene resins containing chiral polyamine chains. *Tetrahedron* **1998**, *54,* 3581-3588.

55- Sans, V.; Gelat, F.; Karbass, N.; Burguete, M. I.; García-Verdugo, E.; Luis, S. V. Polymer Cocktail: A Multitask Supported Ionic Liquid-Like Species to Facilitate Multiple and Consecutive C-C Coupling Reactions. *Adv. Synth. Catal.* **2010**, *352*, 3013-3021.

56- Rebek, J.; Gaviña, F. Three-phase test. Detection of free cyclobutadiene. *J. Am. Chem. Soc.*, **1975**, *97*, 3453-3456.

57- Gaviña, F.; Luis, S. V.; Costero, A. M.; Burguete, M. I.; Rebek, J. Allosteric cooperativity and transport: studies in a circulating system. *J. Am. Chem. Soc.* **1988**, *110*, 7140-7143

58- Deppmeier, B. J.; Driessen, A. J.; Hehre, T. S.; Hehre, W. J.; Johnson, J. A.; Klunzinger, P. E.; Leonard, J. M.; Pham, I. N.; Pietro, W. J.; Jianguo, Y. Spartan '08, build 132 (Mar 27 2009), Wavefunction Inc., Irvine CA, 2009.

59- Halgren, T. A. Merck molecular force field. I. Basis, form, scope, parameterization, and performance of MMFF94. *J. Comput. Chem.* **1996**, *17*, 490-519.

6.2. Supporting information
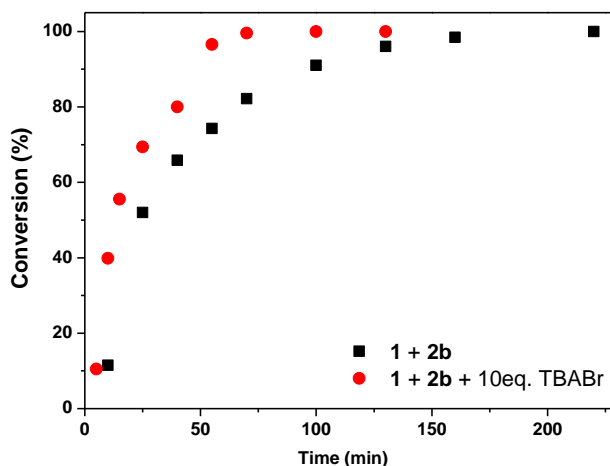
Figure S6.1. Kinetic profiles (reverse phase HPLC) obtained for the conversion of **2b**. Conversions determined with a predetermined calibration curve for **2b**. Reaction conditions: CH_3CN (3 mM), 82 ºC (reflux), 6 equivalents of Cs_2CO_3.
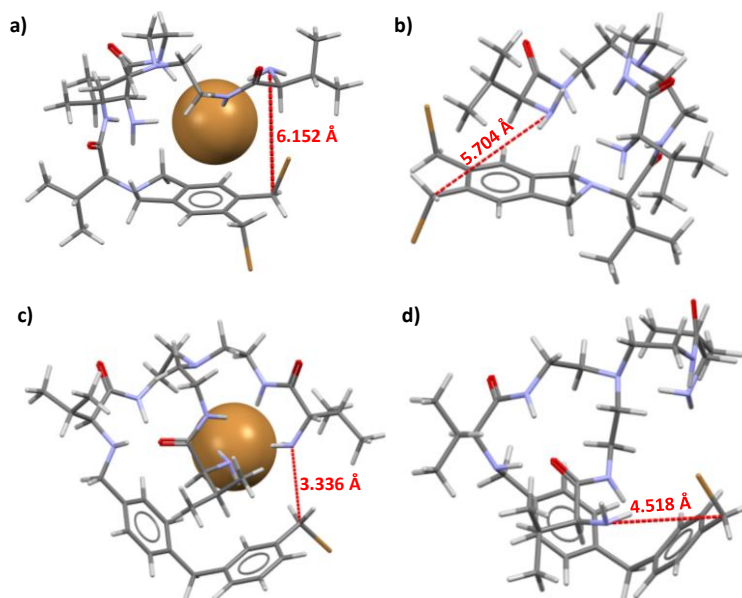
Figure S6.2. Most stable conformation obtained for the reaction intermediates of the macrocyclization process in the presence (a and c) and absence (b and d) of bromide anion. Reaction intermediates for **3a** (a and b) and for **3b** (c and d). Distances between the reactive groups ($H_2N\cdots CH_2Br$) have been highlighted in red. Molecular models calculated using Spartan08' at the MMFF level of theory.
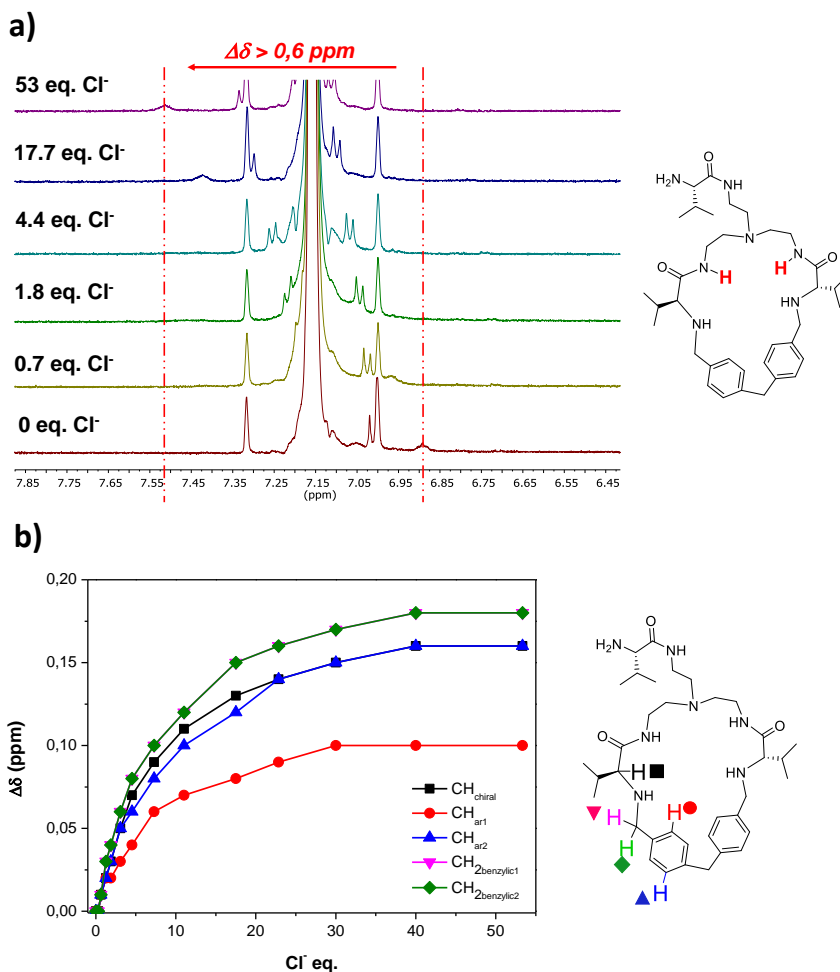
Figure S6.3. H NMR titration experiments for **3b** (0.5 mM in C_6D_6, 400 MHz, room temperature) using increasing amounts of NBu_4Cl (80 mM in C_6D_6). a) Partial ^{1}H NMR spectra highlighting the downfield shift experienced by the amide protons; initial and final positions marked with a red line. b) Downfield shift experienced by other characteristic protons of **3b**. The protons studied have been highlighted with different colours.
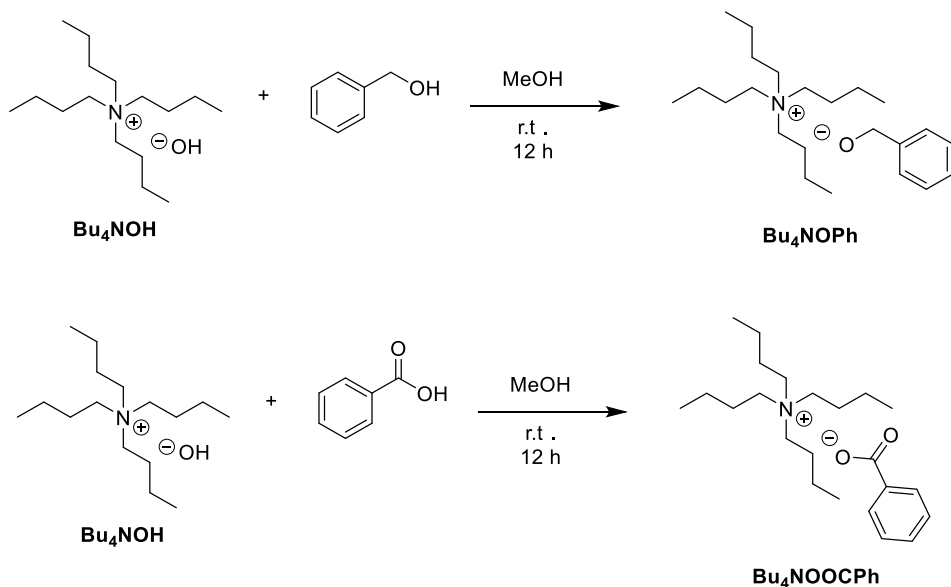
Scheme S6.1. Synthesis of the tetrabutylammonium salts of the analogues of the anionic intermediates: **Bu₄NOPh** and **Bu₄NOOCPh**. The water formed in the reaction was removed by evaporation at 80 °C under reduced pressure.
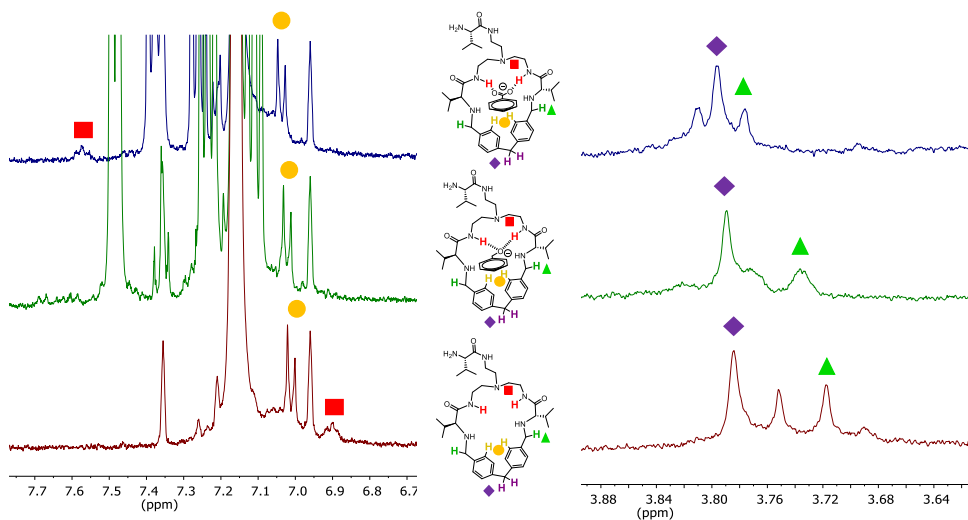
Figure S6.4. Partial ^{1}H NMR (400 MHz, C$_6$D$_6$) spectra for the following 1 mM solutions of **3b**: alone (red spectrum); + 10mM **Bu₄NOPh** (green spectrum); + 10 mM in **Bu₄NOOCPh** (dark blue spectrum). The different signals have been colour coded in agreement with colours assigned to the hydrogen atoms in the structures.

TOF MS ES(-) Predicted for $C_{43}H_{62}N_7O_5^-$
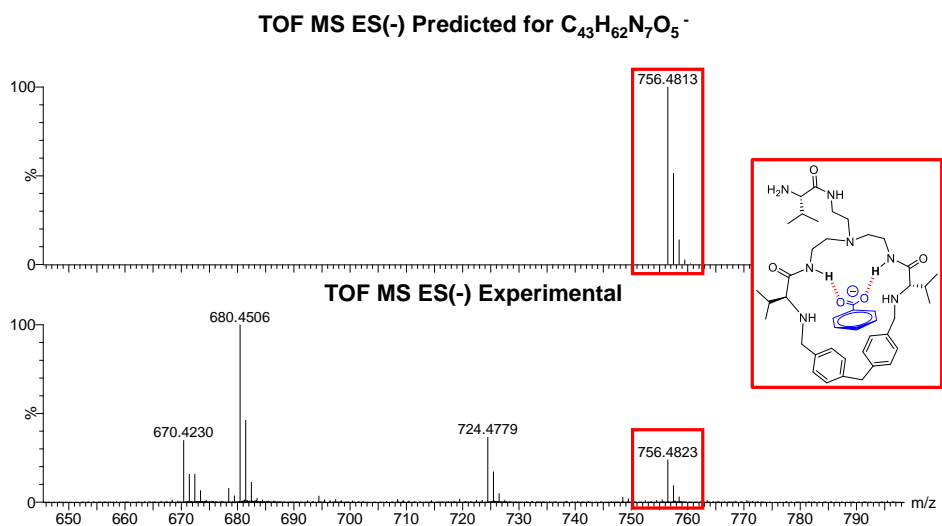
Figure S6.5. HRMS (ESI-) analysis of a 1:10 mixture **3b** : **Bu$_4$NOOCPh** in methanol. Below: experimental mass spectrum. Above: predicted mass spectrum for the supramolecular complex.

Table S6.1. Elemental analysis (EA) results for the immobilization of tributylamine on the Merrifield resin **4** (3.9 mmol Cl/g).[a]

Entry	Resin	Eq. tributylamine	EA N(%)	Theoretical N(%)
1	**4**	0	0	0
2	**5a**	1	3.3	3.2
3	**5b**	0.9	2.5	3.0
4	**5c**	0.7	2.0	2.5
5	**5d**	0.5	1.7	2.0
6	**5e**	0.3	1.0	1.3

[a] The theoretical values have been calculated assuming that all the equivalents added of tributylamine were anchored on the support.
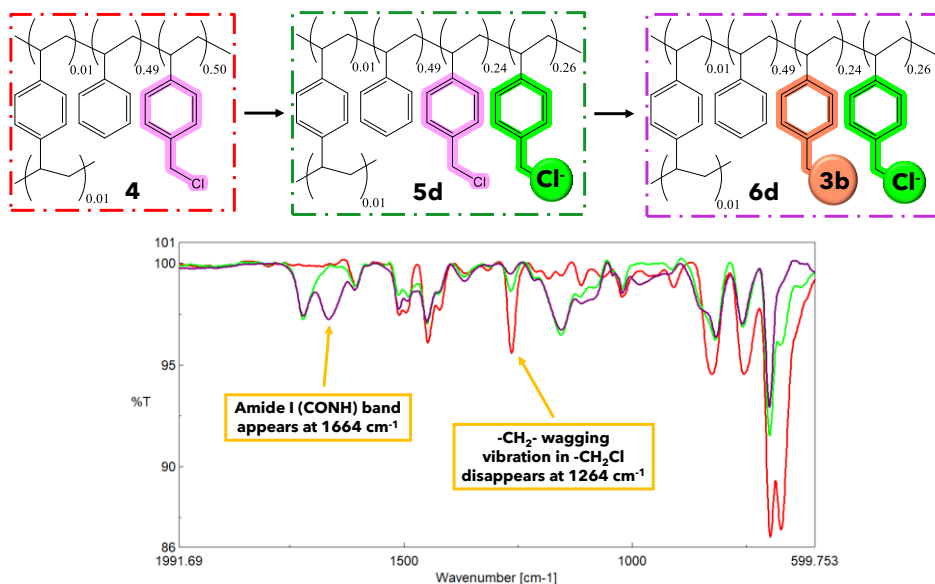
Figure S6.6. ATR-FT-IR partial spectra for the multifunctional resin **6d** (purple), the starting Merrifield resin **4** (red) and the intermediate resin **5d** (green). The disappearance of the band at 1264 cm^{-1} for chloromethylated groups and the appearance of the band at 1664 cm^{-1} for the pseudopeptidic macrocyclic fragments have been highlighted in orange. The composition in DVB, PS and in the two catalytic species has been included.
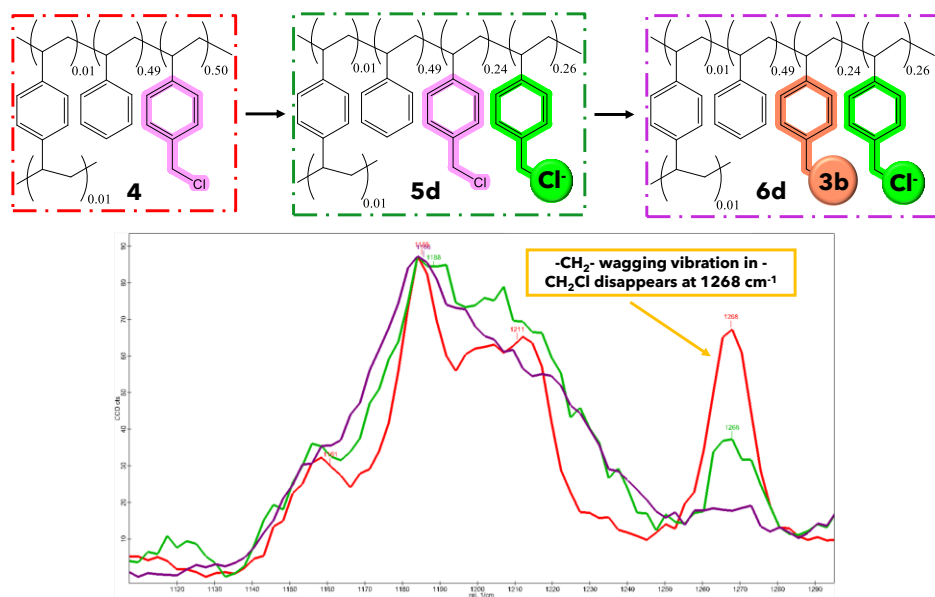
Figure S6.7. Partial RAMAN spectra for the multifunctional resin **6d** (purple), the starting Merrifield resin **4** (red) and the intermediate resin **5d** (green). The disappearance of the C-Cl band at 1268 cm^{-1} has been highlighted in orange. The composition in DVB, PS and in the two catalytic species has been included.
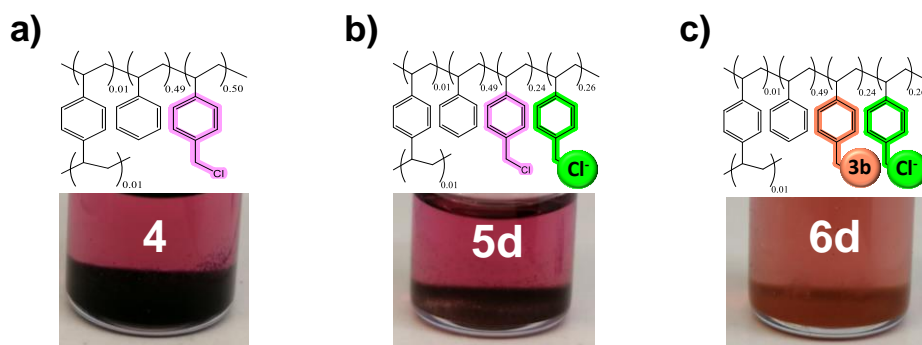
Figure S6.8. NBP tests for a) **4**, b) **5d** and c) **6d**. The appearance of a purple colour in the resin beads is indicative of the presence of chloromethyl groups in the polymeric beads.
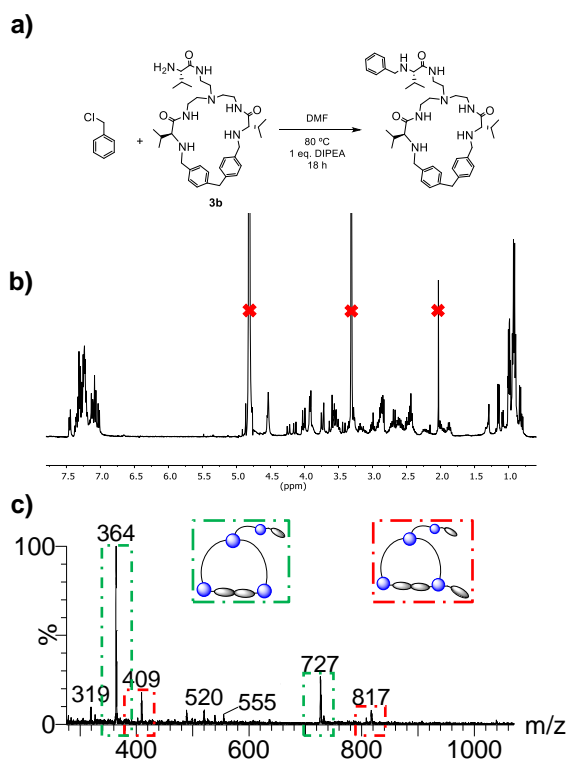
Figure S6.9. a) Homogenous reaction between **3b** and chloromethyl benzene in DMF (80 °C for 18 h). b) ¹H NMR (400 MHz, CD₃OD) spectrum for the reaction crude of the substitution reaction between **3b** and chloromethyl benzene. Peaks corresponding to residual solvents have been marked with red crosses. c) HRMS (ESI+) for the reaction crude of the substitution reaction between **3b** and chloromethyl benzene. Monocationic and dicationic peaks corresponding to the mono- and disubstituted species highlighted in green and red, respectively; only one of the possible substitution isomers has been indicated in the generic structures depicted.
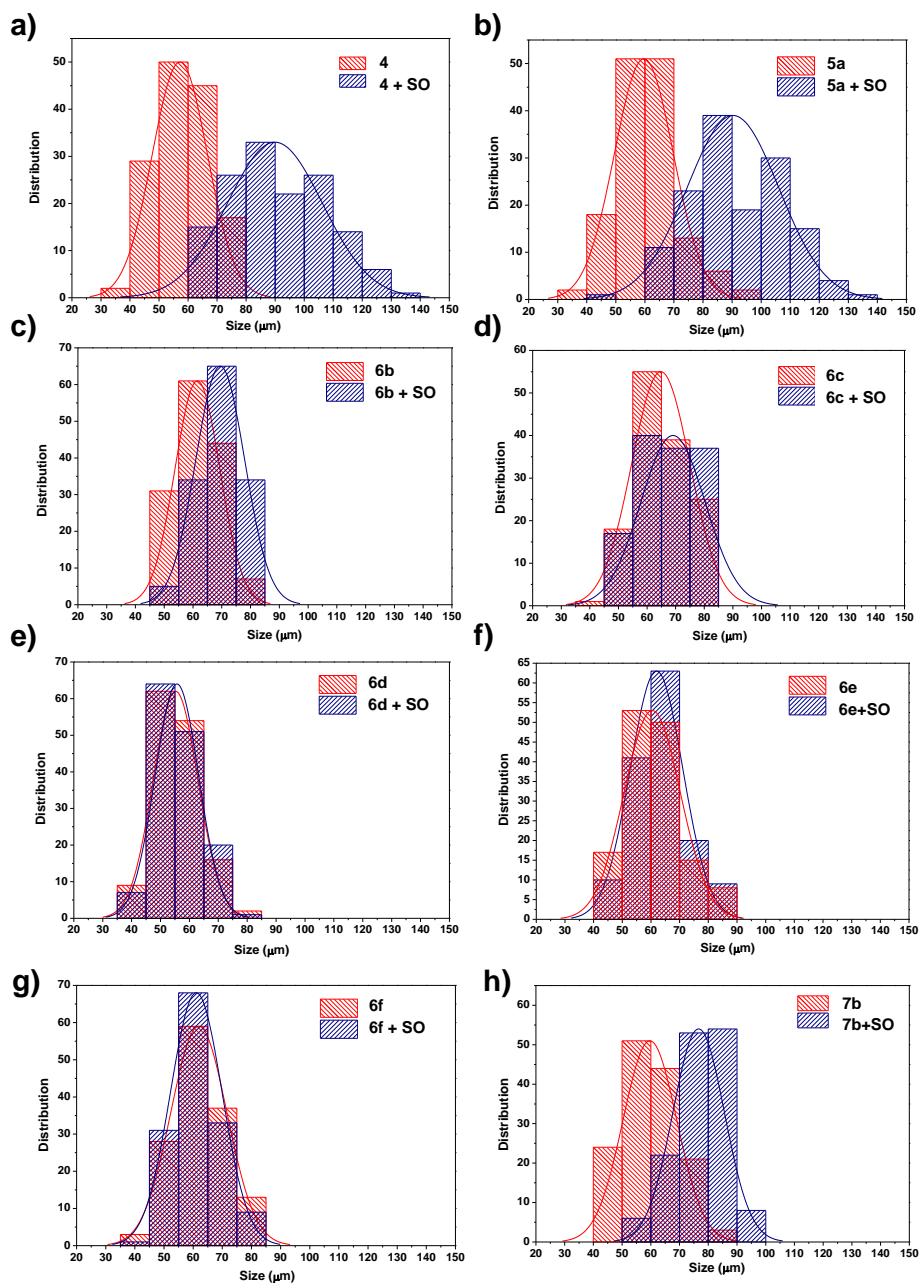
Figure S6.10. Particle size histograms obtained by optical microscopy in the swelling experiments for the different resins in styrene oxide (SO). Resins: a) **4**, b) **5a**, c) **6b**, d) **6c**, e) **6d**, f) **6e**, g) **6f**, and h) **7b**. Total counts >150 in all cases.

Table S6.2. Comparison of the efficiency for some of the best reported multifunctional polymers as heterogeneous supramolecular catalysts.[a]

Ref.	mol%	solvent	T (ºC)	pCO$_2$ (bar)	Time (h)	Yield (%)	TON [b]	TOF (h^{-1}) [b]
Mirabaud et al. [c),d)]	2	MEK	80	10	18	78	39	2.2
Dong et al.[e)]	4	-	100	12	12	95	24	2.0
Desens et al.[f)]	2	-	100	10	3	89	45	14.8
This work	0.12	-	100	balloon	5	85	709	141.8

[a] All the experiments correspond to styrene oxide as substrate. The reported structures have been summarized in Figure S11. [b] TON and TOF values have been calculated with the data supplied in the publications. [c] Bu$_4$NI (2 mol%) was used as homogenous co-catalyst. [d] A. Mirabaud, A. Martinez, F. Bayard, J.-P. Dutasta,, V. Dufaud, *New J. Chem.* **2018**, *42*, 16863-16874. [e] T. Dong, Y.-J. Zheng, G.-W. Yang, Y.-Y. Zhang, B. Li, G.-P. Wu, *ChemSusChem* **2020**, *13*, 4121–4127. [f] W. Desens, C. Kohrt, M. Frank, T. Werner, *ChemSusChem* **2015**, *8*, 3815–3822.
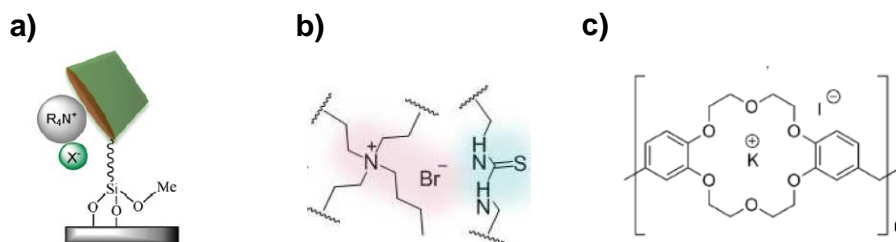
Figure S6.11. General structures of the heterogenous supramolecular organocatalysts reported for the CO$_2$ cycloaddition to epoxides and included in Table S2. a) *Mirabaud et al.* b) *Dong et al.* c) *Desens et al.*
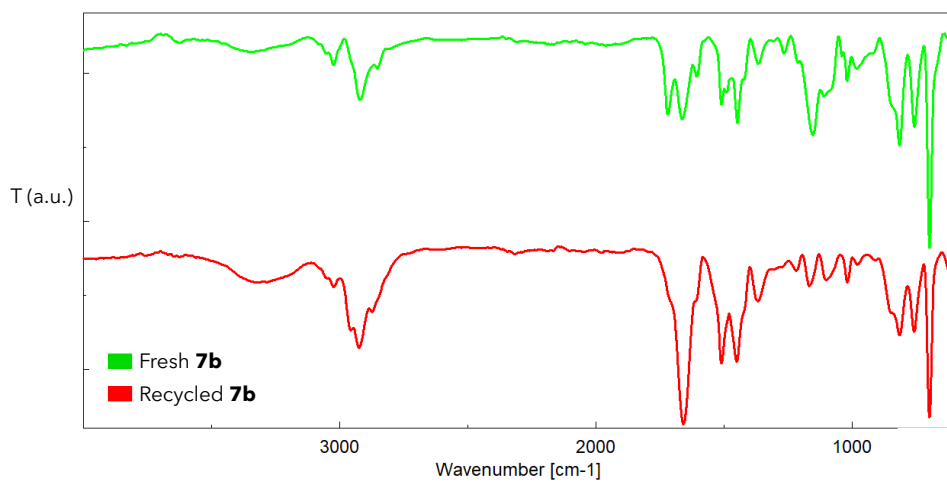
Figure S6.12. ATR-IR spectra comparison between a freshly prepared **7b** sample (above, green) and the resin after reused for 5 cycles (below, red).
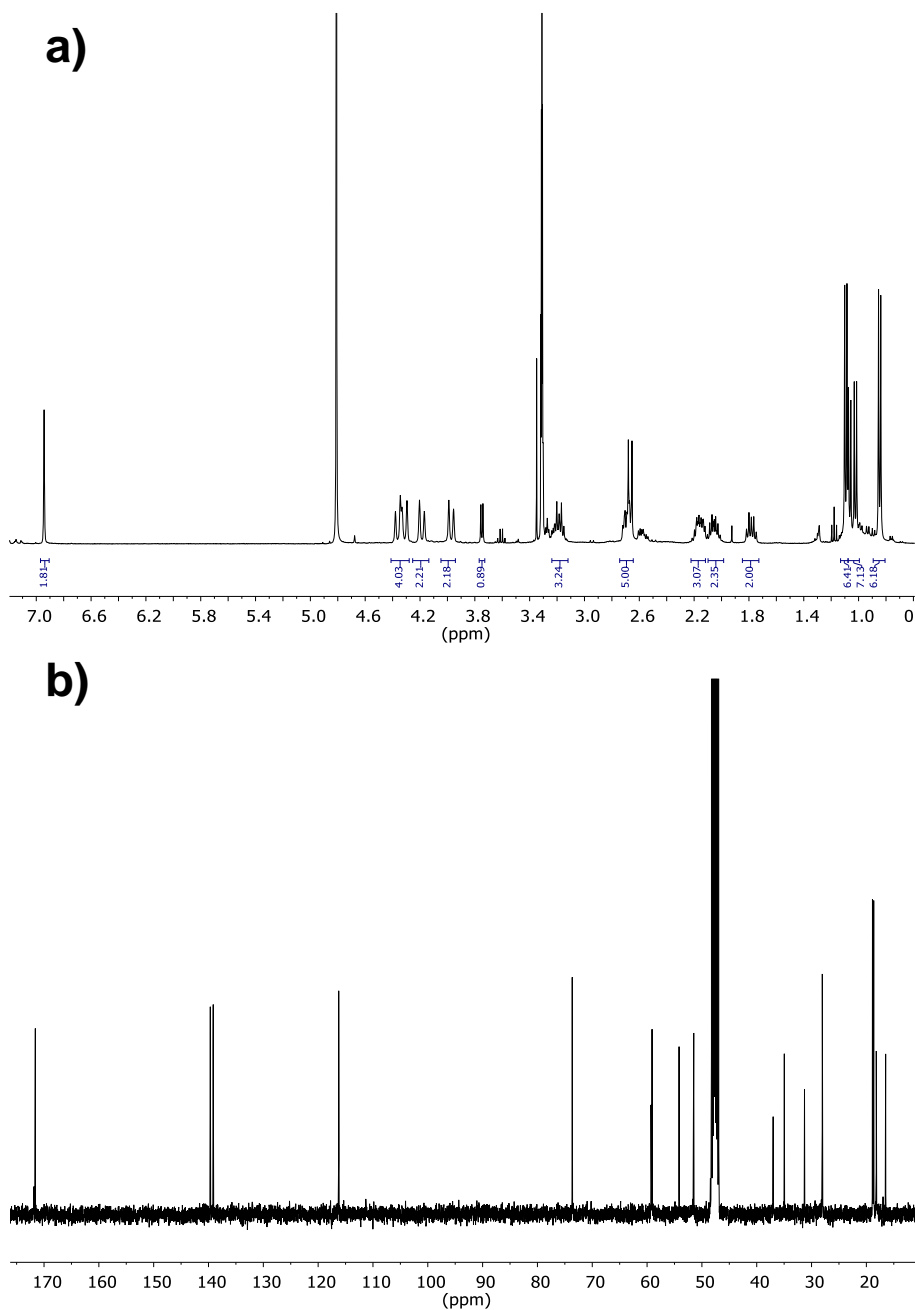
Figure S6.13. Spectroscopic data for **3a**. a) ¹H NMR (400 MHz, CD₃OD); b) ¹³C{¹H} NMR (100 MHz, CD₃OD).
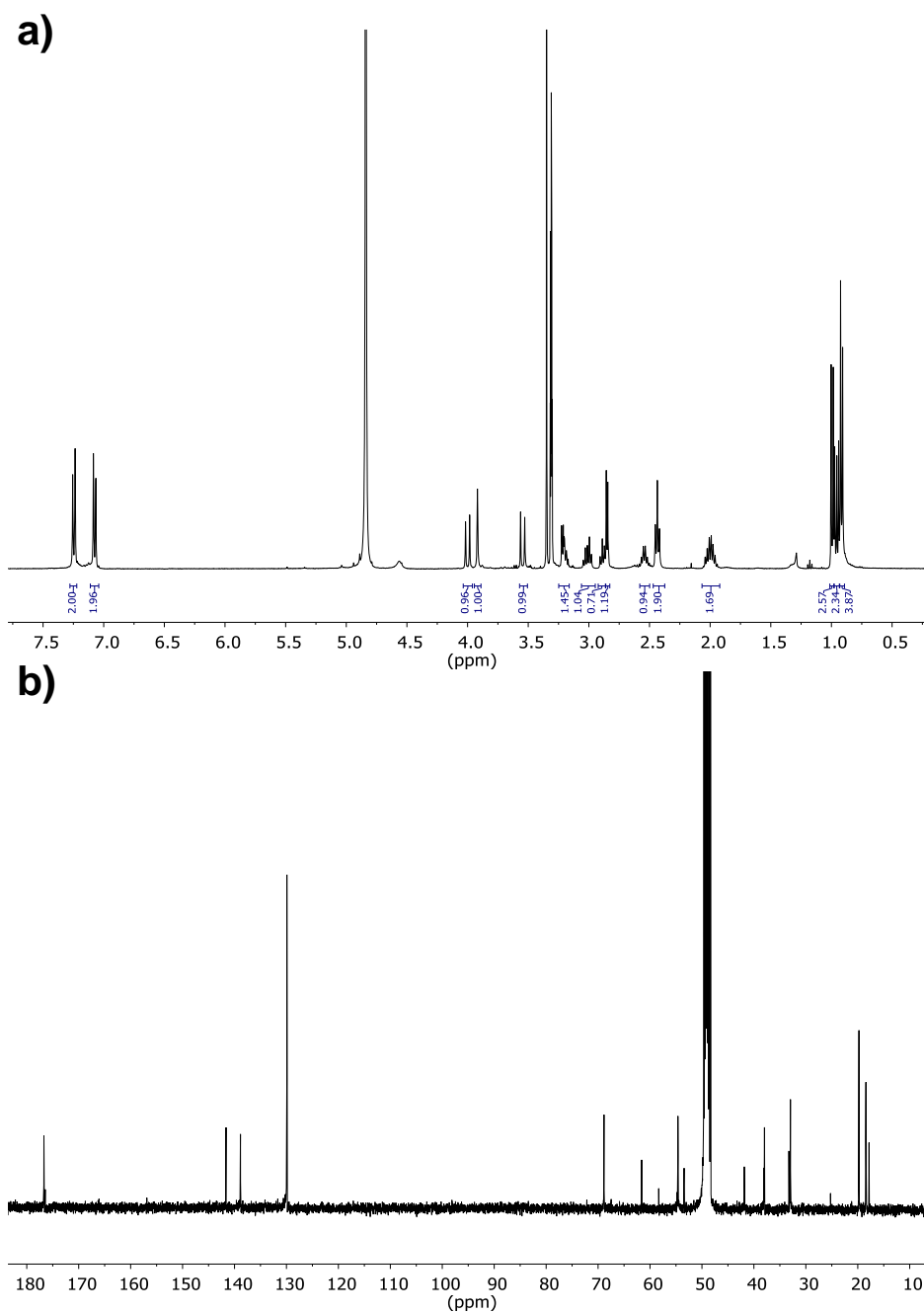
Figure S6.14. Spectroscopic data for **3b**. a) ^{1}H NMR (400 MHz, CD$_3$OD); b) ^{13}C{^{1}H} NMR (100 MHz, CD$_3$OD).

Chapter 7

Highly Active and Enantioselective Multifunctional One-Component Supramolecular Catalysts for the Cycloaddition of CO_2 to Epoxides
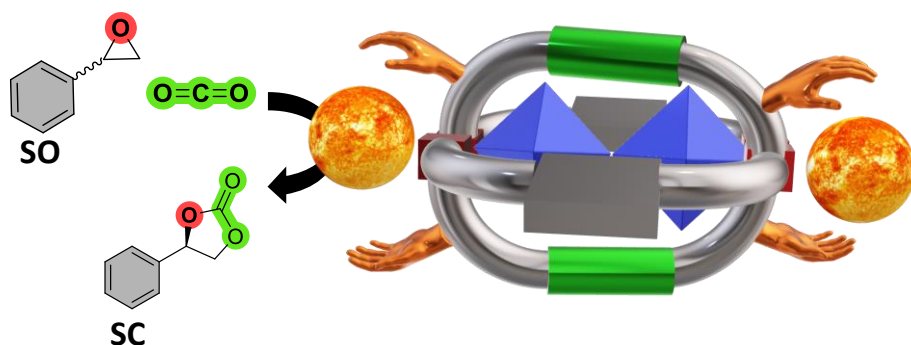
7.1. Main text

7.1.1. Abstract

A series of multifunctional catalysts based on novel pseudopeptidic [2+2] macrocycles have been obtained with high selectivity through the dynamic self-assembly of the different components into a well-defined individual supramolecular species. The coordination of two Zn^{2+} ions within the chiral cavity leads to octahedral homobimetallic complexes able to promote remarkable activities in the cycloaddition of CO_2 to epoxides even at mild conditions (1 bar CO_2 and 60 ºC), without the need of any auxiliary co-catalysts. The whole catalytic cycle was dominated by cooperative non-covalent forces involving multiple functional sites, displaying an enzyme-like catalytic behaviour. In these supramolecular catalysts the zinc cores act as Lewis acid sites, while the location of two iodide counterions outside the coordination sphere renders active "naked" nucleophiles. The chiral environment associated to the amino acid sidechains in this preorganized catalytic system provides recognition sites for efficient kinetic resolution. In the case of the sluggish styrene oxide substrate, the highest selectivity factor reported to date was attained.

7.1.2. Introduction

One of the major challenges facing the global chemical community is reducing atmospheric carbon dioxide.[1] Fortunately, CO_2 can be seen as a cheap, abundant, and nontoxic substance that can lead, in combination with other simple molecules, to added-value chemical products, offsetting the energetic and economic costs of CO_2 capture.[2] Still, its valorisation requires the development of effective catalysts to overcome the elevated CO_2 thermodynamic stability.[3] In this regard, enzymes pave the way for an effective and controlled activation and conversion of CO_2 under moderate conditions, as evidenced during cellular metabolism.[4,5] However, several critical issues hamper the large-scale implementation of enzymatic systems.[6] Thus, the design of new active and stable catalysts able to mimic enzymatic behaviours for CO_2 transformation is of high interest.[7,8] A plethora of synthetic supramolecular

systems has been proposed as efficient bioinspired catalysts for carbon dioxide activation and conversion.[6,9] Among the different added-value products that have been obtained using CO_2, cyclic carbonates (CC) are one of the most popular due to their numerous industrial applications.[10] CC can be obtained through CO_2 cycloaddition to epoxides, with the most common catalytic approach being the use of two-component catalytic systems based on the combination of Lewis acids or bases with co-catalysts that act as the nucleophilic source (Figure 7.1a).[11] In such two-component systems, Lewis acid centres activate the C-O bond of the epoxide (Figure 7.1a1), whereas the presence of Lewis bases facilitates CO_2 activation (Figure 7.1a2).[12,13,14] Some host-guest supramolecular two-component systems have also been described, under both homogenous and heterogenous conditions, obtaining promising results in terms of catalytic activity.[15,16,17,18] Nonetheless, it should be noted that the most active catalysts of this class operate in the presence of huge excess of co-catalysts.[19] Addition of such auxiliary components increase the waste in the process and demands more purification steps, hindering the industrial application of this approach.

In this regard, the design of one-component catalytic systems based on a single molecular or supramolecular species and not requiring any additional co-catalyst is a greener aproach representing a current hot topic.[20,21] Commonly, the two required functional sites are included in the same molecule and connected through covalent bonds using chemical spacers that modulate the conformational features of the final catalytic species (Figure 7.1b).[22,23,24,25,26,27] However, attaining optimally preorganized scaffolds involves the use of complex structures that require multistep syntheses and tedious purification protocols.[28] In addition, most of these one-component systems suffer from low activity at mild conditions (*i.e.*, room temperature and 1 bar), needing high catalyst loadings to achieve good conversions.[29]

Inspired by all these precedents, we envisaged that a suitable design of macrocyclic pseudopeptidic Zn(II)-complexes could promote major advantages in this research field. We report herein the synthesis of a novel series of multifunctional homobimetallic complexes as one-component supramolecular catalysts, bearing

within their structure Lewis acid sites (*i.e.,* Zn^{2+} and amide groups), Lewis basic sites (*i.e.,* amine groups), chiral centres (*i.e.,* associated to the amino acid sidechains), and activated nucleophiles (*i.e.,* iodide anions). The conformationally constrained macrocyclic structure rendered the optimal spatial distribution for cooperation between all active sites, showcasing an enzymatic behaviour (Figure 7.1c).[30] The strong synergic effect between the different functionalities led to remarkable results in terms of activity and enantioselectivity, with the catalytic mechanism being governed by supramolecular interactions.

Previous work:

a) Two-component catalytic systems

a1) (**Nu + LA**)　　　　a2) (**Nu + LB**)
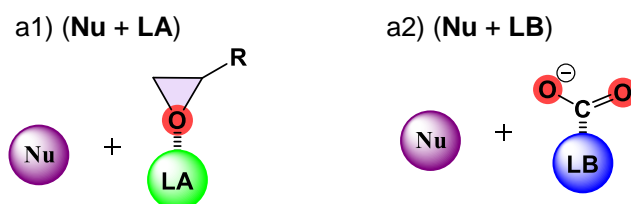
b) Covalently-linked bifunctional one-component catalysts

b1) (**Nu···LA**)　　　　b2) (**Nu···LB**)
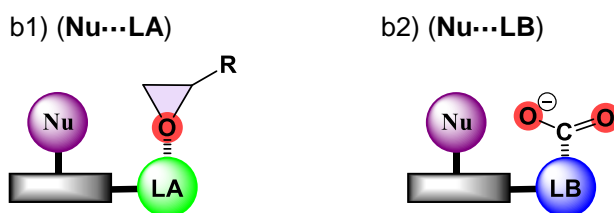
c) This work : Multifunctional one-component supramolecular catalysts
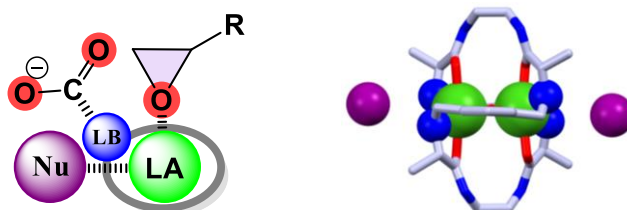
Figure 7.1. Schematic representation for the proposed approaches for the catalytic cycloaddition of CO_2 to epoxides [LA = Lewis acid site, LB = Lewis base, and Nu = nucleophile]. a) Two-component catalytic systems. b) Covalently-linked bifunctional two-component catalysts. c) Multifunctional one-component supramolecular catalysts here presented.

7.1.3. Experimental section

General.

NMR experiments were carried out at 500, 400 or 300 MHz for ^{1}H and 125, 100 or 75 MHz for [13]C. Chemical shifts are reported in ppm from tetramethylsilane using the solvent resonance as the internal standard. Fourier transform infrared spectra (FT-IR) were recorded using an attenuated total reflection (ATR) adapter. Circular dichroism (CD) spectra were recorded using Peltier set-up for precisely controlling the temperature. High resolution mass spectrometry (HRMS) was recorded with a Q-TOF instrument.

Open-chain pseudopeptidic precursors were prepared following literature procedures.[32]

General procedure for the cycloaddition of CO_2 to styrene oxide.

8.7 mmol of epoxide and 0.0044 mmol (or 0.0087 mmol for 1 mol% experiments) of the catalyst were loaded into a Berghof R-300 high-pressure reactor. The reaction vessel was then connected to a pressurized CO_2 source and a back-pressure regulator. The system was purged with 2 bar of CO_2 for 5 minutes, and the final pressure was adjusted to 1 bar. Subsequently, the reaction temperature was risen to the desired temperature and kept at that temperature for the desired time, at 200 rpm stirring. After reaction, the set-up was cooled down to 30 °C and the excess of CO_2 was released carefully. At the end of the reaction, an aliquot of the resulting mixture was analysed by ^{1}H NMR spectroscopy to determine the conversion and by chiral GC to determine the enantiomeric excess of the cyclic carbonate. The experimental procedures were replicated for all experiments. The average deviation of styrene carbonate formation was less than 5%.

General procedure for the ^{1}H NMR conversion determination.

^{1}H NMR spectra were recorded by diluting 20 µL of the reaction crude with 580 µL of $CDCl_3$. The signals δ (ppm) for SO are: 2.76 (t, 1H), 3.10 (t, 1H), and 3.82 (t, 1H) for the CH and CH_2 groups and 7.22−7.38 (m, 5H) for the phenyl group. The

signals δ (ppm) for the cyclic styrene carbonate are: 4.29 (t, 1H) and 4.82 (t,1H) for the CH_2 (methylene), 5.70 (t, 1H) for the CH (methine), and 7.22−7.38 (m, 6H) for the phenyl group. The conversions were measured by NMR integration, considering the signals at 5.70 and 3.82 for SO and SC, respectively (see Figure S7.21 for an example).

General procedure for enantiomeric excess determination by GC.

The enantiomeric purities for the cyclic carbonates were determined by GC using a chiral column (SUPELCO 24304 β-cyclodextrin120, 30 x 0.25 x 0.25 FILM). The samples were prepared diluting 10 μL of the reaction crude with 990 μL of CH_3CN. The peak at 30.9 min was assigned to (*R*)-SC and the peak at 31.2 min was assigned to (*S*)-SC. The peaks of the initial styrene oxide enantiomers appeared at 11.9 min and 12.1 min for (*R*)-SO and (*S*)-SO, respectively. See GC enantiomeric excess determination section (Figures S7.22-S7.27) for more details.

General procedure for IR kinetic experiments.

In-situ FTIR spectra were measured for the different solvent-less kinetic experiments. The temperature (60 ºC) was controlled using a Peltier plate, and the CO_2 atmosphere was introduced with a balloon (see Figure S7.5 for experimental set-up). The data collection consisted of measuring an IR spectrum every 5 minutes. The conversions were determined using an appropriate calibration curve.

General procedure for the spectroscopic titration experiments.

^1H NMR (400 MHz) titration experiments were performed by consecutive additions of the guest to a solution of the desired host. The concentration of the host was kept constant during the experiment. The association constants were determined using HypNMR software.[60]

Crystal structures.

Single crystals suitable for X-ray crystallography were obtained by slow evaporation of a methanol solution of **H₂L1**. A suitable crystal was selected and

mounted on a SuperNova, Dual, Cu at zero, Atlas diffractometer. The structure was solved with the SHELXT 2014/5[61] structure solution program and refined with the SHELXL-2018/3[62] refinement package. Artwork representations were processed using MERCURY[63] software. The refined structure of **H₂L1** has been registered in CCDC with the deposition number: 2153938.

Single crystals suitable for X-ray crystallography were obtained for **4-I** by slow evaporation of MTBE in a THF solution of the organometallic complex. The molecular structure was solved and refined as detailed above. The refined structure has been registered in CCDC with the deposition number: 2153936.

See X-ray Characterisation section for more details (see Supplemental CD).

DFT Calculations.

DFT calculations were run with Gaussian 09 (revision B.01).[64] The X-ray geometric structure for **4-I** was used as the starting point for building-up the models. Geometry optimizations were carried out without symmetry restrictions at the B3LYP level,[65] using the Lanl2Dz basis set.[66] Analytical frequency calculations were used to characterise each stationary point as a minimum. These calculations, carried out at 298.15 K, also allowed for obtaining the thermal and entropic corrections required to calculate Gibbs energy differences. See DFT calculations section for energies and more details (see Supplemental CD).

Syntheses of the macrocyclic pseudopeptidic ligands.

*Synthesis of **L1**.* L-Val-derived bis(aminoamide) (0.230 g, 0.891 mmol, 2 eq.) was reacted with 4-tert-Butyl-2,6-diformylphenol (0.192 g, 0.891 mmol, 2 eq.) in the presence of Na_2SO_4, forming a suspension on chloroform (30 mL, 30 mM). After 15 hour of reaction, 10 mL of methanol were added to the reaction crude and a big excess of $NaBH_4$ (16 eq.) was poured into the flask. The resultant white suspension was left stirring at room temperature for 2 hours. After removal of the solvent at reduced pressure, compound **L1** was extracted from the solid using chloroform as solvent to yield a yellowish solid (0.298 g, 0.329 mmol, 74% yield). Characterisation:

^{1}H NMR (400 MHz, CDCl$_3$, 25 °C) δ = 7.45 (s, 4H), 6.90 (s, 4H), 3.67 (s, 8H), 3.42 – 3.31 (m, 4H), 3.23 (d, J = 9.0 Hz, 4H), 2.87 (d, J = 5.3 Hz, 4H), 1.96 (dt, J = 13.1, 6.7 Hz, 4H), 1.16 (s, 18H), 0.87 (d, J = 6.9 Hz, 12H), 0.80 (d, J = 6.8 Hz, 12H); ^{13}C{^{1}H} NMR (400 MHz, DMSO-d$_6$, 25 °C) δ = 173.1, 153.5, 139.8, 124.0, 123.9, 66.9, 49.0, 38.2, 33.5, 31.6, 19.3, 18.5; FT-IR (ATR): 3278, 3056, 2958, 1646, 1533, 1458 cm^{-1}. MS-ESI(+) m/z: 865.8 ([M + H]$^+$); 887.7 ([M + Na]$^+$).

*Synthesis of **L2**.* L-Phe-derived ligand (yellowish solid, 1.030 g, 0.936 mmol, 79% yield) was synthesized following the protocol described for **L1**. Characterisation: ^{1}H NMR (400 MHz, CD$_3$OD, 25 °C) δ = 7.38 – 6.92 (m, 20H), 6.79 (s, 4H), 3.57 (d, J = 12.9 Hz, 4H), 3.43 (d, J = 12.9 Hz, 4H), 3.33 – 3.24 (m, 4H), 3.16 – 3.00 (m, 12H), 2.88 (dd, J = 13.5, 6.2 Hz, 4H), 2.76 – 2.64 (m, 4H), 1.09 (s, 18H); ^{13}C{^{1}H} NMR (400 MHz, CD$_3$OD, 25 °C) δ = 176.1, 155.2, 142.4, 130.3, 130.2, 127.8, 126.6, 125.3, 64.5, 50.3, 40.3, 39.9, 34.7, 32.1; FT-IR (ATR): 3285, 3060, 2952, 1655, 1525, 1454 cm^{-1}. MS-ESI(+) m/z: 1057.6 ([M + H]$^+$); 1079.8 ([M + Na]$^+$).

*Synthesis of **L3**.* D-Phe-derived ligand (yellowish solid, 0.497 g, 0.452 mmol, 75% yield) was synthesized following the protocol described for **L1**. Characterisation: ^{1}H NMR (400 MHz, CD$_3$OD, 25 °C) δ = 7.38 – 6.92 (m, 20H), 6.79 (s, 4H), 3.57 (d, J = 12.9 Hz, 4H), 3.43 (d, J = 12.9 Hz, 4H), 3.33 – 3.24 (m, 4H), 3.16 – 3.00 (m, 12H), 2.88 (dd, J = 13.5, 6.2 Hz, 4H), 2.76 – 2.64 (m, 4H), 1.09 (s, 18H); ^{13}C{^{1}H} NMR (400 MHz, CD$_3$OD, 25 °C) δ = 176.1, 155.2, 142.4, 130.3, 130.2, 127.8, 126.6, 125.3, 64.5, 50.3, 40.3, 39.9, 34.7, 32.1; FT-IR (ATR): 3285, 3060, 2952, 1655, 1525, 1454 cm^{-1}. MS-ESI(+) m/z: 1057.6 ([M + H]$^+$); 1079.8 ([M + Na]$^+$).

*Synthesis of **L4**.* L-Trp-derived ligand (yellowish solid, 0.075 g, 0.060 mmol, 64% yield) was synthesized following the protocol described for **L1**. Characterisation: ^{1}H NMR (400 MHz, CD$_3$OD, 25 °C) δ = 7.40 (d, J = 8.0 Hz, 4H), 7.18 (d, J = 8.1, 4H), 6.96 – 6.89 (m, 8H), 6.86 – 6.79 (m, 8H), 6.72 (s, 4H), 3.48 (d, J = 13.0 Hz, 4H), 3.39 – 3.26 (m, 8H), 3.10 – 2.98 (m, 12H), 2.84 (dd, J = 14.3, 7.7 Hz, 4H), 1.02 (s, 18H).; ^{13}C{^{1}H} NMR (400 MHz, CD$_3$OD, 25 °C) δ = 176.8, 154.5, 143.0, 138.1, 128.7, 126.6, 125.1, 124.7, 122.5, 119.9, 119.5, 112.4, 111.2, 63.6, 50.3, 39.9, 34.7,

32.1, 29.8; FT-IR (ATR): 3404, 3307, 3057, 2955, 1654, 1524, 1457 cm^{-1}. MS-ESI(+) m/z: 1213.7 ([M + H]$^+$); 1235.9 ([M + Na]$^+$).

Syntheses of the organometallic pseudopeptidic complexes.

Synthesis of 1. Ligand **L1** (0.150 g, 0.165 mmol, 1 eq.) was dissolved in 2 mL of MeOH. ZnI$_2$ (0.105 g, 0.330 mmol, 2 eq.) was dissolved in 0.6 mL of MeOH. The methanolic solution of the ligand was added to the ZnI$_2$ solution, leading to the appearance of abundant white precipitate. The white solid was filtered-off using a syringe filter and the resultant colourless solution was dried under reduced pressure and at 45 °C to yield pure **1-I** as a white solid (0.175 g, 0.145 mmol, 88% yield). Characterisation: ^{1}H NMR (400 MHz, DMSO-d_6, 25 °C) δ = 8.58 (s, 4H), 6.86 (s, 4H), 4.71 (d, J = 13.1 Hz, 4H), 3.82 (d, J = 7.3 Hz, 4H), 3.76 (dd, J = 13.5, 3.5 Hz, 4H), 3.25 – 3.18 (m, 8H), 2.94 (d, J = 12.4 Hz, 4H), 2.24 – 2.12 (m, 4H), 1.03 (d, J = 6.9 Hz, 12H), 0.85 (d, J = 6.9 Hz, 12H); ^{13}C{^{1}H} NMR (400 MHz, DMSO-d_6, 25 °C) δ = 174.7, 160.4, 136.5, 128.4, 120.7, 59.6, 53.2, 41.2, 32.4, 31.5, 19.5, 16.7; FT-IR (ATR): 3456, 3249, 3084, 2959, 1624, 1546, 1480 cm^{-1}. HRMS (ESI/Q-TOF) m/z: [M]$^{2+}$ Calcd for C$_{48}$H$_{78}$N$_8$O$_6$Zn$_2$ 495.7353; Found 495.7359. See spectroscopic characterization section for 2D-NMR analyses (Figures S7.28-S7.32).

Synthesis of 2. **2-I** (white solid, 0.422 g, 0.269 mmol, 89% yield) was synthesized following the protocol described for **L1**. The yellowish solid (1.030 g, 0.936 mmol, 79% yield) was used for synthesizing product **2-I** without further purification. Characterisation: ^{1}H NMR (400 MHz, THF-d_8, 25 °C) δ = 7.77 (d, J = 7.6 Hz, 4H), 7.69 (d, J = 7.2 Hz, 8H), 7.24 – 7.14 (m, 12H), 5.95 (s, 4H), 5.71 – 5.57 (m, 4H), 4.60 (d, J = 13.5 Hz, 4H), 3.70 – 3.56 (m, 8H), 3.42 – 3.32 (m, 4H), 2.90 (t, J = 9.3 Hz, 8H), 2.67 (dd, J = 13.5, 3.3 Hz, 4H), 1.09 (s, 18H).;^{13}C{^{1}H} NMR (400 MHz, THF-d_8, 25 °C) δ = 175.8, 160.9, 138.7, 136.2, 130.3, 128.4, 128.1, 126.3, 121.4, 57.6, 51.8, 41.4, 39.4, 33.1, 31.1; FT-IR (ATR): 3417, 3200, 2949, 1626, 1556, 1480 cm^{-1}. HRMS (ESI/Q-TOF) m/z: [M]$^{2+}$ Calcd for C$_{64}$H$_{78}$N$_8$O$_6$Zn$_2$ 591.7353; Found 591.7362. See spectroscopic characterization section for 2D-NMR analyses (Figures S7.33-S7.37).

Synthesis of 3. **3-I** (white solid, 0.134 g, 0.093 mmol, 86% yield) was synthesized following the protocol described for **L1**. The yellowish solid (0.497 g, 0.452 mmol, 75% yield) was used for synthesizing product **3-I** without further purification. Characterisation: ^{1}H NMR (400 MHz, THF-d$_8$, 25 °C) δ = 7.77 (d, J = 7.6 Hz, 4H), 7.69 (d, J = 7.2 Hz, 8H), 7.24 – 7.14 (m, 12H), 5.95 (s, 4H), 5.71 – 5.57 (m, 4H), 4.60 (d, J = 13.5 Hz, 4H), 3.70 – 3.56 (m, 8H), 3.42 – 3.32 (m, 4H), 2.90 (t, J = 9.3 Hz, 8H), 2.67 (dd, J = 13.5, 3.3 Hz, 4H), 1.09 (s, 18H).;^{13}C{^{1}H} NMR (400 MHz, THF-d$_8$, 25 °C) δ = 175.8, 160.9, 138.7, 136.2, 130.3, 128.4, 128.1, 126.3, 121.4, 57.6, 51.8, 41.4, 39.4, 33.1, 31.1; FT-IR (ATR): 3417, 3200, 2949, 1626, 1556, 1480 cm^{-1}. HRMS (ESI/Q-TOF) m/z: [M]$^{2+}$ Calcd for C$_{64}$H$_{78}$N$_8$O$_6$Zn$_2$ 591.7353; Found 591.7362. See spectroscopic characterization section for 2D-NMR analyses (Figures S7.33-S7.37).

Synthesis of 4. **4-I** (white solid, 0.052 g, 0.033 mmol, 82% yield) was synthesized following the protocol described for **1-I**. Characterisation: ^{1}H NMR (400 MHz, THF-d$_8$, 25 °C) δ = 9.92 (s, 4H), 8.19 (s, 4H), 7.55 (d, J = 2.5 Hz, 4H), 7.38 (d, J = 7.9 Hz, 4H), 7.23 (d, J = 8.1 Hz, 4H), 6.90 (t, J = 7.6 Hz, 4H), 6.73 (t, J = 7.5 Hz, 4H), 5.64 (s, 4H), 5.24 (d, J = 2.4 Hz, 4H), 4.67 – 4.57 (m, 4H), 3.73 (m, 4H), 3.07 (dd, J = 14.1, 4.1 Hz, 4H), 2.90 (dd, J = 13.4, 3.4 Hz, 4H), 2.83 (d, J = 12.7 Hz, 4H), 0.66 (s, 18H);^{13}C{^{1}H} NMR (400 MHz, THF-d$_8$, 25 °C) δ = 176.1, 160.9, 136.7, 128.2, 127.6, 126.9, 121.2, 120.9, 118.6, 118.0, 110.9, 110.2, 56.6, 52.5, 41.3, 32.6, 30.9, 30.1; FT-IR (ATR): 3491, 3428, 3223, 3083, 2959, 1627, 1551, 1478 cm^{-1}. HRMS (ESI/Q-TOF) m/z: [M]$^{2+}$ Calcd for C$_{72}$H$_{82}$N$_{12}$O$_6$Zn$_2$ 669.7571; Found 669.7568. See spectroscopic characterization section for 2D-NMR analyses (Figures S7.38-S7.41).

7.1.4.   Results and discussion

The new family of macrocyclic compounds was synthesized *via* imine condensation of the open-chain C_2 pseudopeptidic bisaminoamides **B** with 5-(tert-butyl)-2-hydroxyisophthalaldehyde (**DA**) followed by *in-situ* reduction (Scheme 7.1). The dynamic nature of the imine bonds allowed for the formation of thermodynamically favoured [2+2] macrocycles, overcoming the production of side

products of oligomeric/polymeric nature.[31] The high efficiency of the macrocyclization reaction can be related with the adoption of the optimal U-turn preorganization for the open chain bisaminoamides, favoured by the aprotic apolar solvent used, namely CHCl₃.[32] Indeed, when the condensation reaction was carried out with 1,8-diaminooctane, instead of the pseudopeptide, mainly the formation of oligomer/polymers was observed, ratifying the postulated role of intramolecular hydrogen bonds promoted by the amide groups in the macrocyclization step (Figure S7.1).[33] It must be highlighted that high isolated yields were achieved for all the pseudopeptidic macrocycles, without the need of using auxiliary templating agents (Table S7.1), even at relatively high concentrations (30 mM).[34]
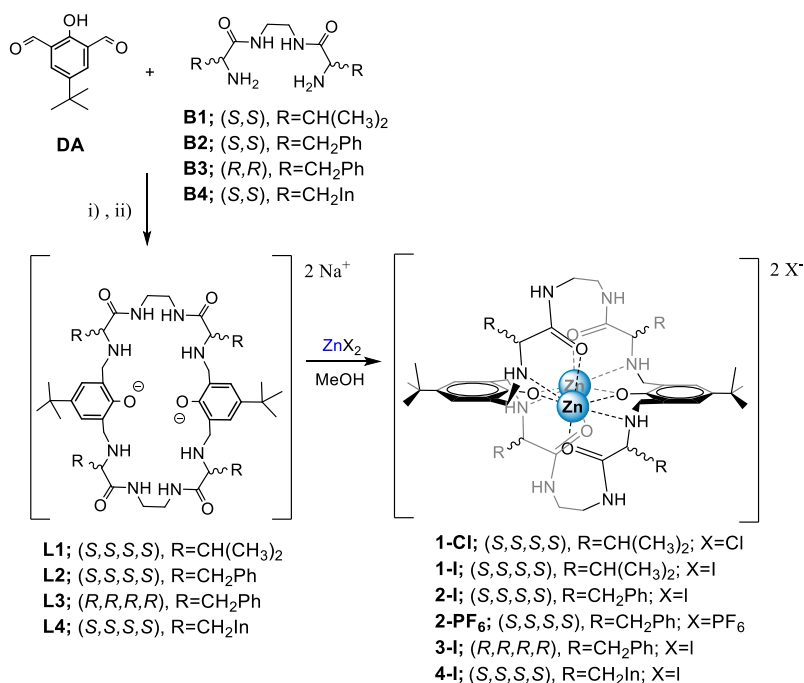
Scheme 7.1. Synthetic route to produce the macrocyclic organometallic species **1-4**. i) CHCl₃ (30 mM concentration for each reagent), Na₂SO₄ at 25 °C for 15 h. ii) MeOH, NaBH₄ excess at 25 °C for 2 h. The metal-complexation step was carried out at 25 °C.

Crystals suitable for X-ray diffraction measurement were grown for the **L1** macrocycle with protonated phenols (**H₂L1**). The solid-state structure revealed a highly twisted conformation involving intramolecular ($d_{HN\cdots OC}$ = 2.78 Å, 92%

vdW$_{N,O}$) and intermolecular (d$_{HN\cdots OC}$ = 2.94 and 2.84 Å, 96 and 93% vdW$_{N,O}$, respectively) hydrogen bonds between the amide groups of the pseudopeptidic chains (Figure S7.2).[35]

The sodium salts of macrocycles **L1-L4** were then reacted with ZnX$_2$ salts, leading to the formation of binuclear pseudopeptidic complexes **1**-**4** in yields in the 80-90% range (Scheme 7.1). The solid-state structure of **4-I** provided unambiguous evidence for complex formation (Figure 7.2a). The two phenoxy-groups act as bridges between the two Zn cores, as previously reported for related systems.[36,37] One amino nitrogen atom of each pseudopeptidic moiety completed the equatorial coordination plane of the metal (Figure 7.2b).
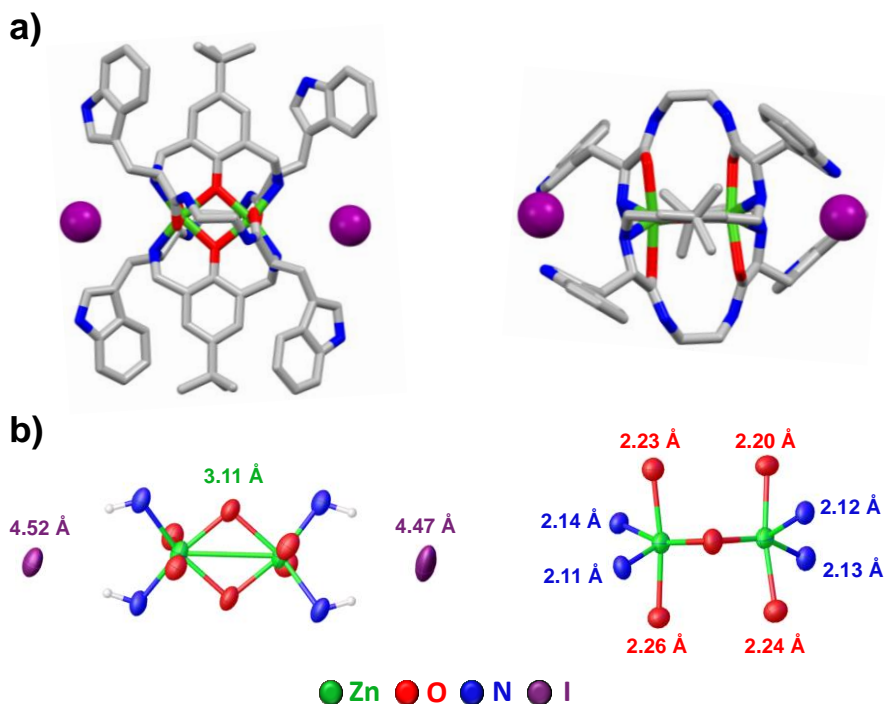
Figure 7.2. Solid-state structure obtained for **4-I.** (a) Side and top-view. Hydrogen atoms and solvent molecules have been removed for clarity. Iodide anions are highlighted in violet. (b) Representation of the distorted octahedral coordination spheres for Zn^{2+} ions. Distances between atoms and metallic cores have been highlighted in different colours. The intermetallic Zn-Zn distance has been marked in green.

In this case, in contrast to the hitherto described molecular structures, the counterion is not coordinated to the metallic sites. Instead, the oxygen atom of the four amide groups is further complexing the apical positions of the metallic centre, resulting in a distorted octahedral coordination sphere for each Zn^{2+} (Figure 7.2b). Consequently, the iodide anion is located out-of-sphere, stabilized by hydrogen bonds with the acid hydrogen atoms of the secondary amines ($d_{N\cdots I}$ = 3.69 Å, 105% $vdW_{N,I}$). Interestingly, the iodide anions are closely surrounded by the constrained chiral environment of the pseudopeptidic fragments (Figure 7.2a). The crystal structure of **4-I** also exhibits an extremely long, and therefore labile, zinc–iodide bond, with an average distance between ions of 4.49 Å (Figure 7.2b).

This opened the way for using these metal complexes as multifunctional one-component catalysts for the cycloaddition of CO_2 to epoxides. Compounds **1** were selected for an initial evaluation of their potential catalytic activity. The reaction between styrene oxide (SO) and CO_2 under solvent-less conditions was selected as the benchmark reaction. Table 7.1 summarises the results obtained for the different conditions assayed. Complex **1-I** showed remarkable activity leading to quantitative conversions in only 1 hour (entry 5, Table 7.1) with a TOF value of 198 h^{-1}, while the zinc salts in the absence of macrocyclic ligand showed low or no activity despite the elevate temperature employed (entries 1-3, Table 7.1). When **1-Cl** was used as catalyst, the performance suffered a significant decrease (see entries 6 and 8 in Table 7.1). This activity decrease was assigned to the lower nucleophilicity of chloride anions as compared to iodide anions.

As expected, lower temperatures afforded lower conversions into the desired styrene carbonate (SC) (entries 9-12, Table 7.1). Notwithstanding, **1-I** afforded a 90% conversion in only 3 hours at 60 ºC and 1 bar of CO_2, which represents an extraordinary value considering the moderate reactivity of SO (entry 9, Table 7.1). This valine-derived catalyst was found to be active even at room temperature, obtaining a 23% conversion, with excellent selectivity, after 15 h of reaction (entry 12, Table 7.1). These results highlight the exceptional activity of these pseudopeptidic multifunctional complexes, even in the absence of any co-catalyst.

Table 7.1. Catalytic results obtained for zinc complexes **1** in the cycloaddition of CO_2 to styrene oxide under solvent-less conditions.[a]

Entry	Cat. (mol%)	Temp. (ºC)	Time (h)	Conversion (%)[b]
1	ZnI_2 (1)	100	3	14
2	ZnI_2 (1)	100	1	3
3	$ZnCl_2$ (1)	100	3	0
4	**1-I** (0.5)	100	3	>99
5	**1-I** (0.5)	100	1	>99
6	**1-Cl** (0.5)	100	3	53
7	**1-I** (0.5)	80	1	>99
8	**1-Cl** (0.5)	80	3	14
9	**1-I** (0.5)	60	3	90
10	**1-I** (0.5)	60	1	31
11	**1-I** (0.5)	40	3	14
12	**1-I** (0.5)	r.t.	15	23

[a] Reaction conditions: styrene oxide (4.35 mmol), 1 bar of CO_2 (autoclave). [b] Conversions determined by ^1H NMR, selectivity for styrene carbonate was always > 99.9% when using pseudopeptidic complexes. Formation of side-products (mainly diol species) was detected when using ZnI_2.

One may presume that these systems, being active under mild conditions and with a well-defined chiral environment, could provide enantiodiscrimination during the cycloaddition of CO_2 to styrene oxide. Chiral epoxides and cyclic carbonates are important intermediates in the production of pharmaceutical and biological compounds.[38,39] Traditionally, enantiopure cyclic carbonates are prepared by enzymatic hydrolysis of racemic epoxides or by the cyclization of chiral diols with highly toxic triphosgene.[40,41] In the search of less hazardous methodologies, the kinetic resolution of racemic epoxides in the presence of carbon dioxide has been exploited, as this is a greener alternative presenting 100% atom economy.[19,42,43,44,45,46,47] The main hurdle in such catalytic approach is the harsh conditions often required for overcoming the inertness of CO_2, which in turn adversely affects the enantiomeric purity of the products.[48] Thus, we decided to evaluate the potential of the macrocyclic complex (**1-I**) for the kinetic resolution of

racemic SO. GC analyses permitted the quantification of the enantiomeric excess for SC. The use of enantiomerically enriched SO mixtures allowed to observe that kinetic resolution of racemic oxiranes was occurring (Figure S7.3). At 40 °C, 0.5 mol % of **1-I** and 1 bar CO_2, conversions after 15 hours increased with the initial amount of the *R*-enantiomer present in the mixture. Indeed, conversions ranged from 7% for pure *S*-enantiomer to 19% for pure *R*-enantiomer, indicating a faster reaction with (*R*)-SO. In addition, for those enantioenriched mixtures, the percentage of (*R*)-SC found was always higher than the percentage of the *R*-enantiomer in the starting SO, corroborating the kinetic resolution of racemic SO.

The nature of pseudopeptidic sidechains was then examined. Results in Table 7.2 illustrate that the amino acid residue was clearly affecting to both activity and enantiopreference of the process. In terms of catalytic performance, the best results were detected for the phenylalanine bimetallic complex, following the trend Phe > Val > Trp (**2-I** > **1-I** > **4-I**, see entries 1-7 in Table 7.2). This result suggests that π-interactions can be involved in the reaction mechanism, stabilizing transition states and reaction intermediates (*vide infra*). A preferential formation of (*R*)-SC was generally observed (entries 1-6 and 8-12 in Table 7.2). Interestingly, when the macrocyclic complex **3-I** displaying the (*R,R,R,R*) configuration was used, the formation of (*S*)-SC was instead favoured (Table 7.2, compare entries 5 and 7). Therefore, the enantioselectivity attained in the reaction was a direct result of the chirality introduced by the amino acid moieties of the complexes. This is of key importance as the enantiomeric preference of the reaction outcome can be easily tuned by simply modifying the chirality of the precursors.

The high activity of the systems allowed to decrease the temperature to r.t. providing more efficient kinetic resolutions with reasonable conversions and leading to better enantioselectivities and *s*-factors (entries 8-12 in Table 7.2). An increase in the reaction time to 24 h resulted in an *s*-factor as high as 9.5 for **2-I**. To the best of our knowledge, this is the highest *s*-factor reported to date for the kinetic resolution of styrene oxide (see Table S7.2 and Figure S7.4).

Table 7.2. Effect of the amino acid sidechain in the catalytic kinetic resolution of styrene oxide by cycloaddition of CO_2 under solvent-less catalysed by zinc iodide pseudopeptidic macrocyclic complexes.[a]

Entry	Cat.	Temp. (ºC)	Time (h)	Conv. (%)[b]	e.e. (%)[c]	s[f]
1	**1-I**	60	1	31	21[d]	2.4
2	**2-I**	60	1	38	30[d]	2.2
3	**4-I**	60	1	15	12[d]	1.9
4	**1-I**	40	4	14	39[d]	2.4
5	**2-I**	40	4	27	58[d]	4.6
6	**4-I**	40	4	9	29[d]	1.9
7	**3-I**	40	4	25	56[e]	4.2
8	**1-I**	r.t.	15	21	49[d]	3.3
9	**2-I**	r.t.	15	23	68[d]	6.4
10	**4-I**	r.t.	15	6	34[d]	2.0
11	**2-I**[g]	r.t.	15	52	55[d]	6.2
12	**2-I**	r.t.	24	45	69[d]	9.5

[a] Reaction conditions: styrene oxide (4.35 mmol), 0.5 mol% of catalyst, 1 bar of CO_2 (autoclave). [b] Conversions determined by ^1H NMR, selectivity for styrene carbonate was always > 99.9 %. [c] Enantiomeric excess determined by GC analyses. [d] Enantiomeric excess for (R)-styrene carbonate. [e] Enantiomeric excess for (S)-styrene carbonate. [f] $s = \ln[(1-c(1+ee)]/\ln[1-c(1-ee)]$, where c is the conversion and e.e. is the enantiomeric excess. [g] 1 mol% of catalyst.

A series of terminal epoxide substrates were then studied for the formation of their cyclic carbonates in the presence of CO_2 and **2-I** (Table S7.3). At 80 °C and under 1 bar of CO_2, all epoxides were smoothly converted into the desired organic carbonates with excellent conversions (> 90%). In addition, although the use of solvent (THF) was in some cases necessary to prevent solidification of the reaction mixture, complex **2-I** was still able to promote kinetic resolutions with enatioselectivities of *ca.* 40% e.e. and *s*-factors of 2.4-2.9 at 40 °C for the different substrates assayed.

Based on the obtained results and the solid-state structure of the complex (Figure 7.2), we can propose that the crowded coordination sphere of the Zn^{2+}

metallic cores allowed for the presence of "naked" iodide anions enabling their role as nucleophiles in a highly efficient ring-opening step.[15] The synergies between the metallic core and the "naked" iodide anion were demonstrated by additional catalytic experiments (Table S7.4). The parent unit **L2**, lacking both the nucleophile source and Zn^{2+} centres, did not promote the formation of styrene carbonate. Addition of 1 mol% of iodide anion as its tetrabutylammonium salt in the presence of 0.5 mol% of **L2** only resulted in a 2% yield, suggesting that the metallic core is of paramount importance for the activation of the substrates under such mild reaction conditions. As expected, when **2-PF$_6$** was used in the reaction, only minor traces of SC were detected. This result indicates that the presence of an activated nucleophile is a requirement for triggering the catalytic cycle. All these evidences reflect that the observed activity and enantioselection involves a tight cooperativity between the different catalytic sites of the one-component system: Lewis acid and basic centres, nucleophile and metallic core, all preorganized with an optimal spatial disposition within the chiral complex (Figure 7.1).

Several spectroscopic experiments were designed for gaining additional insights into mechanistic aspects. The reaction order for **2-I** was determined by *in-situ* FTIR spectroscopy at 60 °C in the presence of a CO_2 balloon (Figure S7.5).[49] The aftermath of the kinetic study revealed a first-order dependence on the bimetallic catalytic species (Figure S7.6 and S7.7).[50] Conformational information was gathered by measuring ^{1}H NMR spectra for **2-I** in different solvents. Figure 7.3 shows that the structure of the complex is conformationally very rigid, as demonstrated by the noteworthy anisochrony observed for the diastereotopic Ar-CH$_2$-NH$_{amine}$ methylene protons (orange signals in Figure 7.3). Besides, in the presence of solvents containing Lewis basic groups, the signals for the amide protons (green signals in Figure 7.3) appeared at lower fields, following the expected basicity trend (DMSO > acetone > THF >> ACN). This observation can be explained by the formation of hydrogen bonds between the acidic amide protons and the basic donor sites of the solvents, as observed in the solid-state structure of **4-I** (Figure S7.8).[51]
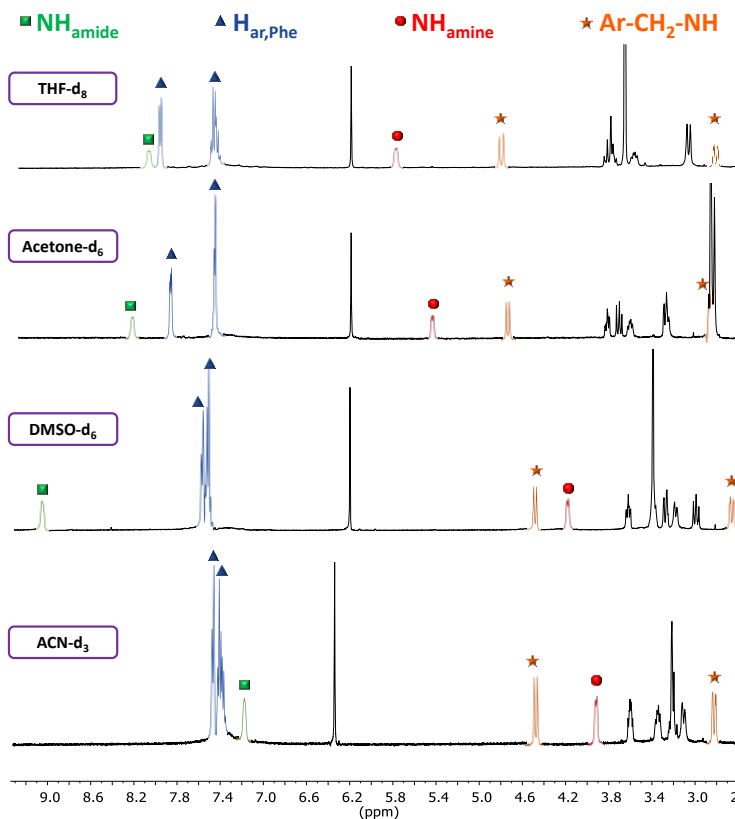
Figure 7.3. ^{1}H NMR (400 MHz, 25 °C) spectra comparison for **2-I** (2 mM) in different deuterated solvents. Spectra from top to bottom: THF, acetone, DMSO, and ACN, respectively. The signals for the protons discussed in the text have been highlighted with different colours in the spectra.

The acidic proton signals for the coordinated secondary amines (red signals in Figure 7.3) did not respond to such basicity trend. Instead, they appeared at much lower fields in the presence of THF/acetone than for DMSO. Comparing the shifts with the ones obtained for the barely preorganized conformation in acetonitrile, $\Delta\delta$ values of +1.8, +1.5, and +0.2 ppm were found for the NH$_{amine}$ signals in THF, acetone, and DMSO, respectively. These differences can be assigned to the polarity of the solvents. For instance, DMSO presents a higher relative polarity than THF (0.444 *vs* 0.207), and thus it promotes a better solvation for the iodide counterions.[52] Hence, the protons of the amino groups are less influenced by the electronegative anions in the most polar solvents like DMSO and ACN (Figure 7.3). On the other

hand, poor solvation of the negatively charged iodide ions results in tight hydrogen bonding with the acidic protons of the coordinated amines (see Figure 7.3 and Figure S7.8). These non-covalent interactions between the anions and the amine hydrogen atoms further rigidify the whole structure of the bimetallic pseudopeptidic complex, as corroborated by the significantly different electronic environment experienced by the aromatic protons of the phenylalanine sidechains in THF and acetone (blue signals, Figure 7.3). Considering the structural similarities between THF and oxiranes, it may be predicted that the catalytically active conformation of the pseudopeptidic complexes in SO must be like the one found in THF. ^{1}H NMR titration experiments of **2-I** with styrene oxide and THF showed similar chemical shift variations (Figure S7.9), corroborating this assumption. Therefore, the efficiency of the catalyst in the kinetic resolution of epoxides could be explained by the rigidized sidechains of the α-C chiral centres of the complex, that are located in the surroundings of the activated nucleophilic anion (see Figure 7.1 for representation).

The recognition capability of the pseudopeptidic complex was assayed in the presence of the two enantiomers of the substrate, namely (*S*)-SO and (*R*)-SO. The association constants for the equimolecular **2-I** : SO system determined by ^{1}H NMR titration experiments revealed a slight preference for the interaction with (*R*)-SO over its (*S*)-enantiomer (Figures S7.10 and S7.11). This observation could be the result of additional π-π interactions between the pseudopeptidic sidechain and the aromatic moiety of the epoxide (see Figure 7.4c). However, the relatively small difference between the two constants, 16 ± 1 M^{-1} and 8 ± 1 M^{-1} for the (*R*) and (*S*) enantiomers, cannot explain by itself the enantiomeric excess obtained during the catalytic conversion (see for instance Entry 12, Table 7.2). It must be mentioned, however, that this enantiomeric preference could be even more pronounced in the supramolecular complexation of the reaction intermediates and the transition states (see Figure 7.4). Conformational changes for **2-I** in the presence of (*R*)-SO were also monitored using circular dichroism (CD). Interestingly a significant decrease was observed, upon addition of (*R*)-SO, in the intensity of the negative band centred at 215 nm and associated to the absorption of amide groups (Figure S7.12).[53] This result

is consistent with a change in the chiral environment of the amide moieties upon hydrogen bonding with the basic oxygen atom of the epoxide.[17] As expected for this molecular recognition process, a red-shift was concomitantly detected in the UV absorption signal for the amide band (Figure S7.13).

The capacity of these complexes to activate carbon dioxide molecules during the catalytic reaction was also analysed. The presence of amino groups in the macrocyclic structure could promote some further activation of carbon dioxide molecules.[54] ^{1}H NMR for **2-I** in the presence of CO_2 (10 bar) allowed the identification of some unexpected species. Initially, the characteristic signals for **2-I** and THF suffered minor changes under the influence of CO_2 (Figure S7.14). Most noticeable differences were detected for the protons located near the secondary amino groups (E, F and G in Figure S7.14) and the amide protons (A in Figure S7.14). This could be related with a change in the coordination sphere of Zn^{2+}. Monitoring the pressurized sample over time led to the detection of new species in which the symmetrical conformation of **2-I** seemed to be distorted, with the appearance of multiple signals in the 6.5 - 7.5 ppm region (Figure S7.15). Besides, some additional peaks were perceived in the 8.0 – 9.8 ppm region, likely distinctive of the formation of carbamate derivatives (Figure S7.16). For this reaction to occur, however, the amino groups should decoordinate the metal to perform the nucleophilic attack on the electrophilic carbon atom of CO_2.[55] The resulting carbamate species shall be stabilized by coordination of the negatively charged oxygen atom with the Zn^{2+} ion (Figure S7.17).[56] Although the chemical structure of such complex species was not fully elucidated, MS-ESI(+) analyses performed immediately after depressurization permitted for the identification of [**2-I**·CO_2] species, with one carbon dioxide molecule coordinated to **2-I** (Figure S7.18). Increasing the MS voltage reduced the abundance of these [**2-I**·CO_2] species, demonstrating the lability of the supramolecular adducts (Figure S7.19). In addition, the signals for these species rapidly decreased with time. The same trend was reflected in the ^{1}H NMR spectrum, observing the disappearance of the unsymmetrical signals upon depressurization (Figure S7.20).

All these experimental data allow for the postulation of a plausible mechanism for the catalytic CO_2 conversion in the presence of styrene oxide (Figure 7.4a). After the preferent recognition of (*R*)-SO by the organometallic species (adduct **A**), the "naked" iodide anion attacks to the α-C of the oxirane, as previously reported for aromatic epoxides.[57] This initial step led to the alkoxylate intermediate, which was likely interacting by means of hydrogen bonds with the acidic hydrogen atoms of the coordinated NH groups (**B**). Additional hydrophobic interactions with the amino acid residues could further stabilise this intermediate. At this point, decoordination and carbamate formation occur in the presence of carbon dioxide, resulting in the species described as **C**. Nucleophilic attack of the alkoxylate to the electrophilic carbon of the activated CO_2 molecule allowed for the formation of the carboxylate **D** that experiences a ring-closing step, yielding the desired (*R*)-styrene carbonate (**E**).

Preliminary DFT calculations were performed for the two enantiomers of relevant species **B** and **D**, as well as for the initial reactants interaction complex (RIC) (**A** in Figures 7.4b and 7.4c). In all cases, the supramolecular adducts resulting from the reaction with (*R*)-SO were more stable than the ones calculated for the interaction with the (*S*)-enantiomer. As surmised, the preorganization of the different components in the RIC **A** was facilitated by non-covalent forces, namely hydrogen bonds, electrostatic, and π···π interactions. The preferential recognition of (*R*)-SO was assigned to the presence of attractive edge-to-face aromatic interactions (for the closest C_{ar}, d_{C-C} = 3.99 Å, Figure 7.4c).[58] Such a favourable interaction was not possible in the presence of (*S*)-SO (see Figure 7.4b for energy differences). A similar scenario was found for the alkoxylate intermediate **B**, although in this case the reaction with (*R*)-SO was only favoured by 0.5 kcal/mol. Calculations indicate that one of the sidechains experiences a conformational change relative to the one present in **2-I** for the anionic intermediates (**B** and **D**) resulting from (*R*)-SO, most likely to maximize the attractive forces between the catalyst and those intermediates.

This catalytic behaviour of the bimetallic pseudopeptidic complexes herein described can thus be compared to enzyme-like catalytic processes promoting

superior specificity by means of non-covalent interactions between the substrate and elegantly preorganized scaffolds of the biocatalysts.[30,59]
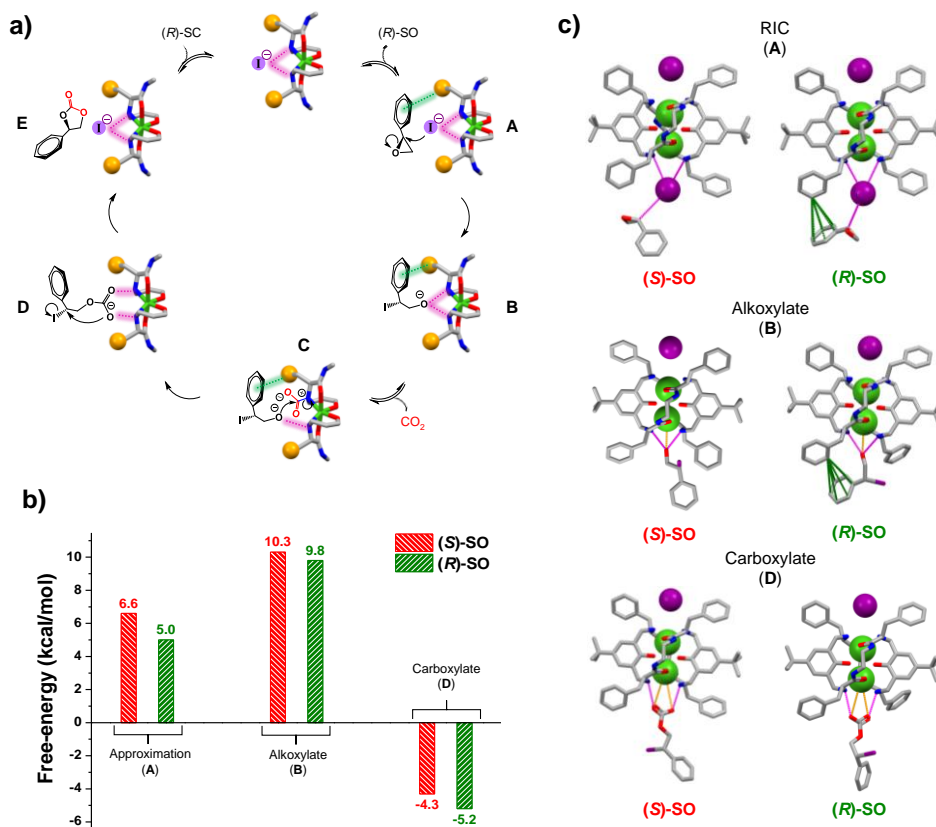
Figure 7.4. a) Postulated mechanism for the enantioselective cycloaddition of CO_2 to styrene oxide in the presence of the one-component bimetallic Zn^{2+} catalysts. The symmetry equivalent (half-molecule) of the pseudopeptidic organometallic macrocycle has been represented with 3D sticks. The sidechains of the amino acid fragments have been represented with orange balls. b) Free-energies obtained, considering the two initial SO enantiomers, for the most relevant mechanism steps: RIC (**A**), alkoxylate (**B**), and carboxylate (**C**). Red bars correspond to energies obtained starting from (*R*)-SO and green bars correspond to energies from (*S*)-SO. c) DFT models calculated for the most relevant species involved in the catalytic cycle. Hydrogen bonds highlighted with discontinuous magenta lines. Electrostatic interactions highlighted with discontinuous orange lines. Aromatic interactions highlighted with discontinuous green lines.

7.1.5.   Conclusions

The present results highlight the high level of functional preorganization that can be achieved with systems derived from relatively simple pseudopeptidic macrocycles. The precise structural design of the one-component system here considered rendered activated nucleophiles and supramolecularly-active acid and basic centres in close proximity within a well-defined chiral cavity, leading to remarkable activity and enantioselectivity without the need of any additional co-catalyst. This opens the way for developing new bioinspired catalytic systems showcasing enzymatic behaviours in challenging CO_2 sustainable transformations

7.1.6.   References

1- de Kleijne, K.; Hanssen, S. V.; van Dinteren, L.; Huijbregts, M. A. J.; van Zelm, R.; de Coninck, H. Limits to Paris compatibility of CO_2 capture and utilization. *One Earth* **2022**, *5*, 168-185.

2- Peplow, M. The race to upcycle CO_2 into fuels, concrete and more. *Nature* **2022**, *603*, 780-783.

3- Mikkelsen, M.; Jorgensen, M.; Krebs, F. C. The teraton challenge. A review of fixation and transformation of carbon dioxide. *Energy Environ. Sci.* **2010**, *3*, 43-81.

4- Shi, J.; Jiang, Y.; Jiang, Z.; Wang, X.; Wang, X.; Zhang, S.; Han, P.; Yang, C. Enzymatic conversion of carbon dioxide. *Chem. Soc. Rev.* **2015**, *44*, 5981-6000.

5- Long, N.V.D.; Lee, J.; Koo, K.-K.; Luis, P.; Lee, M. Recent Progress and Novel Applications in Enzymatic Conversion of Carbon Dioxide. *Energies* **2017**, *10*, 473.

6- Sahoo, P.C.; Kumar, M.; Puri, S.K.; Ramakuma, S.S.V. Enzyme inspired complexes for industrial CO2 capture: Opportunities and challenges. *J. CO2 Util.* **2018**, *24*, 419-429.

7- Artz, J.; Müller, T. E.; Thenert, K.; Kleinekorte, J.; Meys, R.; Sternberg, A.; Bardow, A.; Leitner, W. Sustainable Conversion of Carbon Dioxide: An Integrated Review of Catalysis and Life Cycle Assessment. *Chem. Rev.* **2018**, *118*, 434-504.

8- Moller, F.; Piontek, S.; Miller, R.G.; Apfel, U.P. From Enzymes to Functional Materials—Towards Activation of Small Molecules. *Chem. Eur. J.* **2018**, *24*, 1471-1493.

9- Gamba, I. Biomimetic Approach to CO_2 Reduction. *Bioinorganic Chem. Appli.* **2018**, *2018*, 1.

10- Guo, L.; Lamb, K. J.; North, M. Recent developments in organocatalysed transformations of epoxides and carbon dioxide into cyclic carbonates. *Green Chem.* **2021**, *23* ,77-118.

11- North, M.; Pasquale, R. Mechanism of Cyclic Carbonate Synthesis from Epoxides and CO_2. *Angew. Chem. Int. Ed.* **2009**, *48*, 2946-2948.

12- Pescarmona, P. P. Cyclic carbonates synthesised from CO2: Applications, challenges and recent research trends. *Curr. Opin. Green Sustain.* **2021**, *29*, 100457.

13- Aomchad, V.; Cristòfol, A.; Monica, F.D.; Limburg, B.; D'Elia, V.; Kleij, A. W. Recent progress in the catalytic transformation of carbon dioxide into biosourced organic carbonates. *Green Chem.* **2021**, *23*, 1077-1113.

14- Whiteoak, C. J.; Kielland, N.; Laserna, V.; Escudero-Adán, E. C.; Martin, E.; Kleij, A. W. A Powerful Aluminum Catalyst for the Synthesis of Highly Functional Organic Carbonates. *J. Am. Chem. Soc.* **2013**, *135*, 1228-1231.

15- Mirabaud, A.; Mulatier, J.-C.; Martinez, A.; Dutasta, J. P.; Dufaud, V. Investigating Host–Guest Complexes in the Catalytic Synthesis of Cyclic Carbonates from Styrene Oxide and CO_2. *ACS Catal.* **2015**, *5*, 6748-6752.

16- Martínez-Rodríguez, L.; Garmilla, J. O.; Kleij, A. W. Cavitand-Based Polyphenols as Highly Reactive Organocatalysts for the Coupling of Carbon Dioxide and Oxiranes. *ChemSusChem* **2016**, *9*, 749-755.

17- Esteve, F.; Altava, B.; Burguete, M. I.; Bolte, M.; García-Verdugo, E.; Luís, S. V. Pseudopeptidic macrocycles as cooperative minimalistic synzyme systems for the remarkable activation and conversion of CO_2 in the presence of the chloride anion. *Green Chem.* **2020**, *22*, 4697-4705.

18- Mirabaud, A.; Martinez, A.; Bayard, F.; Dutasta, J.-P.; Dufaud, V. A new heterogeneous host-guest catalytic system as an eco-friendly approach for the synthesis of cyclic carbonates from CO_2 and epoxides. *New J. Chem.* **2018**, *42*, 16863-16874.

19- Ren, W.-M.; Wu, G.-P.; Lin, F.; Jiang, J.-Y.; Liu, C.; Luo, Y.; Lu, X.-B. Role of the co-catalyst in the asymmetric coupling of racemic epoxides with CO_2 using multichiral Co(iii) complexes: product selectivity and enantioselectivity. *Chem. Sci.* **2012**, *3*, 2094–2102.

20- Takaishi, K.; Nath, B. D.; Yamada, Y.; Kosugi H.; Ema, T. Unexpected Macrocyclic Multinuclear Zinc and Nickel Complexes that Function as Multitasking Catalysts for CO_2 Fixations. *Angew. Chem. Int. Ed.* **2019**, *58*, 9984-9988.

21- Wu, X.; Chen, C.; Guo, Z.; North, M.; Whitwood, A. C. Metal- and Halide-Free Catalyst for the Synthesis of Cyclic Carbonates from Epoxides and Carbon Dioxide. *ACS Catal.* **2019**, *9*, 1895-1906.

22- Ema, T.; Miyazaki, Y.; Shimonishi, J.; Maeda, C.; Hasegawa, J.-Y. Bifunctional Porphyrin Catalysts for the Synthesis of Cyclic Carbonates from Epoxides and CO_2: Structural Optimization and Mechanistic Study. *J. Am. Chem. Soc.* **2014**, *136*, 15270–15279.

23- Li, P.; Cao, Z. Catalytic coupling of CO_2 with epoxide by metal macrocycles functionalized with imidazolium bromide: insights into the mechanism and activity regulation from density functional calculations. *Dalton Trans.* **2019**, *48*, 1344-1350.

24- Esteve, F.; Escrig, A.; Porcar, R.; Luis, S. V.; Altava, B.; García-Verdugo, E. Immobilized Supramolecular Systems as Efficient Synzymes for CO_2 Activation and Conversion. *Adv. Sustainable Syst.* **2022**, 2100408.

25- Desens, W.; Kohrt, C.; Frank, M.; Werner, T. Highly Efficient Polymer-Supported Catalytic System for the Valorization of Carbon Dioxide. *ChemSusChem* **2015**, *8*, 3815-3822.

26- Hao, Y.; Yan, X.; Chang, T.; Liu, X.; Kang, L.; Zhu, Z.; Panchal, B.; Qin, S. Hydroxyl-anchored covalent organic crown-based polymers for CO_2 fixation into cyclic carbonates under mild conditions. *Sustain. Energy Fuels* **2022**, *6*, 121-127.

27- Longwitz, L.; Steinbauer, J.; Spannenberg, A.; Werner, T. Calcium-Based Catalytic System for the Synthesis of Bio-Derived Cyclic Carbonates under Mild Conditions. *ACS Catal.* **2017**, *8*, 665-672.

28- Maeda, C.; Mitsuzane, M.; Ema, T. Chiral Bifunctional Metalloporphyrin Catalysts for Kinetic Resolution of Epoxides with Carbon Dioxide. *Org. Lett.* **2019**, *21*, 1853–1856.

29- Cavalleri, M.; Panza, N.; di Biase, A.; Tseberlidis, G.; Rizzato, S.; Abbiati, G.; Caselli, A. [Zinc(II)(Pyridine-Containing Ligand)] Complexes as Single-Component Efficient Catalyst for Chemical Fixation of CO_2 with Epoxides. *Eur. J. Org. Chem.* **2021**, *19*, 2764-2771.

30- Raynal, M.; Ballester, P.; Vidal-Ferran, A.; van Leeuwen, P. W. N. M. Supramolecular catalysis. Part 2: artificial enzyme mimics. *Chem. Soc. Rev.* **2014**, *43*, 1734-1787.

31- Kołodziejski, M.; Stefankiewicz, A. R.; Lehn, J.-M. Dynamic polyimine macrobicyclic cryptands – self-sorting with component selection. *Chem. Sci.* **2019**, *10*, 1836−1843.

32- Becerril, J.; Bolte, M.; Burguete, M. I.; Galindo, F.; Garcia-España, E.; Luis, S. V.; Miravet, J. F. Efficient Macrocyclization of U-Turn Preorganized Peptidomimetics: The Role of Intramolecular H-Bond and Solvophobic Effects. *J. Am. Chem. Soc.* **2003**, *125*, 6677-6686.

33- Esteve, F.; Altava, B.; Bolte, M.; Burguete, M. I.; García-Verdugo E.; Luis, S. V. Highly Selective Anion Template Effect in the Synthesis of Constrained Pseudopeptidic Macrocyclic Cyclophanes. *J. Org. Chem.* **2020**, *85*, 1138-1145.

34- Martí-Centelles, V.; Pandey, M. D.; Burguete, M. I.; Luis, S. V. Macrocyclization Reactions: The Importance of Conformational, Configurational, and Template-Induced Preorganization. *Chem. Rev.* **2015**, *115*, 8736-8834.

35- Alvarez, S. A cartography of the van der Waals territories. *Dalton Trans.* **2013**, *42*, 8617-8636.

36- Kember, M. R.; White, J. P.; Williams, C. K. Di- and Tri-Zinc Catalysts for the Low-Pressure Copolymerization of CO_2 and Cyclohexene Oxide. *Inorg. Chem.* **2009**, *48*, 9535–9542.

37- Deacy, A. C.; Durr, C. B.; Williams, C. K. Heterodinuclear complexes featuring Zn(ii) and M = Al(iii), Ga(iii) or In(iii) for cyclohexene oxide and CO_2 copolymerisation. *Dalton Trans.* **2020**, *49*, 223-231.

38- Nicolaou, K. C.; Couladouros, E. A.; Nantermet, P. G.; Renaud, J.; Guy, R. K.; Wrasidlo, W. Synthesis of C-2 Taxol Analogues. *Angew. Chem. Int. Ed. Engl.* **1994**, *33*, 1581-1583.

39- Song, C. E.; Lee, S.-G. Supported Chiral Catalysts on Inorganic Materials. *Chem. Rev.* **2002**, *102*, 3495–3524.

40- Kang, S. K.; Jeon, J. H.; Nam, K. S.; Park, C. H.; Lee, H. W. Regioselective Protection of Triols to Cyclic Carbonates. *Synth. Commun.* **1994**, *24*, 305-312.

41- Matsumoto, K.; Fuwa, S.; Kitajima, H. Enzyme-mediated enantioselective hydrolysis of cyclic carbonates. *Tetrahedron Lett.* **1995**, *36*, 6499-6502.

42- Zhou, H.; Zhang, H.; Mu, S.; Zhang, W.-Z.; Ren, W.-M.; Lu, X.-B. Highly regio- and stereoselective synthesis of cyclic carbonates from biomass-derived polyols via organocatalytic cascade reaction. *Green Chem.* **2019**, *21*, 6335–6341.

43- North, M.; Quek, S. C. Z.; Pridmore, N. E.; Whitwood, A. C.; Wu, X. Aluminum(salen) Complexes as Catalysts for the Kinetic Resolution of Terminal Epoxides via CO_2 Coupling. *ACS Catal.* **2015**, *5*, 3398−3402.

44- Maeda, C.; Ogawa, K.; Sadanaga, K.; Takaishi, K.; Ema, T. Chiroptical and catalytic properties of doubly binaphthyl-strapped chiral porphyrins. *Chem. Commun.* **2019**, *55*, 1064-1067.

45- Fu, X.; Jing, X.; Jin, L.; Zhang, L.; Zhang, X.; Hu, B.; Jing, H. Chiral basket-handle porphyrin-Co complexes for the catalyzed asymmetric cycloaddition of CO_2 to epoxides. *Chin. J. Catal.* **2018**, *39*, 997-1003.

46- Liu, S.; Suematsu, N.; Maruoka, K.; Shirakawa, S. Design of bifunctional quaternary phosphonium salt catalysts for CO_2 fixation reaction with epoxides under mild conditions. *Green Chem.* **2016**, *18*, 4611-4615.

47- Ema, T.; Yokoyama, M.; Watanabe, S.; Sasaki, S.; Ota, H.; Takaishi, K. Chiral Macrocyclic Organocatalysts for Kinetic Resolution of Disubstituted Epoxides with Carbon Dioxide. *Org. Lett.* **2017**, *19*, 4070-4073.

48- Roy, T.; Kureshy, R. I.; Khan, N. H.; Abdi, S. H. R.; Bajaj, H. C. Asymmetric cycloaddition of CO_2 and an epoxide using recyclable bifunctional polymeric Co(iii) salen complexes under mild conditions. *Catal. Sci. Technol.* **2013**, *3*, 2661-2667.

49- Al-Qaisi, F. M.; Nieger, M.; Kemell, M. L.; Repo, T. J. Catalysis of Cycloaddition of Carbon Dioxide and Epoxides Using a Bifunctional Schiff Base Iron(III) Catalyst. *ChemistrySelect* **2016**, *3*, 545-548.

50- Clegg, W.; Harrington, R. W.; North, M.; Pasquale, R. Cyclic Carbonate Synthesis Catalysed by Bimetallic Aluminium-Salen Complexes. *Chem. Eur. J.* **2010**, *16*, 6828-6843.

51- Gorla, L.; Martí-Centelles, V.; Altava, B.; Burguete, M. I.; Luis, S. V. The role of the side chain in the conformational and self-assembly patterns of C_2-symmetric Val and Phe pseudopeptidic derivatives. *CrystEngComm* **2019**, *21*, 2398-2408.

52- Reichardt, C. *Solvents and Solvent Effects in Organic Chemistry*, Wiley-VCH Publishers, 3rd ed., 2003.

53- Kelly, S. M.; Jess, T. J.; Price, N. C. How to study proteins by circular dichroism. *Biochim. Biophys. Acta* **2005**, *1751*, 119-139.

54- Wang, L.; Zhang, G.; Kodama, K.; Hirose, T. An efficient metal- and solvent-free organocatalytic system for chemical fixation of CO_2 into cyclic carbonates under mild conditions. *Green Chem.* **2016**, *18*, 1229-1233.

55- Notni, J.; Schenk, S.; Görls, H.; Breitzke, H.; Anders, E. Formation of a Unique Zinc Carbamate by CO_2 Fixation: Implications for the Reactivity of Tetra-Azamacrocycle Ligated Zn(II) Complexes. *Inorg. Chem.* **2008**, *47*, 1382-1390.

56- Siegelman, R. L.; McDonald, T. M.; Gonzalez, M. I.; Martell, J. D.; Milner, P. J.; Mason, J. A.; Berger, A. H.; Bhown, A. S.; Long, J. R. Controlling Cooperative CO_2 Adsorption in Diamine-Appended Mg2(dobpdc) Metal–Organic Frameworks. *J. Am. Chem. Soc.* **2017**, *139*, 10526-10538.

57- Castro-Gómez, F.; Salassa, G.; Kleij, A. W.; Bo, C. A DFT Study on the Mechanism of the Cycloaddition Reaction of CO_2 to Epoxides Catalyzed by Zn(Salphen) Complexes. *Chem. Eur. J.* **2013**, *19*, 6289–6298.

58- Jennings, W. B.; Farrell, B. M.; Malone, J. F. Attractive Intramolecular Edge-to-Face Aromatic Interactions in Flexible Organic Molecules. *Acc. Chem. Res.* **2001**, *34*, 885–894.

59- Kuah, E.; Toh, S.; Yee, J.; Ma, Q.; Gao, Z. Enzyme Mimics: Advances and Applications. *Chem. Eur. J.* **2016**, *22*, 8404-8430.

60- Frassineti, C.; Ghelli, S.; Gans, P.; Sabatini, A.; Moruzzi, M.S.; Vacca, A. Nuclear magnetic resonance as a tool for determining protonation constants of natural polyprotic bases in solution. *Analytical Biochemistry*, **1995**, *231*, 374-382.

61- Sheldrick, G. M. A short history of SHELX. *Acta Crystallogr. A,* **2008**, *64*, 112-122.

62- Sheldrick, G. M. Crystal structure refinement with SHELXL. *Acta Crystallogr. C,* **2015**, *71*, 3-8.

63- Macrae, C. F.; Bruno, I. J.; Chisholm, J. A.; Edgington, P. R.; McCabe, P.; Pidcock, E.; Rodriguez Monge, L.; Taylor, R.; van de Streek, J.; Wood, P. A. New Features for the Visualization and Investigation of Crystal Structures. *J. Appl. Crystallogr.* **2008**, *41*, 466-470.

64- Frisch, M. J.; Trucks, G. W.; Schlegel, H. B.; Scuseria, G. E.; Robb, M. A.; Cheeseman, J. R.; Scalmani, G.; Barone, V.; Mennucci, B.; Petersson, G. A.; *et al.* Gaussian 09, Revision B.01 (Gaussian, Inc), **2010**.

65- Becke, A. D. Density-functional thermochemistry. III. The role of exact exchange. *J. Chem. Phys.* **1993**, *98*, 5648-5652

66- Chiodo, S.; Sicilia, E. LANL2DZ basis sets recontracted in the framework of density functional theory. *J. Chem. Phys.* **2006**, *125*, Article number: 104107.

7.2.   Supporting information

a)

b)

Expected [M+H]⁺: 637.6 m/z
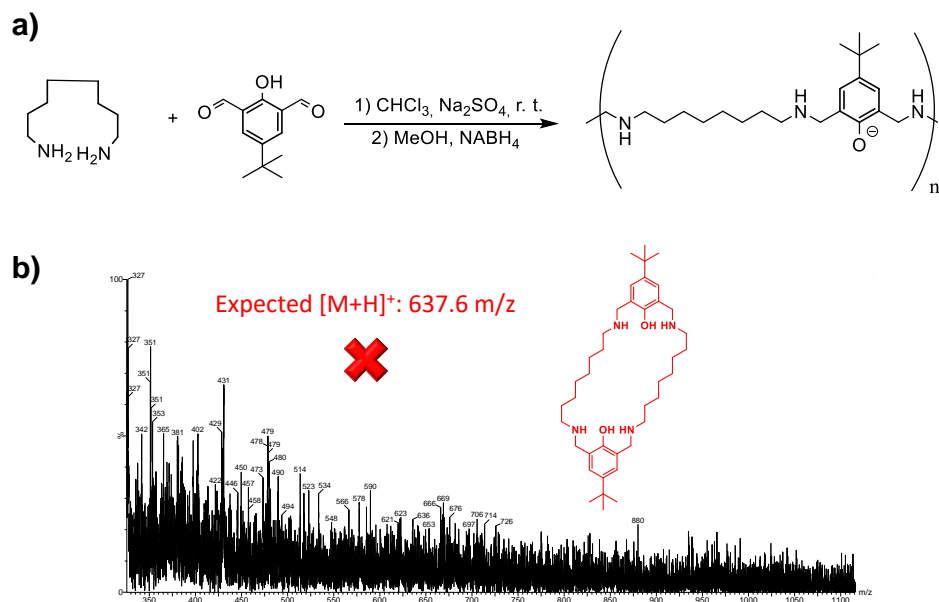
Figure S7.1. a) Attempted synthesis of a non-pseudopeptidic macrocyclic ligand. Unidentified polymers with low solubility in common organic solvents were afforded instead. b) ESI(+) spectrum (MeOH) obtained for the reaction crude, displaying the absence of the expected m/z peaks.

Table S7.1. Isolated yields found for the different macrocyclic ligands.[a]

Entry	Ligand	Isolated yield (%)
1	**L1**	74
2	**L2**[b]	79[b]
3	**L3**	75
4	**L4**	64

[a] Yields determined after the in-situ imine reduction using NaBH₄ .[b] It must be noted that the synthesis of **L2** was carried out at gram scale, maintaining the efficiency of the two-step reaction.
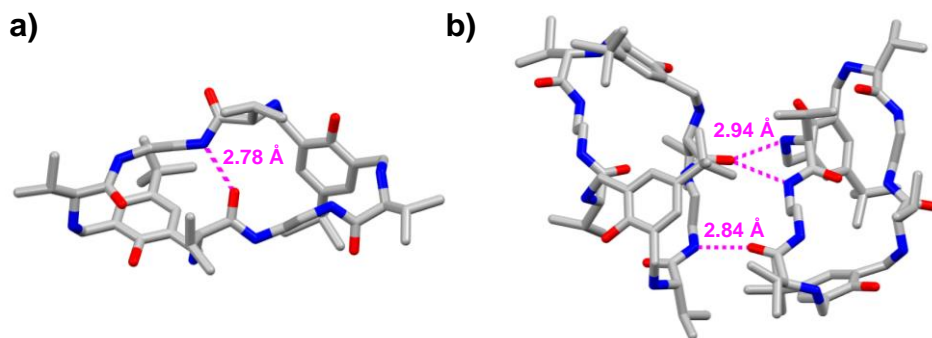
Figure S7.2. X-Ray for the macrocycle **H₂L1.** a) Stick representation of the molecular structure found for **H₂L1**, highlighting the HN⋯CO intramolecular hydrogen bond in pink. b) Stick representation of two vicinal molecules, highlighting the three HN⋯CO intermolecular hydrogen bonds in pink. Hydrogen atoms and solvent molecules have been removed for clarity. Colour code: C(grey), N(blue), O(red). See X-Ray experimental section for more details. CCDC number: 2153938.

Entry	Percentage of R isomer in SO (%)	Conv. (%)	Percentage of R Isomer in SC (%)
1	100	19	96
2	75	17	87
3	50	14	73
4	25	12	47
5	0	7	7
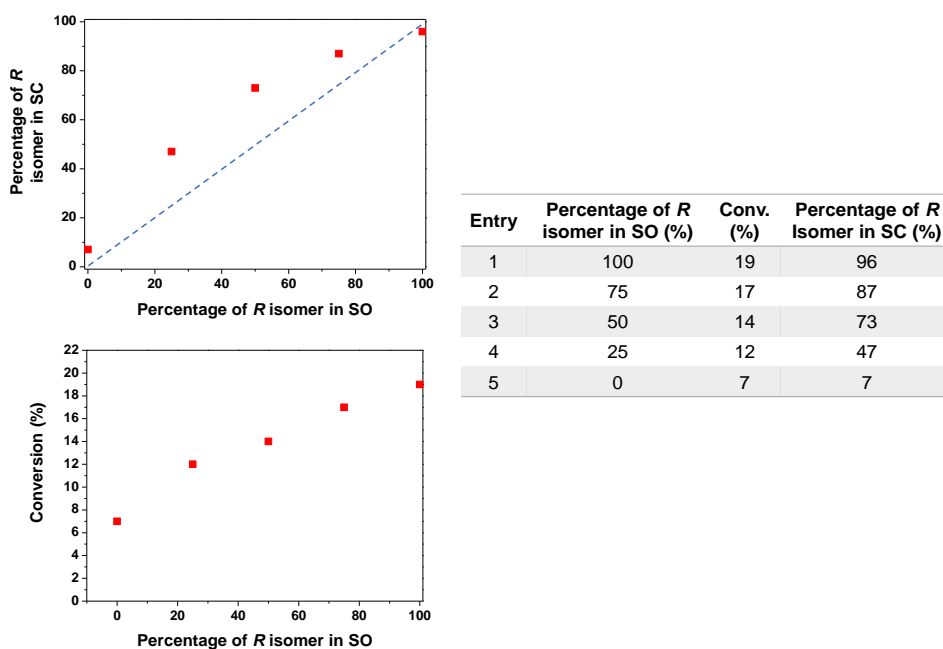
Figure S7.3. Cycloaddition of carbon dioxide to enriched chiral mixtures of styrene oxide. Reaction conditions: 0.5 mol % **1-I**, solvent-less, 1 bar of CO_2 at 40 °C for 4 h. SO: styrene oxide. SC: styrene carbonate. The percentage of R isomer in SO corresponds to the abundance of this enantiomer in the initial enantiomerically enriched mixture of SO.

Table S7.2. Comparison of catalytic results reported to date for the kinetic resolution of styrene oxide with CO_2.

Ref.	Cat. (mol%)	Co-cat (mol%)	t (h)	P (bar)	T (°C)	Conv. (%)[b]	e. e. (%)[c]	s[d]	TOF (h⁻¹)	TOF co-cat (h⁻¹)
A	2	-	6	1	25	13	6	1.1	1.1	-
B	1	-	24	1	60	26	22	1.7	1.1	-
C	0.05	TBAB (0.1)	24	17	50	27	54	4.1	22.5	11.3
D	0.1	TBAF (0.2)	16	8	25	39	3.3	1.1	24.4	12.2
E	2.5	TBAB (2.5)	3	1	25	21	6	1.1	2.8	2.8
F	0.05	PTAT (0.1)	1.5	5	0	5	6	1.0	66.7	33.3
G	0.1	TBAL-TAR (0.1)	72	7	25	27	3	1.1	3.8	3.8
H	0.1	TBAF (0.2)	18	12	25	37	0	-	20.6	10.3
I	0.1	-	48	6	20	13	9	1.2	2.7	-
J	0.1	PPN-DNP (10)	24	n.c.[a]	0	12	68	5.4	5.0	0.5
K	0.5	TBAC (1)	140	10	25	36	0	-	0.5	0.3
L	1	TEAB (1.5)	30	20	25	10	74	7.3	0.3	0.2
M	0.2	-	48	17	30	9	59	4.1	0.9	-
This work (2-I)	**0.5**	**-**	**1**	**1**	**60**	**38**	**30**	**2.2**	**76.0**	**-**
	0.5	**-**	**4**	**1**	**40**	**27**	**58**	**4.6**	**13.5**	**-**
	0.5	**-**	**24**	**1**	**25**	**45**	**1**	**9.5**	**3.8**	**-**

[a] The amount of CO_2 accounts for 0.5-0.6 equivalents in comparison with styrene oxide. See Figure S7.4 for general structures.

REFERENCES TABLE S7.2.

A – M. A. Emelyanov, N. V. Stoletova, A. F. Smolyakov, M. M. Ilin, V. I. Maleev, V. A. Larionov, *Inorg. Chem.* **2021**, *60*, 13960−13967.

B – Y.-D. Li, D.-X. Cui, J.-C. Zhu, P. Huang, Z. Tian, Y.-Y. Jia, P.-A. Wang, *Green Chem.* **2019**, *21*, 5231–5237.

C – C. Maeda, K. Ogawa, K. Sadanaga, K. Takaishi, T. Ema, *Chem. Commun.* **2019**, *55*, 1064-1067.

D- Z. Zhu, Y. Zhang, K. Wang, X. Fu, F. Chen, H. Jing, *Catal. Commun.* **2016**, *81*, 50-53.

E- M. North, S. C. Z. Quek, N. E. Pridmore, A. C. Whitwood, X. Wu, *ACS Catal.* **2015**, *5*, 3398−3402.

F- L. Jin, Y. Huang, H. Jing, T. Chang, P. Yan, *Tetrahedron: Asymmetry*, **2008**, *19*, 1947-1953.

G- S. Zhang, Y. Huang, H. Jing, W. Yao, P. Yan, *Green Chem.* **2009**, *11*, 935–938.

H- P. Yan, H. Jing, *Adv. Synth. Catal.* **2009**, *351,* 1325–1332.

I- T. Chang, L. Jin, H. Jing, *ChemCatChem* **2009**, *1*, 379–383.

J- W.-M. Ren, G.-P. Wu, F. Lin, J.-Y. Jiang, C. Liu, Y. Luo, X.-B. Lu, *Chem. Sci.* **2012**, *3*, 2094-2102.

K- X. Fu, X. Jing, L. Jin, L. Zhang, X. Zhang, B. Hu, H. Jing, *Chinese J. Catal.* **2018**, *39*, 997-1003.

L- J. Qin, V. A. Larionov, K. Harms, E. Meggers, *ChemSusChem* **2019**,*12*, 320–325.

M- C. Maeda, M. Mitsuzane, T. Ema, *Org. Lett.* **2019**, *21*, 1853-1856.
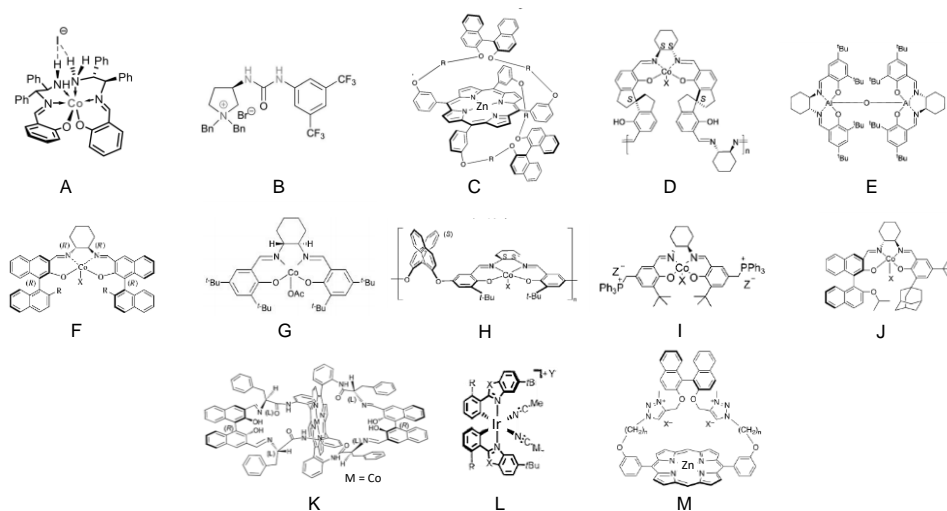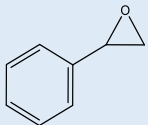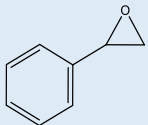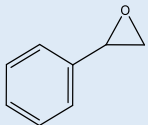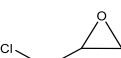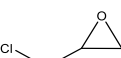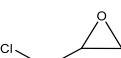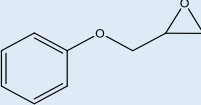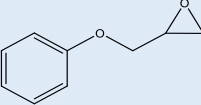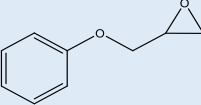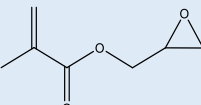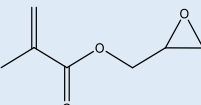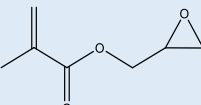
Figure S7.4. Cycloaddition of carbon dioxide to enriched chiral mixtures of styrene oxide. Reaction conditions

Table S7.3. Substrate scope for the CO_2 cycloaddition to epoxides in the presence of **2-I**.[a]

Entry	Epoxide	Solvent	Temp. (ºC)	Time (h)	Conv. (%)[b]	e. e. (%)[c]	s[d]
1		-	80	1	> 99	n.m.	n.m.
2		-	40	15	21	68	6.3
3		THF	40	15	16	66	5.5
4		-	80	1	> 99	n.m.	n.m.
5		-	40	15	6	35	2.1
6		THF	40	15	7	48	2.9
7		-	80	1	91	n.m.	n.m.
8		-	40	15	11	22	1.6
9		THF	40	15	12	26	1.8
10		-	80	1	> 99	n.m.	n.m.
11		-	40	15	24	38	2.5
12		THF	40	15	18	35	2.2
13		-	80	1	95	n.m.	n.m.
14		-	40	15	5	35	2.1
15		THF	40	15	10	40	2.4

[a] Reaction conditions: epoxide (4.35 mmol), 1 bar of CO_2 (autoclave), and 0.5 mol% **2-I**. In the experiments where THF was used it was introduced in a 50%$_{v/v}$ proportion. [b] Conversions determined by ^{1}H NMR, selectivity for the cyclic carbonates was always > 99.9 %. [c] Enantiomeric excess determined by GC analyses. For high temperature assays (T = 80 ºC) the enantiomeric excess was not measured (n.m.). [d] $s = \ln[(1-c(1+ee)]/\ln[1-c(1-ee)]$, where c is the conversion and ee is the enantiomeric excess.

Table S7.4. Catalytic results obtained for the cycloaddition of CO_2 to styrene oxide at r.t.[a]

Entry	Cat. (mol%)	Conv. (%)[b]	e. e. (%)[c,d]
1	**2-I** (0.5)	23	68
2	**L2** (0.5)	0	0
3	**L2** (0.5) + TBAI (1)	2	4
4	TBAI (1)	3	0
5	**2-PF$_6$** (0.5)	trace	0

[a] Reaction conditions: styrene oxide (4.35 mmol), 1 bar of CO_2 (autoclave) at r.t. for 15 h. [b] Conversionss determined by ^{1}H NMR, selectivity for styrene carbonate was always > 99.9 %. [c] Enantiomeric excess determined by GC analyses. [d] Enantiomeric excess for (R)-styrene carbonate.carbonates was always > 99.9 %. [c] Enantiomeric excess determined by GC analyses. For high temperature assays (T = 80 ºC) the enantiomeric excess was not measured (n.m.). [d] $s = \ln[(1-c(1+ee)]/\ln[1-c(1-ee)]$, where c is the conversion and ee is the enantiomeric excess.

Figure S7.5. Experimental set-up for the FTIR spectroscopy kinetic analyses. The temperature was maintained constant at 60 ºC with the aid of an auxiliar peltier. CO_2 was introduced in the system with a balloon. The reaction was performed under solvent-less conditions.
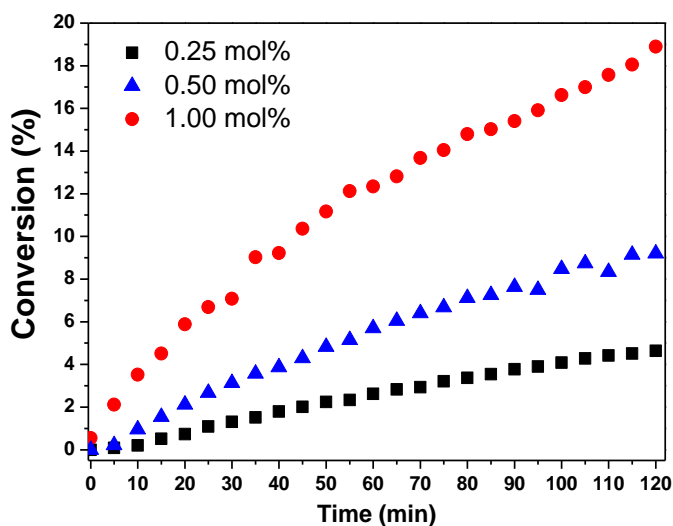
Figure S7.6. FTIR conversions for the kinetic experiments in the presence of **2-I.** Reaction conditions: styrene oxide (solvent-less), 60 ºC, CO_2 balloon. Conversions were determined with the appropriate calibration, using the IR band at 1039 – 1099 cm^{-1} (vC-O asymmetric vibration) for the formation of styrene carbonate. Catalytic loading: 1 mol% (red points), 0.5 mol% (blue points) and 0.25 mol% (black points).

% mol	[cat]	Log [cat]	K_{obs}	Log K_{obs}
0.5	43	1.633	0.0008	-3.0970
0.25	21.5	1.332	0.0004	-3.398
1	86	1.934	0.0019	-2.721

y = 1,124x - 4,908
R^2 = 0,996
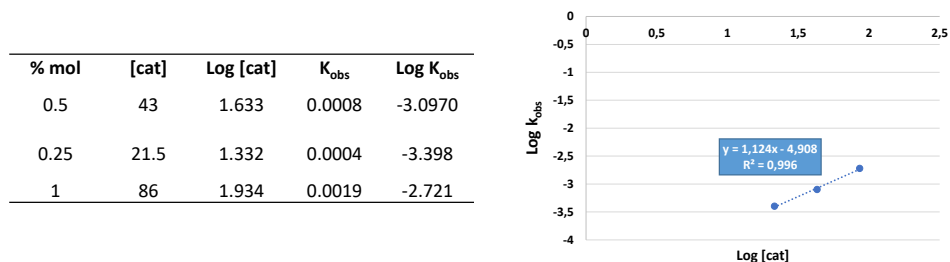
Figure S7.7. Results obtained for the in-situ FTIR kinetic experiments in the presence of **2-I**. Reaction conditions: styrene oxide (solvent-less), 60 °C, CO_2 balloon. The reaction was performed at 1 mol%, 0.5 mol% and 0.25 mol% for **2-I**. A first-order dependence is observed for the catalyst, as corroborated by the slope in the linear regression of the graph (right).
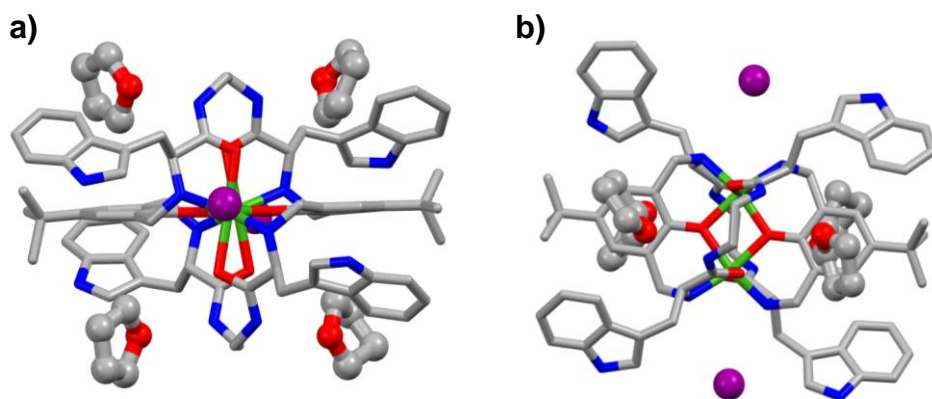
Figure S7.8. Representation of the THF solvent molecules found in the solid-state structure for **4-I**. The Lewis basic O atoms of the solvents are hydrogen bonded to the acidic amide groups (average $O \cdots N_{amide}$ distance = 2.9 Å, 95% $vdW_{N,O}$). a) Side-view. b) Top-view. Hydrogen atoms and disorder have been removed for clarity. Spacefill model for THF molecules and stick model for the organometallic scaffold. Colour code: green for Zn, purple for I, blue for N, red for O, grey for C. CCDC number: 2153936.
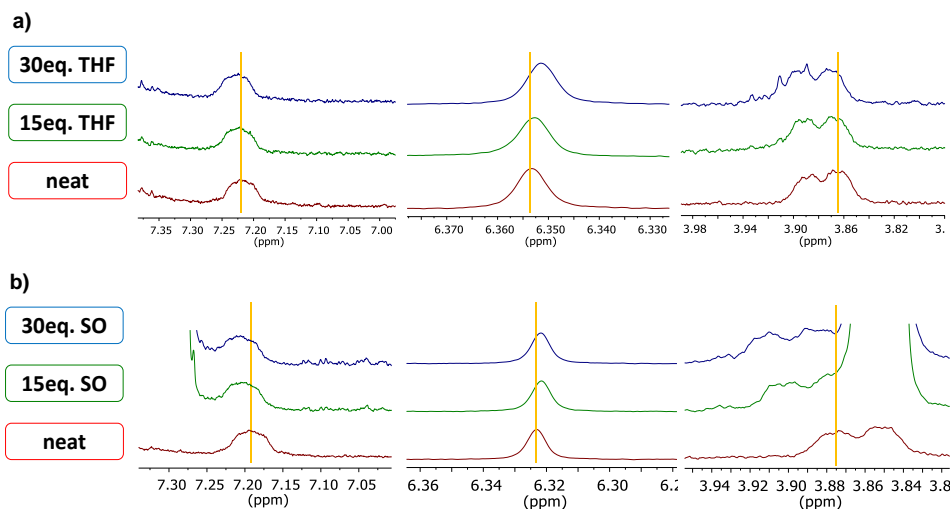
Figure S7.9. Partial ^{1}H NMR (400 MHz, CD$_3$CN, 25 ºC) spectra for **2-I** (2 mM) in the presence and absence of a) THF and b) styrene oxide, "SO". The shifts of the different protons have been highlighted with an orange line. Amide NH signal: 7.35 – 7.00 ppm; Aromatic C-H signal: 6.30 – 6.37 ppm; Amine NH signal: 3.82 – 3.98 ppm. The concentration of the organometallic host was maintained constant during the experiment.
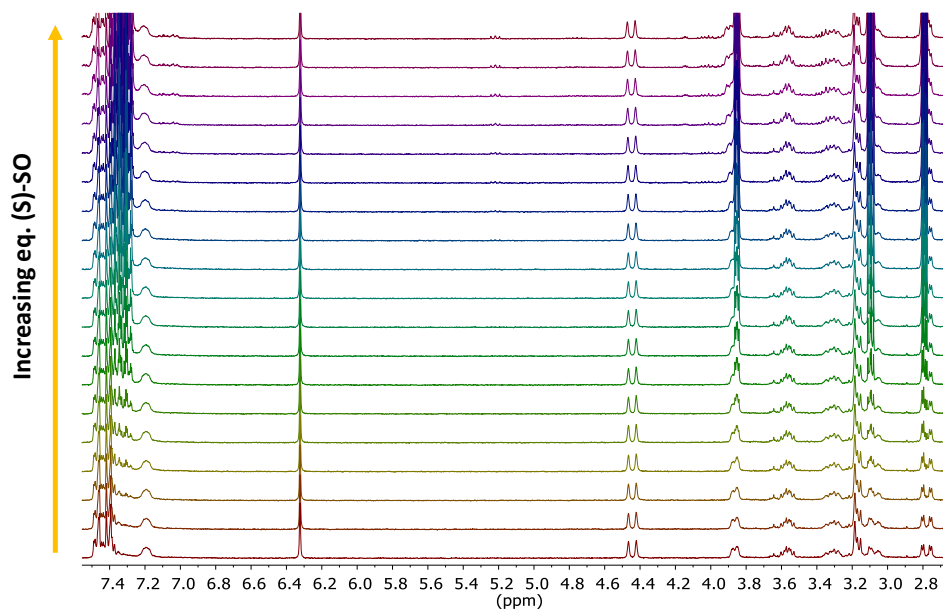
Figure S7.10. Partial ^{1}H NMR (400 MHz, CD$_3$CN, 25 ºC) spectra for the titration experiment of **2-I** (2 mM) with increasing amount of (*S*)-SO. From bottom to top: 0, 0.3, 0.5, 0.8, 1.1, 1.6, 2.1, 2.8, 3.7, 4.6, 6.1, 7.6, 10.3, 12.7, 16.7, 22.2, 27.3, 30.8 equivalents of SO added. SO abbreviation stands for styrene oxide. The concentration of the organometallic host was maintained constant during the experiment.

eq guest	Ar-CH₂-NHamine		NHamide		NHamine	
	Δδ (ppm) (R)-SO	Δδ (ppm) (S)-SO	Δδ (ppm) (R)-SO	Δδ (ppm) (S)-SO	Δδ (ppm) (R)-SO	Δδ (ppm) (S)-SO
30.8	0.0084	0.0061	0.0232	0.0123	0.0564	0.0329

(R) - SO

β (1 : 1)	16 M⁻¹
σ	1 M⁻¹

(S) - SO

β (1 : 1)	8 M⁻¹
σ	1 M⁻¹

Figure S7.11. Chemical shifts (ppm) determined for **2-I** (2 mM) in the presence of 30.8 equivalents of either (*R*)-SO or (*S*)-SO. The association constants measured using HypNMR software for 1 : 1 supramolecular complexes have also been included with their respective error.
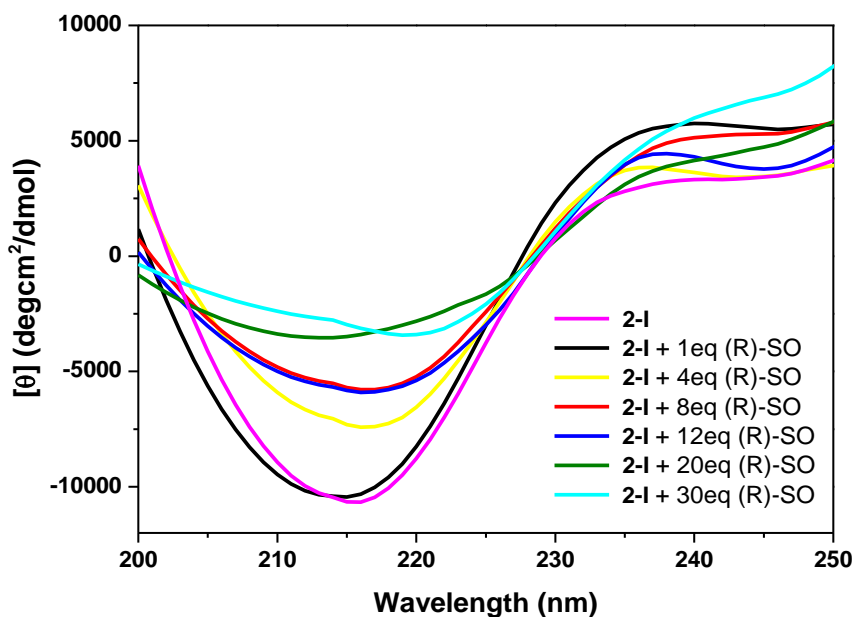
Figure S7.12. CD spectra (CH₃CN, 25 °C) for the titration experiment of **2-I** (0.01 mM) with increasing amounts of (*R*)-SO. SO abbreviation stands for styrene oxide. The concentration of the organometallic host was maintained constant during the experiment.
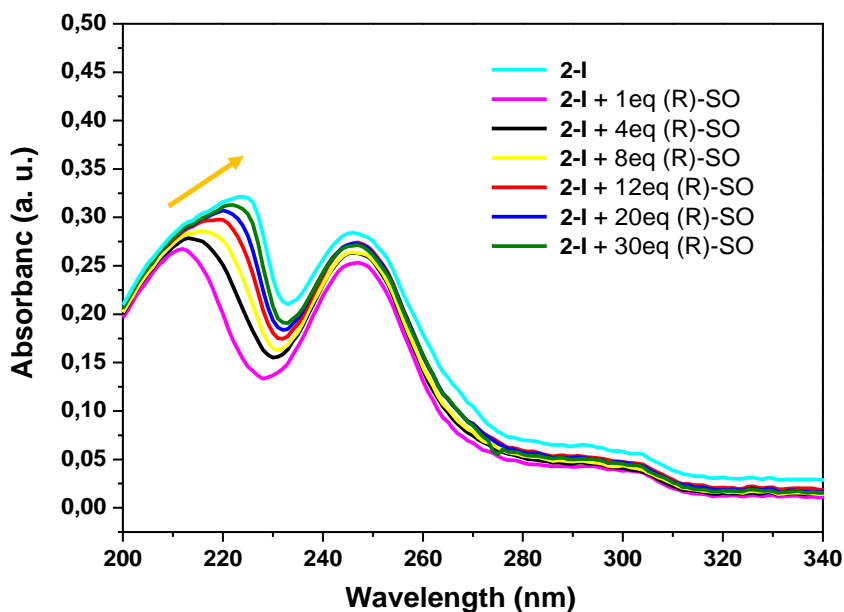
Figure S7.13. UV-Vis spectra comparison (CH₃CN, 25 ºC) for the titration experiment of **2-I** (0.01 mM) with increasing amounts of (R)-SO. The concentration of the organometallic host was maintained constant during the experiment. The red-shift observed for the amide band has been highlighted with an orange arrow.
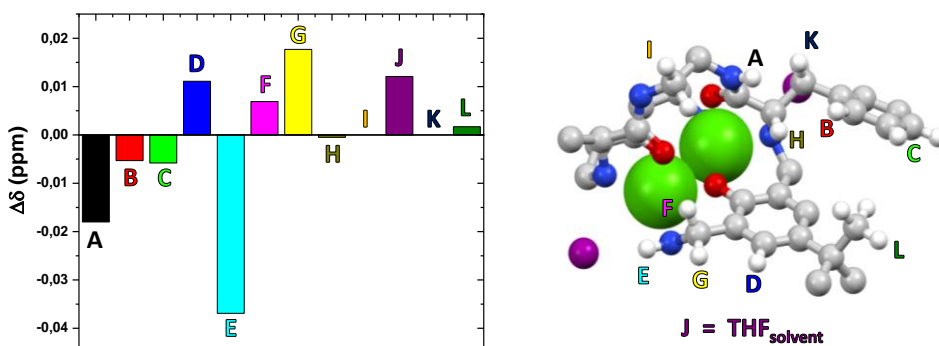
Figure S7.14. ^{1}H NMR (500 MHz, 25 ºC, THF) shifts observed for the characteristic signals of **2-I** (10 mM) and for the methylene protons attached to the O atom of THF (marked as purple J in the figure) in the presence of 10 bar of CO_2. The shifts were determined after 2 h exposure to the CO_2 atmosphere. The spacefill model on the right highlights the hydrogens (white balls) studied in the experiment, which have been identified with different letters and colours.

Figure S7.14. ^{1}H NMR (500 MHz, 25 ºC, THF) shifts observed for the characteristic signals of **2-I** (10 mM) and for the methylene protons attached to the O atom of THF (marked as purple J in the figure) in the presence of 10 bar of CO_2. The shifts were determined after 2 h exposure to the CO_2 atmosphere. The spacefill model on the right highlights the hydrogens (white balls) studied in the experiment, which have been identified with different letters and colours.
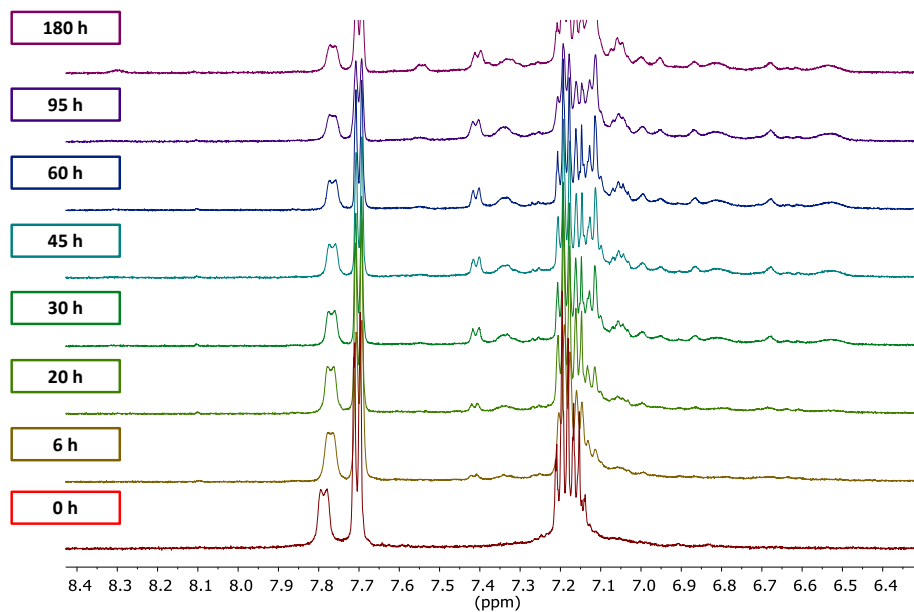
Figure S7.15. Time evolution of the partial ^{1}H NMR (500 MHz, 25 ºC, THF-d8) spectra for the aromatic region of **2-I** (10 mM) in the presence of CO_2 (10 bar). The appearance of unsymmetrical signals can be appreciated in the 7.5 – 6.5 ppm region.
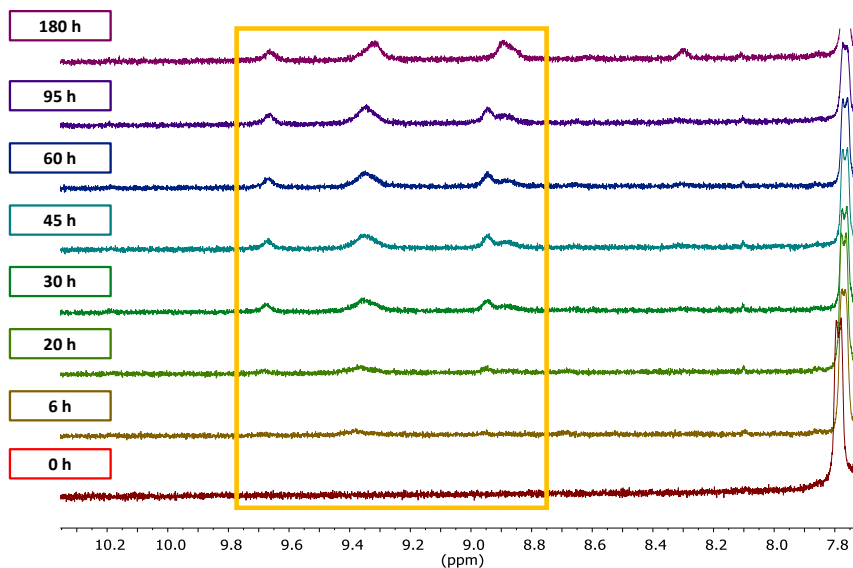
Figure S7.16. Time evolution of the partial ^1H NMR (500 MHz, 25 °C, THF-d_8) spectra for **2-I** (10 mM) in the presence of CO_2 (10 bar). The appearance of broad peaks has been assigned to the acidic protons of the carbamate species ($HN^+R_1R_2CO_2$), which can be hydrogen bonded with the iodide anion and the amide groups of the pseudopeptidic scaffold.
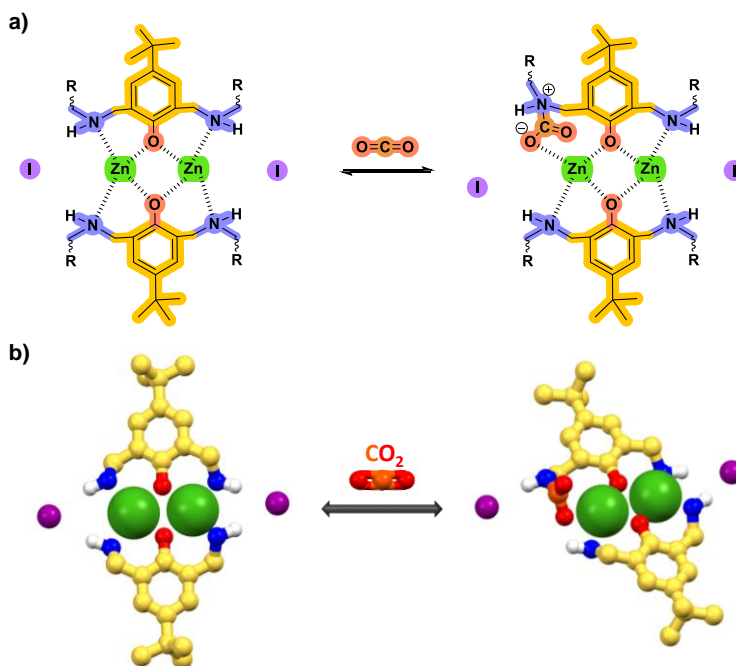
Figure S7.17. CO_2 activation by the bimetallic scaffold by means of the reversible formation of carbamate species. (a) ChemDraw model. (b) Ball and stick representation.
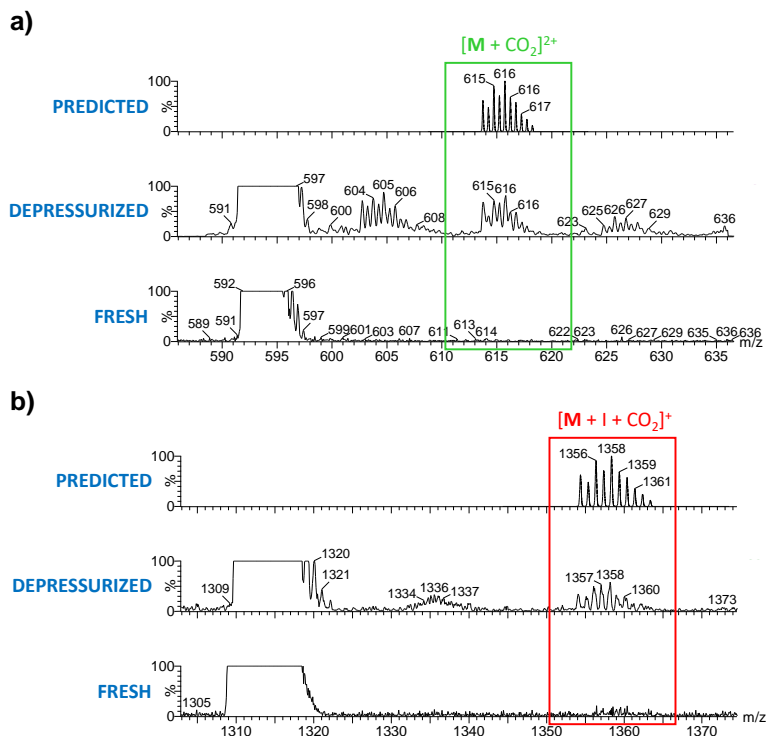
Figure S7.18. MS(ESI+, 20 V) spectra comparison for fresh **2-I** sample (THF-d$_8$, 10 mM) and **2-I** after depressurization. a) 585 – 635 m/z range. b) 1300 – 1370 m/z range. The predicted isotope model for the species with CO_2 has been included. The diprotonated peak for $[M + CO_2]^{2+}$ has been highlighted in green. The monoprotonated peak for $[M + I +CO_2]^+$ has been highlighted in red.
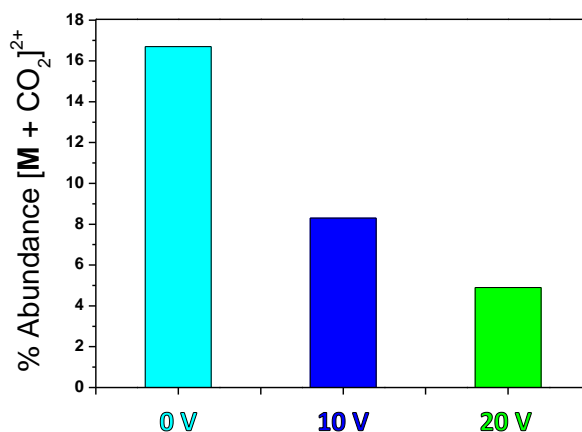
Figure S7.19. Abundance for $[M + CO_2]^{2+}$ calculated by MS(ESI+) at different voltages. **M** corresponds to dicationic **2**. Abundances calculated as: (Intensity$[M + CO_2]^{2+}$ / Intensity$[M]^2$) x 100.
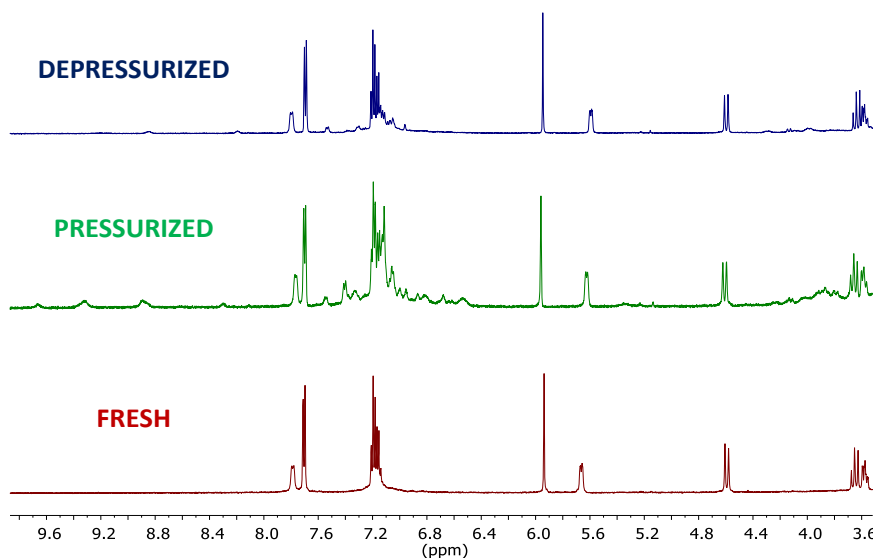
Figure S7.20. ^{1}H NMR (500 MHz, THF-d$_8$, 25 ºC) spectra for fresh sample of **2-I** (red spectrum), **2-I** after 180 h at 10 bar CO_2 (green spectrum), and **2-I** after 24 h of depressurization (blue spectrum).
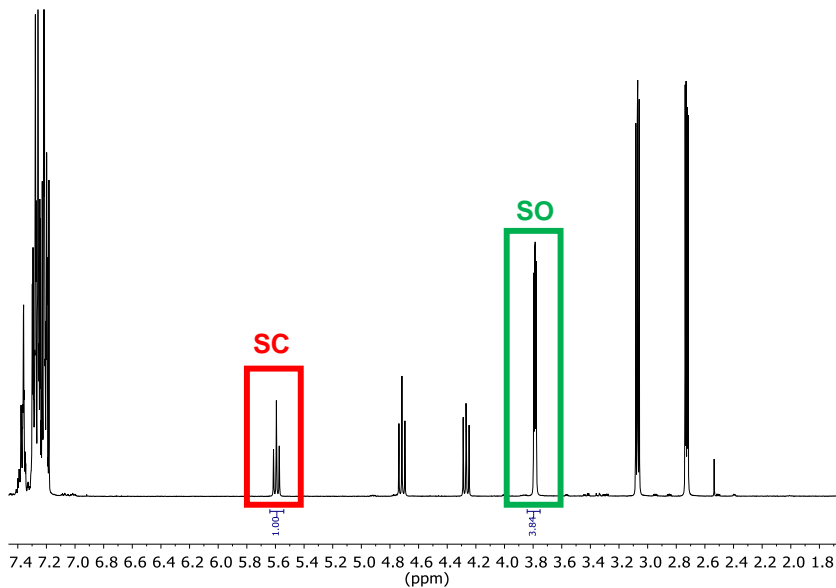
Figure S7.21. Example of the conversion determination by ^{1}H NMR (400 MHz, CDCl$_3$, 25 ºC). The conversion is determined by NMR integration as follows: C (%) = [Isc / (Isc + Iso)]x 100. The Isc corresponds to the integration of the signal for SC (5.6 ppm, highlighted in red). The Iso corresponds to the integration of the signal for SO (3.8 ppm, highlighted in green). It must be noted that the selectivity was > 99.9% for the desired styrene carbonate.
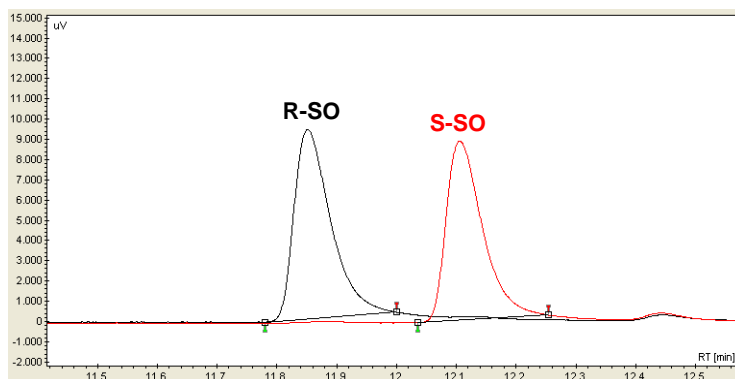
Figure S7.22. GC chromatograms separately obtained for the optically pure *R*-SO (black chromatogram) and *S*-SO (red chromatogram).
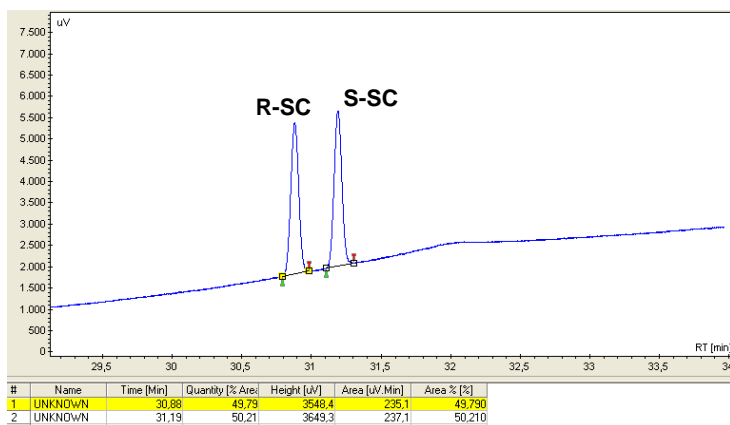
Figure S7.23. GC chromatogram obtained for a racemic mixture of styrene carbonate (SC). The racemic mixture was obtained by reacting styrene oxide in the presence of 2 mol% TBAI, at 100 ºC for 5 h in the presence of 1 bar of CO_2.
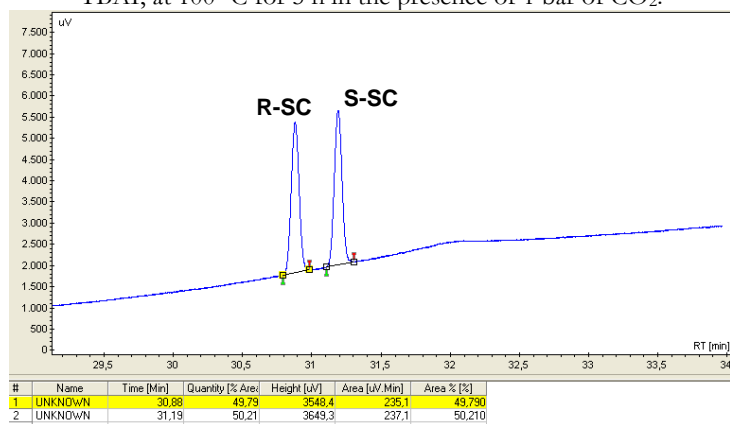
Figure S7.24. GC chromatogram obtained for the reaction crude using *S*-SO as reagent. Reaction conditions: 0.5 mol % **1-I**, solvent-less, 1 bar of CO_2 at 40 ºC for 4 h.
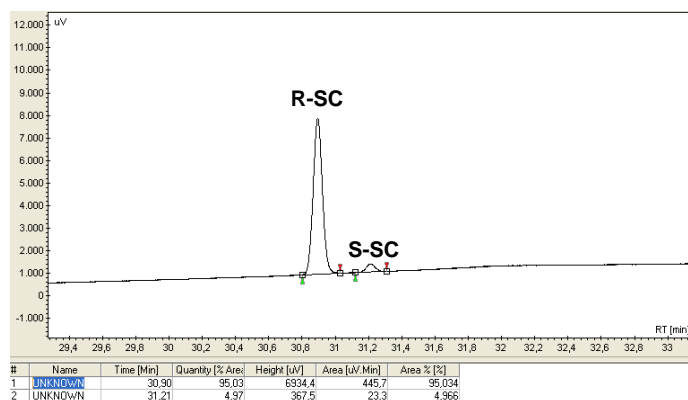
Figure S7.25. GC chromatogram obtained for the reaction crude using *R*-SO as reagent. Reaction conditions: 0.5 mol % **1-I**, solvent-less, 1 bar of CO_2 at 40 ºC for 4 h.
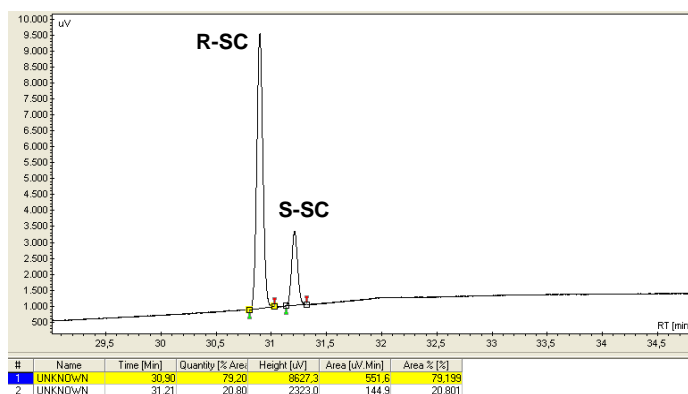
Figure S7.26. GC chromatogram obtained for the reaction crude using racemic SO as reagent. Reaction conditions: 0.5 mol % **2-I**, solvent-less, 1 bar of CO_2 at 40 ºC for 4 h. Enantiomeric excess *R*-SC: 58 %.
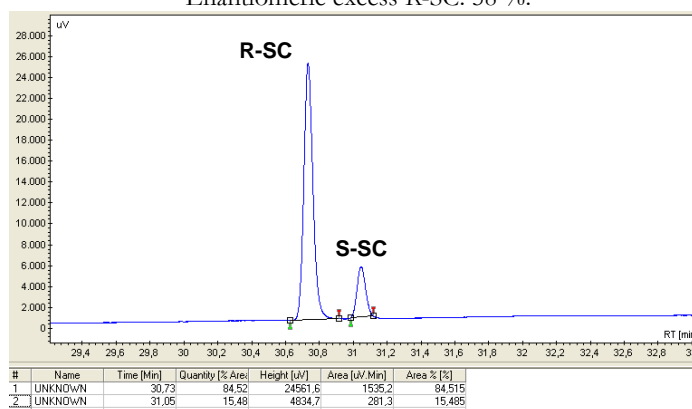
Figure S7.27. GC chromatogram obtained for the reaction crude using racemic SO as reagent. Reaction conditions: 0.5 mol % **2-I**, solvent-less, 1 bar of CO_2 at 25 ºC for 24 h. Enantiomeric excess *R*-SC: 69 %.
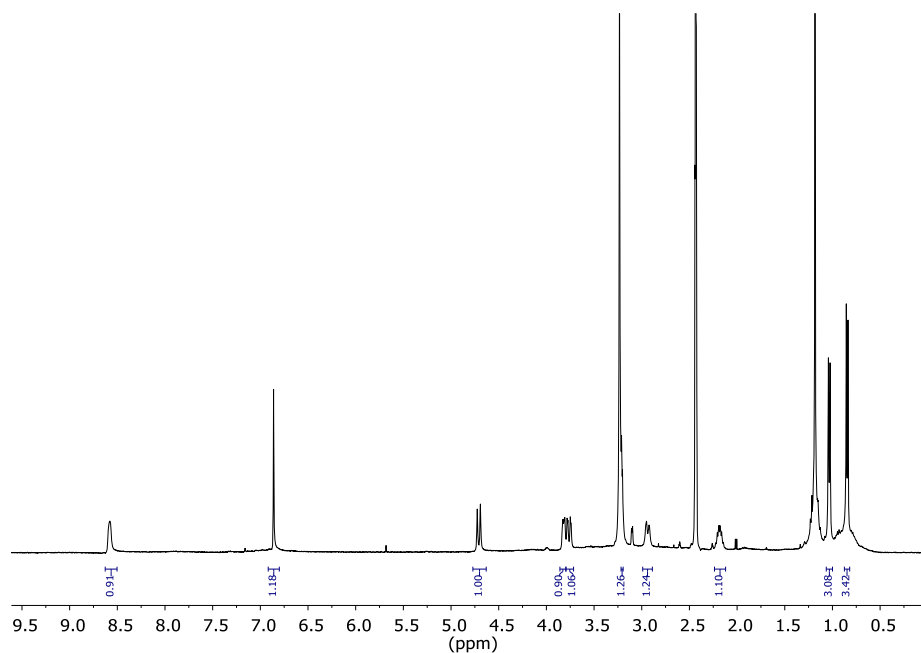
Figure S7.28. ^{1}H NMR (400 MHz, DMSO-d$_6$, 25 °C) for **1-I** (5 mM).
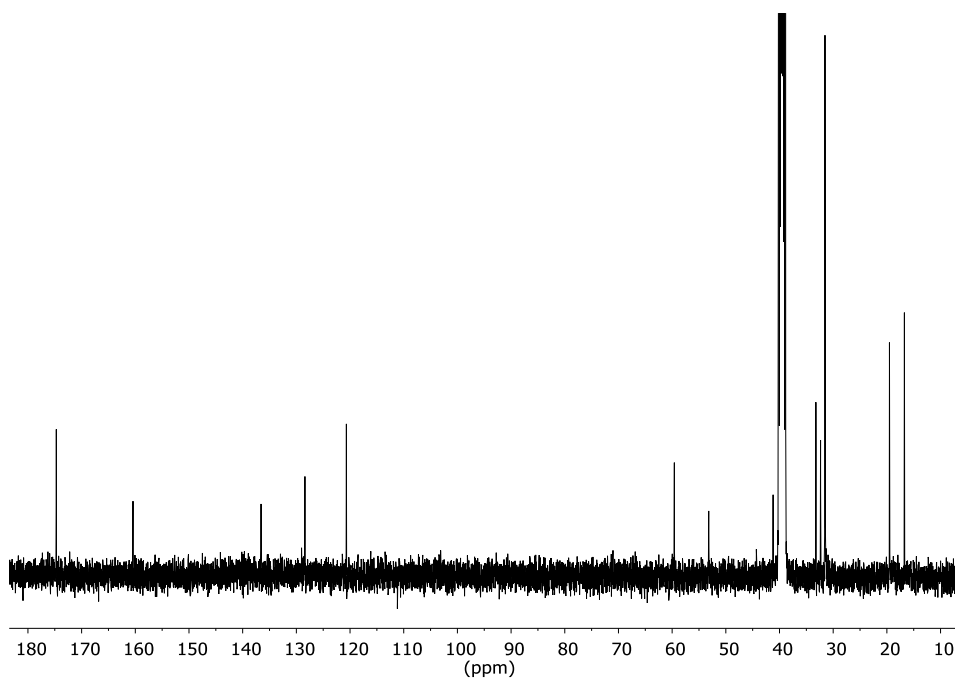
Figure S7.29. ^{13}C{^{1}H} NMR (400 MHz, DMSO-d$_6$, 25 °C) for **1-I** (5 mM).
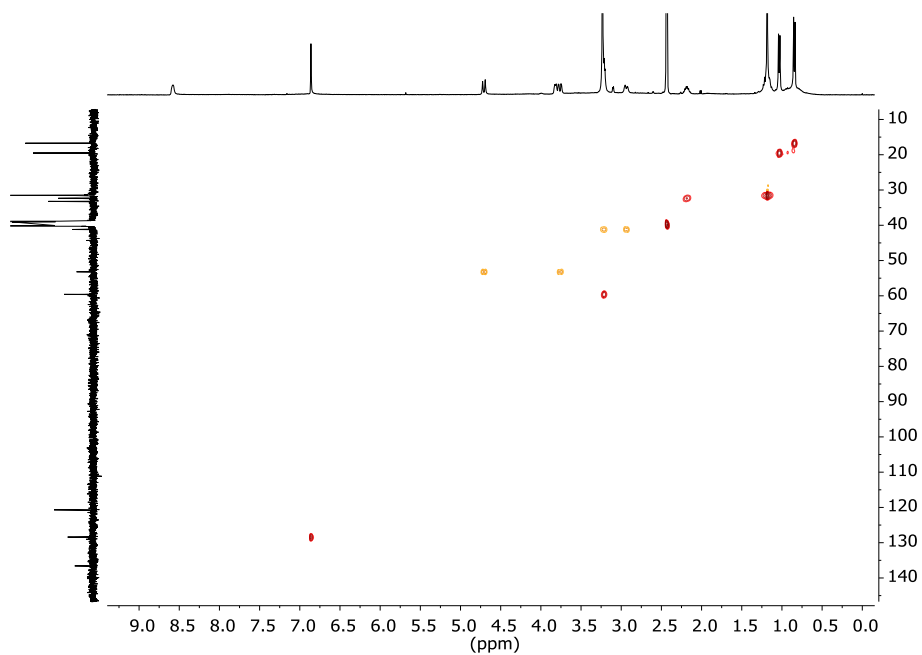
Figure S7.30. 2D HSQC NMR (400 MHz, DMSO-d_6, 25 °C) for **1-I** (5 mM).
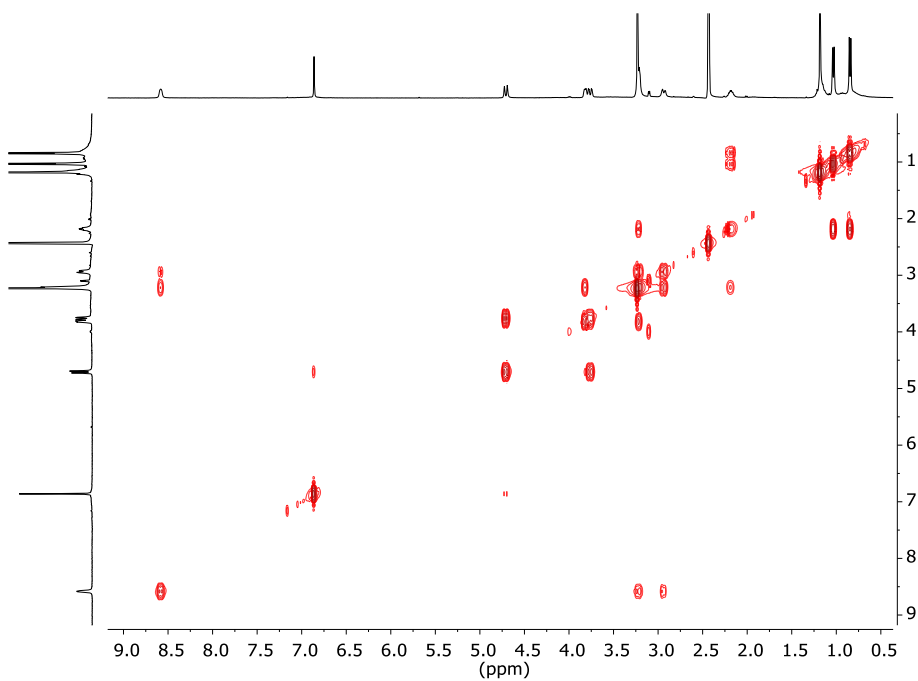
Figure S7.31. 2D COSY NMR (400 MHz, DMSO-d_6, 25 °C) for **1-I** (5 mM).
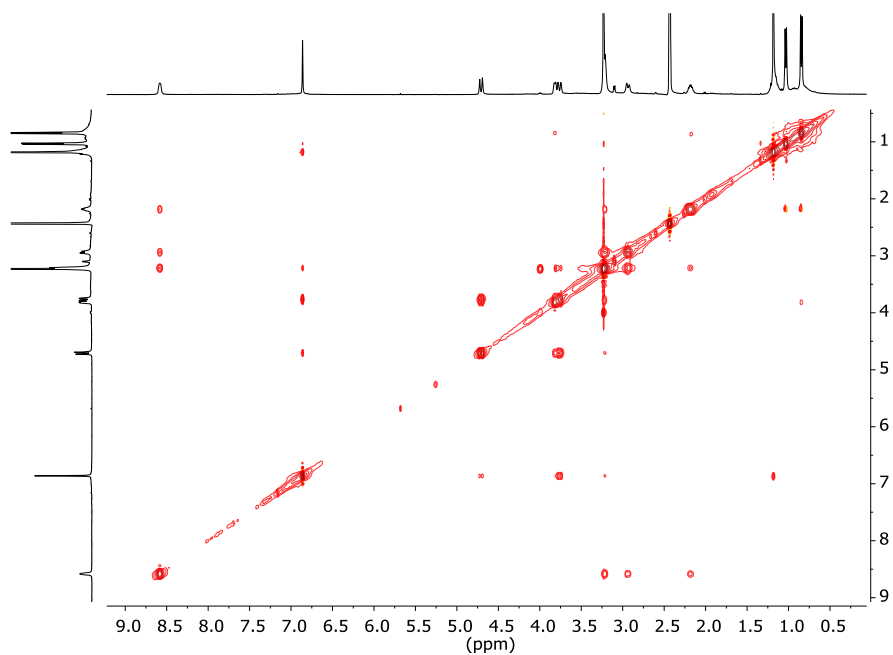
Figure S7.32. 2D NOESY NMR (400 MHz, DMSO-d_6, 25 °C) for **1-I** (5 mM).
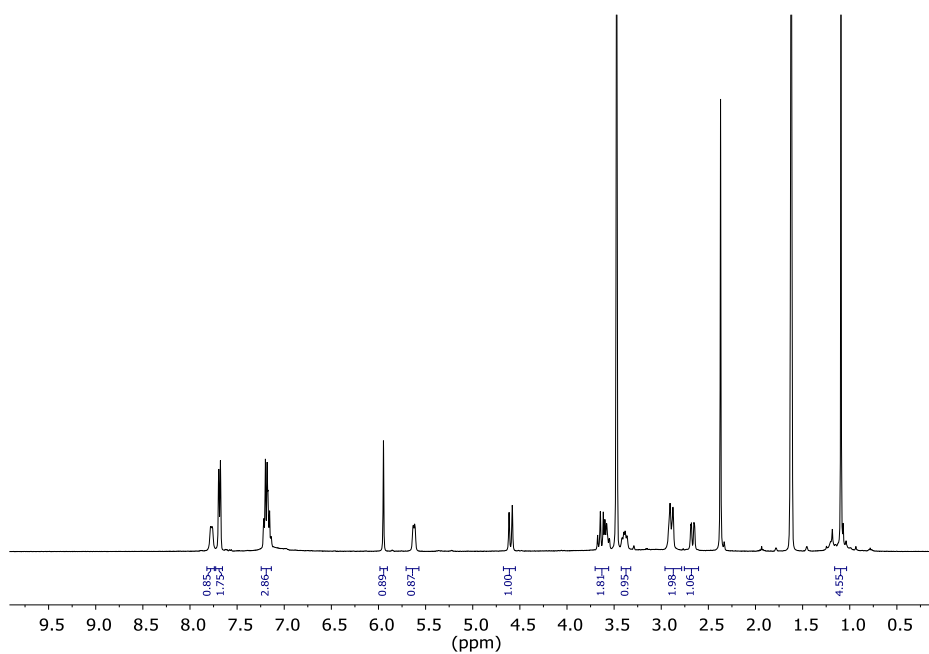
Figure S7.33. ^{1}H NMR (400 MHz, THF-d_8, 25 °C) for **2-I** / **3-I** (5 mM).
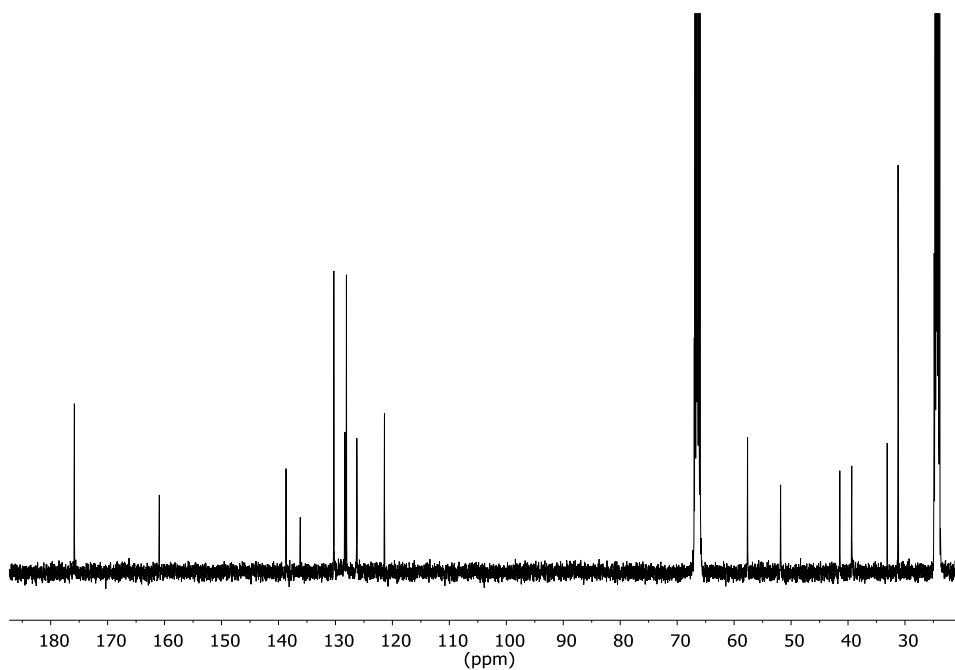
Figure S7.34. $^{13}C\{^1H\}$ NMR (400 MHz, THF-d$_8$, 25 °C) for **2-I / 3-I** (5 mM).
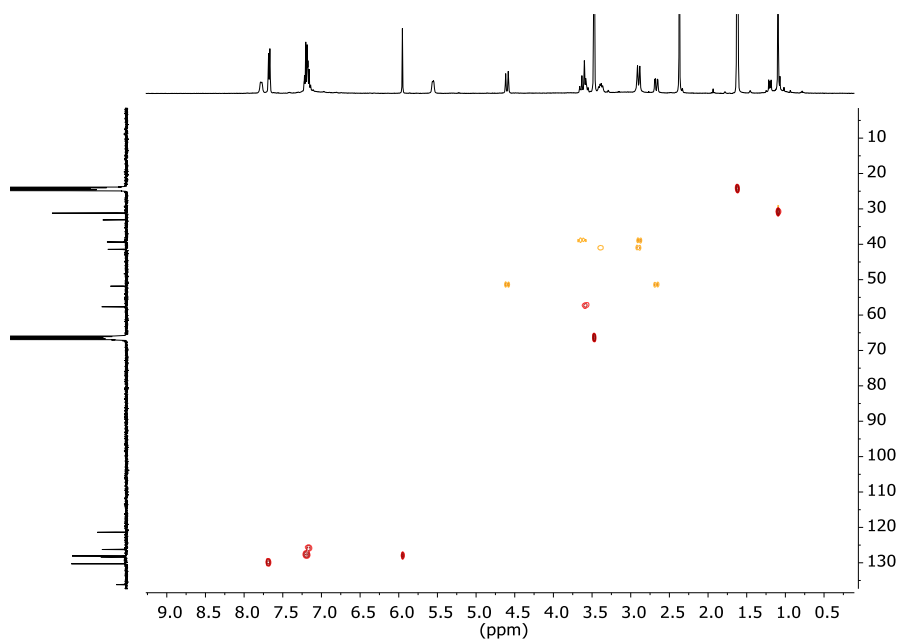
Figure S7.35. 2D HSQC NMR (400 MHz, THF-d$_8$, 25 °C) for **2-I / 3-I** (5 mM).
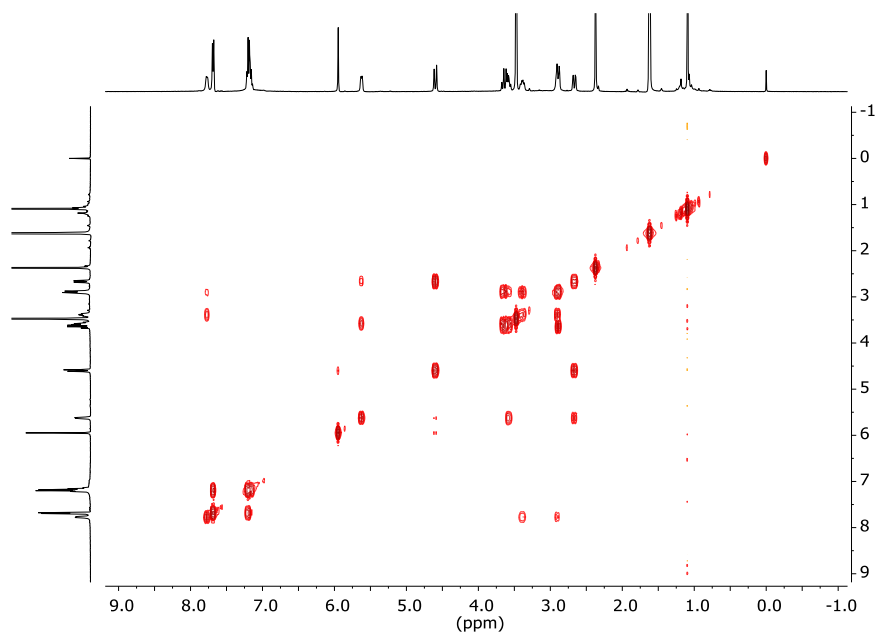
Figure S7.36. 2D COSY NMR (400 MHz, THF-d$_8$, 25 °C) for **2-I** / **3-I** (5 mM).
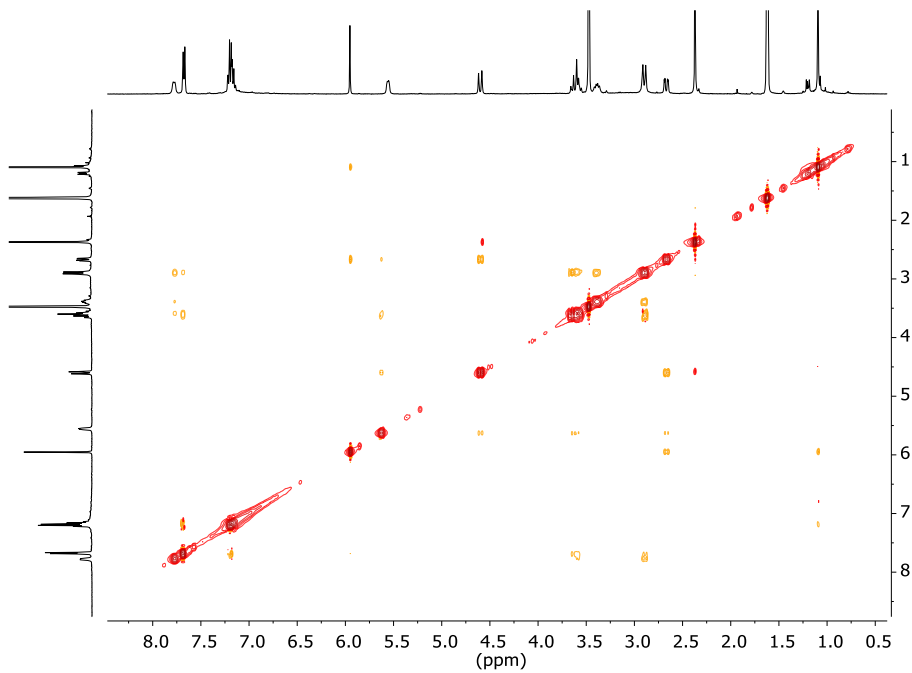
Figure S7.37. 2D NOESY NMR (400 MHz, THF-d$_8$, 25 °C) for **2-I** / **3-I** (5 mM).
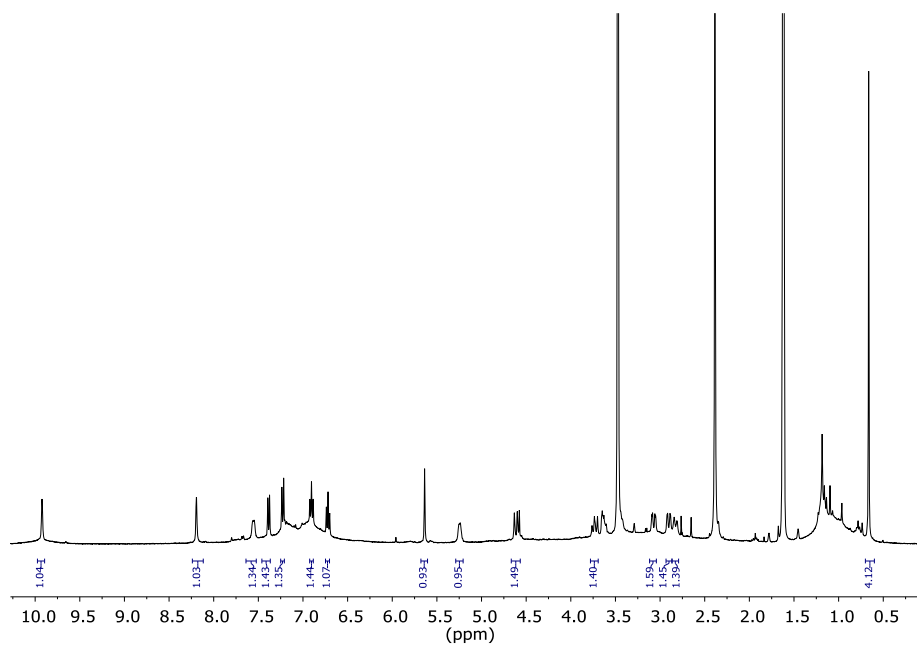
Figure S7.38. ^{1}H NMR (400 MHz, THF-d$_8$, 25 °C) for **4-I** (5 mM).
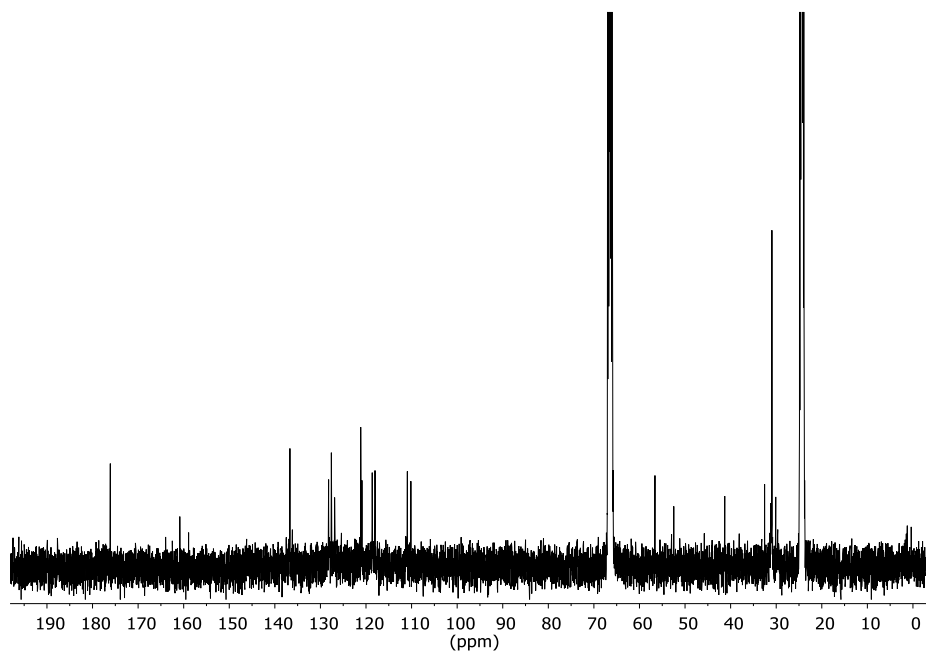
Figure S7.39. ^{13}C{^{1}H} NMR (400 MHz, THF-d$_8$, 25 °C) for **4-I** (5 mM).
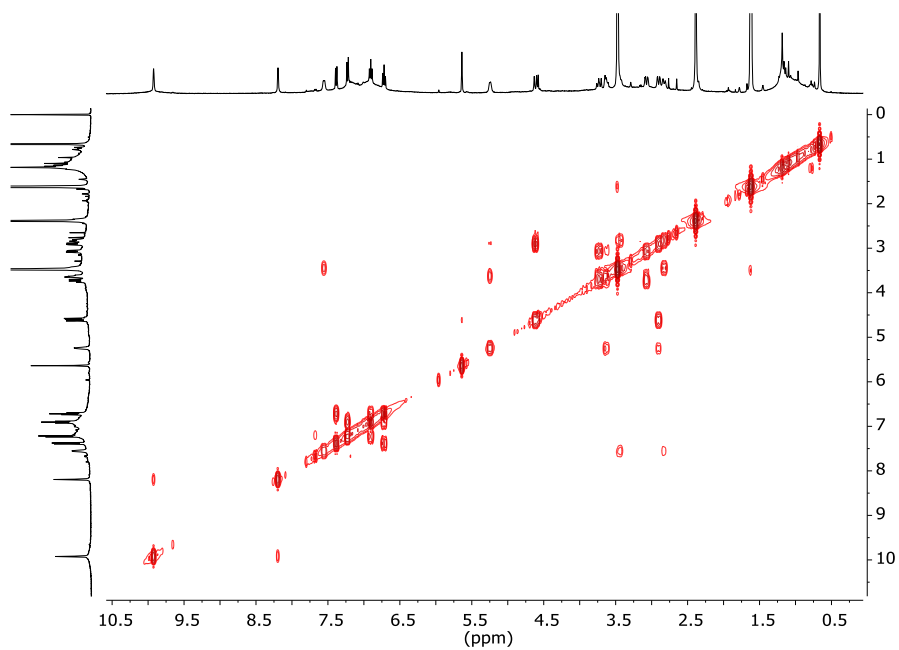
Figure S7.40. 2D COSY NMR (400 MHz, THF-d$_8$, 25 °C) for **4-I** (5 mM).
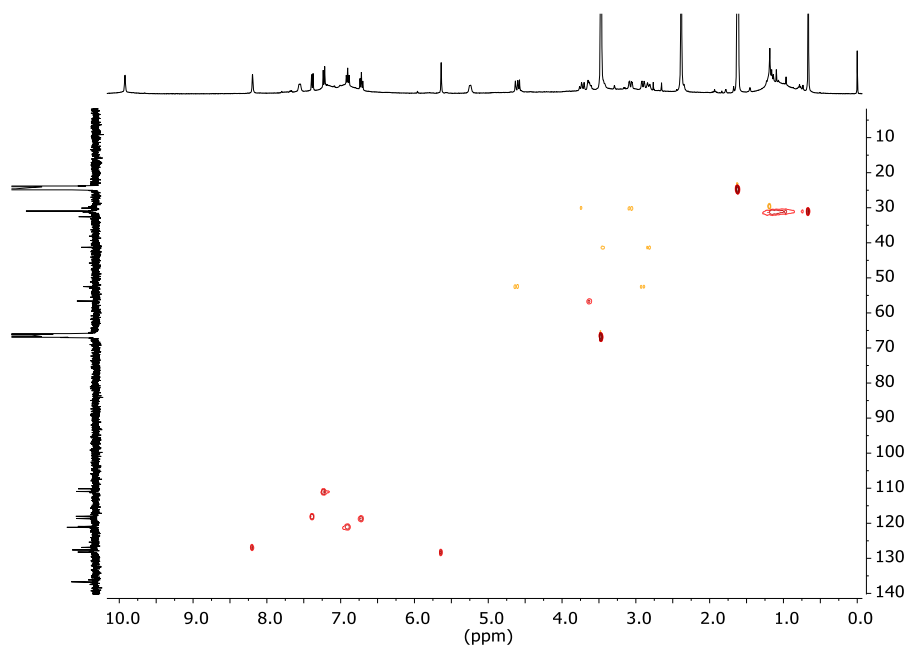
Figure S7.41. 2D HSQC NMR (400 MHz, THF-d$_8$, 25 °C) for **4-I** (5 mM).

Chapter 8

Doubly Chiral Pseudopeptidic Macrobicyclic Molecular cages: Water-assisted Dynamic Covalent Self-Assembly and Chiral Self-sorting

WATER-ASSISTED SELF-ASSEMBLY and CHIRAL SELF-SORTING

COMPONENTS

DYNAMIC SCRAMBLING
SELF-ASSEMBLING

DOUBLY-HOMOCHIRAL
CRYPTANDS
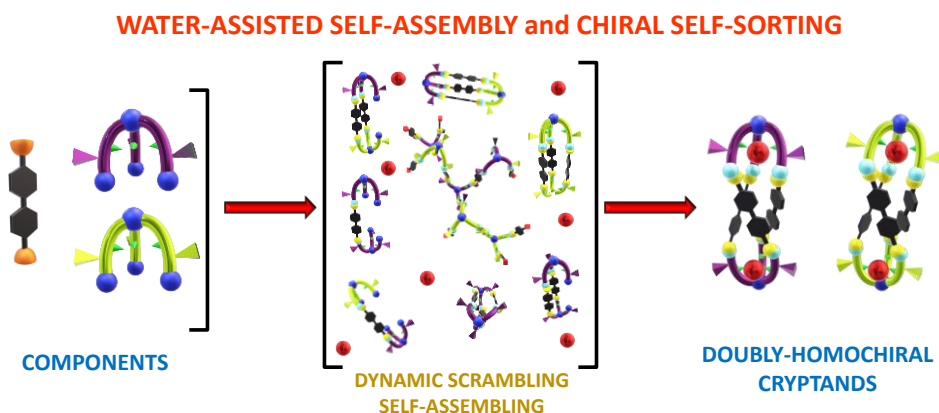
8.1. Main text

8.1.1. Abstract

Taking advantage of the dynamic covalent chemistry approach, four different cages were synthesized by condensation of tripodal pseudopeptides with 4,4'-biphenyldicarboxyaldehyde. Whereas undesired products of polymeric nature were obtained in polar solvents, the [3+2] cryptand-type macrobicyclic architectures were obtained in excellent yields using chloroform as solvent, even at relatively high concentrations. The presence of two encapsulated water molecules may provide a positive template effect in the low polarity medium. The final macrobicycles display a combination of two types of chirality: D,L chirality due to the asymmetric α-C centres and P,M helical chirality. The homochiral helicity found for all the enantiomerically pure molecular cages indicates strong chirality induction by the asymmetric α-C. Besides, the self-sorting properties of the different chiral pseudopeptides have been studied, resulting in high-fidelity homo-self-sorting. DFT calculations point out that the self-sorting outcome may also be a direct result of the encapsulation of two water molecules within the cavity.

8.1.2. Introduction

Since the birth of supramolecular chemistry, a wide range of macrocycles and macrobicycles (such as cryptands) have been designed and used for sophisticated applications.[1-4] Nonetheless, the synthesis of preorganized three-dimensional species is generally challenging, as the macrocyclization steps must always overcome the competing oligomerization/polymerization processes.[5-8] Dynamic covalent chemistry (DCvC), in particular imine formation, offers a thermodynamically-driven approach that may minimize the generation of such by-products.[9-14] One of the merits of using DCvC is that, the reversible nature of dynamic bond allows for the occurrence of component exchange, structural rearrangement and error checking, providing the ideal scenario for self-sorting processes.[15-19]

Several inspiring self-sorting examples have been previously reported based on differences in cation coordination preferences.[20-23] Nevertheless, the assembly of biological supramolecular structures makes mainly use of organic non-covalent interactions such as hydrogen bonding, donor-acceptor interactions and Van der Waals forces.[24] This high-fidelity molecular recognition is responsible for events as crucial as the formation of a DNA double helical structure and the folding of polypeptide chains into proteins with remarkable selectivity.[25] In conjunction with the forces between components, the medium, in particular water molecules, may serve as supramolecular vectors affecting the stability, structure, dynamics, and functions of biomolecules.[26] Examples of self-sorting experiments between organic components based on such type of supramolecular interactions are rather scarce in the literature.[27-30]

Among the diverse self-sorted examples described to date, chiral self-sorting, i.e., the selection for a supramolecular assembly of an interaction partner with a specific chirality from a complex mixture of possible partners, is of paramount relevance as chirality is an omnipresent property in Nature.[31] In fact, in the course of evolution one type of chirality has been favoured in the build-up of the biological molecules making up living organisms, with L-amino acids as the main component of proteins and enzymes and D-sugars as the main components of DNA and RNA.[32] Appropriate design of chiral self-sorting systems may shed light on the formation of complex molecular architectures,[33] allowing for the gradual development of applications involving chiral chemical entities.[34] In this respect, pseudopeptidic compounds could have major advantages, as they present high functional density for potential noncovalent interactions, together with their inherent chirality provided by the amino acid scaffolds.[35] Hence, they could contribute to an understanding of the biomolecular processes.[36]

Herein we report the highly selective formation of cryptand-type macrobicyclic pseudopeptides upon condensation of the tripodal components bearing **L** or **D** valine **V** or phenylalanine **F** amino acid residues (**LTV** / **DTV** / **LTF** / **DTF**) with 4,4'-biphenyldicarboxyaldehyde (**A**) (Scheme 1). These cryptands present enhanced

chiroptical properties compared to their corresponding pseudopeptidic precursors because of the higher rigidity prompted by the non-covalent intramolecular interactions. Furthermore, in view of the presence of six imine groups, we have also investigated the DCvC behaviour of these novel pseudopeptidic molecular cages in competition experiments with the parent tris(2-aminoethyl)amine (TREN) as well as the related self-sorting properties.

LTV ; (*S,S,S*), R=CH(CH₃)₂
DTV ; (*R,R,R*), R=CH(CH₃)₂
LTF ; (*S,S,S*), R=CH₂Ph
DTF ; (*R,R,R*), R=CH₂Ph

A

(LTV)₂A₃ ; (*S,S,S,S,S,S*), R=CH(CH₃)₂
(DTV)₂A₃ ; (*R,R,R,R,R,R*), R=CH(CH₃)₂
(LTF)₂A₃ ; (*S,S,S,S,S,S*), R=CH₂Ph
(DTF)₂A₃ ; (*R,R,R,R,R,R*), R=CH₂Ph
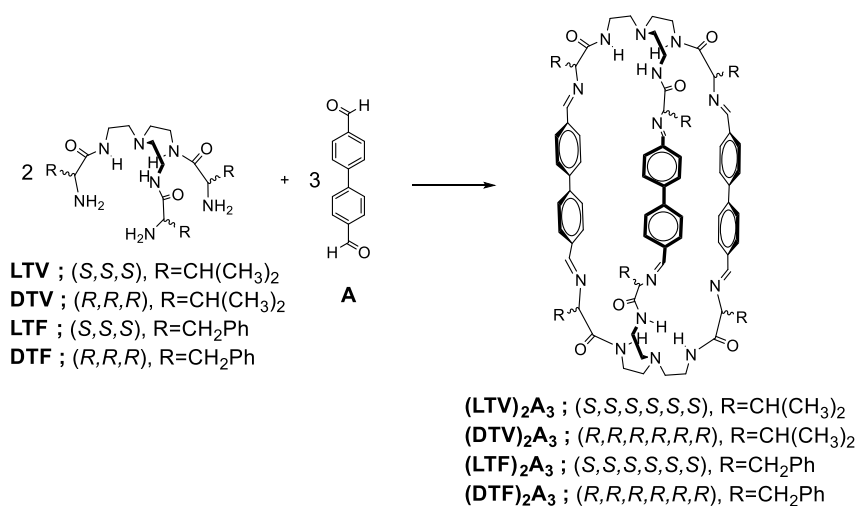
Scheme 8.1. Molecular structures of the tripodal pseudopeptides (**LTV, DTV, LTF, DTF**) and the selected dialdehyde (**A**), together with the generated [3 + 2] homoleptic imine-based organic macrobicyclic cryptand cages. **V** (valine) and **F** (phenylalanine) indicate the amino acid used for the preparation of the tripodal pseudopeptidic component. **D** and **L** indicate the amino acid enantiomer used for the preparation of the tripodal pseudopeptidic component.

8.1.3.   Experimental section

General.

NMR spectra were recorded on Bruker Avance 400 (400 MHz for ¹H and 100 MHz for ¹³C{¹H}), Bruker Avance III plus 400 (400 MHz for ¹H and 100 MHz for ¹³C{¹H}), and Bruker Ascend Spectroscope Avance Neo-500 MHz (500 MHz for ¹H and 125 MHz for ¹³C{¹H}) instruments. MestReNova 10 software was used for the treatment of the NMR spectra. Chemical shifts are given in ppm. Residual solvent

peaks were taken as reference (CDCl$_3$:7.26 ppm). NMR tubes were sealed with Teflon caps to avoid evaporation of solvent and changes in concentration. Quantitative ^{1}H NMR were measured using the integration of the residual solvent peaks as internal standard. The error in ^{1}H NMR integration amounts to ± 5% (the error bars in the quantitative NMR graphs account for 5% of each data point). The coupling constants (J) are listed in Hz. Peaks are described as singlet (s), doublet (d), triplet (t), doublet of doublets (dd) and multiplet (m). Unless otherwise noted, spectra were recorded at 25 °C.

HRMS-ESI (High-Resolution Mass Spectrometry-Electro-Spray Ionisation) mass spectra were recorded by direct injection into a ThermoFisher Exactive Plus EMR Orbitrap mass spectrometer. The CD spectra were recorded on CD-ORD J-1500 (Jasco).

Commercially available chemicals were purchased from Sigma-Aldrich, Alfa Aesar, Fluorochem, TCI and were used without further purification. Solvents and reagents of pharmaceutical grade quality were purchased from Carlo Erba, and solvents of spectroscopic grade were purchased from Sigma-Aldrich and Fisher Chemical. CDCl$_3$ was purchased from Euriso-TOP and filtered through basic alumina to remove traces of acidity before use. CD$_3$CN was purchased from Euriso-TOP.

General Synthetic Procedures.

Synthesis of (LTV)$_2$A$_3$. **LTV** (0.220 mg; 0.496 mmol) was dissolved in CHCl$_3$ (15 mL), then **A** (0.156 g; 0.744 mmol) in CHCl$_3$ (18 mL) was added dropwise over 5 min. The resulting clear, colourless solution was stirred for 72 h at room temperature. Then, 0.2 g of Na$_2$SO$_4$ were added to the solution to remove as much water as possible. The suspension was filtered off and the resulting solution was dried at reduced pressure and low temperature (ca. 5-10 °C) to afford pure (**LTV**)$_2$**A$_3$** as a white solid. Yield: 0.259 g (74%); ^{1}H NMR (500 MHz, 25 °C, CDCl$_3$) δ 8.25 (s, 1H), 8.00 (s, 1H), 7.72 (d, J = 8.1 Hz, 2H), 6.48 (d, J = 7.8 Hz, 2H), 3.96 (t, J = 11.2 Hz, 1H), 3.62 (d, J = 7.9 Hz, 1H), 3.03 – 2.90 (m, 1H), 2.61 (d, J = 3.7 Hz, 2H), 2.22 (d,

J = 7.1 Hz, 1H), 1.04 (d, *J* = 6.7 Hz, 3H), 0.81 (d, *J* = 6.6 Hz, 3H). $^{13}C\{^1H\}$ NMR (125 MHz, 25 °C, CDCl$_3$) δ 172.1, 162.9, 143.3, 134.6, 128.8, 127.9, 84.8, 57.2, 37.4, 33.0, 19.7, 19.6. HRMS (ESI+) m/z: [M+2H]$^{2+}$ calcd 705.4361, found 705.4387.

Synthesis of **(DTV)$_2$A$_3$**: **DTV** (0.226 g; 0.510 mmol) was dissolved in CHCl$_3$ (16 mL), then **A** (0.160 g; 0.765 mmol) in CHCl$_3$ (18 mL) was added dropwise over 5 min. The resulting clear, colourless solution was stirred for 72 h at room temperature. Then, 0.2 g of Na$_2$SO$_4$ were added to the solution to remove as much water as possible. The suspension was filtered off and the resulting solution was dried at reduced pressure and low temperature (ca. 5-10 °C) to afford pure (**DTV**)$_2$**A$_3$** as a white solid. Yield: 0.284 g (81%); ^1H NMR (500 MHz, 25 °C, CDCl$_3$) δ 8.25 (s, 1H), 8.00 (s, 1H), 7.72 (d, *J* = 8.1 Hz, 2H), 6.48 (d, *J* = 7.8 Hz, 2H), 3.96 (t, *J* = 11.2 Hz, 1H), 3.62 (d, *J* = 7.9 Hz, 1H), 3.03 – 2.90 (m, 1H), 2.61 (d, *J* = 3.7 Hz, 2H), 2.22 (d, *J* = 7.1 Hz, 1H), 1.04 (d, *J* = 6.7 Hz, 3H), 0.81 (d, *J* = 6.6 Hz, 3H). $^{13}C\{^1H\}$ NMR (125 MHz, 25 °C, CDCl$_3$) δ 172.1, 162.9, 143.3, 134.6, 128.8, 127.9, 84.8, 57.2, 37.4, 33.0, 19.7, 19.6. HRMS (ESI+) m/z: [M+2H]$^{2+}$ calcd 705.4361, found 705.4387.

Synthesis of **(LTF)$_2$A$_3$**: **LTF** (0.298 g; 0.507 mmol) was dissolved in CHCl$_3$ (16 mL), then **A** (0.159 g; 0.761 mmol) in CHCl$_3$ (18 mL) was added dropwise over 5 min. The resulting clear, colourless solution was stirred for 40 h at room temperature. Then, 0.2 g of Na$_2$SO$_4$ were added to the solution to remove as much water as possible. The suspension was filtered off and the resulting solution was dried at reduced pressure and low temperature (ca. 5-10 °C) to afford pure (**LTF**)$_2$**A$_3$** as a white solid. Yield: 0.379 g (88%); ^1H NMR (500 MHz, 25 °C, CDCl$_3$) δ 8.33 (dd, J = 7.9, 4.4 Hz, 1H), 7.64 – 7.50 (m, 3H), 7.09 – 6.99 (m, 3H), 6.88 (t, J = 7.5 Hz, 2H), 6.07 (d, J = 7.8 Hz, 2H), 4.21 (dd, J = 11.1, 2.6 Hz, 1H), 4.01 – 3.89 (m, 1H), 3.65 (dd, J = 13.4, 2.5 Hz, 1H), 3.05 – 2.94 (m, 1H), 2.94 – 2.79 (m, 2H), 2.64 – 2.54 (m, 1H). $^{13}C\{^1H\}$ NMR (125 MHz, 25 °C, CDCl$_3$) δ 172.9, 163.7, 143.3, 136.9, 134.1, 130.2, 128.8, 128.4, 128.0, 126.7 128.8, 127.9, 77.9, 56.8, 42.1, 39.1, 29.9. HRMS (ESI+) m/z: [M+2H]$^{2+}$ calcd 849.4372, found 849.4356.

*Synthesis of **(DTF)₂A₃:*** **DTF** (0.290 g; 0.493 mmol) was dissolved in $CHCl_3$ (15 mL), then **A** (0.155 g; 0.740 mmol) in $CHCl_3$ (18 mL) was added dropwise over 5 min. The resulting clear, colourless solution was stirred for 40 h at room temperature. Then, 0.2 g of Na_2SO_4 were added to the solution to remove as much water as possible. The suspension was filtered off and the resulting solution was dried at reduced pressure and low temperature (ca. 5-10 °C) to afford pure **(DTF)₂A₃** as a white solid. Yield: 0.377 g (90%); ^{1}H NMR (500 MHz, 25 °C, $CDCl_3$) δ 8.33 (dd, J = 7.9, 4.4 Hz, 1H), 7.64 – 7.50 (m, 3H), 7.09 – 6.99 (m, 3H), 6.88 (t, J = 7.5 Hz, 2H), 6.07 (d, J = 7.8 Hz, 2H), 4.21 (dd, J = 11.1, 2.6 Hz, 1H), 4.01 – 3.89 (m, 1H), 3.65 (dd, J = 13.4, 2.5 Hz, 1H), 3.05 – 2.94 (m, 1H), 2.94 – 2.79 (m, 2H), 2.64 – 2.54 (m, 1H). ^{13}C{^{1}H} NMR (125 MHz, 25 °C, $CDCl_3$) δ 172.9, 163.7, 143.3, 136.9, 134.1, 130.2, 128.8, 128.4, 128.0, 126.7 128.8, 127.9, 77.9, 56.8, 42.1, 39.1, 29.9. HRMS (ESI+) m/z: [M+2H]$^{2+}$ calcd 849.4372, found 849.4356.

X-Ray Crystallography.

LTV and **(LTF)₂A₃** X-Ray diffraction data was obtained on a 4-circle Xcalibur EosS2 diffractometer (Agilent Technologies) equipped with a CCD detector. CCDC numbers: 2143486 and 2143485, respectively. **DTV**, **(DTF)₂A₃** and **(DTV)₂A₃** X-Ray diffraction data was obtained on a SuperNova-Dual diffractometer (Agilent Technologies) equipped with an Atlas CCD detector. CCDC numbers: 2143483, 2143482, and 2143484, respectively. The structures were solved with the SHELXT 2014/5[77] structure solution program and refined with the SHELXL-2018/3[78] refinement package. Artwork representations were processed using MERCURY[79] software. See Supplemental CD for details.

DFT Calculations.

DFT calculations were run with Gaussian 09 (revision B.01).[80] Geometry optimizations were carried out without symmetry restrictions at the B3LYP level,[81] using the Lanl2Dz basis set.[82] Analytical frequency calculations were used to characterise each stationary point as a minimum. These calculations, carried out at

298.15 K, also allowed for obtaining the thermal and entropic corrections required to calculate Gibbs energy differences. See Supplemental CD for details.

The X-ray geometric structures for the homochiral species were used as the starting point for Montecarlo conformational searchers. The most stable conformation was initially determined at the MMFF level of theory, and then the DFT models were calculated. The same procedure was followed for the heterochiral species, starting from the X-ray geometry of the homochiral species, and then modifying the three chiral centres of one of the cage lids

8.1.4.   Results and discussion

8.1.4.1.   Synthesis and characterisation of the pseudopeptidic cryptands

The reactions examined involved four pseudopeptidic tripodal compounds derived from natural L-valine and L-phenylalanine, as well as from their corresponding D-enantiomers. The syntheses of the different tris(aminoamides) followed previously reported procedures.[37] For the valine derivatives, **DTV** and **LTV**, details of their solid state structures were established by single crystal X-ray crystallography (Figure S8.1a and S8.1b, respectively). Both structures present a highly symmetric fully expanded conformation, with the arms of the pseudopeptide located in the same horizontal plane. The angles between the three different arms are of 112.9(2)°, almost equivalent to the theoretical distribution for a trigonal planar molecular geometry (120.0°). The adoption of such expanded conformation can be explained by the low-energy packing accomplished in solid-state, as the neighbouring molecules of the valine-derived tripodal compounds are interacting by means of parallel intermolecular hydrogen bonding (Figure S8.1c).[38,39] Indeed, the calculated N$\cdots$O distance in the solid-state structures for the three symmetric intermolecular hydrogen bonds formed was 2.835(7) Å (HN$\cdots$O=C bonding, 90% vdW$_{N,O}$).[40,41] Hence, both **LTV** and **DTV** formed β-sheet-like self-assembled crystalline solids.[42,43]

The synthesis of macrobicyclic structures from two tripodal triamine and three dialdehyde components involves the formation of six imine groups by reversible amine-aldehyde condensations in a multiple dynamic covalent process allowing for error correction in the course of the reaction.[13,14,15,17] Despite the unfavourable extended spatial conformation seen in the solid-state for the pseudopeptidic precursors, their capability to form cryptands was evaluated by reacting each of them with 4,4'-biphenyldicarboxyaldehyde (Scheme 8.1). First, the reaction conditions were optimized using **LTV** as the triamino compound and **A** as the dialdehyde. When the reaction was performed in acetonitrile (3 mM in **LTV** and 4.5 mM in **A**), a substantial polymeric precipitate was formed after 15 h at room temperature. This yellowish material was only soluble in a 50 mol% solution of trifluoroacetic acid in wet CDCl$_3$, allowing for identification of the characteristic ^{1}H NMR signals for **LTV** and **A**. This result agrees with the formation of a highly crosslinked imine-based polymer, undergoing acid-catalysed hydrolysis.[44] Performing the reaction in CD$_3$CN at 25 °C allowed real time monitoring the imine formation reactions (Figure S8.2). After 15 h, some yellowish precipitate was formed, while the solution contained a complex mixture of unreacted reagents (ca. 30%), unidentified intermediates, and 10% of the desired cryptand. After 10 days at room temperature, the reaction led to 14% of unreacted **A** and ca. 30% of **(LTV)$_2$A$_3$** as the predominant product in solution. The presence of **(LTV)$_2$A$_3$** was also corroborated by HRMS (Figure S8.3). Diffusion-ordered spectroscopy (^{1}H DOSY NMR) for the isolated homoleptic l-valine-derived molecular cage provided a diffusion coefficient of $7.08 \cdot 10^{-6}$ cm^{2}s^{-1} (Figure S8.4), corresponding to a molecular volume of 3037 Å^3.[45]

When the reaction was performed in CDCl$_3$ at room temperature (3 mM in **LTV**, 4.5 mM in **A**) no precipitation was observed even after 5 days of reaction. ^{1}H NMR revealed the formation of the desired cryptand almost quantitatively (93% NMR yield) after 4 days (Figure 8.1a). Conversion of **A** was higher than 90% after 8 h, and complete after 20 h. Thus, the consumption of **A** occurred much faster than the appearance of the **(LTV)$_2$A$_3$** product. This behaviour indicated the occurrence of multiple condensation reactions generating initially different intermediates. This

double macrocyclization process was also followed by HRMS analysis. Although HRMS analyses are not fully quantitative, they can be very useful for studying the appearance and disappearance of different components in the course of the reaction.[15] Indeed, Figure 8.1b shows the relative distribution for the detected intermediates present at different reaction times, together with the formation of the desired [3+2] cage.
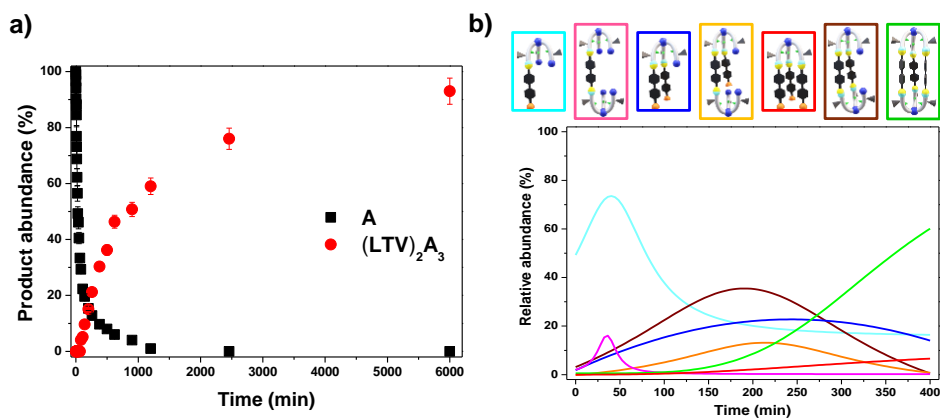
Figure 8.1. a) Kinetic profile (^{1}H NMR, 400 MHz) for the formation of **(LTV)$_2$A$_3$**. Amount of conversion of **A** and yields for **(LTV)$_2$A$_3$** determined with NMR integration. Reaction conditions: room temperature, 3 mM in **LTV** and 4.5 mM in **A** in CDCl$_3$. b) Trends in product distribution calculated for the different reaction times obtained from non-linear fitting of HRMS data.

The evolution with time of the different signals in the ^{1}H NMR spectra afforded valuable information (Figure S8.5a). After 2 h, once the characteristic signals for the macrobicycle **(LTV)$_2$A$_3$** were well displayed in the spectra, the signal corresponding to water started to shift to higher δ values ($\Delta\delta_{44h}$ = +0.4 ppm, orange discontinuous lines in Figure S8.5a). This observation suggests the existence of strong interactions between the molecular cage and water molecules, with the hydrophobic medium likely favouring the encapsulation of H$_2$O molecules tightly hydrogen bonded to the pseudopeptidic moieties of the cage. Therefore, water molecules, as released in the condensation steps, could act as a thermodynamic template,[46,47,6] stabilizing the structure of **(LTV)$_2$A$_3$** and thus favouring its formation, possibly in an autocatalytic fashion.[48,49] No significant shift was observed for water molecules in the experiment

in acetonitrile (($\Delta\delta_{10days}$ = +0.02 ppm), suggesting that water templation is much less effective in more polar solvents (Figure S8.5b).

Due to random twisting motions around the axis of the bridgehead nitrogens, the spectrum of **(LTV)₂A₃** appears as highly symmetrical, as only a single set of signals is observed, for example, for the imine protons (marked as I in Figure S8.6) and the proton of the stereogenic carbons (C in Figure S8.6). The two doublets distinctive of para-substituted aromatic rings (A and B, Figure S8.6) appearing at 7.42 and 6.48 ppm, respectively, reveal the existence of very different electronic environments for both hydrogen atoms, with one of them substantially shielded. It suggests a significant twisting around the N---N bridgehead axis of the three-dimensional molecular cage with the involvement of π-π intramolecular interactions. It was especially noticeable in the signals of the protons of the methylene group attached to the NH of the amide groups, appearing as diastereotopic protons (E and E' in Figure S8.6). The amide protons (D in Figure S8.6) increase their hydrogen bonding in the cage, as their signal appears at higher δ values than in the open-chain **LTV** (7.98 ppm vs 7.67 ppm, 1.5 mM in CDCl₃).

The outcome of the self-sorting in the present system may result from its response to solvent effectors. When the reaction is carried out in a polar solvent such as acetonitrile, products of polymeric nature are generated. Precipitation of such polymers traps the system out-of-equilibrium, and thus without sorted outcome. This shortcoming can be addressed by changing the solvent to chloroform, which keeps the various intermediates in solution and allows for reaching equilibrium, possibly also facilitated by the template effect of encapsulated water molecules, as found in the crystal structures (Figure 8.2).

Under these optimized conditions, the condensation reactions between **A** and the other pseudopeptidic reagents, **DTV**, **LTF** and **DTF**, were studied separately. All the macrobicyclization reactions afforded the corresponding cryptand with isolated yields higher than 80% for a 3 mM concentration in the triamine (Entries 1-4, Table 8.1). Interestingly, a 5-fold increase in concentration did not result in any

significant decrease in yields (Entries 5-8 in Table 8.1), emphasizing the robust fidelity of the reagents to self-assemble in such [3+2] architectures. Regarding the effect of changing the amino acid sidechain, slightly better results were observed for phenylalanine derivatives (**(LTF)₂A₃** and **(DTF)₂A₃**).

Table 8.1. Isolated yields obtained in the condensation reactions between **A** and the four different pseudopeptidic tripodal compounds.

Entry	Macrobicycle	Conc (mM)[a,b]	Isolated yield (%)[c]
1	**(LTV)₂A₃**	3	85
2	**(LTF)₂A₃**	3	90
3	**(DTV)₂A₃**	3	87
4	**(DTF)₂A₃**	3	92
5	**(LTV)₂A₃**	15	74
6	**(LTF)₂A₃**	15	88
7	**(DTV)₂A₃**	15	81
8	**(DTF)₂A₃**	15	90

[a] Solvent: CHCl₃, reaction temperature: 25 ºC, reaction time: 5 days. [b] Concentration of the tripodal open-chain pseudopeptide. [c] Pure products were isolated after Na₂SO₄ filtration and solvent evaporation, not needing further purification.

Crystals suitable for X-ray diffraction were obtained for **(DTV)₂A₃**, **(LTF)₂A₃** and **(DTF)₂A₃**. These solid-state structures provided unambiguous evidence for cage formation (Figure 8.2). In all cases, the hydrophobic sidechains (isopropyl and benzyl groups for valine and phenylalanine derivatives, respectively) are located in the outer part of the cryptand. In the same way, the three biphenyl fragments are arranged in a helical disposition involving intramolecular π-π interactions. Thus, in the case of **(LTF)₂A₃,** the three interacting aromatic bridges adopt two circular edge-tilted-T arrangement with the angles between the centroids of the benzene rings (61.22(2)º, 60.70(2)º, and 58.08(2)º) defining two essentially equilateral triangles (Figure S8.7a).[50] For each set of three aromatic rings, the smallest intramolecular H_{Ar}-centroid distances were of 2.8321(10), 2.7072(9), and 2.8671(10) Å, corroborating the definition of a slightly distorted equilateral triangle. Overall, the lines connecting the

centroids in the two sets of benzene rings identify a Star of David (Figure S8.7b).[51-53]
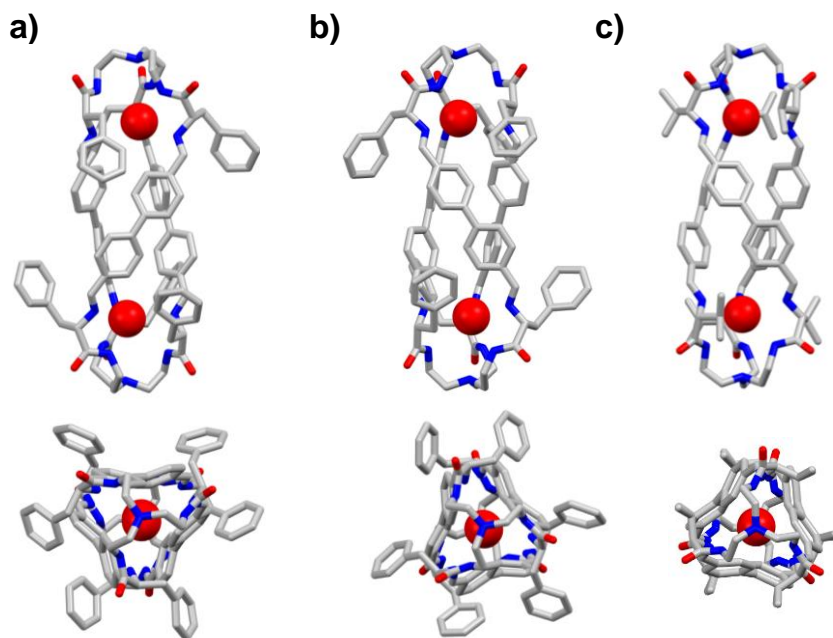
Figure 8.2. Solid-state molecular structures of **(LTF)₂A₃** and **(DTF)₂A₃** and **(DTV)₂A₃** (from left to right) showing also the helical chirality enforced by the asymmetric α-C centre as obtained for a) M-**(LTF)₂A₃,** b) P-**(DTF)₂A₃** and c) P-**(DTV)₂A₃**. Side-view (top) and front-view (bottom) have been represented in all cases. Hydrogen atoms, non-essential solvent molecules and disorder have been removed. Oxygen atoms of the encapsulated water molecules have been represented in space-filling mode for clarity. See supplemental information for crystallographic details.

A similar scenario is found for **(DTV)₂A₃,** although in the valine-derived cryptand the shortest H_{Ar}-centroid distances are slightly larger (2.9980(18) Å). These CH···π interactions are in good agreement with the observed ^{1}H NMR shift of the aromatic proton appearing at 6.48 and 6.07 ppm for **(LTV)₂A₃/(DTV)₂A₃** and **(LTF)₂A₃/(DTF)₂A₃,** respectively (Figures S8.27 and S8.33). The aromatic sidechains of the phenylalanine derivative also display π-π interactions with the bisphenyl bridging units. The shortest distance between the H_{Ar} of phenylalanine and the closest aromatic carbon of the biphenyl bridge is of 2.731(2) Å. These additional interactions can help to stabilize the three-dimensional structure, explaining the

higher yields observed in comparison with the valine derivatives (see Table 8.1). The polar groups of the pseudopeptidic units are predominantly facing the cavity, creating two hydrophilic pockets in a cage with a strongly hydrophobic surface. Two molecules of water are encapsulated inside the polar terminal pockets (Figures 8.2 and S8.8), hydrogen bonded to the protons of the amide groups (distance $O_{water} \cdots N_{amide}$ = 3.063(6) Å, 97% $vdW_{N,O}$ for $(LTF)_2A_3/(DTF)_2A_3$ and 3.062(5) Å, 97% $vdW_{N,O}$ for $(DTV)_2A_3$) and with the basic nitrogen atom of the imine groups (distance $O_{water} \cdots N_{imine}$ = 3.050(7) Å, 97% $vdW_{N,O}$ for $(LTF)_2A_3/(DTF)_2A_3$ and 3.037(4) Å for $(DTV)_2A_3$, 96% $vdW_{N,O}$). This finding is in accordance with water acting as thermodynamic template. Additional intramolecular hydrogen bonds are found between the NH group of the amides and the N atom of the imines, with distances $N_{amide} \cdots N_{imine}$ of 2.732(4) Å (82% $vdW_{N,N}$) for $(LTF)_2A_3/(DTF)_2A_3$ and 2.787(6) Å (84% $vdW_{N,N}$) for $(DTV)_2A_3$ (Figure S8.8). The intermolecular interactions between water and cage were further corroborated by variable temperature ^{1}H NMR spectroscopy, observing a shift towards lower δ for the water signal and for the NH protons of the amides with increasing temperatures (Figure S8.9).

Especial attention should be paid to the twisted conformation adopted by the cryptands. Solid state structures of the pseudopeptidic macrobicycles demonstrate that, in each of the framework of the cages, the three biphenyl units adopt the same rotational conformation, namely either P for clockwise rotation ($(DTF)_2A_3$ and $(DTV)_2A_3$) or M for anti-clockwise rotation ($(LTF)_2A_3$ and $(LTV)_2A_3$). Each homoleptic cage thus has helical homochirality, namely P_3 or M_3,[54-55] which is driven by the orientation adopted by the three aromatic units because of the aforementioned intramolecular CH$\cdots$π interactions. This propeller-shaped central aromatic moiety can find similarities with secondary structures found in Nature,[17,56] as for example the DNA triple helix or the collagen triple helix.[57-59]

We envisaged at this point that such chiral environment should result in strong CD differences for the cryptands. The two enantiomers for each pseudopeptidic cage presented mirror-like CD spectra (Figure 8.3), expressed through a cotton effect

centred at 309 nm, corresponding to the UV absorption for the conjugated central aromatic units.[60-62]
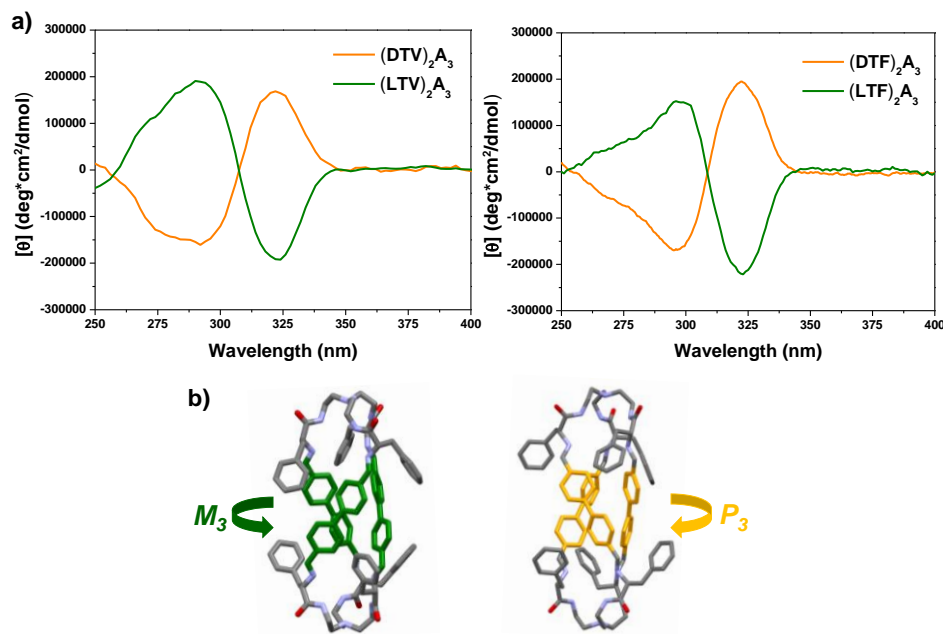
Figure 8.3. a) CD spectra comparison (CHCl$_3$, 0.015 mM, 25 ºC) for **(LTV)$_2$A$_3$** / **(DTV)$_2$A$_3$** (left) and **(LTF)$_2$A$_3$** / **(DTF)$_2$A$_3$** (right). The superposition of the spectra for each separated enantiomer reflects mirror-like CD. b) Representation of solid-state structures found for **(XTF)$_2$A$_3$** (**X= D** or **L**) showing the helical chirality enforced by the asymmetric α-C chirality: M-**(LTF)$_2$A$_3$** (left) and P-**(DTF)$_2$A$_3$** (right). Solvent molecules and hydrogen atoms have been removed for clarity. The aromatic biphenyl bridges have been coloured depending on the rotational chirality.

The Cotton effect was positive in the case of the homoleptic l-cryptands (**(LTF)$_2$A$_3$** and **(LTV)$_2$A$_3$**) and negative for their enantiomeric molecular cages (**(DTF)$_2$A$_3$** and **(DTV)$_2$A$_3$**). Hence, the helical arrangement was endowed by the intramolecular and intermolecular (with water) supramolecular interactions and the rotational homochirality, was governed by the chirality of the initial pseudopeptide. It agrees with the solid state structure for the pseudopeptidic based cryptands compared to that reported for the cage prepared from TREN and **A**, in which the bridging units were barely twisted.[17]

8.1.4.2. Competition studies with the parent achiral component TREN (T)

After the successful synthesis, isolation, and characterisation of the four homoleptic cages X_2A_3 (X = LTV, DTV, LTF, DTF), we carried out competition experiments for two different tripodal amines: LTV and tris(2-aminoethyl)amine (TREN, T). One may consider T to be more reactive than LTV, as the steric hindrance resulting from the α-substitution in the pseudopeptide might decrease its reactivity. Besides, the nitrogen atoms of the terminal amino groups in LTV could be acting as hydrogen bond acceptor in intramolecular interactions, decreasing their nucleophilicity. The initial experiment involved a 3 : 2 : 2 mixture of A (4.5 mM), T (3 mM) and LTV (3 mM) using CDCl$_3$ as solvent (Figure 8.4).
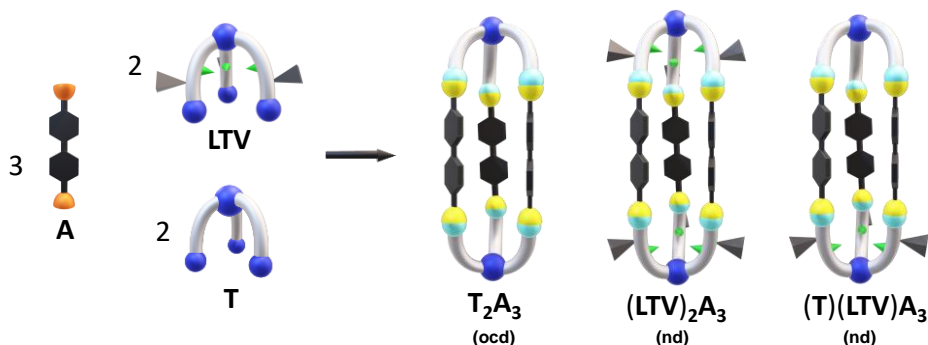
Figure 8.4. Competition experiment between **T** and **LTV** using **A** as the dialdehyde. Reaction conditions: CDCl$_3$, 25 ºC, 3 mM for **LTV**, 3 mM for **T**, 4.5 mM for **A**. The abundance of each species was determined by NMR integration. Note: (ocd), only compound detected; (nd), not detected.

In line with the expected tendency, the only cryptand appreciably present in solution after 41 h of reaction was T_2A_3, with all the initial T reagent being consumed (Figure S8.10). In good agreement with this result, the homoleptic cage $(LTV)_2A_3$ and the mixed heteroleptic cage $(T)(LTV)A_3$ were not detectable in the ^{1}H NMR spectrum, whereas 95% of the initial LTV was still present unreacted. Comparing the kinetic profiles for each separated macrocyclization, noteworthy differences were observed. For instance, the consumption of the aldehyde was slightly faster in the presence of T than for its competitor LTV, confirming the higher nucleophilicity of

T over the open-chain tripodal pseudopeptide (Figure S8.11a). In terms of the yield for the respective cages, the formation of **T₂A₃** was also kinetically favoured, as yields higher than 50% were achieved after only 50 min, while it took 600 min for reaching such yields for **(LTV)₂A₃** (Figure S8.11b). The product distribution was stable for more than 10 days, without any exchange between components occurring. This observation suggested that the homoleptic cage **T₂A₃** was also the thermodynamically favoured product.

8.1.4.3. Effect of the sidechain in the self-sorting between components
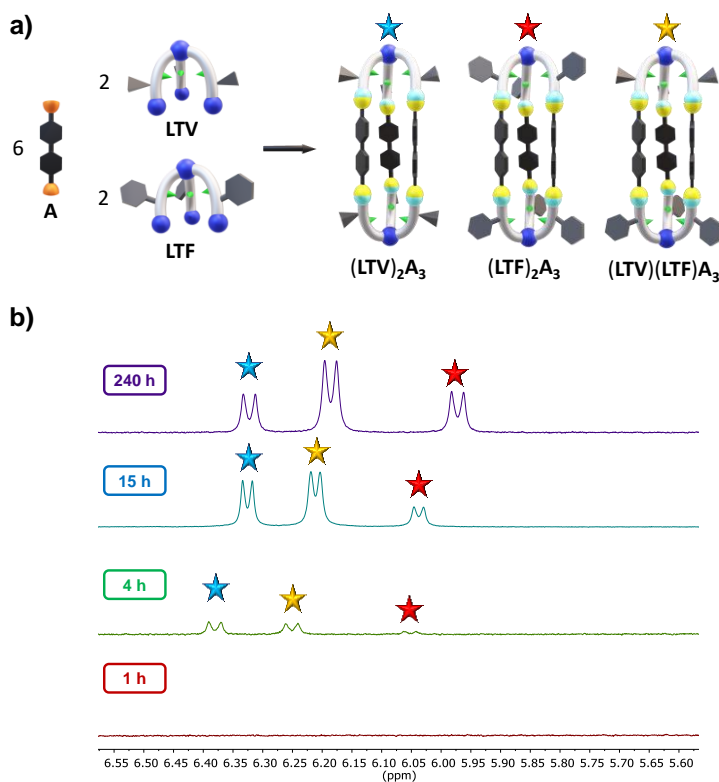
Figure 8.5. Self-sorting experiment between **LTV** and **LTF** using **A** as the dialdehyde. a) Representation of the self-sorting experiment between **LTV** and **LTF** using **A** as the dialdehyde. Reaction conditions: CDCl₃, 25 ºC, 3 mM for **LTV**, 3 mM for **LTF**, 9 mM for **A**. b) Partial ¹H NMR (400 MHz, CDCl₃, 25 ºC) spectra for the self-sorting experiment at 1 h (red spectrum), 4 h (green spectrum), 15 h (light blue spectrum), and 240 h (purple spectrum).

The effect of the amino acid sidechain in the reactivity and self-sorting properties of the cryptands was also studied. This experiment seemed more challenging, as the reactivity of the tripodal pseudopeptides **LTV** and **LTF** was expected to be similar. The self-sorting experiment was performed using a 2 : 2 : 6 mixture (**LTV** : **LTF** : **A**) in CDCl$_3$ at room temperature (Figure 8.5a). Monitoring the product distribution by ^{1}H NMR spectroscopy showed that the homoleptic cage **(LTV)$_2$A$_3$** was formed prior to the homoleptic **(LTF)$_2$A$_3$** one (Figure 8.5b), the NMR yields being respectively 11% and 5% after 4 h. In addition to the characteristic peaks of the homoleptic cages, a new signal at 6.20 ppm was assigned to the heteroleptic **(LTV)(LTF)A$_3$** species. The final ^{1}H NMR spectrum indicated that these three products embraced a statistical distribution, namely 1:2:1, as confirmed by NMR integration. The same statistical distribution was also observed in the HRMS analysis of the crude after 10 days of reaction (Figure S8.12). This result highlights that the sidechain did not trigger significant changes in the energy distribution between homoleptic and heteroleptic compounds.

To probe whether the distribution observed for the self-sorting experiment corresponded to the thermodynamically favoured distribution, we envisaged that mixing two equimolar solutions of pure **(LTF)$_2$A$_3$** and **(LTV)$_2$A$_3$** should result in the formation of the heteroleptic cage over time. This process would be possible through component exchange in presence of a nucleophile or hydrolysis and further rearrangement of the components, permitted by the dynamic nature of the imine bonds. Similar exchange processes have been already established for dynamic macrocycles and cryptands.[15,17] Thus, pseudopeptides **LTV** and **LTF** were first reacted separately with **A** (3 mM for the pseudopeptide and 4.5 mM for the dialdehyde, CDCl$_3$, 25 ºC) for 72 h prior to combining the two reaction samples. The resulting mixture was left to equilibrate, monitoring the change in the product distribution over 12 days (Figure S8.13). The increase in concentration of **A** over time suggested that the error-checking was occurring through hydrolysis and further rearrangement of the components. Although the self-sorting experiment was not completed in the time-range monitored, a final distribution of 30 : 33 : 37 was

observed for **(LTV)₂A₃** : **(LTV)(LTF)A₃** : **(LTF)₂A₃**, suggesting that the three cryptands presented similar energies. HRMS analysis of the final reaction mixture (12 days of reaction) corroborated the formation of the heteroleptic cryptand (Figure S8.14).

Performing the competition experiment in the presence of a defect of dialdehyde (3 mM for **LTV**, 3 mM for **LTF** and 4.5 mM for **A**), the kinetic preferences of the macrocyclization were also determined (Figure S8.15a). The signals characteristic of **(LTV)₂A₃** were the first to be detectable in the ¹H NMR spectra (Figure S8.15b). The heteroleptic cage was the second macrobicycle to be formed, whereas the homoleptic **(LTF)₂A₃** cage was only detected after 8 h. The corresponding kinetic profiles suggest that the pseudopeptide **LTV** must be somewhat more nucleophilic and/or less sterically hindered than **LTF** (Figure S8.15c). The kinetic profiles for the separated synthesis of **(LTF)₂A₃** and **(LTV)₂A₃** confirmed the higher reactivity of **LTV** as indicated at short times by the faster consumption of **A** (Figure S8.16). Inspired by previous studies where the introduction of external chemical species resulted in interesting changes in selectivity,[63-65] the effect of anionic species as chemical effectors in the competition experiment was assayed, but only minor changes were observed in the final distributions after 8 days of reaction (Table S8.1).

8.1.4.4.   Effect of component chirality in the self-sorting processes

The macrobicyclic compounds **(LTX)₂A₃** and **(DTX)₂A₃** (**X=V** or **F**) combine remarkable chirality features of two types: asymmetric α-C D,L chirality and helical P,M chirality due to twisting around the N---N bridgehead axis enforced by the asymmetric α-C centre in opposite directions for D and L. Figures 8.2 and 8.3 show the corresponding molecular structures in the solid state for M-**(LTF)₂A₃**, P-**(DTF)₂A₃** and P-**(DTV)₂A₃**. These observations, together with the spectroscopic data found, suggest a strong helical chirality induction.[66,67] A related homochiral

induction by asymmetric α-C centers is found in trinuclear double stranded helicates,[68] and in the formation of chiral tetrahedral cages.[69]

The information gathered from ^{1}H NMR, CD and solid state analyses, indicated that the helical macrobicycles here described could promote chiral self-sorting. Several examples can be found in the literature describing homochiral rearrangements in the syntheses of highly twisted molecules or pinwheel-shaped structures.[70-72] The formation of helical architectures generally results in homo-self-sorting, as the arrangement in the heteroleptic species would always lead to a helical conflict, coming at high energy costs.[32]

The self-sorting between **LTV** and **DTV** was first considered. Reacting a mixture of the enantiomeric tripodal pseudopeptides with **A** could produce either homochiral (homo-self-sorting) or heterochiral (hetero-self-sorting) macrobicycles (Figure 8.6).[73,74]
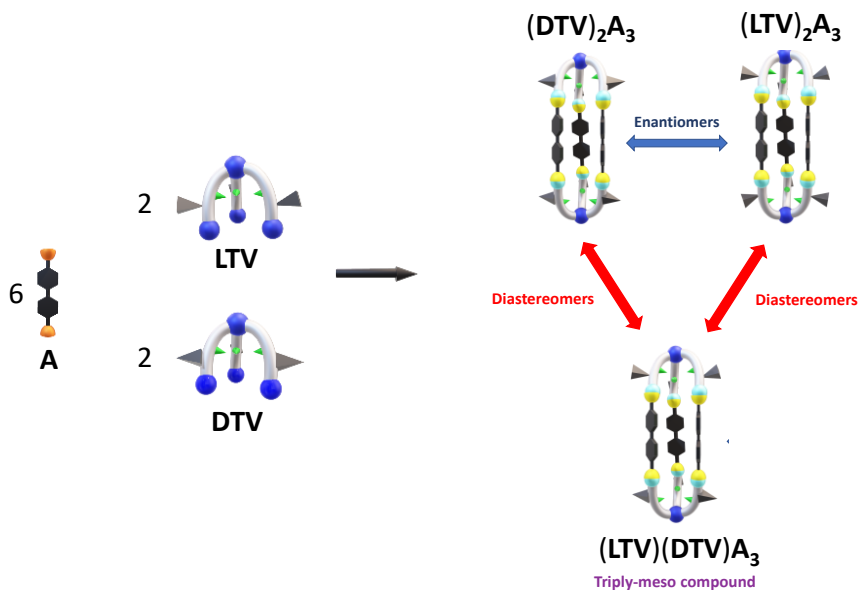
Figure 8.6. Self-sorting experiment between **LTV** and **DTV** using **A** as the dialdehyde, leading to two homoleptic/homochiral enantiomers **(DTV)$_2$A$_3$**, **(LTV)$_2$A$_3$** and a heteroleptic/heterochiral triply-meso diastereomer **(LTV)(DTV)A$_3$**. Reaction conditions: CDCl$_3$, 25 ºC, 3 mM **LTV**, 3 mM **DTV**, 9 mM **A.**

The heterochiral **(LTV)(DTV)A₃** assembly represents the unusual case of a triple stranded meso structure, diastereomeric with respect to the homochiral assemblies. It must be noted that ^{1}H NMR spectroscopy can only quantify the homochiral/heterochiral ratio, namely $(\mathbf{(LTV)_2A_3} + \mathbf{(DTV)_2A_3}) / \mathbf{(LTV)(DTV)A_3}$. ^{1}H NMR spectra for the reaction mixture at different times (Figure S8.17) allowed identifying new signals assignable to the heterochiral cage. After 19 h of reaction, a product distribution of 59 : 41 (homochiral : heterochiral) was determined, the homochiral being favoured. Thereafter, a progressive decrease in the concentration of the heterochiral species was observed over time (Figure S8.18). After 13 days at room temperature, the heterochiral cage was still present in the reaction mixture, with a 90 : 10 homo- to heterochiral ratio. HRMS analyses corroborated that the major compounds during the rearrangement were the homochiral/heterochiral cages of same mass, being the three components characterised by m/z peaks at 1410.9 and 705.4 m/z, for $[M+H]^+$ and $[M+2H]^{2+}$ respectively (Figure S8.19). Carrying out the experiment in the presence of 10 mol% of TFA resulted in a ca. 2.6 times faster homochiral self-sorting, as the redistribution was catalysed by the acid (Figure S8.20).

Interestingly, one of the signals assigned to the aromatic protons of the biphenyl groups of the heterochiral cages did not show the characteristic δ shift observed in homochiral cryptands (compare B and B' signals in Figure S8.21). This suggests that the heterochiral species does not induce a helical twisting with π-π stacking as a result of the opposite twisting preference of the heterochiral (**LTV**) and (**DTV**) lids. The self-sorting process should be even more efficient between **LTF** and **DTF**, as these phenylalanine-derived macrobicycles presented a more pronounced helical conformation due to the additional π-interactions with the aromatic sidechains. In agreement with this hypothesis, when reacting a **LTF** : **DTF** : **A** mixture (2 : 2 : 6 equivalents respectively) the evolution of the peaks for the different species showed a significantly faster rearrangement, shifting from an initial 60 : 40 homochiral : heterochiral distribution to the final 96 : 4 distribution in less than 3 days (Figure S8.22).

DFT calculations for the homochiral and heterochiral macrobicylic cages were carried out to estimate energy differences for valine and phenylalanine derivatives. All conformation optimizations were calculated for the isolated molecules, providing endergonic formation energies for the cryptands (Figure 8.7a). Energy diagrams for the isolated compounds do not agree with experimental results, as, for instance, the heterochiral cage was calculated to be almost 10 kcal/mol more stable for the valine cryptand. However, taking into account the observed binding of water molecules inside the cavity of the ditopic cryptand cage, the energies for the most stable conformation of the macrobicycles were calculated with two molecules of water encapsulated within the hydrophilic pockets (Figure 8.7b).
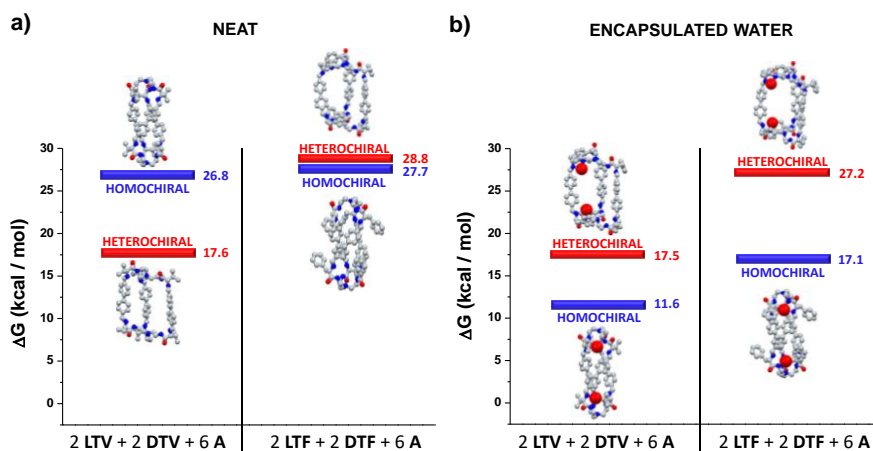
Figure 8.7. Most stable conformation (DFT, B3LYP, LANL2DZ, Gaussian09) for the homochiral and heterochiral cryptands a) in the absence and b) in the presence of two water molecules. Free energies (kcal/mol) have been calculated from the formation energies of the reaction components. See computational section in supplemental information for more details.

The trapped water molecules were clearly stabilizing the homochiral cages, decreasing their energy by 15.2 and 10.6 kcal/mol for **(LTV)$_2$A$_3$** and **(LTF)$_2$A$_3$**, respectively. This stabilization was much lower for the heterochiral cage, in which the weaker host-guest noncovalent interactions barely modified the initial energy (< 2 kcal/mol). This role of the water molecules was confirmed by ^{1}H NMR experiments, revealing a significant shift towards higher δ values of the water signal

as the system underwent the heterochiral to homochiral change (Figure S8.23). It must be noted that the encapsulation of water seemed more efficient for the valine cryptand, $\Delta\delta_{H2O}$ = +1.1 ppm for **(LTV)$_2$A$_3$** and +0.35 ppm for **(LTF)$_2$A$_3$**, which correlates well with the energy reduction estimated upon water binding.

The energy differences between the homochiral and heterochiral cages in the presence of water were of 5.9 and 10.1 kcal/mol for the valine and phenylalanine macrobicycles respectively. These values are in agreement with the self-sorting experiments for the systems, revealing a higher predominance of the homochiral cage -under the same conditions- for the phenylalanine derivative (Figures S8.18 and S8.22). These results indicate that the encapsulation of water played a crucial role in the self-sorting outcome, showcasing a non-biological example of the role of water in shaping sophisticated tertiary and quaternary structures found in proteins.[75]

The former results highlight the key role of the side chain of the constituent amino acid in these processes. The efficient encapsulation of H_2O can be associated to the hydrophobicity of the side chains in Val and Phe derivatives. The higher efficiency observed for Val can reflect the higher hydropathy of its side chain.[76] It must be noted, besides, that the folding of the benzyl group to maximize the aromatic-aromatic interactions leads to a less efficient hydrophobic shielding of the pseudopeptidic fragment interacting with the water molecule in **XTF$_2$A$_3$** and can also disturb the hydrogen bond interactions associated to this encapsulation. Hence, the strong hydrophobic surface of **XTV$_2$A$_3$** enhances water encapsulation and, thus, homo-chiral self-sorting. In agreement with this, experiments carried out with glycine (less hydrophobic and lacking chirality) and tryptophane (significantly more hydrophilic)[76] did not produce in an efficient way the desired molecular cages (only complex mixtures of products were obtained).

Considering this effective chiral self-sorting, one may surmise that the same pronounced helical twisting induced by the chiral centers could also affect the self-sorting of two tripodal pseudopeptides with different sidechains and opposite chirality. When components **LTV**, **DTF** and **A** were mixed in a 2 : 2 : 6 ratio in

CDCl$_3$, the self-sorting of the system was clearly apparent in the ^{1}H NMR spectra. Figure 8.8 shows the evolution of the spectra over time, with the formation of both **(LTV)$_2$A$_3$** and **(DTF)$_2$A$_3$**. In excellent accordance with the kinetic preferences of **LTV** over **DTF**, the **(LTV)$_2$A$_3$** macrobicycle was formed earlier than its phenylalanine analogue. The spectrum of the reaction outcome after 3 days was a superimposition of the spectra from the individual reactions for the preparation of the homoleptic/homochiral cryptands under similar experimental conditions, revealing the absence of heteroleptic cage **(LTV)(DTF)A$_3$**. This efficient self-recognition process was confirmed by HRMS analysis, observing that after 78 h the two major products were the homoleptic cages, with only traces of the heteroleptic species detected (Figure S8.24).
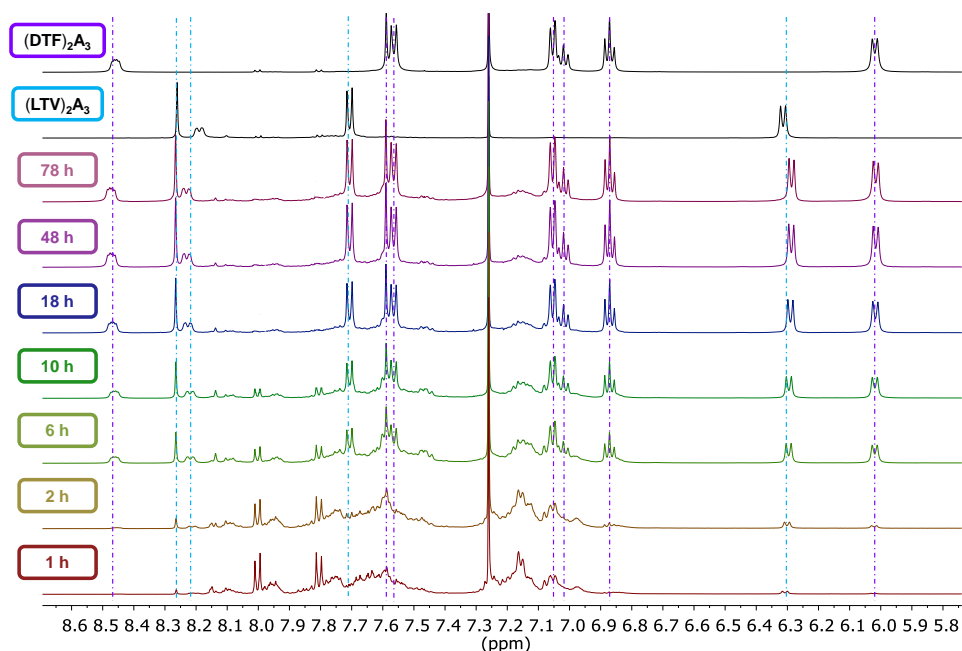
Figure 8.8. Partial ^{1}H NMR (500 MHz, CDCl$_3$, 25 ºC) spectra for the self-sorting experiment at different times. Reagents: **LTV**, **DTF** and **A** (3 mM, 3 mM and 9 mM, respectively). The two black spectra on top correspond to the pure macrobicycles (1.5 mM each), highlighting the signals for **(LTV)$_2$A$_3$** (blue lines) and **(DTF)$_2$A$_3$** (purple lines).

The intramolecular noncovalent forces, and thus the helical chirality of the architecture, appear to be responsible for reaching such high-fidelity self-sorting.

Performing the process with the alternative mixture of compounds, namely **DTV** : **LTF** : **A** reacting in a 2 : 2 : 6 ratio, resulted as expected in the same homo-self-sorting, with the spectrum of the final reaction mixture being a superimposition of **(DTV)₂A₃** and **(LTF)₂A₃**. Therefore, the intrinsic chirality of the secondary structure was able to promote excellent selectivities in the self-sorting between components. As evidence of chirality driven self-recognition, when all four tripodal reagents were mixed in the presence of **A** in a 2 : 2 : 2 : 2 : 12 ratio (**LTV** : **DTV** : **LTF** : **DTF** : **A**), the statistical distribution previously observed for the sidechain self-sorting experiment (see for instance Figure 8.5) was obtained (Figure S8.25). Hence, the system was able to perform chirality self-sorting towards homochiral compounds but did not distinguish between the sidechains of the valine or phenylalanine derived species.

8.1.5.   Conclusions

In conclusion, the work presented herein describes the efficient synthesis of novel chiral pseudopeptidic macrobicycles. Whereas products of polymeric nature are favoured in polar solvents, the cage structure is obtained in almost quantitative yields in homogeneous solution where equilibrium can be achieved. This high efficiency is due to a large extent to the positive template effect of water molecules bound in the three-dimensional cavities formed by the tripodal capsules at each end of the macrobicyclic structure, as revealed in the solid state by radiocrystallography and ¹H NMR spectroscopy. The present pseudopeptidic cages display helical chirality and a preorganized cavity for molecular recognition of polar substrates in hydrophobic media, adding value to their straightforward synthesis via imine condensation.

The pseudopeptidic dynamic library responded primarily to chirality features, as high-fidelity chiral homo-self-sorting was achieved for the mixtures. Such fidelity is remarkable for such complex multicomponent systems made up from purely organic building blocks that differ in chirality, with structures presenting similar binding sites.

The encapsulation of discrete water molecules appears to be the main driving force for this error-checking process, thus stressing the role of the aqueous medium in the formation efficiency and selectivity as well as in the determination of structural features of complex three-dimensional architectures in biomolecules.

8.1.6.   References

1- Yu, J.; Qi, D.; Li, J. Design, synthesis and applications of responsive macrocycles. *Commun Chem.* **2020**, *3*, Article number: 189.

2- Pinalli, R.; Pedrini, A.; Dalcanale, E. Biochemical sensing with macrocyclic receptors. *Chem. Soc. Rev.* **2018**, *47*, 7006-7026.

3- Marsault, E.; Peterson, M. L. Macrocycles Are Great Cycles: Applications, Opportunities, and Challenges of Synthetic Macrocycles in Drug Discovery. *J. Med. Chem.* **2011**, *54*, 7, 1961–2004.

4- Dietrich, B.; Viout, P.; Lehn, J.-M. *Macrocyclic Chemistry: Aspects of Organic and Inorganic Supramolecular Chemistry*, VCH: 1993.

5- Yang, J.-M.; Yu, Y.; Rebek Jr, J. Selective Macrocycle Formation in Cavitands. *J. Am. Chem. Soc.* **2021**, *143*, 2190–2193.

6- Martí-Centelles, V.; Pandey, M. D.; Burguete, M. I.; Luis, S. V. Macrocyclization Reactions: The Importance of Conformational, Configurational, and Template-Induced Preorganization. *Chem. Rev.* **2015**, *115*, 8736–8834.

7- Vilar, R. Anion Templates in Synthesis and Dynamic Combinatorial Libraries. *Struct. Bonding* **2008**, 129, 175–206.

8- Rossa, L.; Vögtle, F. Synthesis of Medio- And Macrocyclic Compounds By High Dilution Principle Techniques. In *Cyclophanes I. Topics in Current Chemistry*, Vol. 113; Vögtle, F., Ed.; Springer: Berlin, Heidelberg, 1983.

9- Lei, Y.; Chen, Q.; Liu, P.; Wang, L.; Wang, H.; Li, B.; Lu, X.; Chen, Z.; Pan, Y.; Huang, F.; Li, H. Molecular Cages Self-Assembled by Imine Condensation in Water. *Angew. Chem. Int. Ed.* **2021**, *60*, 4705–4711.

10- Abet, V.; Szczypinski, F. T.; Little, M. A.; Santolini, V.; Jones, C. D.; Evans, R.; Wilson, C.; Wu, X.; Thorne, M. F.; Bennison, M. J.; Cui, P.; Cooper, A. I.; Jelfs, K.

E.; Slater, A. G. Inducing Social Self-Sorting in Organic Cages To Tune The Shape of The Internal Cavity. *Angew. Chem. Int. Ed.* **2020**, *59*, 16755–16763.

11- Komáromy, D.; Nowak, P.; Otto, S. *Dynamic Covalent Chemistry: Principles, Reactions and Applications*. Wiley: 2017.

12- McKee, V.; Nelson, J.; Town, R. M. Caged oxoanions. *Chem. Soc. Rev.* **2003**, *32*, 309-325.

13- McDowell, D.; Nelson, J.; McKee, V. A furan-derived schiff-base crypt and incorporating the trans,trans dicarbimine link. *Polyhedron* **1989**, *8*, 1143-1145.

14- Jazwinski, J.; Lehn, J.-M.; Lilienbaum, D.; Ziessel, R.; Guilhem, J.; Pascard, C. Polyaza Macrobicyclic Cryptands: Synthesis, Crystal Structures of a Cyclophane Type Macrobicyclic Cryptand and of its Dinuclear Copper(i) Cryptate, and Anion Binding Features. *J. Chem. Soc., Chem. Commun.* **1987**, 1691-1694.

15- Yang, Z.; Lehn, J.-M. Dynamic Covalent Self-Sorting and Kinetic Switching Processes in Two Cyclic Orders: Macrocycles and Macrobicyclic Cages. *J. Am. Chem. Soc.* **2020**, *142*, 15137−15145.

16- Greenaway, R. L.; Santolini, V.; Szczypiński, F. T.; Bennison, M. J.; Little, M.; Marsh, A.; Jelfs, K. E.; Cooper, A. I. Organic Cage Dumbbells. *Chem. Eur. J.* **2020**, *26*, 3718−3722.

17- Kolodziejski, M.; Stefankiewicz, A. R.; Lehn, J.-M. Dynamic Polyimine Macrobicyclic Cryptands − Self-Sorting with Component Selection. *Chem. Sci.* **2019**, *10*, 1836−1843.

18- Vantomme, G.; Lehn, J.-M. Reversible Adaptation to Photoinduced Shape Switching by Oligomer-Macrocycle Interconversion with Component Selection in a Three-State Constitutional Dynamic System. *Chem. Eur. J.* **2014**, *20*, 16188−16193.

19- Acharyya, K.; Mukherjee, S.; Mukherjee, P. S. Molecular Marriage through Partner Preferences in Covalent Cage Formation and Cage-to-Cage Transformation. *J. Am. Chem. Soc.* **2013**, *135*, 554− 557.

20- Ayme, J.-F.; Lehn, J.-M.; Bailly, C.; Karmazin, L. Simultaneous Generation of a [2 × 2] Grid-Like Complex and Linear Double Helicate: a Three-Level Self-Sorting Process. *J. Am. Chem. Soc.* **2020***, 142,* 5819−5824.

21- Roberts, D. A.; Pilgrim, B. S.; Nitschke, J. R. Covalent Post-Assembly Modification in Metallosupramolecular Chemistry. *Chem. Soc. Rev.* **2018**, *47*, 626−644.

22- Wood, C. S.; Ronson, T. K.; Belenguer, A. M.; Holstein, J. J.; Nitschke, J. R. Two-Stage Directed Self-Assembly of a Cyclic [3]catenane. *Nat. Chem.* **2015**, *7*, 354−358.

23- Beves, J. E.; Campbell, C. J.; Leigh, D. A.; Pritchard, R. G. Tetrameric Cyclic Double Helicates as a Scaffold for a Molecular Solomon Link. *Angew. Chem. Int. Ed.* **2013**, *52*, 6464−6467.

24- Uhlenheuer, D. A.; Petkau, K.; Brunsveld, L. Combining supramolecular chemistry with biology. *Chem. Soc. Rev.* **2010**, *39*, 2817-2826.

25- Safont-Sempere, M. M.; Fernández, G.; Würthner, F. Self-Sorting Phenomena in Complex Supramolecular Systems. *Chem. Rev.* **2011**, *111*, 5784-5814.

26- Levy, Y.; Onuchic, J. N. Water and proteins: A love-hate relationship. *Proc. Natl. Acad. Sci. U.S.A.* **2004**, *101*, 3325-3326.

27- Zhao, X.; Wang, H.; Li, B.; Zheng, B.; Yang, D.; Xu, W.; Li, X.; Yang, X.-J.; Wu, B. Narcissistic self-sorting in anion-coordination-driven assemblies. *Chem. Commun.* **2021**, *57*, 6078-6081.

28- Coubrough, H. M.; van der Lubbe, S. C. C.; Hetherington, K.; Minard, A.; Pask, C.; Howard, M.; Fonseca Guerra, J.C.; Wilson, A. J. Supramolecular Self-Sorting Networks using Hydrogen-Bonding Motifs. *Chem. Eur. J.* **2019**, *25*, 785–795.

29- Aratsu, K.; Prabhu, D. D.; Iwawaki, H.; Lin, X.; Yamauchi, M.; Karatsu, T.; Yagai, S. Self-sorting regioisomers through the hierarchical organization of hydrogen-bonded rosettes. *Chem. Commun.* **2016**, *52*, 8211-8214.

30- Wu, A.; Isaacs, L. Self-Sorting: The Exception or the Rule?. *J. Am. Chem. Soc.* **2003**, *125*, 4831-4835.

31- Chen, Y.; Qian, C.; Zhao, Q.; Cheng, M.; Dong, X.; Zhao, Y.; Jiang, J.; Wang, L. Adjustable chiral self-sorting and self-discriminating behaviour between diamond-like Tröger's base-linked cryptands. *Chem. Commun.* **2019**, *55*, 8072-8075.

32- Liu, M.; Zhang, L.; Wang, T. Supramolecular Chirality in Self-Assembled Systems. *Chem. Rev.* **2015**, *115*, 7304−7397.

33- Jedrzejewska, H.; Szumna, A. Making a Right or Left Choice: Chiral Self-Sorting as a Tool for the Formation of Discrete Complex Structures. *Chem. Rev.* **2017**, *117*, 4863−4899.

34- Brandt, J.; Salerno, F.; Fuchter, M. The added value of small-molecule chirality in technological applications. *Nat. Rev. Chem.* **2017**, *1*, 0045.

35- Luis, S. V.; Alfonso, I. Bioinspired Chemistry Based on Minimalistic Pseudopeptides. *Acc. Chem. Res.* **2014**, *47*, 112–124.

36- Solà, J.; Jimeno, C.; Alfonso, I. Exploiting complexity to implement function in chemical systems. *Chem. Commun.* **2020**, *56*, 13273-13286.

37- Martí, I.; Rubio, J.; Bolte, M.; Burguete, M. I.; Vicent, C.; Quesada, R.; Alfonso, I.; Luis, S. V. Tuning Chloride Binding, Encapsulation, and Transport by Peripheral Substitution of Pseudopeptidic Tripodal Small Cages. *Chem. Eur. J.* **2012**, *18*, 16728–16741.

38- Gorla, L.; Martí-Centelles, V.; Altava, B.; Burguete, M. I.; Luis, S. V. The role of the side chain in the conformational and self-assembly patterns of C_2-symmetric Val and Phe pseudopeptidic derivatives. *CrystEngComm* **2019**, *21*, 2398–2408.

39- Herschlag, D.; Pinney, M. M. Hydrogen Bonds: Simple after All?. *Biochemistry* **2018**, *57*, 3338−3352.

40- White, N. G.; Serpell, C. J.; Beer, P. D. Structural Study of Triazole and Amide Containing Anion-Templated Pseudorotaxanes. *Cryst. Growth Des.* **2014**, *14*, 3472-3479.

41- Alvarez, S. A cartography of the van der Waals territories. *Dalton Trans.* **2013**, *42*, 8617-8636.

42- Song, Z.; Fu, H.; Wang, R.; Pacheco, L. A.; Wang, X.; Lin, Y.; Cheng, J. Secondary structures in synthetic polypeptides from N-carboxyanhydrides: design, modulation, association, and material applications. *Chem. Soc. Rev.* **2018**, *47*, 7401-7425.

43- Davis, J. M.; Tsou, L. K.; Hamilton, A. D. Synthetic non-peptide mimetics of α-helices. *Chem. Soc. Rev.* **2007**, *36*, 326–334.

44- Belowich, M. E.; Stoddart, J. F. Dynamic imine chemistry. *Chem. Soc. Rev.* **2012**, *41*, 2003–2024.

45- Morris, K. F.; Johnson, C. S. Diffusion-ordered two-dimensional nuclear magnetic resonance spectroscopy. *J. Am. Chem. Soc.***1992**, *114*, 3139-3141.

46- Bru, M.; Alfonso, I.; Burguete, M. I.; Luis, S. V. Anion-Templated Syntheses of Pseudopeptidic Macrocycles. *Angew. Chem. Int. Ed.* **2006**, *45*, 6155–6159.

47- Curtis, N. F. Macrocyclic coordination compounds formed by condensation of metal-amine complexes with aliphatic carbonyl compounds. *Coord. Chem. Rev.* **1968**, *3*, 3-47.

48- Blackmond, D. G. Autocatalytic models for the origin of biological homochirality. *Chem. Rev.* **2020**, *120*, 4831–4847.

49- Bissette, A. J.; Fletcher, S. P. Mechanisms of autocatalysis. *Angew. Chem. Int. Ed.* **2013**, *52*, 12800–12826.

50- Jennings, W. B.; Farrell, B. M.; Malone, J. F. Attractive Intramolecular Edge-to-Face Aromatic Interactions in Flexible Organic Molecules, *Acc. Chem. Res.* **2001**, 34, 885–894.

51- Song, B.; Zhang, Z.; Wang, K.; Hsu, C.-H.; Bolarinwa, O.; Wang, J.; Li, Y.; Yin, G.-Q.; Rivera, E.; Yang, H.-B.; Liu, C.; Xu, B.; Li, X. Direct Self-Assembly of a 2D and 3D Star of David. *Angew. Chem. Int. Ed.* **2017**, *56*, 5258–5262.

52- Leigh, D. A.; Pritchard, R. G.; Stephens, A. J. A Star of David catenane. *Nat. Chem.* **2014**, *6*, 978-982.

53- Hasenknopf, B.; Lehn, J.-M.; Kneisel, B. O.; Baum, G.; Fenske, D. Self-Assembly of a Circular Double Helicate. *Angew.Chem. Int. Ed. Engl.* **1996**, *35*, 1838-1840.

54- Chen, Y.; Wu, G.; Chen, B.; Qu, H.; Jiao, T.; Li, Y.; Ge, C.; Zhang, C.; Liang, L.; Zeng, X.; Cao, X.; Wang, Q.; Li, H. Self-Assembly of a Purely Covalent Cage with Homochirality by Imine Formation in Water. *Angew. Chem. Int. Ed.* **2021**, *60*, 18815–18820.

55- Gidron, O.; Jirásek, M.; Trapp, N.; Ebert, M.-O.; Zhang, X.; Diederich, F. Homochiral [2]Catenane and Bis[2]catenane from Alleno-Acetylenic Helicates - A Highly Selective Narcissistic Self-Sorting Process. *J. Am. Chem. Soc.* **2015**, *137*, 12502-12505.

56- Kramer, R.; Lehn, J.-M.; De Cian, A.; Fischer, J. Self-Assembly, Structure, and Spontaneous Resolution of a Trinuclear Triple Helix from an Oligobipyridine Ligand and Ni" Ions. *Angew. Chem. Int. Ed. Engl.* **1993**, *32*, 703-706.

57- Shoulders, M. D.; Raines, R. T. Collagen structure and stability. *Annu. Rev. Biochem.* **2009**, *78*, 929–958.

58- Felsenfeld, G.; Davies, D. R.; Rich, A. Formation of a three-stranded polynucleotide molecule. *J. Am. Chem. Soc.* **1957**, *79*, 2023-2024.

59- Felsenfeld, G.; Rich, A. Studies on the formation of two- and three-stranded polyribonucleotides. *Biochim. Biophys. Acta* **1957**, *3*, 457-468.

60- Ranjbar, B.; Gill, P. Circular Dichroism Techniques: Biomolecular and Nanostructural Analyses- A Review. *Chem. Biol. Drug Des.* **2009**, *74*, 101−120.

61- Bulheller, B. M.; Miles, A. J.; Wallace, B. A.; Hirst, J. D. Charge-transfer transitions in the vacuum ultraviolet of protein circular dichroism spectra. *J. Phys. Chem. B* **2008**, *112*, 1866−1874.

62- Kelly, S. M.; Jess, T. J.; Price, N. C. How tostudy proteins by circular dichroism. *Biochim. Biophys. Acta* **2005**, *1751*, 119−139.

63- Holub, J.; Vantomme, G.; Lehn, J.-M. Training a Constitutional Dynamic Network for Effector Recognition: Storage, Recall, and Erasing of Information. *J. Am. Chem. Soc.* **2016**, *138*, 11783−11791.

64- Bru, M.; Alfonso, I.; Bolte, M.; Burguete, M. I.; Luis, S. V. Structurally disfavoured pseudopeptidic macrocycles through anion templation. *Chem. Commun.* **2011**, *47*, 283-285.

65- Beer, P. D.; Sambrook, M. R.; Curiel, D. Anion-templated assembly of interpenetrated and interlocked structures. *Chem. Commun.* **2006**, *20*, 2105–2117.

66- Howlader, P.; Ahmed, S.; Mukherjee, P. S. Guest-Induced Enantioselective Self-Assembly of a Pd6 Homochiral Octahedral Cage with a C3-Symmetric Pyridyl Donor. *J. Am. Chem. Soc.* **2020**, *142*, 20968-20972.

67- Wu, G.; Chen, Y.; Fang, S.; Tong, L.; Shen, L.; Ge, C.; Pan, Y.; Shi, X.; Li, H. Self-Assembled Cage for Wide-Scope Chiral Recognition in Water. *Angew. Chem. Int. Ed.* **2021**, *60*, 16594–16599.

68- Zarges, W.; Hall, J.; Lehn, J.-M.; Bolm, C. Helicity Induction in Helicate Self-Organisation from Chiral Tris(bipyridine) Ligand Strands. *Helv. Chim. Acta* **1991**, *74*, 1843-1852.

69- Yan, L.-L.; Tan, C.-H.; Zhang, G.-L.; Zhou, L.-P.; Bünzli, J.-C.; Sun, Q.-F. Stereocontrolled Self-Assembly and Self-Sorting of Luminescent Europium Tetrahedral Cages. *J. Am. Chem. Soc.* **2015**, *137*, 8550-8555.

70- Wang, J.; Zhao, H.; Chen, M.; Jiang, Z.; Wang, F.; Wang, G.; Li, K.; Zhang, Z.; Liu, D.; Jiang, Z.; Wang, P. Construction of Macromolecular Pinwheels Using Predesigned Metalloligands. *J. Am. Chem. Soc.* **2020**, *142*, 21691–21701.

71- Beaudoin, D.; Rominger, F.; Mastalerz, M. Chiral Self-Sorting of [2+3] Salicylimine Cage Compounds. *Angew. Chem. Int. Ed.* **2017**, *56*,1244–1248.

72- Shi, X.; Fettinger, J. C.; Cai, M.; Davis, J. T. Enantiomeric Self-Recognition: Cation-Templated Formation of Homochiral Isoguanosine Pentamers. *Angew. Chem., Int. Ed.* **2000**, *39*, 3124−3127.

73- Wang, X.; Peng, P.; Xuan, W.; Wang, Y.; Zhuang, Y.; Tian, Z.; Cao, X. Org. Narcissistic chiral self-sorting of molecular face-rotating polyhedra. *Biomol. Chem.* **2018**, *16*, 34–37.

74- Beuerle, F.; Klotzbach, S.; Dhara, A. Let's Sort It Out: Self-Sorting of Covalent Organic Cage Compounds. *Synlett* **2016**, *27*,1133–1138.

75- Ernst, J. A.; Clubb, R. L.; Zhou, H.-X.; Gronenborn, A. M.; Clore, G. M. Demonstration of Positionally Disordered Water Within a Protein Hydrophobic Cavity by NMR. *Science* **1995**, *267*, 1813-1817.

76- Kyte, J.; Doolittle, R. F. A Simple Method for Displaying the Hydropathic Character of a Protein. *J. Mol. Biol.* **1982**, *157*, 105-132.

77- Sheldrick, G. M. A short history of SHELX. *Acta Crystallogr., Sect. A: Found. Crystallogr.* **2008**, *64*, 112-122.

78- Sheldrick, G. M. Crystal structure refinement with SHELXL. *Acta Crystallogr., Sect. C: Struct. Chem.* **2015**, *71*,3-8.

79- Macrae, C. F.; Bruno, I. J.; Chisholm, J. A.; Edgington, P. R.; McCabe, P.; Pidcock, E.; Rodriguez-Monge, L.; Taylor, R.; van de Streek, J., Wood, P. A. Mercury

CSD 2.0 – new features for the visualization and investigation of crystal structures. *J. Appl. Crystallogr.* **2008**, *41*, 466-470.

80- Frisch, M. J.; Trucks, G. W.; Schlegel, H. B.; Scuseria, G. E.; Robb, M. A.; Cheeseman, J. R.; Scalmani, G.; Barone, V.; Mennucci, B.; Petersson, G. A.; *et al.* Gaussian 09, Revision B.01 (Gaussian, Inc), **2010**.

81- Becke, A. D. Density-functional thermochemistry. III. The role of exact exchange. *J. Chem. Phys.* **1993**, *98*, 5648-5652

82- Chiodo, S.; Sicilia, E. LANL2DZ basis sets recontracted in the framework of density functional theory. *J. Chem. Phys.* **2006**, *125*, Article number: 104107.

8.2. Supporting information
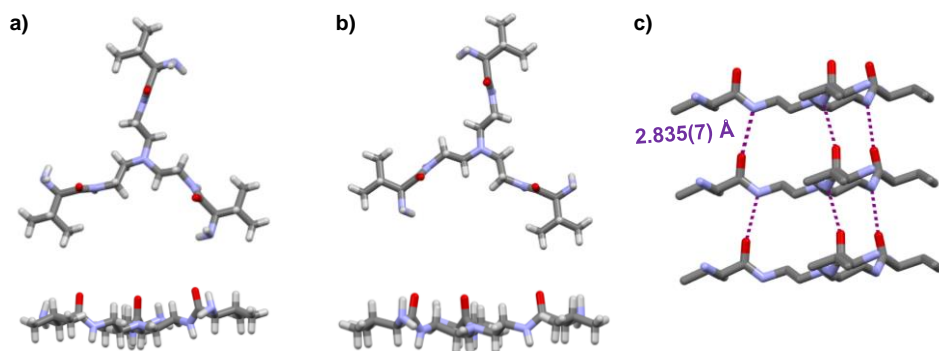
Figure S8.1. Solid state X-ray molecular structures of the valine-derived precursors. a) **DTV** [above: top view; below: side view]. b) **LTV** [above: top view; below: side view]. c) Packing diagram obtained for three vicinal **LTV** molecules. Hydrogen atoms have been omitted. Intermolecular HN···O=C hydrogen bonding and the corresponding N···O distance have been highlighted in purple. Atom colour code: red, O; blue, N; grey, C; white, H. Disordered water molecules have been omitted for clarity
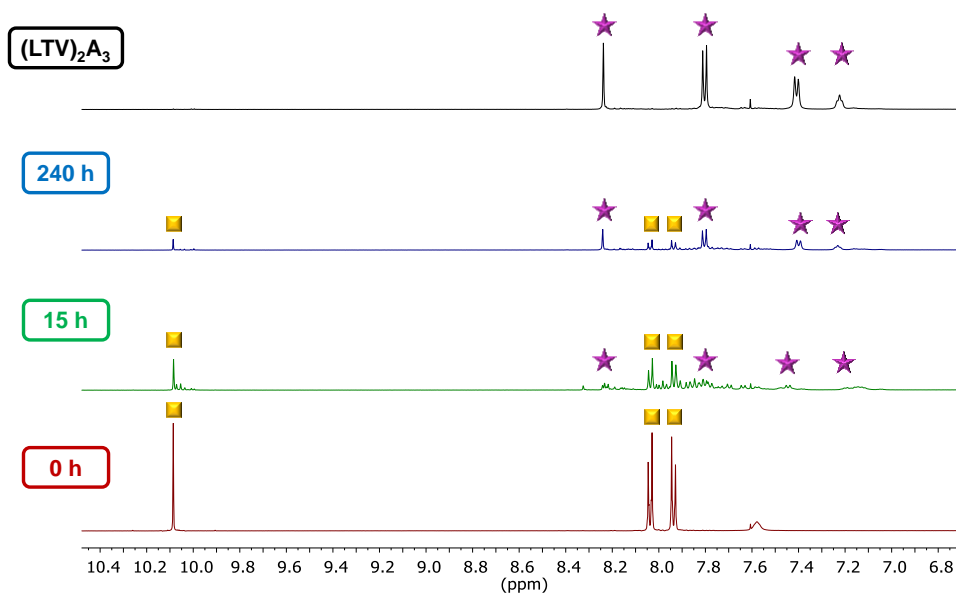
Figure S8.2. Partial ^{1}H NMR (500 MHz, CD$_3$CN, 25 °C) spectra for the condensation reaction between **LTV** (3 mM) and **A** (4.5 mM). The CH$_3$CN signal was used as internal standard for the experiment. The signals for **A** and **LTV** have been highlighted with orange squares and purple stars, respectively. The spectrum for pure (**LTV)$_2$A$_3$** (black spectrum) in CD$_3$CN (1.5 mM) has been included on top for comparison.
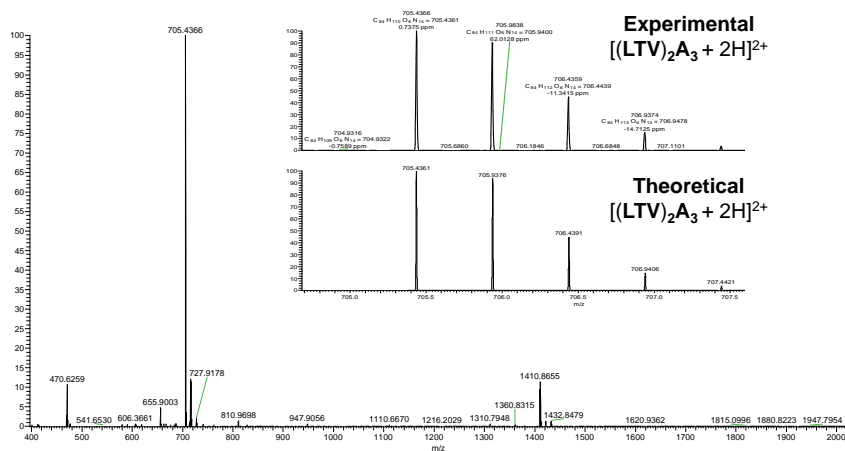
Figure S8.3 HRMS (CD$_3$CN, direct infusion) spectrum of the reaction crude after 4 days for the condensation between **LTV** and **A** (3 mM and 4.5 mM, respectively). The predicted and experimental isotopic patterns for the diprotonated [(**LTV**)$_2$**A**$_3$ + 2H]$^{2+}$ species have been included in the insets.
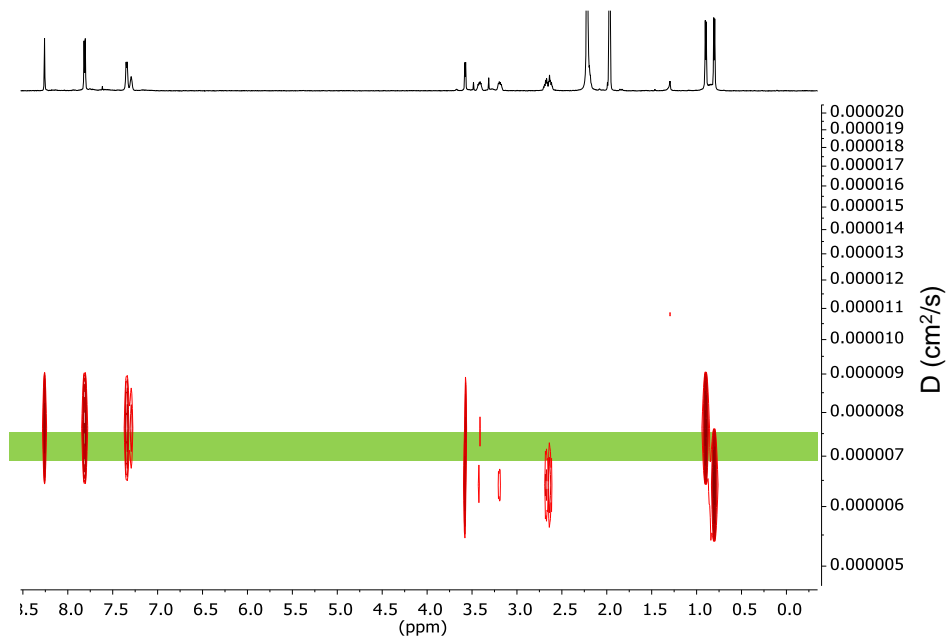
Figure S8.4. 2D DOSY (500 MHz, 25 ºC) experiment for (**LTV**)$_2$**A**$_3$ in CD$_3$CN (1.5 mM). The average diffusion coefficient obtained for the macrobicycle has been highlighted with a green bar.
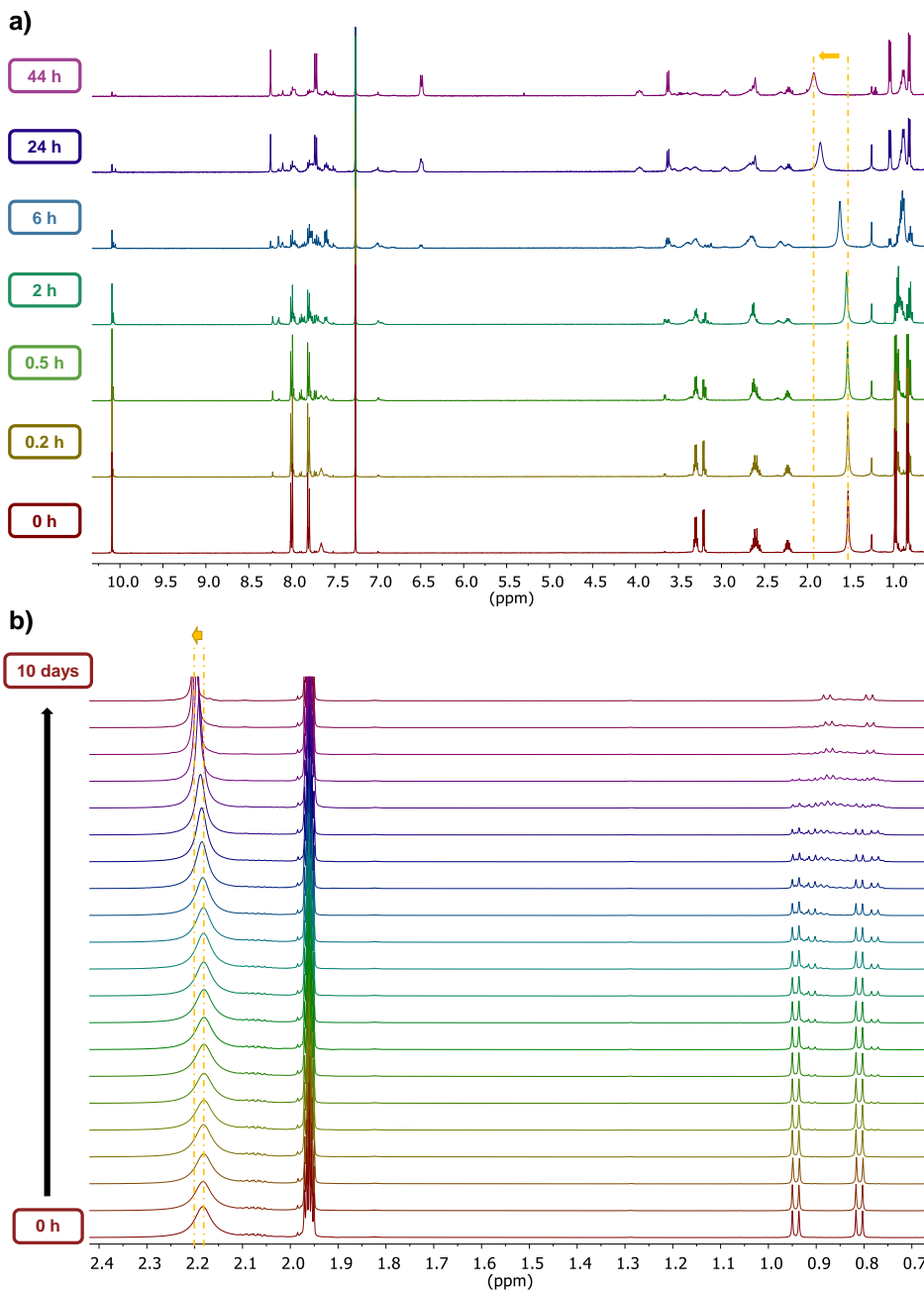
Figure S8.5. a) ^{1}H NMR (400 MHz, CDCl$_3$, 25 ºC) spectra for the condensation between **LTV** (3 mM) and **A** (4.5 mM). The CHCl$_3$ signal was used as internal standard for the experiment. The noteworthy shift (+0.4 ppm) for the water signal has been highlighted with an orange arrow. b) ^{1}H NMR (500 MHz, CD$_3$CN, 25 ºC) spectra for the condensation between **LTV** (3 mM) and **A** (4.5 mM). The modest shift (+0.02 ppm) for the water signal has been highlighted with an orange arrow.
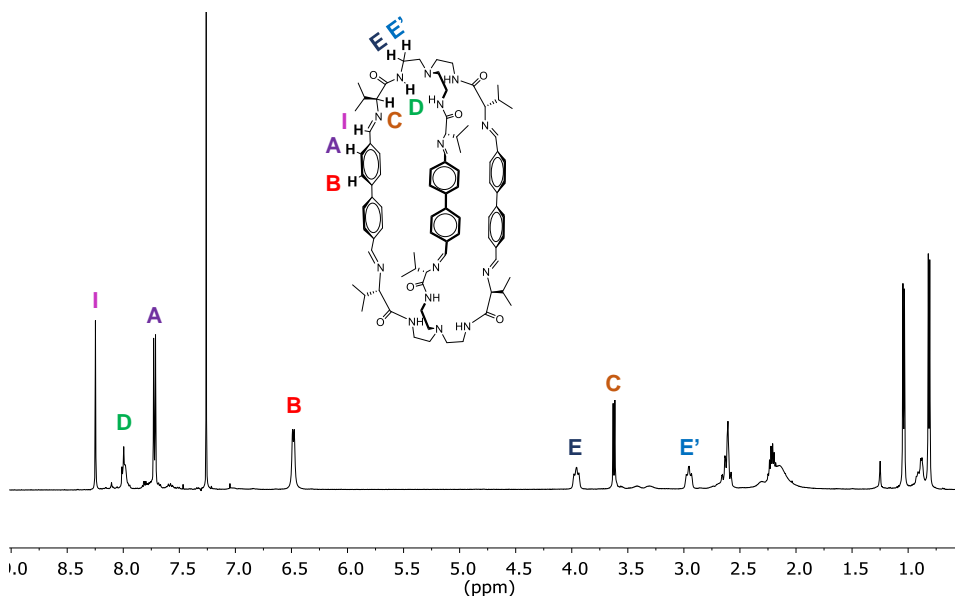
Figure S8.6. ¹H NMR (400 MHz, CDCl₃, 25 ºC) recorded for (**LTV**)₂**A₃** (1.5 mM). The most characteristic peaks for the symmetric macrobicycle have been highlighted with letters of different colours. These signals were assigned with the aid of 2D NMR spectra (see Figures S28-31).
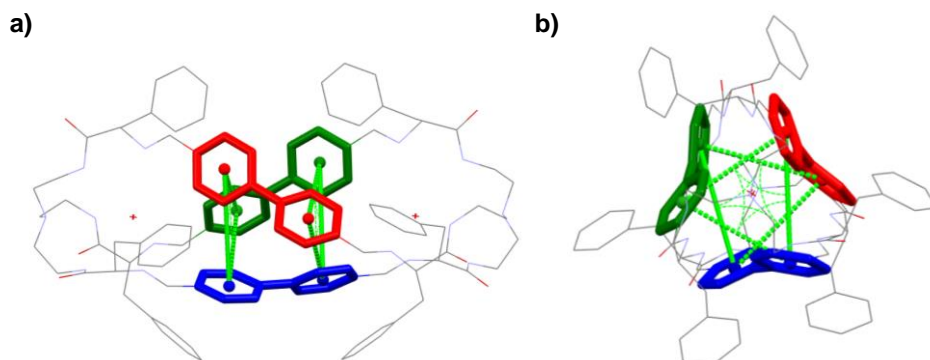
Figure S8.7. Wireframe representation of the solid-state structure found for (**LTF**)₂**A₃**. a) side-view and b) top-view of the cryptand. The biphenyl scaffolds (sticks model) for each bridging unit have been highlighted with differentiated colours. The centroids of the aromatic rings are represented with spheres of the colours of the corresponding ring. Angles and distances between centroids have been coloured in light green. Disorder, hydrogen atoms, and solvent molecules have been removed for clarity.
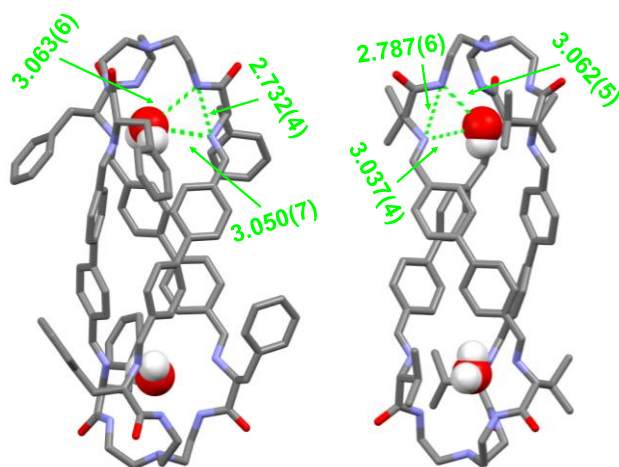
Figure S8.8. Stick representation of the water encapsulated within the cryptand cavity of (**LTF**)₂**A₃** (left) and (**LTV**)₂**A₃** (right). The water molecules are displayed using space fill mode. Hydrogen bond distances (N⋯O and N⋯N distances) have been highlighted in green. Disorder, solvent molecules, and non-essential hydrogen atoms have been emitted for clarity.
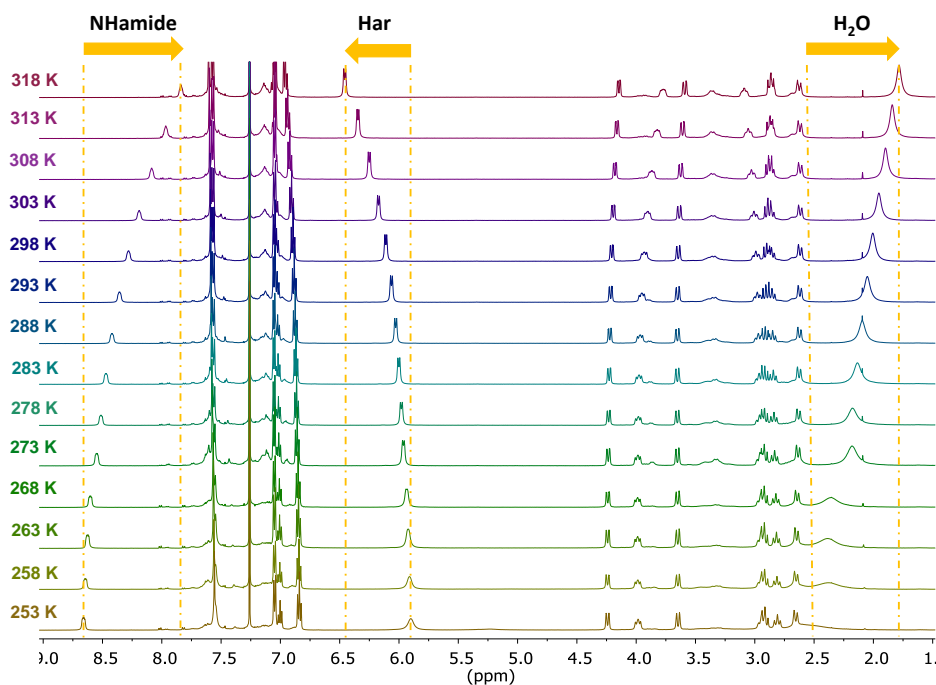
Figure S8.9. Variable temperature ¹H NMR (500 MHz, CDCl₃) for (**LTF**)₂**A₃** (3 mM). The shifts towards lower δ for water and amide, and towards higher lower δ for the aromatic signals have been highlighted with orange arrows.
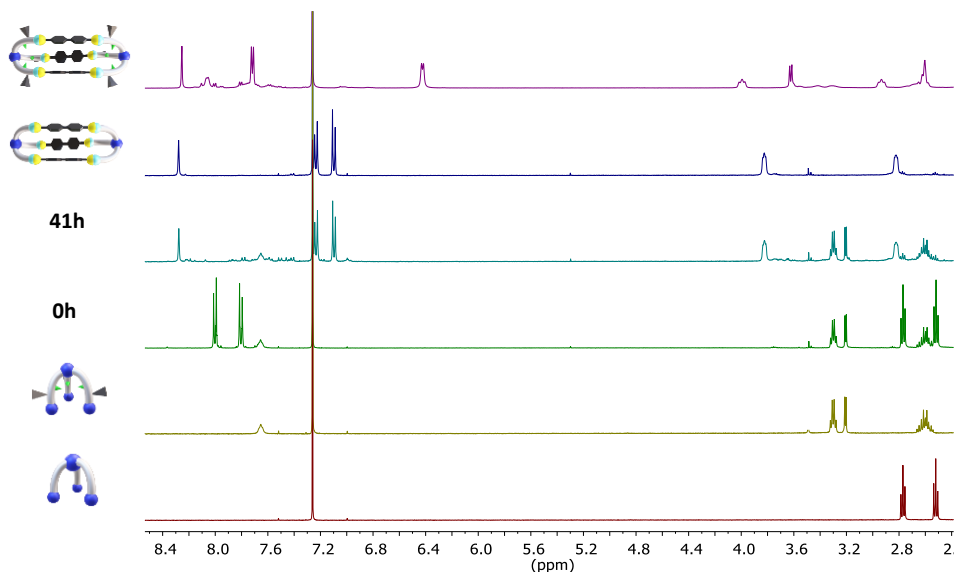
Figure S8.10. Partial ^{1}H NMR (400 MHz, CDCl$_3$, 25 °C) spectra for the different components (**T** in red, **LTV** in yellow, **T$_2$A$_3$** in dark blue and (**LTV**)$_2$**A$_3$** in purple) and the competition experiment NMR sample after mixing (green spectrum) and after 41 h of reaction (light blue spectrum). Competition experiment reaction conditions: 3 mM **LTV**, 3 mM **T**, 4.5Mm **A**, CDCl$_3$, 25 °C.
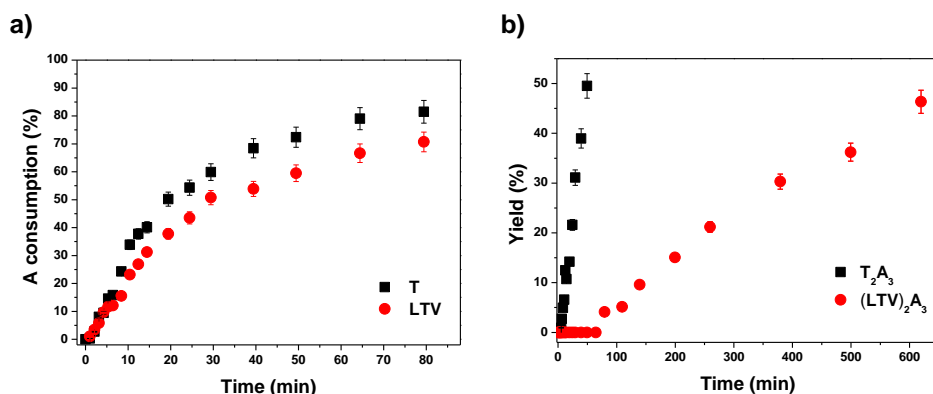
Figure S8.11. Kinetic profiles for the separated synthesis of **T$_2$A$_3$** (black squares) and (**LTV**)$_2$**A$_3$** (red circles). a) Consumption of **A**; b) formation of the respective cryptands up to 50% yields. Data determined by NMR integration. Reaction conditions: room temperature, 3 mM for **LTV** / **T** and 4.5 mM for **A** in CDCl$_3$ (25 °C).
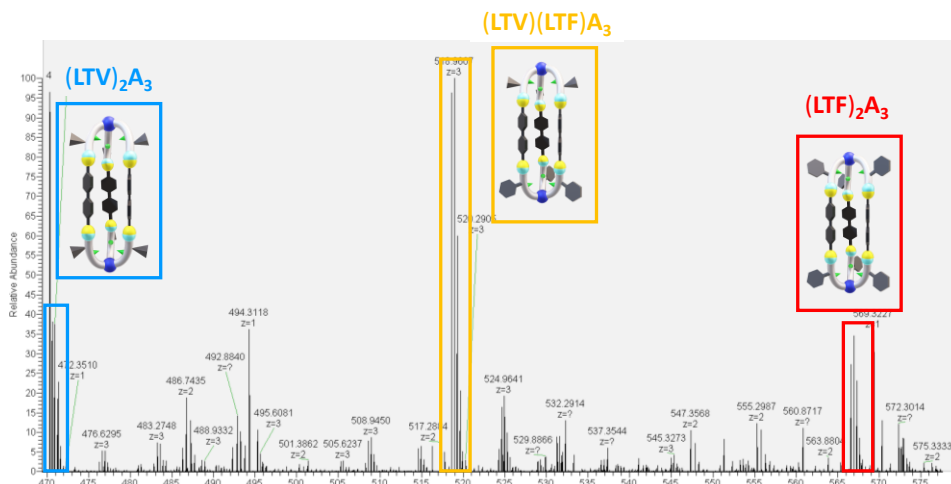
Figure S8.12. HRMS (range 470 – 580 m/z) spectrum for the self-sorting experiment between **LTV** : **LTF** : **A** (3 mM, 3 mM and 9 mM in CDCl$_3$, 25 ºC). The spectrum was recorded after 10 days of reaction, when the system had reached equilibrium. The peaks highlighted correspond to the triprotonated [cryptand + 3H]$^{3+}$ species. Colour legend: blue for the homoleptic (**LTV**)$_2$**A**$_3$, yellow for the heteroleptic (**LTV**)(**LTF**)**A**$_3$, and red for the homoleptic (**LTF**)$_2$**A**$_3$.
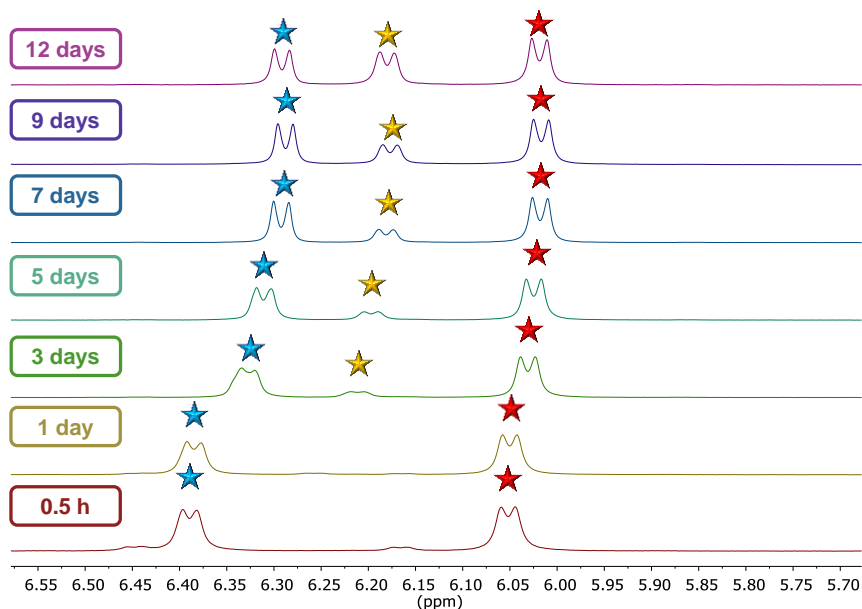
Figure S8.13. Partial ^{1}H NMR (500 MHz, CDCl$_3$, 25 ºC) spectra for the exchange experiment between (**LTV**)$_2$**A**$_3$ (blue star) and (**LTF**)$_2$**A**$_3$ (red star). The signal for the generated heteroleptic (**LTV**)(**LTF**)**A**$_3$ is highlighted with a yellow star. The initial concentration of the cryptands was of 1.5 mM for each homoleptic species. Red stars: (**LTF**)$_2$**A**$_3$. Blue stars: (**LTV**)$_2$**A**$_3$.
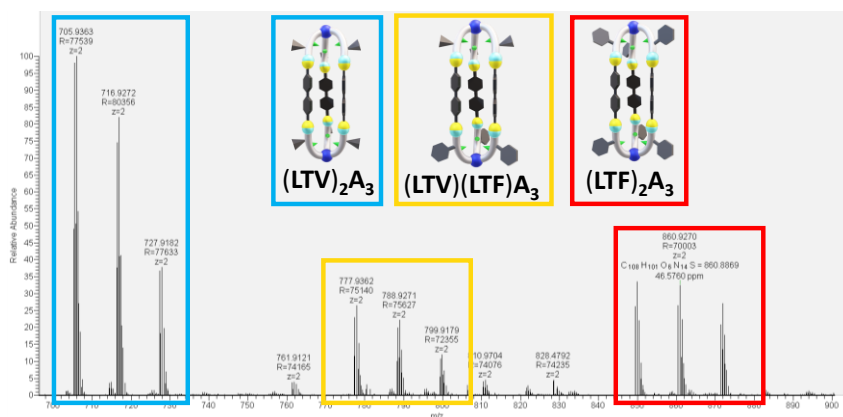
Figure S8.14. HRMS (range 700 – 900 m/z) for the exchange experiment between **(LTV)₂A₃** and **(LTF)₂A₃** (1.5 mM each in CDCl₃, 25 ºC). The spectrum was recorded after 12 days of reaction. The peaks highlighted correspond to the dicharged [cryptand + 2H]²⁺, [cryptand + H + Na]²⁺, and [cryptand + 2 Na]²⁺ species. Colour legend: blue for the homoleptic **(LTV)₂A₃,** yellow for the heteroleptic **(LTV)(LTF)A₃,** and red for the homoleptic **(LTF)₂A₃.**
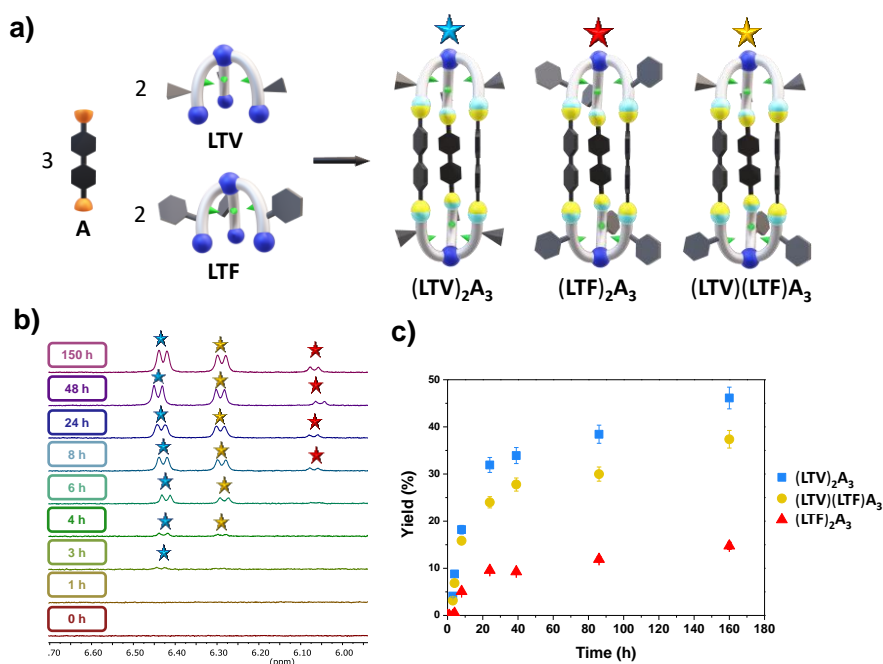
Figure 8.15. a) Representation of the competition experiment between **LTV**, **LTF** and **A** (3 mM, 3 mM and 4.5 mM respectively). Reaction conditions: CDCl₃, 25 ºC. b) Partial ¹H NMR (400 MHz, CDCl₃, 25 ºC) spectra for the competition experiment. The signals correspond to the aromatic protons of **(LTV)₂A₃** (blue stars), **(LTF)₂A₃** (red stars) and **(LTV)(LTF)A₃** (yellow stars). c) Yields for the desired cryptands, as determined by NMR integration.
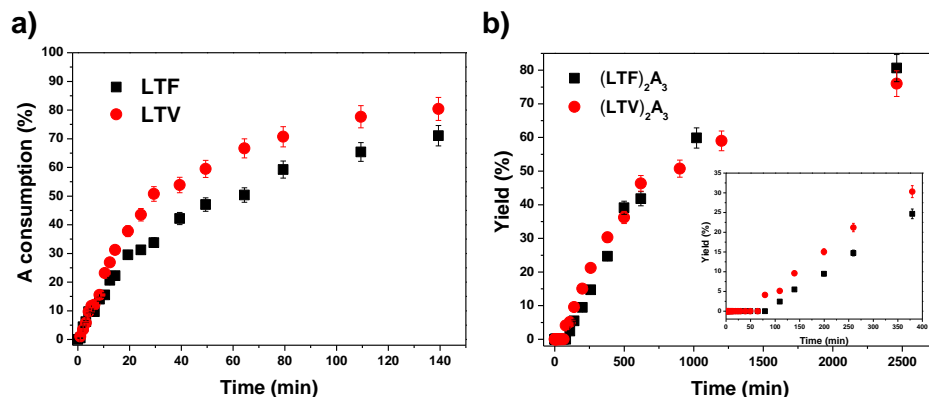
Figure S8.16. Kinetic profiles for the separated synthesis of (**LTF**)$_2$**A**$_3$ (black squares) and (**LTV**)$_2$**A**$_3$ (red circles). a) Consumption of **A**; b) formation of the cryptands (inset showing the experimental data at short reaction time 0-400 min). Data determined by NMR integration. Reaction conditions: room temperature, 3 mM for **LTV** / **LTF** and 4.5mM for **A** in CDCl$_3$.

Table S8.1. Results of the competition experiment between **LTV** and **LTF** in the presence of anions.

Effector	Temp. (ºC)[a]	Yield (LTV)$_2$A$_3$ (%)	Yield (LTV)(LTF)A$_3$ (%)	Yield (LTF)$_2$A$_3$ (%)
neat	25	47	38	15
	5	50	40	10
NBu$_4$Cl 3 mM	25	52	37	11
	5	58	34	8
NBu$_4$NO$_3$ 3 mM	25	58	33	9
	5	50	38	12

[a] Reaction conditions: 3 mM for **LTV** / **LTF** and 4.5 mM for **A** in CDCl3 for 8 days. Yields for the desired cryptands have been determined with NMR integration.
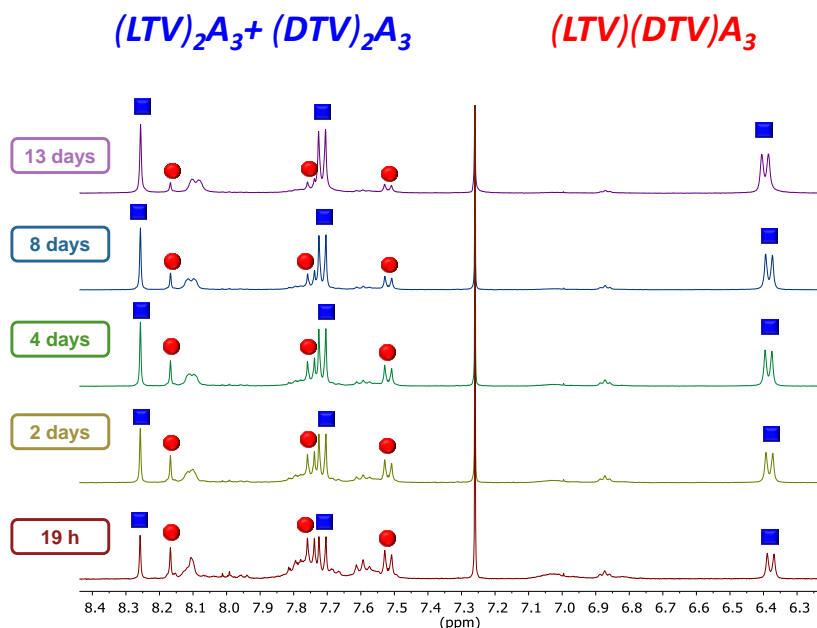
Figure S8.17. Partial ^{1}H NMR (400 MHz, CDCl$_3$, 25 °C) spectra for the valine-derived chiral self-sorting experiment. The signals corresponding to the mixture of homochiral cages (($\mathbf{LTV}$)$_2\mathbf{A_3}$ + ($\mathbf{DTV}$)$_2\mathbf{A_3}$) are marked with blue squares, and the ones for the heterochiral cage ($\mathbf{LTV}$)($\mathbf{DTV}$)$\mathbf{A_3}$ with red circles.
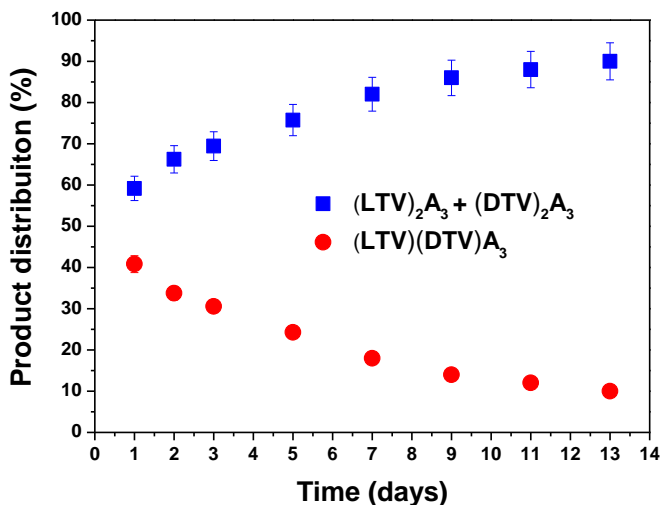
Figure S8.18. Product distribution evolution for the self-sorting experiment between $\mathbf{LTV}$ (3 mM), $\mathbf{DTV}$ (3 mM) and $\mathbf{A}$ (9 mM). Reaction conditions; CDCl$_3$, 25 °C. The values corresponding to the mixture of homochiral cages (($\mathbf{LTV}$)$_2\mathbf{A_3}$ + ($\mathbf{DTV}$)$_2\mathbf{A_3}$) are represented by blue squares, and the ones for the heterochiral cage ($\mathbf{LTV}$)($\mathbf{DTV}$)$\mathbf{A_3}$ by red circles. Product distribution determined by NMR integration.
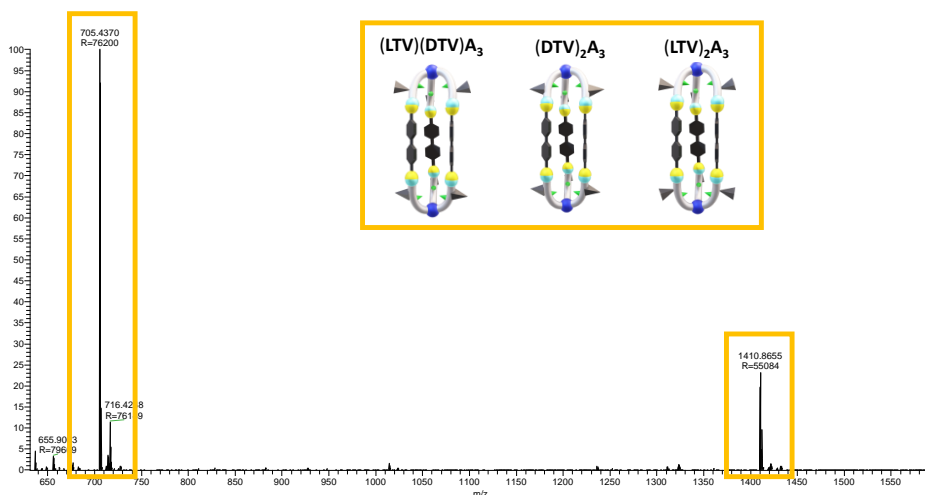
Figure S8.19. HRMS for the reaction crude after 3 days in the self-sorting experiment between **LTV** (3 mM), **DTV** (3 mM) and **A** (9 mM). Reaction conditions; CDCl₃, 25 ºC. The characteristic peaks of the equimassic cryptands ((**LTV**)$_2$**A**$_3$, (**DTV**)$_2$**A**$_3$, (**LTV**)(**DTV**)**A**$_3$) are highlighted in orange.
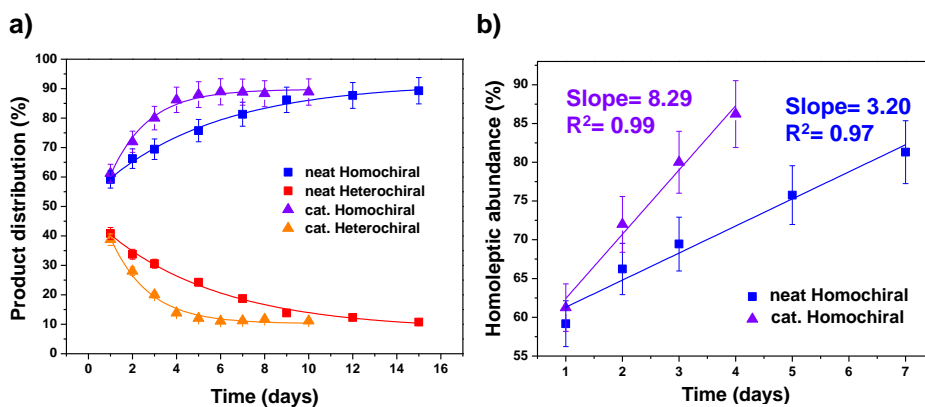
Figure S8.20. a) Product distribution comparison for the catalysed (10 mol% TFA) *vs.* uncatalysed self-sorting experiment between **LTV** (3 mM), **DTV** (3 mM) and **A** (9 mM). Reaction conditions; CDCl₃, 25 ºC. Uncatalysed: values corresponding to the mixture of homochiral cages ((**LTV**)$_2$**A**$_3$ + (**DTV**)$_2$**A**$_3$) are represented with blue squares, and the ones for the heterochiral cage (**LTV**)(**DTV**)**A**$_3$ with red squares. Catalysed: values corresponding to the mixture of homochiral cages ((**LTV**)$_2$**A**$_3$ + (**DTV**)$_2$**A**$_3$) are represented with purple triangles, and the ones for the heterochiral cage (**LTV**)(**DTV**)**A**$_3$ with orange triangles. b) Linear ranges for the homochiral abundance in the TFA catalysed (purple triangles) and uncatalysed (blue squares) self-sorting. Product distributions have been determined by NMR integration.
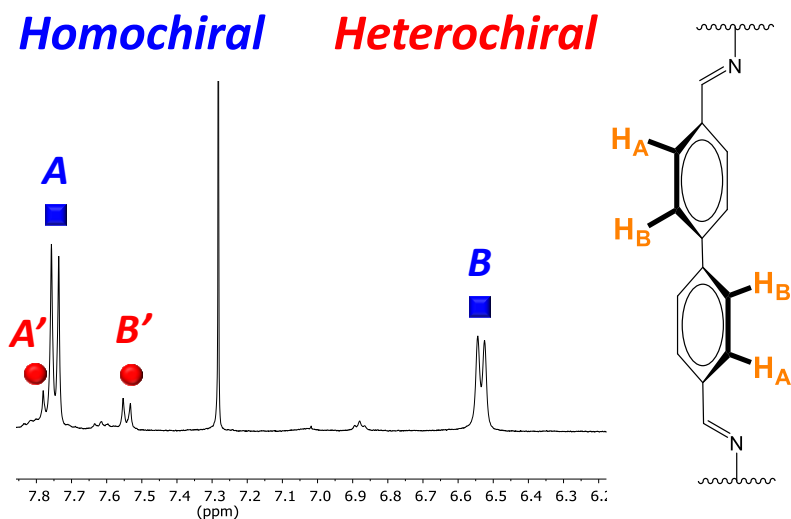
Figure S8.21. Partial ^{1}H NMR (400 MHz, CDCl$_3$, 25 °C) spectrum for the aromatic A and B protons of the bisphenyl bridges. The signals (A and B) corresponding to the homochiral cages (**LTV**)$_2$**A**$_3$ + (**DTV**)$_2$**A**$_3$ are marked with blue squares. The signals (A' and B') corresponding (**LTV**)(**DTV**)**A**$_3$ are marked with red circles.
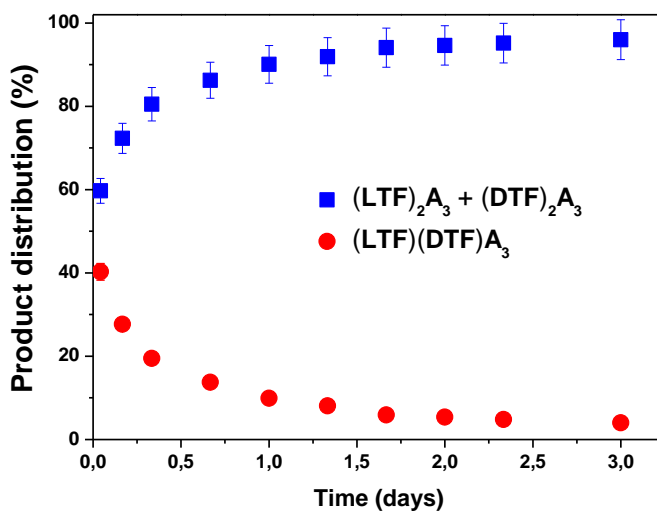
Figure S8.22. Product distribution evolution for the self-sorting experiment between **LTF** (3 mM), **DTF** (3 mM) and **A** (9 mM). Reaction conditions; CDCl$_3$, 25 °C. The values corresponding to the mixture of homochiral cages ((**LTF**)$_2$**A**$_3$ + (**DTF**)$_2$**A**$_3$) are represented with blue squares, and the ones for the heterochiral cage (**LTF**)(**DTF**)**A**$_3$ with red circles. Product distributions have been determined with NMR integration.

a) 2 **LTV** + 2 **DTV** + 6 **A**
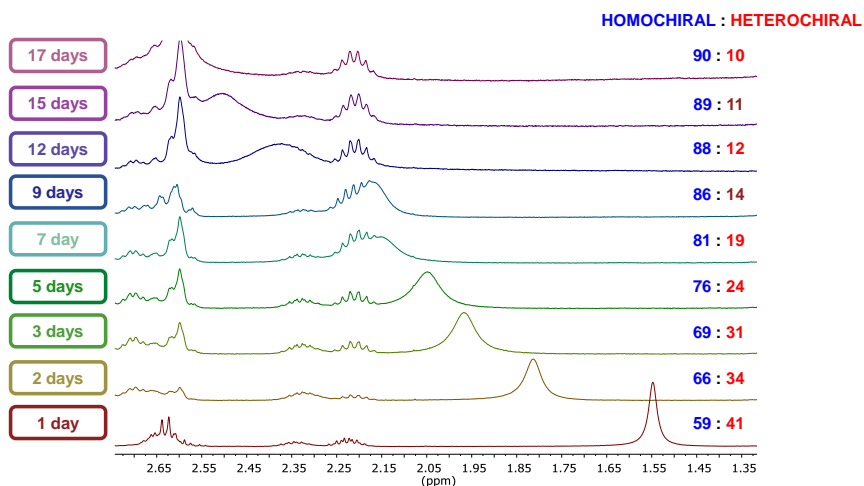
b) 2 **LTF** + 2 **DTF** + 6 **A**
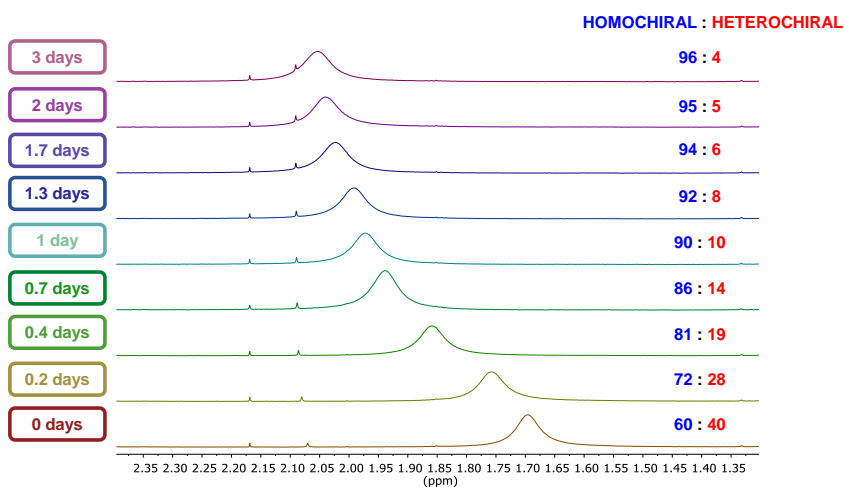
Figure S8.23. ^{1}H NMR partial spectra (400 MHz, CDCl$_3$, 25 °C) displaying the downfield shift experienced by water molecules in the chiral self-sorting experiment for a) **LTV** (3 mM) + **DTV** (3 mM) + **A** (9 mM), and b) **LTF** (3 mM) + **DTF** (3 mM) + **A** (9 mM).
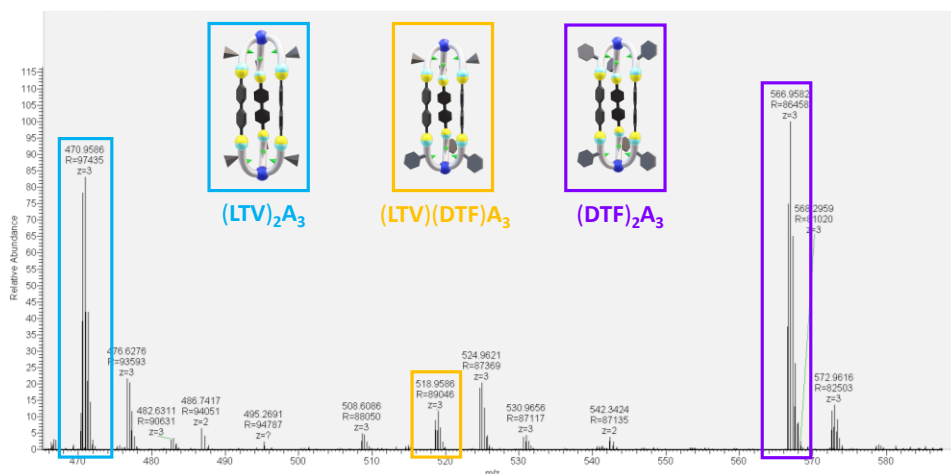
Figure S8.24. HRMS (range 460 – 600 m/z) spectrum for the reaction crude of the self-sorting experiment between **LTV**, **DTF** and **A** (3 mM, 3 mM and 9 mM, respectively, in CDCl$_3$, 25 ºC, 78 h). The peaks highlighted correspond to the tricharged [cryptand + 3H]$^{3+}$ species. Colour legend: blue for the homoleptic (**LTV**)$_2$**A**$_3$, yellow for the heteroleptic (**LTV**)(**DTF**)**A**$_3$ and purple for the homoleptic (**DTF**)$_2$**A**$_3$.
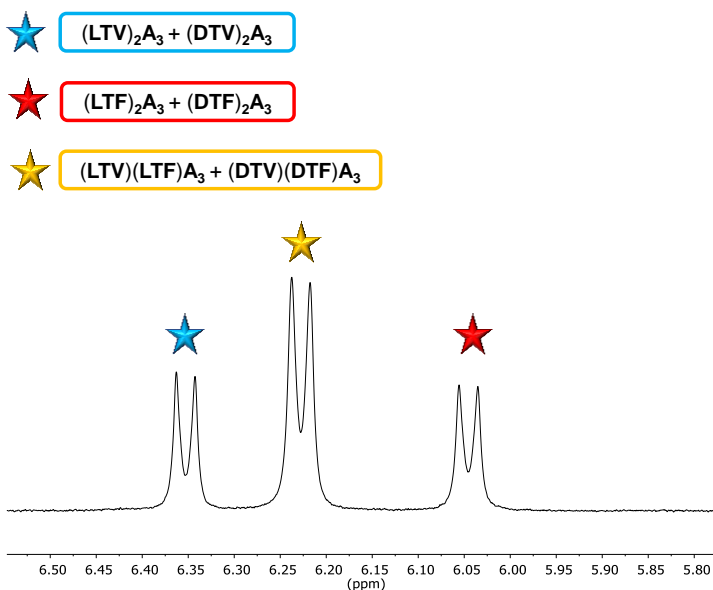
Figure S8.25. Partial ^{1}H NMR (400 MHz, CDCl$_3$, 25 ºC, 78 h) spectrum for the self-sorting experiment between **DTV** : **LTV** : **DTF** : **LTF** : **A** (2 : 2 : 2 : 2 : 12). The signals correspond to the aromatic protons of the enantiomeric pairs: (**LTV**)$_2$**A**$_3$ + (**DTV**)$_2$**A**$_3$ (blue stars), (**LTF**)$_2$**A**$_3$ + (**DTF**)$_2$**A**$_3$ (red stars) and (**LTV**)(**LTF**)**A**$_3$ + (**DTV**)(**DTF**)**A**$_3$ (yellow stars).
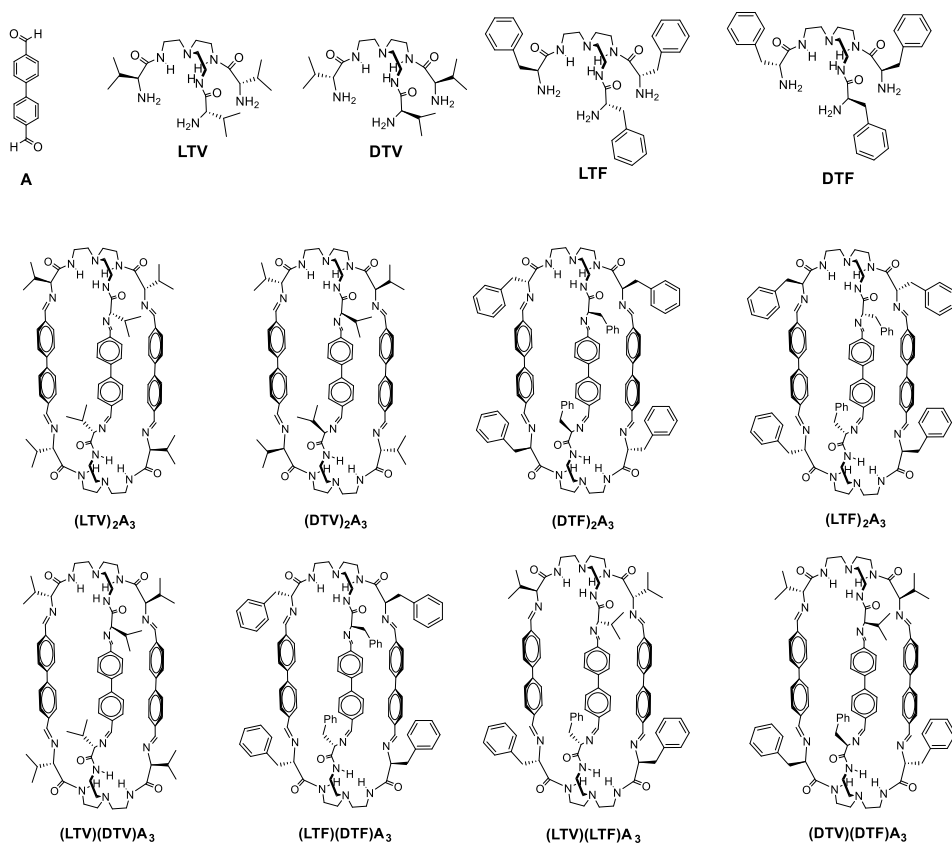
Figure S8.26. Aldehyde, amines and macrobicyclic cages that have been used in this work.
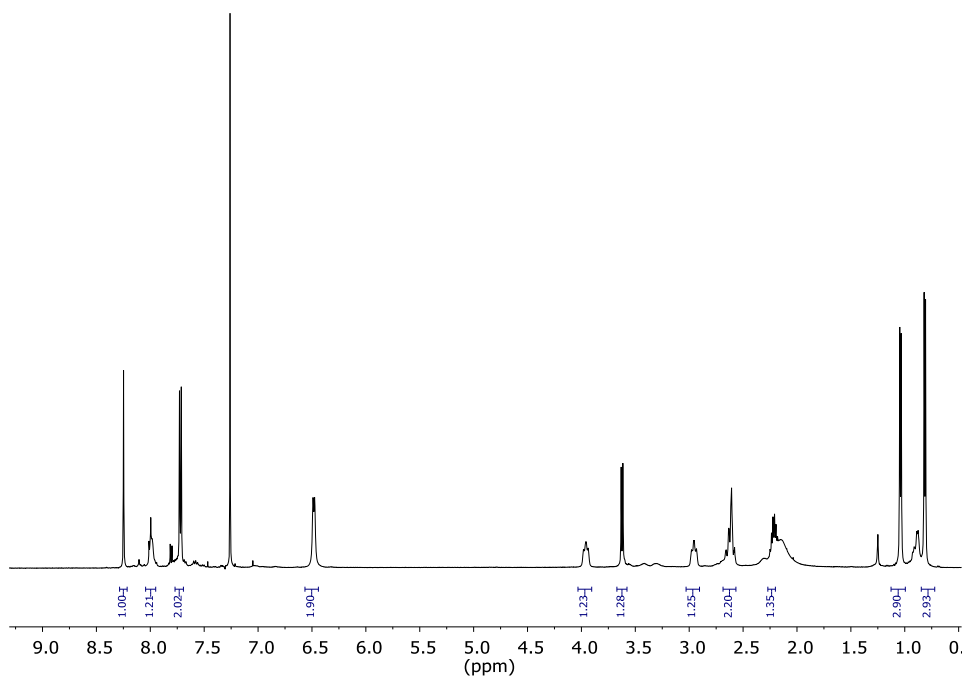
Figure S8.27. ^{1}H NMR (500 MHz, 25 ºC, CDCl$_3$) spectrum for **(LTV)$_2$A$_3$** / **(DTV)$_2$A$_3$** (1.5 mM).
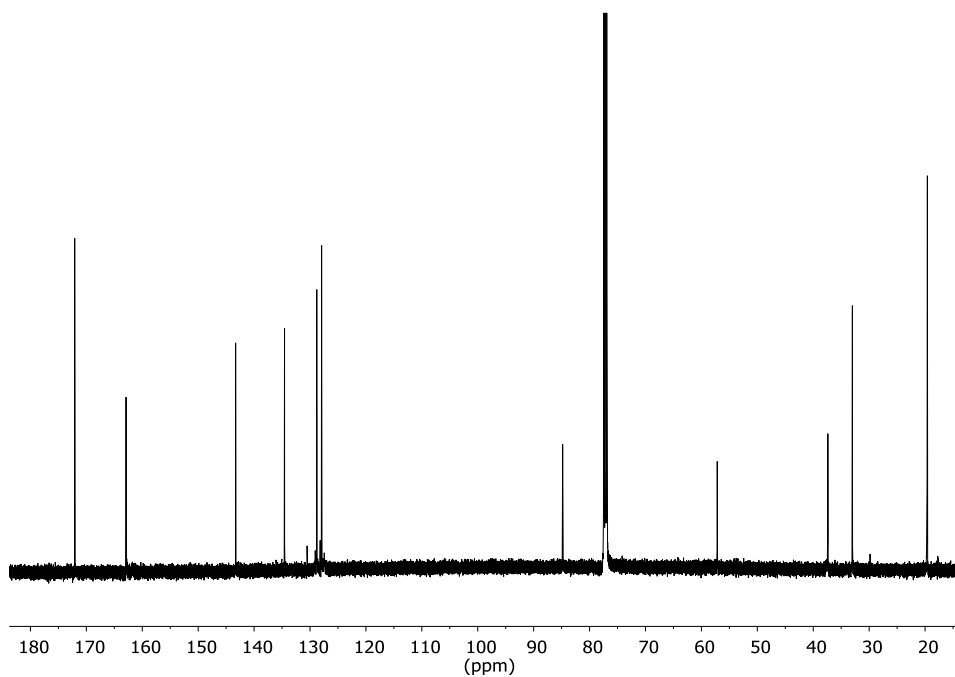
Figure S8.28. ^{13}C{^{1}H} NMR (125 MHz, 25 ºC, CDCl$_3$) spectrum for **(LTV)$_2$A$_3$** / **(DTV)$_2$A$_3$** (1.5 mM).
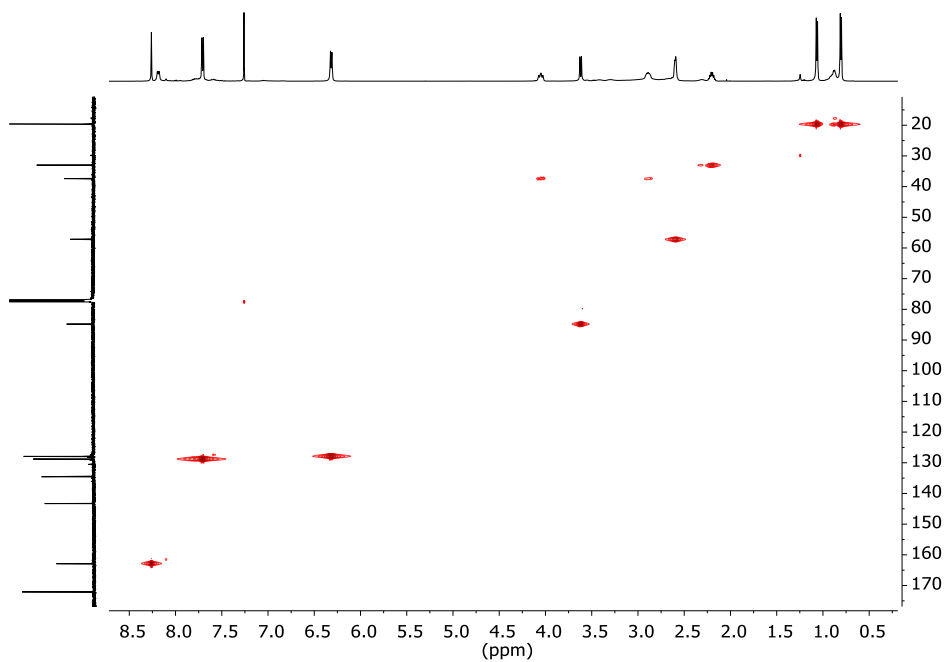
Figure S8.29. HSQC NMR (500 MHz, 25 ºC, CDCl$_3$) spectrum for **(LTV)$_2$A$_3$ / (DTV)$_2$A$_3$** (1.5 mM).
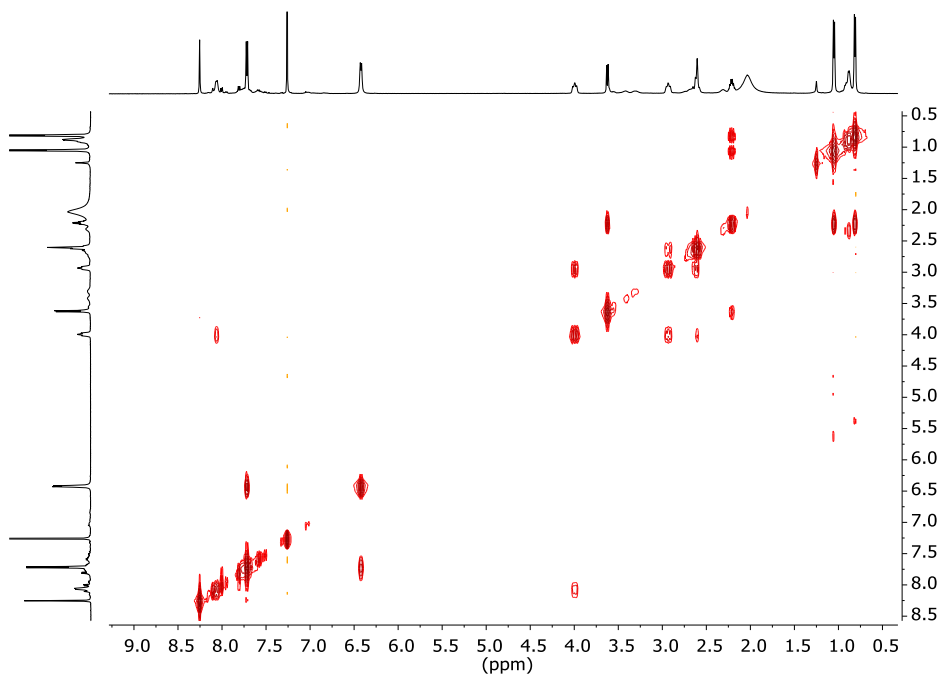
Figure S8.30. COSY NMR (500 MHz, 25 ºC, CDCl$_3$) spectrum for **(LTV)$_2$A$_3$ / (DTV)$_2$A$_3$** (1.5 mM).
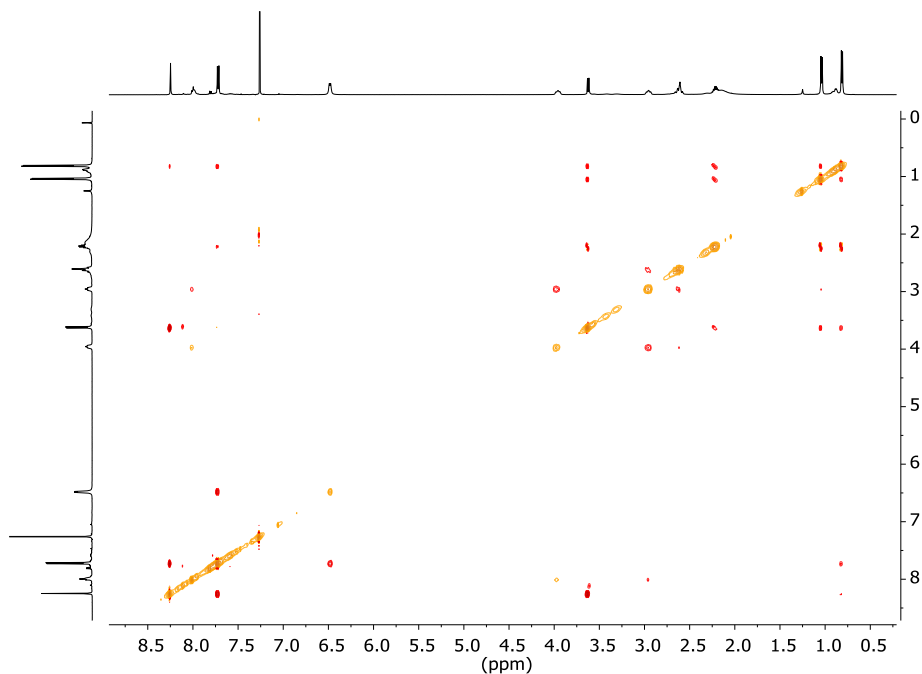
Figure S8.31. ROESY NMR (500 MHz, 25 ºC, CDCl$_3$) spectrum for **(LTV)$_2$A$_3$** / **(DTV)$_2$A$_3$** (1.5 mM).

Figure S8.32. HMBC NMR (500 MHz, 25 ºC, CDCl$_3$) spectrum for **(LTV)$_2$A$_3$** / **(DTV)$_2$A$_3$** (1.5 mM).

Figure S8.33. ^{1}H NMR (500 MHz, 25 °C, CDCl$_3$) spectrum for **(LTF)$_2$A$_3$ / (DTF)$_2$A$_3$** (1.5 mM).
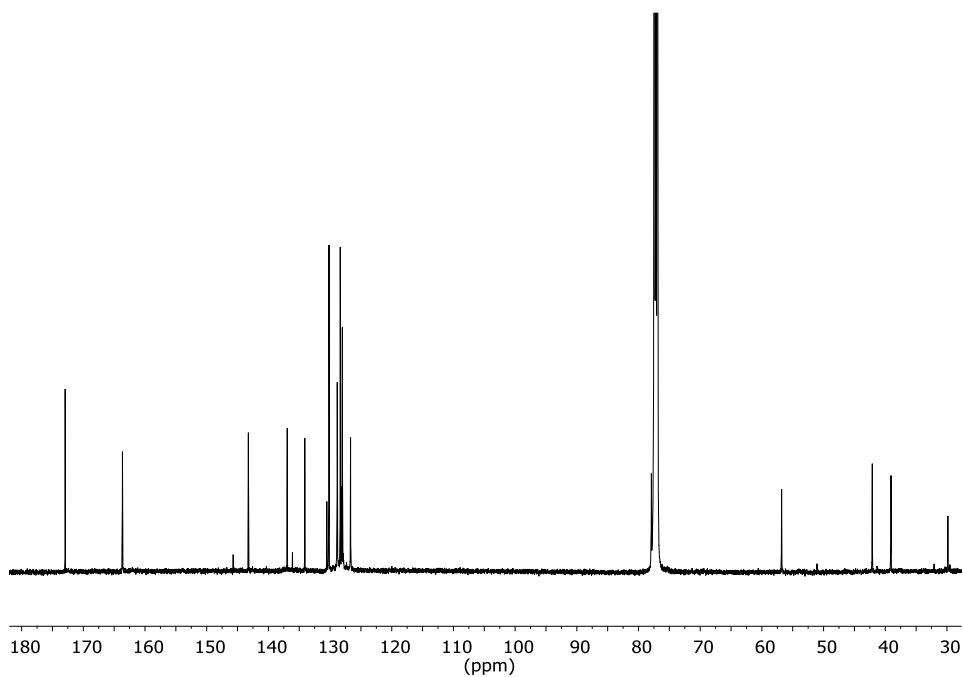
Figure S8.34. ^{13}C{^{1}H} NMR (125 MHz, 25 °C, CDCl$_3$) spectrum for **(LTF)$_2$A$_3$ / (DTF)$_2$A$_3$** (1.5 mM).
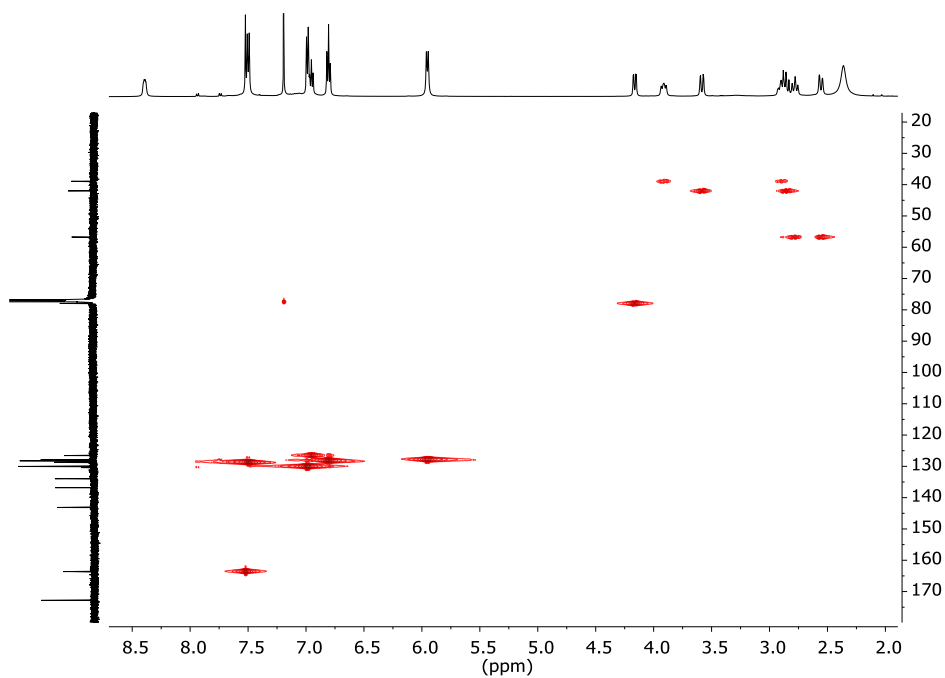
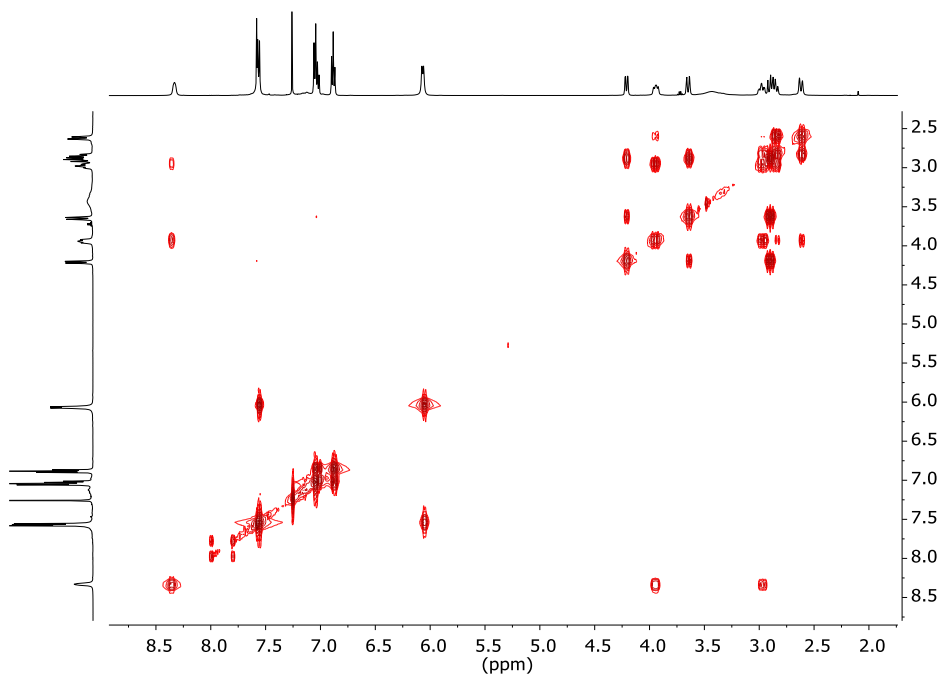**Figure S8.35.** HSQC NMR (500 MHz, 25 ºC, CDCl₃) spectrum for **(LTF)₂A₃** / **(DTF)₂A₃** (1.5 mM).

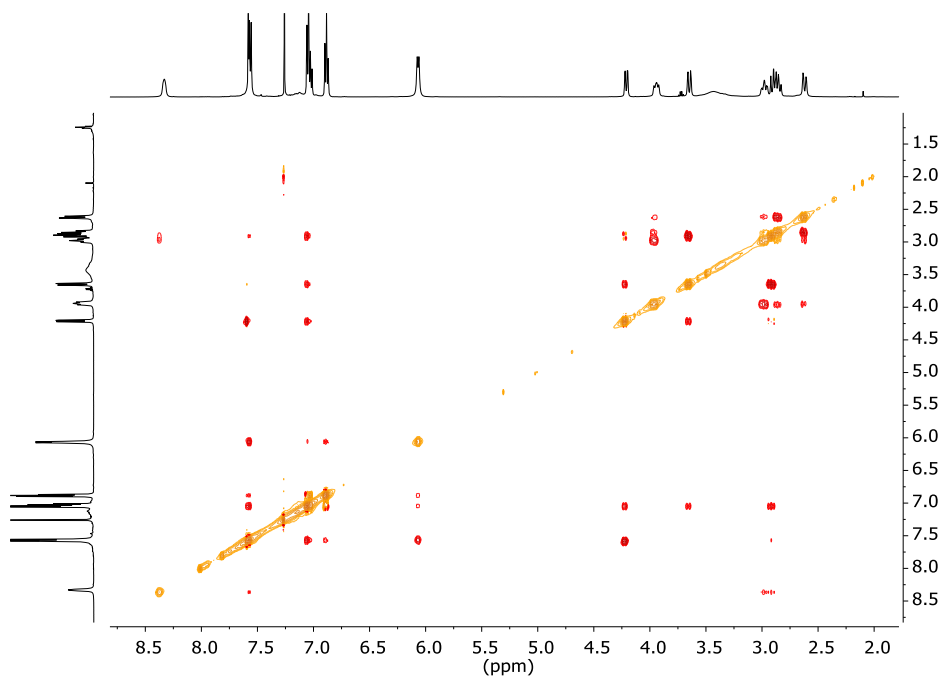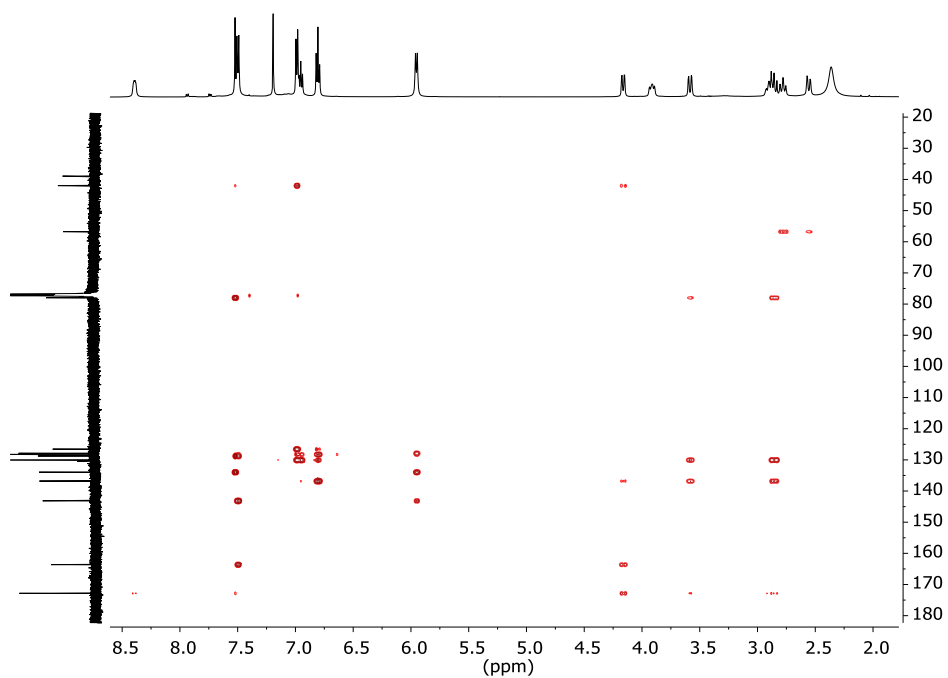**Figure S8.36.** COSY NMR (500 MHz, 25 ºC, CDCl₃) spectrum for **(LTF)₂A₃** / **(DTF)₂A₃** (1.5 mM).

Figure S8.37. ROESY NMR (500 MHz, 25 °C, CDCl$_3$) spectrum for **(LTF)$_2$A$_3$** / **(DTF)$_2$A$_3$** (1.5 mM).

Figure S8.38. HMBC NMR (500 MHz, 25 °C, CDCl$_3$) spectrum for **(LTF)$_2$A$_3$** / **(DTF)$_2$A$_3$** (1.5 mM).
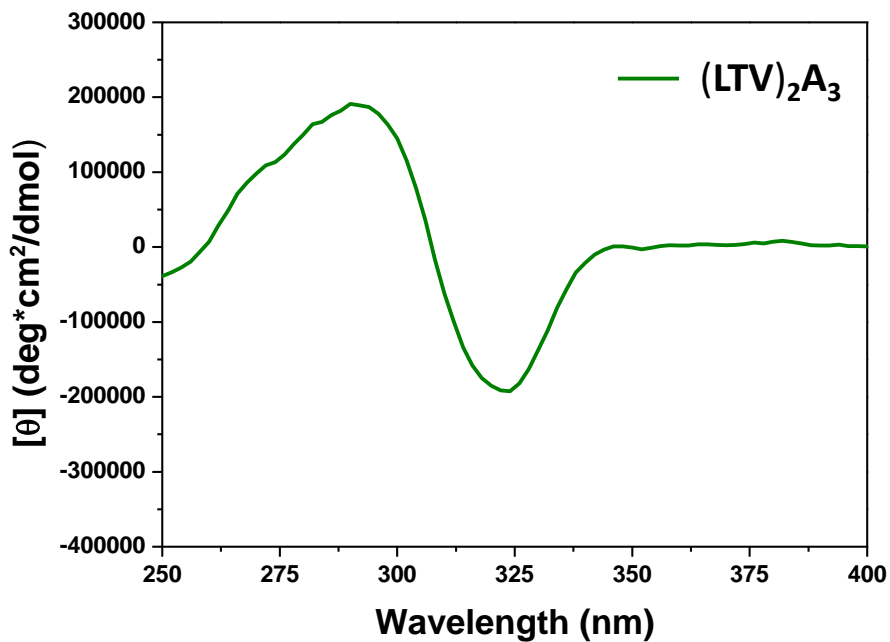
Figure S8.39. Circular dichroism (25 °C, CDCl$_3$) spectrum for **(LTV)$_2$A$_3$** (0.015 mM).
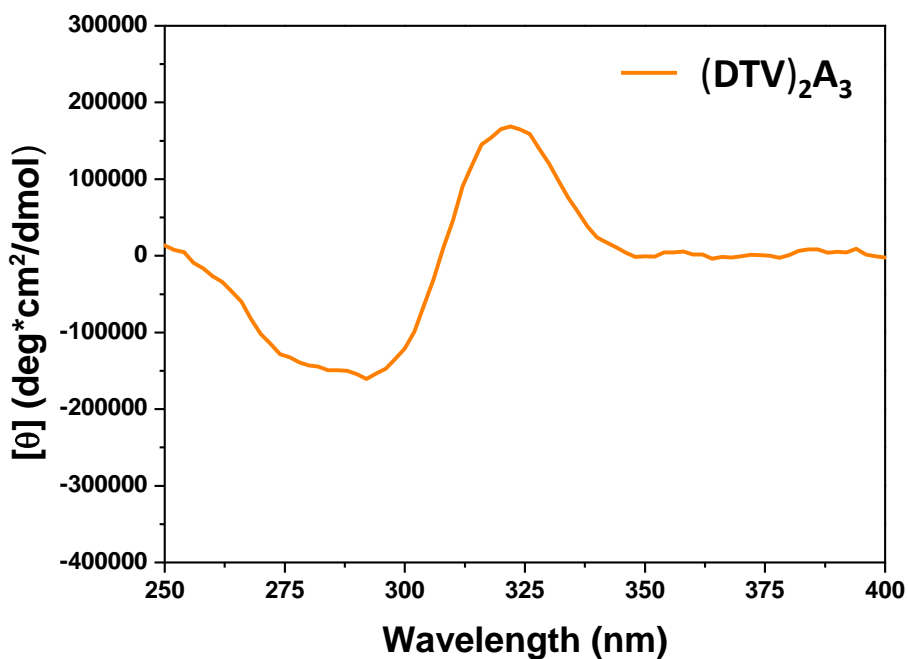
Figure S8.40. Circular dichroism (25 °C, CDCl$_3$) spectrum for **(DTV)$_2$A$_3$** (0.015 mM).

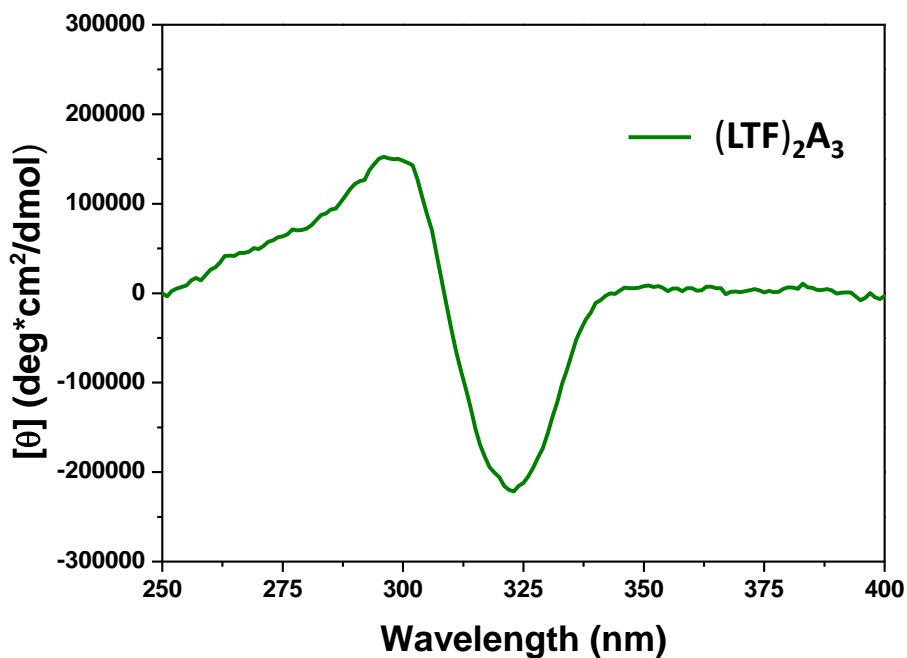**Figure S8.41.** Circular dichroism (25 °C, CDCl$_3$) spectrum for **(LTF)$_2$A$_3$** (0.015 mM).
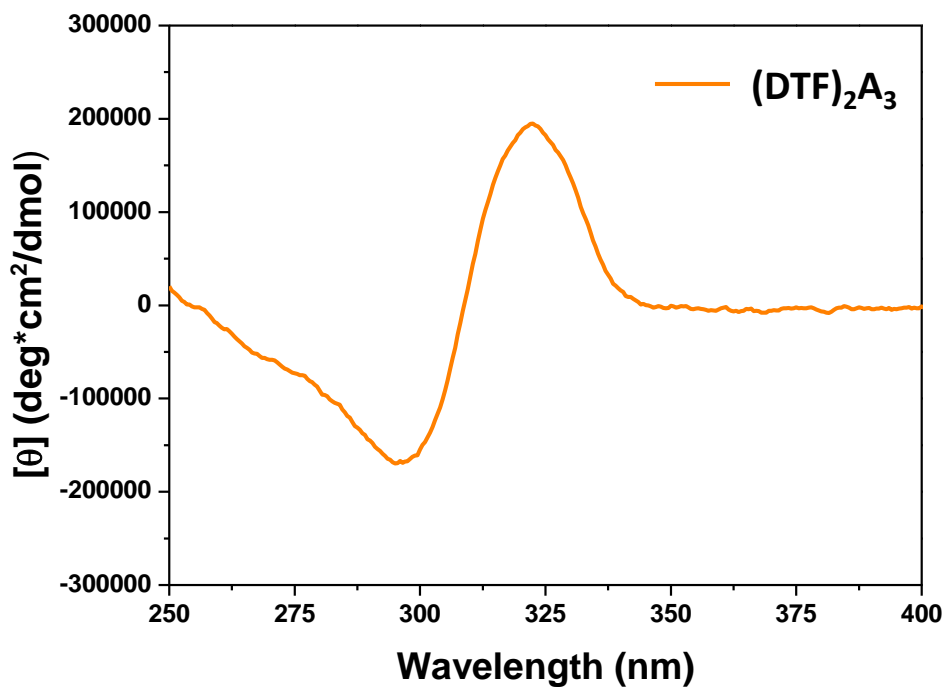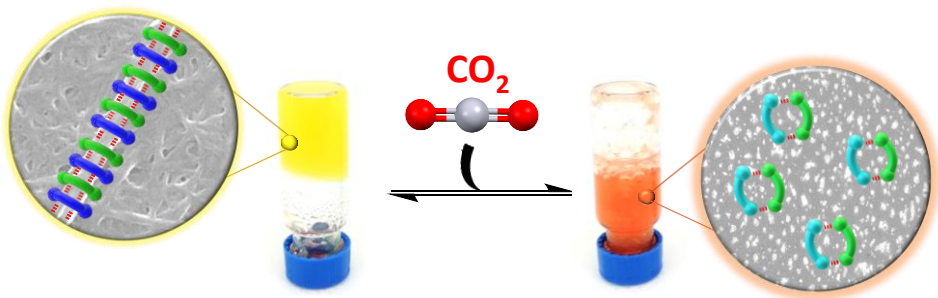

Figure S8.42. Circular dichroism (25 °C, CDCl$_3$) spectrum for **(DTF)$_2$A$_3$** (0.015 mM).

Chapter 9

Unravelling the supramolecular driving forces in the formation of CO_2-responsive pseudopeptidic low molecular weight hydrogelators

9.1. Main text

9.1.1. Abstract

A new family of C_2-symmetric pseudopeptides with high functional density for supramolecular interactions has been synthetized through the attachment of four amino acid subunits to a diamino aliphatic spacer. The resulting open-chain compounds present remarkable properties as low molecular weight hydrogelators. The self-assembled 3D-networks could be characterised by SEM analyses observing regular nanofibers with 80-100 nm diameters. Spectroscopic and molecular modelling experiments revealed the presence of strong synergic effects between H-bonding and π-π interactions, with best results obtained for the homoleptic tetra-pseudopeptide derived from L-Phe. In addition, these bioinspired hydrogels presented pH and CO_2 responsive sol-gel transitions. The formation of ammonium carbamate derivatives in the presence of carbon dioxide triggered a conformational change in the pseudopeptide that was detrimental for its adequate self-assembly. To the best of our knowledge, this are the first low molecular weight hydrogelators that are responsible to carbon dioxide.

9.1.2. Introduction

aSoft materials based on low molecular weight gelators (LMWG) have received significant attention in the last two decades, as they present some interesting features such as well-defined molecular weights, easy structural tuneability, and their capacity to form relatively regular nanostructures.[1,2,3,4] The strength of their 3D-networks, and thus, the critical gelation concentration (CGC) of the corresponding supramolecular gels, is extremely dependent on the intermolecular non-covalent interactions present.[5,6,7]

Gels formed in aqueous systems, i.e., hydrogels, are of special interest due to the wide variety of applications possible, ranging from tissue engineering,[8,9] and controlled drug delivery,[10,11,12] to nanoscale electronics,[13] and actuators.[14,15]

Minimalistic pseudopeptidic systems combining amino acid moieties and simple abiotic fragments are very attractive because of their highly tuneable character and their potential biocompatibility and biodegradability.[16,17,18,19]

In this regard, C_2-symmetric pseudopeptidic compounds displaying apolar spacers have shown remarkable gelating behaviours in different solvents,[20] with the presence of additional functional components like urea fragments significantly increasing the stability of the resulting supramolecular gels.[21,22] Introduction in the apolar spacers in such pseudopeptides of polar functionalities has shown to afford efficient hydrogelators with pH-responsive self-assembling properties.[23] Related approaches have allowed, for instance, the development of bioinspired hydrogels as controlled drug release systems.[24]

The dynamic nature of the different intermolecular interactions involved in the formation of the polymeric supramolecular structure enables, upon exposure to external stimuli, reversible sol-gel transition.[25,26,27,28] Unsurprisingly, many efforts have been devoted to the design of hydrogels that exhibit promising switchable properties on the basis of their different applications.[29,30,31] On this behalf, CO_2 is an ideal candidate for acting as stimulus because it is a non-toxic, cheap, and abundant species. Therefore, several CO_2-switchable soft materials have been precisely designed, promoting interesting advantages in the fields of chemosensors, absorbents, and drug delivery.[32,33,34,35,36,37,38] Nevertheless, to the best of our knowledge, all those reported systems are either based on polymeric materials, or the reported LMWGs are only suitable for the gelation of organic solvents, hampering their use for biological applications. An additional hurdle of amino-based CO_2 absorbents is the large energy consumption associated with high temperatures required for desorption, stressing the need for the development of more efficient systems.[39]

Taking these inspiring precedents into account, we report herein the preparation of open-chain C_2-symmetric pseudopeptides containing four amino acid units within their structure. These simple compounds can be used to generate stable hydrogels

which self-assembly is governed by π-π interactions and H-bonding.[40,41] The resultant supramolecular materials display promising properties for reversible, CO_2 controlled hydrogelation. They present a rapid and isothermal CO_2 absorption at room temperature, with the subsequent CO_2 desorption from the resulting ammonium carbamate derivative upon heating at temperatures > 70 ºC, which defines a change in the self-assembly process.

9.1.3. Experimental section

General.

Reagents and solvents were purchased from commercial suppliers and used without further purification. Deionized water was obtained from a MilliQ equipment (Burlington, MA, USA).

NMR experiments were carried out on a Varian INOVA 500 spectrometer (500 MHz for ^{1}H and 125 MHz for ^{13}C), on a Bruker 400 (400 MHz for ^{1}H and 100 MHz for ^{13}C), or on a Bruker 300 (300 MHz for ^{1}H and 75 MHz for ^{13}C). Chemical shifts are reported in parts per million using the solvent residual peak as the reference. ATR FT-IR spectra were acquired on a JASCO 6200 equipment having a MIRacle Single Reflection ATR Diamond/ZnSe accessory. Samples were directly deposited onto the ATR sample holder, and the FT-IR spectra were collected. The raw IR data were processed with JASCO spectral manager software. UV–Vis absorption measurements were carried out on a Hewlett-Packard 8453 spectrophotometer, having a controlled temperature system.

Gelation experiments.

In a typical experiment, a weighted amount of the LMWG was mixed with 1 mL of the selected solvent in a 1.5 mL glass vial. Gelation was defined when a homogeneous mixture was obtained exhibiting no gravitational flow upon inversion of the vial. For organic/water solvent mixtures, the LMWG was first dissolved in the

corresponding amount of the organic solvent (DMSO or EtOH) and MilliQ water was subsequently added.

Rheological experiments.

The different gels were characterised using a controlled stress AR-2000 rheometer from TA Instruments. A Peltier holder with a plate geometry (60 mm diameter, 500 μm gap) was used for all samples. Frequency sweeps were performed in the angular frequency range 0.1–100 rad/s with the instrument in oscillatory mode at 25 °C. Strain sweeps were performed using a frequency of 1 rad/s in an amplitude sweep range of 0.01% - 80% with the instrument in oscillatory mode at 25 °C.

Molecular modelling.

Lowest energy conformations for the different species considered were calculated at the MMFFaq level of theory using Spartan08.[42] Stationary points were confirmed by subsequent frequency calculation. All vibrational frequencies were positive. See supporting information for cartesian coordinates.

Synthetic protocols.

The C₂-symmetrical bis(aminoamides) (**4**) were prepared as previously reported.[43]

*Synthesis of Cbz-N protected tetra-pseudopeptidic intermediates (**5**).*

*Synthesis of **5a**.* **2a** (7.741 g, 10.686 mmol) was dissolved in anhydrous DME (150 mL) at 0 °C in a two-necked round-bottomed flask (500 mL) using a N₂ atmosphere. A DME solution (150 mL) of **4a** (3.02 g, 11 mmol) was then added dropwise. The reaction mixture was stirred at 0 °C for 1 h and at 25 °C for 18 h. Subsequently, the white suspension was heated for 6 h at 40-50 °C. The resultant white precipitate was filtered-off and washed with cold water and cold methanol. The solid product was dried overnight under reduced pressure at 50 °C to yield **5a** as a white solid. Yield (7.09 g, 9.79 mmol, 89.0%). The product was used for the subsequent step without further purification.

*Synthesis of **5b**.* Intermediate **5b** was successfully synthesized following the same procedure as described for **5a** but using **2b** instead of **2a** and **4b** instead of **4a**. Yield (3.473 g, 3.804 mmol, 87.0%). The product was used for the subsequent step without further purification.

*Synthesis of **5c**.* Intermediate **5c** was successfully synthesized following the same procedure as described for **5a** but using **2b** instead of **2a** and **4c** instead of **4a**. Yield (3.186 g, 3.330 mmol, 76.9%). The product was used for the subsequent step without further purification.

*Synthesis of **5d**.* Intermediate **5d** was successfully synthesized following the same procedure as described for **5a** but using **2b** instead of **2a** and **4d** instead of **4a**. Yield (2.209 g, 2.192 mmol, 81.6%). The product was used for the subsequent step without further purification.

*Synthesis of **5e**.* Intermediate **5e** was successfully synthesized following the same procedure as described for **5a** but using **2b** instead of **2a**. Yield (4.931 g, 6.001 mmol, 90.9%). The product was used for the subsequent step without further purification.

*Synthesis of **5f**.* Intermediate **5f** was successfully synthesized following the same procedure as described for **5a** but using **4b** instead of **4a**. Yield (1.238 g, 1.506 mmol, 63.2%). The product was used for the subsequent step without further purification.

*Synthesis of tetra-pseudopeptidic compounds (**6**).*

*Synthesis of **6a**.* **5a** (0.676 g, 0.932 mmol) was suspended on methanol (150 mL) in a 250 mL two-necked round-bottomed flask, using an ultrasonic bath. After obtaining a N_2 atmosphere, Pd/C (0.198 g, 0.092 mmol) was poured into the flask while nitrogen was being flushed. The nitrogen balloons were then replaced by ones filled with hydrogen and the mixture was stirred for 24 h. The suspension was filtered through a Celite® layer, and the adsorbent was washed with methanol. The final solution was evaporated under reduced pressure to yield pure **6a** as a white solid. Yield (0.346 g, 0.758 mmol, 81.3%); mp 228-229 ºC; $[\alpha]_D^{25} = -7.32°$ ($c = 0.1$, DMSO); ATR-FTIR: 3278, 3050, 1634, 1537 cm^{-1}; ^{1}H NMR (400 MHz, CD$_3$OD) δ 0.85 – 0.99

(m, 24H), 1.95 (m, 4H), 3.08 (t, J = 14.94, 14.94 Hz, 2H), 3.17 (dd, J = 5.46, 14.16 Hz, 2H), 3.24 (d, J = 6.55 Hz, 2H), 4.01 (d, J = 7.07 Hz, 2H); $^{13}C\{^1H\}$ NMR (75 MHz, CD₃OD) δ 16.1, 17.3, 18.4, 18.5, 30.4, 31.8, 38.6, 58.8, 60.1, 172.6, 175.8; HRMS (ESI/Q-TOF) m/z: [M + H]⁺ Calcd. for $C_{22}H_{44}N_6O_4$ 457.3502; Found 457.3498.

*Synthesis of **6b**.* **6b** was successfully synthesized following the same procedure as described for **6a** but using **5b** instead of **5a**. Yield (0.331 g, 0.510 mmol, 82.5%); mp 193-195 °C; $[\alpha]_D{}^{25}$ = -3.42° (c = 0.05, DMSO); ATR-FTIR: 3282, 3042, 1648, 1535 cm⁻¹; ¹H NMR (300 MHz, CD₃OD) δ 2.41 – 3.13 (m, 12H), 3.40 – 3.51 (m, 2H), 4.36 – 4.48 (m, 2H), 6.95 – 7.29 (m, 20H); $^{13}C\{^1H\}$ NMR (75 MHz, CD₃OD) δ 37.6, 38.7, 40.3, 54.5, 56.0, 126.4, 126.5, 128.1, 128.2, 129.0, 129.0, 136.9, 137.3, 172.3, 175.0; HRMS (ESI/Q-TOF) m/z: [M + H]⁺ Calcd. for $C_{38}H_{44}N_6O_4$ 649.3502; Found 649.3508.

*Synthesis of **6c**.* **6c** was successfully synthesized following the same procedure as described for **6a** but using **5c** instead of **5a**. Yield (1.269 g, 1.837 mmol, 78.4%); mp 152-154 °C; $[\alpha]_D{}^{25}$ = -6.21° (c = 0.05, DMSO); ATR-FTIR: 3283, 3042, 1639, 1529 cm⁻¹; ¹H NMR (400 MHz, CD₃OD) δ 0.99 (tt, J = 10.2, 6.3 Hz, 2H), 1.16 – 1.30 (m, 4H), 2.50 - 2.64 (m, 2H), 2.75 – 3.03 (m, 10H), 3.44 (dd, J = 7.8, 5.4 Hz, 2H), 4.45 (t, J = 7.4 Hz, 2H), 7.21 – 7.01 (m, 20H); $^{13}C\{^1H\}$ NMR (100 MHz, CD₃OD) δ 25.0, 29.8, 39.4, 40.2, 42.0, 55.8, 57.4, 127.8, 127.9, 129.5, 129.6, 130.5, 138.2, 138.8, 172.9, 176.5; HRMS (ESI/Q-TOF) m/z: [M + H]⁺ Calcd. for $C_{41}H_{50}N_6O_4$ 691.3972; Found 691.3973.

*Synthesis of **6d**.* **6d** was successfully synthesized following the same procedure as described for **6a** but using **5d** instead of **5a**. Yield (0.485 g, 0.662 mmol, 70.1%); mp 138-141 °C; $[\alpha]_D{}^{25}$ = -3.02° (c = 0.05, DMSO); ATR-FTIR: 3272, 3085, 1654, 1542 cm⁻¹; ¹H NMR (400 MHz, CD₃OD) δ 1.01 - 1.18 (m, 10H), 1.26 (p, J = 7.7, 6.9 Hz, 4H), 2.51 – 2.65 (m, 2H), 2.76 – 3.03 (m, 10H), 3.44 (dd, J = 7.7, 5.5 Hz, 2H), 4.45 (t, J = 7.3 Hz, 2H), 7.20 – 7.01 (m, 10H); $^{13}C\{^1H\}$ NMR (100 MHz, CD₃OD) δ 27.8, 30.2, 39.4, 40.4, 42.1, 55.8, 57.4, 127.8, 127.9, 129.5, 129.6, 130.5, 138.2, 138.8, 172.3,

176.5; HRMS (ESI/Q-TOF) m/z: [M + H]+ Calcd. for $C_{44}H_{56}N_6O_4$ 733.4441; Found 733.4449.

*Synthesis of **6e**.* **6e** was successfully synthesized following the same procedure as described for **6a** but using **5e** instead of **5a**. Yield (0.263 g, 0.475 mmol, 77.4%); mp 207-209 °C; $[\alpha]_D^{25}$ = -1.75° (*c* = 0.05, DMSO); ATR-FTIR: 3280, 3085, 1636, 1546 cm^{-1}; ^{1}H NMR (400 MHz, DMSO-d_6) δ 0.80 (dd, *J* = 6.8, 5.0 Hz, 6H), 1.92 (h, *J* = 6.6 Hz, 2H), 2.63 (dd, *J* = 13.4, 8.5 Hz, 2H), 2.99 (dd, *J* = 13.5, 4.3 Hz, 2H), 3.11 (s, 4H), 3.46 (dd, *J* = 8.6, 4.3 Hz, 2H), 4.10 (t, *J* = 7.3 Hz, 2H), 7.38 – 7.14 (m, 10H), 7.96 (d, *J* = 9.0 Hz, 2H), 8.03 (s, 2H); ^{13}C{^{1}H} NMR (100 MHz, DMSO-d_6) δ 18.5, 19.6, 31.3, 41.1, 56.5, 57.7, 126.6, 128.6, 129.8, 139.1, 171.4, 174.4; HRMS (ESI/Q-TOF) m/z: [M + H]+ Calcd. for $C_{30}H_{44}N_6O_4$ 553.3497; Found 553.3503.

*Synthesis of **6f**.* **6f** was successfully synthesized following the same procedure as described for **6a** but using **5f** instead of **5a**. Yield (0.428 g, 0.774 mmol, 63.5%); mp 184-189 °C; $[\alpha]_D^{25}$ = -8.2° (*c* = 0.05, DMSO); ATR-FTIR: 3282, 3083, 1636, 1535 cm^{-1}; ^{1}H NMR (300 MHz, DMSO-d_6) δ 0.56 (dd, *J* = 6.8, 1.5 Hz, 6H), 0.73 (d, *J* = 6.9 Hz, 6H), 1.81 (tdd, *J* = 6.8, 4.7, 2.0 Hz, 2H), 2.58 (dd, *J* = 13.3, 8.3 Hz, 2H), 2.76 – 2.88 (m, 2H), 2.91 – 2.97 (m, 4H), 3.04 (d, *J* = 3.2 Hz, 2H), 4.43-4.52 (m, 2H), 7.18 – 7.27 (m, 10H), 7.90 (d, *J* = 5.9 Hz, 2H), 8.05 (s, 2H); ^{13}C{^{1}H} NMR (75 MHz, DMSO-d_6) δ 17.0, 17.1, 19.9, 31.5, 38.5, 126.7, 128.5, 129.6, 138.2, 171.6, 174.7; HRMS (ESI/Q-TOF) m/z: [M + H]+ Calcd. for $C_{30}H_{44}N_6O_4$ 553.3497; Found 553.3508.

9.1.4. Results and discusión

9.1.4.1. Synthesis of the pseudopeptidic compounds and gelation properties as LMWGs

The synthesis of the different C_2-symmetric tetra-pseudopeptides **6a-f** is shown in Scheme 1. Compounds **4a-d** were obtained following the previously reported synthetic procedure (Scheme 9.1).[43] Briefly, the first step consisted in the synthesis of the activated esters of the l-amino acids, using DCC as the coupling agent. The

resulting activated esters **2a-b** were reacted with the desired diamine to yield the N-Cbz-protected pseudopeptides **3**. The deprotection step to afford compounds **4** relied on the use of HBr/HAc (33%) solution. An additional coupling step with either **2a** or **2b** afforded the N-protected tetra-pseudopeptides **5**. Subsequent hydrogenation in the presence of palladium on activated carbon led to the desired deprotected tetra-pseudopeptides **6**. The overall yields to produce **6** from compounds **1** ranged from 20% to 40%.
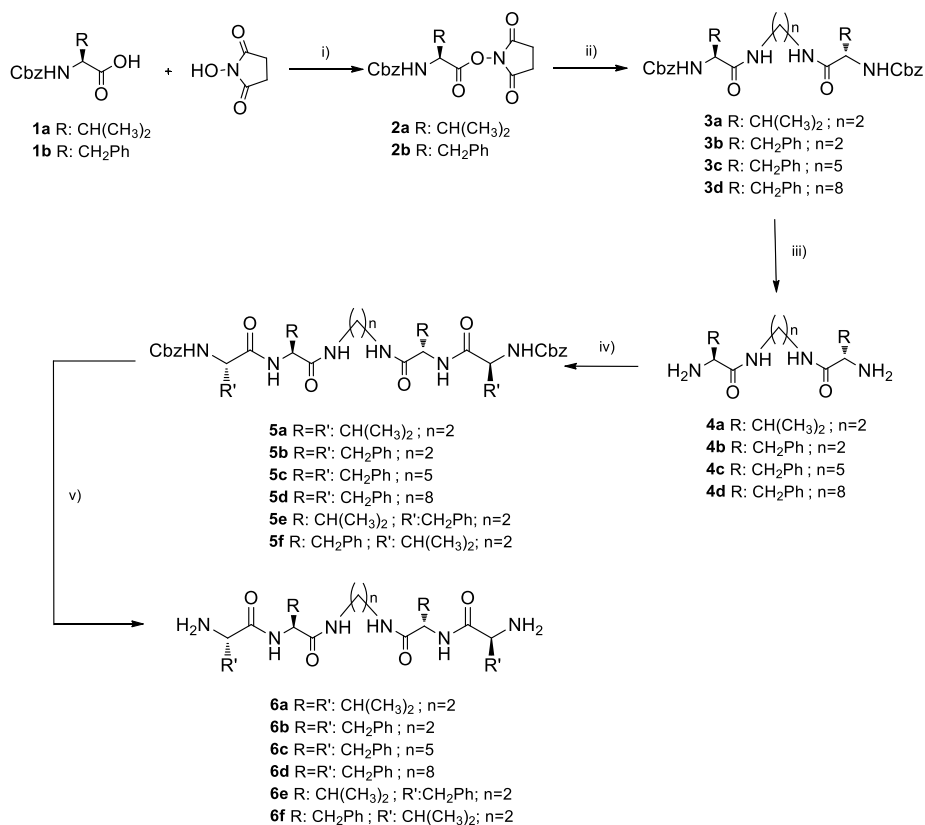
Scheme 9.1. Synthesis of tetra-pseudopeptidic compounds. i) DCC, 0 °C, 16 h. ii) dry DME, ethylene diamine, r.t., 18 h. iii) HBr/HAc (33%), 3 h. iv) dry DME, **2**, r.t., 18 h. v) H₂, Pd/C, MeOH.

The gelation properties of the tetra-pseudopeptidic compounds **6a-f** were assayed in different aqueous mixtures and in water. As shown in Table 9.1, the nature of the amino acid sidechain plays a critical role in the self-assembly behaviour. As a

matter of fact, the phenylalanine derivative **6b** formed gels in water mixtures and in water at 1 mg/mL (entries 2, 17 and 20, Table 9.1), while the valine derived compound **6a** was not able to yield hydrogels under analogous conditions (entries 1, 18 and 19, Table 9.1). These results suggested that π-π interactions could be a major requirement for the 3D-network to grow. Interestingly, when the gelation properties for compound **6b** were assayed in H_2O:DMSO (90:10, v/v), an instantaneous gelation process was observed, without the need of any external stimuli. On the other hand, when the experiments were performed in EtOH:H_2O mixtures, sonication was always needed to obtain similar hydrogels.

The key role of aromatic interactions in the aggregation capacity of these pseudopeptides was confirmed by the results obtained for the heteroleptic compounds **6e** and **6f** containing only two aromatic groups in the sidechains instead of the four displayed by **6b**. When 1 mg of **6e** or **6f** were dissolved in H_2O:DMSO (90:10, v/v), a clear solution was obtained, thus revealing a lower gelating ability (entries 7 and 9, Table 9.1). When the concentration of the heteroleptic compounds was increased to 5 mg/mL, this triggered the formation of a weak hydrogel for **6f** (entry 10, Table 9.1), whereas the **6e** sample appeared still as a clear solution (entry 8, Table 9.1). Interestingly, a weak gel was obtained when mixing equimolar amounts of **6e** and **6f** (0.5 mg/mL each), inferring that the two-component mixture was able to self-assemble in fibrillar aggregates (entry 11, Table 9.1).

Besides, the effect of the length of the aliphatic spacer in the gelation ability was also evaluated. Previous studies of related pseudopeptides demonstrated that depending on the length of the alkyl aliphatic spacer, the amide groups can be in -*syn* or -*anti* disposition,[44] which affects their self-assembly behaviour. Dissolving 1 mg of **6c**, having three additional methylene groups in the spacer over **6b**, in 100 μL of DMSO and adding 900 μL of water led to the formation of a weak gel upon sonication. In order to obtain a stronger gel, 3 mg of **6c** were required (entries 3,4, Table 9.1). Compound **6d**, containing an even longer spacer (n = 8), was only able to promote the formation of weak gels even at 5 mg/mL (entries 5, 6, Table 9.1). Thus, the compound with the shorter aliphatic spacer (n = 2) **6b** presented the best

gelation properties in aqueous media, most likely as a direct result of the optimal preorganization of the aromatic moieties of the sidechains.

Table 9.1. Gelation properties of compounds **6a-6f** in aqueous solutions.[a]

Entry	Comp.	Solvent(s)	Proportion (v/v)	Conc. (mg/mL)[b]	Result
1	**6a**	H_2O : DMSO	90 : 10	1	S
2	**6b**	H_2O : DMSO	90 : 10	1	G[d]
3	**6c**	H_2O : DMSO	90 : 10	1	wG[d]
4	**6c**	H_2O : DMSO	90 : 10	3	G[d]
5	**6d**	H_2O : DMSO	90 : 10	1	wG[b]
6	**6d**	H_2O : DMSO	90 : 10	5	wG[c]
7	**6e**	H_2O : DMSO	90 : 10	1	S
8	**6e**	H_2O : DMSO	90 : 10	5	S
9	**6f**	H_2O : DMSO	90 : 10	1	S
10	**6f**	H_2O : DMSO	90 : 10	5	wG[c]
11	**6e+6f**	H_2O : DMSO	90 : 10	0.5+0.5	wG
12	**6b**	H_2O : DMSO	50 : 50	1	wG[c]
13	**6a**	H_2O : EtOH	90 : 10	1	I
14	**6b**	H_2O : EtOH	90 : 10	1	I
15	**6b**	H_2O : EtOH	70 : 30	1	wG[c]
16	**6b**	H_2O : EtOH	70 : 30	0.5	wG[c]
17	**6b**	H_2O : EtOH	50 : 50	1	G[c]
18	**6a**	H_2O : EtOH	50 : 50	1	S
19	**6a**	H_2O	-	1	I[b]
20	**6b**	H_2O	-	1	G[b]

[a] The gel formation was qualitatively analysed by the vial inversion technique. I: Insoluble, S: Soluble, WG: Weak Gel, G: Gel. [b] Heating at 90 °C for 5 minutes. [c] Ultrasonication for 5 minutes. [d] Instantaneous formation of gel.

SEM experiments provided additional insights into the microstructure of the hydrogels. Thus, SEM images for the dried gel of **6b** obtained in H_2O:DMSO (90:10

v/v) allowed to observe the presence of a well-defined interpenetrated network of regular nanofibers, displaying diameters of 80-100 nm (Figure S9.1).[45]

Vial inversion analyses allowed for the quantification of the critical gelation concentration (CGC), which is defined as the minimum amount of gelator required to gelate 1 mL of solvent at a given temperature.[12] Data presented in Table S9.1 permitted the assignment of a CGC for compound **6b** lower than 0.6 mg/mL (see also Figure S9.2). This value demonstrates the remarkable gelation properties of **6b**, belonging to the class of superhydrogelators.[46] UV-VIS spectroscopy was also used to determine the CGC for **6b** (Figure 9.1). The formation of the gel could be straightforwardly monitored by measuring the absorption changes at 600 nm. A sigmoidal curve is observed with an inflexion point being ca. 0.4 mg/mL. This concentration is in good agreement with the value determined by vial inversion method.
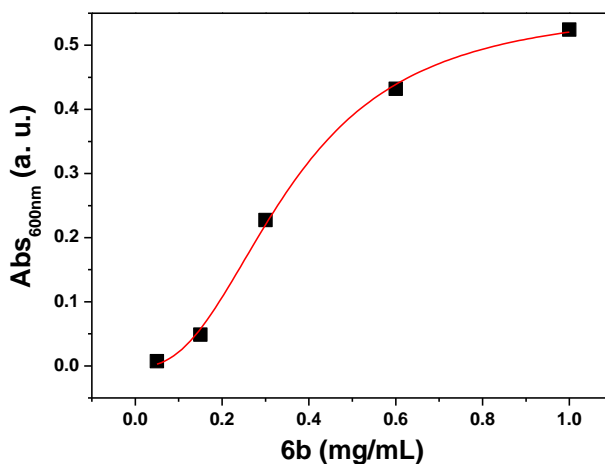
Figure 9.1. UV absorption at 600 nm for **6b** at different concentrations in H_2O:DMSO (90:10). The red line corresponds to the sigmoidal fitting calculated using Origin Software.

The thermal stability of the gel formed from **6b** (H_2O:DMSO (90:10 v/v), 1 mg/mL) was likewise investigated using the vial inversion test (Table S9.2). The hydrogel was stable until 85 °C, temperature at which the soft material started to lose viscosity. This finding was assigned to some evaporation of the water present in the initial solvent mixture. The mechanical properties of this hydrogel (H_2O:DMSO

(90:10 v/v)) were studied using rheological measurements. A typical LMWG presents a storage and a loss modulus (G´ and G´´, respectively), which are frequency independent, and will break at relatively low strain.[47] Figure 9.2 displays the rheological results obtained for **6b** (1 mg/mL). The storage modulus (G') of the gel was much higher than the loss modulus (G") over the whole range of frequency swept, which is characteristic of gel-like materials (Figure 9.2a). The strain sweep measurement (Figure 9.2b) showed that both the storage and loss moduli of the gel remained constant up to 10 Pa of stress (3.6% strain), corresponding to the so-called linear viscoelastic region (LVER). Furthermore, the average complex viscosity of the hydrogel was quantified, obtaining a value of 113 Pa·s.
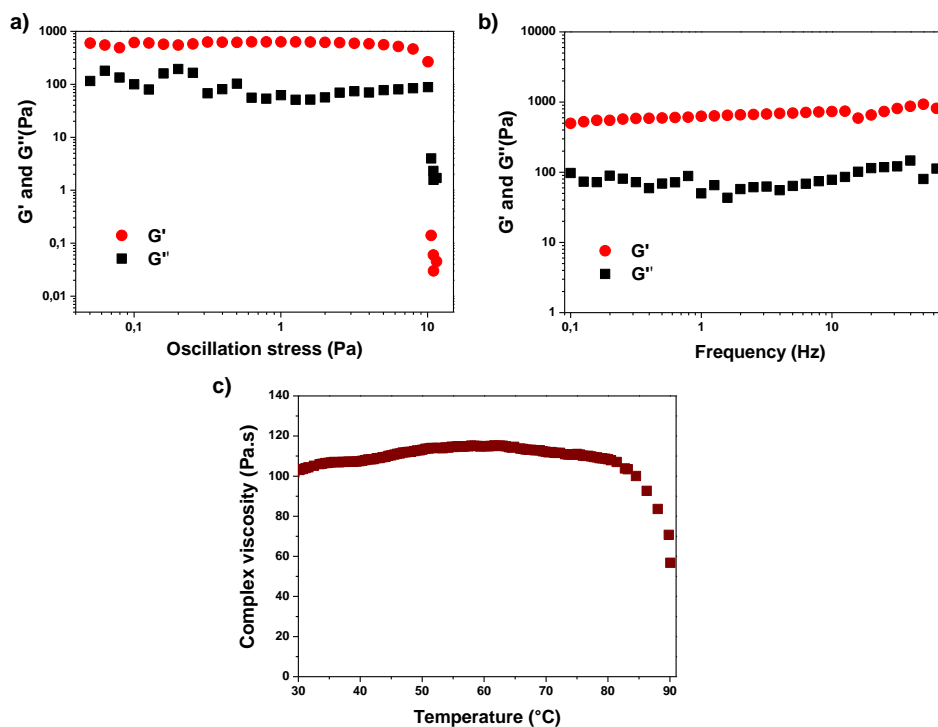
Figure 9.2. Rheological measurements for the hydrogel from **6b** (1 mg/mL, H₂O:DMSO (90:10 v/v)). a) Amplitude sweeps with 1 Hz at 25 °C; b) Frequency sweeps with 0.1 Pa strain at 25 °C; c) Dependence of complex viscosity with the temperature using a heating rate of 0.2 °C/min and a constant frequency of 1 Hz and 0.1% strain.

By heating the sample prepared *in-situ* on the Peltier geometry, it was possible to evaluate the effect of temperature in the mechanical properties of the

pseudopeptidic soft material. For instance, observing the complex viscosity trend with temperature, a linear range was obtained from 25 to 85 °C (Figure 9.2c). When the temperature reached values higher than 83 °C, a clear decrease in the viscosity was appreciated, indicating that the sample was losing its gel-like properties. Hence, the critical gelation temperature (CGT) was identified as 83 °C, value within the same range that the one obtained by the vial inversion method (see Table S9.2). The material can be classified as a thixotropic gel because, upon shaking the vial, the sample became much more fluid than in its static state. The same rheological experiments were also performed for **6b** at higher gelator concentrations (5 mg/mL in H_2O:DMSO (90:10 v/v)). Not surprisingly, the resulting gel presented a higher complex viscosity, with an average value of 1640 Pa·s. This stronger gel was able to resist oscillation strains of ca. 40 Pa, corroborating the tougher properties of the gel at higher concentrations (Figure S9.3).

Next, we decided to analyse whether an external stimulus could induce a gel-sol transition. Considering the functional groups present in the chemical structure of **6b**, pH appeared as a good candidate, as the pseudopeptide presented terminal amino groups (basic) and amide groups (slightly acidic). Therefore, vial inversion tests were carried out for samples at different pH values, controlled by commercially available buffers (Figure S9.4). Results presented in Table 9.2 revealed that the higher the pH was, the more favourable was the formation of the gel. These pH-dependent results indicate the participation of the terminal amino groups in the formation of the non-covalent network, as when these groups were in their fully protonated form, a completely transparent solution was obtained. Interestingly enough, some crystallization could be observed in the sample at pH 1 after aging the vial for one week. SEM images of the resulting crystalline solid revealed the formation of fibre-like crystals, which were likely the result of the formation of diprotonated ammonium salts for **6b** (Figure S9.5). Therefore, the protonation of the primary amines led to a detrimental conformational change, precluding the formation of the 3D supramolecular network. It must be noted, however, that **6b** is able to form weak

gels even at physiological pH (Table 9.2, vial 4), opening a wide scope for future applications in areas such as drug delivery.

Table 9.2. Gelation properties as a function of pH in H_2O:DMSO (90:10 v/v) for **6b** (1 mg/mL).[a]

Vial	Buffer (mM)	pH	Result
1	– [b]	1	S
2	Citrate (20)	4	wG
3	Citrate (20)	6	wG
4	Phosphate (30)	7	wG
5	HEPES (20)	8	G

[a] Gel formation was qualitatively analysed by the vial inversion technique. [b] The sample at pH = 1 was prepared by adding 20 µL of concentrated HCl. I: Insoluble, S: Soluble, WG: Weak Gel, G: Gel. The buffers were commercially available and, when needed, the pH was adjusted using NaOH or HCl. See Figure S9.4 for vial inversion tests.

9.1.4.2.   Supramolecular driving forces

Seeking for relevant information about the supramolecular interactions that governed the formation of these soft materials, a series of ^1H NMR and theoretical studies were undertaken. First of all, increasing amounts of water were added to a 3 mM solution of **6b** in DMSO-d_6 and ^1H NMR spectroscopy allowed for observing some relevant changes observed for the characteristic signals of the pseudopeptide. Indeed, most of the peaks of **6b** broadened with the addition of water, suggesting the formation of intermolecular polymeric aggregates. An upfield shift was observed for the proton signals of the central amide groups (green triangles in Figure 9.3) indicating a different involvement in hydrogen bonding in the supramolecular aggregates.

In a similar manner, the protons corresponding to the aromatic moieties experienced a shift towards lower δ, especially noticeable for the protons assigned to the aromatic ring of the central amino acid scaffolds, suggesting their participation in hydrophobic interactions. Besides, the methylene protons of the aliphatic central spacer and the benzylic protons also experienced a different electronic environment

in the aggregates, as evidenced by the upfield shift for the central methylene protons (orange discontinuous lines, Figure S9.6).
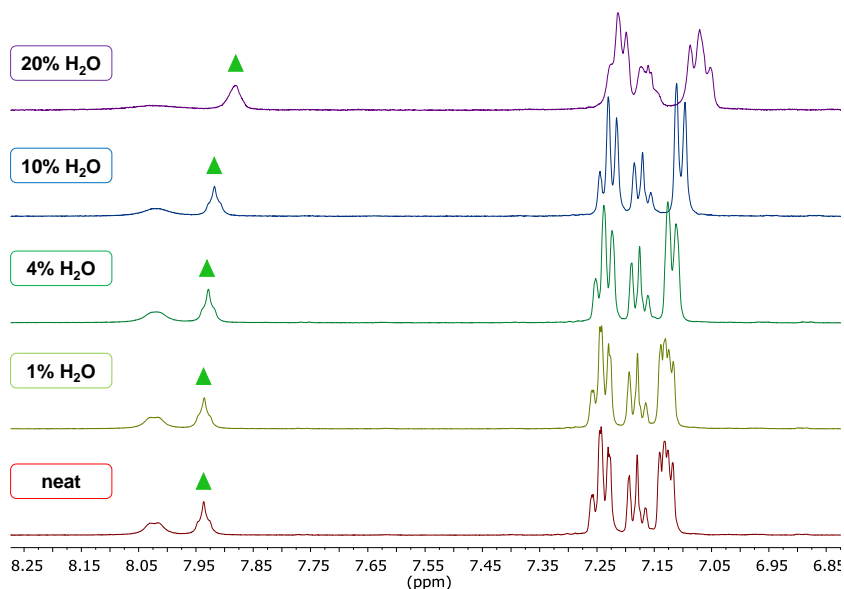

Figure 9.3. Partial ^{1}H NMR (500 MHz, DMSO-d_6) spectra for the titration of **6b** (3 mM) with increasing amounts of water. The water content is indicated as v/v (%). The signal for the central amide groups has been marked with green triangles.

In terms of the signals for the protons of the water molecules, a progressive downfield evolution could be observed, shifting from 3.35 to 3.93 ppm ($\Delta\delta = +0.58$ ppm) when the amount of water reached 20% v/v (purple discontinuous lines, Figure S9.6). This change in the electronic environment was likely the result of water entrapment in the three-dimensional network formed, increasing their H-bonding. Interestingly, analogous experiments performed for **6f** revealed less pronounced shifts for both water molecules and signals from the heteroleptic pseudopeptide (Figure S9.7 and S9.8). As a matter of fact, the signal for water shifted $\Delta\delta = +0.28$ ppm. Albeit the aromatic protons of **6f** also shifted towards lower δ values in the presence of water, the shift was much less significant than the one observed for **6b** (Figure S9.8). This indicates that the homoleptic tetra-phenylalanine derived pseudopeptide promoted higher efficiencies in forming the supramolecular

aggregates, in good accordance with trends found in gelation studies (see for instance Entries 2 and 9 in Table 9.1).

Variable temperature ^1H NMR experiments corroborated the fundamental role of intermolecular hydrogen bonding and π-π interactions in the self-assembly of the pseudopeptides. Important conformational information was gathered when the sample containing a 3 mM solution of **6b** in H_2O:DMSO (20:80) was heated from 30 to 80 °C. As expected, the proton signals of the amide groups and water experienced an upfield shift as temperature increased (*ca.* $\Delta\delta$ = -0.24 and -0.35 ppm for NH$_{amide}$ and H_2O, respectively), suggesting their participation through hydrogen bonding interactions within the supramolecular network of aggregates (Figure 9.4a and Figure S9.9).
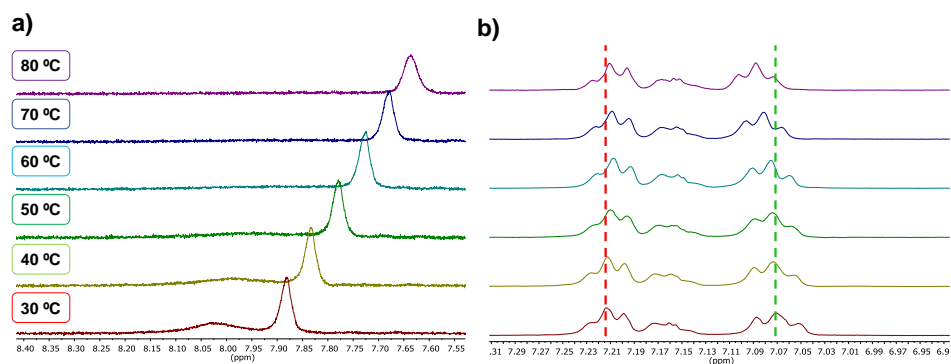
Figure 9.4. Partial ^1H NMR (500 MHz, DMSO-d_6) spectra for the variable temperature experiments of **6b** (3 mM, H_2O:DMSO, 20:80). a) Amide group region. b) Aromatic region.

A different scenario was observed on behalf of the signals for the aromatic units. The multiplet appearing at 7.21 ppm undergone a minor upfield shift, as marked with a discontinuous red line in Figure 9.4b. On the other hand, a more pronounced change was noted for the signal appearing at 7.07 ppm at 30 °C, but with the opposite direction than the one found for the signal at 7.21 ppm. This trend is in good agreement with interconnected π systems, where one of the aromatic units acts as the π-donor and the other one as the π-acceptor.[48] Additionally, the protons of the chiral carbon centres, the methylene protons of the central spacer, and the benzylic protons experienced a small shift ($\Delta\delta$ = +0.03 ppm, discontinuous orange lines, Figure S9.9).

Molecular modelling for **6b**, **6e**, and **6f** unravelled the importance of synergic π-
π interactions, only affordable in the case of **6b**. All the models were based on
molecular mechanics at the MMFFaq level of theory, taking into account the water
solvation (see experimental section for more details). Calculating the most stable
conformation for the dimers of each tetra-pseudopeptide, noteworthy disparities
were found. For instance, the two modelized molecules of **6b** adopt a β-sheet spatial
disposition stabilized by means of intermolecular hydrogen bonds involving the
central amide groups of the pseudopeptidic scaffolds. Additionally, the hydrophobic
aromatic units are located in the outer part of the molecules, intermolecularly
interacting through π-π forces (Figure 9.5a). Therefore, the conformation adopted
allows for the construction of bigger self-assembled supramolecular structures,
leading to the formation of fibre-like aggregates (Figure 9.5d). On the other hand,
the modelized dimers for the heteroleptic tetra-pseudopeptides rather embraced a
tangled conformation, only stabilized through intermolecular hydrogen bonding
between the amide groups, precluding an efficient extension of the network to form
gels (Figure 9.5b, 9.5c, and 9.5e).
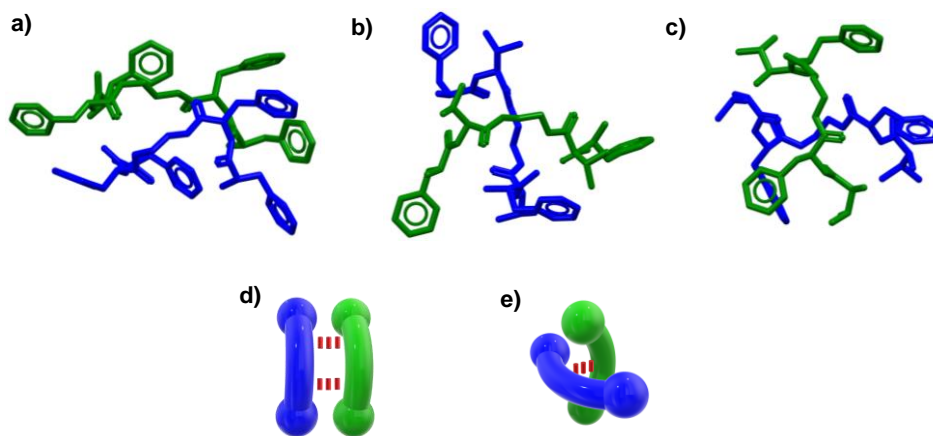
Figure 9.5. Most stable conformations (Spartan08', MMFFaq) obtained for the dimers of a)
6b, b) **6e**, and c) **6f**. d) Representation of the parallel β-sheet, and e) the tangled dimeric
assemblies.

  The non-covalent interactions governing the gel formation for **6b** were studied
in higher detail. The four amide groups (presenting an -*anti* disposition) of each of

the pseudopeptidic molecules are highly interconnected with the analogues of the neighbouring molecule, leading to the formation of parallel hydrogen bonds (Figure 9.6a). The average distance between the O···N atoms involved in the interaction is 2.780 Å (90 % vdW$_{N,O}$),[49] suggesting a strong interaction even in competitive polar media. In terms of the hydrophobic interactions between the dimeric species, four different intermolecular edge-to-face π-π interactions have been detected (Figure 9.6b). Besides, weak intramolecular NH··· π forces were identified between the phenyl rings of the phenylalanine sidechains and the acidic NH proton of the amide groups, further stabilising the whole system (Figure 9.6c).[50]
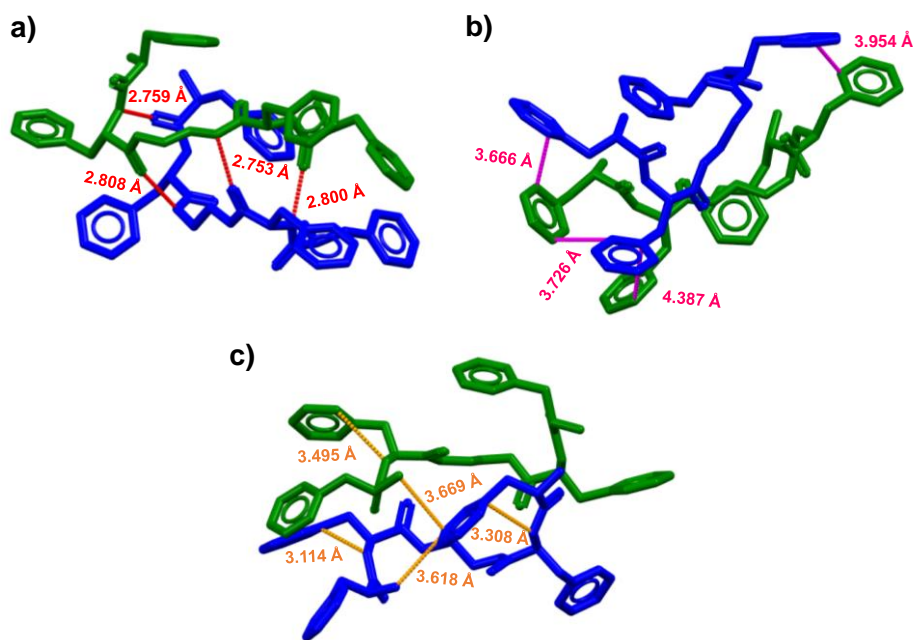
Figure 9.6. Non-covalent forces identified in the most stable conformation obtained for the dimer of **6b** (Spartan08', MMFFaq). a) Intermolecular hydrogen bonding between the amide groups of the two different molecules. Bonds and distances have been highlighted in red. Measured distances correspond to O···N bonds in the C=O···N-H entities. b) Intermolecular edge-to-face π-π interactions between the dimeric molecules. Bonds and distances have been highlighted in pink. Measured distances correspond to the closest aromatic carbons between the vicinal rings. c) Intramolecular NH··· π interactions between the aromatic rings and the acidic NH protons of the amide groups. Bonds and distances have been highlighted in orange. Measured distances correspond to the closest aromatic carbon to the N atom of the amides.

9.1.4.3. CO_2 stimulus responsiveness

In view of these promising results, we envisaged that the soft materials could experience reversible gel-to-sol transition triggered by carbon dioxide. It is well known that the solubility of carbon dioxide in water leads to a noteworthy decrease in the pH, reaching values between 3.5 and 4.[51] In addition, amines have been widely used as chemical absorbents of carbon dioxide.[52] The interaction of CO_2 with unhindered primary amines is known to generate ammonium carbamate species, because primary amines are more basic and nucleophilic than water.[53,54]

We performed ^{1}H NMR analyses in DMSO-*d₆* as solvent to get information about the formation of ammonium carbamate products.[55] For comparison, the spectrum of the diprotonated [**6b**·2HCl] species in DMSO was also recorded. Significant differences were observed when comparing the spectra of freshly prepared **6b** with the one for [**6b**·2HCl] and that for **6b** after bubbling a CO_2 balloon for 5 mins (Figure S9.10). For **6b**-CO_2, the downfield shift for the proton of the stereogenic carbon (from δ = 3.42 to 4.10 ppm), together with the appearance of new signals at 6.62, 8.24, and 8.59 ppm could indicate the formation of the ammonium carbamate derivative. While the methylene protons of the central spacer shifted towards lower δ values for [**6b**·2HCl], no shift was observed for **6b**-CO_2. Furthermore, a significant downfield shift of the aromatic protons and an increase in the anisochrony of the benzylic protons was observed for **6b**-CO_2, the latter attributed to the lack of free rotation. As expected, the signals of these CO_2-derived species decreased with time, even at room temperature, indicating that the interaction with carbon dioxide was reversible (see Figure S9.11). This quite fast dynamic equilibrium in the NMR tube precluded its study by ^{13}C NMR. Two main approaches have been established in literature for the formation of carbamate derivatives for diamino compounds: intramolecular asymmetric carbamate salts (Figure S9.12a), and dimeric symmetric carbamate species (Figure S9.12b).[53] As the ^{1}H NMR spectrum of **6b** in the presence of CO_2 does not reflect a complex mixture of asymmetric signals, the formation of the dimeric symmetric ammonium carbamate species can be considered.

When CO_2 was bubbled into the **6b** gel sample (1 mg/mL in H_2O:DMSO, 90:10 v/v) a transition from gel to weak gel was clearly observed by vial inversion. Determining the pH before and after the CO_2 adsorption, values of 8.5 and 5.3 were obtained, respectively. Thus, selecting an appropriate pH indicator, it was possible to design a colorimetric probe for the gel-sol transition. Gelation of an aqueous solution of methyl red in DMSO (10% v/v) with **6b** (1 mg/mL) led to the expected yellowish gel (Figure 9.7a-left). After bubbling carbon dioxide, a change in the colour of the sample was observed, shifting from yellow to orange (Figure 9.7a-right). Besides, comparing the rheological properties of a freshly prepared **6b** gel (1 mg/mL in H_2O:DMSO 90:10 v/v) and the sample after CO_2 absorption, the storage modulus (G') decreased more than one order of magnitude. The complex viscosity presented an average value of 5.2 Pa·s, which is more than 20 times smaller than the viscosity of the original gel (113 Pa·s). The formation of a weaker CO_2-absorbed soft material was also corroborated with the values of the oscillation strain required for breaking down the gel. Whereas an oscillation strain of 10 Pa was necessary for the gel-liquid transition in the freshly prepared gel, a strain of only 0.7 Pa was necessary for the ammonium carbamate-derived sample (Figure 9.7b).

Generally, the desorption of CO_2 is controlled by temperature for most of the systems reported to date. This is the consequence of ammonium carbamate decomposition at high temperatures, releasing carbon dioxide and the free amino groups.[56] We speculated whether our bioinspired materials could promote hydrogel recovery upon increasing temperatures. The CO_2 absorption was conducted at 25 °C under atmospheric conditions and the desorption was carried out at temperatures between 30 to 80 °C. To precisely study the reversibility of the system, we determined the desorption temperature by *in-situ* pH measurements for the sample. The pH of the gel drastically decreased from 8.48 to 5.43 in less than 100 seconds upon CO_2 bubbling. At the same time, the viscosity of the system was clearly reduced after the addition of carbon dioxide. Once the gel had been depleted, we studied the pH variations at different temperatures, providing an insight into the CO_2 desorption efficiency (Figure 9.7c). Interestingly, at temperatures > 70 °C, a significant increase

in pH could be appreciated, indicating the decomposition of the carbamate species. To our delight, this system was thus able to promote CO_2 desorption at relatively low temperatures, considering that the ammonium carbamate species are formed from primary amino groups.[39] The efficient CO_2 release was assigned to the thermodynamically favoured recovery of the supramolecular gel.
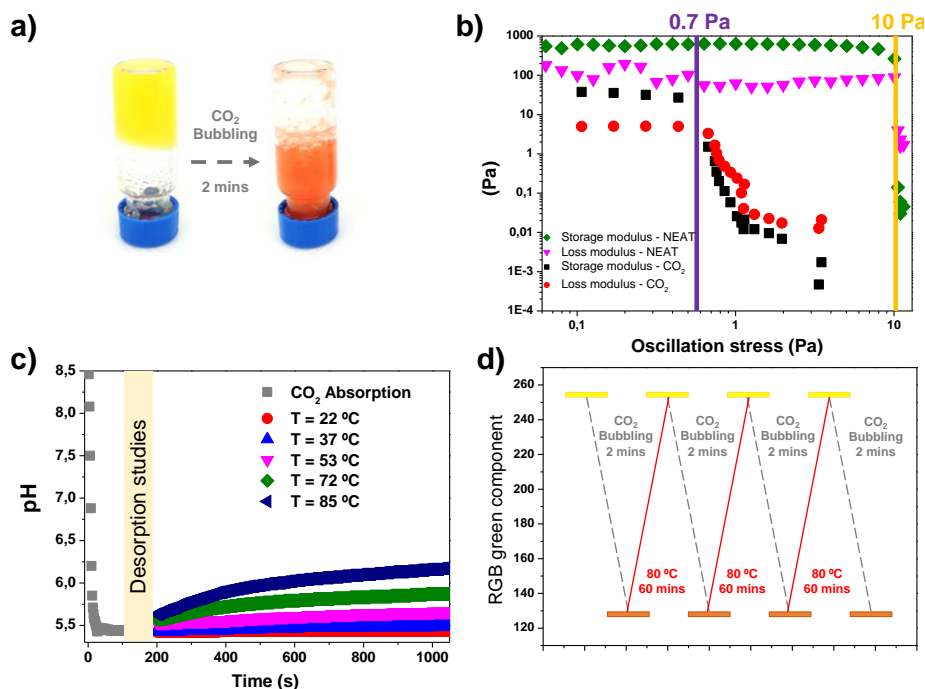

Figure 9.7. a) Vial inversion test for the methyl red containing samples before (left) and after (right) CO_2 incorporation (1 mg of **6b** in 1 mL of H_2O(methyl red):DMSO (90:10)). b) Storage and loss modulus representation for neat (green and pink, respectively) and CO_2-rich (black and red, respectively) samples. The oscillation stress required for the gel to liquid transition has been highlighted in purple for the CO_2-rich sample and in orange for the freshly prepared **6b** hydrogel. c) CO_2 absorption/desorption results obtained *via* in-line monitorization of pH for **6b** gel (1 mg in 1 mL of H_2O:DMSO, 90:10). d) Cycles for the CO_2 absorption/desorption – hydrogel depletion/formation obtained for **6b** by measuring the RGB green component observed (1 mg of **6b** in 1 mL of H_2O:DMSO, 90:10)

Subsequently, we designed a suitable cycle for studying the hydrogel destruction/formation using CO_2 as an external stimulus, obtaining promising results in terms of reversibility (Figure 9.7d). The experiment relied on simple colorimetric analyses using methyl orange as pH indicator. An orange weak gel was observed after

CO_2 absorption, resulting in a RGB green component value of 128. Contrarily, a yellowish colour (RGB green component = 255) could be observed when the hydrogel was recovered after heating at 80 °C for 60 minutes.

Hence, the formation of the carbamate species was clearly affecting the outcome of the self-assembly of the pseudopeptide. We calculated the most stable conformation for the proposed ammonium carbamate symmetric dimeric derivatives at the MMFFaq level of theory. Interestingly, albeit some intermolecular hydrogen bonding interactions were found between the amide groups and the carbamate scaffolds, only one intermolecular π-π interaction was detected, supporting the hypothesis that such aromatic forces are essential for affording the supramolecular 3D-network (Figure S9.13a). The dimeric ammonium carbamate derivative displayed tight electrostatic interaction between the terminal ammonium and carbamate groups (Figure S9.13b), leading to the formation of discrete supramolecular architectures and, thus, precluding the formation of bigger aggregates (Figure S9.13c).

9.1.5.   Conclusions

Novel open-chain pseudopeptides have been successfully synthesized. These bioinspired species have demonstrated promising properties as low molecular weight hydrogelators, with CGC values as low as 0.6 mg/mL. The nature of supramolecular interactions governing gel formation was elucidated, revealing strong cooperativity between hydrogen bonding and π-π forces. Modification of the sidechain composition and the aliphatic spacer length allowed for modulating the properties of the final materials. The presence of terminal amino groups in their basic form was found crucial for efficient self-assembly. Gel-sol transitions could be easily triggered by pH modification, obtaining the toughest materials under basic conditions (pH > 8). Besides, the high tendency of primary amines to react with carbon dioxide permitted to assay the CO_2-responsiveness of these soft materials. In this regard, remarkable results were obtained with desorption temperatures of ca. 70 °C, assigned to the thermodynamically favoured recovery of the supramolecular gel.

9.1.6. References

1- Dastidar, P. Supramolecular gelling agents: can they be designed?. *Chem. Soc. Rev.* **2008**, *37*, 2699-2715

2- Buerkle, L. E.; Rowan, S. Supramolecular gels formed from multi-component low molecular weight species. *Chem. Soc. Rev.* **2012**, *41*, 6089-6102.

3- Draper, E. R.; Adams, D. J. How should multicomponent supramolecular gels be characterised?. *Chem. Soc. Rev.* **2018**, *47*, 3395-3405.

4- Chivers, P. R. A.; Smith, D. K. Shaping and structuring supramolecular gels. *Nat. Rev. Mater.* **2019**, *4*, 463-478.

5- Levin, A.; Hakala, T. A.; Schnaider, L.; Bernardes, G. J. L.; Gazit, E.; Knowles, T. P. J. Biomimetic peptide self-assembly for functional materials. *Nat. Rev. Chem.* **2020**, *4*, 615-634.

6- Wang, D. X.; Wang, M. X. Exploring Anion−π Interactions and Their Applications in Supramolecular Chemistry. *Acc. Chem. Res.* **2020**, *53*, 1364-1380.

7- Stankovic, I. M.; Niu, S. Q.; Hall, M. B.; Zaric, S. O. Role of aromatic amino acids in amyloid self-assembly. *Int. J. Biol. Macromol.* **2020**, *156*, 949-959.

8- Song, J.; Michas, C.; Chen, C. S.; White, A. E.; Grinstaff, M. W. From Simple to Architecturally Complex Hydrogel Scaffolds for Cell and Tissue Engineering Applications: Opportunities Presented by Two-Photon Polymerization. *Adv. Healthcare Mater.* **2020**, *9*, 1901217.

9- Cheng, W.; Ding, Z.; Zheng, X.; Lu, Q.; Kong, X.; Zhou, X.; Lumand, G.; Kaplan, D. L. Injectable hydrogel systems with multiple biophysical and biochemical cues for bone regeneration. *Biomater. Sci* **2020**, *8*, 2537-2548.

10- Li, Z.; Huang, J.; Wu, J. pH-Sensitive nanogels for drug delivery in cancer therapy. *Biomater. Sci.* **2021**, *9*, 574-589.

11- Hoffman, A. S. Hydrogels for biomedical applications. *Adv. Drug Delivery Rev.* **2012**, *64*, 18-23.

12- Mayr, J.; Saldias, C.; Diaz, D. D. Release of small bioactive molecules from physical gels. *Chem. Soc. Rev.* **2018**, *47*, 1484-1515.

13- Guo, V. H.; Bae, J.; Fang, Z. W.; Li, P. P.; Zhao, F.; Vu, G. H. Hydrogels and Hydrogel-Derived Materials for Energy and Water Sustainability. *Chem. Rev.* **2020**, *120*, 7642-7707.

14- Chen, J.; Leung, F. K. C.; Stuart, M. C. A.; Kajitani, T.; Fukushima, T.; van der Giessen, E.; Feringa, B. L. Artificial muscle-like function from hierarchical supramolecular assembly of photoresponsive molecular motors. *Nat. Chem.* **2018**, *10*, 132-138.

15- Nele, V.; Wojciechowski, J. P.; Armstrong, J. P. K.; Stevens, M. M. Tailoring Gelation Mechanisms for Advanced Hydrogel Applications. *Adv. Funct. Mat.* **2020**, *30*, 2002759.

16- Fleming, S.; Ulijn, R. V. Design of nanostructures based on aromatic peptide amphiphiles. *Chem. Soc. Rev.* **2014**, *43*, 8150-8177.

17- Dou, X-Q.; Feng, C-L. Amino Acids and Peptide-Based Supramolecular Hydrogels for Three-Dimensional Cell Culture. *Adv. Mater.* **2017**, 29, 1604062.

18- Ramalhete, S. M.; Nartowski, K. P.; Sarathchandra, N.; Foster, J. S.; Round, A. N.; Angulo, J.; Lloyd, G. O.; Khimyak, Y. Z. Supramolecular Amino Acid Based Hydrogels: Probing the Contribution of Additive Molecules using NMR Spectroscopy. *Chem. Eur. J.* **2017**, *23*, 8014-8024.

19- Das, T.; Häring, M.; Haldar, D.; Díaz, D. D. Phenylalanine and derivatives as versatile low-molecular-weight gelators: design, structure and tailored function. *Biomater. Sci.* **2018**, *6*, 38-59.

20- Zanna, N.; Merlettini, A.; Tomasini, C. Self-healing hydrogels triggered by amino acids. *Org. Chem. Front.* **2016**, *3*, 1699-1704.

21- Steed, J. W. Anion-tuned supramolecular gels: a natural evolution from urea supramolecular chemistry. *Chem. Soc. Rev.* **2010**, *39*, 3686-3699.

22- Valls, A.; Castillo, A.; Porcar, R.; Hietala, S.; Altava, B.; García-Verdugo, E.; Luis, S. V. Urea-Based Low-Molecular-Weight Pseudopeptidic Organogelators for the Encapsulation and Slow Release of (R)-Limonene. *J. Agric. Food Chem.* **2020**, *68*, 7051-7061.

23- Rubio, J.; Alfonso, I.; Burguete, M. I.; Luis, S. V. Interplay between hydrophilic and hydrophobic interactions in the self-assembly of a gemini amphiphilic pseudopeptide: from nano-spheres to hydrogels. *Chem. Commun.* **2012**, *48*, 2210-2212.

24- Valls, A.; Burguete, M. I.; Kuret, L.; Altava, B.; Luis, S. V. Open chain pseudopeptides as hydrogelators with reversible and dynamic responsiveness to pH, temperature and sonication as vehicles for controlled drug delivery. *J. Mol. Liq.* **2022**, *348*, 118051.

25- Raza, F.; Zhu, Y.; Chen, L.; You, X.; Zhang, J.; Khan, A.; Waseem Khan, M.; Hasnat, M.; Zafar, H.; Wu, J.; Ge, L. Paclitaxel-loaded pH responsive hydrogel based on self-assembled peptides for tumor targeting. *Biomater. Sci.* **2019**, *7*, 2023-2036.

26- Meng, F.; Ni, Y.; Ji, S.; Fu, X.; Wei, Y. Dual Thermal-and pH-responsive Polypeptide-based Hydrogels. *Chin. J. Polym. Sci.* **2017**, *35*, 1243-1252.

27- Shaikh, H.; Rho, J. Y.; Macdougall, L. J.; Gurnani, P.; Lunn, A. M.; Yang, J.; Huband, S.; Mansfield, E. D. H.; Peltier, R.; Perrier, S. Hydrogel and Organogel Formation by Hierarchical Self-Assembly of Cyclic Peptides Nanotubes. *Chem. Eur. J.* **2018**, *24*, 19066-19074.

28- Chu, C.-W.; Stricker, L.; Kirse, T. M.; Hayduk, M.; Ravoo, B. J. Light-Responsive Arylazopyrazole Gelators: From Organic to Aqueous Media and from Supramolecular to Dynamic Covalent Chemistry. *Chem. Eur. J.* **2019**, *25*, 6131-6140.

29- Wang, H.; Heilshorn, S. C. Adaptable Hydrogel Networks with Reversible Linkages for Tissue Engineering. *Adv. Mater.* **2015**, *27*, 3717.

30- Chen, W. H.; Liao, W.-C.; Sohn, Y. S.; Fadeev, M.; Cecconello, A.; Nechushtai, R.; Willner, I. Stimuli-Responsive Nucleic Acid-Based Polyacrylamide Hydrogel-Coated Metal–Organic Framework Nanoparticles for Controlled Drug Release. *Adv. Funct. Mater.* **2018**, *28*, 1705137.

31- Doring, A.; Birnbaum, W.; Kuckling, Responsive hydrogels – structurally and dimensionally optimized smart frameworks for applications in catalysis, micro-system technology and material science. D. *Chem. Soc. Rev.* **2013**, *42*, 7391-7420.

32- Han, D.; Boissiere, O.; Kumar, S.; Tong, X.; Tremblay, L.; Zhao, Y. Two-Way CO_2-Switchable Triblock Copolymer Hydrogels. *Macromolecules* **2012**, *45*, 7440-7445.

33- Zhang, L.; Qian, J.; Fan, Y.; Feng, W.; Tao, Z.; Yang, H. A facile CO_2 switchable nanocomposite with reversible transition from sol to self-healable hydrogel. *RSC Adv.* **2015**, *5*, 62229-62234.

34- Jie, K.; Zhou, Y.; Yao, Y.; Shi, B.; Huang, F. CO_2-Responsive Pillar[5]arene-Based Molecular Recognition in Water: Establishment and Application in Gas-Controlled Self-Assembly and Release. *J. Am. Chem. Soc.* **2015**, *137*, 10472-10475.

35- Nagasawa, Y.; Seida, Y.; Gotoh, T.; Furuya, E. Influence of Hydrophobicity of Backbone Polymer in Thermo-Responsive Hydrogel with Immobilized Amine on Cycle Capacity for Absorption and Recovery of CO_2. *Polymers* **2019**, *11*, 1024.

36- Lin, S.; Theato, P. CO_2-Responsive Polymers. *Macromol. Rapid Commun.* **2013**, *34*, 1118-1133.

37- Jia, Y. G.; Zhang, M.; Zhu, X. X. CO_2-Switchable Self-Healing Host–Guest Hydrogels. *Macromolecules* **2017**, *50*, 9696-9701.

38- Satav, S. S.; Bhat, S.; Thayumanavan, S. Feedback Regulated Drug Delivery Vehicles: Carbon Dioxide Responsive Cationic Hydrogels for Antidote Release. *Biomacromolecules* **2010**, *11,* 1735-1740.

39- Rao, A. B.; Rubin, E. S. A Technical, Economic, and Environmental Assessment of Amine-Based CO_2 Capture Technology for Power Plant Greenhouse Gas Control. *Environ. Sci. Technol.* **2002**, *36*, 4467–4475.

40- Allix, F.; Curcio, P.; Nghi Pham, Q.; Pickaert, G.; Jamart-Gregoire, B. Evidence of Intercolumnar π−π Stacking Interactions in Amino-Acid-Based Low-Molecular-Weight Organogels. *Langmuir* **2010**, *26*, 16818–16827.

41- Ghosh, S.; Adler-Abramovich, L.; Gazit, E.; Verma, S. Spacer driven morphological twist in Phe-Phe dipeptide conjugates. *Tetrahedron* **2013**, *69*, 2004-2009.

42- Calculated using Spartan08 software at the MMFFaq level of theory. Deppmeier, B. J.; Driessen, A. J.; Hehre, T. S.; Hehre, W. J.; Johnson, J. A.; Klunzinger, P. E.; Leonard, J. M.; Pham, I. N.; Pietro W. J.; Jianguo, Y. Spartan '08, build 132 (Mar 27 2009), Wavefunction Inc.: Irvine CA, 2009.

43- Becerril, J.; Bolte, M.; Burguete, M. I.; Galindo, F.; García-España, E.; Luis, S. V.; Miravet, J. F. Efficient Macrocyclization of U-Turn Preorganized Peptidomimetics: The Role of Intramolecular H-Bond and Solvophobic Effects. *J. Am. Chem. Soc.* **2003**, *125*, 6677–6686.

44- Gorla, L.; Martí-Centelles, V.; Altava, B.; Burguete, M. I.; Luis, S. V. The role of the side chain in the conformational and self-assembly patterns of C2-symmetric Val and Phe pseudopeptidic derivatives. *CrystEngCom* **2019**, *21*, 2398–2408.

45- Becerril, J.; Escuder, B.; Miravet, J. F.; Gavara, R.; Luis, S. V. Understanding the Expression of Molecular Chirality in the Self-Assembly of a Peptidomimetic Organogelator. *Eur. J. Org. Chem.* **2005**, *3*, 481-485.

46- Murata, K.; Aoki, M.; Suzuki, T.; Harada, T.; Kawabata, H.; Komori, T.; Ohseto, F.; Ueda, K.; Shinkai, S. Thermal and Light Control of the Sol-Gel Phase Transition in Cholesterol-Based Organic Gels. Novel Helical Aggregation Modes As Detected by Circular Dichroism and Electron Microscopic Observation. *J. Am. Chem. Soc.* **1994**, *116*, 6664-6676.

47- Yan, C.; Pochan, D. Rheological properties of peptide-based hydrogels for biomedical and other applications. *Chem. Soc. Rev.* **2010**, *39*, 3528-3540.

48- Lin, C.; Skufca, J.; Partch, R. E. New insights into prediction of weak π–π complex association through proton-nuclear magnetic resonance analysis. *BMC Chemistry* **2020**, *14*, 66.

49- Alvarez, S. A cartography of the van der Waals territories. *Dalton Trans.* **2013**, *42*, 8617-8636.

50- Alfonso, I.; Burguete, M. I.; Galindo, F.; Luis, S. V.; Vigara, L. Molecular Rotors as Simple Models to Study Amide NH-Aromatic Interactions and Their Role in the Folding of Peptide-like Structures. *J. Org. Chem.* **2007**, *72*, 7947-7956.

51- Peng, C.; Crawshaw, J. P.; Maitland, G. C.; Martin Trusler, J. P.; Vega-Mazza, D. The pH of CO_2-Saturated Water at Temperatures Between 308 K and 423 K at Pressures up to 15 MPa. *J. Supercrit. Fluids* **2013**, *82*, 129-137.

52- Wang, M.; Lawal, A.; Stephenson, P.; Sidders, J.; Ramshaw, C. Post-combustion CO2 capture with chemical absorption: a state-of-the-art review. *Chem. Eng. Res. Des.* **2011**, *89*, 1609−1624.

53- Heldebrant, D. J.; Koech, P. K.; Ang, M. T. C.; Liang, C.; Rainbolt, J. E.; Yonker, C. R.; Jessop, P. G. Reversible zwitterionic liquids, the reaction of alkanol guanidines, alkanol amidines, and diamines with CO_2. *Green Chem.* **2010**, *12*, 713–721.

54- Said, R. B.; Kolle, J. M.; Essalah, K.; Tangour, B.; Sayari, A. A Unified Approach to CO2–Amine Reaction Mechanisms. *ACS Omega* **2020**, *5*, 26125−26133.

55- Note: studies in D_2O or D_2O/DMSO-d_6 mixtures could not be performed due to gel formation.

56- Hampe, E. M.; Rudkevich, D. M. Exploring reversible reactions between CO_2 and amines. *Tetrahedron* **2003**, *59*, 9619-9625.

9.2. Supporting information
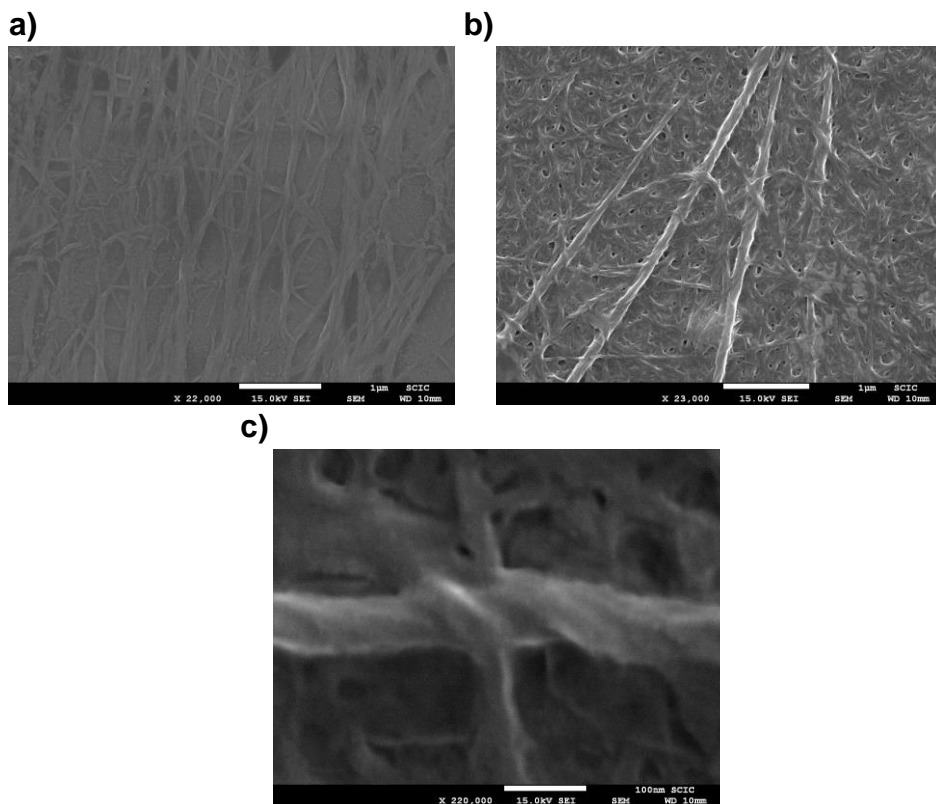
Figure S9.1. SEM images for the dried sample of **6b** (1 mg/mL) in DMSO:H_2O (10:90).

Table S9.1. Gelation properties for compound **6b** in DMSO:H_2O (10:90) at different concentrations.[a]

Entry	w/v (mg/mL)	mM	Result [a]
1	1.00	1.55	G
2	0.80	1.23	wG
3	0.60	0.91	wG
4	0.30	0.48	S
5	0.15	0.24	S
6	0.05	0.07	S

[a] Vial inversion method used for qualitative analyses. S: Soluble, wG: Weak Gel, G: Gel.
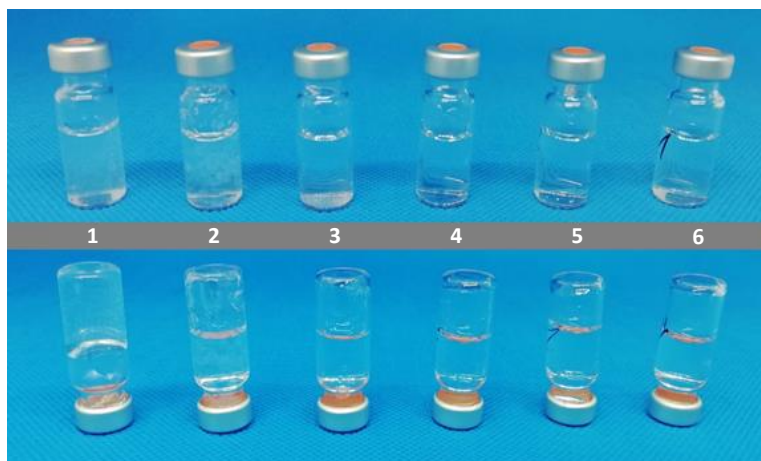
Figure S9.2. Vial inversion test pictures for determining the CGC of **6b** in H_2O:DMSO (90:10). The white numbers correspond to their assigned entry in Table 9.2.

Table S9.2. Thermal stability results for the hydrogel of **6b** (1 mg/mL in H_2O:DMSO 90:10).[a]

Temperature (ºC)	Result
25	G
30	G
35	G
40	G
45	G
50	G
55	G
60	G
65	G
70	G
75	G
80	G
85	G
90	wG

[a] The gel formation was qualitatively analysed by the vial inversion technique. I: Insoluble, S: Soluble, wG: Weak Gel, G: Gel. The sample was heated using an oil bath on a heating mantle.
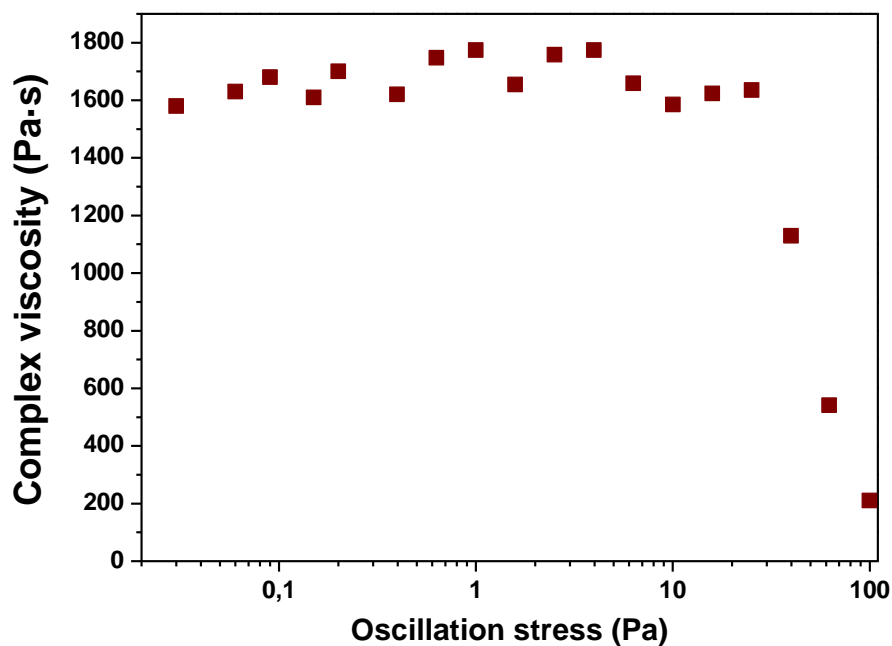
Figure S9.3. Rheological measurements (amplitude sweeps) for the hydrogel from **6b** (5 mg/mL, H$_2$O:DMSO (90:10 v/v). The complex viscosity has been represented *vs* the oscillation stress. The frequency was set to 1 Hz.
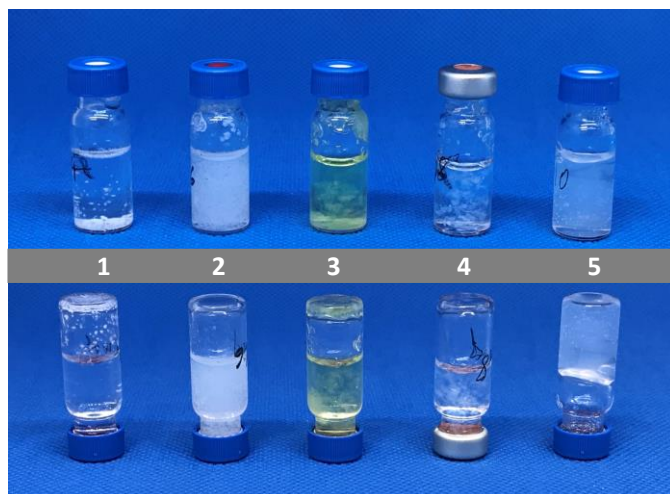
Figure S9.4. Effect of the pH in the gel formation for **6b** (1 mg/mL, bufferH$_2$O:DMSO 90:10). Vial pictures at pH: 1 (vial 1), 6 (vial 2), 7 (vial 3), 4 (vial 4), and 8 (vial 5). The vial at pH = 7 has a yellowish colour because the buffer used (Aldrich) presented a yellow colour for easy recognition.
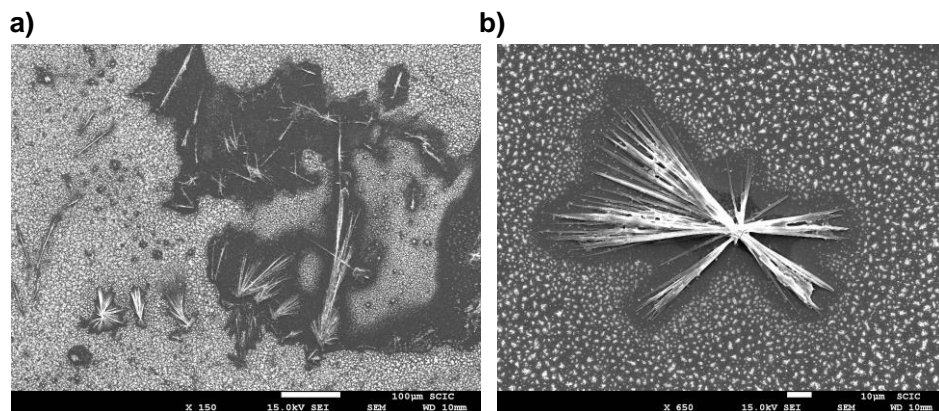
Figure S9.5. SEM images for the crystals obtained for a dried sample of **6b** (1 mg/mL) in DMSO:H$_2$O (10:90) at pH = 1. The crystalline solid has been assigned to the diprotonated [**6b**·2HCl] species.
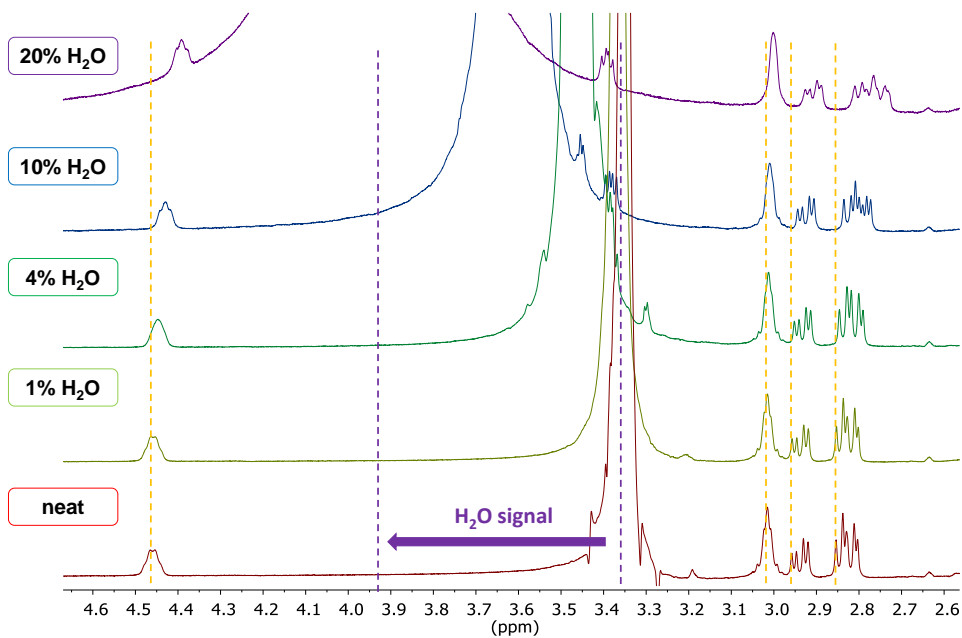
Figure S9.6. Partial ^{1}H NMR (500 MHz, DMSO-d_6) spectra for the titration of **6b** (3 mM) with increasing amounts of water. The water content has been indicated as v/v (%).
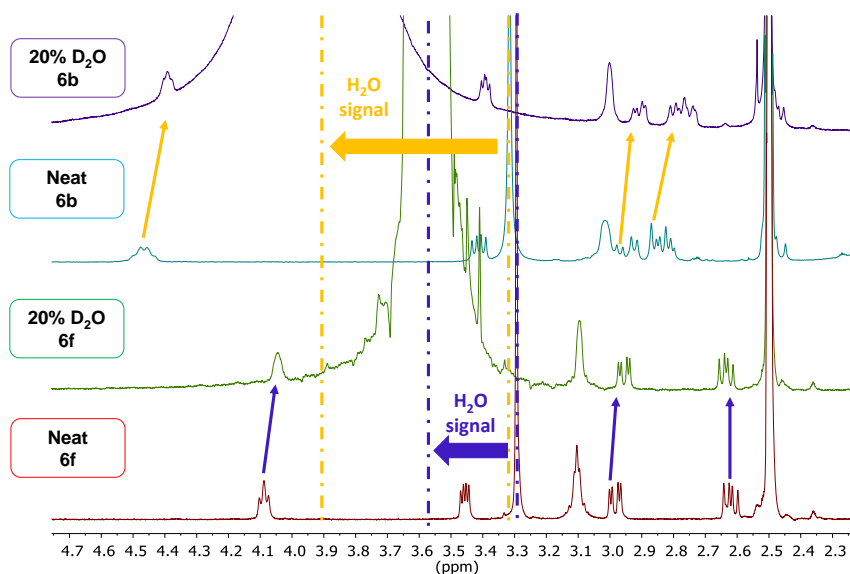
Figure S9.7. Partial ¹H NMR (500 MHz, DMSO-*d₆*, 3 mM) spectra for **6b** (above) and **6f** (below) in the presence and absence of H_2O. The spectra display the 4.7 – 2.3 ppm region. The water content has been indicated as v/v (%). The most relevant shifts have been highlighted in blue and orange for **6f** and **6b**, respectively.
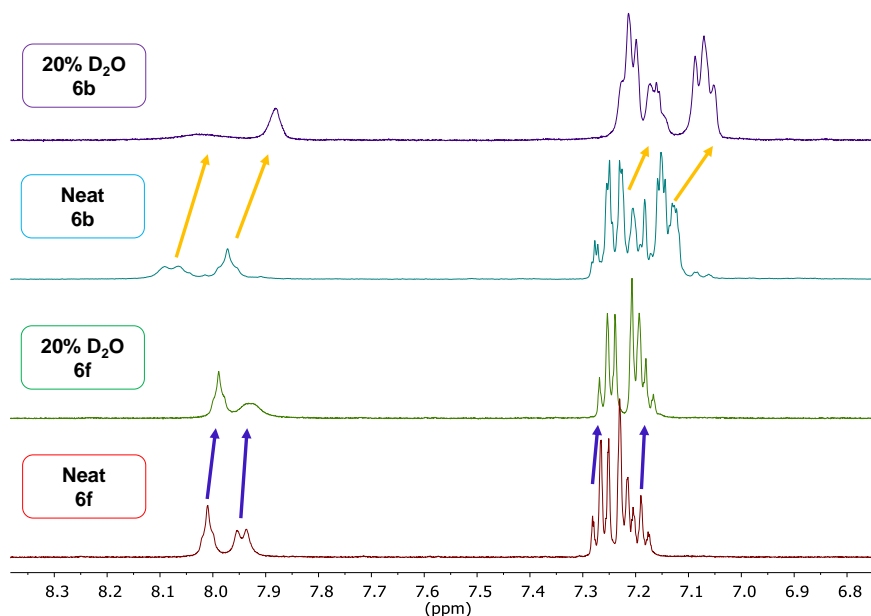
Figure S9.8. Partial ¹H NMR (500 MHz, DMSO-*d₆*, 3 mM) spectra for **6b** (above) and **6f** (below) in the presence and absence of H_2O. The spectra display the 8.3 – 6.8 ppm region. The water content has been indicated as v/v (%). The most relevant shifts have been highlighted in blue and orange for **6f** and **6b**, respectively.
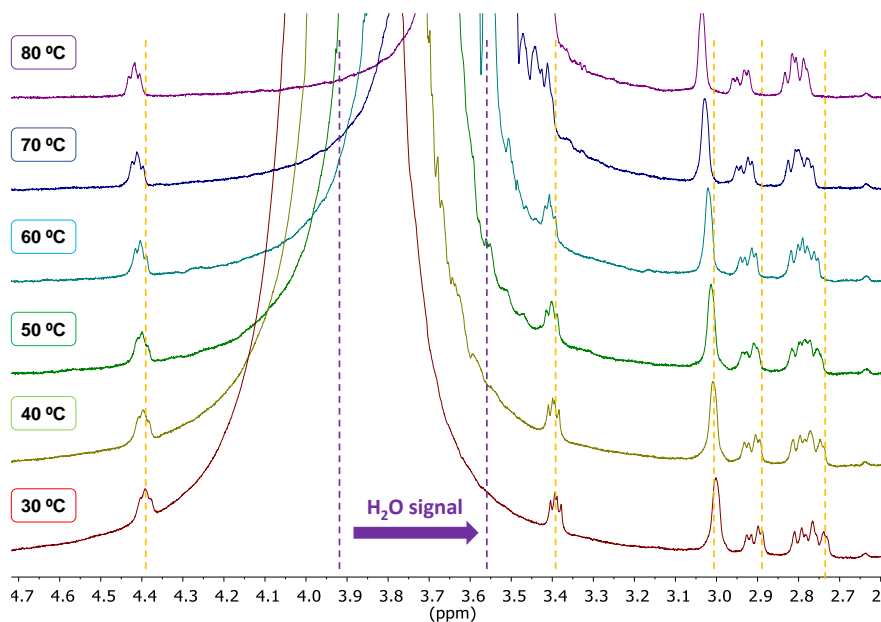
Figure S9.9. Partial ^{1}H NMR (500 MHz, DMSO-d_6) spectra for the variable temperature experiments of **6b** (3 mM, H_2O : DMSO, 20 : 80). The spectra display the 4.7 – 2.6 ppm region. Water shift has been highlighted in purple. Shifts for the characteristic protons of **6b** are highlighted in orange.
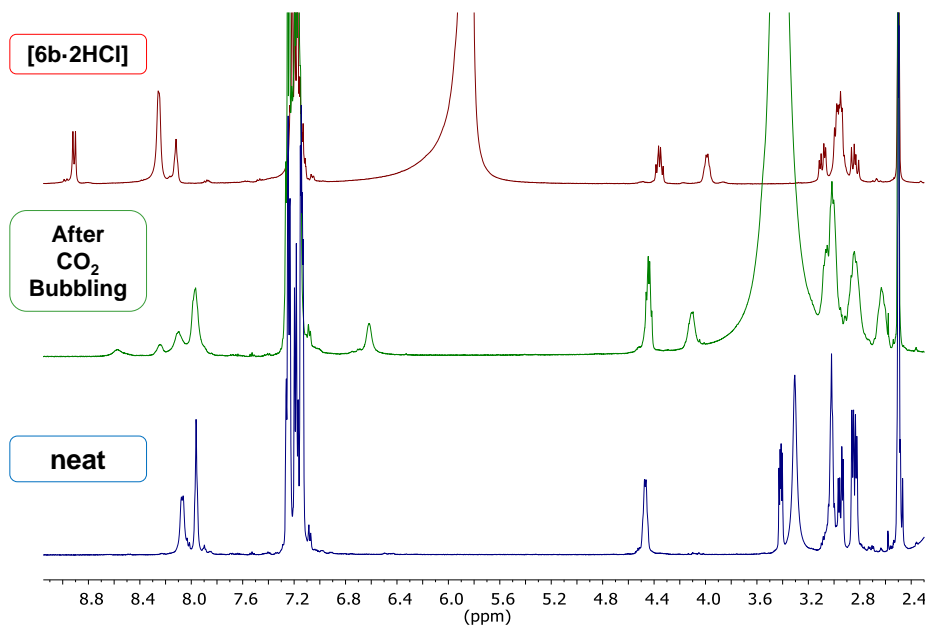
Figure S9.10. Partial ^{1}H NMR (500 MHz, 35 mM in **6b**, DMSO-d_6) spectra for neat **6b** (blue spectrum), **6b** sample after CO_2 bubbling (green spectrum), and [**6b·2HCl**] (red spectrum).
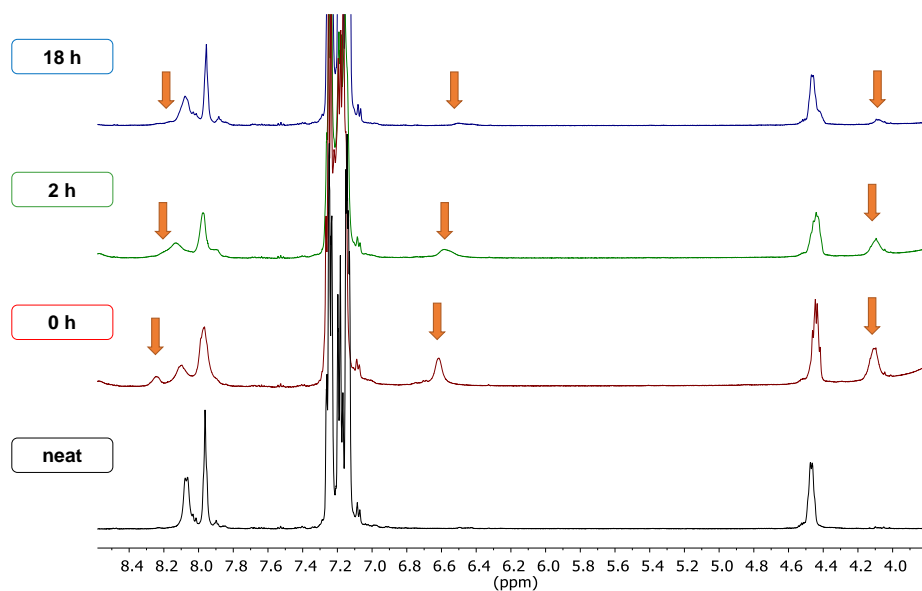
Figure S9.11. Time evolution of the partial ¹H NMR (500 MHz, 35 mM in **6b**, 25 ºC, DMSO-*d₆*) spectra for **6b** at different times after bubbling CO₂. The signals highlighted with orange arrows have been assigned to the metastable carbamate-derived species.

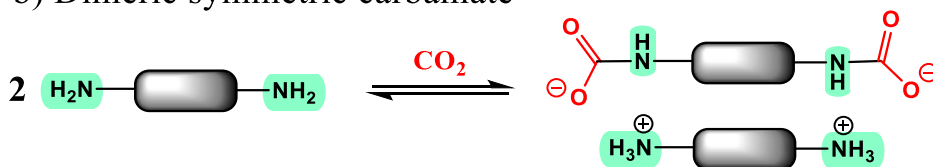## a) Intramolecular asymmetric carbamate
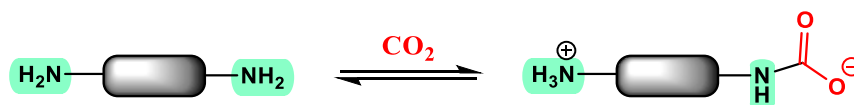
b) Dimeric symmetric carbamate

Figure S9.12. Main approaches described for the CO₂ absorption using diamino compounds. a) Intramolecular asymmetric ammonium carbamate formation. b) dimeric symmetric ammonium carbamate formation.
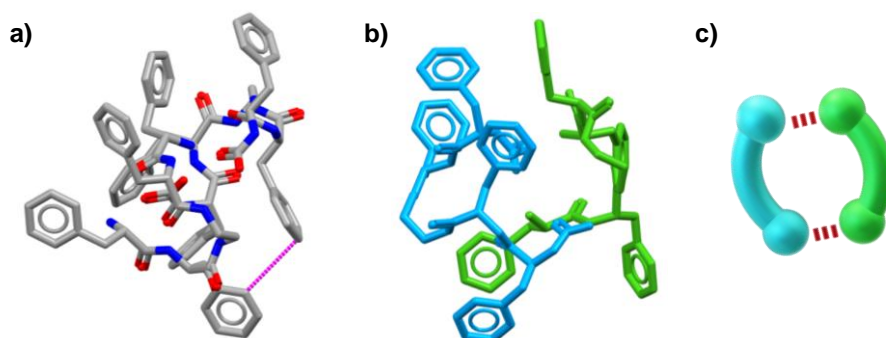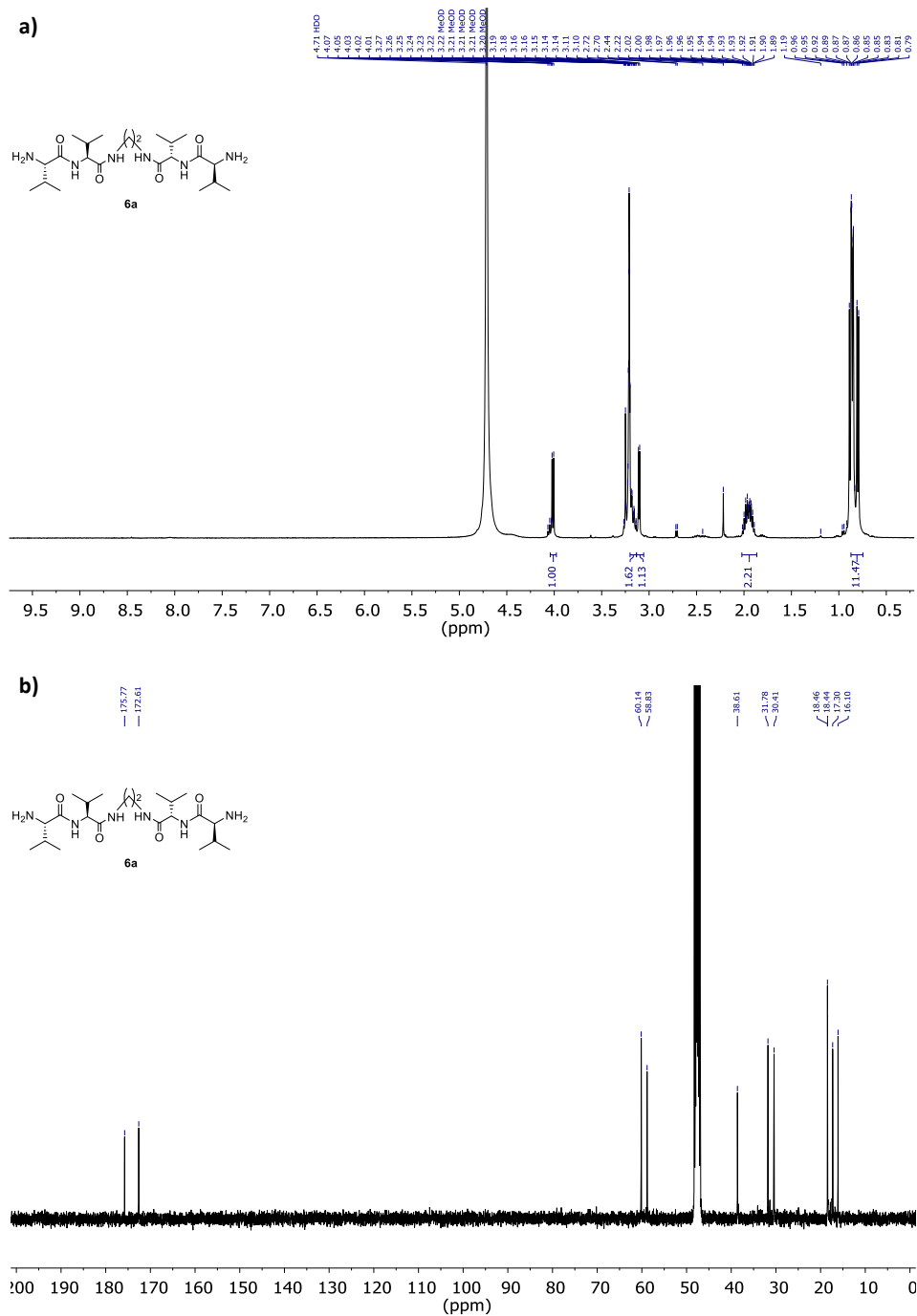
Figure S9.13. a) Most stable conformation obtained for the **6b**-CO_2 ammonium carbamate-derived symmetric dimer (Spartan08', MMFFaq). The presence of only one π-π interaction has been highlighted with a discontinuous magenta line. b) Most stable conformation obtained for the **6b**-CO_2 ammonium carbamate-derived symmetric dimer, with each one pseudopeptidic molecule coloured in green and the other one in light blue (Spartan08', MMFFaq). c) Representation of the supramolecular macrocyclic conformation adopted by the dimeric ammonium carbamate derivative. Electrostatic interactions have been highlighted with discontinuous red lines.
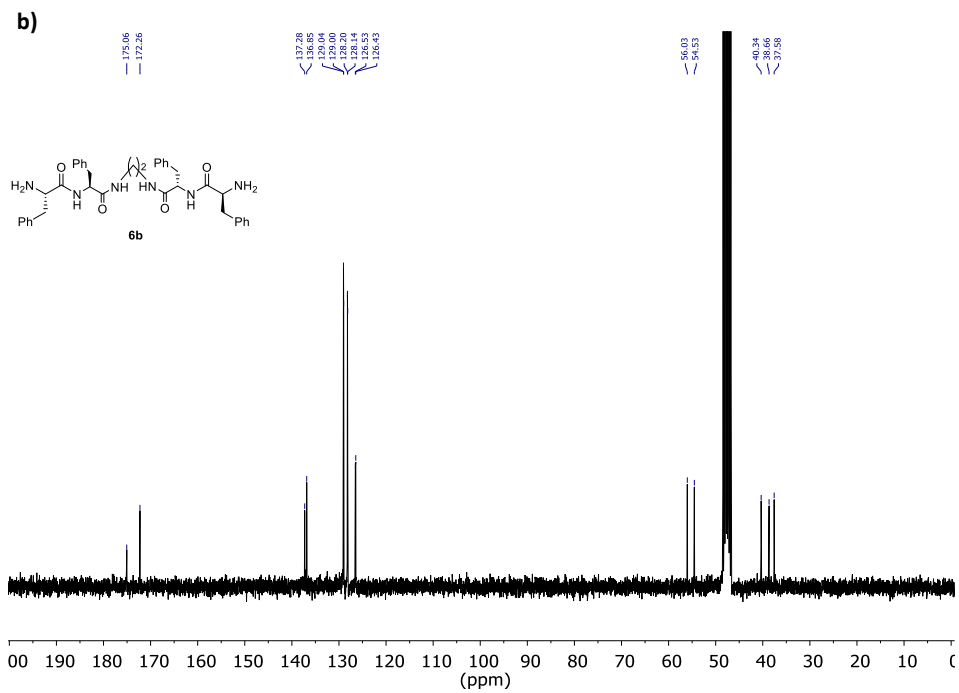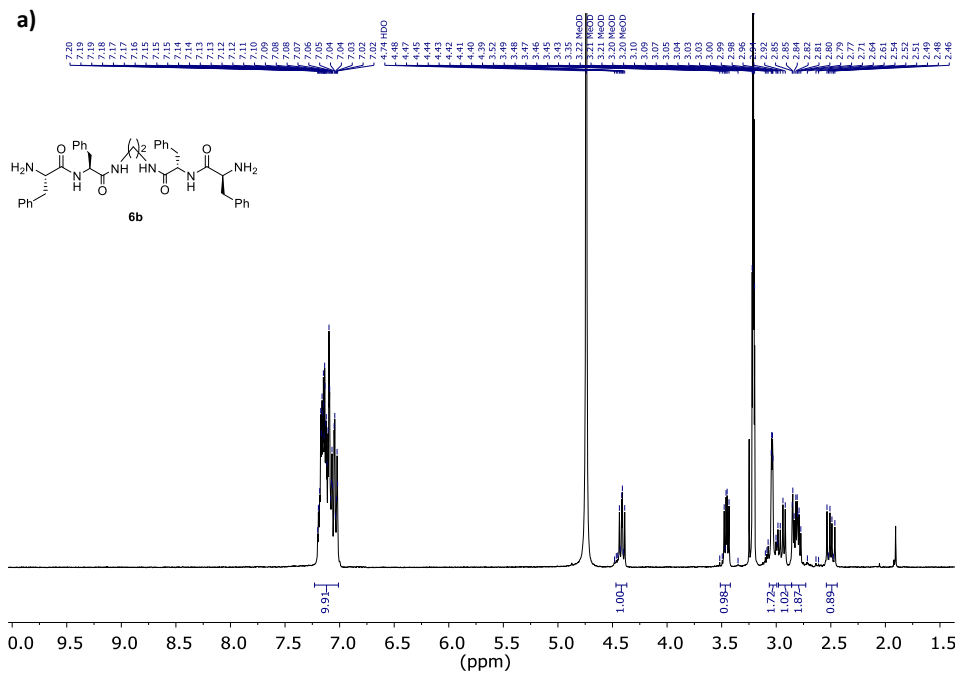
a)

b)

Figure S9.14. a) ¹H NMR (400 MHz, CD₃OD) for **6a** (7 mM). b) ¹³C{¹H} NMR (75 MHz, CD₃OD) for **6a** (10 mM).

a)

b)

Figure S9.15. a) ^{1}H NMR (300 MHz, CD$_3$OD) for **6b** (7 mM). b) ^{13}C{^{1}H} NMR (75 MHz, CD$_3$OD) for **6b** (7 mM).

a)

b)
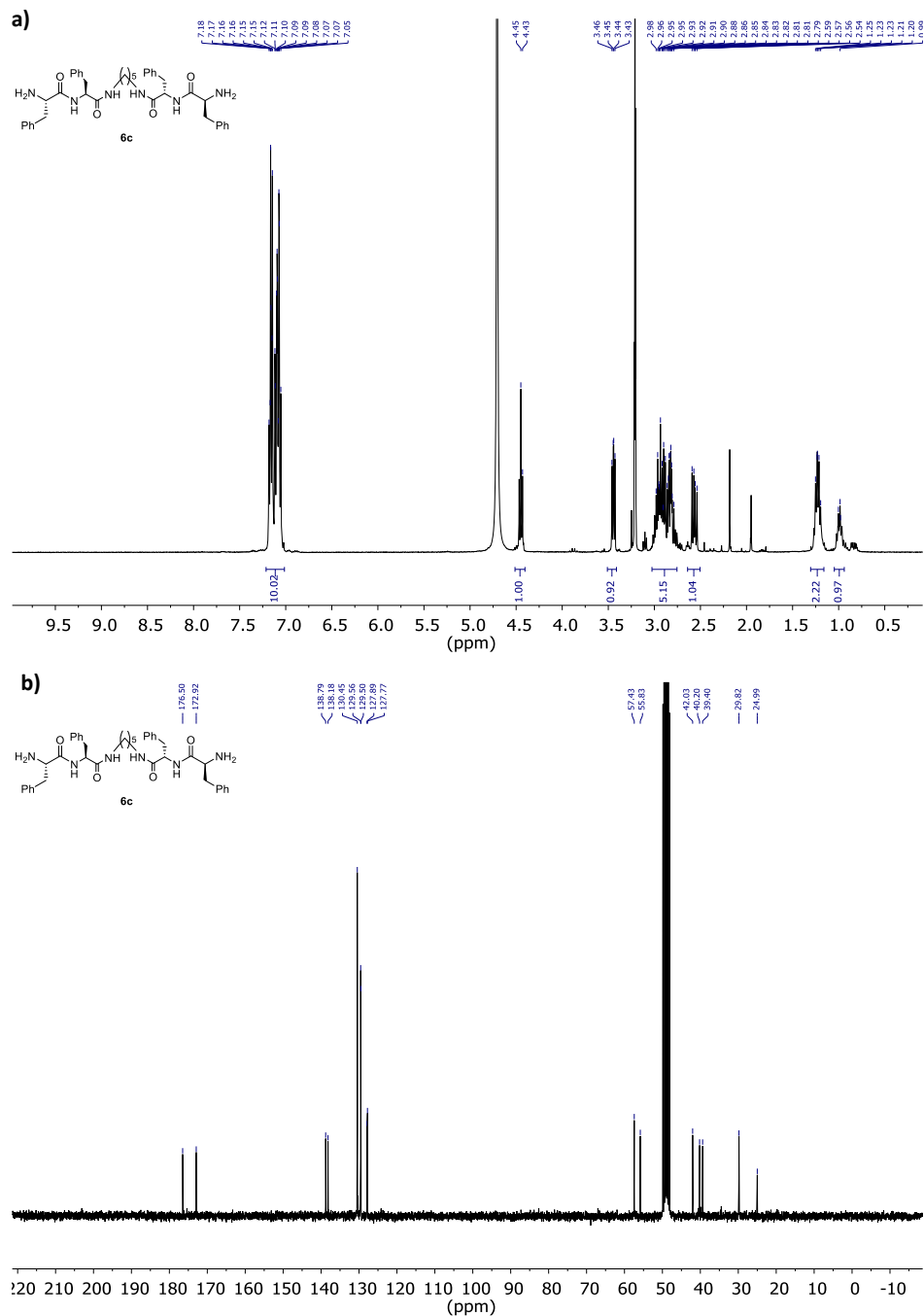
Figure S9.16. a) ^{1}H NMR (400 MHz, CD$_3$OD) for **6c** (10 mM). b) ^{13}C{^{1}H} NMR (100 MHz, CD$_3$OD) for **6c** (10 mM).

Figure S9.17. a) ¹H NMR (400 MHz, CD₃OD) for **6d** (7 mM). b) ¹³C{¹H} NMR (100 MHz, CD₃OD) for **6d** (7 mM).
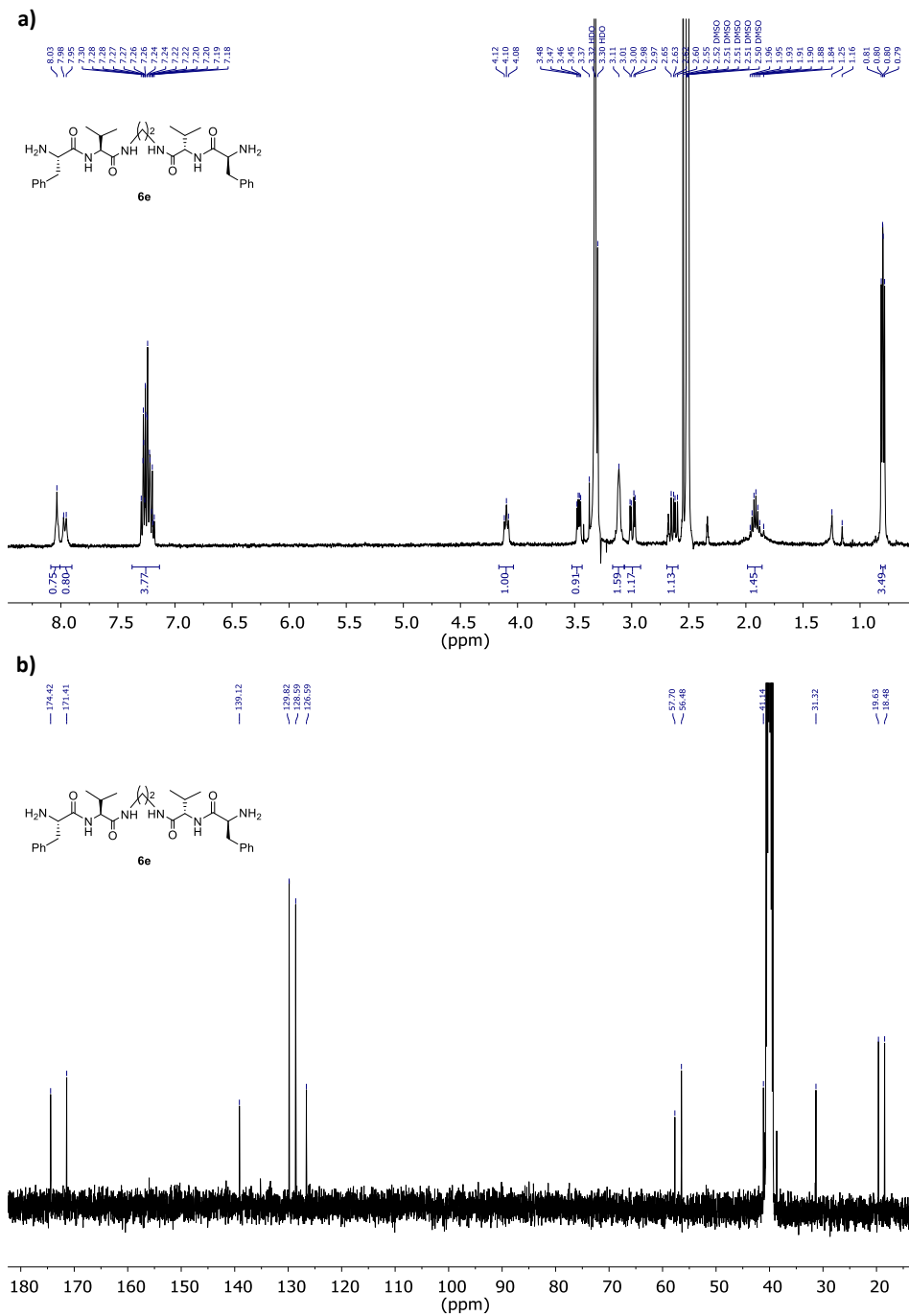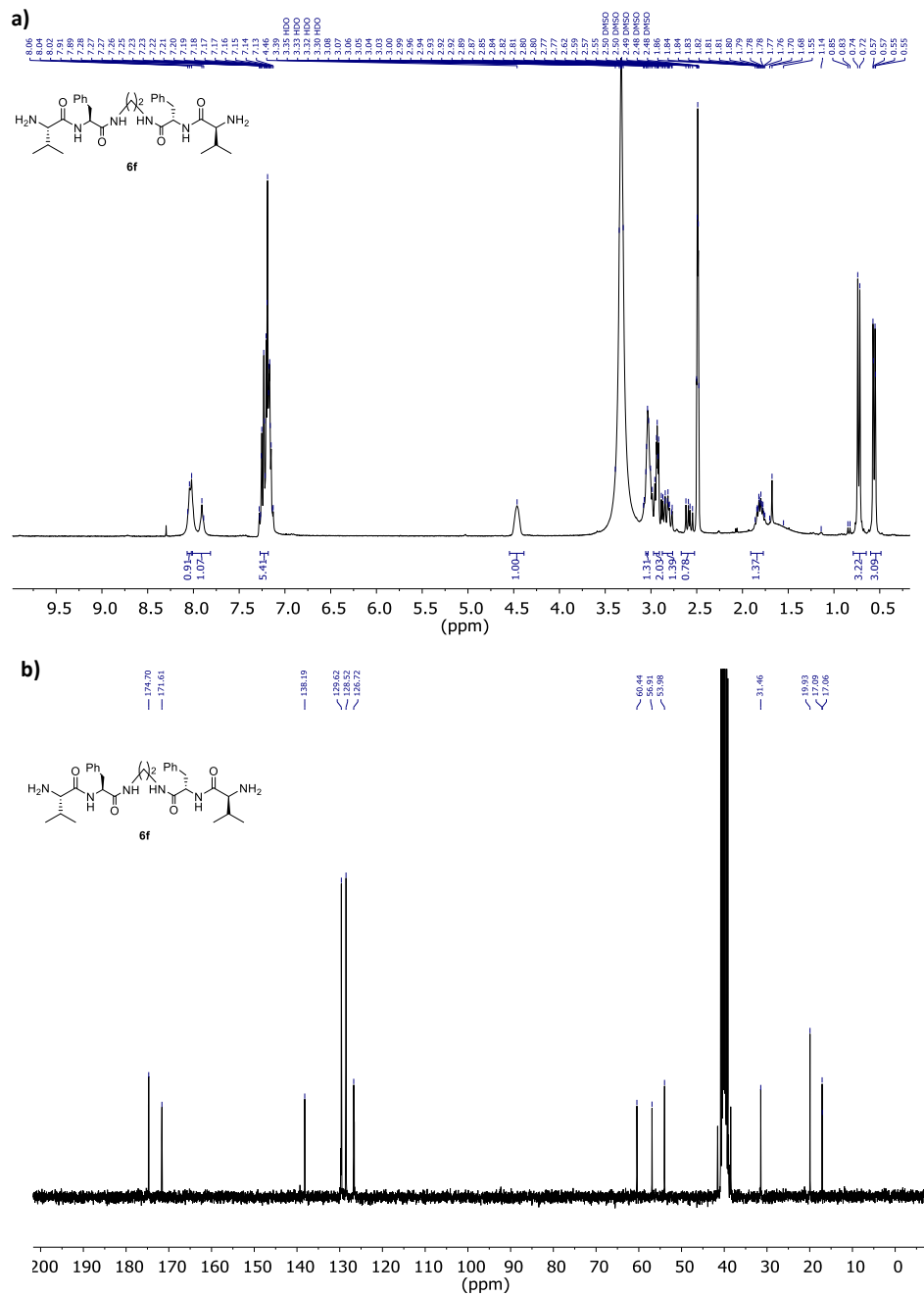
a)

b)
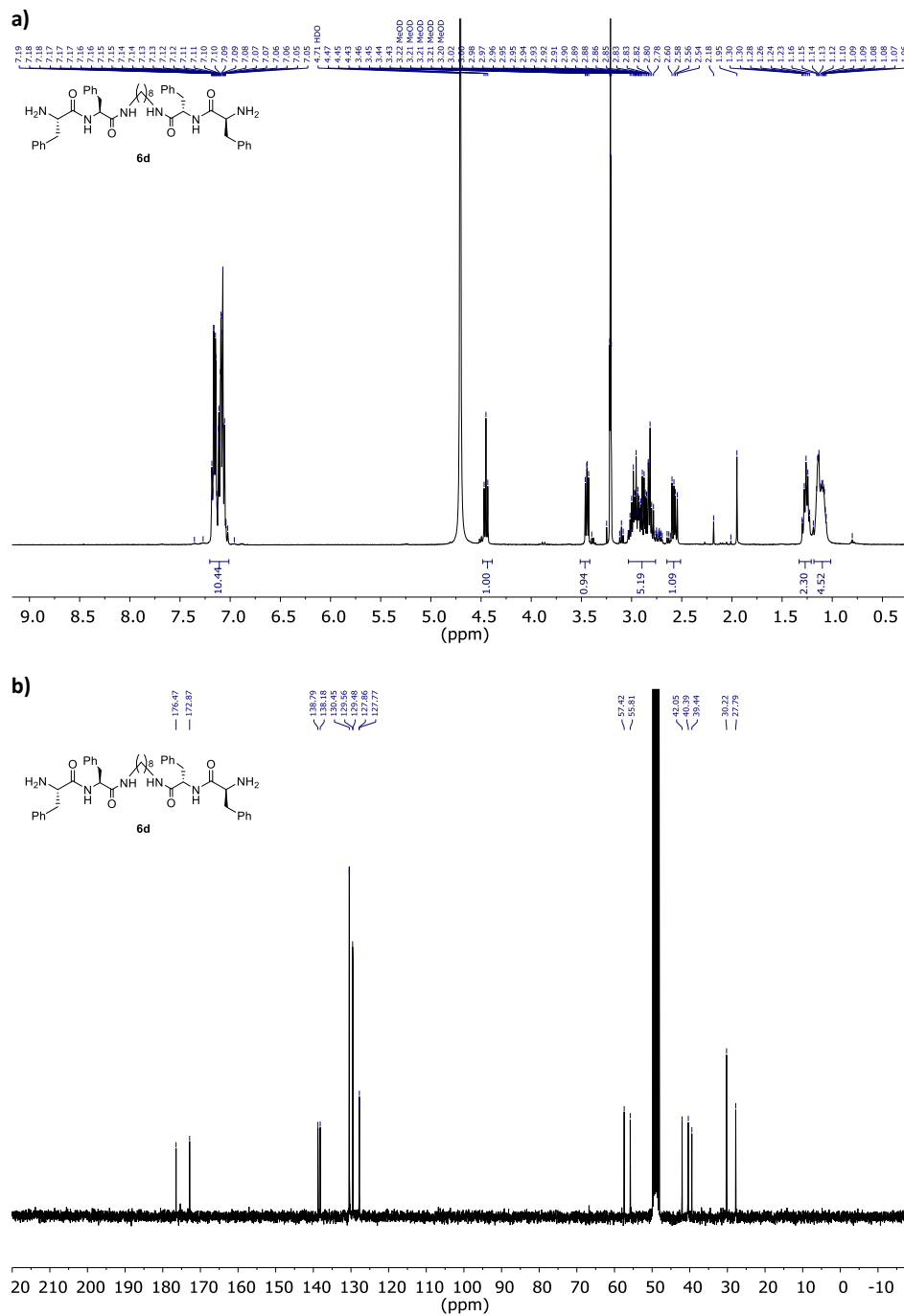
Figure S9.18. a) ^{1}H NMR (400 MHz, DMSO-d$_6$) for **6e** (4 mM). b) ^{13}C{^{1}H} NMR (100 MHz, CD$_3$OD) for **6e** (4 mM).

a)

b)

Figure S9.19. a) ^{1}H NMR (300 MHz, DMSO-d_6) for **6f** (10 mM). b) ^{13}C{^{1}H} NMR (75 MHz, CD$_3$OD) for **6f** (10 mM).

Chapter 10

Conclusions

The main conclusions for the work here presented have been included in each of the chapters. Nonetheless, it is worth to highlight the most relevant conclusions encompassing the different projects.

➢ In the field of macrocyclization reactions, a series of preorganized pseudopeptidic macrocycles have been successfully synthesized. The final compounds present high functional density close to the rigidized cavity, making them ideal candidates for supramolecular applications. Besides, the exploration of sustainable techniques for increasing the cyclization efficiency has also been explored. For instance, the implementation of templating agents has been studied for both irreversible (S_N2 reactions, Chapter 3) and dynamic (imine condensation, Chapter 8) macrocyclizations. Flow chemistry has been proved as a useful tool for improving the productivity of the reactions (Chapter 4), permitting a noteworthy decrease as well in the environmental impact.

➢ Regarding the catalytic properties of the macrocycles, we have designed three different generations of efficient synzymatic systems. The first generation encompassed the use of constrained macrocyclic pseudopeptides that were able to activate the catalytic pool in the presence of the Cl^- anion. The presence of amide groups, tertiary amines, and the cavity seemed to play a crucial role in the enzyme-like catalysis (Chapter 5). A second generation of organocatalysts was designed in order to decrease the waste generated in the catalytic process. The macrocyclic structure was modified by incorporating a pendant arm that facilitated the immobilization of the pseudopeptides, together with the nucleophile source, onto the same solid support (Chapter 6). This way, the catalytic system did not require any additional co-catalyst, while keeping remarkable activities even at low CO_2 pressures (CO_2 balloon). The third, and final, generation of synzymes embraced bimetallic Zn(II)-complexes obtained from macrocyclic

ligands. The highly crowded coordination sphere obtained for the Zn^{2+} ions allowed for the presence of "naked" iodide anions. Therefore, these systems were able to catalyse the cycloaddition of carbon dioxide to epoxides without the need of additional auxiliary substances. The synergic effect between the metallic core, nucleophilic anions, and active sites of the ligands resulted in the remarkable kinetic resolution of epoxides (Chapter 7). For all the mentioned catalyst generations, the supramolecular interactions responsible for the catalytic activity were investigated.

➢ On behalf of Materials Chemistry, we have described the syntheses of new tetra-pseudopeptidic compounds with promising gelating properties. These low molecular weight gelators can be classified as supergelators, due to the remarkably low concentrations needed for hydrogel formation. The supramolecular driving forces responsible of the self-assembly were studied in detail, highlighting a strong synergic effect between hydrogen bonding and π-π interactions. In addition, these thixotropic gels presented pH-dependent sol-gel transitions, paving the way for the design of CO_2-responsive materials (Chapter 9).